



THÈSE / UNIVERSITÉ DE RENNES 1
sous le sceau de l'Université Européenne de Bretagne

pour le grade de
DOCTEUR DE L'UNIVERSITÉ DE RENNES 1
Mention : Traitement du Signal et Télécommunications

Ecole doctorale MATISSE

présentée par

Faten Mina

Préparée à l'unité de recherche LTSI – Inserm U1099
Laboratoire Traitement du Signal et de l'Image
UFR Informatique-Electronique (ISTIC)

**Modèles
biomathématiques
des effets de la
stimulation électrique
directe et indirecte
sur la dynamique
neuronale.
Application à
l'épilepsie.**

**Thèse soutenue à Rennes
le 3 décembre 2013**

devant le jury composé de :

Jacques DEMONGEOT

Professeur des universités
Université Joseph-Fourrier Grenoble/ rapporteur

Frédéric ALEXANDRE

Directeur de Recherche INRIA
Université de Bordeaux 2/ rapporteur

Fernando LOPES DA SILVA

Professeur émérite
Université d'Amsterdam / examinateur

Arnaud BIRABEN

Praticien hospitalier
CHU de Rennes/ examinateur

Fabrice WENDLING

Directeur de recherche Inserm
Université de Rennes 1/ directeur de thèse

Pascal BENQUET

Maître de conférences
Université de Rennes 1/ co-directeur de thèse

RESUME EN FRANÇAIS

La stimulation cérébrale profonde (SCP) est désormais une option thérapeutique possible pour les patients atteints de troubles neurologiques comme la maladie de Parkinson, des tremblements, la dystonie, l'épilepsie Néanmoins, si la SCP semble être efficace pour corriger des troubles du mouvement (la maladie de Parkinson, la dystonie ...)[1], les résultats obtenus dans le cadre de l'épilepsie sont moins évidents [2]. Une grande variabilité interindividuelle des effets des neurostimulations est souvent rapportée. Alors qu'un protocole de stimulation intracérébral peut diminuer la fréquence de crises d'épilepsie chez un patient donné, une procédure similaire peut au contraire être aggravante chez un autre patient. Cela est vraisemblablement dû, entre autre, au choix des paramètres de stimulation qui se base, en partie, sur certains réglages empiriques identifiés chez les patients parkinsoniens. Cette approche empirique est la conséquence d'une compréhension incomplète des mécanismes neuronaux qui sous-tendent les effets modulateurs de l'activité neuronale induits par la stimulation [3].

CONTEXTE BIOMEDICAL ET ENONCE DU PROBLEME

L'épilepsie est un trouble neurologique qui touche 1% de la population mondiale. Ce syndrome affecte plus particulièrement les enfants, les adolescents et les personnes âgées et la sémiologie des crises diffère d'un patient à un autre. Les crises sont la seule manifestation clinique de la maladie. Elles sont l'expression d'un dysfonctionnement, aigu et transitoire (quelques secondes à quelques minutes) de l'activité électrophysiologique du cerveau, lié à la fois à une hyperexcitabilité et une hypersynchronisation des cellules neuronales.

Sur le plan thérapeutique, les traitements antiépileptiques actuels sont symptomatiques. Ils ne guérissent pas l'épilepsie mais contribuent à la diminution de la fréquence des crises. Cependant, malgré l'existence d'une multitude de médicaments antiépileptiques sur le marché, un tiers des patients épileptiques ne répondent pas aux traitements médicamenteux et sont ainsi considérés pharmaco-résistants. Presque deux tiers de ces patients présentent une forme focale d'épilepsie [4]. L'intervention chirurgicale reste possible pour certains d'entre eux. Pourtant, la résection de la zone épileptogène n'est toujours pas possible pour des considérations anatomiques et fonctionnelles. Dans ce contexte, la SCP représente une alternative thérapeutique. Or, les protocoles de stimulations efficaces ne sont actuellement pas

identifiés. Les efforts cliniques déployés pour les étudier suivent souvent des approches empiriques.

Dans ce contexte, les objectifs de cette thèse sont les suivants :

- 1) Etudier, sur le plan théorique, les effets de la stimulation électrique sur la dynamique neuronale épileptique à partir de modèles biomathématiques
- 2) Progresser dans la compréhension des mécanismes neuronaux qui sous-tendent les effets modulateurs observés.
- 3) Etablir des règles pouvant guider le choix des paramètres de stimulation.
- 4) Procéder à une validation expérimentale, si possible, des résultats théoriques obtenus.

APPROCHE PROPOSEE

Chez les patients épileptiques, les signaux électroencéphalographiques recueillis sur le cuir chevelu ou de manière intracérébrale, même en l'absence de crises, révèlent une dynamique électrique anormale caractérisée par la récurrence d'activités spécifiques. Ces activités, regroupées sous le terme d'activités intercritiques, désigne la dynamique épileptique en dehors des crises. Cette thèse porte notamment sur l'analyse des effets modulateurs de l'activité intercritique par le courant de stimulation.

La méthodologie générale proposée, pour atteindre les objectifs mentionnés, repose sur l'utilisation conjointe de la modélisation biomathématique, l'analyse des signaux réels (cliniques/expérimentaux), l'analyse des systèmes dynamiques non linéaire et l'expérimentation animale. La Figure 1 résume le travail entrepris pendant la thèse et son organisation dans le manuscrit. Deux configurations de SCP sont étudiées dans ce manuscrit : la stimulation indirecte en courant alternatif (Partie 1) et la stimulation directe en courant continu (Partie 2).

Pour chaque configuration, un modèle biomathématique des structures cérébrales impliquées dans les dynamiques épileptiques étudiées est proposé. Mathématiquement parlant, il s'agit d'un système dynamique non linéaire décrit par un ensemble d'équations différentielles ordinaires du premier ordre comportant un terme stochastique (bruit d'entrée). Ensuite, chaque modèle est optimisé pour reproduire plus fidèlement possible les dynamiques temporelles observées dans les signaux électrophysiologiques réels. Pour cette identification de paramètres, des algorithmes de traitement et de caractérisation des signaux ont été développés. Finalement, l'analyse du modèle sous stimulation permet l'identification des mécanismes potentiellement impliqués et de mieux comprendre les effets induits, notamment par rapport aux paramètres utilisés (fréquence, intensité, polarité, durée).

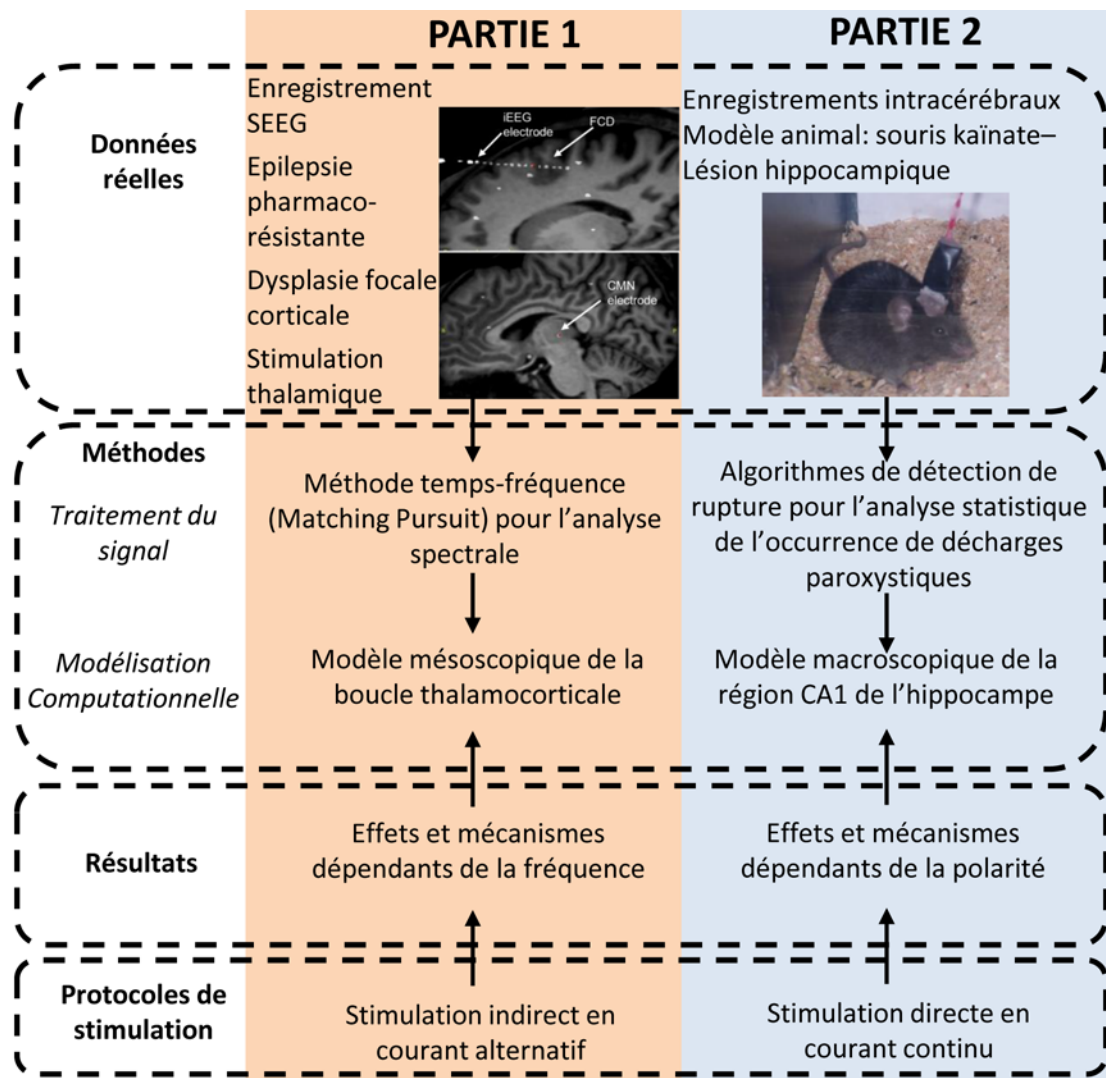


Figure 1. Organisation du manuscrit et travail accompli. La thèse s’organise en deux parties, chacune traitant d’un protocole de stimulation. La Partie 1 concerne la stimulation indirecte en courant alternatif. La Partie 2 concerne la stimulation directe en courant continu. Les deux études utilisent une même approche méthodologique (le traitement du signal et la modélisation computationnelle) et sont aussi fortement liées aux données réelles : soit chez l’homme (Partie 1) soit chez la souris épileptique (Partie 2). Les résultats suggèrent une forte dépendance des effets et des mécanismes de la stimulation sur les paramètres des protocoles utilisés : la fréquence dans le premier cas (Partie 1) et la polarité dans le deuxième (Partie 2).

PARTIE 1 : CAS DE LA STIMULATION INDIRECTE EN COURANT ALTERNATIF (CA)

Dans la première partie de la thèse, un cas particulier de stimulation indirecte en courant alternatif a été étudié. Il s’agit de la stimulation du thalamus dans le cadre d’une épilepsie corticale focale. Cette partie a pour objectif d’étudier les effets de la stimulation électrique d’un noyau gris central l’activité pathologique d’une région néocorticale. La première étape a consisté en la conception d’un modèle mésoscopique de la boucle thalamocorticale. Le modèle proposé est une version étendue de certains modèles préexistants. Il adopte une architecture tri-modulaire semblable à celle généralement utilisée dans les modèles déjà publiés. Cette

architecture est décrite dans la figure 2. Les trois modules (cortical, thalamique, et réticulaire) sont représentés dans le modèle. Chaque module est composé d'une ou plusieurs sous populations neuronales. Plusieurs aspects nouveaux ont été implémentés : (1) la prise en compte des effets de la stimulation au niveau sous-cortical, représentée par une entrée de contrôle en boucle ouverte, (2) la modélisation explicite de deux mécanismes cellulaires (dépression synaptique à court terme (DCT) et l'inhibition antérograde (FFI)) essentiels dans les dynamiques thalamocorticales et (3) une implémentation du compartiment cortical qui reproduit au mieux les dynamiques épileptiques.

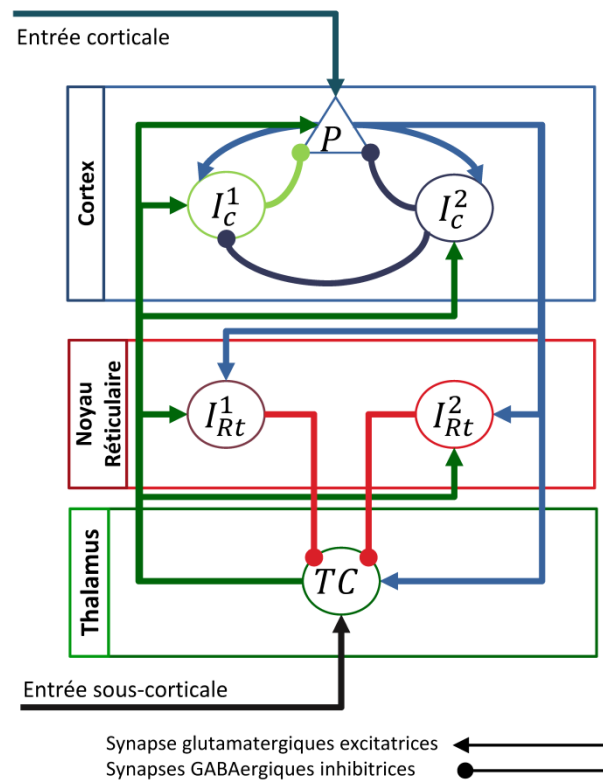


Figure 2. L'architecture tri-modulaire du modèle. Les modules cortical, thalamique, et réticulaire sont représentés dans le modèle. Chacun est composé d'une ou plusieurs sous populations neuronales interconnectées via des synapses excitatrices ou inhibitrices.

Une base de données clinique provenant du bilan pré-chirurgical intracérébral effectué chez un patient présentant une épilepsie pharmacorésistante d'origine corticale focale a été utilisée pour optimiser les paramètres du modèle (distance entre la sortie du modèle et les signaux réels, correspondant à un potentiel de champ local ou local field potential ; LFP). Trois paramètres clés (parmi une quarantaine de paramètres) ont été optimisés, les autres étant réglés selon des considérations physiologiques. L'algorithme automatique d'optimisation a requis la mise au point d'une méthode de traitement et de caractérisation des signaux réels hors et pendant la stimulation thalamique. Cette méthode s'est basée sur une décomposition

atomique adaptative des signaux (Matching Pursuit – MPTK [5]). Il a permis l'évaluation de la distribution de l'énergie du signal dans les sous bandes classiques de l'EEG (δ , ..., γ). Ce même algorithme a été ensuite utilisé pour calculer le vecteur de caractéristiques de la sortie du modèle pour chaque valeur parcourue du vecteur de paramètres. Les paramètres optimaux retenus sont ceux qui minimisent la distance euclidienne entre le vecteur de caractéristiques calculé sur signal simulé et celui calculé sur signal réel.

Le comportement dynamique du modèle optimisé a été ensuite analysé en fonction de la fréquence du signal d'entrée (signal de stimulation) permettant de contrôler les dynamiques simulées. Les portraits de phase ont été explorés. L'intermittence des dynamiques simulées a été quantifiée en fonction de la fréquence de stimulation sur l'intervalle [0.5 ; 150 Hz].

L'algorithme de traitement du signal proposé a permis la classification (k-means ; distance de Mahalanobis) des effets de la SCP observés chez le patient. Les résultats de cette étape ont montré que les effets s'organisent en trois groupes : la stimulation à basses fréquences (SBF ; 2 Hz), la stimulation à moyennes fréquences (SMF ; 50 Hz) et la stimulation à hautes fréquences (SHF ; 70, 100, 150 Hz). Par ailleurs, les effets de la SMF coïncident avec le groupe d'activités interictales observées hors stimulation (HS).

Au niveau modélisation, les résultats de cette étude ont montré la dépendance en fréquence des effets de la stimulation indirecte en CA du thalamus sur la dynamique corticale. Des hypothèses sur plusieurs mécanismes ont pu être formulées. La Figure 3 montre les portraits de phases du modèle pour les quatre conditions de stimulation décrites précédemment (HS, SBF, SMF, et SHF). Ces portraits de phases révèlent les bifurcations, dépendantes de la fréquence du signal de stimulation, des dynamiques modélisées. La stimulation à BF réduit largement l'amplitude des oscillations spontanées dans le modèle observées en condition HS. Par contre, la stimulation à MF aggrave ces oscillations. La stimulation à HF abolit ces oscillations et ramène le comportement dynamique du modèle sur un point fixe qui traduit une activité physiologiquement plus proche de la normale.

Cette approche nous a permis de montrer que le comportement dynamique du système change de manière non linéaire en fonction de la fréquence de stimulation. L'intervalle]20; 60 Hz] conduit à une amplification des oscillations dans le modèle alors que pour des fréquences inférieures à 20 Hz ou supérieures à 60 Hz, ces oscillations « pathologiques » sont largement amorties voire abolies.

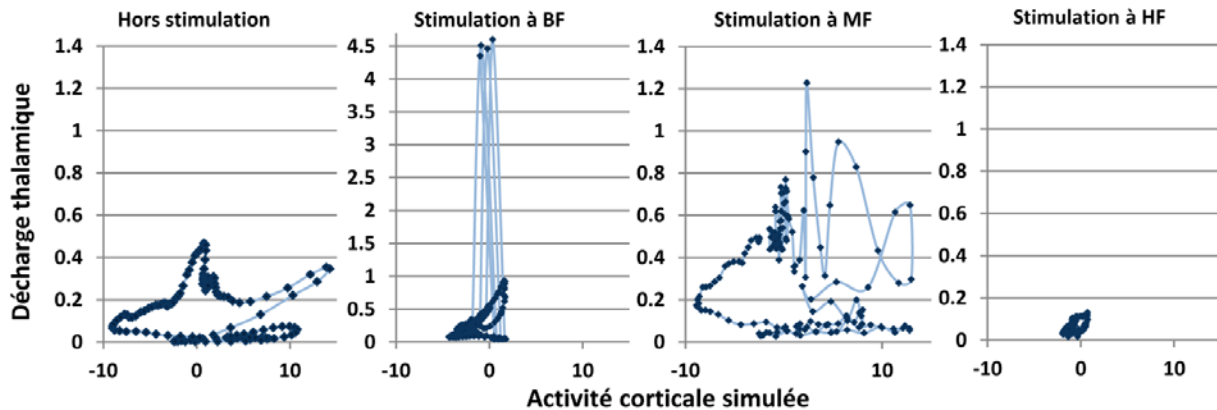


Figure 3. Les portraits de phase du modèle pour les quatre conditions de stimulation : Hors Stimulation (HS), Stimulation à basses fréquences (BF ; ici 2 Hz), à moyennes fréquences (MF ; ici 50 Hz) et à hautes fréquences (HF ici 100 Hz). Le système oscille sur un cycle hors stimulation. Ce cycle est réduit dans le cas de la stimulation à BF, aggravé à MF et aboli à HF. Cela montre que l'entrée de stimulation induit, dans le modèle, le même type de bifurcations que celle observées dans les signaux EEG intracérébraux acquis chez le patient.

L'étude du modèle computationnel a mis en évidence plusieurs mécanismes neurophysiologiques pouvant expliquer les effets dépendants de la fréquence de stimulation. La stimulation thalamique à basse fréquence (BF) inhibe l'activité corticale épileptique en renforçant à la fois l'inhibition interneuronale antérograde corticale et en provoquant une dépression à court terme des synapses excitatrices thalamo-corticales. Ces mécanismes permettent de diminuer l'excitabilité du module cortical observée à BF.

La stimulation à fréquence moyenne (MF) renforce, au contraire, les oscillations épileptiques dans la boucle thalamo-corticale en augmentant la dépolarisation des neurones inhibiteurs lents du module réticulaire et surtout des neurones excitateurs thalamo-corticaux. Enfin, la stimulation thalamique à haute fréquence (HF) réduit l'activité épileptique corticale en supprimant la sortie thalamique (par stimulation des neurones du noyau réticulaires inhibant les cellules thalamo-corticales).

PARTIE 2 : CAS DE LA STIMULATION DIRECTE EN COURANT CONTINU (CC)

Dans la deuxième partie de ma thèse, nous avons étudié les effets de la stimulation directe de la zone épileptogène en courant continu (CC) dans le contexte de l'épilepsie méiale du lobe temporal (EMLT), une forme fréquente d'épilepsie pharmaco-résistante. Dans cette partie, les effets polarisants de la stimulation sont étudiés en fonction de la polarité du courant, au niveau biomathématique et expérimental.

Notre étude se base sur un modèle computationnel d'hippocampe préalablement développé dans notre équipe [6], (structure cérébrale impliquée dans l'initiation des crises dans ce type d'épilepsie).

Nous avons apporté deux modifications au modèle préexistant. Une implémentation de l'interface électrode-électrolyte [7] au niveau des trois sous populations de neurones représentées dans le modèle (cellules pyramidales, interneurons médiant des courants gabaergiques à cinétique lente, et interneurons médiant des courants gabaergiques à cinétique rapide) a été proposée. Le signal de stimulation a été modulé par un coefficient de pondération propre à chaque population avant d'être ajouté au potentiel membranaire moyen. Cette implémentation modifie la polarisation membranaire en fonction de l'entrée de stimulation. D'autre part, nous avons également implémenté une entrée afférente excitatrice au niveau des cellules principales qui permet d'obtenir des transitions dynamiques, entre une activité de fond et une activité à type de décharge épileptique soutenue (quelques secondes). Les lois statistiques qui définissent les caractéristiques d'occurrence de ces décharges (intervalles entre décharges et durée des décharges) ont été identifiées à partir des données expérimentales acquises chez la souris épileptique (modèle kainate *in vivo*). Cela a nécessité la mise au point d'un algorithme de détection et de caractérisation de ces décharges. L'algorithme de Page-Hinkley [8], également utilisé dans notre équipe, a été retenu pour détecter les décharges épileptiques dans les signaux acquis expérimentalement. Il a permis de détecter automatiquement les instants de début et de fin de ces décharges paroxystiques et ainsi d'estimer leur durée.

Les résultats computationnels ont suggéré (1) que les statistiques d'occurrence des décharges paroxystiques suivent une loi gamma (2) et que les effets de la simulation sont dépendants de la polarité du courant injecté. Dans le modèle, deux effets ont été observés. D'une part, une réduction significative de la durée et de l'énergie des décharges paroxystiques pour un courant hyperpolarisant (effet anti-épileptique). D'autre part, une amplification de ces décharges paroxystiques pour un courant dépolarisant (effet pro-épileptique).

Une procédure expérimentale a été entreprise dans le modèle animal pour i) identifier les lois statistiques d'occurrence des décharges épileptiques et ii) (in)valider les hypothèses générées à partir du modèle biomathématique quant aux effets de la stimulation en courant constant sur l'occurrence de ces décharges. Une stimulation de longue durée (50 s) à faible intensité (1 μ A) a été appliquée dans l'hippocampe. L'activité hippocampique (LFP) suivant cette stimulation a été enregistrée et analysée. Les résultats ont montré qu'il existe une polarité de stimulation qui réduit significativement les décharges paroxystiques dans l'hippocampe épileptique, conformément à la prédiction du modèle. Cependant, la polarité inverse n'a pas induit de modifications significatives de l'occurrence de décharges, comme prédit. Une étude préliminaire *in vitro* a montré que les mécanismes qui sous-tendent les effets observés *in vivo* et dans le modèle peuvent être liés à des mécanismes de polarisation de la membrane des neurones. Cependant d'autres mécanismes plus complexes liés aux réseaux neuronaux stimulés semblent aussi être impliqués.

CONCLUSION

Ce travail a permis la caractérisation des effets de deux protocoles différents de stimulation électrique, indirecte et directe.

Dans la première partie du manuscrit on montre que les effets et les mécanismes de stimulation indirecte en courant alternatif sont dépendants de la fréquence choisie. Ce travail représente la première étude qui caractérise les effets de ce type de stimulation sur une plage de fréquences aussi large (0.5 – 150 0Hz). A basse fréquence, les résultats computationnels suggèrent que les stimulations qui diminuent l'activité épileptiques impliquent à la fois la dépression synaptique à court terme et l'inhibition antérograde au niveau thalamocortical. Ces mécanismes jouent un rôle majeur dans la boucle thalamocorticale. Ils interviennent pour affiner la réponse corticale à l'entrée thalamique, comme cela a été montré dans le cadre de l'adaptation sensorielle [9] et dans les dynamiques thalamocorticales [10].

Notre étude montre qu'il existe une plage de fréquence, de valeur intermédiaire (20-60Hz) qui ne diminue pas l'activité épileptique mais qui au contraire peut l'aggraver. Dans la littérature, les mécanismes neurophysiologiques de la stimulation à fréquence intermédiaire ne sont pas bien établis. Pourtant, ces effets sont souvent utilisés en clinique pour déclencher des crises lors de l'exploration pré-chirurgicale afin de localiser la zone épileptogène. D'ailleurs, des stimulations répétitives aux alentours de 60 Hz sont aussi utilisées provoquer une épileptogénèse chez les rongeurs (modèle kindling) [11], ce qui corroborent les résultats décrits dans cette thèse

Enfin les stimulations à hautes fréquences sont également capables de diminuer l'activité épileptique. Nos résultats suggèrent que ce type de stimulation inhibe la structure ciblée en dépolarisant toutes les sous populations de neurones qui la constitue. Cela a été récemment montré par Kendall et al. 2011 [12] dans le cadre de la stimulation thalamique. Ces auteurs ont rapporté l'augmentation du glutamate (un neurotransmetteur excitateur) pendant la stimulation à HF. En même temps, l'activité électrophysiologique de cellules thalamiques a été inhibée.

Dans la deuxième partie du manuscrit, nous nous sommes attachés à tester et à valider expérimentalement des hypothèses générées à partir d'un modèle computationnel sur les effets de stimulations en courant continu de faible intensité. En fait, à part un enregistrement accidentel des effets de la stimulation de longue durée en CC [13], ce type de protocole n'avait jamais été testé *in vivo* et cela malgré un certain nombre d'études *in vitro* qui montrent son efficacité pour la suppression des décharges épileptiques [14-17]. En conclusion, les résultats de cette partie indiquent qu'il existe une polarité de stimulation capable de réduire l'intensité et la

durée totale des décharges épileptiques. Ces résultats confirment la dépendance des effets de la stimulation par rapport à la polarité de stimulation.

RÉFÉRENCES

- [1] G. Pizzolato and T. Mandat, "Deep brain stimulation for movement disorders," *Front Integr Neurosci*, vol. 6, p. 2, 2012.
- [2] M. Rahman, M. M. Abd-El-Barr, V. Vedam-Mai, K. D. Foote, G. J. Murad, M. S. Okun, and S. N. Roper, "Disrupting abnormal electrical activity with deep brain stimulation: is epilepsy the next frontier?," *Neurosurg Focus*, vol. 29, p. E7, Aug 2010.
- [3] C. C. McIntyre and P. J. Hahn, "Network perspectives on the mechanisms of deep brain stimulation," *Neurobiol Dis*, vol. 38, pp. 329-337, 2010.
- [4] I. Gilioli, A. Vignoli, E. Visani, M. Casazza, L. Canafoglia, V. Chiesa, E. Gardella, F. La Briola, F. Panzica, G. Avanzini, M. P. Canevini, S. Franceschetti, and S. Binelli, "Focal epilepsies in adult patients attending two epilepsy centers: Classification of drug-resistance, assessment of risk factors, and usefulness of "new" antiepileptic drugs," *Epilepsia*, vol. 53, pp. 733-740, 2012.
- [5] S. Krstulovic and R. Gribonval, "Mptk: Matching Pursuit Made Tractable," in *IEEE International Conference on Acoustics, Speech and Signal Processing*, Toulouse, 2006, pp. 496 - 499.
- [6] F. Wendling, F. Bartolomei, J. J. Bellanger, and P. Chauvel, "Epileptic fast activity can be explained by a model of impaired GABAergic dendritic inhibition," *European Journal of Neuroscience*, vol. 15, pp. 1499-1508, 2002.
- [7] D. R. Merrill, M. Bikson, and J. G. R. Jefferys, "Electrical stimulation of excitable tissue: design of efficacious and safe protocols," *Journal of Neuroscience Methods*, vol. 141, pp. 171-198, 2005.
- [8] J. Bourien, J. J. Bellanger, F. Bartolomei, P. Chauvel, and F. Wendling, "Mining reproducible activation patterns in epileptic intracerebral EEG signals: application to interictal activity," *Biomedical Engineering, IEEE Transactions on*, vol. 51, pp. 304-315, 2004.
- [9] S. Chung, X. Li, and S. B. Nelson, "Short-term depression at thalamocortical synapses contributes to rapid adaptation of cortical sensory responses in vivo," *Neuron*, vol. 34, pp. 437-46, Apr 25 2002.
- [10] F. Pouille, A. Marin-Burgin, H. Adesnik, B. V. Atallah, and M. Scanziani, "Input normalization by global feedforward inhibition expands cortical dynamic range," *Nat Neurosci*, vol. 12, pp. 1577-85, Dec 2009.
- [11] G. V. Goddard, "Development of epileptic seizures through brain stimulation at low intensity," *Nature*, vol. 214, pp. 1020-1, Jun 3 1967.
- [12] H. L. Kendall, L. H. Frederick, C. Su-Youne, C. L. Dongchul, W. R. David, C. M. Cameron, and C. L. James, "High frequency stimulation abolishes thalamic network oscillations: an electrophysiological and computational analysis," *Journal of Neural Engineering*, vol. 8, p. 046001, 2011.
- [13] S. R. Weiss, A. Eidsath, X. L. Li, T. Heynen, and R. M. Post, "Quenching revisited: low level direct current inhibits amygdala-kindled seizures," *Exp Neurol*, vol. 154, pp. 185-92, Nov 1998.
- [14] M. Bikson, M. Inoue, H. Akiyama, J. K. Deans, J. E. Fox, H. Miyakawa, and J. G. Jefferys, "Effects of uniform extracellular DC electric fields on excitability in rat hippocampal slices in vitro," *J Physiol*, vol. 557, pp. 175-90, May 15 2004.
- [15] J. Maher and R. S. McLachlan, "Febrile convulsions: Is seizure duration the most important predictor of temporal lobe epilepsy?," *Brain*, vol. 118, pp. 1521-1528, December 1, 1995 1995.
- [16] C. Y. Chan, J. Hounsgaard, and C. Nicholson, "Effects of electric fields on transmembrane potential and excitability of turtle cerebellar Purkinje cells in vitro," *J Physiol*, vol. 402, pp. 751-71, Aug 1988.
- [17] R. Mikkelsen, M. Andreassen, and S. Nedergaard, "Suppression of epileptiform activity by a single short-duration electric field in rat hippocampus in vitro," *J Neurophysiol*, vol. 109, pp. 2720-31, Jun 2013.

"Where there is a will, there is a way".

"Progress lies not in enhancing what is, but in advancing toward what will be".
Gibran Khalil Gibran

To the loving memory of my father...

To all the ones who made this accomplishment possible.

Acknowledgments

It is with immense gratitude that I would love to thank all those who took part, directly or indirectly, in the fulfillment of this research work throughout the past three years.

Foremost, I would like to thank Professor Lotfi Senhadji for welcoming me in his research laboratory. I would also like to thank my thesis advisors, Fabrice and Pascal, for their helpful advice and support whenever needed. It was indispensable.

Off course, I would love to thank all the jury members for accepting to participate to my oral presentation; their constructive comments were surely appreciated. Special thanks go to Professor Jacques Demongeot and Professor Frédéric Alexandre for their valuable reports on the dissertation.

Professor Fernando Lopes Da Silva, allow me to thank you for your noble scientific spirit and devotion. I always enjoyed sharing and discussing my research work with you in Manchester, where I first met you, as well as in Rennes during your frequent and appreciated visits to LTSI.

Dr. Biraben, I would like to thank you along with your team members, especially Dr. Pasnicu, for the fruitful collaborative efforts that you maintain with our research team.

For all the mathematical dilemmas I ever had during my thesis, I would love to thank Dr. Jean-Jacques Bellanger for the inspiring discussions he was always ready to indulge in whenever I knocked his door.

Last but not least, I would like to thank all my colleagues for their support and company during these past years. Special thanks to Patricia, Muriel, and Soizic for their logistic support, organizational talents and their kind spirits.

Finally, I praise the patience of my mother and her endless love especially throughout these last eight years. I owe much to you. I also thank my two brothers for their encouragement and their unconditional support throughout my “French experience”. To my love, Haitham, thank you for your devotion, presence, support, help, and love throughout these three years. You always made me feel stronger.

Summary

Introduction	5
Chapter 1: Neuronal Systems – Structure, Function and Control: Background	9
1 Neuronal Dynamics: A Systems View.....	9
2 Assessing Neuronal Function Using Electrophysiology.....	14
3 Controlling (Patho-)physiological Neuronal Dynamics by Electrical Stimulation: State of The Art...	20
Chapter 2: Problem Statement and Objectives	35
1 Problem Statement: Stimulation Parameters, Outcome and Mechanisms.....	35
2 Objectives: Optimize Stimulation Outcome.....	38
3 General Methodology.....	40
Chapter 3: A Computational Model of the Thalamocortical Loop	47
1 Mesoscopic Models of the Thalamocortical Loop.....	47
2 Implementing a Stimulation-Driven Model of Thalamocortical Dynamics.....	50
Chapter 4: Electrophysiological Observations and Signal Analysis for Model Optimization	67
1 The Clinical Observation.....	67
2 Signal Processing.....	69
Chapter 5: Results of Part 1	75
1 Quantification of Stimulation Effects in Real Signals.....	75
2 Reproduction of Real Epileptic LFPs During and in the Absence of Stimulation.....	80
3 Model Analysis.....	82
4 The Mechanisms: Computational Insights.....	89
Conclusion and Discussion on Part 1	92
1 The Model’s Architecture.....	92
2 Signal Processing and Representation.....	94
3 The Frequency-Dependence of The Identified Mechanisms.....	101
4 The Limitations.....	104
5 Conclusion.....	104
Chapter 6: Low-Intensity DC Stimulation of the Ictal Onset Zone – Computational Tools	109
1 DC Stimulation Protocols.....	110
2 A Computational Model of Temporal Lobe Epilepsy.....	115
3 An Experimental Model of Mesio-Temporal Lobe Epilepsy.....	117
4 Methods for Epileptic Signal Analysis.....	120
5 Model Adaptation for the Generation of HPDs.....	126
6 Implementing Stimulation Inputs.....	130
7 Computational Analysis of Stimulation Effects.....	134
Chapter 7: Computational Results of Part 2	137
1 Simulating HPDs.....	137

Chapter 8: Experimental Validation	149
1 Preliminary Safety Test: Stimulation-Induced Heating.....	149
2 The Experimental Protocol.....	152
3 Quantifying Stimulation Effects.....	155
4 Statistical Analysis.....	158
5 The Experimental Observations.....	159
Conclusion and Discussion on Part 2	175
1 Position with Respect to Earlier Studies.....	175
2 Polarization or a Network Effect.....	177
3 Future Implications of the Results.....	178
4 Limitations and Perspectives.....	179
General Conclusion and Perspectives	181
References.....	185
Table Of Contents.....	201
Table of Figures.....	207
Appendix A. Thalamocortical Model Simulink Implementation.....	211
Appendix B. Experimental Signals (Part 2).....	217
Appendix C. Publications.....	225

Introduction

Epilepsy is a neurological disorder characterized by the recurrence of seizures which are the expression of underlying pathological cerebral dynamics. Epilepsy touches about 1% of the world population. In France, about 7 in 1000 individuals suffer from epilepsy with more than 100 new cases declared each year. In fact, given the spectrum of the various forms of seizure semiology and evolution, epilepsy may be referred to as a syndrome rather than a well-defined disease. This diversity reflects the complexity and the multitude of pathophysiological cellular and network processes that underlie epileptic syndromes. This may consequently explain the high percentage (20 – 30%) of drug-resistant epileptic patients who do not benefit from the use of antiepileptic drugs prescribed nowadays. While epilepsy surgery presents a therapeutic alternative for these patients, it implies the resection of the epileptogenic zone and this may not always be possible for anatomical and functional considerations. In this context, deep brain stimulation (DBS) emerges today as a potential antiepileptic alternative for patients with drug-resistant focal epilepsy.

Nevertheless, if DBS seems to be efficient in the context of movement disorders (Parkinson's disease, tremor, dystonia ...), the results obtained in the context of epilepsy are much less evident. Inter-patient variability is often a reported issue of DBS in epilepsy. The same stimulation protocol that may lead to seizure freedom in a patient can double the seizure frequency in another. In fact, this owes to the empirical tuning of stimulation parameters in epileptic patients based on the encouraging empirical results obtained in the context of Parkinson's disease. However, this sub-optimal empirical approach is a direct consequence of the lack of tangible knowledge concerning the mechanisms through which stimulation modulates neural dynamics in general and epileptic dynamics in particular. Indeed, the optimal control of epileptic dynamics by stimulation currents requires a mature understanding of the parameter-dependent stimulation mechanisms involved in neuromodulation. In this account, three fundamental issues should be particularly explored: the choice of the 1) stimulation target, 2) current type (AC vs. DC), 3) stimulation signal parameters (duration, intensity, frequency).

This thesis aims at progressing in the direction of uncovering the mechanisms of neuromodulation by electrical currents and establishing the relationships governing the dependence of these mechanisms on stimulation parameters. Only two possible intracerebral stimulation configurations are explored, indirect AC (alternating current) stimulation and direct DC (direct current) stimulation of the ictal onset zone.

To accomplish these objectives, a general methodology combining computational modeling, signal processing, system analysis and experimental data acquisition was adopted. The first step consisted in proposing a physiologically-plausible model of the brain structure(s) involved in the considered stimulation context. Then, a suitable real electrophysiological dataset was used to optimize the model parameters/structure to guarantee realistic epileptic simulated dynamics. For this, adapted signal processing methodologies were proposed to quantify the real and the simulated electrophysiological signals. Finally, the analysis of the resulting optimized nonlinear dynamical system in response to an adequate stimulation input allowed the establishment of hypothetical stimulation parameter/stimulation effect relationships. Moreover, insights on the underlying mechanisms could be obtained.

In this dissertation, the problem is posed and addressed from a dynamical systems point of view.

The manuscript is organized as follows:

Chapter 1 reviews the state of the art of neuronal systems from three perspectives: structure, function and control. On the structural aspect, a historical note on the evolution of the perception of the central nervous system and neuronal systems is presented. This includes the pioneer modeling attempts of these systems. On the functional aspect, this chapter highlights the importance of electrophysiological signals in interpreting neural function and dysfunction. The biomarkers of dysfunction in certain neurological disorders, particularly in epilepsy, are emphasized. And finally, neural control by stimulation is detailed from a physical as well as a clinical perspective.

In Chapter 2 the problem statement is presented. The objectives of this thesis based on a synthetic view of the state of the art of clinical neurostimulation for epilepsy are then described. This chapter emphasizes the contrast between the variability of the stimulation outcome and the empirical tuning of stimulation parameters. Thereby, an alternative methodology is proposed to study and optimize stimulation protocols.

The rest of the manuscript is divided into two parts.

In part 1 (chapters 3 to 5), the frequency-dependent effects of indirect AC stimulation are addressed. The application context is clinical and relates to thalamic DBS and its modulatory effects on cortical epileptic activity. In chapter 3, a computational mesoscopic lumped-parameter model of the thalamocortical loop is proposed. The proper implementation details of the model are hereby detailed. Chapter 4 presents the clinical dataset used for model optimization. In this chapter, we also describe the time-frequency signal processing methodology used for quantifying the frequency content of the real and simulated signals. This methodology is based on an adaptive time-frequency decomposition algorithm of the processed signals (namely, Matching Pursuit). The detected time-frequency

atoms are arranged in pre-defined frequency bands. Then the spectral distribution is used to elaborate a feature vector (frequency band contribution to the total signal's energy). Calculated on real cortical epileptic signals, this vector was used to optimize the model's output. The optimization algorithms and the stimulation effect tuning are detailed in this chapter. Finally, the results of this first part (Part 1) are presented in chapter 5. They show the bifurcation of the model (in the phase plane) when the frequency of the stimulation input varies. Further analysis of the system's behavior allowed the description of the intermittency in the model's behavior as a function of the stimulation frequency. Finally a number of hypotheses concerning the frequency-dependent mechanisms of thalamic DBS (like feedforward inhibition and short-term depression) were also concluded. The methods used as well as the results obtained in this part are further discussed in the subsequent discussion section.

In part 2 (chapters 6 to 8) the direct DC stimulation of the ictal onset zone is investigated. The study is done in the context of mesio-temporal lobe epilepsy (MTLE), a frequent form of drug-resistant epilepsy. It aims at identifying the polarity-dependent effects of DC stimulation. Chapter 6 presents the computational tools used to accomplish the modeling study. An existing model of the hippocampal CA1 region, developed in our team, was used. The model was amended in order to reproduce dynamical transitions between background activity and sustained epileptic discharges. To proceed, the duration and occurrence times of discharges were identified from real local field potential (LFP) signals recorded in a mouse model of MTLE (also used for experimental tests). Stimulation inputs were also integrated to the pre-existing computational model.

Chapter 7 presents the computational results obtained from the model analysis. From this analysis, an experimental protocol is proposed aimed at attenuating epileptic activity. Chapter 8 reports the experimental validation of the computational model prediction. Results suggest that, for a certain current polarity, low-intensity DC currents applied at the ictal onset zone can significantly diminish the occurrence of hippocampal paroxysmal discharges *in vivo* as predicted computationally. The results of this part are further discussed in the subsequent discussion section.

Finally, this manuscript ends with a general conclusion that summarizes the major findings and suggests some future perspectives and challenges.

Chapter 1: Neuronal Systems – Structure, Function and Control: Background

1 NEURONAL DYNAMICS: A SYSTEMS VIEW

From a systems view, a neuron can be described as a nonlinear dynamical system that can switch state between two states, “resting” and “firing”, depending on the intensity of the incoming disturbances (electrophysiologically termed as postsynaptic potentials; PSPs). Such a transition or bifurcation, is only possible when the neuron is excitable, that is near to the firing threshold. Otherwise, this dynamical system maintains its equilibrium and the neuron remains quiescent. In fact, this systems description of neuronal dynamics is the result of years of experimental observations and debates concerning the structural as well as the functional organization of the central nervous system. Nowadays, computational representations of neuronal dynamics (models) substantiate, on different levels of detail, this systems view. The objectives of these modeling attempts can be classified into major groups: (1) understanding neuronal dynamics; cellular and network, and (2) controlling these dynamics by external stimuli such as electric stimulation and pharmaceutical molecules (medications).

In this chapter, a brief glance at the evolution of the scientific understanding of the structural/functional organization of the nervous system is firstly presented. Then, the various attempts in modeling the underlying neuronal dynamics are reviewed. And finally, the state of the art regarding the control of neuronal dynamics by stimulation is detailed.

1.1 DISCOVERING THE CONCEPT OF THE NEURON

Due to the absence of adequate technology, the nineteenth century witnessed continuous debates on the organization of the nervous system. In fact, one group of researchers, the reticularists, believed that the nervous system was built up of a large network of tissue, or reticulum, of fused processes of nerve cells. On the other hand, the second group argued that the nervous system consisted of interacting distinct nerve cells. However, it was not before the 1870s, when Golgi discovered the Golgi impregnation (staining), that credible evidence concerning the cellular structure of the nervous system became available. Paradoxically, despite discovering a technique that stained neurons in their whole entirety, Golgi still believed that his results prove that the nervous system consisted of a continuous network [1].

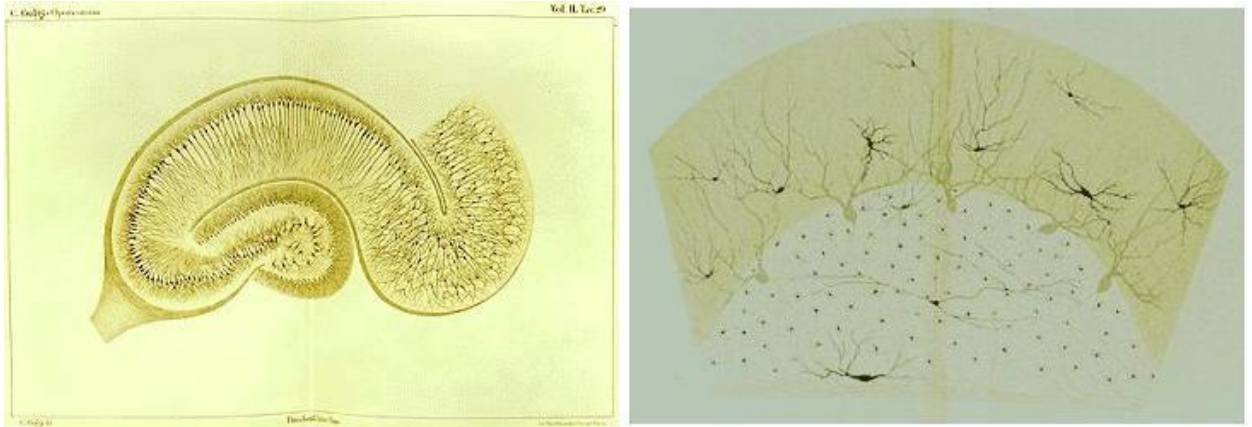


Figure 1. Golgi staining method applied on hippocampal tissue (work of Golgi: <http://neurophilosophy.wordpress.com/2006/08/29/the-discovery-of-the-neuron>).

Later in the late 1880s, Cajal improved the Golgi method and used it to stain a chick cerebellum. Cajal was the first to report that the axons in his samples ended in the gray matter and that their endings coincided with dendritic terminals. Consequently he formulated the law of dynamic polarization according to which information flows in a unidirectional way in a neuron (from the dendrites to the cell body and to the axon). This was probably the first electrophysiological note on neuronal activity viewed at the cellular basis and the incontrovertible evidence on the cellular structure of the nervous system [1].

1.2 THE EARLIEST MODELS OF NEURONAL DYNAMICS

Although that the discovery of the neuron dates back to the end of the nineteenth century, one would imagine that computational models of neurons are much more modern. Nevertheless, the first computational representation of neural behavior is credited to the French neuroscientist Louis Lapicque back in 1907, the integrate-and-fire neural model [2]. This first representation of the neuron as a dynamical system took into consideration its capacitive and resistive properties (see the schema of the authentic model in Figure 2). In fact, for adjusting the parameters of his model, Lapicque developed his proper non polarizable electrodes and experimentally measured neuronal capacitance and resistance. However, this basic neuronal model did not take into consideration realistic electrophysiological elements that underlie neuronal dynamics such as ion channels, transmembrane currents, synaptic transmission, etc.

Later in 1952, Hodgkin and Huxley published a new formalism of neuronal dynamics, the famous Hodgkin-and-Huxley model [3] that remains until today a fundamental work in computational neuroscience. This formalism described the nonlinear electrical dynamics of the excitable membrane of the giant axon of the squid as a function of sodium, potassium and leakage currents. This model, built on the cellular (microscopic) level, was based on previous experimental results [4, 5] that explored the dynamic

electrical characteristics of the squid axon membrane as expressed by the experimental relations between the input current intensity and the membrane potential voltage.

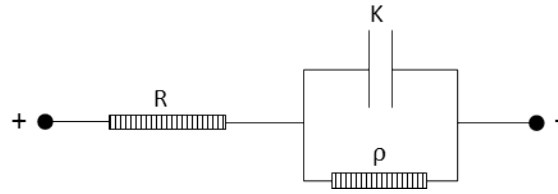


Figure 2. Initial integrate-and-fire model. Adapted from Lapique in 1907 [2].

As the integrate-and-fire model, the Hodgkin-Huxley model relies also on the capacitive properties of the neuronal membrane. However, it takes into consideration the dynamics of ion channels which are also present in the cell membrane. Hodgkin and Huxley's major discovery is that ion channels are controlled by gating variables which depend on the membrane voltage (so called active voltage-dependent ion channels) and which define their conductance g_{ion} . The general equation of the Hodgkin-Huxley single compartment neural model is expressed as:

$$C \frac{dV}{dt} = -I_{leak} - I_{Na} - I_k + I_{inject}$$

or

$$C \frac{dV}{dt} = -g_{leak}(V - E_{leak}) - \bar{g}_{Na}m^3h(V - E_{Na}) - \bar{g}_Kn^4(V - E_K) + I_{inject}$$

where C is the membrane capacitance, V is the difference between the intracellular and the extracellular potential, and I_{leak} , I_{Na} , I_k , I_{inject} are the respective leakage, sodium, potassium and peripheral currents and where E_{ion} denotes the reversal potential the considered ion (also known as the Nernst potential). The leakage current I_{leak} is a lumped representation of all of the time-independent contributions (passive) to the membrane current. These equations show the dependence of the membrane potential V on the activation and inactivation parameters of sodium and potassium ion channels (m, n, h). These parameters are themselves defined by a set of first-order nonlinear differential equations that will not be detailed in this dissertation.

The Hodgkin-Huxley model describes the variation of membrane potential at a certain location on the axon and does not take account of the spatial propagation of action potentials. More sophisticated microscopic neuronal models followed these pioneering works. They actually represent the different neural components (the soma, the dendrites and the axon) in separate distinct compartments. These models are known as multi-compartment models, because each neural component (soma, axon, dendrites) can be represented by one [6] or several compartments [7].

1.3 POPULATIONS OF SINGLE NEURON MODELS

Later on, models were extended to represent networks of interacting neurons in order to study neural network dynamics. On this account, the work of Traub and his colleagues [8] largely contributed this research trend. Using this approach, thousands of single neuron models are interconnected through synapses. Synaptic transmission is modeled by adding synaptic currents I_{syn} to the sum of membrane ion currents. This representation takes into consideration the activated ion channels due to the release of a neurotransmitter in the synaptic cleft. A simple formal model for I_{syn} can be expressed as:

$$I_{syn} = g_{syn}(t) \cdot x \cdot (V - E_{syn})$$

where g_{syn} and E_{syn} determine the characteristics of the modeled synapse (the conductance and the reversal potential respectively) and where x represents the postsynaptic activation in response to presynaptic action potentials.

The high physiological precision of this type of models is not costless. In fact, the higher the complexity of the proposed model the more difficult the mathematical analysis of its behavior. Therefore, at this level of modeling, studying the underlying mechanisms of the modeled processes is not always possible. In this thesis, another type of models was used to study network dynamics: neural mass models.

1.4 NEURAL MASS MODELS

In many brain regions, neurons are organized as homogenous units of similar properties. This fact dates back to the late 1950s when it was evidenced by the pioneer contributions of Mountcastle [9] as well as those of Hubel and Wiesel [10]. These scientists pointed out the existence of cortical neuronal aggregates formed by neighboring neurons lying in narrow vertical columns extending from cortical layer II through VI. These scientific observations proved the hypothesis of the functional organization of these cortical layers into elementary units or populations (cortical columns) that share similar morphological and functional features. In fact, the electrophysiological characterization of these neuronal columns showed that the neurons of each population respond similarly and synchronously to brief peripheral stimuli, and that they consequently share the same dynamics. This discovery led to the computational representation of a neuronal assembly as a single dynamic entity [11], a neuronal population or mass as termed by W. Freeman [12].

The theoretical bases of such macroscopic representations of neuronal populations date back to the early 1970s when Wilson and Cowan first proposed a “macroscopic” deterministic model of neuronal populations’ dynamics [13]. Based on the hypothesis of spatial proximity of the modeled neurons and the redundantly dense inter-neuronal

interaction, this first model only dealt with the temporal dynamics of the neuronal population viewed as a whole. It suggested that the neuronal aggregate can be represented as distinct neural subpopulations (excitatory or inhibitory) interacting through synaptic transmission. Then, a subpopulation can be described as a nonlinear dynamical system of two first-order differential equations. The nonlinearity intervenes at the level of synaptic transmission where threshold and saturation effects are represented. Consequently, the resulting model represents the “average” activity (e.g. average postsynaptic potentials, average firing rate) of the modeled population without explicitly representing the exact activity at the cellular level.

Formally, each subpopulation is built of two functions, the input and the output function or the pulse-to-wave and the wave-to-pulse function as termed by Freeman [12]. The input function transforms the input mean firing rate into a mean postsynaptic potential. This transfer function can be expressed as:

$$H(s) = W / \left(s + \frac{1}{\tau_w} \right)^2$$

where $W \cdot \tau_w^2$ represents the static gain of the synaptic filter H and τ_w represents the time constant (controlling both the rise and decay times) of its impulse response, expressed as:

$$h(t) = \frac{W}{\tau_w} \cdot t \cdot e^{-t/\tau_w}$$

Generally speaking, parameters W and τ_w are adjusted in such a way that the impulse response, $h(t)$, of the filter matches the dynamics of real postsynaptic potentials. When this second-order transfer function is used, it can be easily shown that the decay time of the modeled PSP corresponds then to $3.146 \cdot \tau_w$. (This is further explained in chapter 3).

On the other hand, the output function transforms the sum of mean postsynaptic potentials into an output mean firing rate. This function takes into account the nonlinear characteristics (threshold and saturation effects) of the neural response. Generally, a sigmoidal form is used which can be expressed as:

$$S(v) = \frac{2e_0}{1 + e^{r(v_0-v)}}$$

where $2e_0$ is the maximum firing rate, v_0 is the postsynaptic potential corresponding to a firing rate of e_0 , and r is the steepness of the sigmoid. Indeed, the most valuable contribution of Wilson and Cowan to mesoscopic neuronal modeling is probably the use of the sigmoid function to model the response of a given neuronal population to incoming postsynaptic potentials.

This modeling approach allowed the representation of quite extended neuronal networks with a relatively low computational complexity as compared to the microscopic approach. Following the work of Wilson and Cowan [13], several predictive models of the activity of distinct brain structures were elaborated to analyze their neural dynamics in details. Freeman developed a neural mass model of the olfactory system [14] based on previous histological and physiological studies [15, 16] and furthermore used it to interpret physiological EEG recordings in this system. Freeman and his colleagues proved that their neural mass model can simulate realistic EEG as that observed in distinct compartments like the olfactory bulb or the piriform cortex [17]. However, unlike the Wilson and Cowan model [13], the lumped neuronal aggregates implemented in Freeman's model were either inhibitory or excitatory at a time.

Concurrently, Lopes Da Silva developed a model based on the same concepts [18] to study and explain the mechanisms of generation of the cortical alpha rhythm as experimentally observed in dogs. At the same time, Nunez [19] proposed a neural mass model to study the dynamics of cortical oscillations. Later, these pioneer contributions were further developed and enriched by many research groups in distinct contexts. For instance, this type of modeling proved efficient for studying the state changes in brain dynamics [20], the evoked potentials in the visual cortex [21], the human alpha rhythm [22], the effect of anesthesia on the encephalogram [23] and above all the dynamics of interictal to ictal transition in epilepsy [24-28]. Although the basic input/output functions may slightly vary from one model to another, the level of detail and the general approach remain similar.

In conclusion, all the above models were used to model neuronal dynamics, yet that was not practically possible without the advent of a tool for experimentally assessing neuronal dynamics. As Lapique invented his own electrodes to measure the capacitive characteristics of a neuron in order to adjust the parameters of his model [2], more complex electrophysiology-based techniques were invented prior to the description of electrophysiology-based models.

2 ASSESSING NEURONAL FUNCTION USING ELECTROPHYSIOLOGY

Information transfer and processing in neuronal systems is mediated by electrical currents. Therefore, measuring and interpreting electrophysiological signals can be useful in assessing neural function and thereby dysfunction. This can be particularly helpful for developing a better understanding of the dynamics of neuronal processing as well as the dynamics of neuronal disorders like epilepsy.

Nowadays, electrophysiology-based techniques are used in clinics as well as in laboratories in two different ways. Firstly, in clinics, such techniques constitute

necessary elements of the diagnostic process. They include noninvasive techniques like EEG (electroencephalography), MRI (Magnetic Resonance Imaging), and fMRI (functional MRI) as well as invasive techniques notably intracerebral EEG (iEEG) and ECoG (electrocorticography). Using these diagnostic tools, clinicians look for well-known electrophysiological signatures or biomarkers of neurological disorders in order to further complete the diagnosis (location of affected brain regions, specific subtype of the disorder...). In epilepsy, for example, neurologists use scalp EEG recordings to identify epileptogenic electrophysiological signatures (spikes, spike-wave complexes, paroxysmal discharges ...) in order to define the affected brain regions. Once defined, an intracerebral EEG (iEEG) exploration can be done in order to confirm and delineate the affected regions and to ultimately propose a resective surgery to suppress seizures (if possible). In sleep apnea, clinicians use EEG recordings as well as other multimodal electrophysiological signals (ECG, EMG...) to assess sleep stages and quality and therefore complete the diagnostic process [29].

Secondly, electrophysiology-based techniques are used for the investigation of neuronal function in experimental studies. These techniques vary in function of the experimental procedure (*in vivo* vs. *in vitro*) and the considered level of organization (isolated cells, brain slices, whole structure, whole brain). So while EEG/iEEG or LFP (local field potential) recordings can be used to evaluate the average neuronal activity of large-scale cell aggregates in the living animal (*in vivo*), patch clamp techniques are usually used for single cell electrophysiological recordings. In experimentation, these techniques usually aim at studying new potential biomarkers of known neural disorders [30, 31], or at studying innovative techniques for controlling these pathological dynamics. This is particularly the case of the pioneer studies of the effects of electrical stimulation on epileptic dynamics in animal models (see [32] for review).

It should be noted that these recording techniques can be technically divided into two groups: intracellular and extracellular recording techniques. This generally depends on the size and the position of the recording electrode(s).

2.1 INTRACELLULAR ELECTROPHYSIOLOGICAL RECORDINGS

As intracellular recordings require the presence of the recording electrode in the intracellular space of the neuron, these techniques entail the use of very small electrodes, generally termed microelectrodes. Microelectrodes and microelectrode arrays permit the recording of single-cell membrane dynamics. Many techniques can be classified under this group including the patch-clamp, the current-clamp and the voltage-clamp techniques. However, as these recording techniques are devoted to single-cell preparations, the dynamics of extended systems (neural networks) cannot really be assessed using these techniques.

Nevertheless, at this level, intracellular recordings can be particularly useful in studying the cellular mechanisms of neuronal function/dysfunction and control at the level of a single neuron. Intracellular recordings were used to study the electrophysiological characteristics of excitable tissue. This is for instance the case of cortical malformations (medically termed dysplasia) [33]. In a different context, intracellular recordings were also used to measure the response of different types of neurons (pyramidal cells, basket interneurons ...) to external electric fields [34-36].

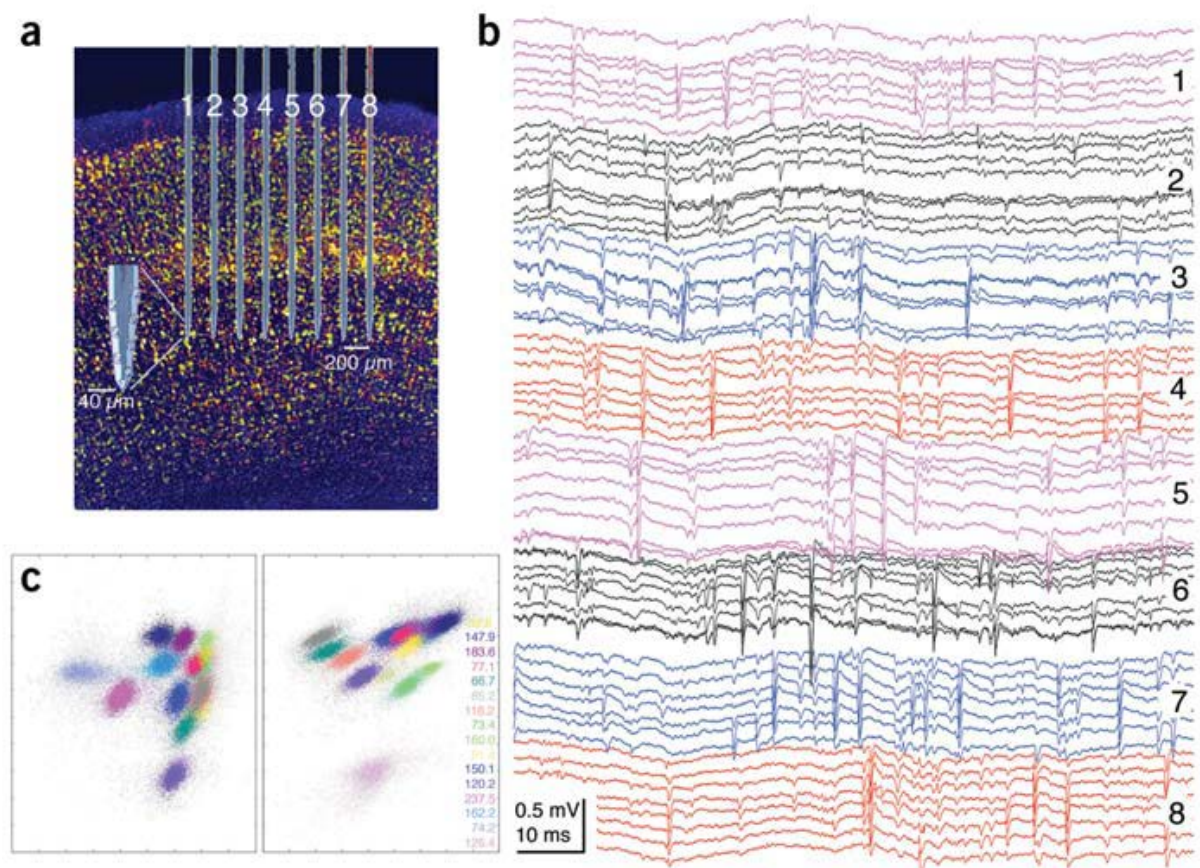


Figure 3. High-density recording of unit activity in the somatosensory cortex of the rat ([37] no requested permission). **(a)** The eight-shank silicon probe system. Each shank is equipped with 8 iridium recording sites at the edges of the tip. Note the micro dimensions of the recording system. **(b)** A sample short recording of both field and unit activity. Each shank recordings (color-coded) correspond to a distinct neural ensemble. This is evidenced by the presence of spikes on several sites of the same shank and the lack of spikes on the sites of other shanks. **(c)** Based on spike occurrence and amplitude, the silicon probe was used to isolate the position of the firing separate neurons. In the figure, a two-dimensional view of the identified clusters (color-coded) at one shank is presented.

2.2 EXTRACELLULAR ELECTROPHYSIOLOGICAL RECORDINGS

Generally speaking, all techniques designed to measure the electrophysiological activity at the systems level are based on the measurement of extracellular fields. In fact, a scalp electrode as well as an intracerebral electrode measures the cumulative electric current contributions of all neighboring active cellular processes. This is expressed as a resultant potential $V_{electrode}$ measured at the recording electrode [38].

EEG/iEEG signals are recorded by relatively large electrodes either at the surface of the scalp (diameter 1 – 15 mm, and thickness ~ 2 mm) or directly through intracerebral cylindrical contacts (diameter ~ 0.8 mm and length ~ 2 mm), whereas lower level extracellular recordings are measured through microwires (diameter ~ 0.1 mm). In any case, recorded signals are extracellular fields. It was originally thought that PSPs were the only contributors to these extracellular signals. But more recent studies showed that unfiltered signals also reflect the summation of APs from nearby cells (located at a few tens of microns from the electrode contact). In particular, the frequency band used to analyse extracellular fields is essential. At low frequency, the filtered signal (i.e. LFP or EEG) is mainly related to slow synaptic events that can be recorded quite far from the sources (even on the scalp). At higher frequencies, the fast extracellular currents involved in the generation APs are visible, especially on electrodes adjacent to recorded cells. This is why, for instance, HFOs [250-600 Hz] are visible on extracellular fields recorded with depth electrodes when the frequency band is broad (up to 2 kHz). See for instance Bedard et al. 2006 [39]: “Local field potentials (LFPs) are routinely measured experimentally in brain tissue, and exhibit strong low-pass frequency filtering properties, with high frequencies (such as action potentials) being visible only at very short distances (approximately 10 micron) from the recording electrode.”

The major advantages of using extracellular techniques to measure network activity are threefold: (1) the mechanisms by which single neuronal currents sum up to a recorded voltage are quite well-understood (2) the state of the neuronal system is not altered (spontaneous recordings *in vivo*) during the recording process and (3) such recordings are the least invasive and the least expensive. So how are extracellular recordings used to assess neural function and dysfunction?

2.3 ASSESSING FUNCTION/DYSFUNCTION USING EXTRACELLULAR SIGNALS (EEG/IEEG)

Information processing in the brain is achieved through neural coding/decoding processes. Communication between functionally connected neural assemblies passes by oscillations and synchronization, which are two essential features of neural (de)coding [40]. Typically, oscillations characterize neuronal information processing in response to a certain stimulus, while the synchronization of oscillations reflects the precise temporal dynamics of neural communications, particularly between distant neural assemblies [41]. These are the working hypotheses of cognitive neurosciences. For example, while an expected visual stimulus invokes an alpha oscillation in the cat cortex, an unexpected one elicits gamma oscillations [40].

2.3.1 ELECTROPHYSIOLOGICAL OSCILLATORY SIGNATURES OF NEURONAL PATHOLOGY (MOVEMENT AND NEUROPSYCHIATRIC DISORDERS)

So, as certain oscillations mark the neural information processing in the normal brain, several neurological disorders are marked by characteristic oscillatory activity (see [41])

for general review). These characteristic electrographic signatures that are recordable by extracellular scalp or intracerebral electrodes contribute to the assessment of neuronal dysfunction in the diseased brain.

Case of Parkinson's disease. Clinical observations as well as animal studies showed that Parkinson patients as well as pathologically equivalent animal models present an abnormal increase in oscillatory β band dynamics in a specific brain motor network connecting the basal ganglia, and particularly the following nuclei GPe, GPi and STN, with the motor cortex [42, 43]. Moreover, this abnormal synchronization is found to be entrained by a basal ganglia pacemaker formed between the subthalamic nucleus (STN) and the external globus pallidus (GPe) [44].

Case of other movement disorders. Recent evidence showed that the abnormal synchronization in the basal ganglia circuits is also a pathophysiological marker of other movement disorders such as dystonia, tremor, and Tourette syndrome (see [41] for review). Apparently, a decrease in the LFP power in the antikinetic frequency band (11 – 30 Hz) compared to an increase in that of the tremor-related band (3 – 10 Hz) is common in patients with movement disorders.

Case of neuropsychiatric disorders. Neuropsychiatric disorders, notably Alzheimer's disease, are characterized by a decrease in cognitive capabilities/function. In terms of the electrographic signature, the disease has been found to be characterized by a widespread decrease in synchronization in the α , β , and γ bands [45] compared to an increase in the δ band synchronization [46]. The loss of β -band synchronization has been shown to be correlated to cognitive impairment in Alzheimer's disease [47].

2.3.2 ELECTROGRAPHIC SIGNATURES OF EPILEPTIC DYNAMICS

Unlike Parkinson's disease, dystonia, and other movement disorders, the electrographic signatures of epileptic dynamics are not unique to all epileptic patients and may vary as a function of time patient-wise. However, epileptic dynamics can be divided into three main categories: interictal, preictal and ictal dynamics. As ictal dynamics refer to the electrographic seizure dynamics, preictal dynamics describe the EEG dynamics just before seizure onset, and finally interictal activity designates electrographic dynamics between two consecutive seizures. Given that epileptic patients may have a seizure frequency inferior to one seizure/week, assessing the epileptiform aspect of the recorded EEG depends generally on the interpretation of interictal dynamics as reflected by interictal epileptiform discharges (Figure 4).

Interictal epileptiform discharges (IEDs) range from transient to more sustained processes observed in the epileptic brain. They can be classified under the following categories:

- Sharp wave: a transient electrographic event with a pointed peak clearly distinguishable from background activity. The duration of a sharp wave ranges between 70 – 200 ms.
- Spike: a sharp wave but with shorter duration (20 – 70 ms).
- Spike-and-wave complex: an electrographic event characterized by a spike followed by a slow wave (positive and/or negative).
- Polyspike-and-slow wave complex: multiple consecutive spike occurrences followed by a slow wave.

IEDs are also termed paroxysmal discharges due to their brutal occurrence (onset and end). These discharges generally occur as rhythmic or semi-rhythmic bursts but also as isolated events. Noteworthy, bursts of rhythmic activity that last as long as a few seconds are often interpreted as electrographic seizures rather than interictal discharges. An increase in the rhythmicity of these discharges may also indicate the close onset of a seizure. The resulting electrographic activity designates **preictal discharges** preceding seizure onset.

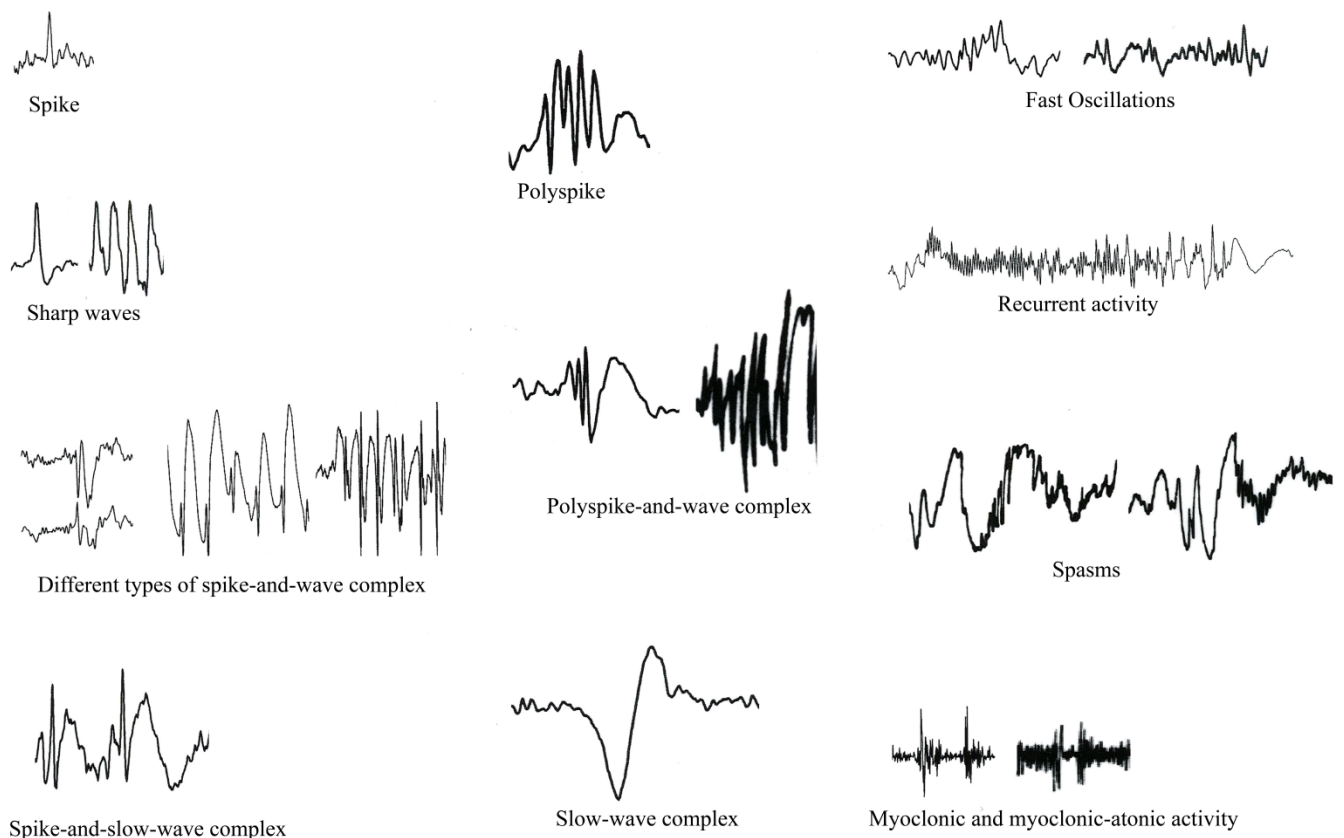


Figure 4. Different Types of epileptic EEG patterns. Adapted and translated from [48]. No permission requested.

IEDs differ by epileptic syndrome. In fact, the morphology of IEDs is as important as the semiology of seizures in determining the type of the considered epileptic syndrome.

While frontal epilepsies are mostly characterized by fast oscillations and slow-wave complexes recorded from the frontal lobe electrodes, parietal-occipital epilepsy is characterized by polyspike-and-wave complexes recorded by the parietal lobe electrodes, and absence seizures are characterized by bursts of spike-and-wave generalized discharges, of frequency 3 – 5 Hz [48].

3 CONTROLLING (PATHO-)PHYSIOLOGICAL NEURONAL DYNAMICS BY ELECTRICAL STIMULATION: STATE OF THE ART

In fact, pathological neuronal dynamics are produced by abnormal neuronal signaling and synchrony as aforementioned. In terms of the control theory, electrical stimulation is the input stimulus aimed at controlling the pathological output of a complex dynamical system, the pathological neural network. As implied, this stimulation input can be simply used in an open-loop configuration when destined at studying the system's response to a given stimulation signal or even in a feedback closed-loop configuration in more advanced applications. Noteworthy, the closed-loop configuration requires a good knowledge of the neural system's response to defined stimulation paradigms. In the literature, open-loop stimulation protocols constitute the majority of existing stimulation trials.

Besides its clinical applications for the control of disease dynamics (epilepsy, Parkinson's disease, tremor, dystonia, depression ...), open-loop noninvasive electrical stimulation, such as transcranial current stimulation (tCS), emerges today as a cognitive enhancement [49] and as a neurohabilitation tool in healthy individuals (see [50, 51] for reviews). Actually, the efficacy of tCS in cognitive function enhancement in healthy subjects is reported for different cognitive tasks (reading, associative language learning, semantic and phonetic fluency, picture naming, recognition memory)[52]. However, a crucial question remains unanswered: how does stimulation exactly modulate neural dynamics in the normal and the diseased brain? Basic insights are based on the modulation of the excitability/inhibition ratio of the stimulated cortical region. tDCS (D=direct) for example is thought to increase (anodal stimulation [53]) or decrease (cathodal stimulation [54]) cortical excitability, thus modulating cortical activity levels. So how does the stimulation input intervene with the intrinsic dynamics of the neural system? And what are the effects of certain parameters of stimulation on the modulatory outcome?

To answer the above questions, the theoretical stimulation-induced electric field formalism following Maxwell's equations and the consequent theoretical effects of stimulation on neural dynamics are first reviewed. Then, actually reported effects of stimulation as a function of stimulation parameters and categories are then presented.

3.1 STIMULATION-INDUCED ELECTRIC FIELD

Neural tissue is surrounded by a low resistivity extracellular medium (about 50 $\Omega \cdot \text{cm}$). Besides, the resistivity of neural tissue itself is relatively low (300 – 800 $\Omega \cdot \text{cm}$). Indeed, stimulation currents injected into neural tissue induce an electric field that may interfere with intrinsic neural currents and properties. Understanding the theoretical effects of induced stimulation fields is essential for deciphering its effects on excitable neural tissue.

3.1.1 IN A VOLUME CONDUCTOR

Given that stimulation frequencies never attain 10 kHz, the current density, the induced potential and the electric field distributions can be estimated using the quasi-static formalism of Maxwell's equations:

$$\nabla \cdot J + \frac{\partial \rho}{\partial t} = 0 \text{ or } \nabla \cdot J = 0 \text{ in a homogeneous medium} \quad (1)$$

$$\nabla \cdot \varepsilon E = \rho \quad (2)$$

$$J = \sigma E \quad (3)$$

$$E = -\nabla V \quad (4)$$

where E ($V \cdot m^{-1}$) is the electric field derived as the gradient of the potential distribution V . J ($A \cdot m^{-2}$) is the current density, and σ ($\Omega \cdot m$), ε ($F \cdot m^{-1}$), and ρ ($C \cdot m^{-3}$) are the conductivity, the permittivity, and the charge density respectively. Solving the above equations is possible when the analytical expression of the voltage distribution V is well-defined. In the case of a monopolar electrode placed in an infinite conductive medium and delivering a current of intensity I , solving Poisson's equation $\Delta V = -\rho/\varepsilon$ (derived from equations (2) and (4)) with a Dirichlet boundary condition $V = 0$ at infinity is sufficient to determine V . The solution is then expressed as:

$$V = 1/4\pi\sigma r \quad (5)$$

In 1976, McNeal derived the same equation of the voltage distribution induced by one monopolar stimulation electrode using an electric network representation of a myelinated fiber [55] and under the assumption that the myelin sheath is a perfect insulator. Evidently, McNeal supposed that the extracellular medium is electrically homogenous. Equation (5) can be generalized to the case of n monopolar electrodes expressed as:

$$\varphi = 1/4\pi\sigma \sum_n I_i/r_i \quad (6)$$

where I_i is the current delivered by the i^{th} electrode, and r_i is the distance of between the latter and the recording point.

Consequently, depending on the stimulation setup, the type and number of stimulation electrodes, it is possible to determine the electric field lines induced in the vicinity of a homogenous conductive medium. It is the induced electrical field that influences neural membrane properties and consequently neural dynamics [36]. More elaborated Bessel-function-based analytical solutions to the Poisson equation in more complex geometries including cylindrical intracerebral electrodes in an infinite medium or multipolar sources in the case of spherical human head models have been derived (see [56] for review).

3.1.2 IN THE VICINITY OF EXCITABLE TISSUE

It is evident that the simplistic geometrical approaches presented in the previous subsection are not representative of the dielectric heterogeneity and the complex geometry that can be encountered in neural tissue. Eventually, when confronted to more realistic geometries and/or heterogeneities in the dielectric properties of the stimulated neural medium, analytical solutions do not generally exist. Numerical methods can be then used, within certain limits, to calculate the induced potential field and consequently the electric field distribution.

Finite element modeling and similar approaches have been generally used to estimate the volume of activated tissue around the stimulation electrodes [57] and to consequently predict the neuronal system's output (spinal cord motoneurons) as a function of stimulation frequency and waveform [58]. Recent studies use these modeling approaches to design and optimize microelectrode array neural prosthesis [59]. These electrical field modeling approaches seem to be promising as model estimations have been recently reported to match the experimentally measured potential field [59].

In conclusion, stimulation currents induce exogenous electric field distributions in the vicinity of neural tissue which leads to the polarization of the membrane potential depending on the orientation and intensity of induced field [36]. This is probably due to the passage of some current lines through the cell bodies of the stimulated neurons, provoking depolarization when the current flows outwards, and hyperpolarization when the current flows inwards (see [60] for review). Moreover, the transmembrane potential variations in response to stimulation currents was computationally modeled and studied in [61, 62]. These studies used detailed multi-compartmental models of the whole neuron [61] or of the neural axon [62] to show that the transmembrane potential (V_m) varies in function of the orientation as well as the intensity of the induced extracellular voltage (V_e). This was expressed as an inhomogeneous equation in [62]:

$$\lambda^2 \Delta^2 V_m / \Delta x^2 - \tau \frac{dV_m}{dt} - V_m = -\lambda^2 \Delta^2 V_e / \Delta x^2 \quad (7)$$

where Δx is the length of the affected axonal compartment, τ is the membrane time constant and λ is the membrane space constant. The latter is a function of the geometric and electrical properties of the membrane. Equation (7) shows that the transmembrane potential depends clearly on the extracellular induced potential distribution and on the directionality of the electrical field; only longitudinal field components exert an effect on transmembrane potential V_m .

Nevertheless, since the effect of stimulation is generally measured on the network level by extracellular recordings, the simple polarization effect may sum up spatially and temporally giving rise to the clinically and experimentally observed complex stimulation-induced network dynamics. Consequently, the response of the neural system to an external stimulus depends largely on its intrinsic properties: structural, electrical and dynamical. Another important extrinsic factor is the way stimulation is applied to the system. In the next subsection, three different parameters of stimulation configuration and their probable contribution to neural modulation are discussed.

3.2 ELECTRICAL STIMULATION CATEGORIES

In practice, the stimulation input intervenes differently with the neural system's dynamics based on the actual implementation of stimulation. Three criteria may have a determinant role; the invasiveness of stimulation (transcranial vs. intracerebral), the choice of the stimulated target whether within or outside the pathological zone (direct vs. indirect stimulation) and the type of the stimulation current (direct current, DC, vs. alternating current, AC).

3.2.1 INTRACEREBRAL VERSUS TRANSCRANIAL CURRENT STIMULATION

Choosing the degree of invasiveness of stimulation usually depends on the clinical context, particularly the location of the desired stimulation target and the type of the pathological dynamics. Transcranial current stimulation (tCS) is generally used for stimulating cortical regions while intracerebral stimulation usually targets deep brain structures. While the membrane polarization effect holds true for both stimulation applications, it is worth noting that stimulation currents induce different field distributions due to the differences in electrode dimensions and the electrode-tissue interface. While tCS employs ring or disc electrodes of 0.4 cm radius at the skin-contact surface, it has been computationally (finite element method) shown that the induced electric field may extend over the cortical surface [63]. Conversely, clinical intracerebral stimulation electrodes (cylindrical contacts 1.5 mm long and 1.27 mm diameter) have been shown to have a local direct effect on the neural ensemble several millimeters around the stimulating electrode [64], while the stimulation current is directly injected into the targeted cerebral structure.

Given its invasiveness, intracerebral stimulation is reserved for the modulation of pathological dynamics and consequently its use has never been reported in healthy

subjects. Transcranial stimulation, on the other hand, has both clinical and cognitive applications as discussed earlier in this section. In the core of this work, only clinical applications of electrical stimulation aiming at modulating pathological dynamics will be discussed.

3.2.2 AC VERSUS DC STIMULATION

In the present clinical context, the degree of invasiveness of the stimulation technique usually determines the stimulation current parameters. Intracerebral stimulation, particularly deep brain stimulation (DBS), is usually associated with AC stimulation and has never been clinically used with DC stimulation signals to the best of our knowledge. High-frequency stimulation (HFS) trains are often reported to modulate disease dynamics in the context of movement disorders encountered in Parkinson's disease, dystonia and tremor (see [65] for review). Nevertheless, more complex results are usually associated to DBS for epilepsy, where the impact of the same stimulation protocol does not seem to have the same effect on epileptic dynamics.

Conversely, tCS is often related to DC stimulation. Transcranial direct current stimulation (tDCS) is currently reported to have positive results on disease dynamics when used for Parkinson's disease, tinnitus, chronic pain, stroke, and even childhood psychosis, as well as on normal cognitive enhancement [50]. Yet, the effectiveness of transcranial alternating current stimulation tACS is also reported in the context of motor, sensory and cognitive processing [51].

The choice of the current type, direct/alternating, is thought to actually determine the way neuronal activity is modulated. The modulatory effects of AC stimulation, whether by sinusoidal waveforms or pulse trains, are highly dependent on several stimulation parameters, particularly, the frequency of the stimulation signal, the targeted cerebral structure and its implication in the pathological network, in the case of pathological dynamics, or a certain cognitive network, in the case of normal dynamics (cognitive enhancement tasks).

Whether transcranial or intracerebral, at low stimulation frequencies (< 10 Hz), AC stimulation has been reported to influence the firing rate of the underlying neuronal systems through frequency-locked entrainment of endogenous oscillations *in vitro* at extremely slow AC stimulation signals (0.075 – 0.375 Hz) [66]. Similarly, the *in vivo* recordings as well as the computational modeling of cortical LFPs in response to thalamic DBS show a frequency-locked modulation of LFP cortical signals related to the frequency of the applied pulse train in the range 1 – 10 Hz [67]. Since, direct thalamocortical pathways exist between the stimulated and the recorded structures, the triggering of endogenous thalamic firing patterns by stimulation frequency is highly probable.

At higher stimulation frequencies, the modulatory effects of AC stimulation signals suggest a depressive inhibitory effect on the cell bodies of the stimulated target [68-71]. The mechanisms of this inhibition are still controversial and will be discussed in chapter 2. Paradoxically, this inhibitory effect is often associated with a recurrent increase of firing of the inhibited structure, with each pulse time-locked to a stimulus pulse [72]. This somato-axonal decoupling of neural cells of the subthalamic nucleus (STN) during HFS was first demonstrated computationally by McIntyre and his colleagues in 2004 [73]. Conversely, a more recent study of the same group showed that the inhibition of pathological oscillations in the thalamocortical loop during HFS was mediated by a stimulation-induced depolarization of the stimulated thalamic nucleus [74]. To conclude, modulatory effects of AC stimulation can vary as a function of the frequency of stimulation. Similarly, distinct cellular mechanisms may be engaged (see chapter 2).

Concerning DC stimulation, it has been reported that transcranial direct currents directly polarize the transmembrane potential of the underlying neural populations depending on the current polarity, cathodal and anodal stimulation [53, 54, 75]. This has been equally established *in vitro* as several studies showed an increase in neuronal excitability during anodal stimulation compared to a decrease in neuronal excitability during cathodal stimulation [34-36, 60]. The effects of DC stimulation can be interpreted as a rebalancing of the excitation/inhibition ratio of the targeted neural system.

3.2.3 DIRECT VERSUS INDIRECT STIMULATION

The last factor that may highly determine the impact of stimulation on neuronal dynamics is the choice of the electrode position with respect to the pathological network. Two possibilities exist. The first one consists in implanting the stimulation electrodes in a structure implicated in the generation of the pathological dynamics, such as the ictal onset zone in partial epilepsies or in a structure of the basal-ganglia network (motor cortex, STN, globus pallidus ...) in Parkinson's disease [76]. In this case, the considered configuration is termed as direct stimulation in this manuscript. The second possibility consists in placing the stimulation electrodes in a cerebral structure presenting efferent outputs to the pathological network. This configuration, termed as indirect stimulation in this dissertation, modulates pathological network dynamics by modulating the synaptic input. So what are the reported effects of both stimulation configurations on disease dynamics?

3.3 STIMULATION FOR MOVEMENT DISORDERS

Despite the empirical approach undertaken to tune the stimulator's parameters, deep brain stimulation for movement disorders is nowadays a highly effective therapeutic procedure. In this section, the pathological network structure of movement disorders is highlighted and then the reported stimulation effects are reviewed.

3.3.1 THE NETWORK STRUCTURE OF MOVEMENT DISORDERS

The pathological oscillatory dynamics associated with movement disorders whether hyperkinetic (e.g. tremor) or hypokinetic (e.g. rigidity) have been shown to propagate over extended cerebral networks essentially including the basal ganglia, the subthalamic nucleus, the striatum, and the motor cortex [42-44]. Figure 5, adapted from [77], presents the block diagram of these interlaced networks. In Parkinson's disease, for example, an excessive synchronization in the basal ganglia – cortical loop with coupled beta band oscillations in the globus pallidus, the motor cortex, and the subthalamic nucleus is often reported [78-81]. This synchronization of neuronal activity is equally reported in the ventrolateral thalamus, ventral anterior thalamus and in the centromedian-parafascicular complex of the thalamus [82]. The pedunclopontine nucleus (PPN) is also thought to be an active element of the dynamical network of Parkinson's disease as well as other movement disorders such as tremor and dystonia [83].

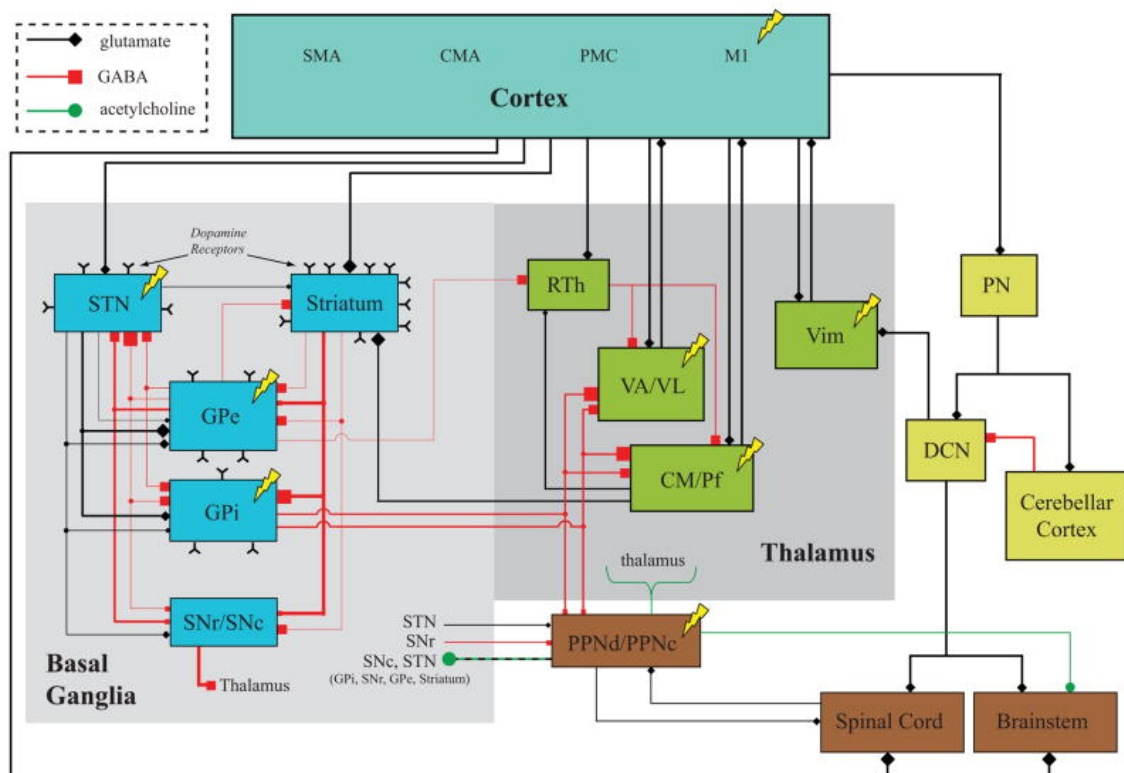


Figure 5. The cerebral network involved in the pathologic dynamics of movement disorders as presented in [77]. The lightning bolts represent actually used targets for neuromodulation. Paradoxically, the stimulation of any of these targets has been reported to alleviate the disease dynamics. The line thickness indicates the relevant proportion of each projection. Colors represent the type of the neurotransmitter-mediated transmission (see legend upper left corner). Line terminals represent the degree of axonal branching of a particular cell type. Abbreviations STN: Subthalamic nucleus, GPe: globus pallidus externus, GPi: globus pallidus internus, SNr: Substantia nigra pars reticulata, SNc: Substantia nigra pars compacta, SMA: supplementary motor cortex, CMA: cingulate motor area, PMC: premotor cortex, M1: primary motor cortex, RTh: reticular nucleus of the thalamus, VA: ventroanterior thalamus, VL: ventrolateral thalamus, CM: centromedian nucleus, Pf: parafascicular nucleus of the thalamus, Vim: ventral intermediate nucleus of the thalamus, PN: pontine nuclei, DCN: deep cerebellar nuclei, PPNd: pedunclopontine nucleus pars dissipatus, PPNc: pedunclopontine nucleus pars compacta.

In effect, the actually used stimulation targets for movement disorders (as indicated in Figure 5) are generally part of the pathological network. In this context, the stimulation configuration that works best is direct stimulation of certain components of the pathological network. Nevertheless, this direct stimulation exerts indirect stimulation effects on the network dynamics leading to the alleviation of motor symptoms.

3.3.2 MODULATORY EFFECTS OF ELECTRICAL STIMULATION

The first modulatory effects of electric deep brain stimulation in the context of Parkinson's disease date back to the 1960s when Hassler and his colleagues [84] reported that high-frequency stimulation (HFS; 25 – 100 Hz) of the globus pallidus suppressed tremor in PD patients whereas low-frequency stimulation (LFS; < 25 Hz) applied at the same location elicited contralateral tremor. Since then, several successive clinical trials (Table 1) showed the effectiveness of electrical stimulation applied to different cerebral structures of the basal ganglia-thalamocortical networks (Figure 5) in the improvement of motor symptoms [85]. In brief, as described in clinical studies of Parkinson, the choice of stimulation parameters relies on the anti-tremor effects of HFS (130 – 185 Hz) in the ventral intermediate nucleus (Vim) of the thalamus reported by Benabid in 1993 [86]. Effectively, stimulation parameters are empirically tuned around these values in order to obtain a visual reduction in motor symptoms [87-92]. This owes to the visible motor symptoms of movement disorders, which allows an online tuning of the stimulator during the surgical procedure.

Table 1 provides a brief list of DBS clinical trials reported between 1960 and 2005. In fact, the table reflects the frequent use of STN, GPe, GPi, and Vim as stimulation targets. The results reported converge to the global effectiveness of HFS (> 100 Hz) STN, GPe and GPi DBS in improving major motor symptoms (tremor, rigidity, akinesia,...). Conversely, Vim stimulation only reduced tremor. This stimulation target seems mostly adapted to tremor-predominant PD and essential tremor patients.

Nevertheless, despite the undeniable advances in stimulation technologies destined at controlling the visible motor symptoms of movement disorders, little work has been done on the modulation of the underlying pathological neural dynamics by stimulation currents (typically the synchronous beta band oscillations propagating in the basal ganglia-thalamocortical network [93]). Consequently, existing DBS solutions are limited to open-loop chronic stimulation. Patients are generally asked to turn off the stimulator overnight to avoid unnecessary use of the stimulator's battery [87-92]. Closed-loop control of the dynamics of movement disorders has been only recently raised [94, 95]. This will require the exploration of the electrophysiological dynamics of pathological neural systems in this particular context which will probably lead to a better understanding of the underlying cellular mechanisms.

3.4 STIMULATION FOR EPILEPSY

Movement disorders are characterized by the continuous clinical manifestations of motor symptoms, whereas the unique clinical manifestation in epilepsy is the recurrence of seizures. Consequently, while stimulation parameters can be tuned as a function of the improvement in motor symptoms in patients with movement disorders, per-operative parameter tuning is almost impossible in epileptic patients. In fact, the literature of DBS for epilepsy shows that some DBS stimulation protocols were initially designed based on empirical insights gained from the previous clinical studies of DBS in the context of movement disorders [96] or epilepsy [97, 98] and/or from experimental trials [99](see [32, 100] for review).

Study	Target	Stimulation Parameters	Reported Results
Hassler et al. 1960 [84]	GP	$f_s < 100$ Hz	$f_s < 25$ Hz elicited contralateral tremor in PD patients $25 < f_s < 100$ Hz suppressed tremor
Benabid et al. 1993 [86]	Vim	P.W. = 60 μ s $f_s = 130 - 185$ Hz $I_s = 0.2 - 1$ mA	Identification of optimal anti-tremor stimulation frequencies in PD, essential tremor, and dyskinesia patients. Best results were obtained for PD patients.
Hubble et al. 1997 [87]	Vim	P.W. = 116.9 ± 86.1 μ s $f_s = 161.9 \pm 29.1$ Hz $V_s = 3.01 \pm 1.05$ V	Significant reduction in motor symptoms in 19 patients with ET and 10 patients with PD over a 3-months follow-up period.
Limousin et al. 1998 [88]	STN	P.W. = 60 μ s $f_s = 130 - 185$ Hz $V_s = 2 - 2.8 \pm 0.6$ V V_s was progressively increased during the long term follow up	Long term improvement in scores for akinesia, rigidity, and tremor of the upper and lower limbs and for impairment in arising from chair, gait, and postural stability in 24 patients when off medications (12-month follow up)
Benabid et al. 2000 [90]	STN	P.W. = 60 μ s $f_s = 130$ Hz $V_s = 2 - 3.5$ V	Cumulative results in reported from 100 clinical cases (5 years follow up): Average % improvement in motor symptoms 41.6% improvement in akinesia 48.6% improvement in rigidity 27% improvement in tremor
Østergaard [92] et al. 2002	STN	P.W. = 60 μ s $f_s = 130 - 200$ Hz $V_s = 3.1 \pm 0.4$ V	Average improvement in motor symptoms in 26/26 PD patients whether on or off medications over a 3-month and a 12-month follow up.
Vesper et al. 2002 [89]	STN	P.W. = 86 – 209 μ s $f_s = 133 - 134$ Hz $V_s = 2.3 - 3.1$ V	Improved motor function over 12-month follow up – Decreasing medication doses (38 patients)
Putzke et al. 2003 [101]	Vim	3 year follow up Parameters were modified over time P.W. ≈ 80 ms $f_s \approx 148 - 165$ Hz $V_s \approx 2.5 - 4$ V	Long-term stability of stimulation-induced reduction in tremor in 19 patients (57 – 98%)
Vitek et al. 2004 [102]	GPi/GPe	P.W. = 200 μ s $f_s < 30, 50, 100, 200,$ and 300 Hz $I_s = 0.25 - 2$ mA	Improvement in motor signs for both GPe and GPi stimulation for $f_s > 100$ Hz. Worsening of motor symptoms was mostly coherent with $f_s \leq 60$ Hz (GPe), or $f_s = 1 - 30$ Hz (GPi)
Hamani et al. 2005 [91]	STN	P.W. = 60 – 120 μ s $f_s = 130 - 185$ Hz $V_s \approx 3$ V	Systematic study of (more than 150 patients) Results after 5 years of stimulation (off medications) 81% improvement in tremor 65% improvement in rigidity 47% improvement in akinesia 39% improvement in postural instability

Table 1. A list of some of DBS clinical studies reported in the context of movement disorders. Stimulation parameters for each study are provided. Abbreviations: P.W.: pulse width, f_s : stimulation frequency, V_s : stimulation voltage, I_s : stimulation current, PD: Parkinson’s disease, ET: Essential tremor.

Ever since the first reported clinical study of deep brain stimulation for epilepsy [103], the golden standard for determining the efficacy of a certain stimulation protocol has been the reduction in the frequency of clinical seizures, of course in the absence of adverse effects (see Table 2). Nevertheless, the well-structured electrographic biomarkers of interictal epileptic dynamics (see section 2.3.2) may allow the study of the modulatory effects of stimulation currents on electrophysiological interictal epileptic dynamics [104, 105], even though this is not always the case in large scale (> 10 patients) clinical studies [106, 107], where the assessment of efficacy relies on subjective patient-reported seizures (statistical analysis of personal seizure diary).

Study	Target	Stimulation	Epilepsy/Seizure Type	Reported Results
Cooper et al. 1973 [103]	Anterior cerebellum	Chronic cerebellar LFS (10 Hz) Unblind study	32 patients with secondary generalized seizures	More than 50% reduction in seizure frequency Seizure suppression in 18/32 patients lasting up to 3 years
Wright et al. 1984 [98]	Cerebellar cortex	Chronic cerebellar LFS (10 Hz), peak $I_s = 1 - 7$ mA Double-blinded study	12 patients with severe epilepsy: Complex partial seizures, complex absence seizures, grand mal, atonic seizures	Only 1 patient out of 12 presented a slight seizure reduction. Results are in contradiction with the results of Cooper et al. [103]
Velasco et al. 1987 [108]	CM	2-hours/day biphasic stimulation (1/5 minutes) P.W. = 0.1 ms $f_s = 60 - 100$ Hz $I_s = 0.8 - 2$ mA 6 to 37 months follow up Unblind study	5 patients with generalized tonic-clonic seizures plus other complex seizures (partial complex, astatic, and myoclonic) Slow interictal dynamics (polyspike wave complex 3 - 4 Hz)	3 months after daily stimulation: 80 - 100% reduction in generalized tonic-clonic seizures 60 - 100% reduction in complex seizures Reduction in IED recorded in the CM as well as by scalp EEG
Fisher et al. 1992 [97]	CM	2-hours/day biphasic stimulation (1/5 minutes) P.W. = 0.9 ms $f_s = 65$ Hz $I_s = 0.7$ mA	7 patients with refractory epilepsy : Generalized or multifocal seizure foci	No significant reduction in seizure frequency was reported in any of the 7 patients.
Benabid et al. 2002 [96]	STN	Chronic HFS 30 months follow up	5 year old girl with a focal centroparietal cortical dysplasia.	Voltage-dependent reduction (80%) of the severity and frequency of seizures.
Velasco et al. 2007 [109]	Hippocampus or Amygdalo-hippocampal junction	Bilateral chronic cyclic stimulation (1 min left - 4 min rest - 1 min right) P.W. = 450 μ s $f_s = 130$ Hz $I_s = 300$ μ A Double-blinded study	9 MTLE patients with/without HS follow up > 18 months Complex partial seizures	Patients without HS (5/9) > 95 % seizure reduction Patients with HS (4/9): 50 - 70 % seizure reduction.

Boëx et al. 2007 [104]	Amygdala/ Hippocampus	P.W.= 450 μ s/phase f_s = 5 or 130 Hz V_s = 1V Stimulation 3 – 6 hours/day	3 patients with MTLE	130 Hz: significant reduction of the interictal spike rate in 2/3 patients, reduction trend in 1 patient 5 Hz: Overall increase in interictal spike rate (trend) in 2/3 patients, no effect in 1 patient.
Miatton et al. 2011 [110]	Hippocampus	Amygdalo- Hippocampal stimulation P.W. = 450 μ s f_s = 130 Hz V_s = 1 – 2.5 V	10 patients with drug-resistant MTLE	53 – 57% reduction in seizure frequency
Valentin et al. 2013 [111]	CM	P.W. = 90 μ s f_s = 60 Hz V_s = 5 V Unblind study	11 patients with frontal epilepsy and generalized seizures	12-months follow up: > 50% seizure reduction 66-months follow up: 5/6 patients had > 50% seizure reduction including 3 seizure free

Table 2. Selected list of clinical trials of DBS for epilepsy. Abbreviations: LFS: low-frequency stimulation, HFS: high-frequency stimulation, I_s : stimulation current, f_s : stimulation frequency, V_s : stimulation voltage, P.W.: pulse width, MTLE: mesial-temporal lobe epilepsy, CM: centromedian thalamic nucleus, STN: subthalamic nucleus, ANT: Anterior thalamic nucleus, HS: hippocampal sclerosis.

Herein, the selected studies presented in Table 2 show the variability of the stimulated targets that could be used in the context of epilepsy. In certain studies [107, 109, 110], the stimulation target is located in the epileptogenic zone; direct stimulation (the hippocampus, the amygdalo-hippocampal junction in temporal lobe epilepsy). In other studies, the stimulation target is external to the pathological region such as the stimulation of STN in the case of a focal centroparietal malformation [96], the stimulation of the CM in case of frontal seizures [111]. The reported results are promising in both direct and indirect stimulation configurations.

Unfortunately, the study of DBS effects on epileptic dynamics will remain empirical as long as no clear guidelines are established for the choice of stimulation type (direct/indirect) as a function of the epilepsy syndrome and its corresponding seizure types. In the following sections, two main categories of epilepsy syndromes are highlighted. Present knowledge concerning their corresponding electrographic interictal dynamics as well as the impact of stimulation currents on these dynamics is hereby reviewed.

Case of focal epileptogenic lesions and malformations. Partial (focal) epilepsy is often associated to acquired brain lesions and inborn malformations [112]. These focal alterations in the structure of the cerebral tissue lead to focal neuronal hyperexcitability that is later on expressed in partial epileptic seizures [113]. The developmental aspect of these epileptic syndromes makes it difficult to attribute particular electrographic patterns for all types of epileptogenic lesions and malformations. Nevertheless, a

certain type of inborn malformations, known as focal cortical dysplasia (FCD), has a confirmed epileptic character with particular epileptiform patterns [114]. Epilepsies associated to focal cortical dysplasias are generally drug-resistant.

The histopathology of FCD [115] reveals an abnormal disorganization of cortical layers associated with hypertrophic or enlarged neural cells often trailing into the white matter. These enlarged neurons, termed balloon cells, are characterized by displaced nucleus, lack of dendrites or axons. In fact, this abnormal chaotic structure of FCDs is of unknown developmental causes and contributes to the hyperexcitability of the lesioned tissue. However, despite this disorganization, FCDs retain sufficient connectives for initiating epileptic seizures [33].

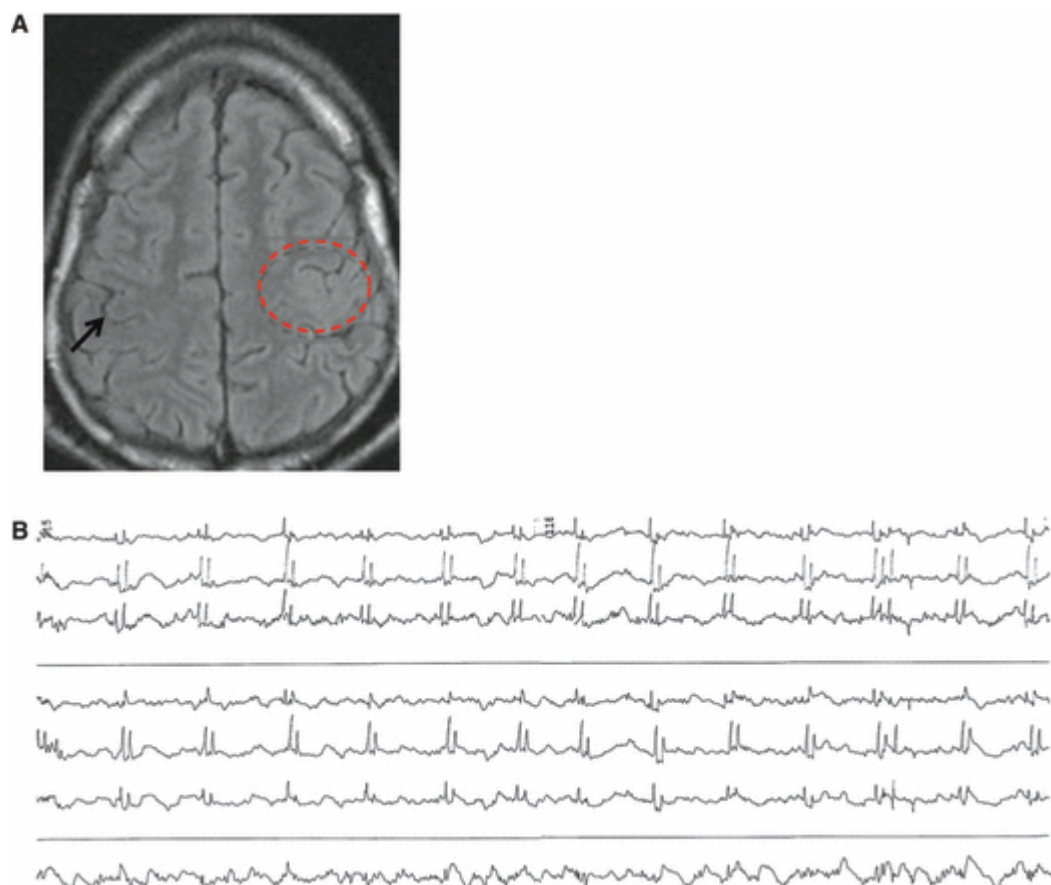


Figure 6. Electrophysiology of focal cortical dysplasia (FCD). **(A)** MRI scan of a patient with drug-resistant epilepsy showing FCD in the right hemisphere (circled knob-shaped) as compared to the normal contralateral cortex (black arrow). **(B)** ECoG recordings of FCD dynamics showing semi-rhythmic continuous spikes and polyspikes. Adapted from [114] without permission.

The electrographic interictal markers of FCD. Clinical studies [112, 114, 116, 117] of FCD's epileptogenicity highlighted its characteristic IEDs (interictal epileptic discharges). EcoG, iEEG, as well as scalp EEG recordings converge to the following set of epileptic dynamics: (1) repetitive electrographic seizures of prolonged rhythmic trains, (2) repetitive bursting discharges, (3) sustained continuous or semi-continuous rhythmic spike or polyspike trains (see Figure 6 [114]).

In view of its developmental aspect, FCDs vary largely among patients particularly in terms of their location in the neocortex and their structure. For this reason, DBS studies in this context are limited to clinical case reports [96, 105].

Case of mesial-temporal lobe epilepsy syndrome.

Temporal lobe epilepsy is the most common form of partial epilepsies in adults (~60% [118]). Mesial-temporal lobe epilepsy (MTLE) constitutes one of the most common forms temporal lobe epilepsies [119]. MTLE is characterized by the recurrence of focal seizures involving mesial temporal lobe structures (hippocampus, amygdala, entorhinal neocortical regions, brainstem, ...). MTLE with hippocampal onset represents 80% of all temporal lobe seizures [118]. Most cases of MTLE are associated with hippocampal sclerosis (HS; 60% - 70% of MTLE patients [120]), and are medically drug-resistant.

The electrographic interictal signatures of MTLE [118]. The interictal epileptic discharges (IEDs) associated with MTLE include recurrent anterior temporal spikes and sharp waves with maximum amplitude at the temporal basal electrodes of EEG scalp recordings. In addition, intermittent slow delta waves are also common at these electrodes. They generally designate electrographic seizures with no clinical manifestations. Otherwise, hippocampal intracerebral recordings showed the recurrence of spontaneous interictal ripples or fast ripples in patients with MTLE [121]. These are termed high-frequency oscillations (HFOs) and are nowadays considered as a potential biomarker of epileptogenicity [122]. Noteworthy, the form of the spikes, sharp and slow delta waves can vary largely among patients.

Finally, drug-resistance in MTLE and its high prevalence among epileptic patients led to the exponential increase in the number of clinical and experimental trials aiming at controlling mesial-temporal epileptic dynamics. Deep brain stimulation of mesial-temporal structure has long been one of the explored trails (see [123] for review). Selected clinical studies are listed in Table 3. The majority of these studies tested the efficacy of high-frequency direct stimulation of the ictal onset zone. Effectively, the choice of the stimulation frequency is usually justified by its anti-tremor effects in Parkinson patients, firstly reported by Benabid et al. in 1993 [86], and by its subsequently reported antiepileptic effects in animal models (see [124] for review) as well as in clinical trials [125]. However, in view of the unresolved problem of resistance to therapy, non-responders or symptom worsening are frequently reported in HFS studies. Overpassing this problem constitutes the ultimate challenge for DBS technologies.

Study	Patients	Stimulation Target	Stimulation Parameters	Stimulation Outcome	Other Remarks
Vnock et al. 2002 [126]	3 patients with MTLE	Amygdala-hippocampal stimulation	$f_s = 130-200\text{Hz}$ PW = 450 μs $V_s = 1\text{V}$	Significant reduction in interictal discharge occurrence and seizure frequency	The stimulation frequency was set to 130Hz for the three patients, but had to be increased to 200Hz in one of them in order to observe antiepileptic effects
Boon et al. 2007 [107]	12 patients with MTLE	Ictal onset zone determined patient-wise	$f_s = 130\text{Hz}$ PW = 450 μs V_s determined patient-wise	Seizure reduction $\geq 50\%$ for 10/12 patients 1/12 patient seizure free (1 year follow up) 1/12 patient 90% seizure reduction 1/12 patient non-responder	Unilateral MTL ictal onset \rightarrow ipsilateral amygdala-hippocampal DBS Bilateral MTL ictal onset \rightarrow bilateral hippocampal DBS
Fisher et al. 2010 [127] (SANTE trial)	110 randomized patients with refractory epilepsy (only 66 MTLE)	Anterior Nucleus of the Thalamus (ANT)	$f_s = 145\text{Hz}$ PW = 90 μs $V_s \approx 5\text{V}$	Patients with temporal seizure onset obtained the highest seizure reduction results 54% of all patients (110) had a seizure reduction $\geq 50\%$	3-month blinded phase ($V_s = 0$ or 5V) followed by 9-month unblinded phase Stimulated 35 patients Control 30 patients
McLachlan et al. 2010 [128]	2 patients with MTLE	Hippocampus (Ictal onset zone)	$f_s = 185\text{Hz}$ PW = 90 μs $V_s \approx 0.5\text{V}$ (tuned minimal value)	33% decrease in seizure frequency during stimulation phase 25% decrease in seizure frequency during the washout phase	3-month chronic stimulation period, followed by 3-month washout period (Bilateral hippocampal stimulation)
Boex et al. 2011 [129]	8 patients with MTLE (2 with HS)	Amygdala-hippocampal stimulation (Ictal onset zone)	$f_s = 130\text{Hz}$ PW = 450 μs $V_s \approx 1-2\text{V}$	67-88% significant seizure reduction in the HS patients (bipolar stimulation 0.5V intensity) 2/8 patients were seizure free 2/8 were non responders 2/8 non-lesional patients > 70% seizure reduction (average follow up 43 months)	The cathode was determined as the closest electrode to the most epileptogenic site and the anode was the one closer to the second most epileptogenic site (patient wise) Inter patient Variability later discussed in function of the location of the stimulating electrodes in [130]
Koubeissi et al. 2013 [131]	11 patients with MTLE	Fornix	$f_s = 1\text{Hz}$ PW = 100 μs (bipolar) $I_s = 8\text{mA/phase}$	92% reduction in seizure frequency lasting two days after the end of stimulation in responding patients (8/11) >75% decrease in spike occurrence during the stimulation sessions	Stimulation sessions done as part of the surgical evaluation of intractable epilepsy
Cukiert et al. 2013 [132]	9 patients with MTLE	Hippocampus (unilateral or bilateral stimulation determined empirically)	$f_s = 130\text{Hz}$ PW = 300 μs $V_s \approx 1-3.5\text{V}$	7/9 patients had a seizure reduction > 60% 4/9 patients had a 100% reduction of generalized tonico-clonic seizures 1/9 only 12% seizure reduction 1/9 was a non-responder	Mean reduction in complex partial seizures for responders: 86.5% Mean reduction in tonico-clonic seizures: 100% (4 of 4 patients)

Table 3. Selected studies of deep brain stimulation for mesial-temporal lobe epilepsy (MTLE)

Chapter 2: Problem Statement and Objectives

Forty years have passed since the first clinical trial of DBS for drug-resistant epilepsy [103] yet, as shown in the previous chapter, deep brain stimulation technologies may reduce seizure frequency but do not cure epilepsy. Actually, on clinical grounds, only three stimulation devices were approved for clinical use in drug-resistant patients throughout these years: the vagus nerve stimulator in 1997 [133], the Medtronic® neurostimulator of the anterior nucleus of the thalamus (ANT) in 2010 [127] and the responsive neurostimulation device RNS Neuropace® in 2013 [134]. Noteworthy, even approved, these devices do not guarantee the improvement in seizure frequency or the absence of adverse side effects. With vagus nerve stimulation, only 39% of the stimulated patients achieved a seizure reduction of at least 50% [133]. With the Medtronic® neurostimulator, only 54% of the patients reported a seizure reduction superior to 50% [127]. The RNS stimulator of Neuropace® has been accorded a mere 37.9% seizure reduction in the stimulated group versus 17% in the control group [134]. In these three cases, a number of complications and seizure worsening has been reported.

1 PROBLEM STATEMENT: STIMULATION PARAMETERS, OUTCOME AND MECHANISMS

The previous chapter shows the contrast between the large number of clinical trials of DBS for epilepsy and the wide spectrum of the possible stimulation outcome (seizure freedom, reduction in seizure frequency, non-responder, seizure worsening). Understanding and resolving this variability can probably lead to an improvement of DBS technologies for epilepsy.

1.1 THE VARIABILITY

As illustrated in Table 2 and Table 3 (previous chapter), the choice of the stimulation parameters remains globally bound to homogenous intervals; in most cases the stimulation frequency is superior to 100Hz, the pulse width is of the order of microseconds, the stimulation current is of the order of milli-amperes and the stimulation voltage is always inferior to 5V. These voltage/intensity parameters depend on the type of the clinical

stimulator used. Although that both current or voltage source stimulators exist in clinics, recent studies highlight the proved safety of current source stimulator as compared to voltage source stimulators [135].

Despite the homogeneity of the stimulation parameters, the stimulation outcome strongly varies among patients (or groups of patients). For the same stimulation trial, very few (< 10 %) patients never experience seizures during the stimulation follow-up (up to 5 years), about half the population (30 – 55 %) report at least 50 % reduction in seizure frequency, about 10 % are non-responders, and few others experience a worsening in seizure frequency and severity (see previous chapter). Many factors may be at the origin of this variability: the choice of the stimulation category (see chapter 1 section 3.2) and parameters, the inter-patient anatomical and pathological differences either on the level of the epileptogenic zone, the seizure semiology or the precision in the position of the stimulating electrodes

The empirical approach usually adopted to determine stimulation parameters ahead of a clinical trial is rather restrictive than constructive. Even the fine tuning of stimulation parameters around a priori fixed values patient-wise does not always guarantee antiepileptic effects. Nevertheless, in view of our current, and still limited, understanding of the mechanisms by which stimulation currents modulate neuronal dynamics, whether normal or pathological, such empirical approach seems clinically the most adapted for drug-resistant patients in whom surgery is contraindicated.

1.2 THE POORLY-UNDERSTOOD MECHANISMS

Today, the precise direct and network mechanisms of neural modulation by DBS remain elusive [77]. The majority of the studies exploring DBS mechanisms usually address those related to HFS (> 100 Hz) given its common use in the clinical context (for examples see [68, 73, 136, 137]). When identified, these mechanisms seem to vary as a function of the employed experimental setup: functional imaging, neurophysiological recording, neurochemistry and biology-inspired computational modeling [138].

Functional imaging studies highlight neural activation in the stimulated network during HFS; thalamic stimulation of patients with essential tremor showed increased activity in the thalamus, the motor cortex, and basal ganglia with respect to baseline activity [139-141]. Regarding neurophysiological observations, the reported results can be divided into two contradictory classes: the inhibition of neuronal activity by HFS versus the increase of neuronal activity by stimulation. These results depend on the recording site. The inhibition of intrinsic neuronal activity was recorded in the stimulated nuclei [69, 142, 143], whereas a

neuronal activation was reported when the stimulation electrodes recorded efferent nuclei of the stimulated target [144, 145]. This indicates that the mechanisms of direct and indirect stimulation can be completely distinct.

Recent evidence from neural network modeling suggests that HFS induces a functional decoupling of the somatic and axonal activity in stimulated neuronal populations [73]. Stimulation may induce the inhibition of intrinsic somatic activity as well as axonal excitation (coupled to the stimulation frequency) at the same time. The origin of the reported somatic inhibition is related to GABAergic (GABA_B) mechanisms. This may imply the dual coexistence of inhibition and excitation in the stimulated nucleus: the inhibition of the intrinsic activity of the latter, versus the activation of its efferent nerve fibers (orthodromic activation), which consequently excites efferent nuclei.

Although that the inhibition of the stimulated target seems to be a probable direct effect of stimulation, the mechanisms underlying this inhibition remain controversial. Among the many studies reported over the last decade, identified mechanisms regarding the inhibitory effect include: local depolarization blockade [68], synaptic depression due to neurotransmitter depletion [146, 147], synaptic inhibition [70], stimulation-induced increase in glutamate levels in the stimulated target and consequent activation of inhibitory neurons (feedback inhibition)[74].

Few studies indirectly addressed the mechanisms of low-frequency stimulation on neural dynamics [148-150]. These studies, initially aimed at studying the mechanisms of cortical adaptation in response to a thalamic stimulation in the context of sensory integration, reported a transient synaptic depression at thalamocortical synapses following trains of thalamic LFS (< 10 Hz). Interestingly, this short-term depression was linked to NMDA receptors formed at the cortical level by ascending thalamocortical fibers [149].

Finally, intermediate-frequency stimulation (IFS; 20 – 60 Hz) has long been used in the context of presurgical evaluation of patients with drug-resistant epilepsy in order to map dysfunctional (the epileptogenic network) and functional brain areas. It has long been observed that this type of stimulation can induce epileptic afterdischarges in animal models of epilepsy [151]. However, to the best of our knowledge, the mechanisms related to these stimulation frequencies have never been specifically explored. A very recent function imaging study shows that maximal cortical activation is attributed to DBS frequencies in the range 40 – 100 Hz [152].

As far as DC stimulation is concerned, stimulation mechanisms are summarized by polarization effects (see chapter 1 section 3.2.2). However, these studies are limited to

transcranial electrical stimulation. DC DBS has never been tested on human patients due to the lack of appropriate knowledge concerning the effective electrical safe dose to be used. DC stimulation is associated with electrode polarization, tissue damage, irreversible charge accumulation, excitotoxicity ... (see [153] for review).

This brief review suggests that the spectrum of involved mechanisms is quite large and that distinct stimulation-induced cellular/network processes can be triggered as a function of stimulation frequency. Besides, the mechanisms underlying frequency-dependent effects remain almost unexplored. This is notably the case of IFS, which is the least associated to possible antiepileptic effects. Similarly, the mechanisms of LFS and DC stimulation remain less explored than those of HFS.

1.3 HOW TO OPTIMIZE STIMULATION

The optimization of stimulation outcome requires a mature understanding of the underlying mechanisms of neuromodulation by electrical currents. Since the present scientific knowledge of these eminent biophysical and neurophysiological processes remains incomplete, the empirical tuning of stimulation parameters cannot be overpassed. Noteworthy, the clinical exploration of all possible ranges of parameters (frequency, current intensity, pulse width ...) and configurations (DC/AC, direct/indirect ...) is practically impossible due to ethical, technical and clinical limitations. Then, the challenge is to define alternative methodologies that allow for the exploration of vast ranges of stimulation parameters and configurations in order to establish a better-defined relationship between stimulation parameters and stimulation effects from the one side and stimulation parameters and mechanisms on the other side

$$outcome = \mathcal{Q}(parameters)$$

$$mechanism = \mathcal{M}(parameters)$$

where \mathcal{Q} and \mathcal{M} represent to-be-defined functions of stimulation parameters. The qualitative or quantitative definition of these relationships/functions can assist the optimization of stimulation protocols.

2 OBJECTIVES: OPTIMIZE STIMULATION OUTCOME

The objectives of this thesis are (1) the development of an alternative computational test ground for studying the mechanisms of generation of real epileptic dynamics in well-defined contexts, (2) the consequent identification of the stimulation parameters-outcome

and the parameters-mechanisms relationships and finally (3) the establishment of guidelines for optimizing stimulation outcome.

2.1 OPTIMIZE STIMULATION PARAMETERS AND EFFECTS

Following the different stimulation configurations, various parameters can be considered for an eventual optimization. During this PhD thesis, my work was focused on two major under-explored stimulation configurations. The first one concerns the case of indirect AC intracerebral stimulation. In this case, the contribution of the stimulation frequency to the modulatory effects is assessed. The second case concerns the DC direct stimulation of the ictal onset zone. Stimulation polarity and duration are particularly studied.

2.1.1 CASE OF INDIRECT AC INTRACEREBRAL STIMULATION

Indirect AC intracerebral stimulation is probably the most common clinical stimulation intervention reported in the context of epilepsy. This stimulation configuration is aimed at modulating the epileptic network activity or the epileptic focus activity by targeting a deep brain (or intracerebral) structure. However, as far as the stimulation parameters are concerned, this configuration is often limited to high-frequency stimulation (HFS; > 100 Hz). In spite of a 10 % rate of non-responders and a 50 % rate of significant reduction in seizure frequency, the effects of lower stimulation frequencies are not seriously explored.

For this stimulation configuration, this work aims at identifying the frequency-dependent stimulation outcome as well as mechanisms on a wider frequency range.

2.1.2 CASE OF DIRECT DC INTRACEREBRAL STIMULATION

DC direct stimulation of the ictal onset zone has never been explored earlier clinically or experimentally *in vivo*. This owes to the monophasic aspect of this type of stimulation that is usually associated with tissue damage [154]. It is proved that at certain current intensities, DC stimulation can provoke electrode polarization through faradaic reactions leading to harmful metal deposit in the stimulated tissue [153]. Other mechanisms related to brain damage by DC stimulation currents include metabolic processes such as excitotoxicity and electrochemical phenomena such as tissue heating [135].

Despite the discouraging assumptions, low-intensity DC direct stimulation is explored in this work. The objective is to assess the contribution of low-intensity current polarity and duration to stimulation outcome in the perspective of translating results to non-invasive tDCS.

3 GENERAL METHODOLOGY

In order to achieve the announced objectives, an interdisciplinary work is undertaken in this thesis. The general methodology relies on the conjoint use of computational modeling, real data acquisition, signal processing, and nonlinear system analysis (Figure 7).

3.1 COMPUTATIONAL MODELING

Computational neuroscience is an interdisciplinary science at the interface of neuroscience, mathematics, physics and engineering. This research domain favors cross-talk among these various disciplines thus allowing the integration of distinct forms of new and detailed knowledge (e.g. experimental neurobiology/neurophysiology, dynamics of “complex” or nonlinear systems, electrical engineering) into a single entity, a computational model. Thereby, the latter can be a useful tool not only to reproduce and explain experimental/clinical observations but also to generate experimentally testable hypotheses about underlying mechanisms. In effect, computational neuroscience encompasses studies ranging from the cellular and molecular levels (microscopic models) to studies at the systems’ level (mesoscopic and macroscopic models). The level of representation actually follows the nature of the studied experimental context and the desired level of exploration of the targeted mechanisms.

In the context of epilepsy, computational neuroscience has been particularly useful. In fact, micro-, macro- and mesoscopic models of epileptic neuronal interactions somehow contributed to our current understanding of major epileptic dynamics particularly in the context of ictal transition and the generation of epileptogenic biomarkers (e.g., high frequency oscillations (HFOs) and spike-wave complexes) [155]. Computational models were later used to predict seizures as well as the efficacy of antiepileptic drugs but with not much success (see [156] for review). Over the past decade, computational modeling particularly gained ground in the domain of “therapeutic” deep brain stimulation (DBS) in an attempt to uncover its underlying mechanisms and therefore optimize its clinical efficiency [157].

Noteworthy, the computational approach is particularly fruitful when it is well grounded in experimental/clinical data [158]. In fact, it has been evidenced that 1300 out of ~600,000 configurations of a four-compartment model could be used to approximate the physiological properties of a biological neuron as simple as the lateral pyloric neuron of the stomatogastric ganglion of decapod crustaceans [159].

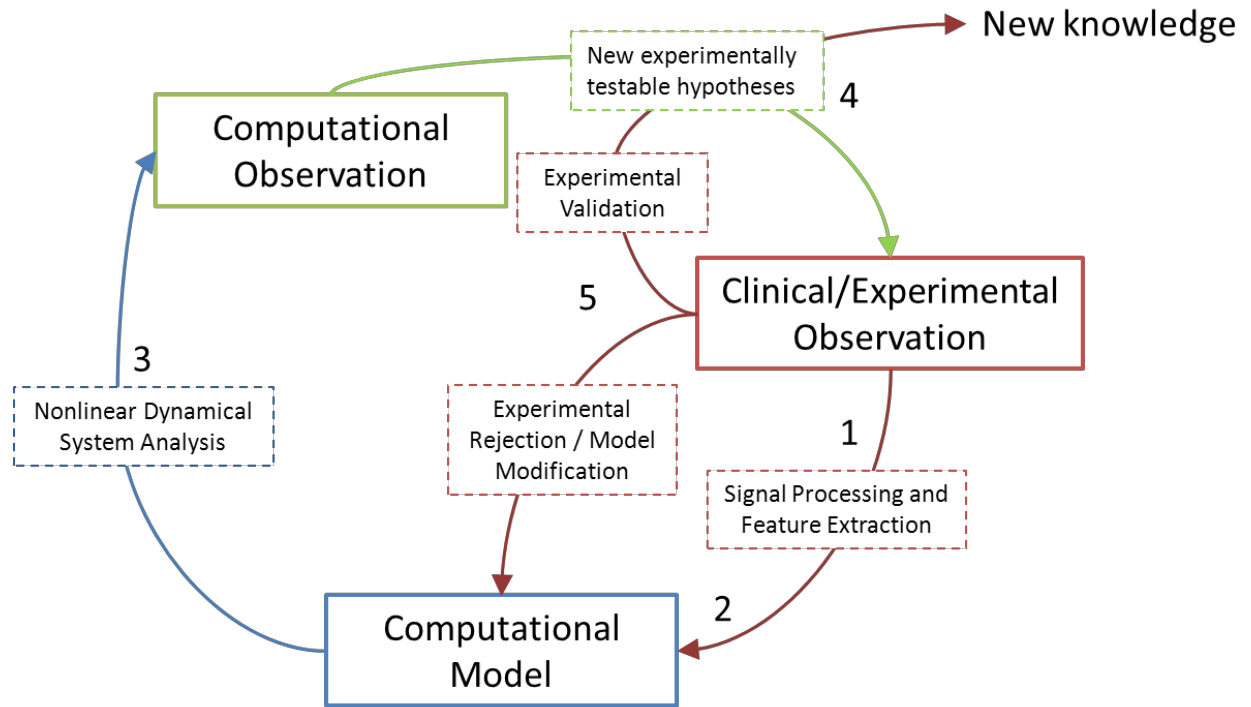


Figure 7. A schematic representation of the general methodology. 1) Real neurophysiological knowledge is used in order to computationally model realistic epileptic dynamics then 2) electrophysiological experimental/clinical data is processed and characterized in order to optimize the model's parameters. 3) The analysis of the resulting nonlinear dynamical system gives rise to computational observations of neurophysiological phenomena (mechanistic insights, physiological processes...). New hypothesis concerning the underlying neurophysiological processes (of neuromodulation in our case) can then be elaborated. 4) The experimental validation of these hypotheses is mandatory for the generation of new knowledge or for the consequent enhancement/modification of the computation model when the tested hypotheses are rejected.

For this reason, a special attention was made in this work to reconcile the computational modeling aspects with the neurosciences experimental/clinical ground reality. Therefore, when considering each stimulation context, a neurophysiology-based model of the concerned brain structure/network is proposed. Similarly, a physiologically-plausible implementation of stimulation inputs is equally included.

3.2 ELECTROPHYSIOLOGICAL DATA ACQUISITION/EXPERIMENTATION AND SIGNAL PROCESSING

Once an adapted model is properly implemented, electrophysiological data is used to optimize the model's parameters. In this work, two data types are used: clinical and experimental electrophysiological signals. Clinical intracerebral EEG (iEEG) signals are recorded during the pre-surgical intracerebral evaluation of the epileptogenic zone in a drug-resistant patient. Experimental LFP signals are acquired as a part of an experimental

setup designed to study epileptic dynamics *in vivo* (mouse model) and to analyze/explain the consequent modulatory effects of DC currents on these dynamics.

Adequate signal processing methods are defined for each data type. A time-frequency adaptive method (Matching Pursuit – MPTK [160]) is used to analyze the frequency content of real iEEG signals and a rupture detection algorithm (Page-Hinkley test) is used to detect transient interictal discharges in experimental LFPs. These different approaches were elaborated to quantify the “epileptic aspect” of actual electrophysiological signals. This aspect was either characterized by its proper spectral distribution when MPTK was used or by the occurrence, intensity and duration of the detected epileptic interictal transients when Page-Hinkley was used. In both cases, the quantified “epileptic aspect” allowed for model parameter optimization (distance between simulated and real signals) and thus for the optimal reproduction of epileptic dynamics in the model based on real data.

3.3 NONLINEAR SYSTEM ANALYSIS

The resulting nonlinear dynamical system is finally analyzed in order to explore the mechanisms of generation of stimulation effects. The phase plane is explored, the activity maps are computed and/or the intermittency of the model’s output is studied as a function of the parameters of the stimulation input.

In the case of AC indirect stimulation, the effect of the frequency of the stimulation signal on the model’s dynamics is defined. Besides, mechanistic insights concerning the observed bifurcations are concluded. In the case of DC direct stimulation, the effect of the polarity of the stimulation input on the model’s dynamics is explored. The sensitivity of these effects to the coefficient of impact on the concerned neuronal subpopulations is also expressed in activity maps. Only for the second stimulation case, the experimental validation of the model’s predictions is accomplished (preliminary experimental study).

3.4 GENERAL OVERVIEW OF THE WORK ACCOMPLISHED DURING THIS PHD THESIS

Figure 8 summarizes the work accomplished during this PhD thesis. It shows the two studied stimulation contexts and their consequent results. As illustrated, both investigations made use of the same family of methods (computational modeling and signal processing). They both relied on real electrophysiological data. Finally, they both implied parameter-dependent effects of stimulation.

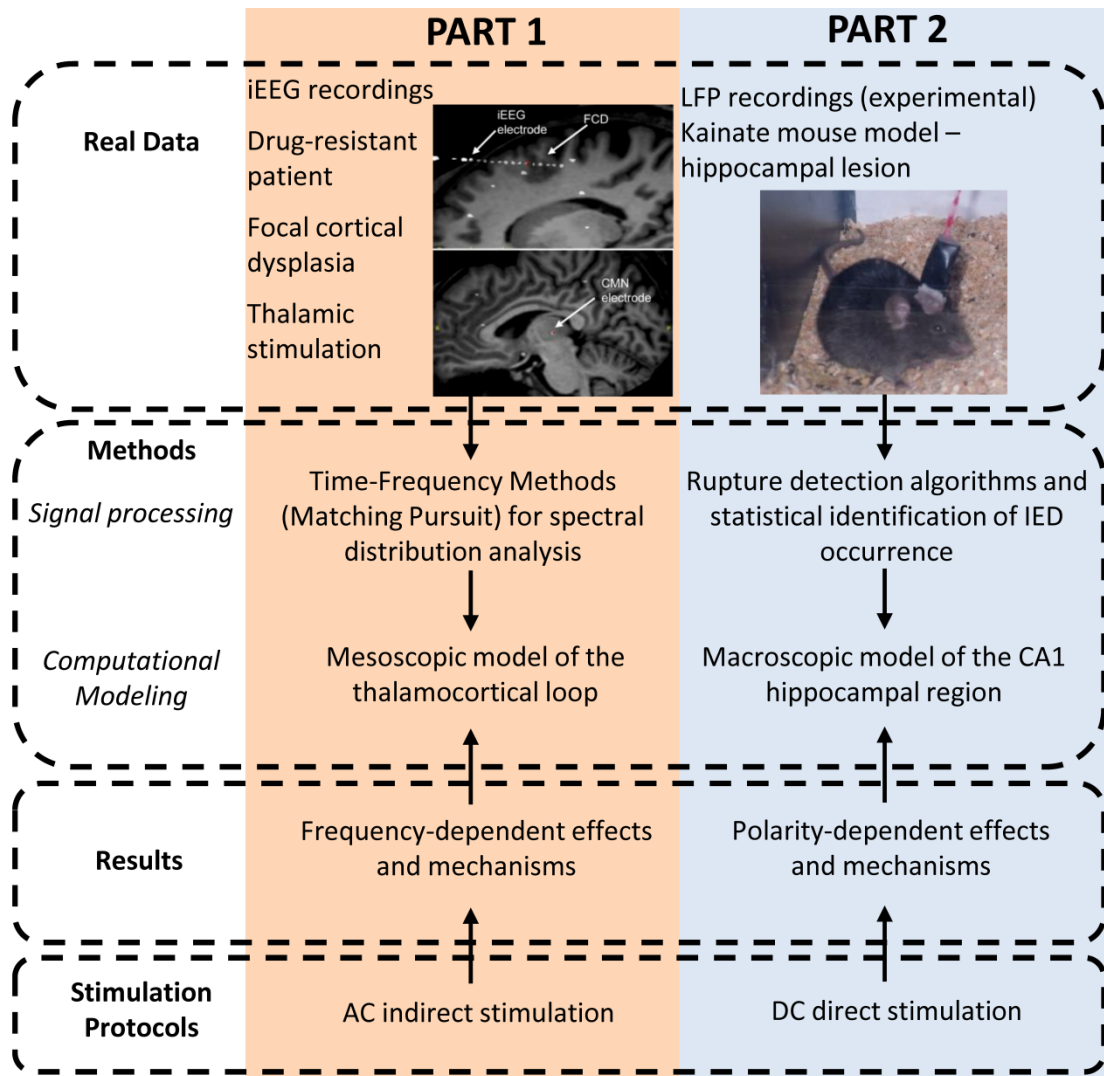


Figure 8. Major contributions and organization of the presented work. In this thesis, two major stimulation protocols were studied in the perspective of a possible clinical translation of the revealed results. The same general methodology was used in these two investigations, described each in a separate part of this dissertation. The first studied stimulation protocol (Part 1, in orange), AC indirect stimulation, involved the development of an extended mesoscopic model of the thalamocortical loop that includes the implementation of major cellular processes (such as feedforward inhibition and short-term depression). The model parameters were then optimized using an adequate clinical dataset observed in the intracerebral EEG (iEEG) recordings of a patient with focal epilepsy. Suitable time-frequency methods (based on Matching Pursuit) were used to characterize the spectral distribution of actual and simulated signals for model optimization. The results suggested frequency-dependent effects and mechanisms of stimulation. The second investigation (Part 2, in blue) of this work concerned the DC direct stimulation protocols. Computationally, an existing model of the hippocampus developed in our team [161] was amended to accomplish this work. The statistical identification of IED occurrence from experimental LFP recordings allowed a better representation of IED occurrence. For this, the Page-Hinkley test was used to detect the peaks of IEDs. The results showed a polarity-dependent modulation of IED occurrence. An experimental protocol was then designed and performed to validate these results.

In Part 1 of this manuscript, AC indirect stimulation protocols are studied particularly in the thalamocortical network. An adequate model of the thalamocortical loop is proposed. It constitutes an extended version of existing models including an explicit implementation of two major cellular mechanisms of cortical adaptation in this network, namely short-term depression and feedforward inhibition. The model makes use of an adequate dataset of clinical intracerebral EEG (iEEG) recordings observed during the preoperative iEEG exploration in a patient with focal epilepsy. The stimulation effects as well as the spontaneous epileptic dynamics observed in this dataset were characterized using an adequate time-frequency signal processing algorithm, based on Matching Pursuit. The quantified features were used to optimize the model's output. The results suggested frequency-dependent effects and mechanisms of stimulation

In the second part of the manuscript (Part 2), the mechanisms and effects of DC direct stimulation protocols are explored. For this, an existing model of the hippocampus [161] developed in our team was adapted to accomplish the computational part of this study. Real LFP recordings in a mouse model (kainate model) of mesial-temporal lobe epilepsy (MTLE) were used to statistically identify the occurrence IEDs in the epileptic hippocampus. This allowed a better representation of the transition between background activity and epileptic discharges in the model. A rupture detection algorithm (Page-Hinkley test) was used to detect the occurrence of these IEDs in real and simulated signals. The results showed a polarity-dependent modulation of IED occurrence in the simulated signals. A polarity-dependent stimulation mechanism (membrane polarization) was implemented to obtain these results. An experimental protocol was then designed to verify the existence of these polarity-dependent effects *in vivo*. The same mouse model was used for this validation. The results are detailed in Chapter 8.

PART 1: FREQUENCY-DEPENDENT EFFECTS OF INDIRECT THALAMIC STIMULATION ON CORTICAL EPILEPTIC DYNAMICS

The objectives of Part 1 can be summarized by (1) understanding the mechanisms of generation of epileptic thalamocortical dynamics, (2) exploring the contribution of the stimulation frequency to the modulation of these dynamics and (3) proposing a clinical implication for the ensued computational results. Firstly, a physiologically-plausible computational model of the thalamocortical loop is proposed. A real clinical dataset of thalamic DBS observed in a patient with drug-resistant epilepsy is then used to optimize the model's parameters to guarantee a realistic epileptic output. For this, a signal processing method based on an adaptive signal decomposition algorithm (Matching Pursuit) is used to characterize real and simulated signals. Later on, an exhaustive optimization procedure is employed to determine the optimal model parameters. And finally, the behavior of the resulting nonlinear dynamical system is analyzed as a function of the frequency of the stimulation input. The results suggest a frequency-dependent modulation of the model's output. Further analysis highlighted frequency-dependent mechanisms of indirect AC stimulation.

Chapter 3: A Computational Model of the Thalamocortical Loop

This chapter first reviews the existing models of the thalamocortical loop. Then our own implementation of a stimulation-driven model of this brain network is detailed. The latter was further used to explore the mechanisms by which DBS modulates epileptic cortical activity.

1 MESOSCOPIC MODELS OF THE THALAMOCORTICAL LOOP

The international league against epilepsy defines epileptic dynamics as related to “abnormal excessive or synchronous neuronal activity in the brain” [162]. Moreover, it is evidenced that thalamocortical dynamics participate into synchronization processes that allow for the generation of normal (e.g. sleep spindles) as well as pathological oscillatory activity (e.g. epileptic discharges) [163]. Given this reported synchrony of neuronal activity in thalamocortical networks, particularly in the epileptic context (e.g. spike-wave epileptic discharges), a particular interest was attributed to the mesoscopic neural modeling in this chapter. Actually, a lumped representation of interacting neuronal populations was adopted for modeling the dynamics of the thalamocortical system in this thesis.

1.1 THE THALAMOCORTICAL LOOP

The thalamus (Figure 9) is a highly compartmentalized midline brain structure of two bilateral halves, lying between the midbrain and the neocortex. It is made up of various nuclei with various and often independent functions. All thalamic nuclei, except the reticular thalamic nucleus (RTN), present reciprocal ipsilateral neuronal projections to particular cortical regions depending on their functions (motor, somatosensory ...). The RTN, which is structurally a thin shell of GABAergic cells surrounding the thalamus, forms efferent inhibitory connections (GABAergic) to the corresponding thalamic nuclei from which it receives glutamatergic input. In the normal brain, all cortical regions receive inputs from the thalamus [164].

Generally speaking, a thalamocortical loop can be defined as the interacting neural system formed by the reciprocal neuronal projections existing between the thalamus and the cortex, passing by the reticular nucleus. Various thalamocortical loops connect different

regions of the cerebral cortex to distinct thalamic nuclei in order to assure certain brain functions (e.g., sleep rhythms, consciousness, sensory integration...). This explains the scientific interest in this type of neuronal networks, and therefore the wholesome of scientific studies, computational included, that it ensued over the past two decades (see [73] for review), especially when it concerns thalamocortical dysfunction (epilepsy, cortical lesions and trauma, tremor... and more recently schizophrenia[165, 166]).

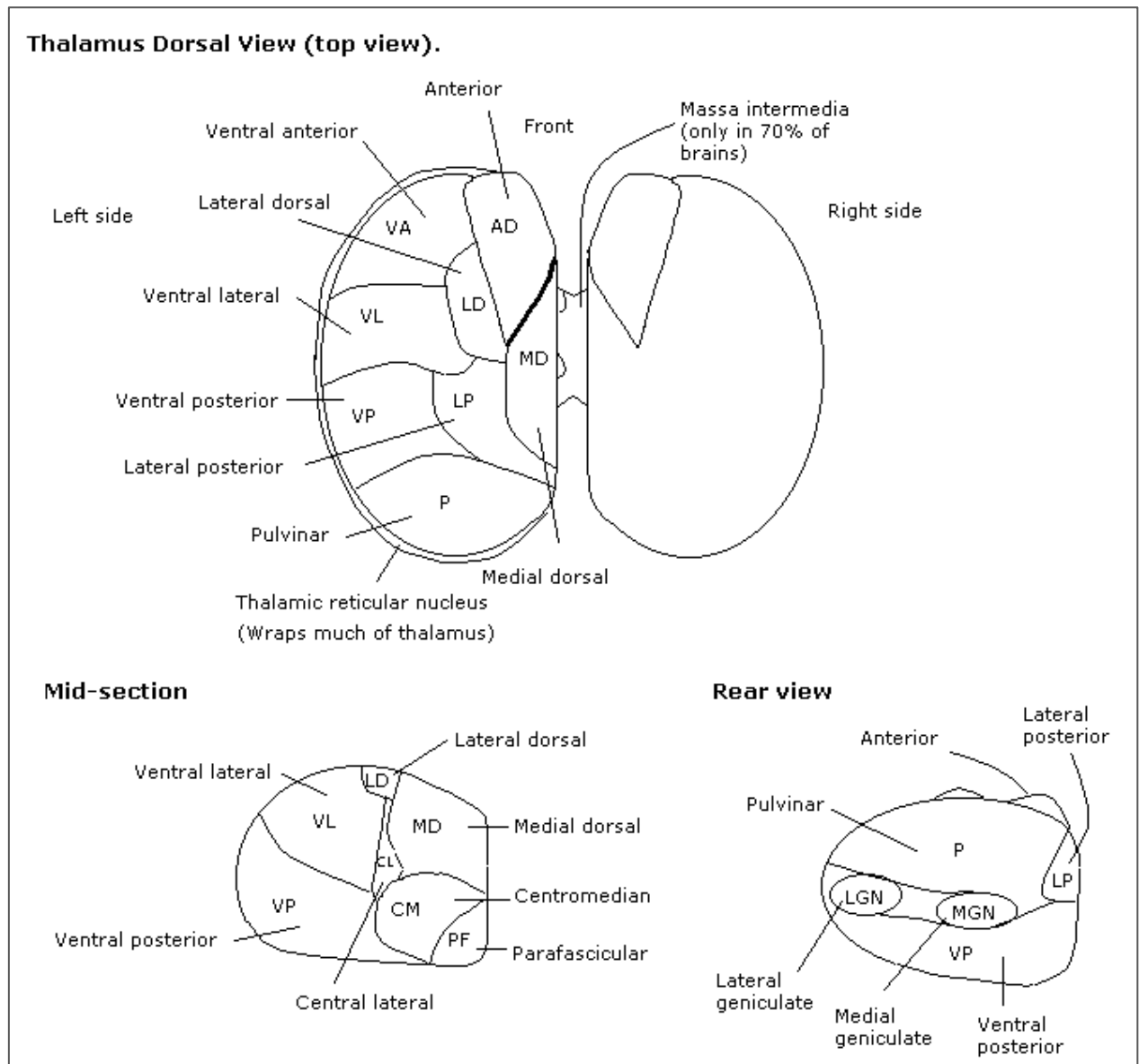


Figure 9. The Thalamic Nuclei (http://en.wikipedia.org/wiki/Thalamic_reticular_nucleus). Dorsal, mid-section and rear view. Note that the thalamic reticular nucleus forms a capsule around the thalamus laterally.

1.2 THALAMOCORTICAL MODELS: STATE OF THE ART

Besides microscopic models, the literature about computational neuroscience is rather rich regarding mesoscopic models of the thalamocortical loop. Models proposed so far share the same generic tri-modular architecture consisting of a cortical, a reticular and a thalamic module (Figure 10). Moreover, one can admit that each of these models can be viewed as an evolution of the preceding ones in an attempt to suitably address the objectives of a particular study. For instance, the models described in [67, 167-169] are extended forms of a sequence of previously published models of cortical dynamics [20, 170, 171] to which a reticular and a thalamic module were added.

Similarly, the thalamocortical model described by Adhikari and his colleagues [67] is the most recent form of Robinson's model [26]. Being the first mesoscopic model to explore thalamic DBS effects on cortical activity, the model contribution included adding a single stimulation input on the thalamic module, herein representing the ventral thalamic nucleus. Formally, the stimulation current was actually summed with the incoming "axonal flux" [67], otherwise termed the incoming firing rate, arriving at the thalamic module.

Equally important, another series of models [27, 172, 173] of the thalamocortical loop evolved in the direction of the thalamic model of Lopes Da Silva [18]. The major advancements introduced by [27] to the initial model of Lopes Da Silva [18] include the extension of the thalamic model into a thalamocortical model by adding a cortical module, and the modeling of the low-threshold calcium current potentially responsible for burst firing in thalamic cells.

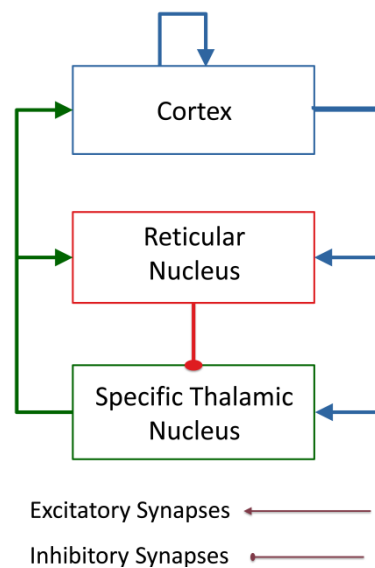


Figure 10. Generic architecture of the thalamocortical model composed of three interconnected modules, a cortical, a thalamic and a reticular module. Each module includes one or several neuronal subpopulations.

2 IMPLEMENTING A STIMULATION-DRIVEN MODEL OF THALAMOCORTICAL DYNAMICS

In order to study the effects and mechanisms of thalamic stimulation on cortical epileptic dynamics, we developed a stimulation-driven model of the thalamocortical loop. The model's architecture is in conformity with the aforementioned previously published models [27, 174-176], yet it included three main adaptations to better account for stimulation-induced dynamics. In brief, these adaptations can be summarized by the implementation of 1) a novel cortical module (to simulate rhythms specific to dysplasia), 2) subcortical stimulation inputs and 3) two cellular mechanisms potentially involved in stimulation-induced dynamics. These mechanisms are the feedforward inhibition (FFI) and the short term depression (STD).

2.1 MODEL ARCHITECTURE

This section provides a detailed overview of the different aspects of the model's architecture, starting from the global network perspective and tracing down to the neuronal subpopulation concept. The proper architecture of each module is then depicted and the different mechanisms explicitly modeled to study the effects of thalamic DBS are equally detailed.

2.1.1 FROM A GLOBAL NETWORK VIEW

From a global perspective, the model architecture was designed of three main blocks, i.e. modules, also present in former models of the thalamocortical loop [26, 27, 167-169, 173]: a cortical, a thalamic and a reticular module. These modules allowed for the physiological representation of the cerebral structures undoubtedly involved in the thalamocortical network dynamics: the cerebral cortex, the thalamus, and the reticular thalamic nucleus. In effect, the cortical, thalamic and reticular modules simulate the dynamics of a cortical neuronal population, a nonspecific thalamic nucleus and the reticular thalamic nucleus, respectively.

2.1.2 ON THE LEVEL OF A SUBPOPULATION

Each module is constituted of one or more subpopulations of neurons each representing an aggregate of highly interconnected neurons sharing the same features and temporal dynamics. A given subpopulation can be either excitatory or inhibitory. Formally, the temporal dynamics of each subpopulation are described by two transfer functions: the input/output functions. The validity of these two functions was experimentally investigated and presented in W. Freeman's "Tutorial on neurobiology: From single neurons to brain

chaos” [12]. This author termed them “pulse-to-wave” and “wave-to-pulse” function respectively.

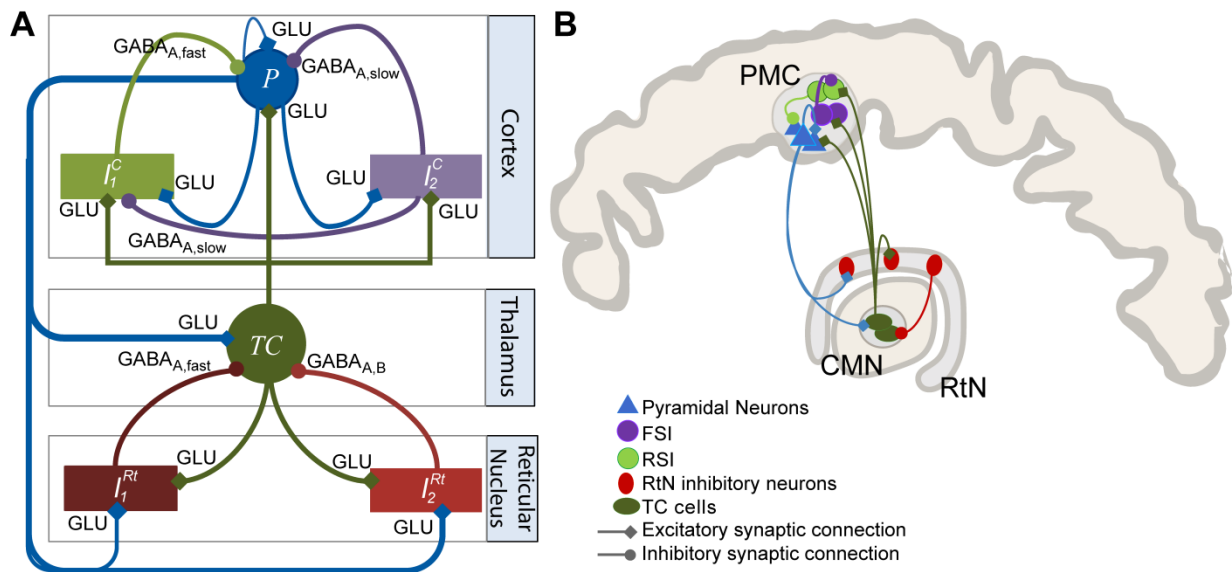


Figure 11. Modeling the thalamocortical loop. **(A)** The tri-modular model architecture inspired from the literature of thalamocortical models and in conformity with **(B)** the corresponding physiological representation.

As its name (pulse-to-wave function) indicates, the input function converts the incoming presynaptic average density of action potentials (pulses) into an average postsynaptic membrane potential (PSP), either excitatory (EPSP) or inhibitory (IPSP) depending on the presynaptic subpopulation. The input function can be mathematically represented by a linear second order low-pass filter as detailed Jansen and Rit [21]:

$$H(s) = W / \left(s + \frac{1}{\tau_w} \right)^2 \quad (8)$$

where s is the Laplace variable, W/τ_w^2 is the filter’s static gain, and $1/\tau_w$ (expressed in s^{-1}) is the filter’s center frequency. The impulse response of this filter is given by:

$$h(t) = \frac{W}{\tau_w} \cdot t \cdot e^{-t/\tau_w} \quad (9)$$

Once the filter parameters W and τ_w are well adjusted, the impulse response $h(t)$ approximates the shape and kinetics of real postsynaptic potentials (PSP). From the physiological point of view, the value assigned to W adjusts the synaptic sensitivity by determining the peak of modeled PSPs. This peak mathematically corresponds to the maximum of the function $h(t)$ and is equal to $W \cdot e^{-1}$. As for parameter τ_w , it is directly

linked to synaptic kinetics i.e. it determines the rise and decay time of the modeled subpopulation. In effect, the rise time (t_{rise}) of $h(t)$ is defined as the time required for $h(t)$ to attain its maximal value. The value of t_{rise} can be derived as follows:

$$\begin{aligned}
 h'(t_{rise}) &= 0 \\
 \Rightarrow e^{-\frac{t_{rise}}{\tau_w}} - \frac{t_{rise}}{\tau_w} \cdot e^{-\frac{t_{rise}}{\tau_w}} &= 0 \\
 \Rightarrow \left(1 - \frac{t_{rise}}{\tau_w}\right) &= 0 \\
 \Rightarrow t_{rise} &= \tau_w
 \end{aligned} \tag{10}$$

Similarly, the decay time t_{decay} can be derived from $h(t)$. As t_{decay} corresponds to the time required by $h(t)$ to fall down to 36% ($1 - e^{-1}$) of its peak, the exact value of t_{decay} can be obtained by graphically solving the function $h(t) = e^{-1} \cdot h(t_{rise})$. The decay time can be thus proven equal to $3.146 \cdot \tau_w$. Indeed, the adequate adjustment of parameter τ_w is indispensable for ensuring physiologically-plausible values of the rise and decay times of modeled PSPs. As a matter of fact, the physiological ranges of values for these parameters can be defined based on studies concerning the *in vitro* features of recorded PSPs (for examples see [177, 178]). Figure 12-A depicts the form taken by the impulse response of filter $H(s)$ in the cortical module.

Finally, it is worth noting that an alternative more detailed implementation of the input function was introduced by Bojak and Liley in [23] and described in detail by Molaei-Ardekani et al. [179]. It replaces the aforementioned mono-exponential impulse response, by a bi-exponential impulse response with two time constants τ_{w1} and τ_{w2} . Therefore, it allows for the separate adjustment of the rise and decay time of the modeled subpopulation, and consequently offers a better approximation of actual PSPs. However, the mono-exponential function proved sufficient for this study.

As for the output function, or the “wave-to-pulse” function, it converts the sum of average excitatory and inhibitory postsynaptic membrane potentials, v , into an average density of outgoing action potentials $S(v)$, also known as the mean firing rate of the concerned subpopulation. Formally, the output function is implemented as a static nonlinear sigmoid of the form:

$$S(v) = \frac{2e_0}{1 + e^{r(v_0 - v)}} \tag{11}$$

where $2e_0$ is the maximum firing rate, v_0 is the postsynaptic potential corresponding to a firing rate of e_0 , and r is the steepness of the sigmoid. Initially proposed by Wilson and Cowan [13], this function accounts for threshold and saturation effects that occur at the somas and initial axonal segments of the modeled neurons. As aforementioned, Freeman could experimentally measure this function *in vitro* owing to the fact that it is a population property [12]. The form of this function is represented in Figure 12-B.

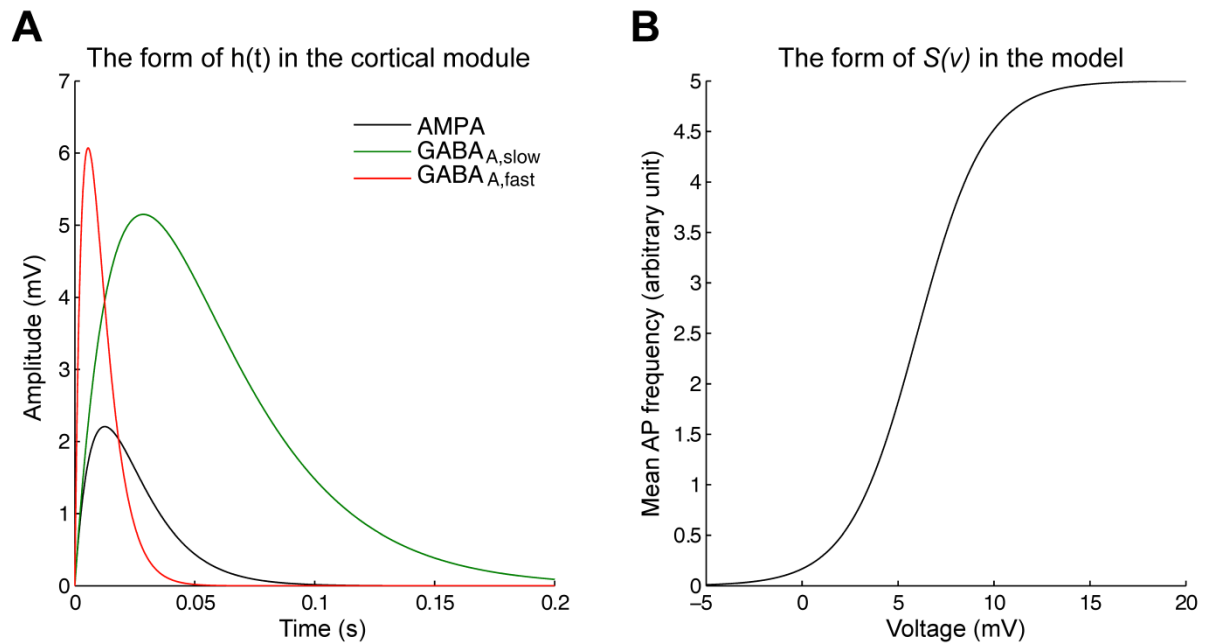


Figure 12. The form of the model's functions in the cortical module. **(A)** The impulse response of the input transfer function in the cortical module for the three types of synaptic transmission represented AMPAergic (A_c and τ_{ac}) and GABAergic transmission (B_c, G_c and τ_{bc}, τ_{gc}) in the three subpopulations. **(B)** The form of the output sigmoidal function in the model.

2.1.3 THE CORTICAL MODULE

The cortical module was designed in accordance with an existing model of the neocortex [180] proven to generate both normal and epileptiform dynamics. Formally, it included a subpopulation of pyramidal principle cells (P ; $W = A_c, \tau_w = \tau_{ac}$ in Equation 8), and two inhibitory subpopulations representing the soma- and proximal-dendrite targeting interneurons (I_1^c , GABA_{A,fast} currents; $W = G_c, \tau_w = \tau_{gc}$ in Equation 8), and the dendrite-targeting interneurons (I_2^c , GABA_{A,slow} currents; $W = B_c, \tau_w = \tau_{bc}$ in Equation 8).

Regarding pyramidal collateral excitation, the implementation followed the model proposed in [21]. Hence the excitatory feedback loop passed by a supplementary excitatory population, P' , analogous to P (P' ; $W = A_c, \tau_w = \tau_{ac}$ in Equation 8). However, unlike P , this population establishes exclusive synaptic projections from and to the subpopulation P . For

simplicity, the model representation (Figure 11) does not schematize P' . However, the Simulink implementation of this module depicted in

takes it into consideration.

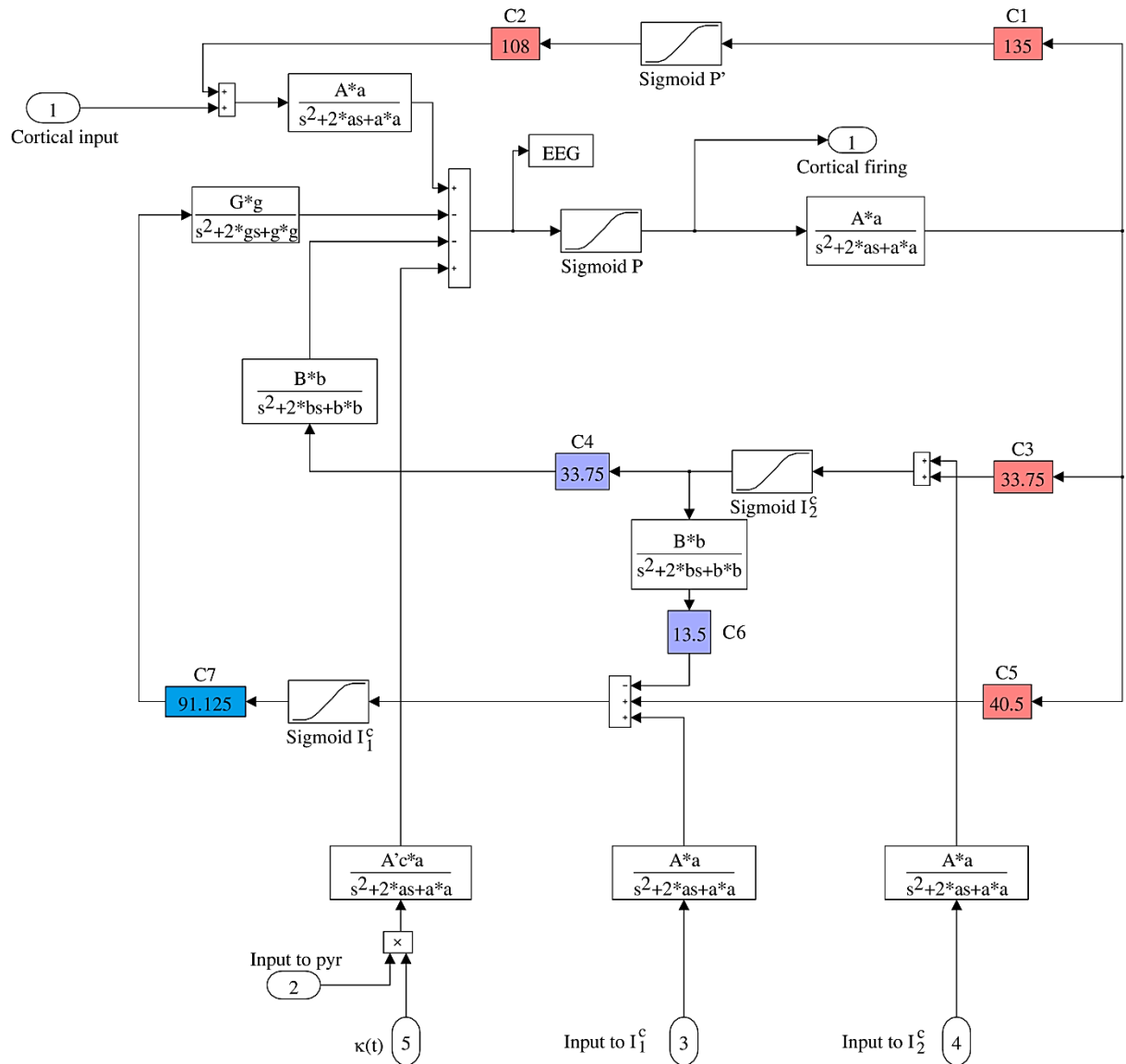


Figure 13. The Simulink implementation of the cortical module. Note the existence of a supplementary excitatory population P' used to model collateral excitation as in [21].

In comparison to other models, the hereby implemented cortical module exhibits extended features. First it integrates cortical inhibition unlike other thalamocortical models [169, 181] that limit this module to a single pyramidal population. Moreover, this cortical inhibition is associated with two types of inhibitory subpopulations instead of a single

inhibitory population as implemented previously [168]. Furthermore, supplementary mechanisms were implemented in the cortical module at the thalamocortical interface, namely feedforward inhibition and short term depression. These will be further detailed in section 2.2.

2.1.4 THE THALAMIC MODULE

The thalamic module was limited to a single excitatory neuronal population (TC ; $W = A_{Th}, \tau_w = \tau_{a_{Th}}$ in Equation 8) highly interconnected with the cortical module. It represents the set of excitatory thalamic cells that innervate the cerebral cortex, termed thalamocortical (TC) cells in neurophysiology. In the model, this subpopulation receives excitatory input from the cortical pyramidal subpopulation P , and sends back excitatory input onto the three cortical subpopulations P , I_1^c and I_2^c . Thalamic inhibition is supplied by the reticular subpopulations which receive excitatory input from the TC cells in return.

2.1.5 THE RETICULAR MODULE

The reticular module was used to simulate the neuronal dynamics of the reticular thalamic nucleus. As confirmed by neurophysiology [182], this nucleus exclusively mediates GABAergic currents. Hence, its implementation comprised two inhibitory neuronal populations I_1^{Rt} and I_2^{Rt} to account for fast (I_1^{Rt} ; $W = G_{Th}, \tau_w = \tau_{g_{Th}}$ in Equation 8) and slow (I_2^{Rt} ; $W = B_{Th}, \tau_w = \tau_{b_{Th}}$ in Equation 8) GABA mediated transmission projecting exclusively onto the thalamic module. As aforementioned, these two subpopulations receive excitatory input from both the thalamic ($W = A_{Th}, \tau_w = \tau_{a_{Th}}$ in Equation 8) and the cortical ($W = A_{Th}, \tau_w = \tau_{a_{Th}}$ in Equation 8) modules.

2.2 IMPLEMENTING PHYSIOLOGICALLY-RELEVANT MECHANISMS

Despite the fact that the model architecture was inspired from existing models, it presented a three-fold novelty: 1) the implementation of thalamocortical feed-forward inhibition, 2) short-term depression and 3) RC depolarizing stimulation effects.

2.2.1 FEED-FORWARD INHIBITION

Cortical interneurons comprise approximately 20% of the cortical neuronal population [183]. These GABAergic cells modulate cortical excitability by two well-known mechanisms: feedback and feedforward inhibition (see [184] for review). Figure 14 illustrates the inter-neuronal projections constituting the hardware of these inhibitory processes. pyramidal principal cells and interneurons exhibit mutual synaptic projections. Interneurons receive excitatory input from principal cells and, in return, they send inhibitory projections onto them. Thus, pyramidal cells excite interneurons and are inhibited by them. This is the mechanism of feedback inhibition.

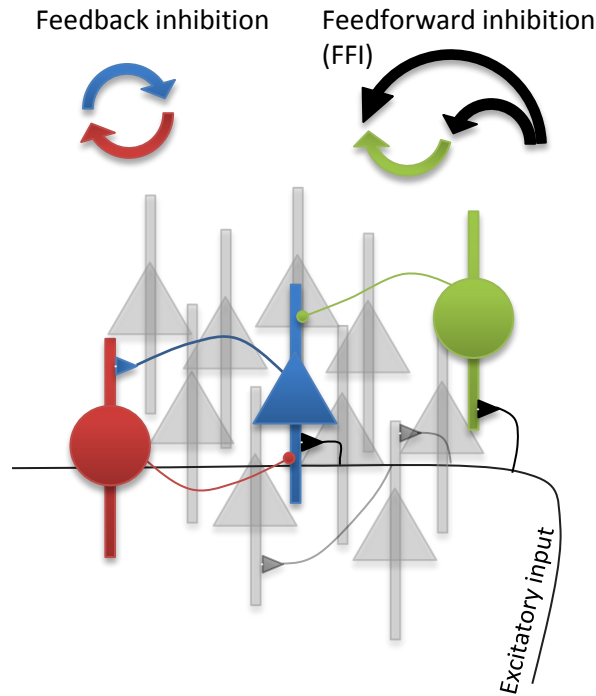


Figure 14. Cortical inhibitory circuits. Feedback inhibition is a local circuit mechanism generated by the mutual projections existing between the principal cells and local interneurons. Pyramidal principal cells send excitatory input onto the local interneurons. In return, interneurons send an inhibitory input onto principal cells. Every time a pyramidal cell excites an interneuron, it gets inhibited in return. Feedforward inhibition relies on long-range excitatory input formed on interneurons and principal cells at the same time. This incoming excitatory input induces in the pyramidal population EPSPs followed by IPSPs lagging by a di-synaptic delay. Depending on the temporal window separating two consecutive incoming action potentials, these EPSPs can be either summed or dampened to induce excitation or inhibition respectively.

On the thalamocortical level, cortical cells receive excitatory input from long-range axons originating from thalamic and other subcortical nuclei as well as from other long-range cortico-cortical axons. These excitatory inputs target cortical principal cells as well as interneurons thus forming feedforward inhibitory circuits (see Figure 14). These afferent thalamocortical fibers form stronger excitatory connections on interneurons than on principal cells. Therefore, the minimal level of thalamocortical input may generate inhibition [185, 186]. As individual EPSPs induced by action potentials coming from individual thalamocortical fibers are insufficient to provoke a cortical firing, the generation of a cortical response to thalamic input necessitates the temporal summation of incoming EPSPs. Consequently, it has been shown that the mechanisms of thalamic feedforward-inhibition depend on the temporal integration window within which these EPSPs can be summated [187]. Formally, at the cortical level, a single EPSP caused by an excitatory thalamic input arrives with a monosynaptic delay at the synaptic terminals formed at both principal cells and interneurons. Consequently, the targeted interneurons induce an IPSP at

the postsynaptic terminal of the principal cells lagging by a di-synaptic delay. In fact, given that the amplitude of the IPSP is way larger than that of the EPSP, the timing of the next EPSP determines summation or damping of EPSPs. Figure 15 describes the possible outcomes in a principal cell due to incoming action potentials (APs) in the presence and absence of FFI. Depending on the timing of the consecutive AP, two induced EPSPs may sum up (Figure 15-E) and thus overpass the AP generation threshold or not (Figure 15-D). Arriving during the prominent IPSP, the EPSP will be dampened and the principal cell cannot overpass the firing threshold. However, arriving just after the first EPSP, the temporal summation of consequent EPSPs is possible and the cell may reach the spike generation threshold [188, 189].

Feed-forward inhibition (FFI) is a thalamocortical regulatory mechanism that has a major role in shaping cortical response to thalamic input [190] in the context of sensory stimuli as well as during spontaneous thalamocortical oscillations [191]. Thus, it may be implicated in the deep brain stimulation mechanisms responsible for modulating epileptic thalamocortical dynamics. These were the arguments for implementing FFI in the model. Physiologically, it implies that the TC cells of the thalamic module extend excitatory projections not only to the pyramidal population (P) but also to the two inhibitory populations I_1^c and I_2^c of the cortical module.

Consequently, simulated thalamocortical impulses elicit synchronous EPSPs in the three cortical subpopulations (P , I_1^c and I_2^c). In response to their activation by this thalamocortical input, I_1^c and I_2^c evoke inhibitory postsynaptic potentials (IPSPs) at their postsynaptic terminals soon after. Eventually, this inhibitory input, arriving onto the P subpopulation with a di-synaptic delay, rapidly dampens the thalamically-evoked EPSPs shortly after their onset thus limiting the temporal integration window of cortical excitability.

Figure 16 shows the outcome, in the model, of a single or two consecutive EPSP(s). These simulations were performed in the model section containing the pyramidal (P) and the fast interneurons (I_1^c) loop. The EPSPs were simulated and input to both populations using a pulse generator and an excitatory H filter. The same EPSP amplitude was used on both subpopulations. We can affirm that the model accounts for the temporal integration window because the time of arrival the second EPSP determines whether consecutive EPSPs sum up (Figure 16-B and C). The major effect that changes in the model, in the presence/absence of FFI is the baseline level of excitability (not illustrated). Peculiarly, the general form and amplitude of the overshoot does not change. In conclusion, it can be deduced that this time dependence can be translated into a frequency-dependence of this mechanism. This was not formally studied in this thesis.

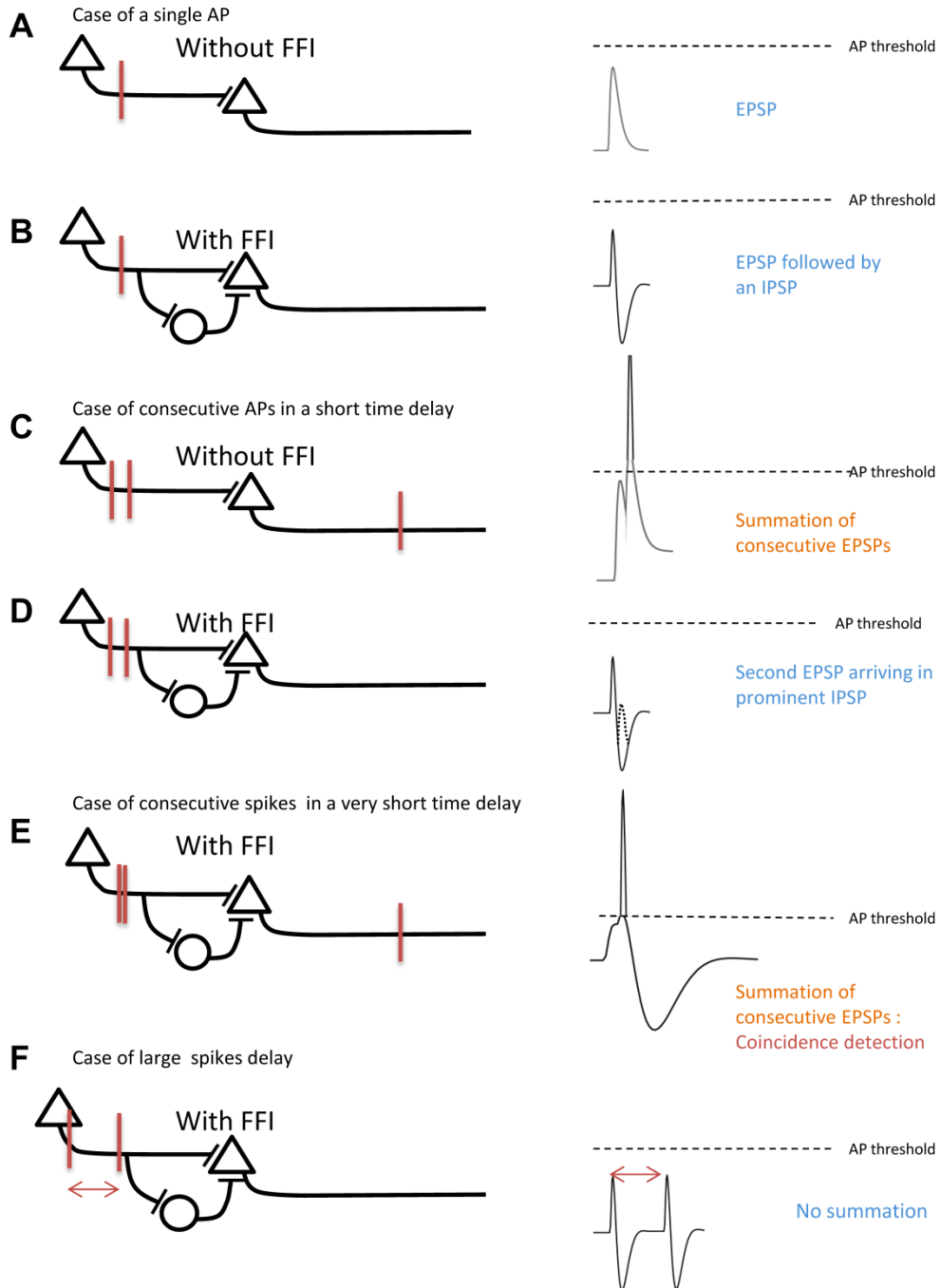


Figure 15. The temporal considerations of feedforward inhibition. **(A)** A single action potential (AP) arriving at a principal cell induces a consequent EPSP which is not sufficient to overpass the AP generation threshold. **(B)** In the presence of FFI, this EPSP will be followed by an IPSP. **(C)** If two APs arrive in a relatively short duration, they may be summed in the absence of FFI. **(D)** However, if the second EPSP is induced during a prominent IPSP, the EPSPs won't sum up, and the AP threshold won't be overpassed. **(E)** However, if the second AP arrives just after the first one, the consecutive EPSPs may also sum up and overpass the AP threshold. **(F)** APs arriving sufficiently far from each other induce independent responses of the same type of that induced in B).

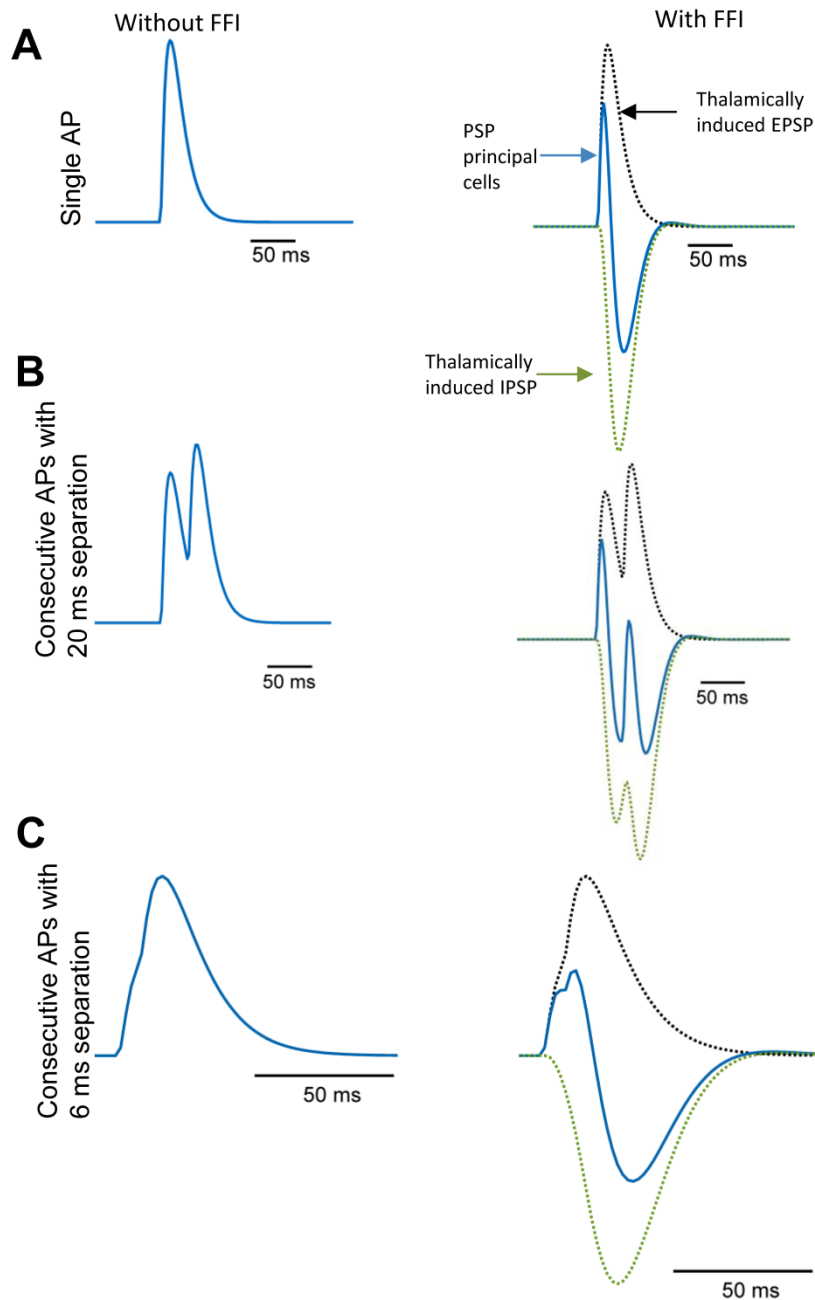


Figure 16. Feedforward inhibition in the model (sample simulations). These signal segments were simulated between the pyramidal (P) and the fast interneurons (I_1^c) subpopulations. Input EPSPs were also simulated. The blue trace refers to the sum of PSPs induced in the principal cell population, in green the induced IPSP and in black the induced EPSP. **(A)** The response to a single EPSP, **(B)** two consecutive EPSPs with 20 ms separation and **(C)** and 6 ms separation. Note that that in case B) the EPSP arrives in the prominent IPSP and is then dampened. In C) the two EPSPs sum up.

2.2.2 SHORT TERM DEPRESSION

Short term plasticity is a mechanism of transient activity-dependent modulation of synaptic efficacy. While short term facilitation indicates a transient increase in synaptic efficacy, short term depression denotes the progressive decrease of synaptic efficacy, and consequently the elicited postsynaptic response, during repetitive presynaptic activity (see [192] for review).

Generally speaking, short term plasticity is often related to cellular interactions lying at the presynaptic terminal. In particular, short term depression is usually related to vesicle depletion due to episodes of repetitive/intense firing as evidenced by experimental studies [193, 194]. Actually, computational implementations of short term depression (STD), based on the vesicle depletion hypothesis, have been frequently used on the microscopic level (see [192] for review). However, to the best of our knowledge, such implementation has not been proposed yet, at mesoscopic or macroscopic level.

As a matter of fact, experimental studies of thalamocortical adaptation indicate that transient episodes of short term depression are induced by thalamic low-frequency stimulation [150]. Speechley and colleagues [149] observed a 40% transient decrease in cortical EPSPs after brief trains of low-frequency stimulation (LFS) in the absence of GABAergic inhibition. Short-term depression is thought to be an essential mechanism of cortical adaptation to thalamic input [150]. Figure 17 (adapted from [150]) depicts experimentally acquired data showing the cortical adaptation to a periodic thalamic bursts of frequency 4 Hz. Note that the cortical responses are rapidly dampened at this stimulation frequency. The responses are barely detectable after 4 s of stimulation (Figure 17-B). Given the importance of this mechanism in thalamocortical dynamics, a macroscopic implementation of STD was attempted in this work based on the experimental results reported by Speechley in 2007. Specifically, a vesicle-depletion model of STD was exclusively implemented at the interface of thalamocortical synapses ($TC \rightarrow P$) since the effects were observed under the effect of a GABA receptor antagonist [149]. Equally, our implementation suggested that intense low-frequency thalamic firing provokes a transient short-term depression in the efficacy of these synapses.

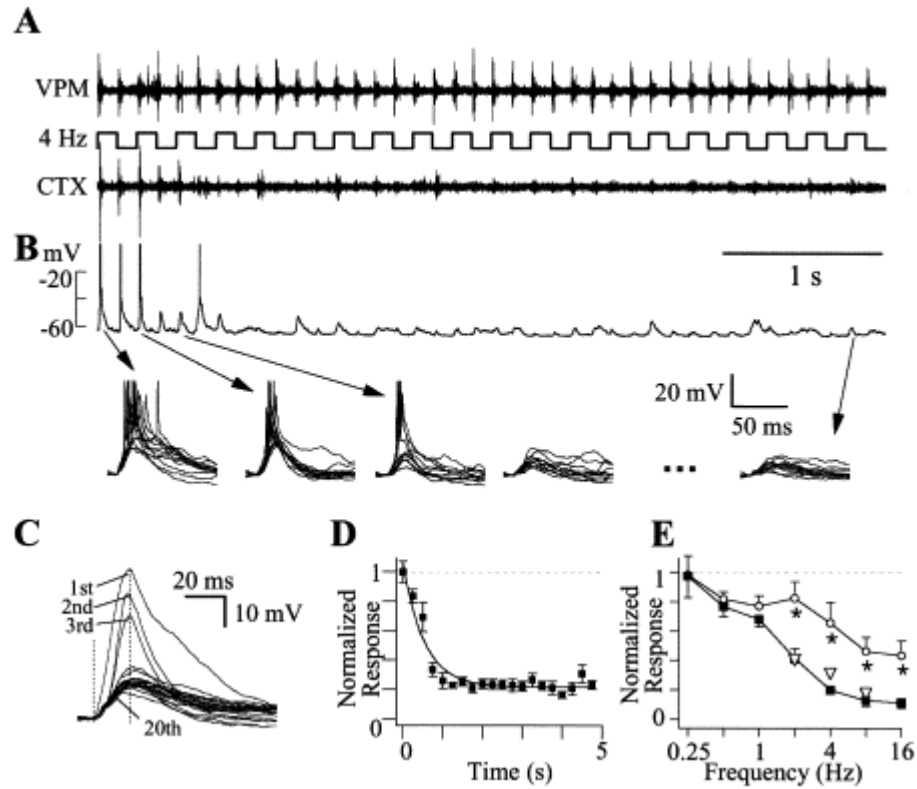


Figure 17. Rapid adaptation of cortical LFP to thalamic input at whisker stimulation of 4 Hz (adapted from [150]). **(A)** Simultaneous recordings from the barrel cortex (CTX) and the thalamus (VPM) during a 4 Hz stimulation of the primary whisker of the rat. Note the rhythmic thalamic activity in response to stimulation and the damping of cortical responses over time. **(B)** Intracellular recording of a cortical pyramidal neuron in the barrel cortex during the same stimulation paradigm. Lower panel, multiple repetitions of the response shown in B. Note the absence of action potentials in the last two illustrated group responses. **(C)** Average of responses shown in B. **(D)** Onset response amplitudes normalized to the first response. **(E)** Frequency dependence of rapid adaptation in barrel cortex. Significant adaptation is reported at 2, 8, and 4 Hz.

Technically, STD was modeled by means of a time-varying function $\kappa(t)$ that determines the normalized efficacy of ($TC \rightarrow P$) synapses. $\kappa(t)$ varies between 0.6 and 1 in function of the intensity/frequency of the mean density of thalamic action potentials $d_{AP}(t)$. The value of $\kappa(t)$ is multiplied by the amplitude of thalamocortical EPSPs at ($TC \rightarrow P$) synapses (determined by $W = A_c'$ in Equation 8) and thus dynamically modulates their efficacy. Formally, the dynamic evaluation of $\kappa(t)$ consists of two steps, filtering then thresholding. First, $d_{AP}(t)$ is low-pass filtered (cutoff frequency $f_c = 10\text{Hz}$) to limit STD effects to low-frequency thalamic input. Then the filtered signal $d_{AP}^f(t)$ is compared to a mean firing threshold ϑ in order to assure that STD can only be produced following a high release of cortical glutamate. Every supra-threshold firing entrains an exponential decrease ($\tau = 8\text{s}$) of $\kappa(t)$ from $\kappa(t_0)$ to 0.6. The duration of this decrease was extended to 0.5s after each thalamic supra-threshold firing. In the absence of this excessive firing, $\kappa(t)$ exponentially

returns to 1 ($\tau = 8$ s) and maintains its value until the next arrival of a supra-threshold firing. $\kappa(t)$ is formally described by the following dynamics:

$$\kappa(t) = \begin{cases} 0.4(d_{AP}^f(t) > \vartheta) \cdot \frac{(u(t) - u(t-0.5))}{2} e^{-t/\tau} + 0.6 \\ 0.4(d_{AP}^f(t) < \vartheta) \cdot (1 - e^{-t/\tau}) + 0.6 \end{cases} \quad (12)$$

where $u(t)$ is the Heaviside function.

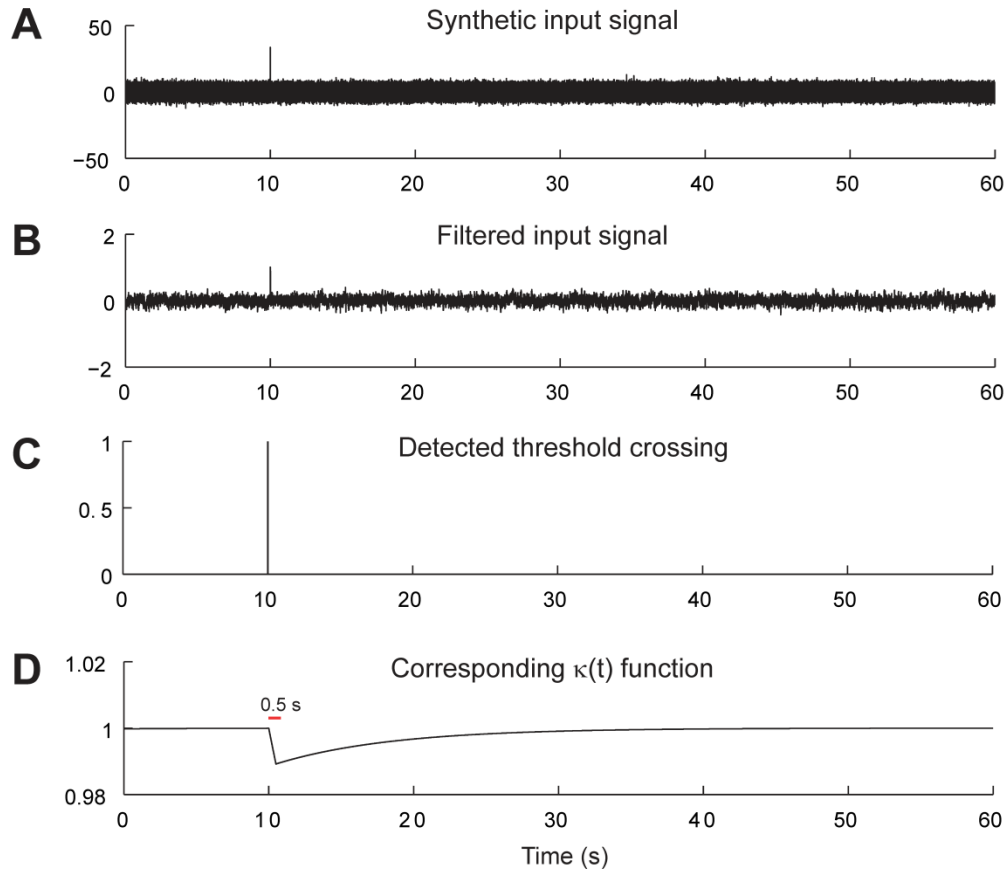


Figure 18. Dynamical response of the $\kappa(t)$ function to one pulse of duration (0.5 ms). **(A)** A synthetic white noise input function was applied to the input of the STD Simulink® block. A pulse was added at $t = 10$ s. **(B)** The first step consists in low-pass filtering this signal. **(C)** Then any threshold crossing is detected. **(D)** This detected event incurs an exponential decrease in the value of $\kappa(t)$ that lasts 0.5 s only. An exponential increase follows the end of this descent. Note that a single pulse cannot cause significant depression.

Figure 18 depicts the dynamical values of $\kappa(t)$ function in response to a synthetic white noise signal including a single pulse occurrence. As illustrated, the input signal is first filtered, then whenever a pulse is detected (Figure 18-C), $\kappa(t)$ undergoes an exponential descent that lasts 0.5 s at the end of which it returns exponentially to its initial value, 1

(Figure 18-D). Noteworthy, a single pulse does not incur significant depression in the value of $\kappa(t)$.

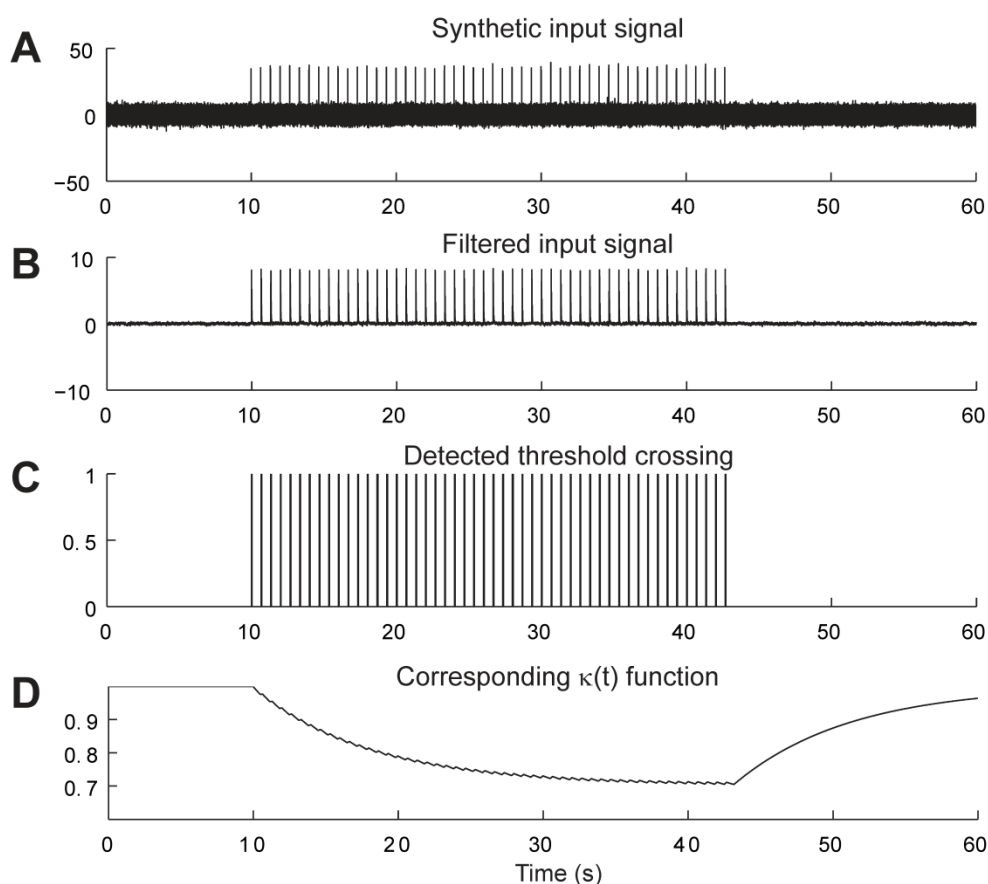


Figure 19. Dynamical response of the $\kappa(t)$ function to a series of pulses arriving at a 1.5 Hz frequency. **(A)** A synthetic white noise input signal was applied to the STD block of the model. A train of pulses at 1.5 Hz was added to this signal. **(B)** First, the signal is filtered. **(C)** Then, any threshold crossing is detected. **(D)** Finally, at each detected crossing, the $\kappa(t)$ function undergoes an exponential decrease from its actual value that lasts only 0.5 s. In this case, the arriving pulses incur a cumulative depression of the value of $\kappa(t)$, which attains the value of 0.7 in 30 s. At the end of this pulse detection, the $\kappa(t)$ function increases exponentially to its initial value.

Figure 19 shows the dynamical values of the $\kappa(t)$ function for a pulse train of duration 30 s and frequency 1.5 Hz. It depicts the cumulative depression incurred due to close pulse repetitions. At the end of the pulse train, the function $\kappa(t)$ restores its initial rest value of 1.

2.2.3 STIMULATION INPUTS

As evidenced by experimental studies, the transmembrane potential of stimulated neurons varies linearly with the intensity of stimulation current (or electric field) which can be either depolarizing or hyperpolarizing depending on current polarity [36, 195]. In effect,

an injected stimulation electric current induces an electric field, which consequently imposes a potential gradient ΔV in the affected space (neural tissue). On the cellular level, at a given point in space, ΔV corresponds to the deviation of the membrane potential V_m from its resting value V_r ; $\Delta V = V_m - V_r$. This linear relationship between the induced electric field \vec{E} and the potential gradient ΔV has been illustrated by the " $\lambda \cdot \vec{E}$ " model [196], where λ is the membrane space constant. This model, well-grounded in the biophysics of compartment models, estimates the membrane potential variation in function of the electric field induced by the electrical stimulation.

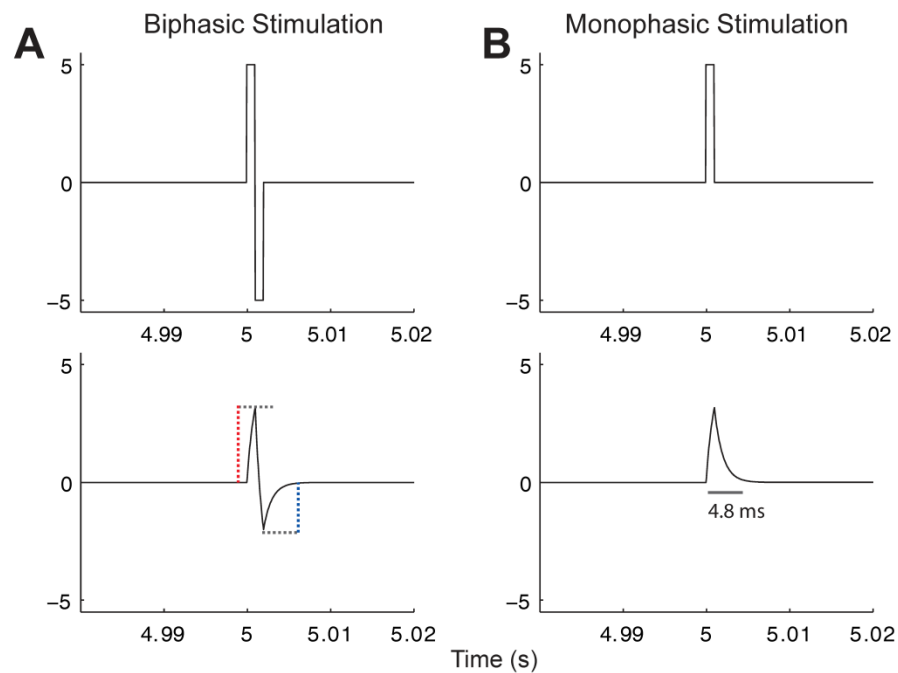


Figure 20. Biphasic versus monophasic pulse stimulation in the model. **(A)** A biphasic pulse stimulation and its corresponding form at the output of the RC low-pass filter block accounting for the electrode-electrolyte interface. Note that the amplitude of the positive part is greater than the negative part. We assume that the effect of a larger positive displacement incurs more effects (related to depolarization) on the model's dynamics that a negative less important displacement. **(B)** A monophasic pulse stimulation was adopted in the model. The 1 ms pulse duration is extended to 4.8 ms by the RC low-pass filter block.

The model presented in this work takes into account this axiom and represents it in a less straightforward approach as space is not represented, conversely to detailed compartment models. Stimulation inputs were integrated in the model at the level of both the thalamic and reticular module. They directly affected the subpopulation mean membrane potential at the level of the sigmoid (output) function. Moreover, to take into consideration a potentially different impact of stimulation on the three concerned subpopulations, the stimulation signal was weighted by a characteristic coefficient at the input of each subpopulation, respectively S_{TC} , S_{Irt1} and S_{Irt2} at the input of TC , I_1^{Rt} and I_2^{Rt} . The stimulation

signal, destined to represent the corresponding $\lambda \cdot \vec{E}$ variation, was modeled as a monophasic pulse train of adjustable frequency, intensity and pulse width. The pulse width was set to 1ms as in clinical DBS. Noteworthy, a monophasic rather than a biphasic pulse train was adopted in the model. Figure 20 illustrates the difference between these two possibilities. We assume that the first pulse polarity (positive) in a biphasic pulse contributes more to the observed response in the model than a negative smaller amplitude negative pulse. This owes to the implementation of an RC block at the interface of the stimulator and the subpopulations accounting for the electrode-electrolyte interface. Thus, the stimulation signal was low-pass filtered ($f_c > 160\text{Hz}$) by this block. The pulse effect was thereby extended to 4.8 ms by this step. This accounts for the average time of repolarization in stimulated sub-populations of cells.

Chapter 4: Electrophysiological Observations and Signal Analysis for Model Optimization

The first step in studying the theoretical effects of stimulation on epileptic neural dynamics is realistically simulating these dynamics in the model. Only then, hypotheses on stimulation effects and subsequent optimized protocols can be made. To proceed, we used a real clinical dataset to tune the model parameters. First, a signal processing algorithm was implemented to quantitatively analyze stimulation effects. Then, the quantified information, expressed as feature vectors, was used to define an optimization procedure aimed at tuning the model parameters in order to guarantee a realistic output.

1 THE CLINICAL OBSERVATION

The clinical dataset used in this study was limited to a unique patient who underwent thalamic DBS during the presurgical intracerebral EEG exploration (iEEG performed under stereotaxic conditions) at the Epilepsy Surgery Unit, Rennes University Hospital [197]. This particular patient was chosen for two main reasons:

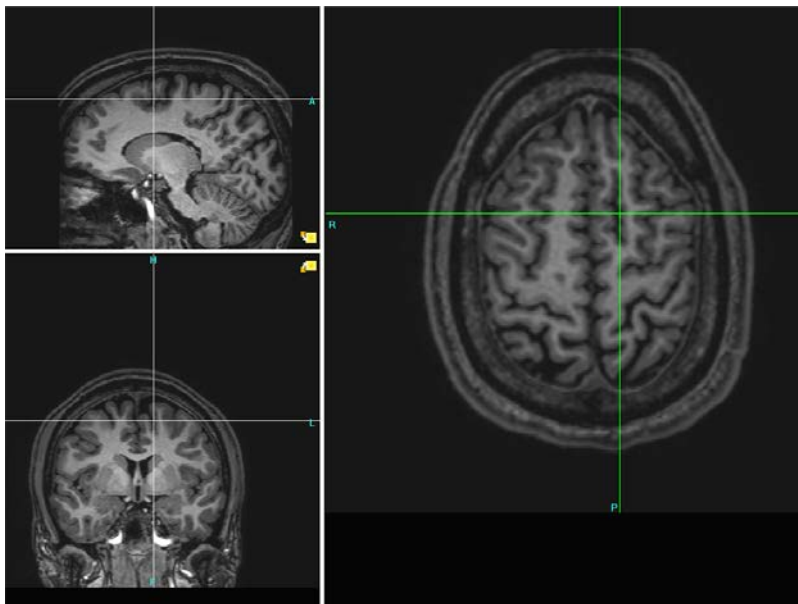


Figure 21. MRI of the Patient showing the location of the focal cortical dysplasia in the premotor cortex of the patient.

- (1) The pronounced frequency-dependent response to stimulation observed during the preoperative diagnostic intracerebral EEG (iEEG) exploration at low-frequency (LFS;

2 Hz), intermediate-frequency (IFS; 50 Hz) and high-frequency (HFS; 70, 100 and 150 Hz) stimulation.

- (2) The existence of the epileptogenic zone in a limited area of the premotor cortex (Figure 21).

This patient suffered from partial drug-resistant epilepsy since the age of two. MRI scans as well as EEG scalp recordings showed the presence of a probable developmental neural malformation in the premotor cortex of the patient. This particular malformation known as focal cortical dysplasia (FCD) is well-known for its epileptogenic electrophysiological signature including (a) continuous rhythmic or semi-rhythmic spikes, (b) paroxysmal bursts of high frequency spikes and (c) recurrent electrographic seizures [114]. Moreover, the continuous rhythmic spiking associated with dysplasia suggests that an “intradysplastic pacemaker” [114] operates in a self-sustained, hyperexcitable and unstoppable fashion and is sufficient to provoke an epileptic syndrome.

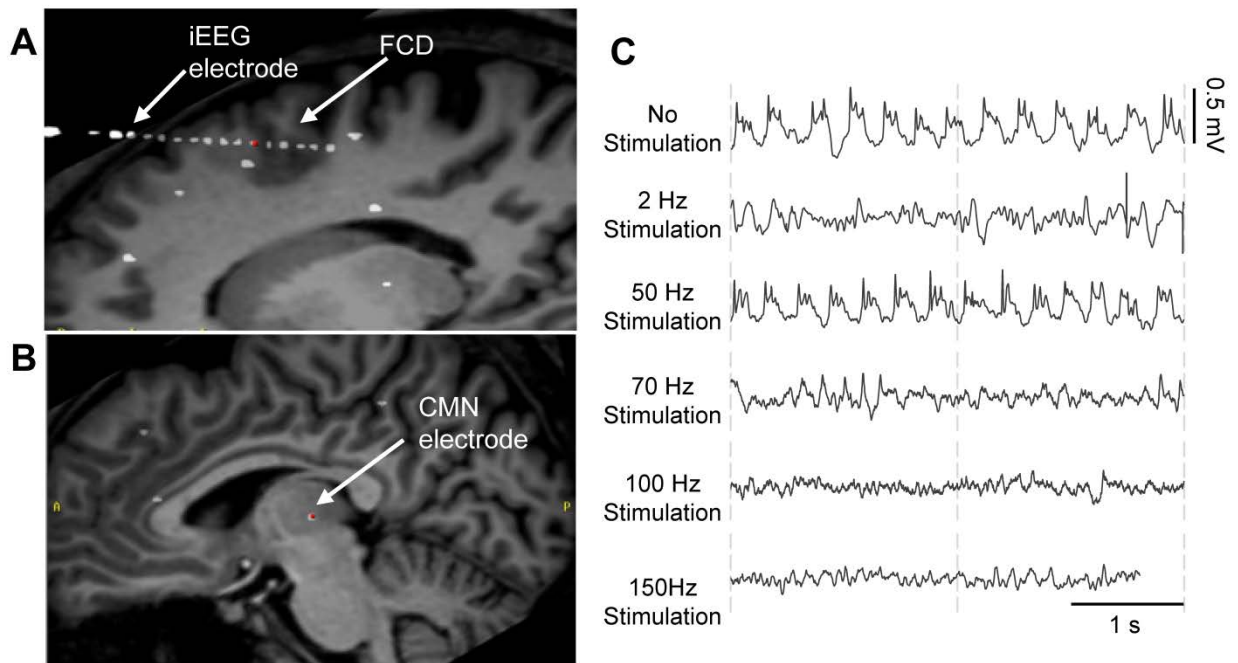


Figure 22. Frequency-dependent stimulation effects: real data. **(A)** Position of the electrode in the FCD. **(B)** Position of the electrode in the CMN. **(C)** Real iEEG segments representing the recorded LFP of the FCD in the absence of stimulation, as well as during the stimulation of CMN at different frequencies.

Based on various clinical studies [198-203] reporting the modulation of epileptic cortical activity by stimulation of the centromedian thalamic nucleus (CMN), it was decided by neurosurgeons to implant a depth electrode in this nucleus (Figure 22-B), as potentially beneficial for the patient who gave his informed consent.

During the presurgical exploration, the stimulation of the CMN induced frequency-dependent modulation of the pathological activity of the FCD (see [197] for more clinical details). Interestingly, low-frequency stimulation (LFS; 2 Hz, 4 mA) as well as high-frequency stimulation (HFS; 70, 100, and 150 Hz, 0.8 mA) desynchronized the pathological rhythmic activity of the FCD while intermediate-frequency (IFS; 50 Hz, 0.8 mA) didn't visibly affect it (Figure 22-C). In fact, assessing the variability of stimulation effects and understanding its intricate causes in function of the frequency of stimulation can move a step further the frequency-dependence of the epileptic system response to the stimulation control input.

Noteworthy, this observation is quite rare since (1) DBS electrodes are rarely implanted in the thalamus for ethical reasons and (2) FCDs vary in type and position in the brain. Their developmental aspect makes it quite impossible to find two epileptic patients presenting exactly the same dysplastic morphology and semiology. And apparently, this highly influences stimulation outcome and leads to a significant inter-patient variability. Moreover, it is uncommon to implant depth-EEG electrodes in this thalamic nucleus. As this is the first reported observation of the effects of CMN stimulation on focal paroxysmal activity in a human patient using depth-EEG electrodes, recruiting more patients with the same clinical semiology was not fruitful. Consequently, this dataset was not only used to quantitatively describe actual stimulation effects but also to automatically optimize the proposed model's output in order to computationally explore their underlying mechanisms.

2 SIGNAL PROCESSING

The use of signal processing techniques was necessary (1) to quantify the clinically-observed effects of stimulation in the real iEEG signals, and (2) to define a suitable feature vector-based cost function for model parameter optimization.

2.1 GENERAL ALGORITHM

The choice of the signal analysis method was driven by the non-stationary aspect of iEEG signals. Consequently, a time-frequency analysis method was privileged. Figure 23-A illustrates the feature extraction methodology that was adopted. iEEG signals recorded in the FCD (which correspond to local field potentials and thus denoted by $LFP_{S_{FCD}}$) in the absence of stimulation and under different stimulation conditions were decomposed using an orthogonal matching pursuit algorithm (Matching Pursuit Toolkit – MPTK – [160]). Consequently, a suitable multi-scalar dictionary of Gabor, Fourier and Dirac atoms was first defined to account for real iEEG signal components.

At its output, the MPTK algorithm provides the table of parameters of the detected time-frequency atoms (~200 atoms for every 3s of iEEG); atom type, central frequency (f), phase (φ), scale (ζ), amplitude (C), and position (p). Identified atoms were then reconstructed using the extracted parameter table and the corresponding analytical expression of the atom type. The general analytical form is given by:

$$C \cdot e^{-\pi((t-p)/\zeta)^2} \cdot \cos(2\pi ft + \varphi)$$

This general expression was used to reconstruct the detected Gabor atoms. Fourier atoms were reconstructed using a similar expression where the Gaussian window is replaced by a rectangular one:

$$C \cdot (u(t - p) - u(t - (p + \zeta))) \cdot \cos(2\pi ft + \varphi)$$

$u(t)$ is the Heaviside function. As for the Dirac it was simply reconstructed by $C \cdot \delta(t - p)$, where $\delta(t)$ is a Dirac at position $p = 0$, and of amplitude $C = 1$.

Finally, the reconstructed atoms were associated to a given frequency band depending on their central frequency. These frequency bands corresponded to the classical EEG bands as defined in healthy adults (δ_1 [0 – 1.9Hz], δ_2 [1.9 – 3.4 Hz], θ_1 [3.4 – 5.4 Hz], θ_2 [5.4 – 7.4 Hz], α_1 [7.4 – 10 Hz], α_2 [10 – 12 Hz], β_1 [12 – 18 Hz], β_2 [18 – 24 Hz], γ [24 – 128 Hz]). Finally, a 9D feature vector \vec{V}_F (Figure 23-A in green) was defined from the normalized energy distribution in these frequency bands, itself computed as the sum of averaged (over time) atom energies relative to the total signal energy. \vec{V}_F can be expressed as follows:

$$\vec{V}_F(i) = \frac{1}{N(i)} \sum_{j=1}^{N(i)} \|s_i(j)\|^2 / \sum_{i=1}^9 \vec{V}_F(i)$$

where N is the number of samples of the decomposed signal, s_i is the reconstructed signal of the i^{th} band (1 to 9 corresponding respectively to δ_1 , δ_2 , θ_1 , θ_2 , α_1 , α_2 , β_1 , β_2 to γ). Noteworthy, the energy of the detected Dirac atoms was automatically attributed to the 9th band for simplicity.

2.2 MATCHING PURSUIT

Matching Pursuit (MP) is part of a class of parsimonious signal analysis algorithms known as atomic decompositions. These algorithms suppose that any signal \mathbf{y} can be expressed as a linear sum of elementary signal components \mathbf{g}_i , called atoms, chosen from a predefined dictionary D :

$$y = \sum_{i=1}^M \omega_i g_i \quad \text{where } g_i \in D \text{ and } \|g_i\| = 1$$

Usually, the predefined dictionary is overcomplete and extremely redundant in this type of applications.

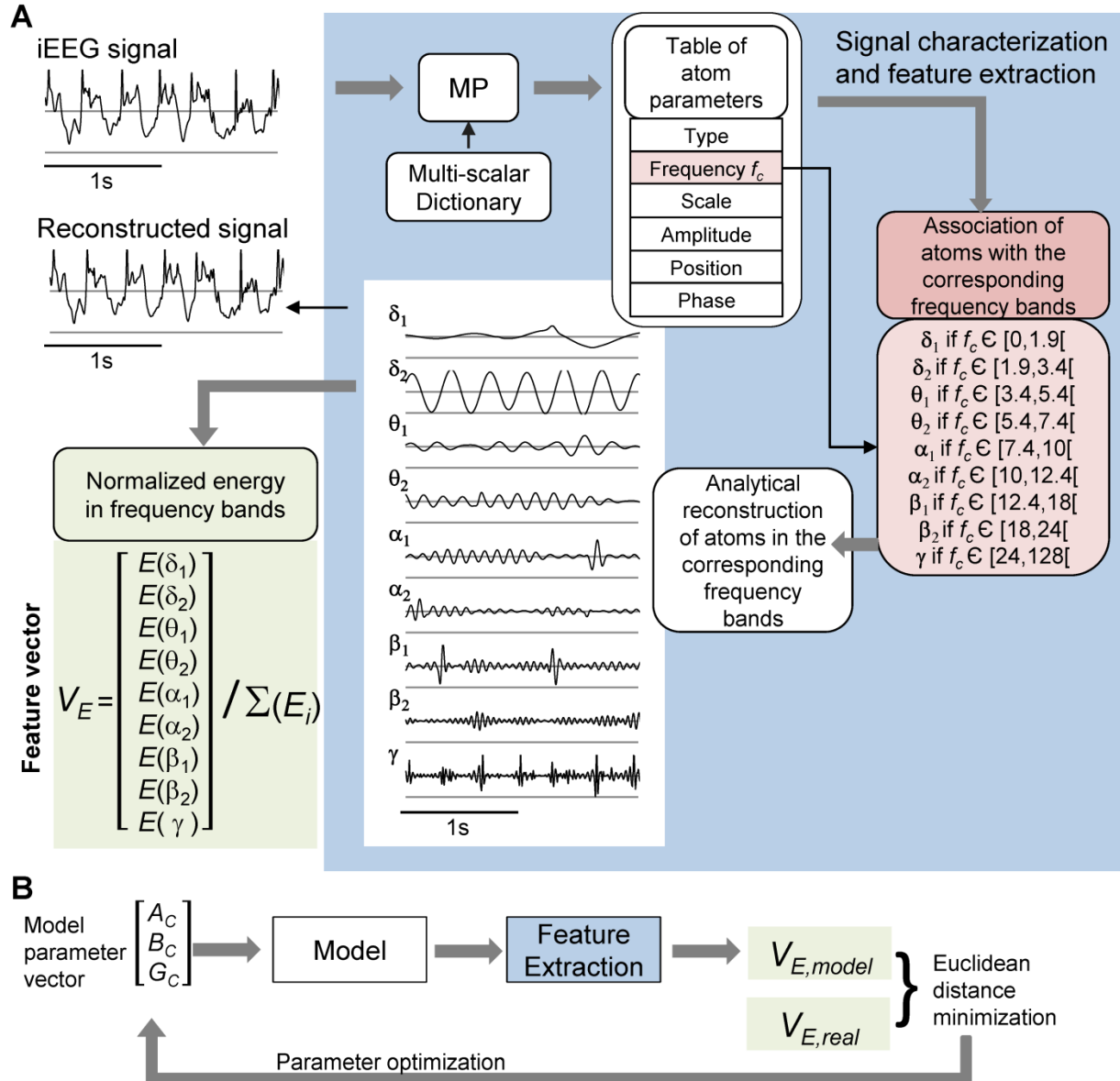


Figure 23. Feature extraction for parameter optimization. **(A)** The feature extraction algorithm. **(B)** The parameter optimization algorithm

First introduced in 1993 by Mallat and Zhifeng [204], matching pursuit (MP) was proposed for pattern extraction in noisy signal applications. It was later used to analyze seizure activity [205] in 1998. Further in 2001, the same Polish group introduced the notion of

stochastic time-frequency dictionaries for matching pursuit [206]. The authors argued that MP must be more and more used to analyze and characterize EEG signals. They introduced the notion of stochastic time-frequency dictionaries for MP to guarantee unbiased MP decompositions. Concurrently, MP was used for encoding audio signals [160]. Later on, its algorithm was adapted to decrease computation time. The fastest existing MP algorithm nowadays is the MPTK of [160].

Basic Algorithm. The basic algorithm of MP operates in the following manner:

- (1) Dictionary definition $D = (g_\gamma(t))_{\gamma \in \Gamma}$ defined in an Hilbert space H , such that $\|g_\gamma\| = 1$, and $\gamma_i = (s_i, u_i, \xi_i)$ is the atom parameter vector (scale s_i , temporal translation u_i , and modulation frequency ξ_i)
- (2) Initialization $i = 0, y_i = y_0 = y$
- (3) Evaluation of the inner product between the signal $y_i(t)$ and each dictionary atom $(g_\gamma(t))_{\gamma \in \Gamma}$, $|\langle y_i, g_\gamma \rangle|$ for every $\gamma \in \Gamma$.
- (4) Choose the dictionary atom that maximizes the inner product.
- (5) Calculate the residual R , which can be expressed as $R = y_i - \langle y_i, g_{\gamma_0} \rangle g_{\gamma_0}$. (R is orthogonal to g_{γ_0}).
- (6) Replace y_{i+1} by R ($y_{i+1} = R$).
- (7) Stop when i) the number of maximal iterations or ii) the desired the energy ratio between the original signal and the current residual is attained. Else repeat steps (3) to (7).

In the initial algorithm the dictionary $D = (g_\gamma(t))_{\gamma \in \Gamma}$ is a countable subset of atoms generated from a single mother wavelet $g(t)$ as follows

$$g_\gamma(t) = \frac{1}{\sqrt{s}} g\left(\frac{t-u}{s}\right) e^{-i\xi t}$$

Current algorithms such as MPTK allow the use of different types of mother wavelets to generate D .

2.3 THE MODEL OPTIMIZATION ALGORITHM FOR SIMULATING EPILEPTIC FCD ACTIVITY

The feature extraction algorithm described earlier in section 2.1 was used to characterize 20 real iEEG signal segments (of duration 5s each) representing the epileptic dynamics of the FCD in the absence of stimulation. The average feature vector, denoted $\vec{V}_{F,real}$, was used for model tuning.

Besides the time constants associated with excitatory/inhibitory postsynaptic potentials which can be physiologically constrained, the model has more than 37 unknown parameters. Moreover, the time needed for the simulation and the characterization of 20s signal is of the order of 2s. Given the computational complexity of an automatic global optimization procedure in these circumstances, some parameters had to be fixed a priori (fixed parameters) while some other parameters were left to vary (free parameters). The free parameters were limited to the average EPSP/IPSP amplitude parameters of the cortical module (A_c, B_c, G_c). This choice was motivated by the real dataset recorded from the thalamocortical system and in which the malformation is limited to the premotor cortex (chapter 4 section 1). Consequently, the equivalent parameters of the thalamic and reticular modules ($A_{Th}, B_{Th}, G_{Th}, A_{Rt}$) were tuned as close as possible to “standard values” usually used in neuronal population models. Noteworthy, the connectivity parameters and the PSP amplitude parameters (A_c, B_c, G_c) are dependent (they are multiplied by each other in the ODEs governing the model’s dynamics). That is, optimizing (A_c, B_c, G_c) can also be interpreted as optimizing the connectivity parameters.

Once the reference feature vector $\vec{V}_{F,real}$ and the free model parameters are defined, the optimization algorithm is executed as described in Figure 23B. For each triplet (A_c, B_c, G_c), the corresponding feature vector $\vec{V}_{F,model}$ was calculated then compared to $\vec{V}_{F,real}$. The optimization procedure aimed at finding the triplet ($\hat{A}_c, \hat{B}_c, \hat{G}_c$) that minimizes a cost function simply corresponding to the Euclidean distance the real and the simulated feature vectors $d(\vec{V}_{F,real}, \vec{V}_{F,model})$ when parameters A_c, B_c and G_c span a predefined range of values according to an exhaustive Brute-Force procedure.

2.4 MODEL TUNING FOR SIMULATING STIMULATION EFFECTS

As mentioned earlier (Chapter 3, section 2.2.3), the modeled stimulation signal is weighted by a characteristic coefficient at the input of each subpopulation, respectively S_{TC} , S_{Irt1} and S_{Irt2} at the input of TC , I_1^{Rt} and I_2^{Rt} . Therefore, based on the hypothesis that stimulation effects depend on the current’s impact on each of the subcortical subpopulations, these three parameters were manually tuned in the range of [-5, 5] each in order to reproduce the desired effects. In fact, this manual procedure was sufficient to reproduce stimulation effects observed in one patient. However, extending the study to a larger group of patients would have made imperative an automated parameter fitting procedure based on the spectral characteristics of real EEG signals.

Noteworthy, impact limits [-5, 5] were chosen based on the fact that the extreme values -5 and 5 are sufficient to reproduce maximum hyperpolarization/depolarization of the

considered subpopulation respectively. However, the same signal processing method described earlier was then used to compare modeled to real signals.

Chapter 5: Results of Part 1

1 QUANTIFICATION OF STIMULATION EFFECTS IN REAL SIGNALS

The application of the aforementioned signal processing algorithm (Chapter 4, section 2) to real iEEG signals confirmed the clinical visual inspection of stimulation effects. Indeed, the energy distribution among the iEEG frequency bands changed significantly depending on stimulation frequency.

1.1 ENERGY DISTRIBUTION

1.1.1 SPONTANEOUS INTERICTAL ACTIVITY ($LFP_{S_{FCD}}$)

The recorded spontaneous activity of the FCD ($LFP_{S_{FCD}}$) presents an abnormal energy distribution as compared to that of a normal iEEG signal. The latter was chosen from the iEEG signals of the same patient recorded on a different electrode far from the FCD, and showing no interictal activity. As Figure 24 shows, the energy distribution of the pathological signal presents a flagrant abnormal peak ($> 60\%$) in the band contribution ($\delta_2 + \theta_1$) corresponding to the frequency range [1.5 – 5.4 Hz]. The γ band contribution (frequency > 24 Hz) seems to double in the pathological context when compared to the normal context.

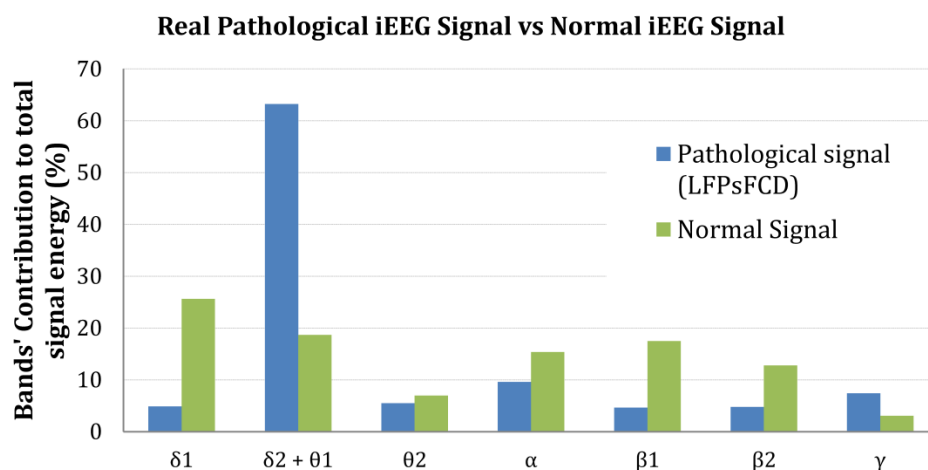


Figure 24. Energy Distribution (%) of Pathological ($LFP_{S_{FCD}}$) Signal vs. Normal Signal. Note the enormous energy peak at $\delta_2 + \theta_2$ band.

Still, the three consecutive peaks of energy of the interictal activity (LFPs_{FCD}) at $\delta_2 + \theta_1$ (1.9 – 5.4 Hz), α (7.4 – 10 Hz), and γ (> 24 Hz) correspond to the three major components of our signal and mark its epileptic aspect. In fact, reconstructing uniquely these three bands well approximates the initial signal (Figure 25). Finally, this characterization was a useful tool for measuring the effectiveness of stimulation effects.

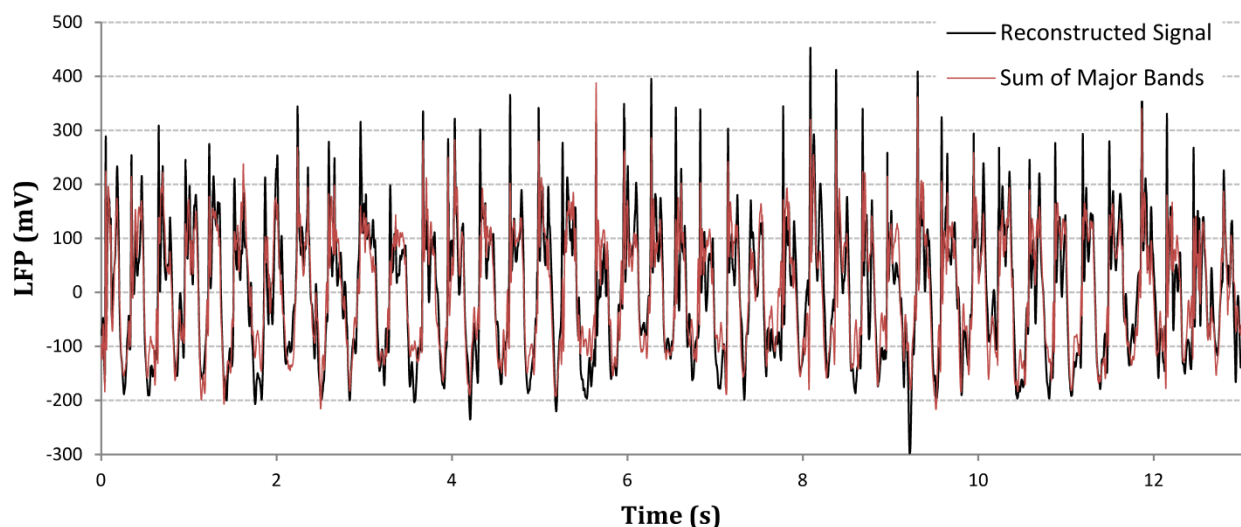


Figure 25. Reconstructed Signal vs. Sum of Major Bands ($\delta_2 + \theta_1$, α , and γ). The sum of the major bands is a sufficient representation of the initial signal.

1.1.2 STIMULATION EFFECTS

As the interictal dynamics of the FCD seem to repeat in a stationary manner with a period of almost 1/3 second, it seems sufficient to consider real activity segments as small as one second for the proposed signal processing algorithm. Given the fact that the patient was stimulated only once at each specified stimulation frequency (2, 50, 70, 100 and 150 Hz), considering real iEEG segments as short as 1 s for the quantitative study was practical.

In practice, 20 real signal segments each of 5 seconds duration representing the interictal FCD dynamics were used to describe the “*No Stimulation*” condition. As for the 2Hz-Stimulation condition, the patient underwent only one thalamic stimulation trial of 60 seconds at a regular frequency of 2Hz. Only 36 seconds of the iEEG signal recorded in the FCD during stimulation were considered for this type of stimulation. However, stimulation segments of 4 seconds each were defined for further analysis using the signal processing algorithm defined earlier. As for the other four reported stimulation frequencies (50, 70, 100, and 150 Hz), the patient underwent only one exploitable stimulation (during interictal activity) of 5s/stimulation frequency. For this, three stimulation cortical iEEG segments of 1.75s each (0.1s overlap) were defined for each stimulation type. Finally, these stimulation

segments were processed, and statistically compared to the “No Stimulation” condition using a t-test.

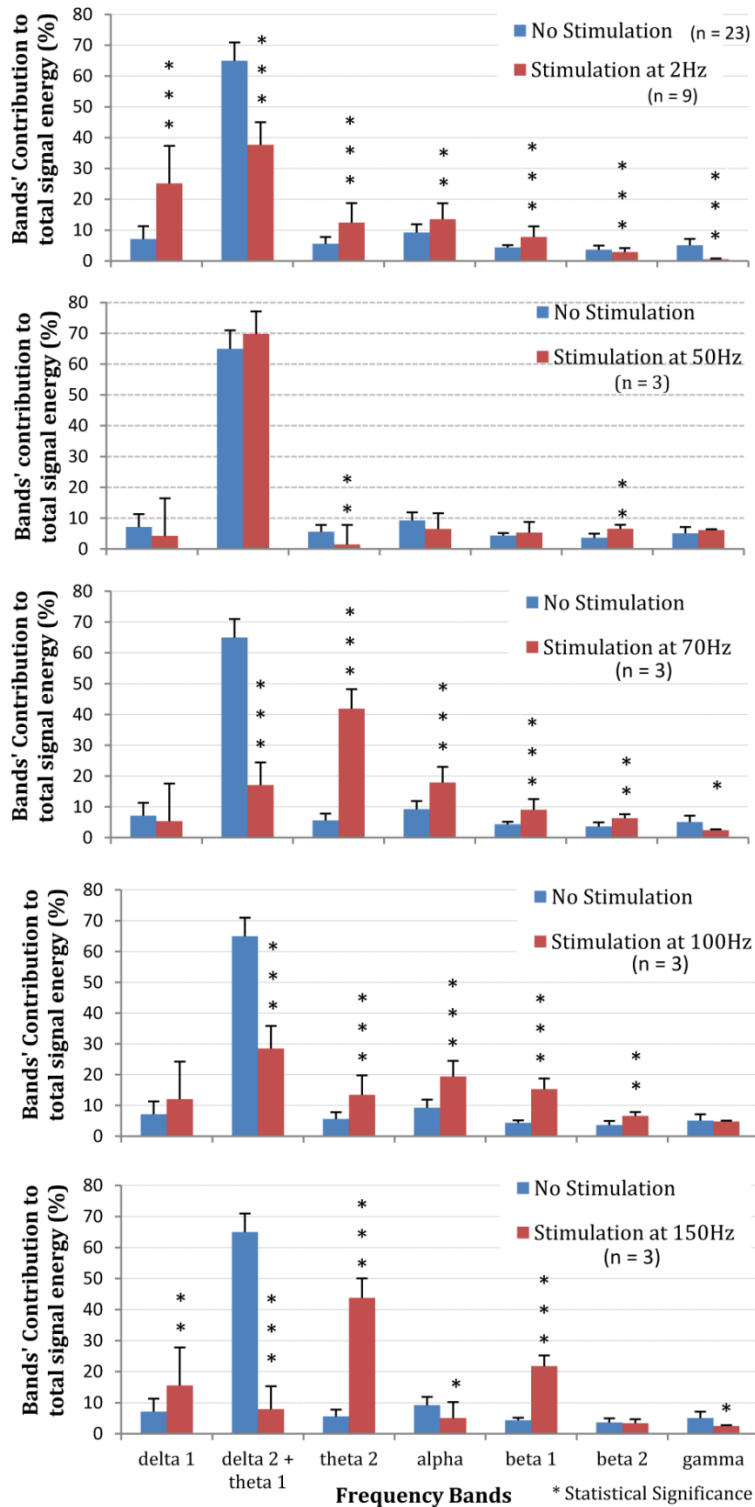


Figure 26. Frequency-dependent modulation of the signal’s energy distribution during stimulation. Each graph represents the distribution of given stimulation condition as compared to the *no stimulation* condition. Note the absence of effect for the 50 Hz stimulation condition.

As demonstrated in Figure 26, stimulation elicits a significant frequency-dependent modulation of the signal energy content. Accordingly, the 2, 70, 100, and 150 Hz stimulation conditions significantly diminish the abnormal “ $\delta_2 + \theta_1$ ” peak present in the spontaneous activity, while the 50 Hz stimulation condition does not affect the contribution of the major frequency bands $\delta_2 + \theta_1$, α , and γ . However, the signal energy redistribution varies as a function of the stimulation frequency. Notably, the decrease in the “ $\delta_2 + \theta_1$ ” peak seems the least important for the 2 Hz stimulation condition. Another “peculiar” peak arises at θ_2 in the case of the 70 Hz and the 150 Hz stimulation conditions. Moreover, the energy distribution of the iEEG signal segments during the 100 Hz stimulation conditions seem to mostly match those of the normal signal presented earlier in Figure 24. Noteworthy, as reported in the clinical report, it is the effects of the 100 Hz stimulation that last the longest (16s) after the end of stimulation compared to 0.5s for the 150 Hz stimulation trial and 2s for the 70 Hz stimulation trial.

1.2 THREE STIMULATION GROUPS

The limited number of experimental observations per stimulation necessitated the use of another form of data analysis and presentation to better mark the stimulation-driven bifurcations in the patient’s thalamocortical system. Consequently, the 9D feature vectors were reduced to 3D feature vectors which then classified by k-means into three groups.

1.2.1 THE 3D SPACE

In order to graphically visualize stimulation effects, a 3D space containing one of the three major LFPs_{FCD} characteristic frequency bands at each axis was defined as follows $(x, y, z) = (E_{\delta_2 + \theta_1}, E_{\theta_2 + \alpha + \beta_1}, E_{\beta_2 + \gamma})$. Consequently, a 3D feature vector (\vec{V}_{F_3D}) was constructed for each signal segment from the initially calculated 9D vector (\vec{V}_F).

$$\vec{V}_{F_3D} = [\vec{V}_F(2) + \vec{V}_F(3), \vec{V}_F(4) + \vec{V}_F(5) + \vec{V}_F(6) + \vec{V}_F(7), \vec{V}_F(8) + \vec{V}_F(9)]$$

The resulting 3D feature vectors were then represented as points in the 3D space as depicted in Figure 27-A. The visual inspection of this representation sounds sufficient to affirm the considerable change caused by the different stimulation frequencies, except for the 50 Hz frequency. Actually, the distribution of points in the 3D frequency space is not random but clustered, indicating that the frequency content of LFPs_{FCD} segments is modulated in function of the stimulation frequency. In addition, some clusters are very close. This is typically the case for i) the no stimulation (yellow) and the 50 Hz stimulation conditions (red) on the one hand, and ii) the 70 Hz (violet) and 150 Hz (cyan) stimulation conditions on the other hand. In this representation, the resemblance between the features

of the spontaneous interictal activity $LFP_{S_{FCD}}$ and that produced at 50 Hz stimulation is made sufficiently evident.

1.2.2 FEATURE VECTOR CLASSIFICATION AND STIMULATION CLUSTERS

To go beyond the visual clustering of the plotted points, the 3D feature vectors were classified into three groups using the k-means algorithm with a Mahalanobis distance. The classification was initialized using Forgy's random initialization method (random choice of initial means) and repeated 1000 times. The clusters that minimize the global intra-cluster inertia were considered as the optimal clusters. These are represented in Figure 27-B.

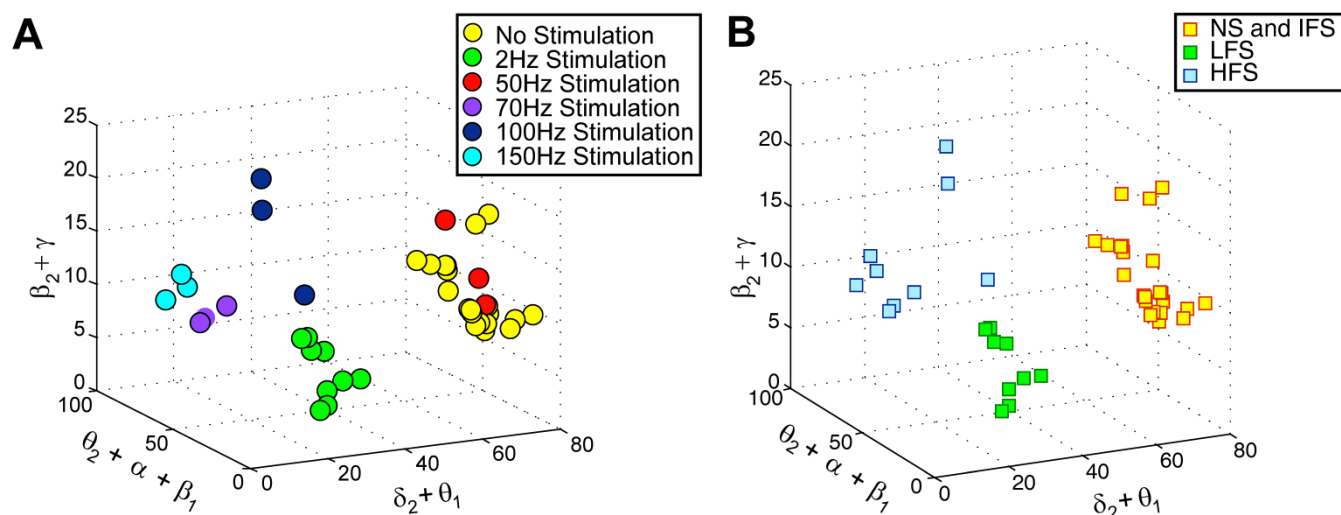


Figure 27. 3D Space and Clustering. **(A)** The projection of 3D feature vectors into the 3D frequency space. **(B)** The k-mean clusters corresponding to stimulation effects. In yellow the co-clustering of the no stimulation (NS) condition and the intermediate-frequency stimulation (IFS; 50 Hz) condition, in green the low-frequency stimulation (LFS; 2 Hz) cluster, and in blue the high-frequency stimulation (HFS; > 70 Hz) cluster.

The 3D feature vectors of real iEEG signal segments were thus automatically classified into three clusters. The first cluster contains those corresponding to iEEG segments recorded during low-frequency stimulation (LFS). The second cluster groups all feature vectors corresponding to segments recorded during high frequency stimulations (HFS, > 70 Hz). And finally, in the third cluster, segments recorded under the no stimulation and the intermediate stimulation frequency (IFS, 50 Hz) conditions are merged together, suggesting that this stimulation frequency does not reduce the “epileptiform aspect” of the activity reflected in the LFP.

In conclusion, this classification procedure allowed the definition of three groups of stimulation effects that will be computationally studied in order to (1) better understand the frequency-dependent mechanisms of action of thalamic stimulation and thus (2)

optimize the stimulation frequency such that epileptic activity is reduced as much as possible.

2 REPRODUCTION OF REAL EPILEPTIC LFPs DURING AND IN THE ABSENCE OF STIMULATION

The model optimization algorithm described earlier in section 2.3 was used to tune the model's output in the absence of stimulation. Then, model parameters for reproducing stimulation effects were tuned manually.

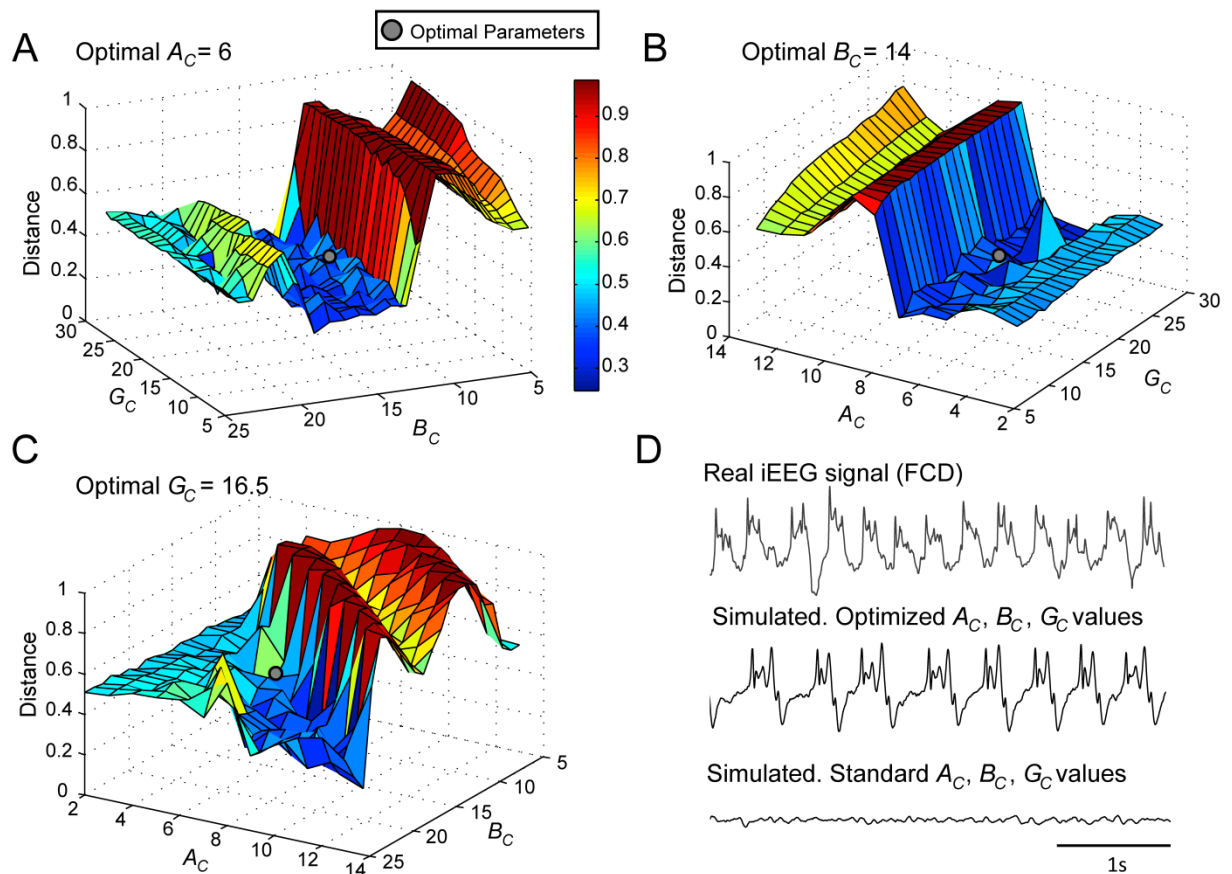


Figure 28. Normalized Euclidean distance between $V_{F,real}$ and $V_{F,model}$. Best fit (gray disk) between simulated and real $LFP_{S_{FCD}}$ was obtained for **(A)** $A_C = 6$, **(B)** $B_C = 14$, and **(C)** $G_C = 16.5$. **(D)** For these modified values of excitation and inhibition, the simulated signal exhibits similar characteristics as the iEEG signal recorded in the FCD. For standard values of excitation and inhibition ($A_C = 3, B_C = 50, G_C = 22$), the model generates background EEG activity.

2.1 SIMULATING EPILEPTIC FCD ACTIVITY

As a first step, we verified the ability of the model to generate signals that resemble those recorded from the FCD in the considered patient ($LFP_{S_{FCD}}$). The optimization procedure, led

us to identify a minimal distance and thus an optimal parameter vector $(\hat{A}_c, \hat{B}_c, \hat{G}_c) = (6, 14, 16.5)$ for which simulated signals under the no stimulation condition have similar features as compared with those of real signals (Figure 28).

2.2 SIMULATING STIMULATION EFFECTS

As mentioned earlier (Chapter 4 section 2.4), stimulation effects were reproduced by manually tuning three model parameters S_{TC} , S_{Irt1} and S_{Irt2} respectively representing the impact of stimulation of the three subcortical subpopulations TC , I_1^{Rt} and I_2^{Rt} . Once determined, these three parameters were considered constant for all stimulation frequencies. Then, the resulting simulated signals (Figure 29) were processed using the same MPTK-based algorithm as that used for processing actual $LFP_{S_{FCD}}$. Similarly, the corresponding 3D feature vectors were later calculated and projected in the same frequency 3D space (Figure 30).

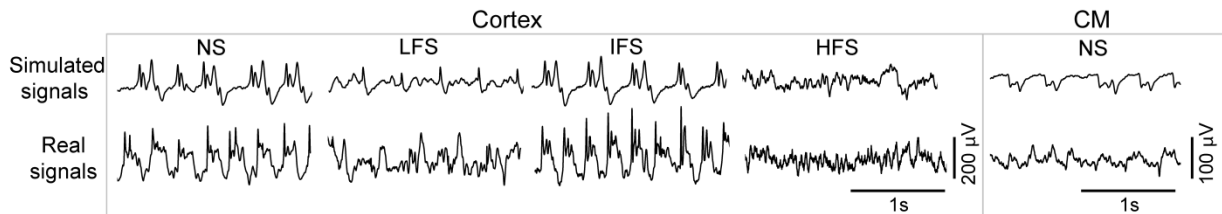


Figure 29. Real and simulated signals for the different stimulation conditions

As shown in Figure 29, although the simulated $LFP_{S_{FCD}}$ do not exactly match actual signals, they present similar features. Indeed, under the no stimulation (NS) and the IFS condition the model generates rhythmic slow oscillations (δ_2) with superimposed faster activity (α and γ), as observed in real data. For LFS and HFS conditions, strong modulation of this activity was also obtained in the model. At LFS, in the model, the slow wave activity was strongly reduced but spike events occurred in the signals at the instant times of stimulation, mimicking, to some extent, comparable events also present in actual $LFP_{S_{FCD}}$. Finally, at HFS, slow oscillations (δ_2) were abolished in the model which generates quasi-normal background activity. This simulated activity was also comparable to real activity observed for HFS stimulation but disclosed visibly less γ activity.

Figure 30 shows the projection of feature vectors of simulated $LFP_{S_{FCD}}$ in the 3D frequency space (“M” triangles). As depicted, simulated signals obtained for LFS, IFS and HFS were close to corresponding clusters obtained from real signals for the exact same computation of feature vectors. Indeed, qualitatively similar bifurcations – to those observed in the real dataset – were produced in the model when similar stimulation conditions were imposed. These bifurcations are quantified in Figure 30.

3 MODEL ANALYSIS

In addition to the manual aspect of the parameter tuning for reproducing the desired stimulation effects, a system analysis study was undertaken in order to:

- (1) Study the stability of the system's output in the neighborhood of its optimal parameters.
- (2) Identify the necessary model conditions for reproducing the simulated stimulation effects.
- (3) Identify the corresponding mechanisms of the simulated stimulation effects in an attempt to optimize stimulation frequency.

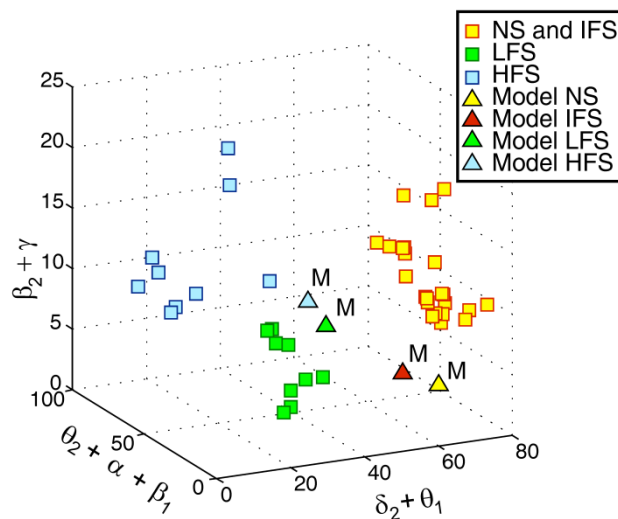


Figure 30. The feature vectors of simulated signals (triangles) projected in 3D frequency space with the feature vectors of real iEEG signals (Squares).

3.1 INDICATIVE STUDY OF PARAMETER SENSITIVITY

The indicative study of parameter sensitivity was done to complement the qualitative aspect of the optimization of stimulation parameters S_{TC} , S_{Irt1} and S_{Irt2} . These three parameters supposed fixed, this study aimed at determining the impact of random changes affecting the parameter vector $\theta = (A_c, B_c, G_c, A_{Th}, B_{Th}, G_{Th}, A_{Rt})$ on the model's output (simulated cortical LFPs). Effectively, this extended parameter vector included the triplet (A_c, B_c, G_c) of EPSP/IPSP amplitude parameters in the cortical module as well as their analogous parameters in the thalamic (A_{Th}, B_{Th}, G_{Th}) and reticular (A_{Rt}) modules. Thus, parameter vector θ determines the excitability properties in the three model modules.

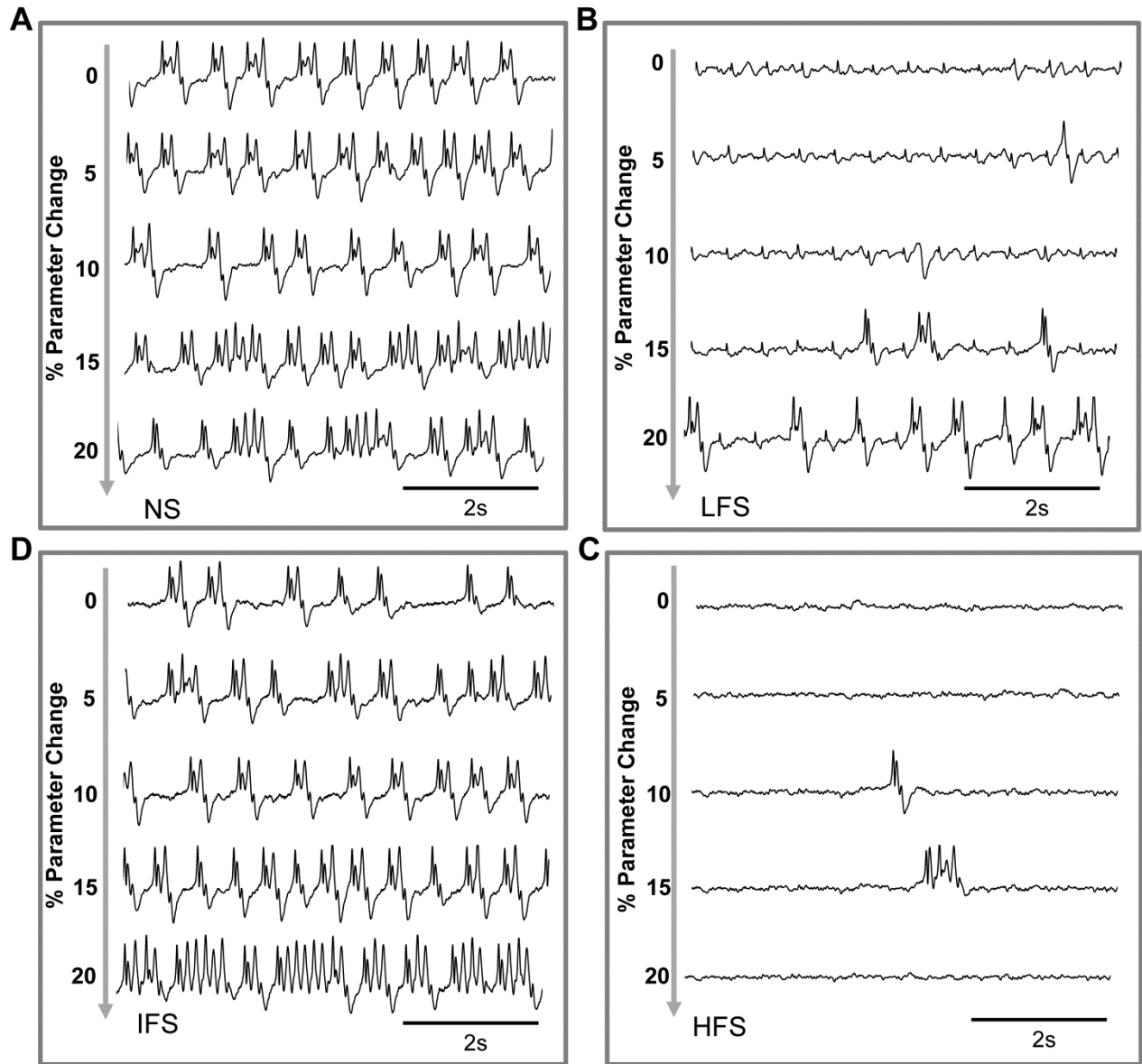


Figure 31. Indicative Study of Parameter Sensibility. Model output sensitivity to variations of excitatory and inhibitory key parameters. Realizations of parameter vector $\theta = (A_c, B_c, G_c, A_{Th}, B_{Th}, G_{Th}, A_{Rt})$ were randomly (uniform law) generated around the optimal parameter vector $\hat{\theta}$ over a variation domain defined by $(1 \pm \mu) \cdot \hat{\theta}$. For $\mu \leq 0.2$ ($\pm 20\%$ variation), stimulation effects are preserved in the model for A) no stimulation, B) low-frequency stimulation, C) intermediate-frequency stimulation, and D) high-frequency stimulation.

Consequently, in order to study the model output robustness, each parameter of vector θ was considered as an independent random variable $\theta(n)$ following the uniform law on the interval $[(1 - \mu) \cdot \hat{\theta}(n), (1 + \mu) \cdot \hat{\theta}(n)]$ where $\mu \in \{0.05, 0.1, 0.15, 0.2\}$ and n is the vector's index. The mean of this uniform law, $\hat{\theta}(n)$, represents the optimal value of its

sense that waveforms are conserved) when parameters stay in the range $[\hat{\theta} \pm \mu \cdot \hat{\theta}]$ with $0 \leq \mu \leq 0.2$ ($\pm 20\%$ variation).

Moreover, the simulated signals for the preceding study ($\mu = 5\%$) were processed and projected in the same 3D space as that of the clusters defined earlier on real signals. As depicted in Figure 32, the 3D feature vectors of the randomly simulated signals remain close enough to the clusters of real quantified stimulation effects. Apparently, minimal variability is evident for the HFS condition.

3.2 MODEL PHASE PORTRAITS

The modulation of the model output features by the stimulation input is linked to the bifurcations of model dynamics induced by this input. Particularly, the modulation of thalamic dynamics is at the heart of the observed effects. Unfortunately, thalamic LFPs are not available in the clinical dataset due to stimulation artefacts. But, the thalamic *TC* firing as well as LFPs are accessible in the model (which is a big advantage) as stimulation-induced artifacts can be easily withdrawn from simulated signals. Moreover, the states of both the thalamic and the cortical modules resume the thalamocortical system's instantaneous state during stimulation. Consequently, the phase space of two model variables a thalamic (*TC* firing) and a cortical (cortical LFP – population *P*) was explored in the four different conditions (NS, LFS (2 Hz), IFS (50 Hz), and HFS (100 Hz)). The phase portraits (*TC* cell firing vs. cortical LFP) illustrated in Figure 33 confirmed the visual inspection of signals simulated at the two modules. For the no stimulation (NS) and for the intermediate frequency stimulation (IFS) conditions, phase portraits were found to be quite similar. They indicated the presence of mixed slow/fast oscillations in both signals. For the low frequency stimulation (LFS) condition, oscillations in the simulated LFP in the FCD were reduced. They came along with short-duration, abrupt and rhythmic augmentations of the *TC* firing corresponding to stimulation pulses. Finally, for the high frequency stimulation (HFS) condition, oscillations in both types of activity stayed confined to small amplitude values.

In conclusion, the phase portraits of two key variables in the model, thalamic firing and cortical local field potential (LFP), prove that stimulation evokes model bifurcations quantitatively similar to those observed in the patient's iEEG signals. Indeed, the cycles in the phase portrait obtained for the NS condition changed into a fixed point under the HFS condition. Along the same line, the LFS phase portrait seems nearer to a fixed point functioning mode when taking the cortical LFP uniquely into consideration. Finally for IFS, the resulting phase portrait denotes an even more oscillatory activity than that of the NS condition.

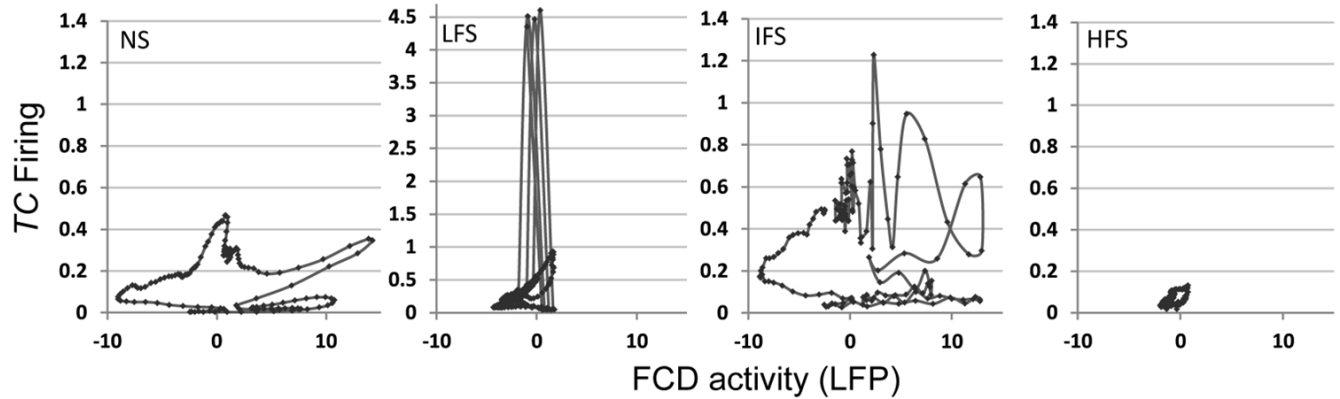


Figure 33. Phase portraits (FCD activity vs. CM firing) for the four stimulation conditions: NS, LFS (2 Hz), IFS (50 Hz), and HFS (100 Hz). During the NS condition, the system oscillates on a limit cycle. Cortical activity is diminished during LFS, whereas thalamic firing increases transiently following stimulation pulses. Cortical activity barely changes during IFS whereas thalamic firing increases. HFS switches the model from a limit cycle functioning mode to a more normal fixed point mode.

3.3 QUANTIFYING MODEL BIFURCATIONS: THE HIGH TO LOW FIRING RATIO (HTOLR)

At this point of the study, the effects of thalamic stimulation on FCD dynamics are well-defined and characterized both in simulated and real signals. Yet, the ultimate question of frequency optimization for clinical use is still immature. For this, we had to quantitatively determine the model output over a large frequency range (0.5 to 150 Hz) rather than at fixed frequency values (2, 50 and 100 Hz). Consequently, a simpler measure of model the output had to be defined. And the final choice was output intermittency.

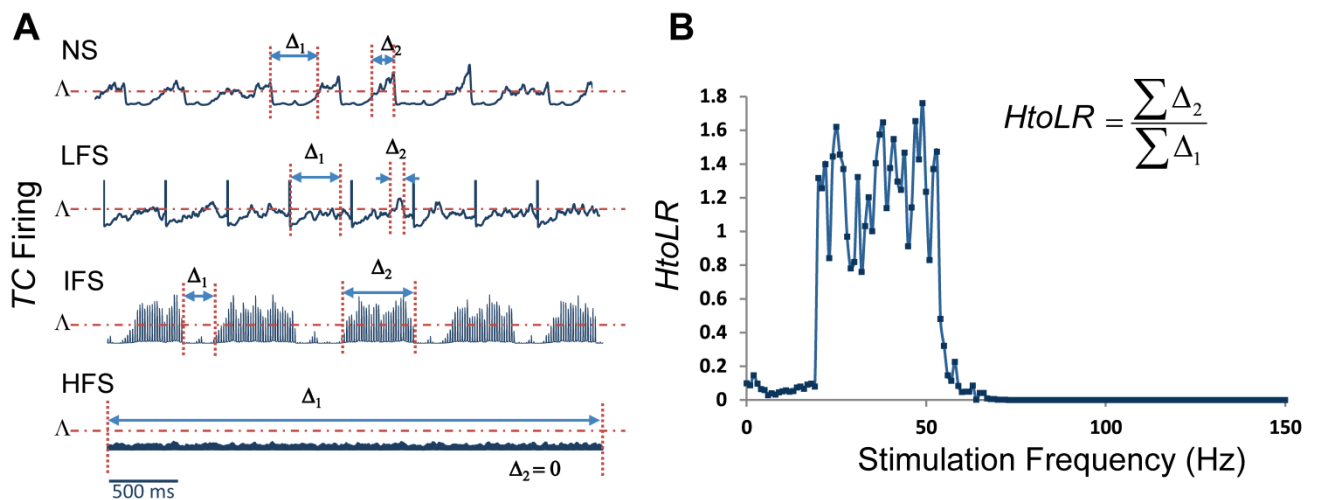


Figure 34. Model intermittency. **(A)** The firing rate of TC cells depends on the frequency of the stimulation input (Δ_1 : time interval for which this firing is lower than a threshold λ , Δ_2 : time interval for which this firing is higher than λ). **(B)** Evolution of the “High to Low Firing Ratio” (*HtoLR*) as a function of stimulation frequency.

In dynamical systems, intermittency is the irregular alteration of phases of apparently periodic and chaotic dynamics. An intermittent phenomenon can be observed in the studied thalamocortical system especially during the NS condition. Measuring this phenomenon provides a simple representation of the model's state (more interestingly the thalamic output) as a function of the frequency of the stimulation input.

First of all, a qualitative inspection of the thalamic firing rate during the four different stimulation conditions was imperative. The corresponding simulated signals, demonstrated in Figure 34-A, show that the thalamic output dramatically differs depending on the stimulation frequency. Under the no stimulation condition (NS), the firing rate continuously oscillates around a certain value (referred to as Λ , Figure 34-A). At LFS, the firing rate was found to be lower, except at the stimulation times where it abruptly and transiently increased. At IFS, a balance was observed between time intervals for which the *TC* firing is above and below Λ . Finally, at HFS, the output of *TC* cells was found to be very low, i.e. systematically under the threshold Λ . Based on these observations, two variables were calculated from the simulated thalamic firing. These correspond to two time intervals, Δ_1 and Δ_2 , for which the *TC* cells firing rate is either below/above the threshold Λ respectively (for illustration see Figure 34-A). These quantities were calculated as a total ($\sum \Delta_1$ and $\sum \Delta_2$) per duration of simulation, the latter being equal for all stimulation conditions. Subsequently, the ratio of these two quantities was calculated for every stimulation frequency in the range 0.5 – 150 Hz. This range was denoted the “*High-to-Low Firing Ratio*” or *HtoLR*.

$$HtoLR = \frac{\sum \Delta_2}{\sum \Delta_1}$$

The *HtoLR* provides an indication on the amount of time the *TC* cells spend at a high firing rate (up state) relatively to the amount of time they spend at a low firing rate (down state). The higher this ratio the higher the proportion of time the system spends at the up state and vice versa.

Figure 34-B provides the evolution of the *HtoLR* when the frequency of the stimulation input changes progressively from 0 to 150 Hz in the model. As depicted, these simulations indicated that three stimulation frequency ranges have different effects on the firing of *TC* cells. First, from 0 to 20 Hz, the down state is predominant. Then, an abrupt jump was observed around 22 Hz indicating that beyond this value, the firing rate dramatically increased. Interestingly, from 55 Hz to 65 Hz, a progressive decrease of the *HtoLR* was observed. Then, after 70 Hz, the ratio is equal to zero indicating that *TC* cells did not fire anymore.

3.4 THE NECESSARY ELEMENTS

A recurrent question asked to any model is the following: what are the elements that are absolutely necessary for the reproduction of the observed effects? In other words, is the proposed model a minimal model that only integrates the essence of observed phenomena? To address this difficult issue, we followed an empirical approach according to which implemented elements/mechanisms were sequentially turned off one at a time to observe the resulting model output.

First of all, removing FFI from the model by removing the thalamic projection onto the two cortical interneurons resulted in the failure to reproduce the LFS effects. Similarly, removing the STD mechanism by establishing a standard h function at the interface of TC and P populations resulted in the failure to reproduce LFS effects. This confirmed that both FFI and STD mechanisms are necessary in the model to suppress the epileptic activity of the FCD when LFS is being utilized.

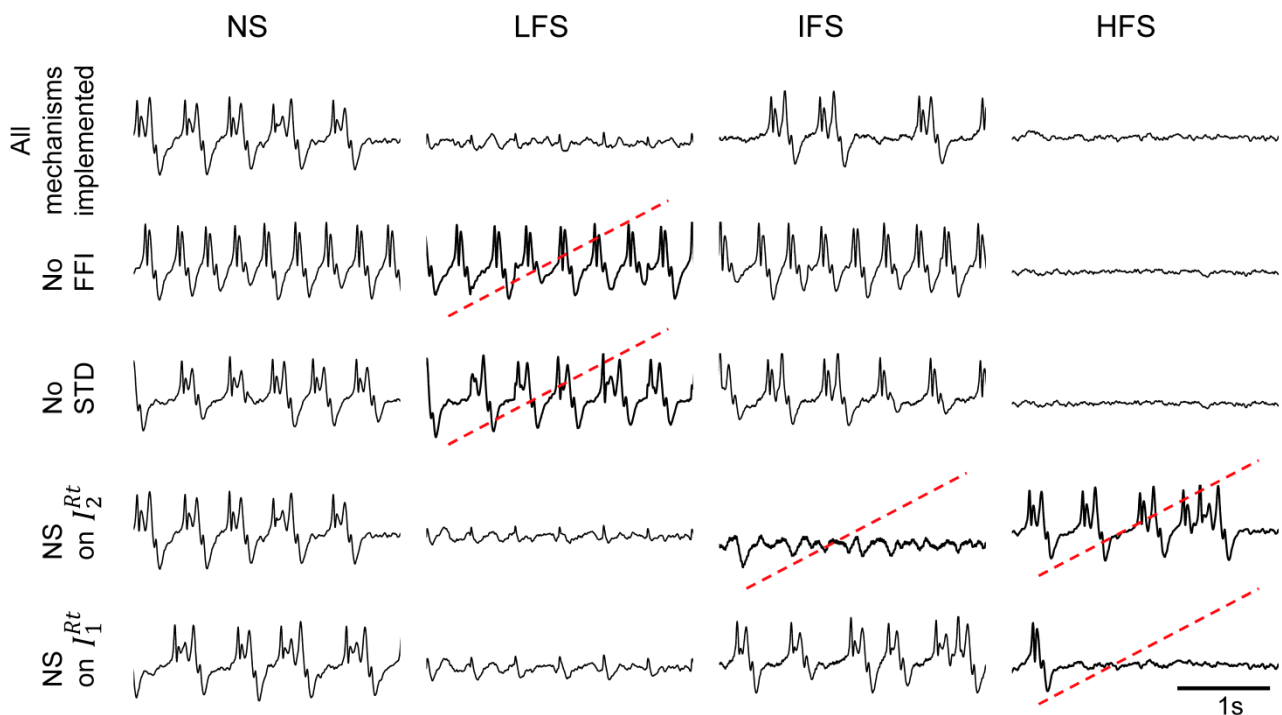


Figure 35. Conditions to reproduce frequency-dependent stimulation effects. Model output in the case where one and only one of the implemented mechanisms (FFI, STD, depolarization of I_{Rt}^2 , and I_{Rt}^1 respectively) is absent. LFS effects are not reproduced when the model does not account for FFI and STD. HFS effects require the depolarization of both reticular populations I_{Rt}^2 and I_{Rt}^1 . Suppression of epileptic activity is observed at IFS when I_{Rt}^2 interneurons are removed. Red dotted lines indicate situations where simulated signals do not match real ones for given stimulation condition.

Secondly, the impact of stimulation on the different subcortical neuronal populations was altered to determine its effects. Two hypotheses were made. The first one suggested that the stimulation current does not affect the dynamics of the fast inhibitory reticular population I_1^{Rt} . Consequently, S_{Irt1} was set to zero thus limiting stimulation effects to the thalamocortical TC population and to the slow inhibitory reticular population I_2^{Rt} . Conversely, the second one suggested that the stimulation currents only impact the thalamocortical TC population and to the fast inhibitory reticular population I_1^{Rt} , and thus S_{Irt2} was set to zero. Running model simulations under the first hypothesis provoked instability of the HFS effect. The model output oscillated from time to time during HFS. Deploying the second hypothesis resulted in an inversion of the effects of IFS and HFS. Results are depicted in Figure 35.

In conclusion, results indicated that the RtN inhibitory interneurons targeting TC cells (both I_1^{Rt} and I_2^{Rt} subpopulations) must be affected (i.e. depolarized) by the stimulation to obtain a suppression of epileptic activity when HFS is being used, as observed in the patient. Third, and interestingly, an unexpected effect was observed at IFS when the depolarization of I_2^{Rt} interneurons was removed from the model. Indeed, epileptic activity was abolished in this case, which is really unlikely to occur during actual stimulation as both subtypes of neurons are expected to be affected by the direct stimulation of the CM thalamic nucleus.

4 THE MECHANISMS: COMPUTATIONAL INSIGHTS

The totality of the preceding results computational and electrophysiological point toward one direction: ***“The frequency of stimulation does matter!”***. One can actually expect to see a nonlinearity of the cortical response to the frequency of thalamic stimulation (Figure 34-B). Moreover, the mechanisms activated by stimulation seem to be themselves frequency-dependent. In the following paragraphs, the mechanisms identified in this study are summarized.

4.1 THE NO STIMULATION “INTERICTAL” DYNAMICS

The spontaneous interictal dynamics observed in the clinical dataset were successfully reproduced in the model by changing the excitability characteristics of the cortical module. Indeed, the optimal parameters vector showed a major increase of 100% in the amplitude of cortical EPSPs A_c , contrasted by a consequent decrease of cortical inhibition (72% and 25% of the values of B_c and G_c respectively).

4.2 LOW-FREQUENCY STIMULATION (LFS, $f < 20$ Hz)

For the low-frequency stimulation (LFS, $f < 20$ Hz) condition, two mechanisms were found to play a major role for the abortion of epileptic activity in the FCD by decreasing cortical excitability: short-term depression (STD, i.e. decreased excitatory synaptic efficacy in thalamus-to-cortex connections) and feed-forward inhibition (FFI, i.e. excitation of inhibitory cortical interneurons by TC cells) (Figure 36-B). Actually, thalamocortical ascending fibers directly target principal pyramidal neurons as well as cortical interneurons inducing EPSPs in pyramidal principal cells as well as GABAergic interneurons [190]. While the arriving EPSPs were weakened by the STD mechanism, the IPSPs mediated to cortical pyramidal by cortical interneurons by FFI refrained cortical excitability.

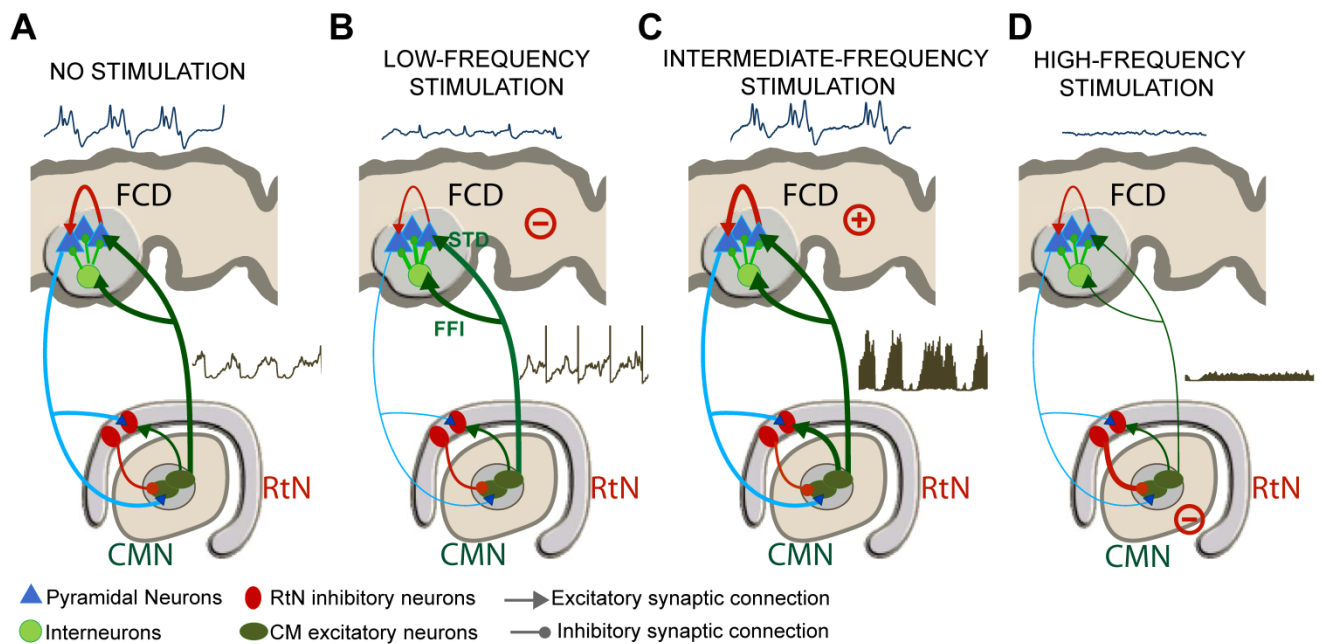


Figure 36. Frequency-dependent mechanisms underlying DBS. **(A)** Under the no stimulation (NS) condition, the thalamocortical loop is responsible for pathological oscillatory rhythms observed in the FCD. **(B)** For low-frequency stimulation (LFS), feed-forward inhibition (FFI, i.e. excitation of inhibitory cortical interneurons by TC cells) and short-term depression (STD, i.e. decreased excitatory synaptic efficacy in thalamus-to-cortex connections) was found to play a major role for the abortion of epileptic activity in the FCD. **(C)** For the intermediate-frequency stimulation (IFS) condition, thalamic output is reinforced (increase of TC cells firing) leading to an increase of the average excitatory post-synaptic potential (EPSP) on cortical pyramidal cells and to no “anti-epileptic” effect. **(D)** For high-frequency stimulation (HFS), the direct and sustained excitation of reticular nucleus (RtN) interneurons leads to dramatic decrease of TC cells firing rate and to a suppression of epileptic activity.

4.3 INTERMEDIATE-FREQUENCY STIMULATION (IFS, $20 < f < 70$ Hz)

For the intermediate-frequency stimulation (IFS, $20 < f < 70$ Hz) condition, results indicated that the thalamic output is reinforced (increase of TC cells firing) and leads to an increase of the average excitatory post-synaptic potential (EPSP) on cortical pyramidal cells (Figure 36-C). This effect corresponds to an increase of the spatiotemporal summation of unitary EPSPs. In this case, both the cortical excitability and the gain in the excitatory thalamocortical loop is increased, leading to “*no antiepileptic*” effect.

4.4 HIGH-FREQUENCY STIMULATION (HFS, $f > 70$ Hz)

Finally, for the high-frequency stimulation (HFS, $f > 70$ Hz) condition, the direct and sustained excitation of reticular nucleus (RtN) interneurons leads to strong inhibition of TC cells and thus to dramatic decrease of their firing rate. Despite the fact that TC neurons are also affected by stimulation, the response of reticular GABAergic neurons to stimulation and the higher efficiency of GABA-mediated currents ensure that IPSPs override EPSPs on TC cells. In this case, the reduced excitatory input to cortical pyramidal cells also leads to a suppression of epileptic activity (Figure 36-D).

Conclusion and Discussion on Part 1

In this study, a computational model of the thalamocortical loop was developed and analyzed in order to interpret the response of a specific neuronal system to an input stimulus, i.e. a pulse train characterized by its frequency. More specifically, this response corresponds to the indirect stimulation response, or in systems terms, the response of a given model's module to an input stimulus affecting another interconnected module. This necessitated the parallel definition of a signal processing methodology capable of precisely describing the real as well as the simulated signal content.

1 THE MODEL'S ARCHITECTURE

In view of the high complexity of the thalamocortical system, performing exactly the same study at the microscopic level would have been much more tedious and of a higher computational complexity. Actually, to our knowledge, the implementation of a microscopic model of focal cortical dysplasia has never been reported. And this is most probably due to the unique "random" architecture (cell types/ neuronal cell orientation/ synaptic projections) of this developmental lesion that would make it quite difficult to model at the cellular level. On the other hand, the advantage of macroscopic modeling is the dramatic reduction in the number of model parameters while staying relatively close to the physiological representation of the considered neuronal system. Only a single constraint remains: in the modeled system, synchronous dynamics of its constituting elements, typically the neuronal cells, is assumed. In fact, in the context of epilepsy, this assumption is common as synchronous continuous rhythmic or semirhythmic spikes and polyspikes constitute an electrophysiological signature of epileptogenic systems in general and of FCD in particular (see Chapter 1 section 3.4).

Regarding the model's architecture, as aforementioned, it followed the same general tri-modular architecture used previously by several research groups to model thalamocortical dynamics [22, 26, 27, 74, 167, 168, 172, 173]. However, the implementation of an alternative version was inevitable in order to:

- (1) guarantee the reproduction of realistic epileptic activity

(2) implement stimulation biophysical effects and stimulation-activated mechanisms

Consequently, the cortical module of the proposed model was extended in order to better approximate the temporal dynamics of epileptic signals recorded in the FCD. This modification consisted in the use of two types of interneurons (mediating GABAergic IPSPs with slow and fast kinetics on cortical principal cells), as reported in a previous study [180]. In effect, previously published models simplified the cortical module to a single population of pyramidal cells [176, 207], or coupled the latter with a single inhibitory subpopulation [175]. It was firstly Suffczynski and his colleagues [27] who implemented two different types of inhibitory GABAergic synapses originating from a single population of interneurons in the cortical module. Similarly, the reticular module was extended into two independent populations of inhibitory neurons instead of a single population as implemented by the preceding models [22, 26, 27, 74, 167, 168, 172, 173]. Effectively, this turned out to be necessary for identifying the mechanisms of stimulation.

In order to account for stimulation effects, the “ $\Delta V = \lambda \cdot E$ ” neural membrane polarization model was adopted [208]. According to this model, the perturbation of the mean membrane potential of a neuron ΔV is a linear function of the induced stimulation electrical field E in its neighborhood, λ is termed “polarization length” [209]. This “ $\lambda \cdot E$ ” assumption was already used in neural mass models in the context of low-intensity direct hippocampal stimulation to anticipate seizures [210] as well as in the analysis of the stimulus-response relationship of DBS in healthy animals [211]. Noteworthy, this assumption is valid for static electric fields. For alternating current stimulation [212], this expression is given by:

$$\Delta V = \lambda \cdot E / \sqrt{(1 + \omega^2 \tau^2)}$$

where $\omega = 2\pi f$ and τ is the polarization time constant. However, in this study, we neglected the extended form supposing that $\Delta V \cong \lambda \cdot E$ for extremely small values of τ . In brief, in the proposed model stimulation inputs were implemented at the level of the mean PSP of each subcortical population. The stimulation impact coefficients were not weighted by frequency-dependent coefficient to represent the complete form of the “ $\lambda \cdot E$ ” model. And this issue should probably be taken into consideration in future studies.

However, it is worth mentioning that in our model, the three subtypes of neurons (TC cells and both subpopulations of inhibitory neurons in the RtN) are depolarized by the stimulation, as suggested in [179] and conversely to [211] where only principal cells are impacted.

Concerning the implemented mechanisms, it is worth noting that short-term depression has never been implemented on the macroscopic level before. The cellular aspect of synaptic depression makes its implementation less evident on this modeling level. However, this becomes possible when short-term depression is regarded as part of the postsynaptic dynamics directly related to the mean firing rate at the population's input. From the same perspective, Modolo and his colleagues [213] modeled long-term plasticity in a neural mass model of cortical dynamics. Finally, concerning feed-forward inhibition (FFI), even though it basically existed in a previously published model [27], it was never explored as a potential mechanism involved in deep brain stimulation.

2 SIGNAL PROCESSING AND REPRESENTATION

In a fundamental reference on electrophysiology [214], Prof. F. Lopes Da Silva writes: "Every experienced electroencephalographer has his or her personal approach to EEG interpretation. (...) there is an element of science and an element of art in a good EEG interpretation; it is the latter that defies standardization". In this study, time-frequency parameterization of EEG data (MP) was used to calculate the spectral estimate of EEG data; real and simulated. As this choice is not as common for EEG analysis, it is hereby discussed and justified by scientific arguments.

2.1 USING FFT – COMPARING THE OPTIMAL MODEL OUTPUTS

It should be noted that spectral estimates (precisely, the power spectrum) were already used in the characterization of real datasets for optimizing model parameters [215]. This was equally the first method that we attempted to use in this study. Using the Fast Fourier transform, the average power spectrum from 0 to 150 Hz was calculated (256 data points were calculated on a 4s window for 50% overlap). This spectrum was then transformed into a 9D feature vector representing the normalized power in the classical iEEG bands.

In order to test the precision of this approach, the cortical module was uniquely considered in the absence of stimulation. An average power spectrum of a simulated signal of 20s duration was calculated. The average power spectrum replaced the feature vector $\vec{V}_{F,real}$ in the model optimization procedure presented in chapter 4, section 2.3. During the first test, the variance of the unspecific cortical input ($p(t)$) was set to zero. Using the simulated signal as a reference signal for parameter optimization, the FFT-based feature vector was sufficient for the identification of the exact parameters used for simulating this signal. However, when the variance of the input white noise $p(t)$ was increased to 3, the identified optimal parameters didn't match those used for simulating the reference signal.

This was the reason that put at doubt the precision of the FFT-based feature vector for model optimization.

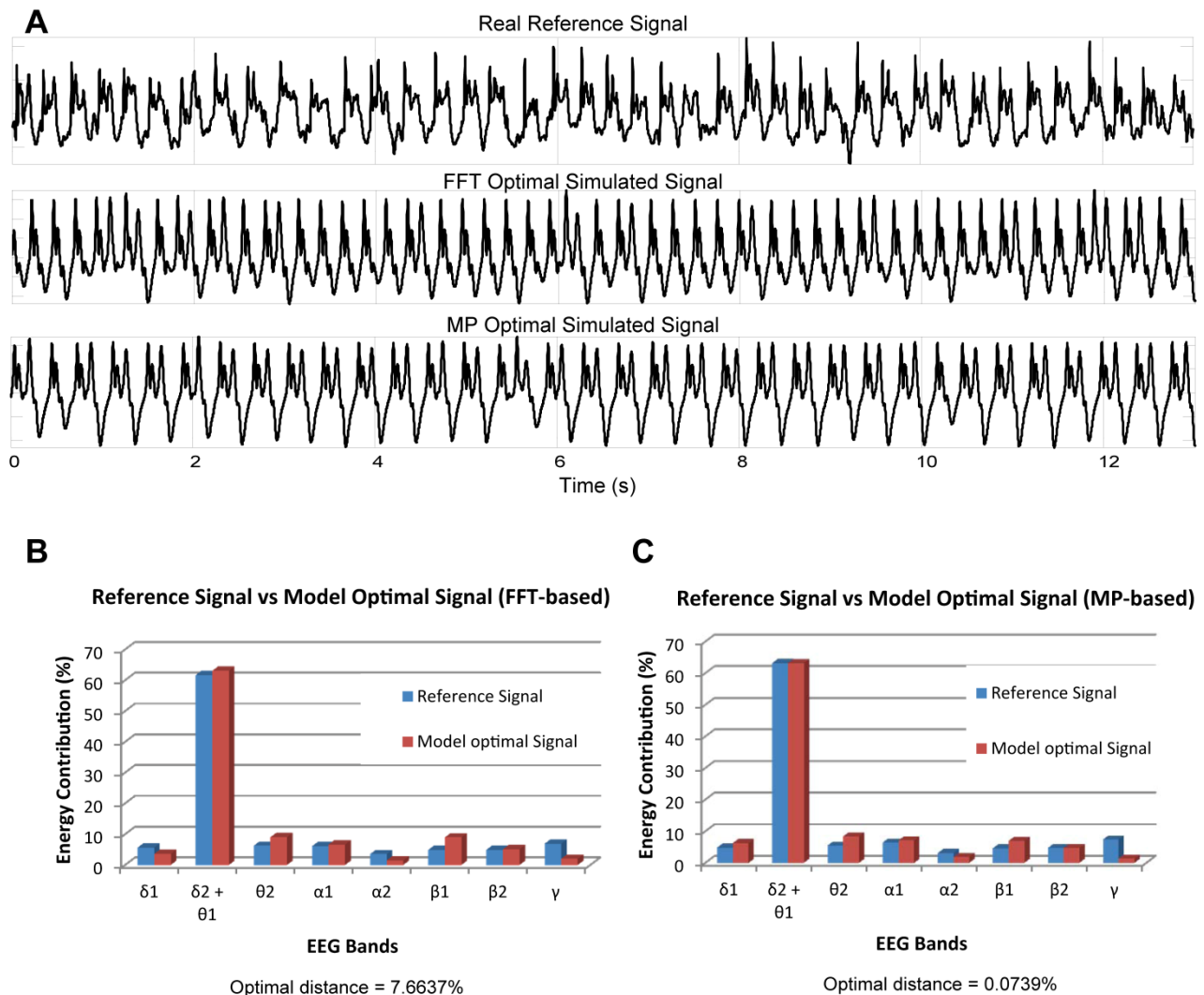


Figure 37. Optimizing the model output: MP vs. FFT. **(A)** The plot of the real reference signal and the optimal simulated signals obtained using the FFT-based feature vector (classical power spectrum) and the MP-based feature vector respectively. Note that the first simulated signal seems to be significantly faster than the real signal. The second simulated signal seems to better match real dynamics. **(B)** The bar plot of the FFT-based feature vectors of the real reference signal and the model optimal signal. **(C)** The bar plot of the MP-based feature vectors of the real reference signal and the model optimal signal. The optimal distance obtained is less than that measured for the FFT-based feature vectors.

To confirm these doubts, test simulations were run at the end of this study in order to compare the optimal model signal for the “no stimulation” condition using the MP-based feature vector versus the power spectrum feature vector. The visual inspection of these signals confirmed that the MP-based feature vector is better adapted to optimize model

parameters and that the resulting simulated signal better resembles the real one (Figure 37-A). Moreover, while the energy distribution of both feature vectors (MP-based and FFT-based) does not seem to vary drastically, the Euclidean distance between the optimal and the reference signal is much smaller in the case of the MP-based feature vector (Figure 37-B and C).

2.2 CLASSICAL TIME FREQUENCY APPROACHES – THE LIMITATIONS

Actually, when the FFT-based characterization failed to meet the required precision, the classical time-frequency methods (Wigner-Ville transform, periodogram, wavelet decompositions) were all considered as possible alternatives. However, the Wigner-Ville transform and the periodogram were not explored for the following reasons:

- (1) They are time-shift dependent. Thus, it is not evident to calculate the distance between 2D feature vectors of out of phase signals using these transforms.
- (2) This could have been done by considering only the average energy content as a function of the frequency. But, this would have eventually led to the same observations obtained for the FFT-based feature vector.

For these reasons, we only explored the wavelet decompositions.

The first tackled algorithm was the discrete wavelet transform (DWT) using daubechies 4 wavelets. Using this algorithm, the choice of the frequency bands was limited to the dyadic scale. As shown in

Figure 38, we could not obtain the 9D feature vector but a 5D feature vector. This 5D vector corresponds to the approximate definitions of the bands (δ , θ , $\alpha + \beta_1$, β_2 and γ).

Surely, this method imposed also a minimum number of samples available in order to attain the lowest band decompositions (δ and θ). This thereby constrained the data analysis procedure (at least 2^{10} samples/ decomposed signal). Each 4s ($f_s = 256$ Hz) of stimulation were then treated as an inseparable signal, and the population of stimulation signals was diminished into a unique signal segment/stimulation frequency. However, the basic problem was that using these approximations, the distinct features observed in the real iEEG signals during the different stimulation trials were rendered less obvious (Figure 39). Following these results, LFS effects can be then misinterpreted as ineffective.

One can argue that the continuous wavelet transform (CWT) would have solved the problem of band definition. Yet, this does not resolve the problem of the minimal number of samples required for each decomposition. And it was for this reason that this approach was not pushed further.

Apart from these fruitless trials with wavelet decompositions, the major drawbacks of using wavelet decompositions go beyond the aforementioned constraints. P. Durka compared these algorithms against adaptive approximations and matching pursuit in [216]. In this work, orthogonal wavelet decompositions (e.g. DWT) are shown to be time-shift variant, i.e, the same signal is decomposed differently if a time shift is added (see [216] for illustrations). However, although that this limitation is not present in the CWT, other problems arise, notably the occurrence of cross terms and the highly redundant representation.

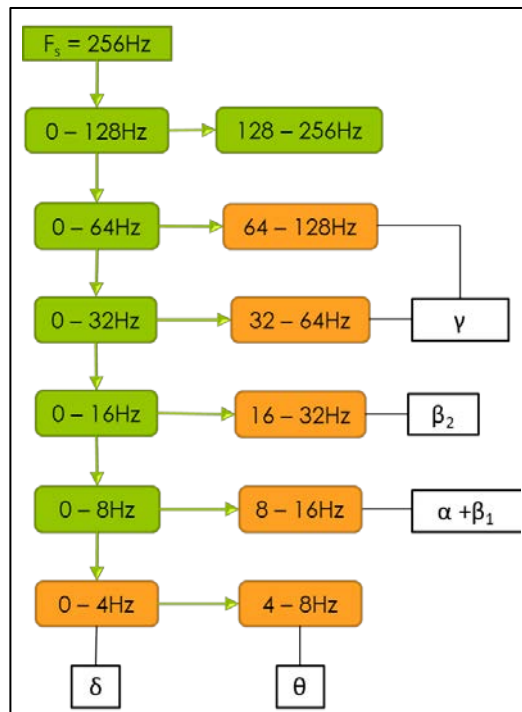


Figure 38. The dyadic scale used for the DWT and the corresponding decomposed frequency bands (δ , θ , $\alpha + \beta_1$, β_2 and γ).

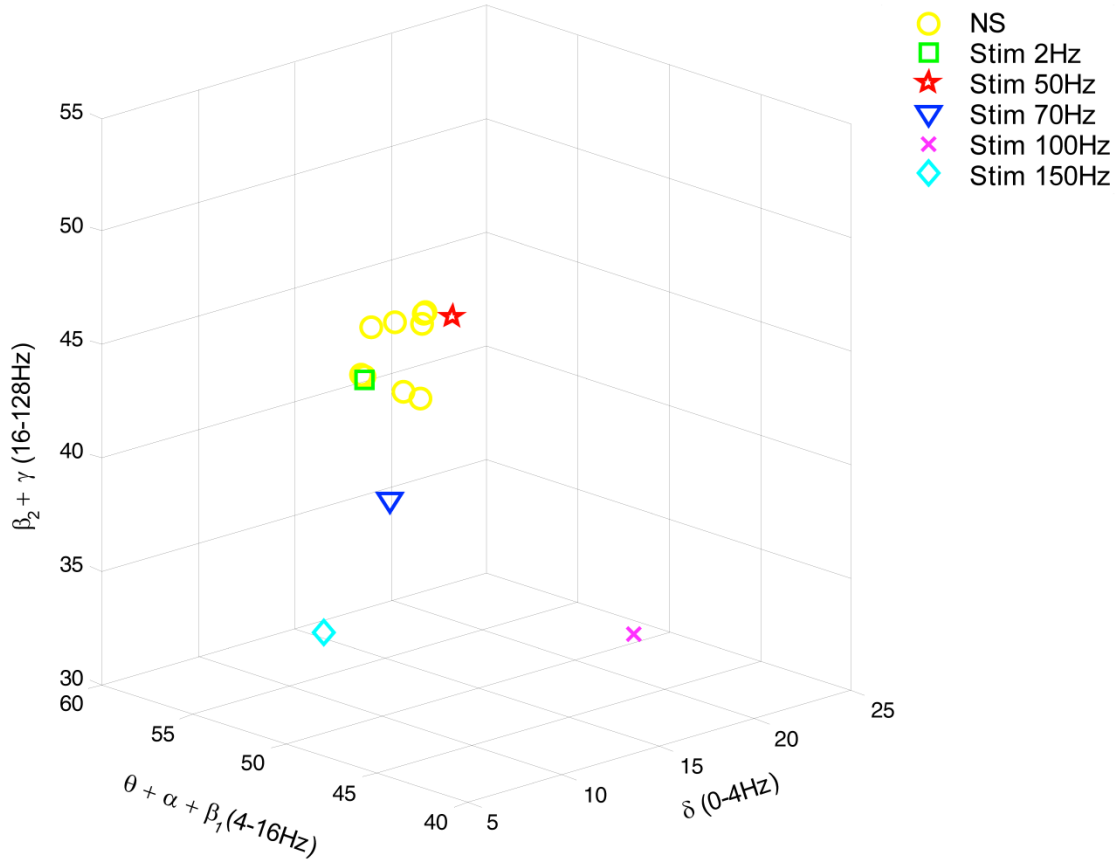


Figure 39. The 3D frequency space as made possible by the DWT transform. The 3D feature vector corresponding to the LFS condition coincides with the feature vectors of the NS effects. The characteristic peak at the $\delta_2 + \theta_1$ band does not exist for the feature vectors of the NS condition. This seems to have been replaced by high-frequency components at the β_2 and γ bands.

2.3 THE ADVANTAGES OF MATCHING PURSUIT (MP)

Besides the lack of cross terms, matching pursuit (as an adaptive time-frequency parameterization) exhibits several advantages over classical time-frequency representations. These advantages include (1) a high time and frequency resolution, (2) an exact characterization of the frequency, position, amplitude, width (scale), and phase of the detected structures (atoms), and finally (3) the possibility of using different atom types in the same decomposition (Fourier, Gabor, Dirac, ...).

The aforementioned characteristics of MP are the reasons behind the precision of the method, its time-shift invariance, and its transversal usability in different contexts (from audio applications such as audio signal coding to biomedical applications such as EEG analysis).

The possibility of detecting a diverse mixture of atoms is illustrated in Figure 40. Four synthetic signals were generated, two sin waves of frequency 5 and 10 Hz respectively, and two symmetric Gabor atoms of duration 12 s and frequency 12 Hz (Figure 40-A). These atoms were summed up into a test signal (Figure 40-B). This signal was decomposed using a properly defined dictionary and the detected atoms were analytically reconstructed in the corresponding bands. Figure 40-C shows 8 different bands with the corresponding reconstructed atoms. The sin wave of frequency 5 Hz was reconstructed in the $\delta_2 + \theta_1$ band, the sin wave of frequency 10 Hz was reconstructed in the α_1 band (7.4 – 10 Hz), and finally the two Gabor atoms were exactly detected and reconstructed in their corresponding position in the α_2 band (10 – 12.4 Hz). Noteworthy, the MP-based feature vector was calculated for both the initial and the reconstructed signal. These two were exactly equal.

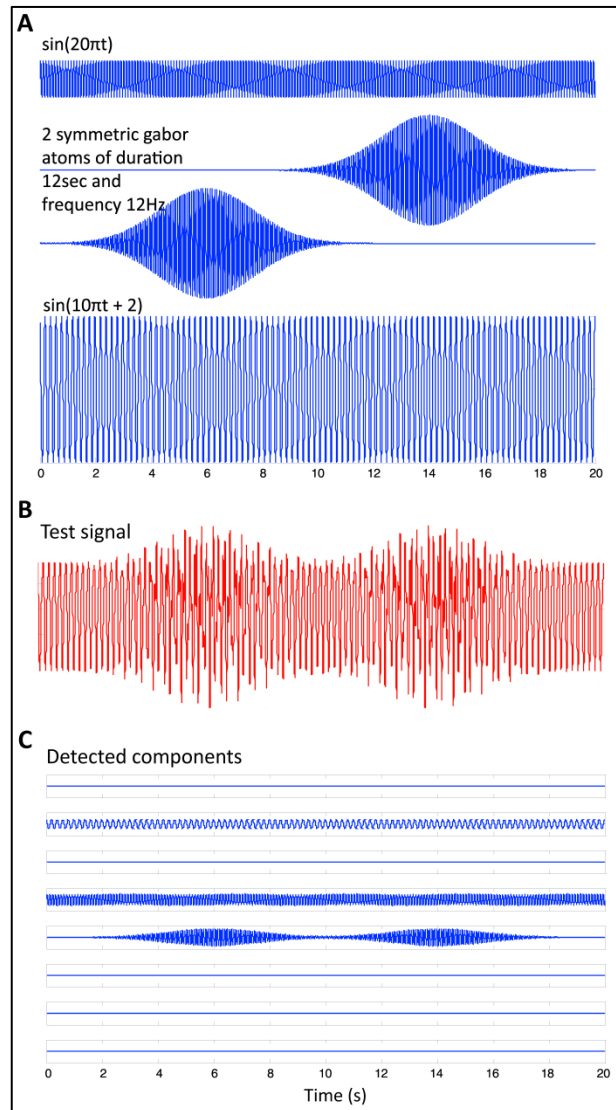


Figure 40. MP precisely detects different signal components. **(A)** Synthetic atoms used for testing MP and are summed together in a **(B)** test signal. **(C)** The detection of the initial atoms and their reconstruction in the corresponding frequency bands.

The high precision and the malleability of the MP decompositions were behind the choice of using it in this study. After all, using this type of decompositions, no constraints were imposed on the definition of the considered frequency bands. Moreover, defining the δ_1 band between 0.1 and 1.9 Hz offered an alternative method to de-trend the signal.

2.4 THE 3D SPACE

Even though the 3D signal representation could have been illustrated using a principal component analysis (PCA) algorithm, we opted for a more physiologically-relevant representation based on the energy content in aggregates of iEEG bands. However, it should be noted that the same clear separation between the stimulation conditions was also obtained using PCA (Figure 41). In this dimension reduction, simulated signals under the four stimulation conditions were also taken into consideration.

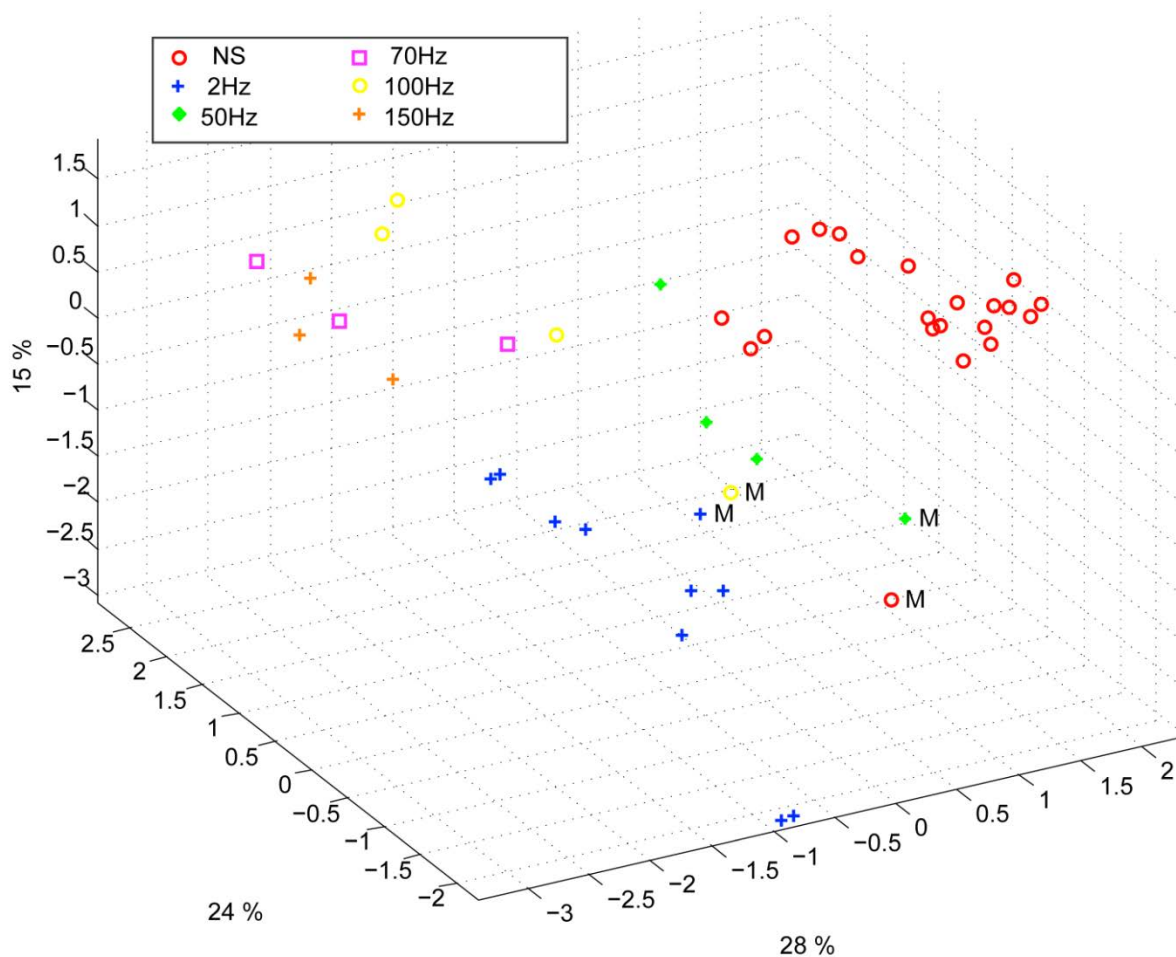


Figure 41. PCA automatic dimension reduction from 9D to 3D feature vectors. The space of the three principal components shows a clear separation between the stimulation groups. Note that, with this representation the IFS group seems dispatched from the NS group. The simulated signals remain relatively close to their corresponding groups.

3 THE FREQUENCY-DEPENDENCE OF THE IDENTIFIED MECHANISMS

Besides all the technical and methodological aspects presented in this study, its major contribution remains the identification of probable mechanisms responsible for the actually observed stimulation effects. More precisely, its ultimate novelty resides in the fact that it addresses these mechanisms on a large frequency range [0.5 – 150 Hz] compared to previous studies that usually address high-frequency stimulation (> 100 Hz) [74, 217] or less often low-frequency stimulation (< 10 Hz). On the other side, no previous studies addressed systematically the mechanisms of intermediate-frequency stimulation (\approx 50 Hz). Nonetheless, conducting this study over this extended frequency range remains built on a valid electrophysiological observation [197] recorded in the cortex of a drug-resistant epileptic patient during the pre-surgical evaluation that made use of intracerebral recordings.

3.1 THE NO STIMULATION CONDITION

As demonstrated in the model, under the NS condition, excitation among pyramidal cells had to be increased and inhibition had to be reduced in the cortical compartment for producing “pathological” oscillatory rhythms, as observed in the FCD of the patient. As these results point out the cortical origin (FCD) of these abnormal dynamics they do not neglect the involvement of the thalamocortical loop in their generation. In fact, these findings are in line with histological studies showing that these typical oscillations are generated in altered brain tissue, where inhibition is partially deteriorated or dysfunctional [218], and where excitation is heavily increased [33]. In addition to neuron alterations in the dysplastic tissue [115], FCD must keep sufficient projections to - and input from - other brain structures (in this case, the thalamus) in order to propagate its pathological dynamics [33]. As mentioned before, the presence of connections with subcortical structures was a necessary condition in the model for producing pathological oscillations resembling those actually recorded in the FCD.

3.2 THE LOW-FREQUENCY STIMULATION CONDITION

As revealed by the model, the mechanisms of action of low-frequency stimulation (LFS) seem to be of higher complexity when compared to those of high-frequency stimulation (HFS). In fact, the implication of a dual mechanism of FFI and STD is but a highly probable hypothesis. As aforementioned, the coexistence of these two mechanisms in the model was the necessary condition for the reproduction of LFS effects. However, as it was computationally possible to increase the impact of STD by making the depressive effect on thalamocortical synapses last longer (in time) or be of higher intensity (> 40% depression of

the amplitude of cortical EPSPs), this study respects the reported physiological limits of this phenomenon following a thalamic electrical LFS [150]. In the same experimental context as [150], LFS trains in adult anaesthetized rats provoked transient long-term depression of thalamocortical synapses; this was measured by up to 40% drop in cortical EPSPs after LFS trains and under the effect of GABA antagonist [149]. Otherwise, STD could have solely explained the effects of LFS if a higher depression in the amplitude of corticothalamic EPSPs was computationally allowed in our study.

As mentioned above, while respecting the imposed physiological limit of STD, the LFS effects could not be reproduced by the model without incorporating also FFI. Actually, thalamocortical ascending fibers directly target pyramidal neurons as well as cortical GABAergic interneurons inducing EPSPs in both cell types [190]. In the model, while less efficient (STD) thalamic EPSPs arrive directly onto pyramidal neurons, IPSPs induced by thalamic stimulation also arrive on pyramidal neurons (FFI) lagging by 1 to 2ms. This short latency between the onset of thalamocortical excitation and the onset of feed-forward inhibition presents a temporal “window of opportunity” for pyramidal cells to integrate excitatory and inhibitory inputs, thus keeping the transmembrane potential below firing threshold. In the literature, neuroanatomical and neurophysiological studies [184] showed the functional importance of FFI in regulating cortical dynamics by controlling cortical excitability [219]. And it is the dual FFI and STD that regulates cortical excitability during LFS in our model.

3.3 THE INTERMEDIATE-FREQUENCY STIMULATION CONDITION

Provided that no previous studies addressed the mechanisms of intermediate-frequency stimulation (IFS, $20 < f < 70$ Hz), it is directly enriching to computationally prove that this stimulation frequency increases the magnitude of thalamic firing and enhances corticothalamic oscillations. The paradox is that its only necessary condition is the depolarization of reticular slow inhibitory neurons I_2^{Rt} by stimulation. As depolarizing inhibitory populations by stimulation current normally increases the inhibitory drive, depolarizing this particular population seems to increase the amplitude of the intermittency in thalamic firing. In this case, both cortical as well as thalamic excitability increased.

Nevertheless, it is worth noting that 50 Hz stimulation frequency is classically used during the pre-surgical evaluation of patients with intractable partial epilepsy in order to trigger seizures and delineate the epileptogenic zone [220, 221]. The same frequency range is also known to provoke afterdischarges and was actually used in the kindling model of epilepsy [151, 222].

3.4 THE HIGH-FREQUENCY STIMULATION CONDITION

Finally, concerning high-frequency stimulation (HFS, $f > 70$ Hz), several studies (for review see [223]) addressed its probable mechanisms. However, as the experimental context (epilepsy, Parkinson, dystonia ...) and the stimulated target (GPe, STN, ...) vary from one study to another, the identified mechanisms also vary and are sometimes contradictory. Today, the mechanisms by which DBS modulates neuronal dynamics, whether normal or pathological remain controversial [223]. Whether HFS acts by local depolarization blockade [68], synaptic depression due to neurotransmitter depletion [146, 147], or synaptic inhibition [70] or whether it disrupts the thalamocortical network's dysrhythmia [74, 217] the answer is far from being definitive.

In our study, the significant reduction of thalamic firing due to HFS seems to explain abolishment of the cortical pathological oscillations as well as those of the thalamocortical network. Actually, this result corroborates reported stimulation studies where HFS (>100 Hz) was associated with significant decrease in epileptiform discharges in vitro, and reduction in seizure frequency in responding patients [106, 198].

Concerning the underlying mechanism, our model suggested that this antiepileptic effect relies completely on the depolarization of both types of reticular inhibitory neural populations. This hypothesis is in line with recent findings suggesting that HFS of the globus pallidus (GPi) in dystonia patients decreased its firing by stimulation-evoked GABA release from afferent fibers and thereby the enhancement of inhibitory synaptic transmission by HFS [71]. Similarly, HFS (100 Hz – 130 Hz) of the STN neurons in vitro showed a suppression of the activity of the majority of neurons by the reinforcement of inhibitory responses [70]. Other HFS studies also provided evidence on the inhibition of GPi output during HFS in human patients [69] as well as the disruption thalamocortical network's dysrhythmia [74, 217].

3.5 THE STIMULATION EFFECTS CURVE

In conclusion, the aspiration of any DBS researcher, whether a physicist an engineer or a clinician, is to draw a clear relationship between the parameters and the effects of stimulation. In this study, it was possible to draw such a relationship in the form of the *HtoLR* curve that indicates that the effects of stimulation are probably non-linearly related to the frequency of the stimulation signal. Moreover, there might be a critical frequency range to avoid per patient in order to optimize stimulation effects. The remaining challenge is how to generalize this type of curves over the different brain regions and for any patient at any time.

4 THE LIMITATIONS

Just like any study, this one has its limitations. Starting by to the level of modeling, the model predicts macroscopic effects of the frequency-dependent mechanisms of thalamic DBS. In fact, the mesoscopic level does not allow the exploration of the elementary cellular mechanisms underlying the “radical” stimulation-evoked bifurcations of the neural dynamics in the thalamocortical system. In other words, the proposed model cannot predict whether the thalamocortical pathological delta waves of the FCD are caused by the interplay of cellular currents – namely the hyperpolarization-activated cation current I_h and the transient low-threshold Ca^{2+} current – or other microscopic electrophysiological mechanisms [224]. Similarly, the model cannot predict if similar-level mechanisms reinforce thalamocortical oscillations during IFS. Shortly, the dynamics of specific neural currents and their implication in DBS mechanisms cannot be explained using this type of models.

Moreover, the representation of neurons as neuronal populations does not allow the testing of the hypotheses of direct activation of neuronal axons by stimulation versus somatic inhibition [223], neither the mechanisms of orthodromic/antidromic propagation of action potentials due to stimulation [225-227]. On a more macroscopic scale, the model cannot study the different effects of DBS in function of the structural properties of the targeted neurons; axonal nodes, branching points, and the diameter of daughter branches. Besides, the model does not integrate the spatial anatomy of cortical layers and different thalamic nuclei. It is limited to one cortical column, one homogeneous neural population of a thalamic nucleus, and two representative neural populations of the reticular nucleus. And thereby, it does not take into consideration the orientation of the stimulation electrode nor the induced electric field with respect to the axonal orientations.

Finally, the fact that this work takes into consideration only one dataset clinically observed in a single epileptic patient is also a weak point of this study. This is due to the fact that such informative clinical datasets stay relatively rare since many conditions have to be met (patient candidate to surgery, presence of a FCD, electrodes positioned in appropriate structures). However, as the goal of this study was to computationally explore the effects of thalamic stimulation on cortical dynamics in order to develop a more profound comprehension of the underlying network mechanisms this clinical limitation can be considered secondary.

5 CONCLUSION

Nowadays, DBS for epilepsy is still in its early stages of development. However, in spite of the unfortunate lack of tangible results concerning its effects on epileptic dynamics, we

believe that deep brain stimulation techniques hold a high unexploited “*antiepileptic*” potential that may be useful in patients with drug-resistant partial epilepsy and in whom surgery is contraindicated. Thus, resolving the issue of **optimizing** stimulation protocols (parameters) turns out to be equally urgent as crucial. On this account, computational models constitute effective as well as simplifying tools that provide an efficient framework to i) account for the many and essential factors that may intervene during stimulation procedures and ii) analyze the links between these factors in a formal manner. This computational approach is particularly fruitful when the developed models are well grounded in experimental/clinical data [179]. However, as this study experimentally relies on a unique dataset recorded from a single patient, further experimental validation was sought. Consequently, an equivalent animal model of FCD was searched in vain as the existing dysplasia models are not focal but extended over the whole cortex (see review in [228]). As this solution was not possible, an alternative experimental test was defined in order to verify the exactitude of the manner stimulation was implemented in the model. The consequent results and observations are in Part 2.

At this stage, the face value of the model is satisfactory. However, the experimental validation of the model predictions is the missing block in this study. Eventually, the next step is obviously to test the model predictions using animal models. At an early stage, experiments can be undertaken in healthy rodents with electrodes implanted in the cerebral cortex and in the thalamus. Hence, the modulation of cortical rhythms during/after direct thalamic stimulation at various frequencies and for controlled vigilance states (sleep, awake, resting, and exploratory) can be assessed in control conditions. In these controls, some drugs can be used to alter some parameters related to synaptic transmission (in a more or less specific manner) which have a correspondence in the model, on the other hand. Then, refined experimental models could be introduced to get closer to the epilepsy context including models of developmental dysplastic lesions (see review in [228]). Hopefully, this combined computational/experimental approach will be helpful in disclosing some of the highly intricate effects of DBS either at the local or at the network level.

PART 2: POLARITY-DEPENDENT EFFECTS OF DC HIPPOCAMPAL STIMULATION ON HIPPOCAMPAL EXCITABILITY

The objective of Part 2 is exploring the polarization effects of direct current (DC) stimulation on the dynamics of hippocampal paroxysmal discharges in the context of mesial temporal lobe epilepsy. Three stimulation parameters are particularly addressed: current polarity, duration and intensity. In order to fulfill this objective, a physiologically-relevant computational model of the hippocampal CA1 region is firstly adopted. Then, a real dataset of experimentally recorded HPDs in an animal model of mesial temporal lobe epilepsy is used to implement a realistic algorithm of HPD generation in the aforementioned computational model. For this, a rupture detection method based on the Page-Hinkley test is used to characterize HPD occurrence, duration and intensity in the real signals. Furthermore, the statistical laws governing the generation of HPDs are identified and implemented in the model. Later on, stimulation inputs are integrated to the model by modeling the electrode-electrolyte interface. Finally, the resulting nonlinear dynamical system is analyzed as a function of the polarity of the stimulation input. The computational results suggest a polarity-dependent modulation of the HPD occurrence; one polarity diminishes HPD duration, intensity and occurrence and the opposite polarity significantly increases these HPD features.

Experimentally, a stimulation protocol is proposed to verify the model's predictions. Preliminary safety tests concerning stimulation-induced heating are performed before the experimental test of low-intensity DC stimulation in vivo. Experimental results suggest that for every stimulated animal there exists a polarity that diminishes HPD duration, intensity and occurrence, as predicted by the model. Nonetheless, the opposite polarity does not seem to influence HPD generation. Moreover, stimulation duration seems to be primordial for assuring stimulation safety as well as stimulation results. Complimentary intracellular recordings are presented to show that neuronal polarization of all circuit components (interneurons as well as CA1 principal cells) may explain these results.

Chapter 6: Low-Intensity DC Stimulation of the Ictal Onset Zone – Computational Tools

Mesio-temporal lobe epilepsy (MTLE) syndrome constitutes the most common form of focal drug-resistant epilepsies (~20% of epileptic patients). It is characterized by the recurrence of focal seizures in the mesio-temporal limbic structures [119] and is often associated with hippocampal sclerosis (45% to 70% of MTLE patients variable from one study to another [229-231]). The origin of MTLE is thought to be a neural accident occurring in early childhood [232](such as febrile seizures, head trauma, intracerebral infections or ischemic episodes [233, 234]). This initial insult is generally followed by years of latency before the onset of the first spontaneous seizure [234]. As patients with MTLE respond poorly to antiepileptic drugs, defining alternative therapeutic interventions is of significant importance.

A recent study [131] reported a long lasting 92% reduction of seizure frequency following low-frequency stimulation (LFS; 1 Hz) of the fornix in 8 patients with MTLE. As this is the unique population study of the effects of LFS on seizure frequency in MTLE patients, other less conventional stimulation protocols such as the low-intensity DC stimulation of the seizure onset zone has never been clinically tested or reported. In this view, hippocampal deep brain DC stimulation may convey an unexplored antiepileptic alternative for MTLE patients with hippocampal sclerosis, especially the non-responders to other types of stimulation. However, the particularity, as well as the difficulty, of this procedure is the definition of the sufficient “electric dose” to be locally delivered to the diseased hippocampus in order to control its epileptic dynamics without provoking collateral damages. In Part 2 of this thesis manuscript, this particular type of stimulation is explored in order to study (1) its possible experimental implementation, (2) its effects on epileptic dynamics, and (3) its probable risks and limitations.

In this chapter, we first address the state of the art of low-intensity DC stimulation and its theoretical as well as experimental effects on neuronal dynamics and properties. Then, we propose a computational and an animal model in order to computationally reproduce the epileptic activity observed in the experimental model and to further explore the effects of DC stimulation currents on these epileptic dynamics.

1 DC STIMULATION PROTOCOLS

Several studies provide experimental *in vitro* evidence of the polarizing effects of weak steady electric currents/fields on neuronal excitability [36, 235-240]. In the following sections, these effects are firstly revised and then a thorough discussion of a possible *in vivo* application is presented.

1.1 *IN VITRO* EFFECTS OF DC ELECTRIC FIELDS: STATE OF THE ART

Whether using CA1 pyramidal cell cultures, as in [239], or hippocampal slices, as in [36], the aforementioned studies confirm that DC electric fields can depolarize/hyperpolarize the impacted neuronal populations. Moreover, the advantages of using hippocampal slices reside in the laminar (radial) organization of the hippocampal region (Figure 42) which is as simple as that of the columnar organization of the cerebral cortex. This well-defined organization allows the study of the effects of a DC field in function of the orientation of the stimulated neurons without modifying the network structure.

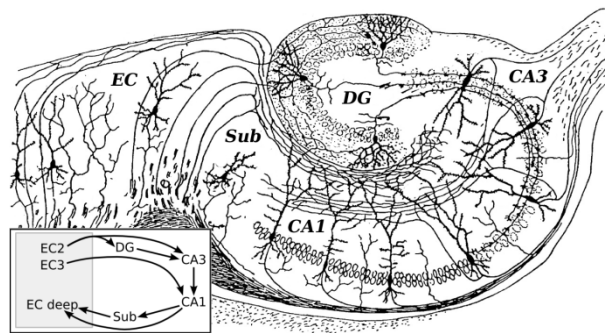


Figure 42. Schematic representation of the hippocampal organization [241].

In the most recent among the cited studies [36], the authors succeeded in measuring the “linear” relationships between the extracellular stimulation field and the neuron response. This was done in hippocampal rat slices. The most prominent results are hereby listed:

- (1) Large negative fields (cathode at the alveus side of CA1) of intensity beyond -80 mV mm^{-1} induced epileptiform discharges in 19 out of the 24 tested slices (extracellular recording). However, positive fields never induced such discharges over the tested intensity range ($< 200 \text{ mV mm}^{-1}$).
- (2) As negative/positive fields increased/decreased the amplitude of population spikes (extracellular recording) evoked by the stimulation of the oriens interneurons (OR), both polarities increased the amplitude of population spikes evoked by the stimulation of LM interneurons (the interneurons of stratum lacunosum-moleculare).

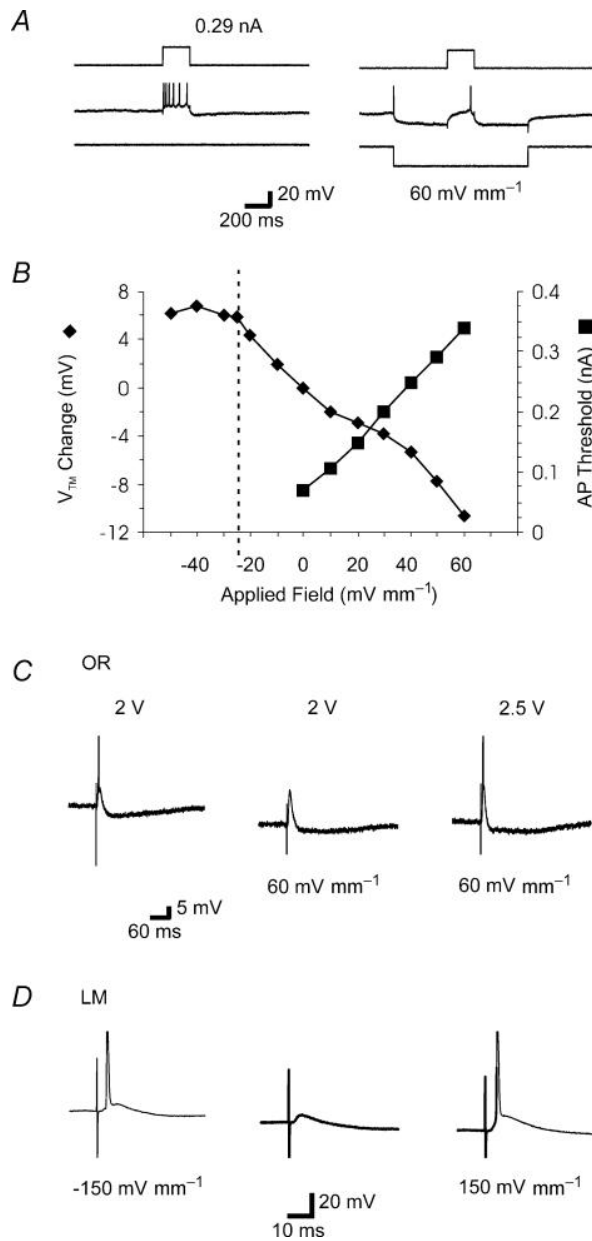


Figure 43. Effects of uniform weak DC electric field on single CA1 neurons. **(A)** In the presence of a positive field CA1 neurons fire less action potentials. **(B)** The linear relationship between transmembrane potential/ AP threshold and applied field intensity. **(C)** The generation of AP is hindered in oriens interneurons (OR) in presence of a positive field. **(D)** The presence of a large uniform electric field is sufficient to increase the amplitude of the stimulation-evoked AP in LM interneurons for both polarities. Adapted from [36].

(3) Intracellular recordings showed that negative applied fields on single CA1 pyramidal cells increased their transmembrane threshold while decreasing the threshold for action potential generation (AP threshold). Positive applied fields led to opposite observations. The figure illustrating the effects on CA1 pyramidal cells is adapted from [36] and presented in Figure 43.

These results remain in accordance with previous studies of the same group confirming that currents parallel to the cell axis (termed “soma-depolarizing currents”) increase neural excitability when the stimulation field makes the apical dendrites layer more positive than the cell body layer. Similarly, currents perpendicular to the cell axis had no pertinent effect on the neuronal response [240]. The proved effect of field polarity in depolarizing/hyperpolarizing CA1 pyramidal cells *in vitro* constitutes the major motivation for testing the validity of this hypothesis in a computational model of the CA1 region and *in vivo* later on.

1.2 THE HYPOTHETICAL BASIS OF NEURONAL POLARIZATION BY DC CURRENTS

Polarizing stimulation operates in function of the polarity and orientation of the applied electric field/current (see [60] for review). As aforementioned, this was proved experimentally by several studies [36, 235-240]. This was also demonstrated computationally by modeling the effect of the stimulation field on single cells [61]. Considering a simplified version of the Hodgkin-Huxley model, a cell compartment can be modeled as a capacitor C_m in parallel with a series combination of a battery E_r and a resistor R_m simulating the combined resistance at rest of all membrane ion channels (Figure 44-A).

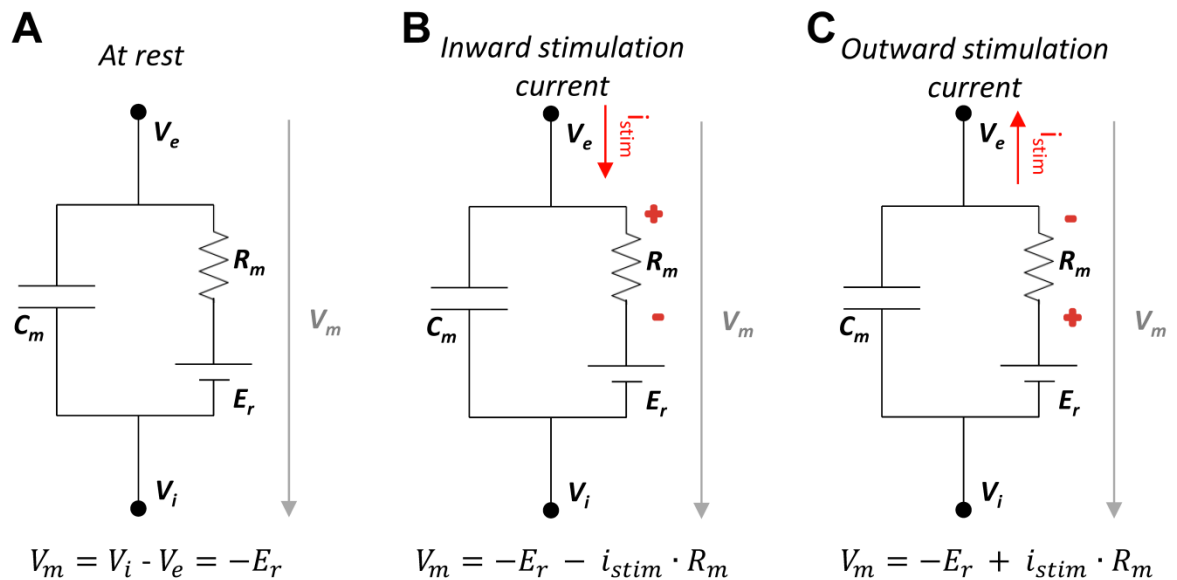


Figure 44. Computational effects of current polarity on neural excitability. **(A)** At rest the transmembrane potential V_m is equal to the resting potential E_r . **(B)** An inward current flowing across the membrane decreases V_m by $-i_{stim} \cdot R_m$. It then hyperpolarizes the membrane at this point. **(C)** Conversely, an outward current flowing out of the membrane increases V_m by $i_{stim} \cdot R_m$ thus causing membrane depolarization.

At rest, the transmembrane potential V_m , defined as the difference between the intracellular potential V_i and the extracellular potential V_e , is equal to the resting potential E_r . When neurons are placed under the effect of an electric field, current lines will flow through the conductive medium (brain tissue) following the Maxwell equations (see Chapter 1 section 3.1). Some of the current lines will pass through the cell bodies. In this case, it has been evidenced that inward stimulation currents will generate hyperpolarization by driving the transmembrane potential away from threshold (Figure 44-B). Conversely, outward stimulation currents will cause depolarization by driving the transmembrane potential nearer to threshold (Figure 44-C) [60]. Note that the global effect

is driven by the hyperpolarization/depolarization of the soma (AP generation site) and not the dendrites.

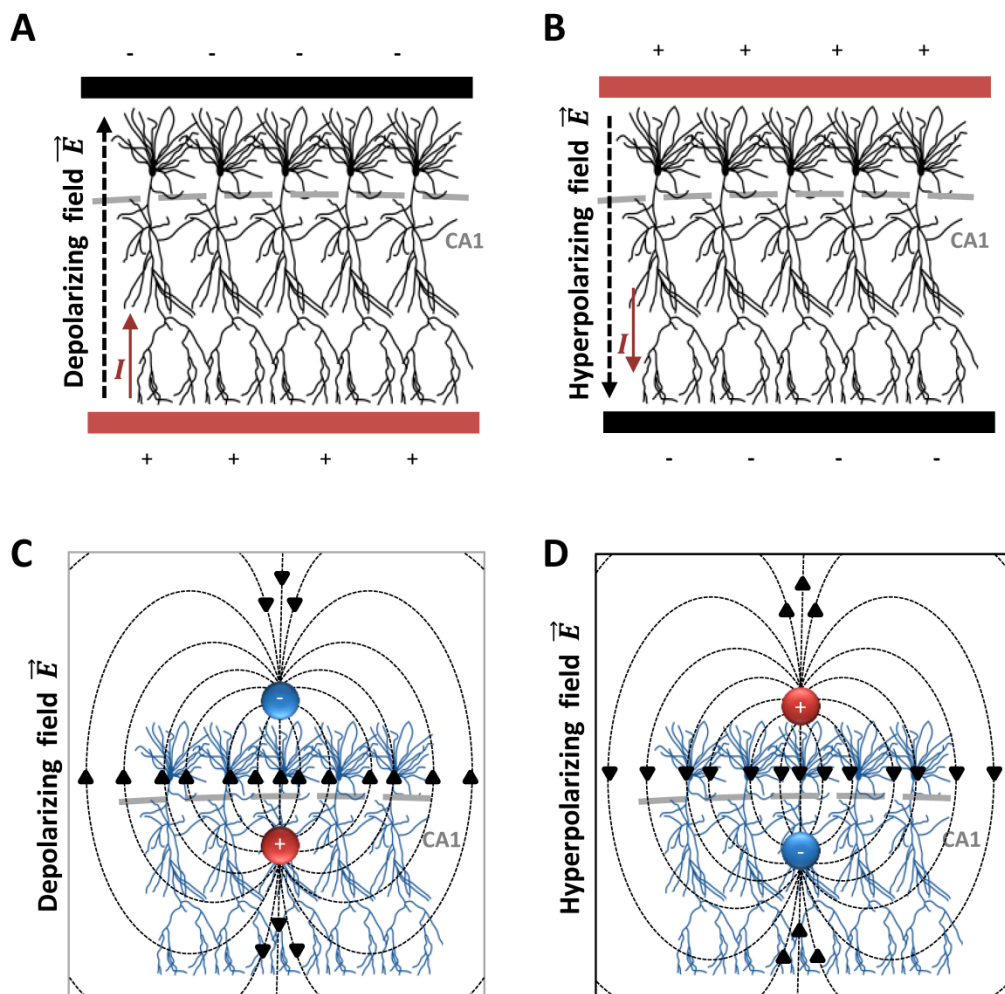


Figure 45. Schematic representation of the effects of injected currents on neuronal excitability as a function of electrode types and polarity. In the case of large field electrodes: **(A)** the depolarizing field and the **(B)** hyperpolarizing field configurations. In the case of localized bipolar electrodes: **(C)** the depolarizing field and the **(D)** hyperpolarizing field configurations.

Stimulation electrodes are usually of two types: either large field electrodes (usually used in *in vitro* setups), or localized field electrodes, monopolar or bipolar (usually used in *in vivo* setups). In the case of field electrodes (*in vitro*; see Figure 45-A and B), the effect of the induced uniform electric field depends on the position of the parallel plates with respect to the somato-dendritic axis. In consequence, stimulation has no effect if current lines are perpendicular to the cell axis, and conversely, it exerts a maximum effect on neuronal excitability when these lines are parallel to the cell axis. In Figure 45-A, the current enters the cell through the apical dendrites and leaves it in the somatic and basilar region

generating depolarization. The global effect of the field is a depolarizing effect. Conversely, in Figure 45-B, the current enters the cell through the soma and basal dendrites generating somatic hyperpolarization and therefore abolishing neural firing.

As for bipolar electrodes (Figure 45-C and D), for simplicity, the induced electric field lines can be considered equivalent to those generated by an electric dipole in a homogenous medium. In such a configuration, neurons lying between the two electrodes receive the maximum polarizing effects if the axis joining the two electrodes lies perfectly parallel to the somato-dendritic axis. Nevertheless, in the neighborhood of the electrodes, neurons may have a higher probability of falling on a field lines aligned with their axes especially when neuronal orientation is uncertain (*in vivo* electrode implantation) or highly variable (in the case of interneurons for example). Yet, in the case of well-known structural organizations such as the CA1 region of the hippocampus, it can be assumed that when bipolar electrodes are implanted on the opposite sides of CA1 (stratum pyramidale), the polarity of stimulation can theoretically provoke depolarizing (Figure 45-C) as well as hyperpolarizing electric fields (Figure 45-D) *in vivo*. For this, the anode (\oplus) should be implanted, anatomically, just above the somatic layer. Noteworthy, if the electrodes are implanted on the same side of the CA1 region, the hyperpolarizing effect will be theoretically replaced by a depolarizing effect.

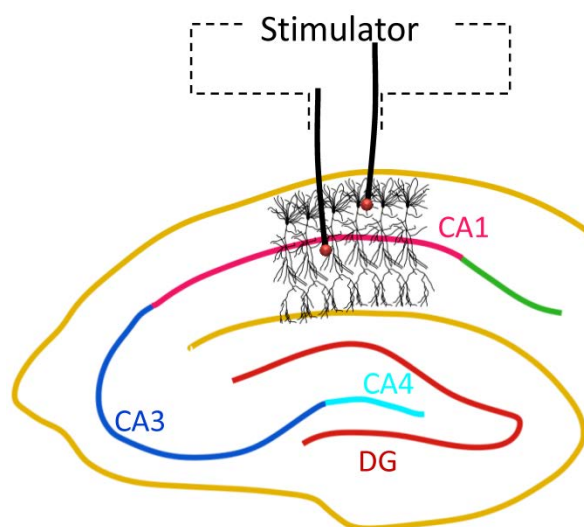


Figure 46. Schematic representation of the stimulation electrodes ideally situated on the two sides of the CA1 region.

A possible *in vivo* implementation of this type of stimulation can be performed by placing the two tips of the bipolar electrode in the hippocampus of epileptic animals. The two tips

should be situated on the opposing sides of the cell bodies layer in the CA1 region (see Figure 46). Consequently, several questions could be experimentally addressed:

- (1) Can *in vivo* DC stimulation modify the excitability of the epileptic hippocampus?
- (2) Do opposite stimulation polarities induce opposite effects *in vivo* (hyperpolarization vs. depolarization)?
- (3) What is the minimal/maximal intensity and duration of stimulation needed to obtain a significant reduction in epileptiform discharges?

Noteworthy, low-intensity DC stimulation has never been intentionally tested *in vivo* given the probable damage associated with monophasic stimulation [154] and related to the irreversible chemical redox reactions that take place at the electrode surface during long duration DC current stimulation [153]. However, it has been reported that DC currents as low as 10 – 15 μ A applied for 15 minutes per day significantly increased the seizure threshold in fully kindled rats [242]. This effect termed “quenching effect” was accidentally obtained due to a DC leak at the stimulator output. Interestingly, the authors reported that the DC stimulation effects were reversible, and that no evident histological or anatomical damage was ensued.

However, before experimentally testing these hypotheses in the freely moving animal, a computational exploration is first performed. The proposed computational model was coupled with real LFP signals recorded in an animal model of MTLE in order to:

- (1) Reproduce realistic epileptic dynamics in the model using real LFP experimental signals.
- (2) Computationally study the effects of stimulation in the model.
- (3) Experimentally validate the model’s predictions later on.

2 A COMPUTATIONAL MODEL OF TEMPORAL LOBE EPILEPSY

Two major approaches are described in the literature for modeling hippocampal dynamics and subsequently simulating the ensued local field potentials (LFPs) contributing to iEEG/EEG recordings. These are the ‘detailed’ versus the ‘lumped’ modeling approaches. Single neuron characteristics, whether structural (axon, dendrites, cell body) or functional (type, specific ion channels, connectivity ...), are taken into consideration in ‘detailed’ models of the hippocampus [7, 243-245]. Conversely, lumped models represent the hippocampal dynamics as the interaction of several neural subpopulations [161], analogous to those introduced in Part 1 chapter 3 section 2.1.2. In the past years, both approaches were developed in our team giving rise to a microscopic detailed [245] and a macroscopic

lumped [161] model of the hippocampus CA1 region. The lumped model of the hippocampus [161] was used for studying effects of direct DC stimulation on hippocampal dynamics.

2.1 COMPUTATIONAL MODEL OF THE HIPPOCAMPUS

The aforementioned population model is more specifically a model of the CA1 region of the hippocampus. In [161], the authors demonstrate that, depending on the excitability/inhibition parameters, this model can reproduce real normal and epileptic dynamics (sporadic spikes, sustained discharges of spikes, slow rhythmic activity ...), actually observed in hippocampal recordings.

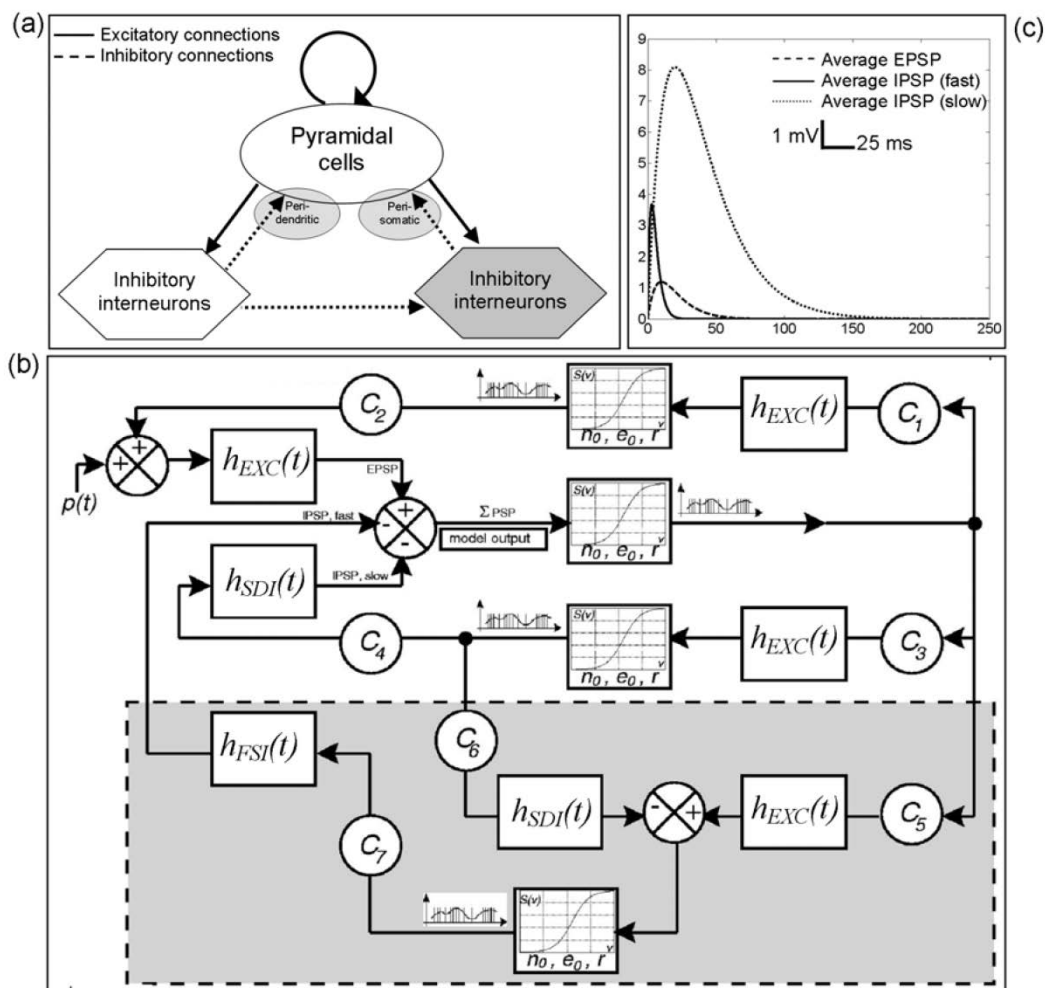


Figure 47. The architecture of the hippocampus model as presented by [161]. **a)** The schematic representation of the model as three interacting subpopulations. The excitatory interactions are represented by a plus sign (+) and the inhibitory by a minus sign (-). **b)** The block diagram of the model. **c)** Impulse response of the synaptic transmission (h) blocks.

2.1.1 General Architecture

The general architecture of the model is provided in Figure 47 (adapted from [161]). As illustrated, it is built of three interacting subpopulations: one pyramidal cell population, and two interneuron populations (both inhibitory, but mediating GABAergic currents with different – slow and fast - kinetics). Each of these populations is described by the two transfer functions introduced in Part 1 chapter 3 section 3.1.2, the input function $h(t)$ and the sigmoidal output function $S(v)$. This system can be described by a set of ten nonlinear first order differential equations (see [161] for details). In this chapter, a real animal model of MTLE is used to include HPD generation to this well-established mesoscopic model of the CA1 region.

3 AN EXPERIMENTAL MODEL OF MESIO-TEMPORAL LOBE EPILEPSY

Animal research has long contributed to the scientific and medical advances we witnessed during the last century, and continues to assist the comprehension and control of the dynamics of diseases nowadays. Most often, this scientific practice is guided by strict ethical frameworks aimed at decreasing unnecessary animal sufferings as well as limiting unnecessary experimentations. In France, the first law code of animal experimentation was introduced in 1976 defining the animal as a “*sensible being capable of feeling pain*”. In 1986, the European Union's Directive 86/609/EEC established a common European chart of animal research regulations. This chart was reviewed and updated in 2013 following the new European Directive 2010/63/UE. From then on, all new experimental protocols/procedures have to be submitted to a regional ethical comity then to a national ethical comity before being approved.

3.1 KAINATE MODEL OF MESIO-TEMPORAL LOBE EPILEPSY

In view of its proved resemblance to human MTLE with hippocampal sclerosis, the kainate mouse model [246] was used in this study to model realistic epileptic hippocampal dynamics and consequently study the effects of DC hippocampal DBS on these dynamics.

3.1.1 MODEL DESCRIPTION

Kainic acid (KA) is a natural chemical first isolated from seaweed (*Digenea simplex*) in Japan back in 1953 [247]. KA is a natural agonist of ionotropic AMPA (α -amino-3-hydroxy-5-methyl-4-isoxazolepropionic acid) and kainate receptors (KAR), the latter discovered later in 1976 [248]. These two types of synaptic receptors constitute along with NMDA (N-Methyl-D-aspartic acid) and metabotropic glutamate receptors the four types of glutamatergic synaptic receptors of the central nervous system. Being an agonist of two main glutamatergic receptors, KA presents an excitatory effect on neuronal function and was

among the first chemoconvulsants used to create rodent models of MTLE. KA is administered systematically or through intracerebral perfusion to incur sustained depolarization in the brain.

The animal model used in this study was first described by Suzuki and his colleagues in 1995 [246]. The actual experimental protocol consisted of the unilateral injection of a small quantity of Kainic acid directly into the dorsal hippocampus of an adult mouse during a stereotactic surgical procedure. Following kainate administration and after awakening from anesthesia, the mice experience a status epilepticus that ends spontaneously after several hours. In most cases, the animal regains a normal behavior. However, over the 3 weeks following the injection, KA induces a set of histological and electrographic alterations in the injected hippocampus. Histologically, KA causes a gradual pattern of cell loss and synaptic reorganization prominent with the hippocampal sclerosis of MTLE patients (see [249] for details on histological modifications).

Concerning the electrographic changes in hippocampal activity, a clear shift towards excessive excitability is evidenced [250, 251]. Typical epileptiform discharges (spike-wave and polyspike-wave discharges) start appearing in the recorded iEEG. These discharges present a sporadic aspect at the beginning of the epileptogenesis (first two weeks after injection) and evolve into epileptiform bursts of high frequency spikes and sharp waves by the end of the third week. These epileptiform discharges, usually termed hippocampal paroxysmal discharges (HPDs), get more frequent throughout epileptogenesis [250].

3.1.2 HIPPOCAMPAL PAROXYSMAL DISCHARGES: SPECIFIC BIOMARKERS OF EPILEPTOGENICITY

A recent study of the intra-hippocampal kainate model classified the epileptogenesis process into six stages depending on certain features of the recorded hippocampal discharges [252]. The illustration published in [252] is presented in Figure 48. In brief, after the KA intra-hippocampal injection and at the end of the subsequent status epilepticus, the activity of the injected hippocampus will change into a chronic epileptiform activity in the three weeks (on average) that follow KA injection. During the first stage of this evolution, no particular epileptiform activity is detected in the recorded iEEG. The arrival of sporadically distributed spikes marks stage 2. When stage 3 is attained, these spikes get organized into brief bursts of spike discharges lasting from 6 to 11s. Then, at stage 4, these discharges start lasting longer (12 to 17s). Finally, the chronic form of epilepsy is attained by stage 5. At this stage, the aforementioned hippocampal discharges last more than 18s. These discharges presenting electrographic seizures are termed **Hippocampal Paroxysmal Discharges** (HPDs). And finally, stage 6 is attained when these HPDs last longer than 40s and are thereby generalized to the cerebral cortex provoking convulsive tonico-clonic seizures.

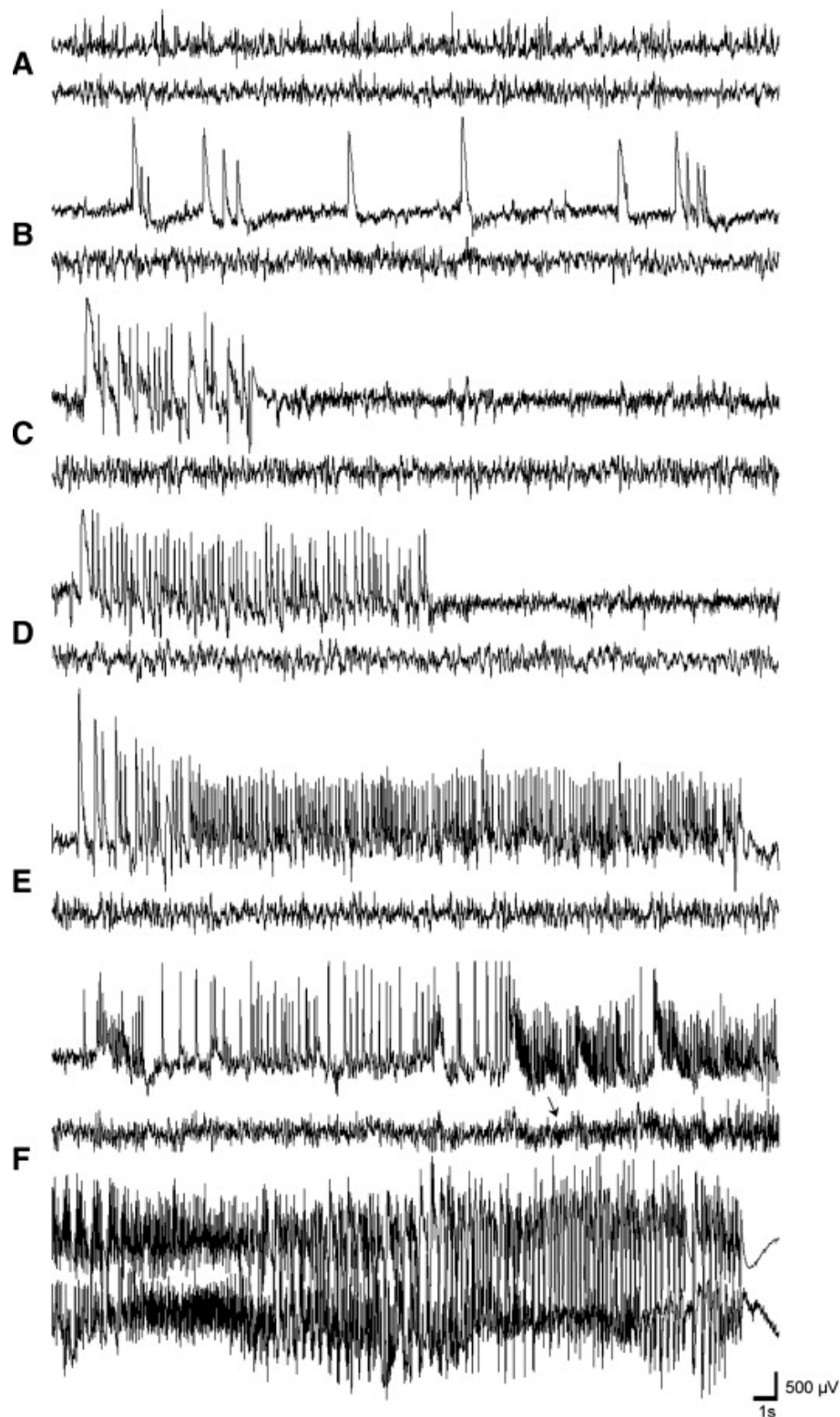


Figure 48. The different electrographic signatures of the different stages of epileptogenesis defined by Heinrich and his colleagues in [252]. EEGs were recorded in injected mice during the first 16 days of epileptogenesis. For each panel, the upper trace represents the EEG recorded in the injected hippocampus and the lower one corresponds to the EEG recorded between the left and right frontoparietal cortical electrodes. (A) Stage 1: Low-voltage background activity in absence of theta oscillations and epileptiform discharges. (B) Stage 2: Sporadic hippocampal spikes. (C) Stage 3: Short hippocampal spike discharges of duration 6 to 11s. (D) Stage 4: Long hippocampal discharges of duration 12 to 17s. (E) Stage 5: Appearing of recurrent hippocampal electrographic seizures of duration superior to 18s. These seizures are defined as hippocampal paroxysmal discharges. (F) Stage 6: The HPDs recorded in stage 5 are prolonged and can last up to 40s. These discharges can propagate to the cerebral cortex. Adapted from [252].

Noteworthy, a more recent study, published by our team, reported that the morphology of sporadic isolated spikes changes with the progression of the disease. An electrophysiological marker of epileptogenesis is proposed [30] as based on the amplitude of the spike and on the area of the negative wave.

In this work, any epileptiform dynamic ranging from the isolated sporadic spike to HPDs will be considered as a marker of the epileptic feature in the diseased hippocampus. At this stage, any stimulation-induced change in the occurrence/characteristics of such events will be considered as potentially interesting.

3.2 EXPERIMENTAL KAINATE PROTOCOL AND SIGNAL ACQUISITION

All the experiments described in this part were conducted on 80 ± 10 days old C57BL/6J (B6) adult male mice housed in individual cages with food and water ad libitum and kept in a $21 \pm 1^\circ\text{C}$ and 12-h light/dark cycle conditions. All animal procedures were conducted in accordance with the European Communities Council Directive of 24 November 1986 (86/609/EEC).

Under general anesthesia conditions (chloral hydrate 400 ml/kg i.p.), the animals undergo intra-hippocampal kainate injection (50 nl of a 20 mM solution of kainic acid (KA), or the equivalent of 20mM of KA) into the right dorsal hippocampus (AP = -2 mm ; ML = -1,5 mm ; DV = -2 mm with bregma as reference according to Franklin & Paxinos atlas). After intra-hippocampal KA injection, a bipolar electrode is inserted into the injected hippocampus just underneath the injection site (AP = -2 mm ; ML = -1,5 mm ; DV = -1,9 mm). Another bipolar electrode is implanted in the contralateral hippocampus and a supplementary monopolar electrode is implanted as a reference. This stereotaxic surgical procedure was performed by the research assistant of the animal experimentation (G. Dieuset) of our laboratory (LTSI).

After three weeks of epileptogenesis, the animals undergo their first iEEG video recording using a video-EEG clinical monitoring system (*Deltamed*). The recorded signals were sampled at 2 kHz, and hardware-filtered by a high-pass filter (0.16 Hz cutoff frequency) integrated into the signal acquisition system. Only animals presenting hippocampal paroxysmal discharges at day 21 after the KA injection were considered for the rest of the stimulation experimental validation protocol described in the next chapter. The recorded baseline LFP signals were then used to model hippocampal discharges in the model.

4 METHODS FOR EPILEPTIC SIGNAL ANALYSIS

Distinct types of epileptic events were observed in the iEEG signals recorded in animals (variable duration spike bursts and hippocampal paroxysmal discharges, isolated single spikes and sharp waves) in short periods of time (1-2 seconds; see Figure 49). Although these different events may be evoked by distinct cellular mechanisms, all of them were considered for quantifying the epileptic character of the recorded signal.

4.1 IEEG SIGNAL QUANTIFICATION

In order to determine the level of excitability of epileptogenic zone (injected hippocampus) as function of time, an iEEG signal quantification procedure was defined. This quantification procedure consisted of three steps:

1. Detecting the occurrence of these epileptic events
2. Defining the relevant features (duration/occurrence/intensity/energy...) that characterize these events
3. Studying the evolution of these features in response to stimulation

4.1.1 DETECTION OF HPDs USING THE PAGE-HINKLEY METHOD

In the literature, many detection algorithms were previously described and used in the context of automated seizure or spike detection (see [253] for review). These algorithms can be categorized into more than 6 groups (methods based on morphological patterns, independent component analysis, or wavelet decompositions, on clustering, or on artificial neural networks,...). Our choice took into account the brutal onset of the encountered epileptic events by a (poly)spike or a sharp wave. For this reason, rupture detection methods were considered. Moreover, given the fact that the Page-Hinkley [254] algorithm was already implemented, tested, and optimized for spike detection in our lab, this choice reduced the algorithm implementation time for the purpose of this work. Consequently, the Page-Hinkley algorithm was used for the detection of the onset of the recorded epileptiform events.

The algorithm. The Page-Hinkley algorithm is a sequential analysis technique (statistical test) initially designed for monitoring change detection [255]. In the following, the Page-Hinkley test (PHT) is used to detect changes in the average of a temporal sequence $\vartheta(t), t \in \{1, \dots, n\}$ representing the LFP recorded in the injected hippocampus.

Consider a sequence $\varepsilon(t), t \in \{1, \dots, n\}$ of n mutually independent random variables following the same normal distribution of mean $\mu = 0$. Then $\vartheta(t), t \in \{1, \dots, n\}$ can be tested against the null hypothesis:

$$H_0 : \vartheta(t) = \mu_0 + \varepsilon(t), t \in \{1, \dots, n\}$$

In this case, H_0 corresponds to the absence of epileptic transients. Whenever H_0 is rejected at instant r , a rupture is detected, and the hypothesis $H_{1,r}$ is retained.

$$H_{1,r} = \begin{cases} \vartheta(t) = \mu_0 + \varepsilon(t), t \in \{1, \dots, r-1\} \\ \vartheta(t) = \mu_1 + \varepsilon(t), t \in \{r, \dots, n\} \end{cases} \quad H_1 = \bigcup_{r=2, \dots, n} H_{1,r}$$

where μ_0 and μ_1 ($\mu_0 < \mu_1$) are the mean values of the corresponding distributions to the absence/ occurrence of a rupture at instant r . While μ_0 and μ_1 , and therefore the average rupture, $\nu = \mu_1 - \mu_0$, for the detection of an epileptic event can be determined (optimized) on a learning dataset *a priori*, r is the only unknown variable to be determined online. In such cases, the maximum likelihood ratio (generally denoted by the Greek letter Λ) is usually employed. Λ is generally expressed as follows:

$$\Lambda = \text{Ln} \left(\frac{\text{likelihood for } H_1}{\text{likelihood for } H_0} \right) = \text{Ln} \left(\frac{L(H_1)}{L(H_0)} \right)$$

In this case, Λ can be expressed as follows:

$$\Lambda_n(r) = \text{Ln} \left(\frac{\prod_{t=1}^{r-1} P_0(\vartheta(t)) \cdot \prod_{t=r}^n P_1(\vartheta(t))}{\prod_{t=1}^n P_0(\vartheta(t))} \right) = \text{Ln} \left(\frac{\prod_{t=r}^n P_1(\vartheta(t))}{\prod_{t=r}^n P_0(\vartheta(t))} \right)$$

where P_0 and P_1 are the probability density distributions of the random variables $\vartheta(t)$, $t \in \{1, \dots, n\}$ in the absence/presence of a rupture. P_0 corresponds to a normal distribution of mean μ_0 ($N(\mu_0, \sigma)$). P_1 corresponds to a normal distribution of mean μ_1 ($N(\mu_1, \sigma)$). Then $\Lambda_n(r)$ can be simply reduced to:

$$\Lambda_n(r) = \frac{\mu_1 - \mu_0}{\sigma^2} \sum_{t=r}^n (\vartheta(t) - \frac{\mu_1 + \mu_0}{2}) = \frac{1}{\sigma^2} S_r^n(\mu_0, \nu)$$

where

$$S_r^n(\mu_0, \nu) = \nu \sum_{t=r}^n \left(\vartheta(t) - \mu_0 - \frac{\nu}{2} \right)$$

Then, maximizing the likelihood ratio $\Lambda_n(r)$ corresponds to maximizing $S_r^n(\mu_0, \nu)$ in order to estimate the instant of rupture:

$$\hat{r} = \underset{2 \leq r \leq n}{\text{argmax}} S_r^n(\mu_0, \nu)$$

Whenever the detected maximum exceeds a fixed threshold s at an instant r , a rupture is declared at this instant. This can be formulated as follows:

$$\Lambda_n(\hat{r}) = \max_{2 \leq r \leq n} S_r^n(\mu_0, \nu) \underset{H_{1,r}}{\overset{H_0}{\leq}} s$$

An equivalent form of the detector can also be expressed as

$$\Lambda_n(\hat{r}) = S_1^n(\mu_0, \nu) - \min_{2 \leq r \leq n} S_1^r(\mu_0, \nu) \underset{H_1}{\overset{H_0}{\leq}} s$$

Note that whenever a rupture is declared, the minimum of $S_1^r(\mu_0, \nu)$ should be recalculated before an upcoming detection. The mean μ_0 is generally estimated online as the mean of the recorded signal over a sliding window of fixed duration or over a window of incremental duration ($t \in \{1, \dots, n\}$). The average rupture amplitude ν is usually fixed as the minimal amplitude of observed rupture events while s is usually optimized to minimize false alarms. The performance of the detector largely depends on the choice of parameters ν and s .

This algorithm is already implemented in our team's EEG analysis software called **Amadeus**. It accounts for a refractory period after the detection of a rupture, i.e. no further detection is allowed in a user-defined time-window after each rupture. Another feature integrated to the detector is a preprocessing step. It aims at increasing the contrast between transient sharp events and background activity through band-pass filtering the signal ($20 < f_{\text{cutoff}} < 80$ Hz). This pass band allows the filtering of much of the background activity while reinforcing the energy of the epileptiform events. Furthermore, the detector's parameters have been previously optimized for the detection of spikes and discharges in clinical EEG [254]. The optimal parameters published in [256] are presented in Table 4 alongside with the parameters that were used in this study. Note that these optimal parameters (Table 4 – second column) were tuned patient-wise depending on the morphology of the detected events [256].

The slight detector parameter tuning (Table 4 – 3rd column) allowed the detection of basically all epileptic events observed in the signals (see Figure 50 for an illustration). Nevertheless, all automatically detected events were then manually verified for non-detections and false alarms (e.g. stimulation artifacts). Periods of amplitude saturation (due to the animal's active exploration of the cage) were excluded a priori.

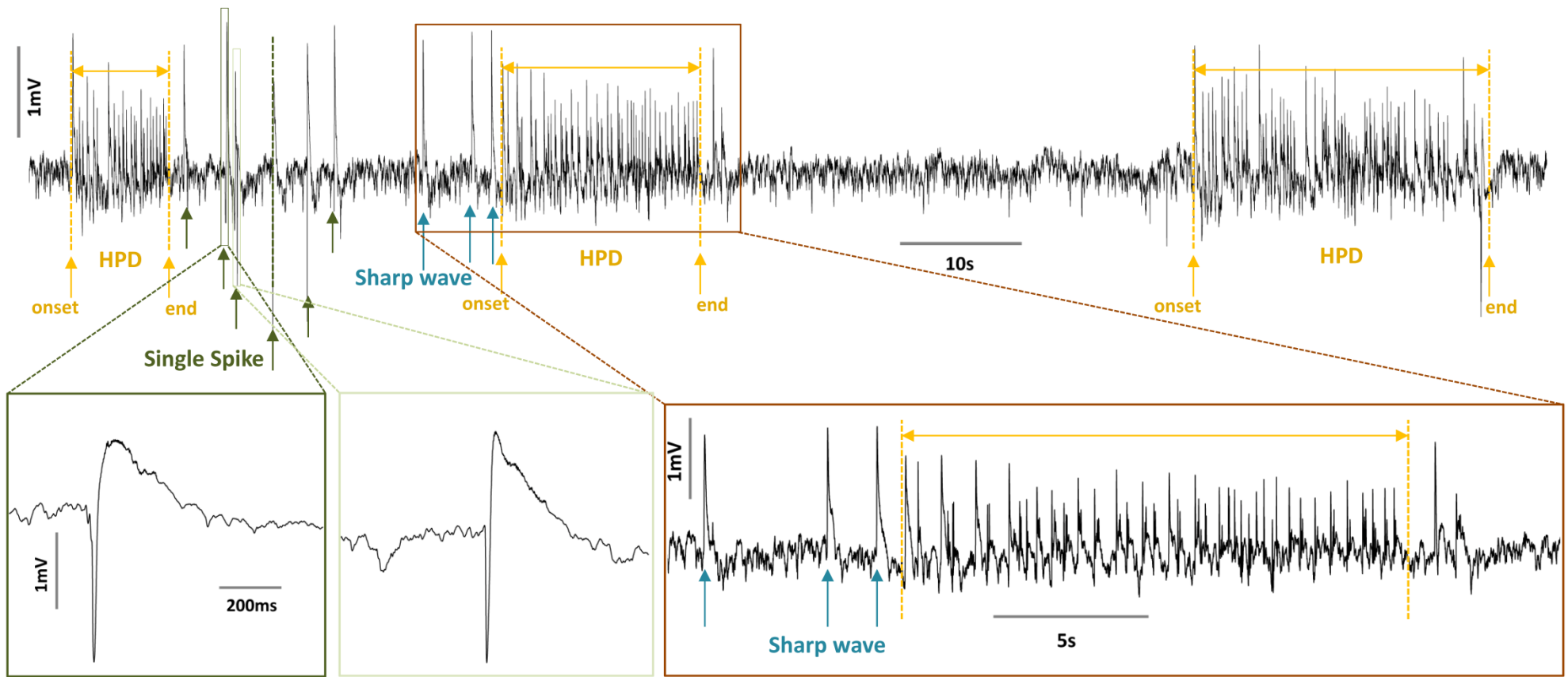


Figure 49. Distinct epileptic events observed in the iEEG of the recorded animals. Upper panel, an example of a 120s-iEEG signal recorded from the injected hippocampus at day 27 (after injection). Hippocampal paroxysmal discharges/spike bursts (yellow arrows), single spikes (green arrows), and sharp waves (blue arrows) can occur in the interval of a minute. Lower panel, zoom on major epileptic events, from left to right, two examples of single spikes and an example of an HPD preceded by three sharp waves. Although that these epileptic events may possibly pass through distinct cellular mechanisms, they were considered equally for quantifying the epileptic character of the recorded signals.

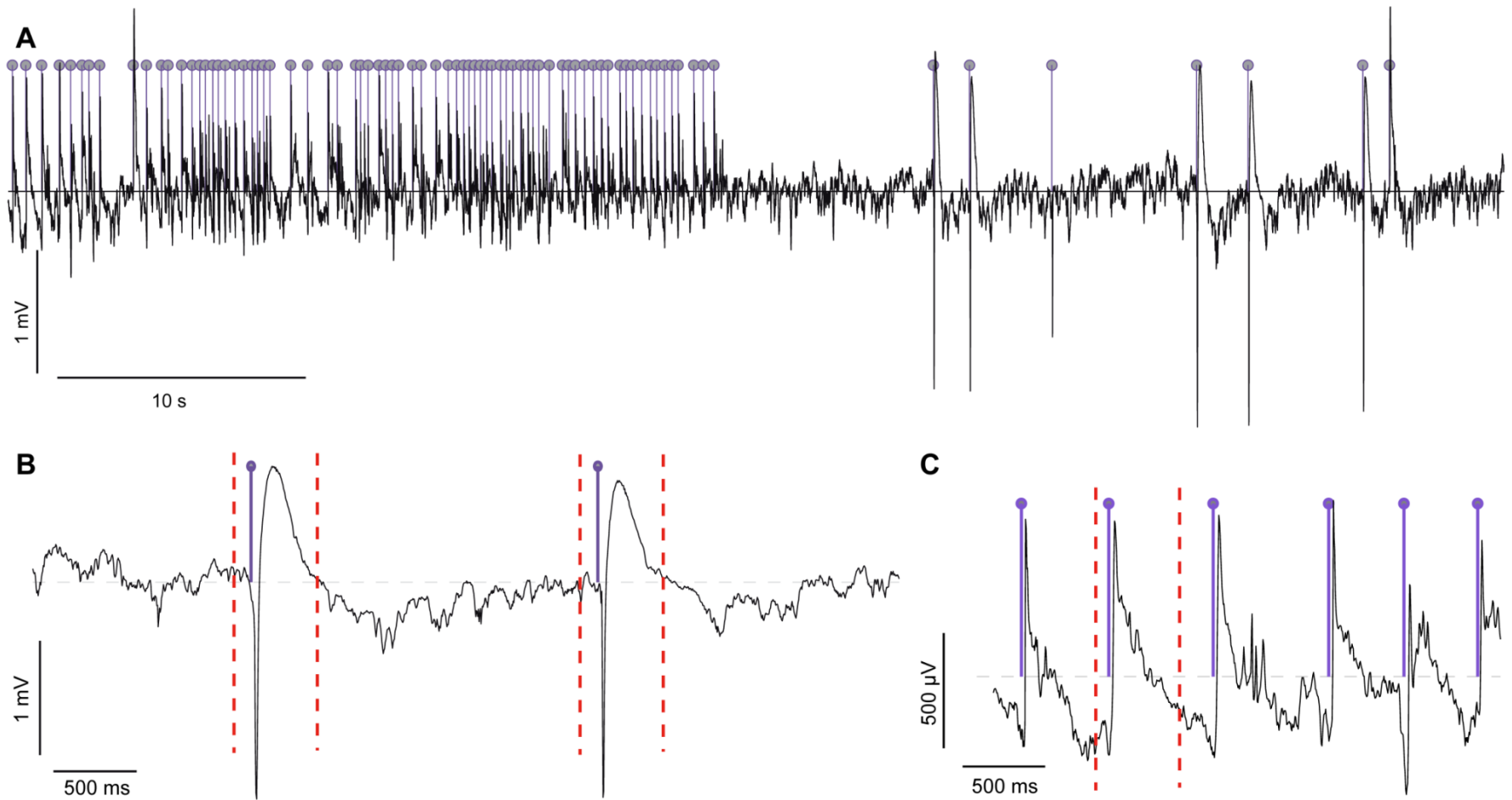


Figure 50. The Page-Hinkley Test. **(A)** A real segment of a non-preprocessed iEEG signal recorded from the injected hippocampus (black). Violet stem plot represents the events detected by the Page-Hinkley algorithm. These correspond to the peaks detected in the epileptic events (isolated single spikes, HPDs, sharp waves, etc.). Further analysis of the occurrence of these peaks allowed the automatic detection of the epileptic event's onset/end, whether it is a discharge or an isolated event. **(B-C)** Axiom (a): an epileptic peak indicates an ongoing epileptic event starting at least 0.1 s ahead of, and lasting at least 0.4 s after, the detected rupture. The dotted lines indicate the time slots attributed to each rupture. **(B)** Case of a paroxysmal spike followed by a negative wave. **(C)** Case of a peak in a continuous discharge.

	Optimal Parameters [256]	Tuned Parameters
Number of pass band filters	3	3
Pass band	20 – 40 Hz	20 – 40 Hz
ν	$10 \cdot \mu_0$	30
s	$20 \cdot \mu_0$	30
Refractory period	0.1 s	0.2 s

Table 4. List of parameters provided and tested in [256] for the detection of clinical epileptic events, as well as the parameters slightly modified for enhancing the detection of epileptic events in experimental iEEG recordings.

As the Page-Hinkley test allowed the detection of the brutal onset (peak) of every epileptic discharge, further processing was needed to detect the onset/end of conventional epileptic events (discharges, spikes, sharp waves, etc.). The event detection algorithm was then built on the following axioms:

- a. Each detected peak reveals an ongoing epileptic event starting at least 0.1 s before and lasting 0.4 s after the detected rupture.
- b. Two consecutive peaks, p_1 and p_2 , are said to belong to the same discharge if their hypothetical time slots (onset-end) overlap or are separated by less than 0.5 s. This is equivalent to Heinrich’s definition for the classification of hippocampal discharges [252], suggesting that if two spikes are separated by less than 1s they belong to the same discharge.
- c. If b. is true, then the detected time slots of p_1 and p_2 are merged into a single slot $[t_{\text{onset}_{p_1}} t_{\text{end}_{p_2}}]$.

Running this algorithm (see pseudo code Table 5) on the recorded LFP signals allowed the detection of the time slots corresponding to epileptic dynamics (all types included).

5 MODEL ADAPTATION FOR THE GENERATION OF HPDs

While the model’s parameters can be adjusted to produce sustained spike discharges or background activity using the activity maps provided in [161], they had to be modified such that the model output dynamically alternates background activity and sustained hippocampal discharges as observed in real LFP signals as illustrated in Figure 49. Consequently, an extension was proposed.

5.1 EXPERIMENTALLY IDENTIFYING THE DURATION AND FREQUENCY OF OCCURRENCE OF HPDs

In order to model the occurrence of HPDs, herein considered of all possible durations (> 0.5 s), two supposedly independent random variables were defined (see Figure 51-A):

- (1) ΔHPD : representing the duration of detected HPDs.
- (2) ΔBKG : representing the inter-HPD intervals as measured between consecutive HPDs.

Consequently, in order to identify the statistical distributions followed by these two random variables, measures of ΔHPD and ΔBKG were estimated from real iEEG recordings, over sufficiently long durations (~ 2 hours) for a given animal. The histograms of the two RV could be plotted (see Figure 51-B and C). At first sight, the identified histograms evoked a possible exponential distribution. However, given that neither the HPD duration nor the inter-HPD duration can be null, a gamma distribution was privileged. The probability density function $f(x, a, b)$ of a random variable X following a gamma distribution is of the form

$$X \sim \Gamma(a, b) \quad f(x, a, b) = \frac{b^a x^{a-1} e^{-bx}}{(a-1)!}$$

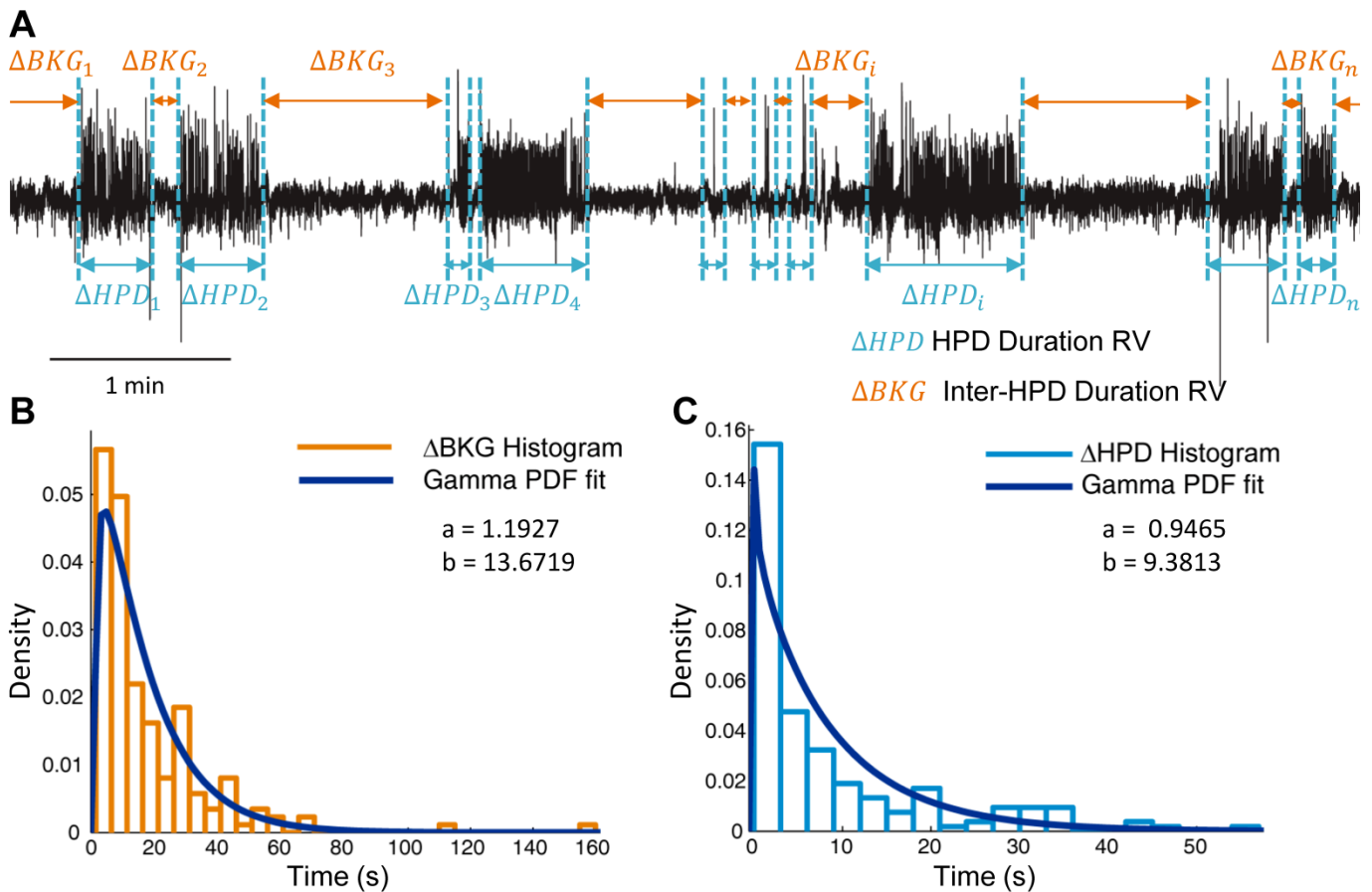


Figure 51. The experimental identification of the statistical laws of ΔHPD and ΔBKG . **(A)** Illustration of different values of the two random variables ΔHPD and ΔBKG . **(B)** The histogram of ΔBKG fitted to a gamma probability density distribution (PDF). **(C)** The histogram of ΔHPD fitted to a gamma probability density distribution (PDF). The fitted distributions' parameters are given in the illustration.

Pseudo Code 1. Epileptic Event Delimitation over a sliding window

Input parameters: the LFP signal $\vartheta(t)$, the peak tag table $\tau_p(t)$ given by Page-Hinkley, duration of sliding window t_{win} , sampling frequency f_s - $\text{length}(LFP) = t_{win} = 60$ s for simulated signals

Output parameters: the event tag table $\tau_{\Delta ED}(t)$ indicating the time slots of detected discharges in t_{win} intervals

```
for j = 0: twin: length( $\vartheta/f_s$ ) - twin
    lower_index = find( $\tau_p > j$ );
    upper_index = find( $\tau_p < j + t_{win}$ );
     $\tau_{pj} = \tau_p(\text{lower\_index} : \text{upper\_index})$ ;
%% Determine the time slots of detected peaks
for i = 1:length( $\tau_{pj}$ )
     $\tau_{\Delta p}(i, 1) = \tau_{pj}(t) - 0.1$ 
     $\tau_{\Delta p}(i, 2) = \tau_{pj}(t) + 0.4$ 
end
%% Determine continuous epileptic events
for i = 1:length( $\tau_{pj}$ )
     $\tau_{\Delta p}(i, 1) = \tau_{pj}(t) - 0.1$ 
     $\tau_{\Delta p}(i, 2) = \tau_{pj}(t) + 0.4$ 
end
detect =  $\tau_{\Delta p}(2: \text{end}, 1) - \tau_{\Delta p}(1: \text{end} - 1, 2)$ ; %% Determine the inter slot duration
decision = detect(:) < 0.5; %% Compare the inter slot duration to 0.5
%% Continuous discharges are then detected by sequences of ones "1"
make_decision = decision(1: end - 1) - decision(2: end);
index_discharge_onset = find(make_decision == -1)+1;
index_discharge_end = find(make_decision == 1)+1;
 $\tau_{\Delta ED, j} = \tau_{\Delta p}$ ; %% Initialize the table of epileptic discharge tags
if index_discharge_onset(1) > index_discharge_end(1) %% The first discharge starts at the first
detected peak
    index_discharge_onset = [1; index_discharge_onset];
end
if length(index_discharge_onset) > length(index_discharge_end) %% The last discharge includes the
last peak
    index_discharge_end = [index_discharge_end; length( $\tau_{\Delta p}$ )];
end
for i = length(index_discharge_end):-1:1
     $\tau_{\Delta ED, j}(\text{index\_discharge\_onset}(i), 2) = \tau_{\Delta p}(\text{index\_discharge\_end}(i), 2)$ ; %% Combine continuous peaks
     $\tau_{\Delta ED, j}(\text{index\_discharge\_onset}(i)+1: \text{index\_discharge\_end}(i)) = []$ ; %% Delete the redundant peaks
end
 $\tau_{\Delta ED}(:, :, \frac{j}{t_{win}} + 1) = \tau_{\Delta ED, j}$ ;
 $\tau_{pjj}(:, :, \frac{j}{t_{win}} + 1) = \tau_{pj}$ ;
End
```

Table 5. Pseudo code for defining the onset and end of isolated (spikes and sharp waves)/continuous epileptic events (discharges). The implementation was done in Matlab®.

Note that, having chosen a gamma distribution, a more or less exponential distribution has not been excluded ($a=1$). Parameter identification has been performed using the Statistics toolbox in Matlab® (GUI fitting tool dfittoll). Moreover, the choice of the gamma function to fit the distribution of the duration of ictal and interictal events has already been reported in [257]. The identified parameters and the fitted probability density functions are illustrated in Figure 51.

5.2 IMPLEMENTING DYNAMICAL CHANGES OF HPDS IN THE MODEL

Early in 1984, Johnston and Brown [258] showed that epileptiform burst discharges in the hippocampus are rather network driven than endogenous. They claimed that network-driven paroxysmal depolarizing shifts (PSDs) underlie these events. Consequently, a non-endogenous implementation of HPD generation is herein proposed.

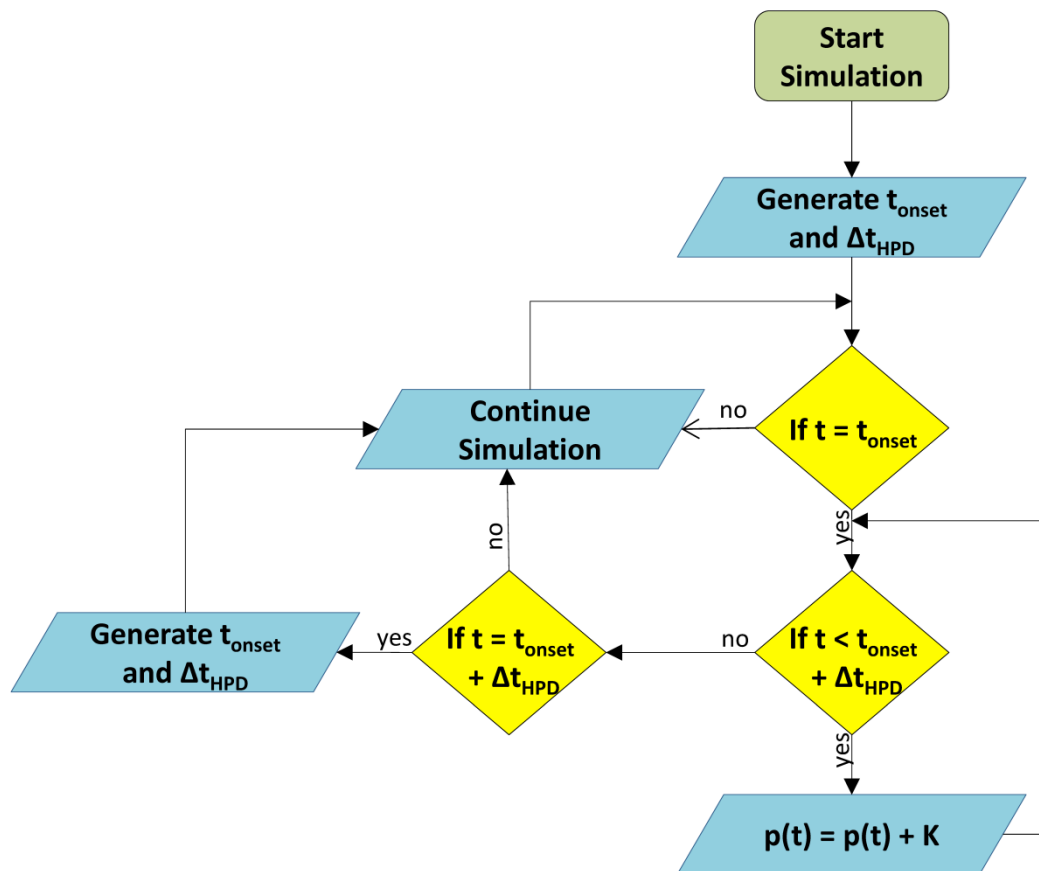


Figure 52. Flowchart of HPD simulation diagram. Adding K to $p(t)$ causes a brutal augmentation of the mean of the noise input to the hippocampal principal cells with a duration Δt_{HPD} . This means an increase in the system's excitability for Δt_{HPD} . An HPD is simulated during this phase.

Given that the previously introduced hippocampus model represents uniquely the CA1 region, a network-driven depolarization of the pyramidal cells of CA1 implied the implementation of an external input PSD signal arriving at the input function (presynaptic terminals) of the pyramidal subpopulation. Then, this external PSD signal was added to the input noise $p(t)$ arriving at the pyramidal subpopulation (see Figure 47) following the algorithm illustrated in Figure 52.

This algorithm, implemented in Simulink®, can be described as follows:

- (1) Initialization: At $t = 0$, generate a value for $\Delta\mathbf{HPD}$ and another for $\Delta\mathbf{BKG}$.
- (2) Dynamically simulate the model till $t = \Delta\mathbf{BKG}$. Between $t = \Delta\mathbf{BKG}$ and $t = \Delta\mathbf{HPD} + \Delta\mathbf{BKG}$, a fixed step K is added to the nonspecific noise $p(t)$.
- (3) The end of the step K triggers the random generator in order to generate the next values of $\Delta\mathbf{HPD}$ and $\Delta\mathbf{BKG}$.
- (4) Again, between $t = t_0 + \Delta\mathbf{BKG}$ and $t = t_0 + \Delta\mathbf{HPD} + \Delta\mathbf{BKG}$, a fixed step K is added to the nonspecific noise $p(t)$. t_0 designates the instant at which the last values of $\Delta\mathbf{HPD}$ and $\Delta\mathbf{BKG}$ were generated.
- (5) Back to step 3
- (6) The simulation can be either manually ended by the user or automatically by Simulink if a simulation time is specified

The sudden arrival of K can be assimilated to the closing and opening of an automatic switch commanded by two random gamma generators, one for generating a random closing time and one for the switch opening time (Figure 53). If the model parameters are tuned such that the model generates isolated spikes from time to time (critical zone of functioning), then an HPD will be generated every time K is added to $p(t)$. This can be done using the activity maps provided with the model implementation by the authors [161]. This implementation takes into consideration the epileptogenicity (increase in excitability) of the injected hippocampus as well as the exogenous cause of paroxysmal depolarization shifts.

6 IMPLEMENTING THE STIMULATION INPUTS

Given the polarizing effects of DC stimulation on the targeted structure (see Chapter 6), stimulation inputs were directly summed to the mean transmembrane potential of the impacted subpopulations. As illustrated in Figure 53, this corresponds to summing stimulation inputs with the mean PSPs just before the sigmoidal output function $S(v)$ of the stimulated subpopulation. Consequently, the subpopulation will be depolarized if a positive long duration pulse is added to its mean transmembrane potential. Conversely, it will be hyperpolarized by a negative long duration pulse. Stimulation inputs were then incorporated in the model at the level of pyramidal cell population as well as the two

inhibitory neural populations. Noteworthy, the same stimulation principle was employed in thalamic DBS in Part 1.

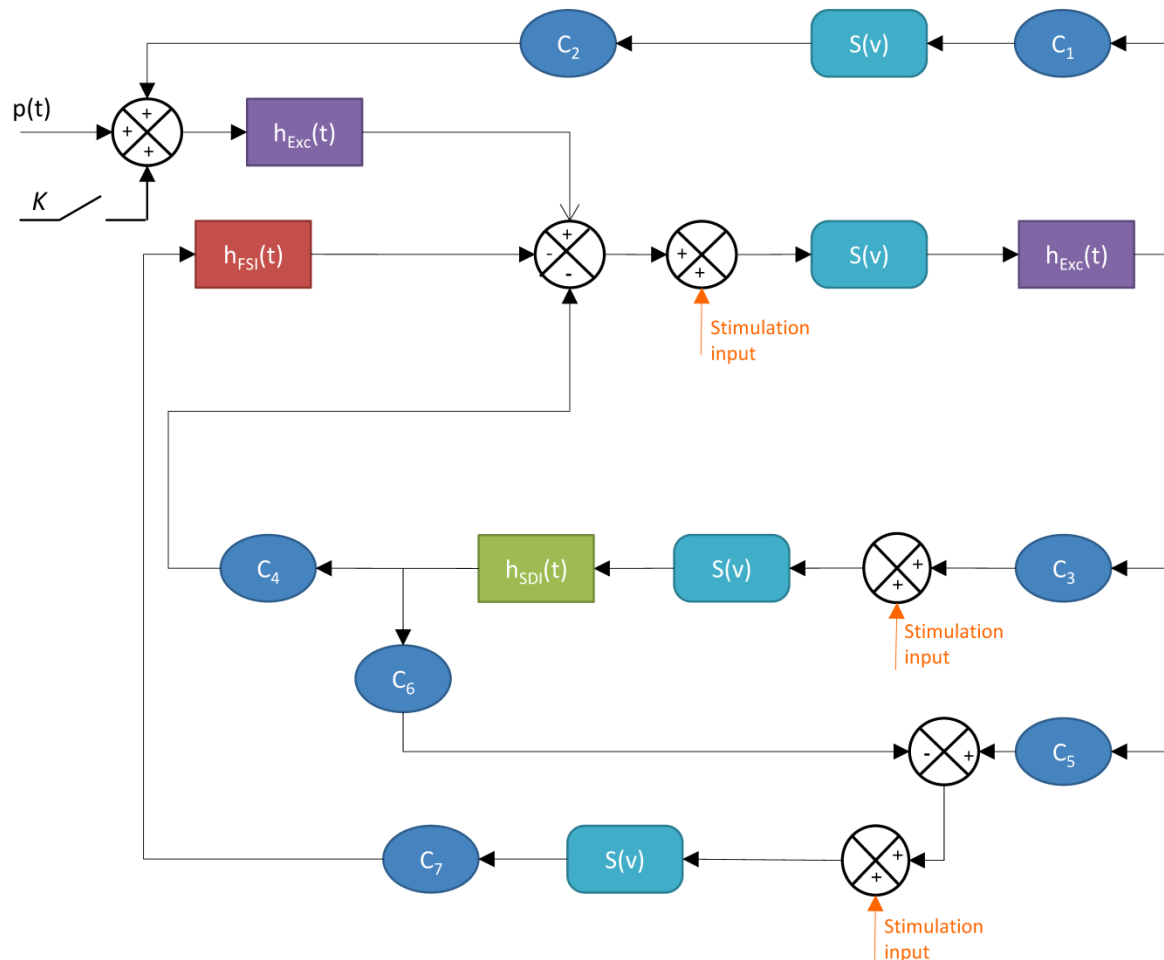


Figure 53. Block diagram of the model indicating the emplacement of stimulation inputs before the sigmoidal function of each population, as well as that of the PSD (paroxysmal depolarization shift) input. The PSD input is schematically represented as a switch K .

However, a more explicit implementation of the electrode-electrolyte interface has been provided for this part. This implementation accounted for the charge accumulation at the interface; it also provided a compensation for possible short-term plastic effects following stimulation. Figure 54 provides a schematic representation of the implemented interface. A faradaic impedance Z_f in parallel with a double layer capacitance C_{dl} model the interface between the cerebral fluid and the implanted electrode. In series with this interface, the solution resistance R_s , also termed the access resistance, represents the resistance of the cerebral fluid/tissue between the two tips of the bipolar electrode. This implementation is in line with the literature of electrode models and stimulation protocols (see [153] for review).

Determining the values of Z_f and C_{dl} depends largely on the chemical composition of the used electrodes. In [153], the authors classify iEEG electrodes into two categories; ideally polarizable versus ideally non-polarizable electrodes. For ideally polarizable electrodes, the value of the faradaic impedance Z_f is infinite. Therefore, such an electrode can be modeled as a pure capacitor in series with the solution resistance R_s . In this case, no electron transfer occurs during an eventual stimulation pulse. Therefore, stimulation is carried out uniquely through capacitive action (see Figure 55 (a) adapted from [153]). Conversely, for an ideally non-polarizable electrode, the faradaic impedance has zero resistance. Therefore, only the solution resistance appears in the model, as current flows readily through faradaic reactions (see Figure 55 (a)). The stimulation current is then accommodated through electron flow (charge injection), charge accumulation as well as metal deposits may form in the stimulated site. This is a desired situation for a recording or reference electrode, so that the electrode potential remains near equilibrium and is not perturbed upon the flow of nearby stimulation currents.

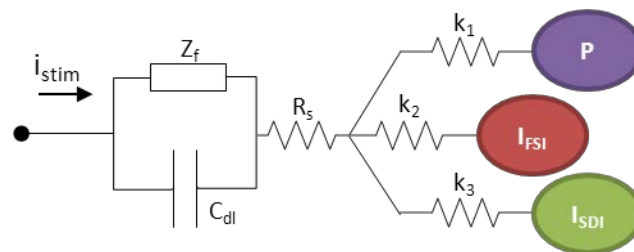


Figure 54. The implementation of the electrode-electrolyte interface in the model. Three resistive components k_1 , k_2 , and k_3 model the distinct stimulation impact on the three subpopulations. Z_f and C_{dl} were tuned manually.

However, ideal electrodes do not exist in real life. So, real electrodes can either be highly polarizable/non-polarizable. A highly polarizable electrode is one that can accommodate a large amount of injected charge on the double layer before Faradaic reactions are initiated, and thus is well-adapted to be used as a stimulation electrode. A highly non-polarizable electrode has a very small faradaic resistance Z_f , and may thereby be irreversibly corroded by the flow of a long-duration stimulation current. Highly polarizable electrodes are characterized by a low exchange current density ($\sim 10^{-9}$ A/cm²), conversely to highly non-polarizable electrodes that are characterized by a large exchange current density ($\sim 10^{-3}$ A/cm²). In conclusion, and according to [153], all real electrodes may be modeled with a finite faradaic impedance Z_f in parallel with a capacitor C_{dl} as shown in Figure 55 (b).

The recording electrodes used in the experimental KA model are made of stainless steel. Actually, stainless steel electrodes are widely used in experimental neuroscience given their inoxidable character when placed in aqueous solutions. The AC-impedance characteristics of stainless steel electrodes are also well studied in function of the frequency of the stimulation current [6-9].

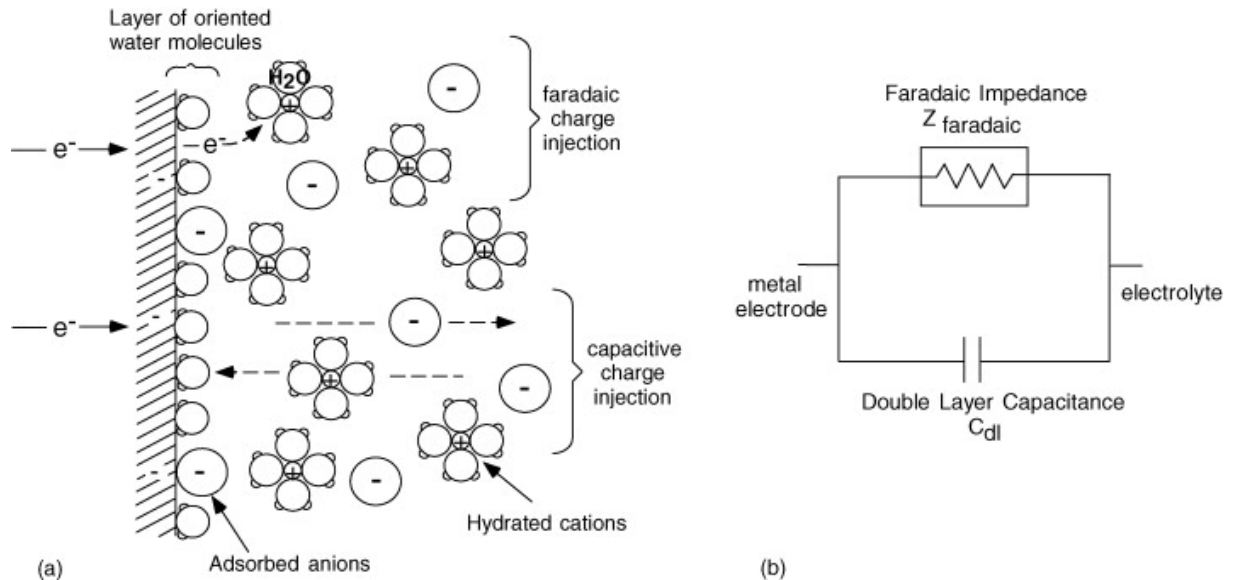


Figure 55. Modeling the electrode-electrolyte solution. (a) Two possible mechanisms of charge injection: faradaic vs. capacitive. (b) General model of a real metal electrode in aqueous solution. Adapted from [153].

For tested frequency ranges of stimulation current (e.g. 0.01 Hz – 1000 kHz or 1 Hz – 10 kHz), the measured impedance (Z_f and C_{dl}) always decreases linearly as a function of the stimulation frequency. At low frequencies, the magnitude of Z_f seems to increase as the intensity of the stimulation current decreases. Similar results are reported for the capacitance of C_{dl} [6, 8]. In an aqueous NaCl solution, the double layer capacitance C_{dl} of a stainless steel electrode is of the order of 10 – 20 mF/cm², and the magnitude Z_f is of the order of 1 M Ω /cm² at a 1 mHz stimulation frequency [6].

In the model, these values were slightly tuned in order to guarantee a compensation for a short-term effect persisting after stimulation. Z_f was tuned to 0.1 M Ω and C_{dl} was tuned to 1 mF. The time constant of RC electrode-electrolyte interface was then 100 s. Finally, considering a 2 S/m average conductivity of grey matter [259], R_s was calculated as the resistance between the two tips of the bipolar electrode each of diameter 125 μ m, and separated by 350 μ m. The retained value was then 18.15 k Ω .

Pseudo Code 2. Measuring the features of epileptic dynamics

Input parameters: the LFP signal $\vartheta(t)$, the peak tag table/ interval τ_{pjj} , duration of sliding window t_{win} , sampling frequency f_s , the event tag table $\tau_{\Delta ED}(t)$

Output parameters: features table $T_{features}$

```
for j = 1:size( $\tau_{\Delta ED}$ , 3) %% For every  $t_{win}$  minute interval
     $T_{features}(1,j) = \text{sum}(\tau_{\Delta ED}(:,2,j) - \tau_{\Delta ED}(:,1,j))$ ; %% First calculated feature, the total duration of
    discharge in the  $t_{win}$  minute interval
     $T_{features}(2,j) = \text{length}(\tau_{\Delta ED}(:,2,j))$ ; %% Second calculated feature, the total number of discharge in
    the  $t_{win}$  minute interval
     $T_{features}(3,j) = \text{length}(\tau_{pjj}(:, :, j))$ ; %% Third calculated feature, the total number of peaks in the
     $t_{win}$  minute interval
     $T_{features}(4,j) = 0$ ; %% Initialization for of fourth feature for calculating the total energy of discharge
    in the  $t_{win}$  minute interval
    for i = 1:length( $\tau_{\Delta ED}(:, :, j)$ )
         $T_{features}(4,j)$ 
            =  $T_{features}(4,j)$ 
            +  $\frac{1}{N} \sqrt{\vartheta(\tau_{\Delta ED}(i,1) * f_s : \tau_{\Delta ED}(i,2) * f_s) .* \vartheta(\tau_{\Delta ED}(i,1) * f_s : \tau_{\Delta ED}(i,2) * f_s)}$ 
            %% N is the number of samples in discharge i.
    end
end
```

Table 6. Pseudo code for measuring the epileptic features of an iEEG signal $\vartheta(t)$. The code was implemented in Matlab®.

7 COMPUTATIONAL ANALYSIS OF STIMULATION EFFECTS

Once the model was tuned for the generation of realistic HPDs similar to those observed *in vivo*, the next step was to study the effects of stimulation in function of its impact (k_1 , k_2 , and k_3) on the three stimulated subpopulations P , I_{FSI} , and I_{HDI} .

As the model was implemented in Simulink®, the used stimulation signal was delivered by a pulse generator, whose intensity and pulse duration were set to $1 \mu\text{A}$ and 50 s respectively. The choice of the intensity was deduced from an experimental study assuming that a $1 \mu\text{A}$ current intensity is the minimum required to diminish epileptiform discharges in the recorded LFP *in vitro* [35]. The model activity maps were then constructed for defined ranges of k_1 , k_2 , and k_3 . These activity maps represented the quantified epileptic features of the simulated LFP in the minute following stimulation.

7.1 QUANTIFYING EPILEPTIC FEATURES IN SIMULATED LFP SIGNALS

In the minute following the end of the simulated stimulation pulse, HPDs were detected using the pseudo code described in Table 5. Once detected, measuring the epileptic features of the simulated LFP signals in each time window ($t_{win} = 60$ s) consisted of measuring, the occurrence of epileptic dynamics, their intensity, and duration. The occurrence was measured as the number of detected discharges/peaks in the processing

window (of duration t_{win}). The duration of these events represented the lumped duration of epileptic dynamics in the same window. And finally, the intensity feature corresponded to the energy of epileptic events in this window. This can be simply expressed as

$$E_{t_{win}} = \sum_{i=1}^D \frac{1}{N(i)} \sqrt{\sum_{j=1}^{N(i)} \vartheta_j^2}$$

where D is the number of detected discharges and $N(i)$ is the number of samples of the i^{th} discharge and ϑ_j is the LFP signal components constituting the j^{th} band. The pseudo code of this algorithm is given in Table 6.

Chapter 7: Computational Results of Part 2

The computational study performed in the previous chapter gave rise to interesting observations concerning the effect of current polarity on hippocampal epileptic dynamics. The hippocampus model [161] was successfully used to reproduce hippocampal paroxysmal discharges in the absence of as well as in response to stimulation. The results are hereby detailed.

1 SIMULATING HPDS

Realistic epileptic hippocampal dynamics could be simulated in the model by manually tuning the parameters A , B , and G corresponding to the amplitudes of the EPSPs/IPSPs that could be generated in the model as well as tuning the parameter K corresponding to the amplitude of the input PSD. The initial values were set according to the model activity maps presented in [161]. As aforementioned, the onset/duration of hippocampal paroxysmal discharges (HPDs) were experimentally identified and parameterized.

Figure 56 presents a 400 s simulated signal segment as well as a real iEEG signal segment corresponding to the no stimulation condition. The simulated and simulated HPDs occurring in these signal segments are also illustrated. It can be assumed that the model can mimic realistic hippocampal activity.

1.1 MODEL ACTIVITY MAPS

In order to estimate the approximate values of k_1 , k_2 and k_3 (Figure 54) necessary for the reproduction of the polarization effects of DC stimulation, the model activity maps were computed on empirically predefined parameter. The activity maps represent the number of detected peaks/min (Figure 57), the total discharge duration/min (Figure 58), the total discharge energy/min (Figure 59) recorded during the minute following a stimulation pulse of duration 50 s and intensity $1 \mu\text{A}$. Five stimulation simulations were performed for each triplet (k_1, k_2, k_3) , then the average of the features computed over the five simulations were traced in the activity maps.

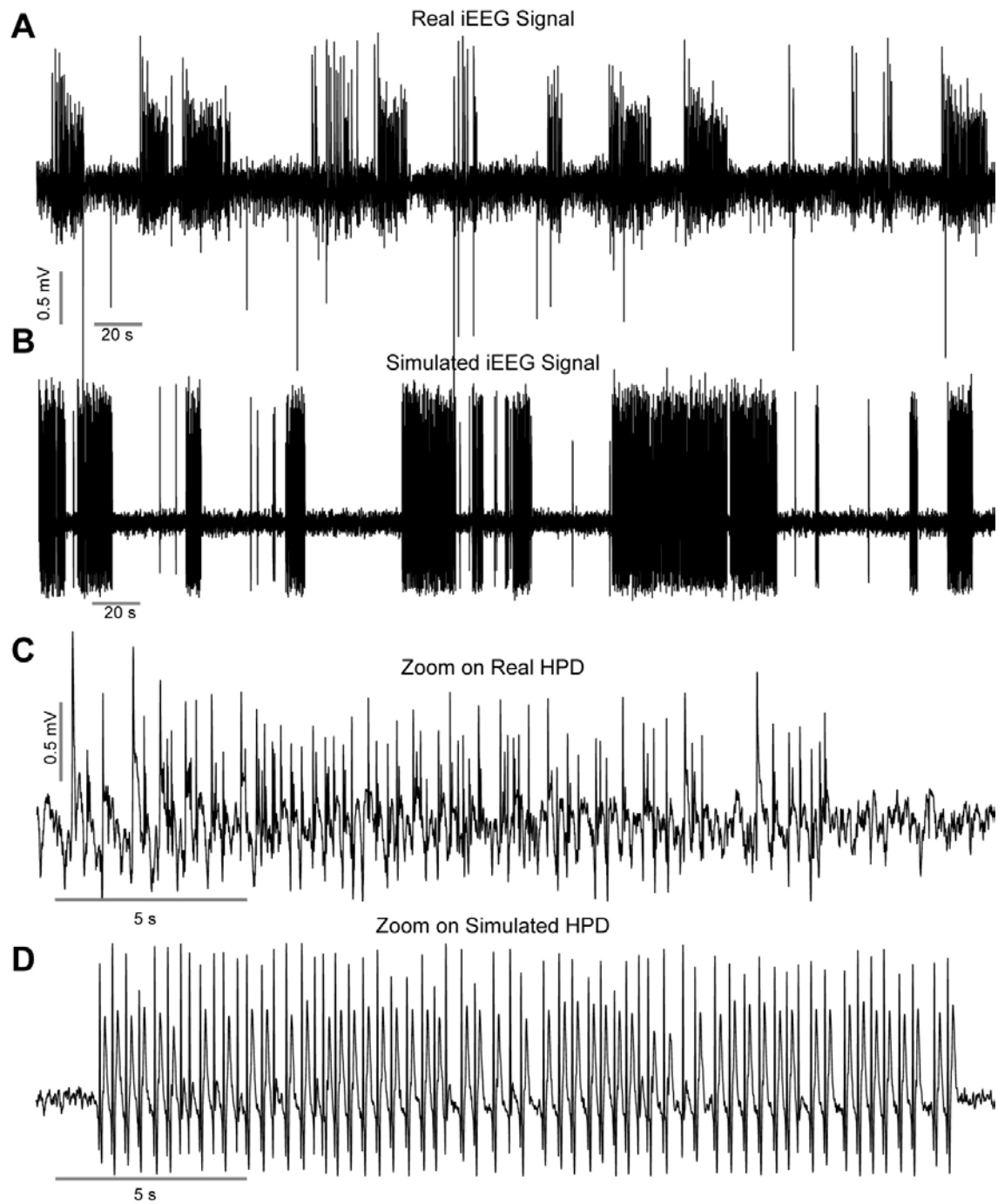


Figure 56. Modeling HPDs. **(A)** Real and **(B)** simulated hippocampal iEEG segments. Note the abrupt passage from background to epileptiform activity in both simulated and real hippocampal LFP. Zoom on a **(C)** real and a **(D)** simulated HPD. Note the spike-and-wave complex in both real and simulated HPDs.

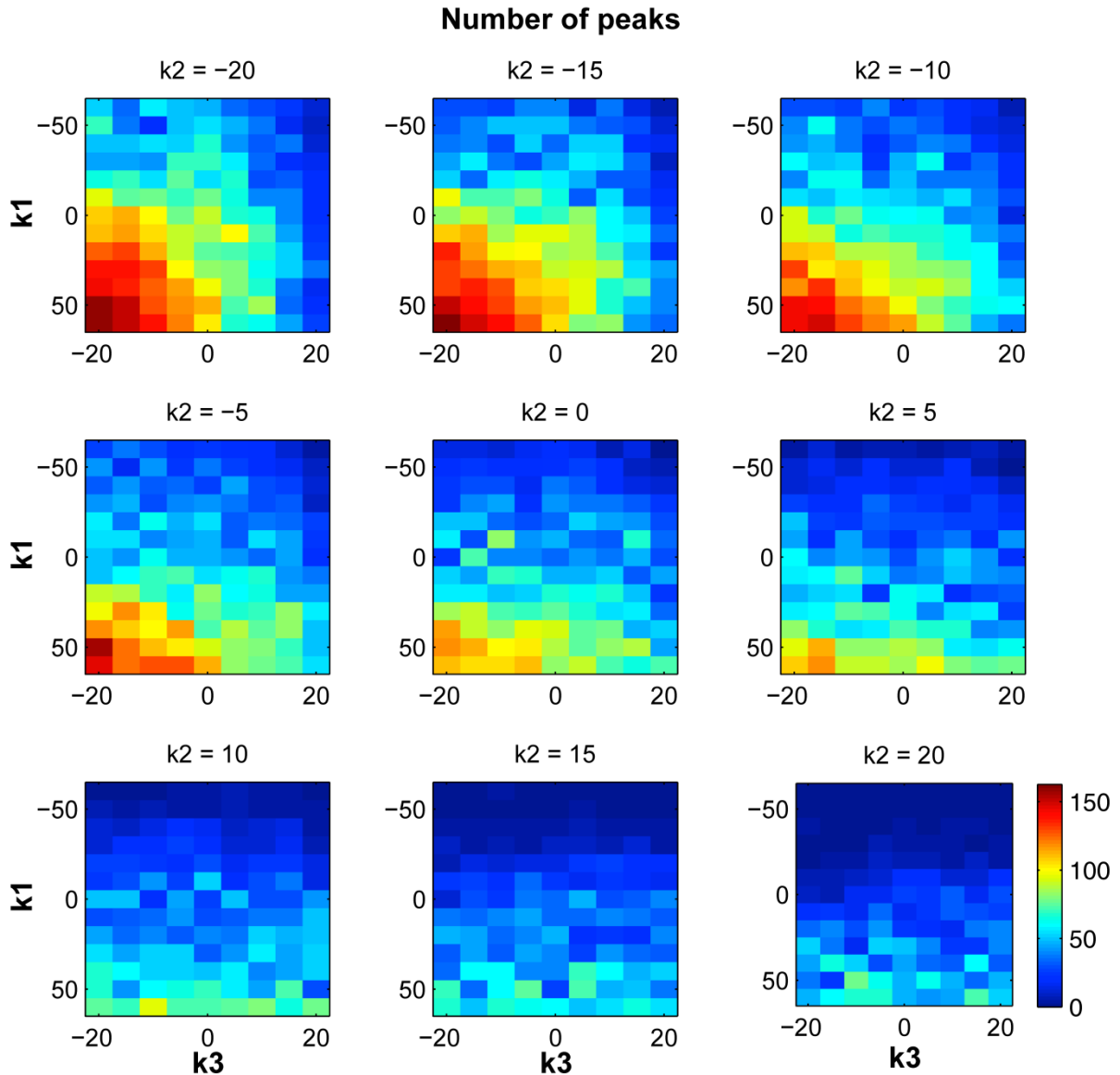


Figure 57. Model activity maps representing the average number of peaks (calculated over 5 simulations) in the minute following a stimulation pulse of duration 50 s and intensity $1 \mu\text{A}$ for different values of k_1, k_2 and k_3 . Note the excessive increase in peak occurrence for extremely negative values of k_2 and k_3 with simultaneous extremely positive values of k_1 and vice versa. It can be concluded that the effect of k_3 is predominant over that of k_2 . It is actually sufficient to obtain an increase/a decrease of peak occurrence even if k_2 is null.

As depicted in the activity maps, the highest levels of excitability in the model are related to the positive values of k_1 , coupled to negative values of k_3 when k_2 is extremely negative (≤ -10 ; bottom lower corners of the maps). Similarly, when the value of k_3 is extremely positive (≥ 10), negative values of k_1 seem sufficient to hyperpolarize the system. To exclude these extreme conditions that were not observed in real iEEG recordings, only

middle panel maps were considered for the optimization of stimulation effects ($k_2 = [-5, 0, 5]$).

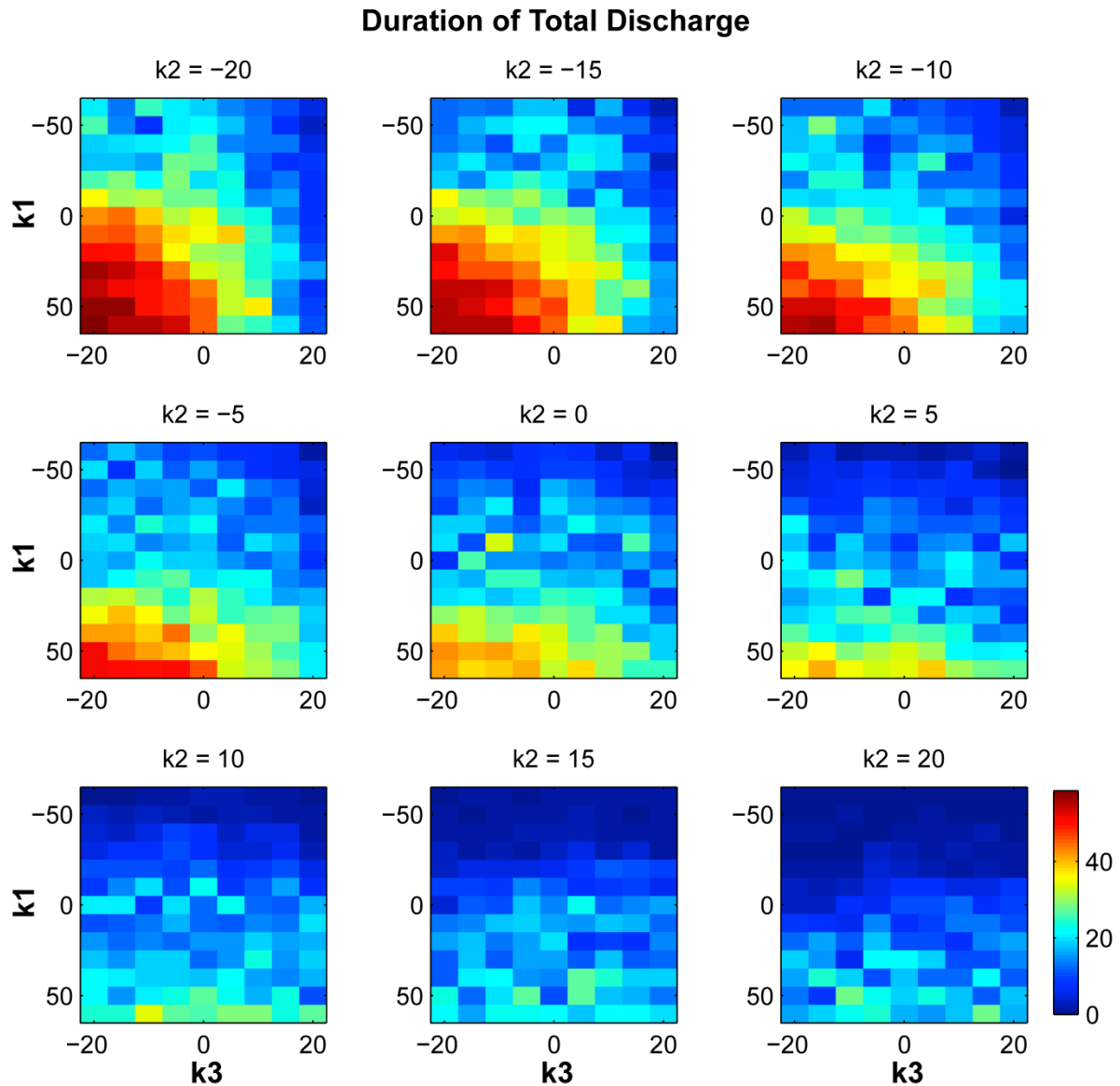


Figure 58. Model activity maps representing the average duration (s) of discharge (calculated over 5 simulations) in the minute following a stimulation pulse of duration 50 s and intensity $1 \mu\text{A}$ for different values of k_1, k_2 and k_3 . Note the excessive increase in HPD duration for extremely negative values of k_2 and k_3 with simultaneous extremely positive values of k_1 and vice versa. It can be concluded that the effect of k_3 is predominant over that of k_2 . It is actually sufficient to obtain an increase/ a decrease in total HPD duration even if k_2 is null.

1.2 SIMULATED STIMULATION EFFECTS

For reproducing stimulation effects, we supposed that inverting the polarity of the stimulation current systematically implies inverting the sign of parameters k_1, k_2 and k_3 . So

the challenge was finding the triplet (k_1, k_2, k_3) that induces model hyperpolarization and consequently the triplet $-(k_1, k_2, k_3)$ that depolarizes the model dynamics in certain limits. The triplet (k_1, k_2, k_3) was set to $(-30, 5, 5)$, in order to avoid the change in the discharge morphology during stimulation. Examples of simulation results are illustrated in figures Figure 60, Figure 61 and Figure 62. Each signal corresponds to the model output during an independent simulation. Note that, in the model, the depolarization effects are more marked than hyperpolarization effects. This could be avoided, if the polarity constraint on interneurons is relaxed. If we suppose that interneurons are always depolarized by stimulation for both polarities given their unstructured organization, the marked stimulation effect can be avoided.

The stimulation effects were then studied as a function of the stimulation polarity in the model. Three groups were defined: the no stimulation group, the hyperpolarizing stimulation group and the depolarizing stimulation group. One hundred simulations were then performed per group. The simulated signals were then analyzed, and the boxplots corresponding to the number of detected peaks/min, the total duration of discharge/min and the discharge energy/min were plotted in Figure 63. The hyperpolarizing polarity seems to divide by two the preceding quantities whereas the depolarizing polarity seems to at least double their values. Using a stimulation current intensity of $0.5 \mu\text{A}$ does not seem to affect the model dynamics. This was verified by tracing the boxplots of 100 trials per group in case the pulse amplitude is set to $0.5 \mu\text{A}$ (not illustrated).

1.3 THE THEORETICAL EQUIPOTENTIAL LINES INDUCED BY STIMULATION

Given the current intensity, the theoretical intra-electrode distance, the induced potential lines can be estimated when considering homogeneous the conductivity of the electrode neighborhood. In a 2D plane, this can be mathematically expressed as:

$$V(r_1, r_2) = \frac{I}{4\pi\sigma} \cdot \left(\frac{1}{r_1} - \frac{1}{r_2} \right)$$

where r_1 and r_2 are the distances between the considered point and the anode or the cathode respectively. Parameter σ corresponds to the conductivity of the considered medium. The theoretical values of function $V(r_1, r_2)$ are depicted in Figure 64. A current, as small as $1 \mu\text{A}$, can induce a potential difference of the order of 10 mV between the tips of the stimulation electrode.

Equipotential lines can be used to estimate the electric field lines as well as the temperature gradient induced by the simulation current. The electric field lines can be classically obtained given the conventional potential-electric field expression $\vec{E} = -\nabla V$.

Figure 65 illustrates the electric field lines that could be determined accordingly. Calculating the electric field density around the stimulation electrodes, it can be shown that the minimal field intensity 0.1 mm away from the electrodes remains as high as 30mV/mm, which is comparable in value to the electric field used in the pilot study discussed earlier in chapter 6 [36].

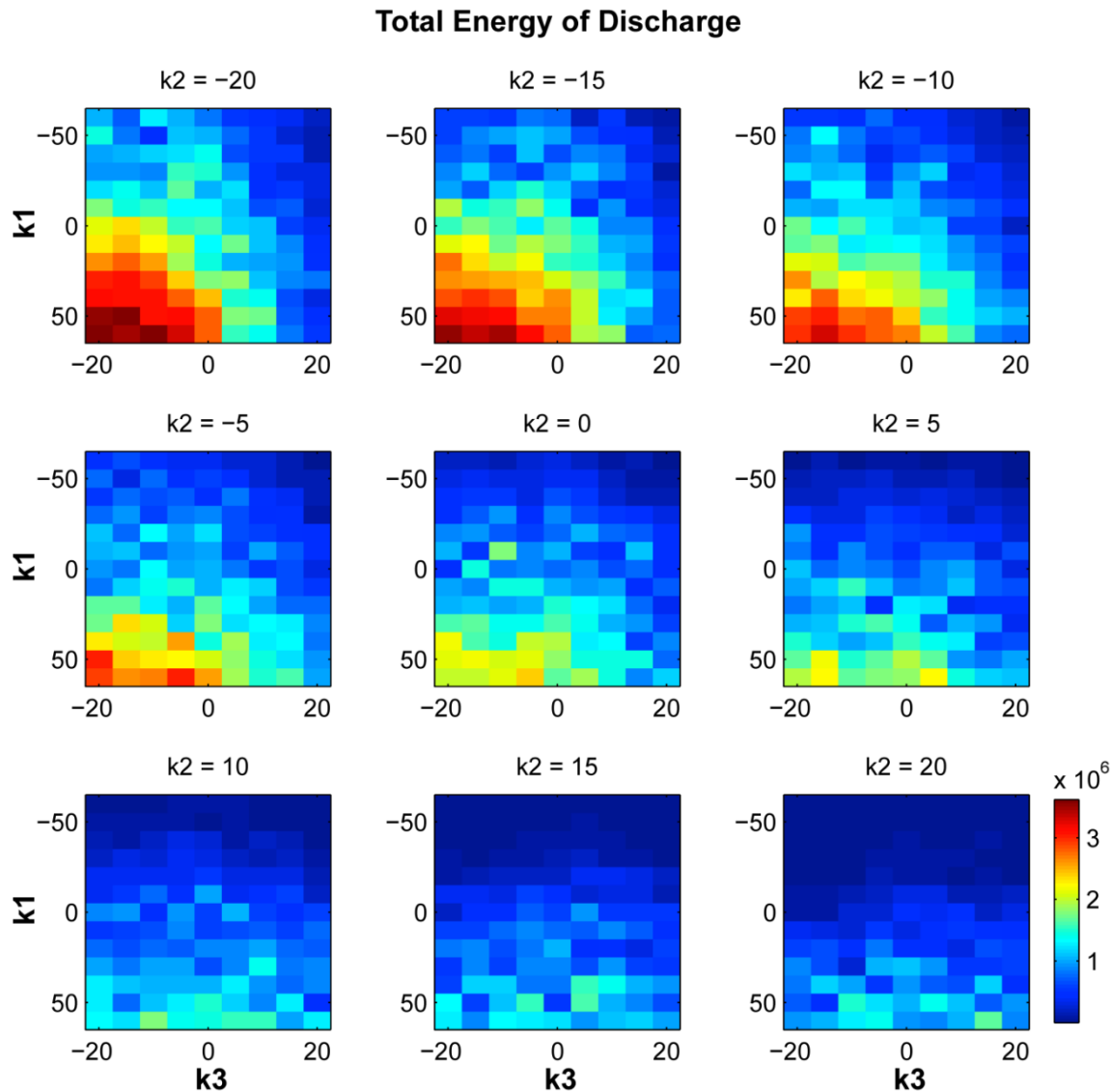


Figure 59. Model activity maps representing the average energy of discharge (calculated over 5 simulations) in the minute following a stimulation pulse of duration 50 s and intensity 1 μ A for different values of k_1, k_2 and k_3 . Note the excessive increase in the energy of total HPDs for extremely negative values of k_2 and k_3 with simultaneous extremely positive values of k_1 and vice versa. It can be concluded that the effect of k_3 is predominant over that of k_2 . It is actually sufficient to obtain an increase/ a decrease in total HPD energy even if k_2 is null.

Concerning the heat diffusion during stimulation, this can be described by the following differential equation [260]:

$$\rho C_p \frac{\partial T}{\partial t} = \nabla(k\nabla T) - \rho_b \omega_b C_b (T - T_b) + Q_m + \sigma |\nabla V|^2$$

where ρ is the brain tissue density, C_p is the specific heat of the brain tissue ($\text{J kg}^{-1} \text{ }^\circ\text{C}^{-1}$), k is the thermal conductivity of the brain tissue ($\text{W m}^{-1} \text{ }^\circ\text{C}^{-1}$), ρ_b is the blood density (kg m^{-3}), ω_b is the blood perfusion ($\text{ml s}^{-1} \text{ ml}^{-1}$), C_b is the specific heat of the blood ($\text{J kg}^{-1} \text{ }^\circ\text{C}^{-1}$), T_b is the body core temperature ($^\circ\text{C}$), Q_m is the metabolic heat source term (W m^{-3}), σ is the conductivity of the brain tissue (S m^{-1}) and ∇V is the potential gradient induced by stimulation. Note that the first term of the equation, $\nabla(k\nabla T)$, represents the dissipation of heat through the thermal conductivity of the brain. The second term represents heat diffusion through blood perfusion, $\rho_b \omega_b C_b (T - T_b)$. The third term represents intrinsic heat generation through metabolic processes, Q_m . Only the last term corresponds to the stimulation induced heating, $\sigma |\nabla V|^2$. It is directly related to the magnitude of the potential gradient induced by the stimulation current.

The simplest thermal model of stimulation can be considered through neglecting metabolic processes as well as blood perfusion. The simplified thermal model can then be expressed as:

$$\rho C_p \frac{\partial T}{\partial t} = \nabla(k\nabla T) + \sigma |\nabla V|^2$$

Considering that the stimulation induced heating reaches its max at a point t_{max} after the onset of the stimulation current. The maximum attained temperature can be then estimated by calculating the steady state solution of the above equation:

$$\nabla(k\nabla T) + \sigma |\nabla V|^2 = 0$$

The implications of the above equation consist in directly relating the process of heat diffusion to the amplitude of the voltage gradient induced by stimulation. The resolution of heat diffusion equations in the context of deep brain stimulation constitutes an uprising concern in the field. Experimental and computational data show that stimulation-induced heating depends on the root mean square voltage (rms) of the stimulation signal [260]. Besides, across a wide range of stimulation wave forms (sine wave, square wave, or DBS stimulation) the peak temperature rise reported for an rms value of 2V is of 0.2°C. Consequently, as long as low-intensity currents are used for DC stimulation protocols, no harmful stimulation-induced heating should be expected in the targeted brain tissue.

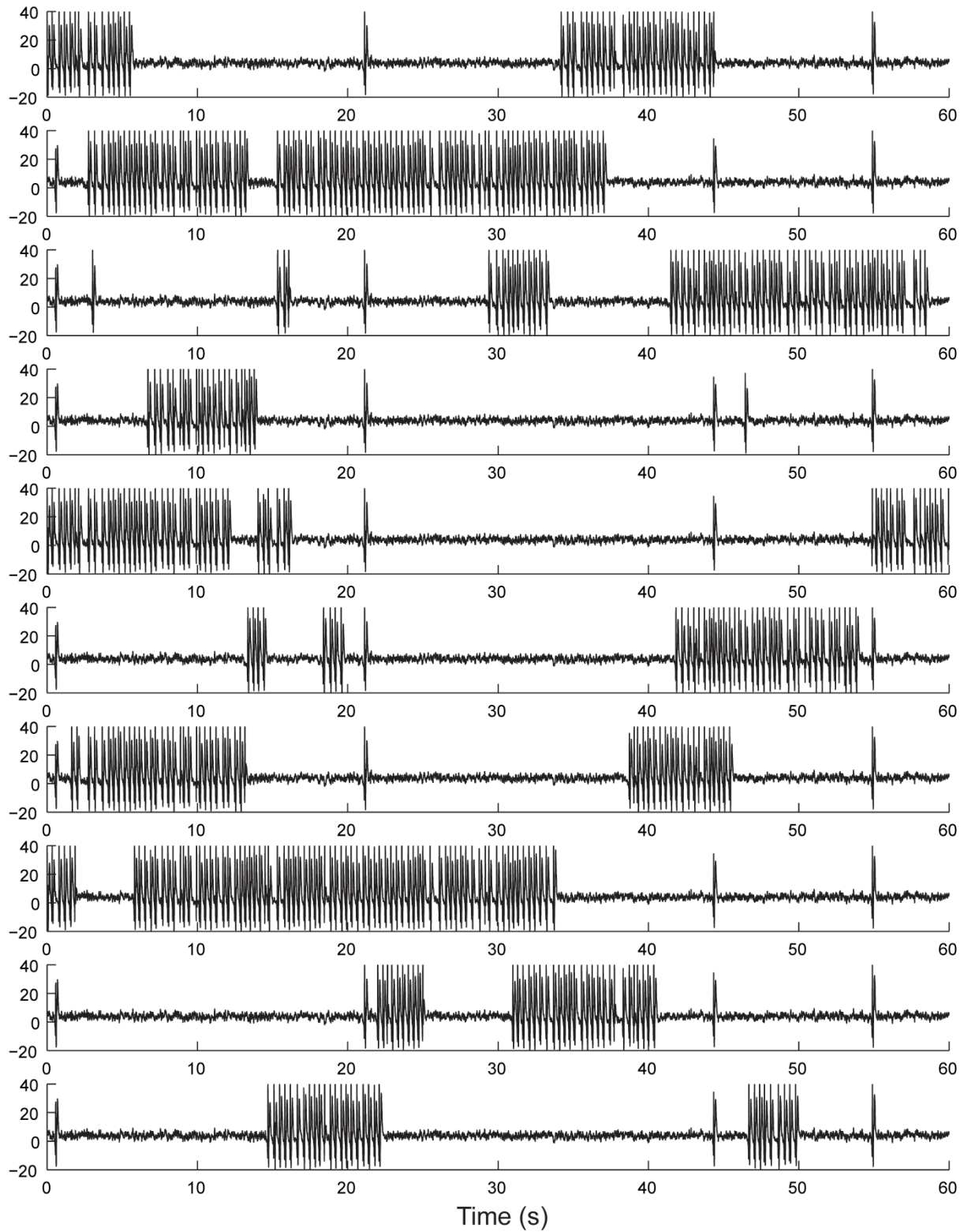


Figure 60. Ten examples of possible model dynamics in the absence of stimulation. Simulated signals correspond to LFPs

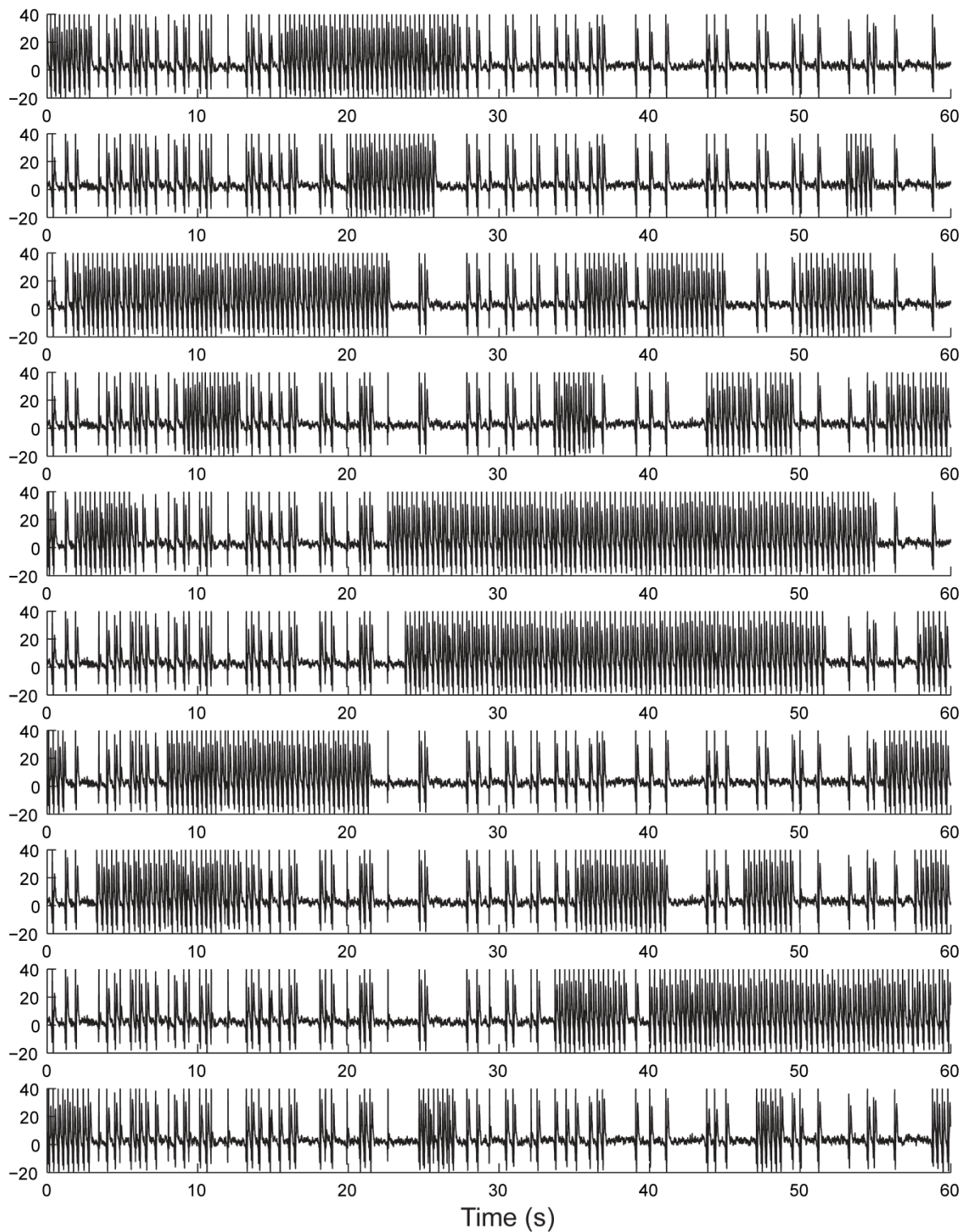


Figure 61. Ten examples of the model output when “depolarizing” stimulation is applied. Note the increase in HPD duration and intensity as well as in peak occurrence.

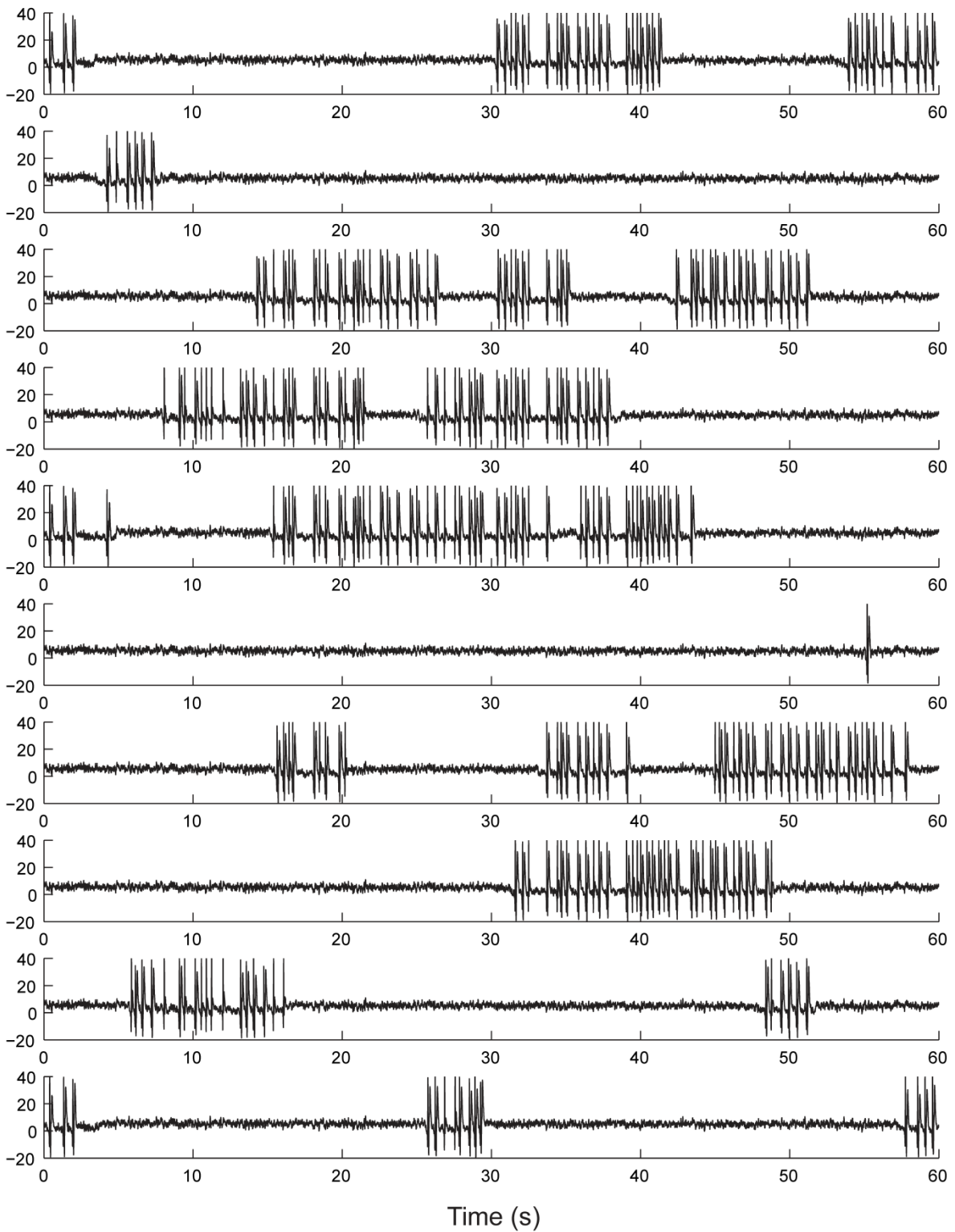


Figure 62. Ten examples of the model output when “hyperpolarizing stimulation” is applied. Note the decrease in HPD duration as well as in peak occurrence.

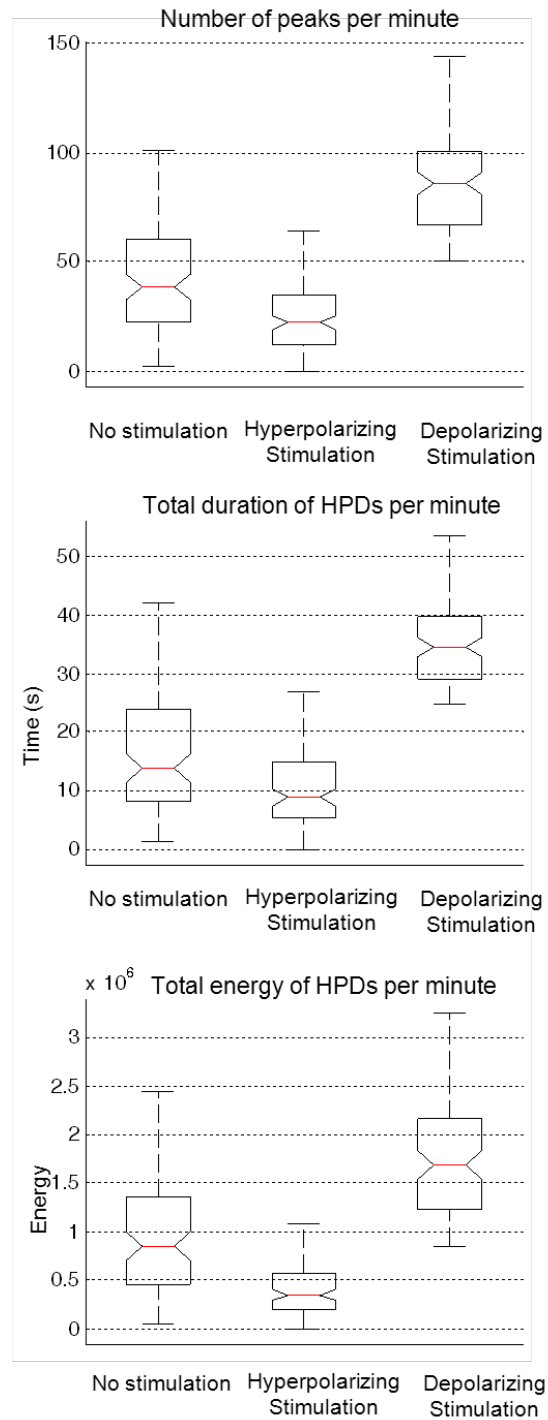


Figure 63. Boxplots of simulated iEEG signals in the absence and during hyperpolarizing and depolarizing stimulation.

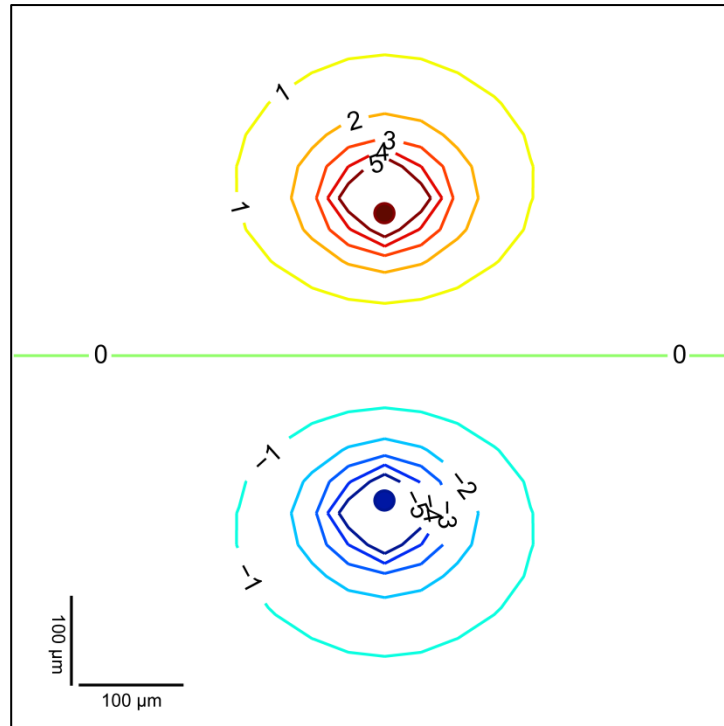


Figure 64. The theoretical equipotential lines induced during the $1\mu\text{A}$ DC stimulation, for an intra-electrode distance of $350\mu\text{m}$ in a homogenous medium of conductance 0.35 S/m . The red and blue spheres represent the anode and the cathode emplacements respectively. The numbers on the potential lines indicate their corresponding value in mV. The maximum induced voltage gradient between the two electrode tips is of the order of 10 mV .

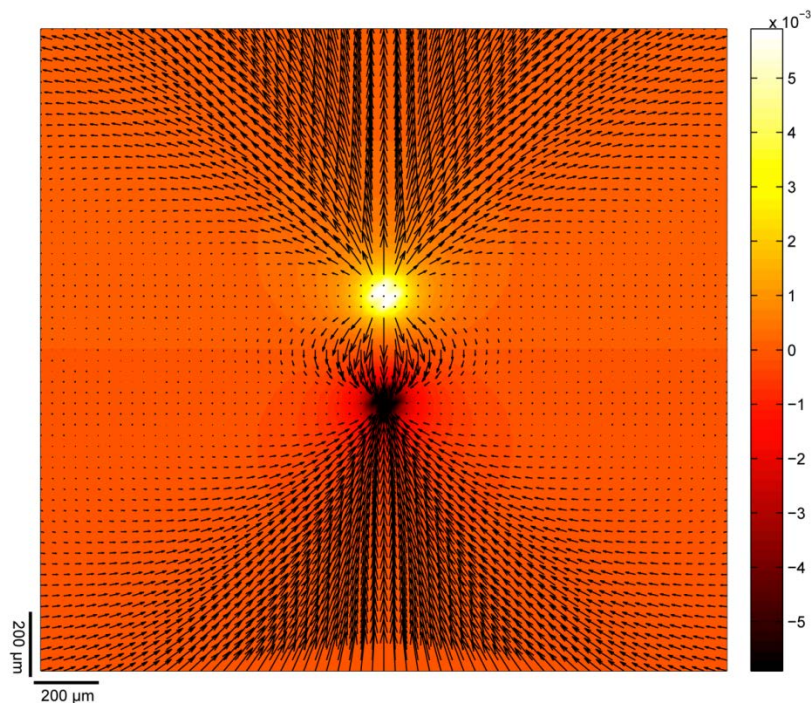


Figure 65. The electric field lines induced by stimulation superimposed over the induced potential map (V).

Chapter 8: Experimental Validation

As the results of the computational study were encouraging (see chapter 8), an experimental procedure was designed to verify the computational predictions as well as the safety of this type of stimulation. Noteworthy, the indirect implication of this experimental validation is the validation of the stimulation inputs implementation in the model: stimulation polarizes the transmembrane potential.

In this chapter, the experimental preliminary safety tests are first explained, and then the *in vivo* experimental setup, including the stimulation protocols and data analysis, is detailed. Finally, the observed experimental results are reported.

1 PRELIMINARY SAFETY TEST: STIMULATION-INDUCED HEATING

DC stimulation may provoke tissue damage through five possible mechanisms: chemical, thermal, mechanical, electroporation, and excitotoxicity [135]. Consequently, a preliminary test protocol was performed before the start of *in vivo* experiments in order to verify thermal “safety” of DC stimulation protocols.

A bipolar stimulation electrode was implanted in a freshly extracted C57BL/6J (B6) mouse brain. The monitor temperature probe of an automatic temperature controller (*TC-324B Warner Instrument Corporation*) was inserted between the two tips of the stimulation bipolar electrode (Figure 66). The experiment was conducted in a temperature controlled room ($21\pm 1^\circ\text{C}$). The test stimulation pulse was only given when the recorded temperature reached a stable baseline in the absence of stimulation.

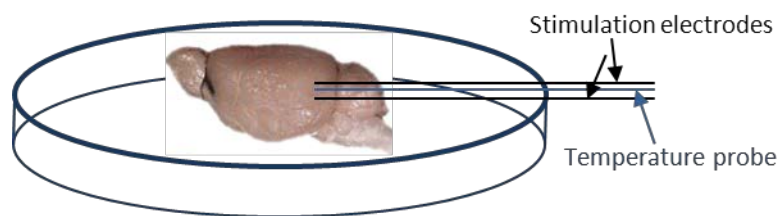


Figure 66. Verifying temperature rise during stimulation. A temperature probe was inserted between the two tips of a bipolar stimulation electrode. These were then implanted in a freshly extracted mouse brain *in vitro*. Temperature change was recorded during long-duration stimulation pulses.

Different stimulation current intensities (0.1mA, 0.5mA, 1mA, 1.5mA, and 4mA) were gradually tested over 100 s durations. After the end of each 100 s pulse, stimulation was paused until the stabilization of the recorded temperature. Each stimulation current intensity was tested twice.

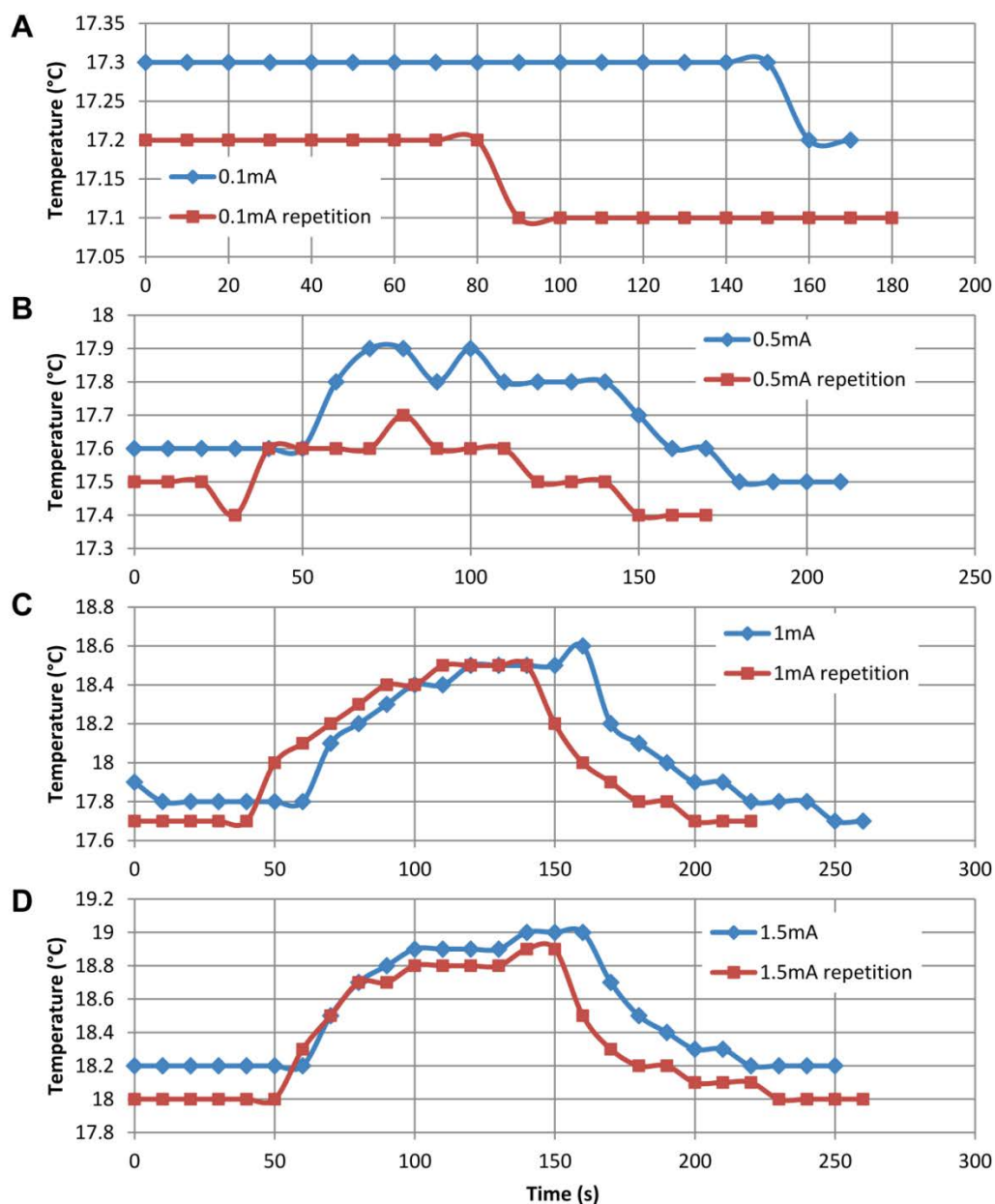


Figure 67. The thermal heating recorded for different stimulation current intensities applied for 100s. **(A)** 0.1 mA, **(B)** 0.5 mA, **(C)** 1 mA and **(D)** 1.5 mA. Each stimulation 100 s pulse was tested twice at every current intensity.

The *in vitro* thermal safety test discarded the neural death risk due to the thermal heating associated to DC stimulation only when stimulation current remained relatively small (< 0.1 mA). The results are illustrated in Figure 67 and Figure 68.

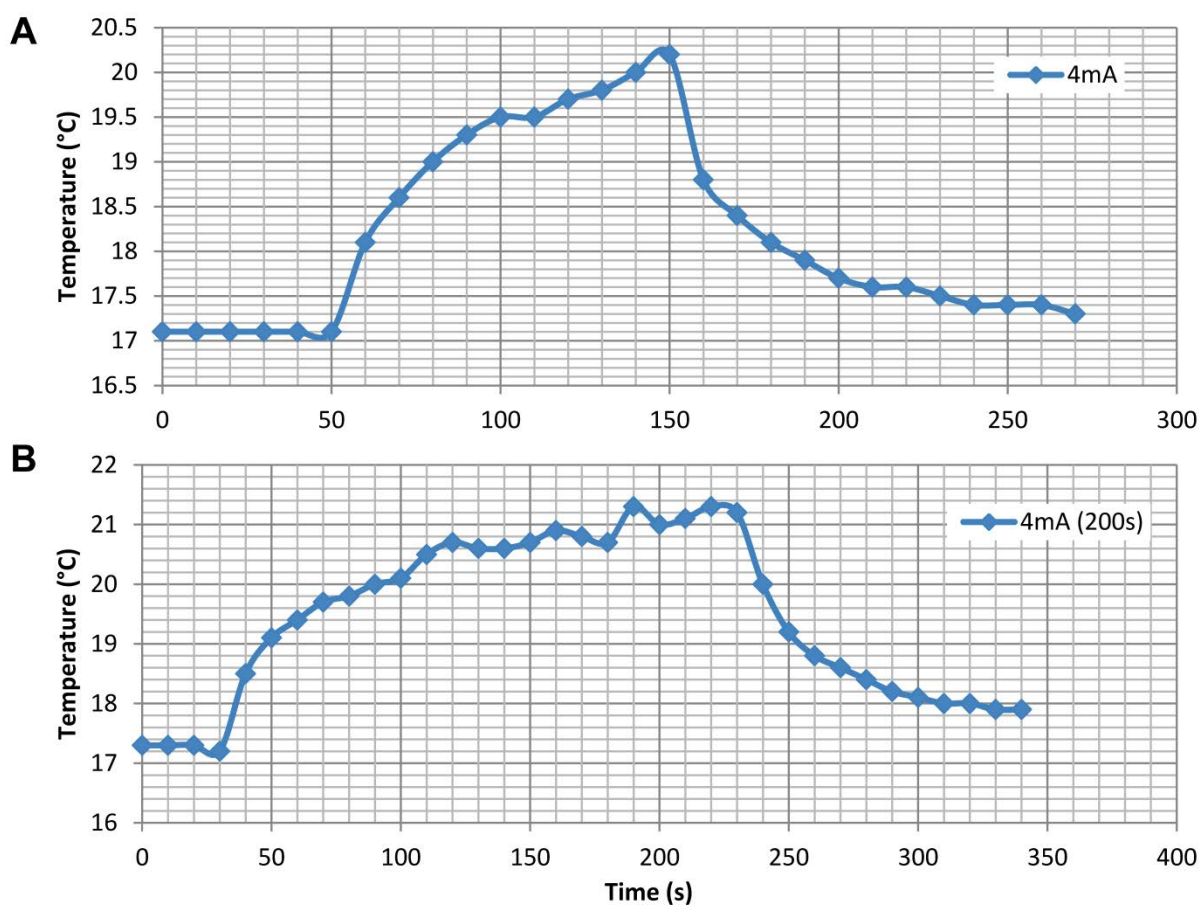


Figure 68. Thermal heating produced by high current intensity DC stimulation (4 mA) applied for **(A)** 100 s and **(B)** 200 s respectively. The recorded temperature elevation is higher than 4°C.

In fact, as no heating was recorded during a stimulation of current intensity 0.1 mA, a 0.5 mA stimulation pulse provoked a temperature elevation of approximately 0.3°C. Moreover, when the stimulation current intensity was increased to 1 – 1.5 mA, a 1°C thermal elevation was recorded. Noteworthy, an increase in temperature of about 1°C can exert profound effects on a single neuron and on the neural network functioning [261-263]. Enormous temperature elevations of approximately 4°C were recorded for currents of 4 mA intensity (Figure 68). Increasing the stimulation duration also contributed to an increase in temperature only if a stable temperature was not reached by the end of 100 s.

After the end of the stimulation pulse, the temperature of the stimulated tissue drops exponentially. It should be noted that, when such experiments are conducted in a freshly

extracted brain, an essential mechanism that contributes to tissue cooling, blood perfusion, is absent and heat is dissipated uniquely through the thermal conductivity of the brain [264].

2 THE EXPERIMENTAL PROTOCOL

At day 27 after the KA intra-hippocampal injection (see chapter 6 section 3.2), the confirmed epileptic animals were scheduled for a 4-hour baseline video-iEEG recording using a clinical monitoring system (*Deltamed*). This was intended for quantifying the basal epileptic activity of each animal before any experiment. After establishing a baseline recording for the considered animal, stimulation sessions were programmed between day 28 and day 40 (after injection) with no *a priori* on electric field polarities with respect to CA1 (due to the uncertainties in the implantation procedure). In effect, due to the possible imprecision of the manual electrode implantation procedure, we could not verify a priori that the implanted electrodes have exactly the configuration illustrated in chapter 6 Figure 46. Each animal underwent 4 to 5 stimulation sessions in order to test the intra-individual variability of the stimulation outcome. A *GRASS Technologies S88X* stimulator was used in all stimulation sessions. The recorded LFPs were sampled at 2 kHz, and hardware-filtered by a high-pass filter (0.16 Hz cutoff frequency) integrated into the signal acquisition system.

2.1 THE PROTOCOL VARIANTS

Three stimulation protocol variants were used. Each animal underwent only one type of protocol variants repeated over 4 to 5 stimulation sessions. These variants denoted P_1 , P_2 and P_3 , are illustrated in Figure 69. Stimulation current was limited to 1 μA , the equivalent to one tenth of the DC current intensity used in [242] and reported to provoke no tissue damage. Similarly, the results of the aforementioned thermal safety tests show that the tissue induced-heating at this low current intensity is negligible. Stimulation duration was limited to an intermittent 400s total per day. In fact, it has been shown that tissue damage increases linearly with stimulation duration when using monophasic HFS (high-frequency stimulation; 130 Hz) [154]. This is related to an irreversible charge accumulation at the cathodal electrode.

To compare, we calculated the total injected charge density during a “safe” stimulation duration (5 minutes) for a maximal allowed current $I_{max} = 100\mu\text{A}$ for a monophasic monopolar high-frequency stimulation (pulse width = 60 μs ; cathodal electrode area = 177 $\cdot 10^{-6}$) as defined by [154], as well as the theoretical total injected current for a DC stimulation of duration 100s, and intensity 1 μA using the following expression for the charge density per phase (as defined in [265]):

$$\text{Charge density} = \frac{\text{current intensity (mA)} \cdot \text{pulse width(ms)}}{\text{cathodal electrode area (cm}^2\text{)}}$$

Evidently, the resulting charge density/phase for DC stimulation (phase = 100 s) turned out to be enormous with respect to the previously calculated “safe” dose. Consequently, we made the following assumption: in monophasic stimulations, the phase (polarity) is never inverted; so charge accumulation may be a consequence of charge accumulation due to consecutive stimulations with the same polarity, which explains the linear relation with stimulation duration [154]. For this, we assume that the total charge density injected during a monophasic stimulation session can be expressed as a function of the total stimulation duration for all stimulation frequencies (DC to HFS):

$$\text{Total Charge density} = \frac{\text{current intensity (\mu A)} \cdot \text{total stimulation duration(s)}}{\text{cathodal electrode area (cm}^2\text{)}}$$

Given this approach, it can be concluded that the maximal harmless total charge density that can be identified from [154] is equal to $1.322 \cdot 10^6 \mu\text{C/cm}^2$. If this is set as a maximal allowed charge density injection, then the maximum allowed DC stimulation time at an intensity of 1 μA should be inferior to 160 seconds (given that the cathodal electrode diameter used in this study is 125 μm) in a relatively short time (< 5 min). This upper stimulation duration was respected in all stimulation protocols.

Protocol P₁. Protocol P₁ consisted of alternating stimulation pulses of inverse polarities, termed S₁/S₂, but of constant duration of 100s. Each two pulses were separated by a period of *no-stimulation* lasting 300s. This silence period was designed for recording the neural system’s response after a stimulation of polarity S₁ or S₂. (S₁ represented by a positive pulse and S₂ by a negative pulse in Figure 69). Alternating pulses of opposite polarities was initially provided for inverting charge accumulation.

Protocol P₂. Since stimulation pulses were separated by a large duration, inverting charge accumulation was probably not guaranteed by inverting stimulation polarities. Consequently, P₂ was rather designed for maximally separating stimulation effect interferences and residuals caused by the succession of S₁/S₂ stimulation pulses. Formally, P₂ consisted of delivering 4 50s-pulses of polarity S₁ each two separated by a 5 minutes *no-stimulation* period. This was followed by a rest period of approximately 1 hour. Then another 4 50s-pulses of polarity S₂ each two separated by a 5 minutes *no-stimulation* period were delivered. Again, the 300s *no-stimulation* period was reserved for recording the system’s response to the delivered stimulation pulse.

Protocol P₃. Finally, in order to conduct a preliminary test on the relation between stimulation duration and efficacy, protocol P₃ was defined. It consisted of delivering consecutive S₁/S₂ pulses separated by a 300s *no-stimulation* period. This was repeated by successively incrementing pulse durations [5, 10, 20, 30, 40, 50s].

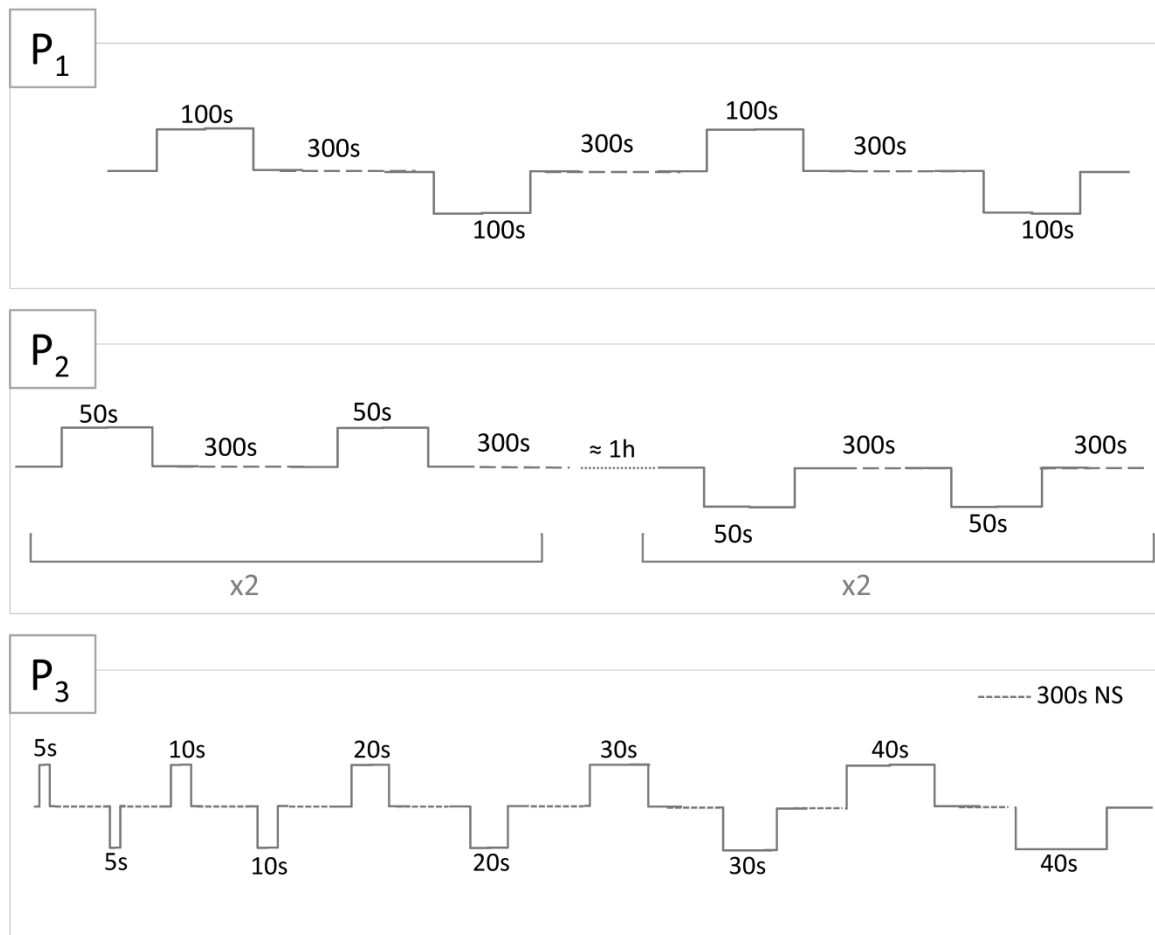


Figure 69. The different stimulation protocols used in this study. In protocol P₁, polarity is inverted at each stimulation pulse. Stimulation duration is fixed to 100 s. In protocol P₂, only one polarity is tested at a time. A “no stimulation” duration of approximately 1 hour is used to separate the polarity trials. Finally, in protocol P₃, the effect of the duration is explored. Stimulation polarity is inverted at every stimulation pulse and pulse duration is gradually increased during the stimulation session. A 300 s no stimulation (NS) duration separates consecutive pulses and is intended for measuring the system’s response.

2.2 DATABASE

Only 5 mice were included in this study, and only one protocol was tested per mouse. Table 7 resumes the protocol used by mouse and the number of repetitions (stimulation sessions) of each protocol. No matter what the protocol used, stimulation responses after each stimulation pulse were supposed independent from all other stimulation trials.

Consequently, each stimulation pulse corresponded to an independent trial of a polarity-specific or (duration-specific) stimulation.

Mouse ID	Protocol	Number of Repetitions
K143	P1	5
K148	P3	5
K155	P2	5
K168	P2	5
K171	P2	5

Table 7. Mouse Database detailing the used protocol variant and the number of repetitions of stimulation sessions.

2.3 HISTOLOGICAL VERIFICATION

Upon the completion of all stimulation sessions, stimulated mice were injected with a lethal dose of chloral hydrate. Their brains were removed from the skull and directly frozen in isopentane (2-methylbutane) at -35°C . The frozen brains were then cut in coronal sections of $20\ \mu\text{m}$ on a cryostat that were collected on gelatin-coated strips.

Then, tissue sections were stained using the Nissl staining method in order to verify (1) the position of the electrodes, (2) the neural dispersion provoked by the perfusion of KA and (3) the absence of collateral damages or neural death that could be provoked by DC stimulation. In brief, the Nissl staining method suggests that brain slides be immersed in a 0.1% cresyl violet solution for 8 minutes, then dehydrated in increasing concentrations of ethanol. Finally, the slides are cleared through the immersion in two consecutive butan-1-ol baths (8 minutes each), and cover-slipped in a resin layer between two glass strips. The histological verification was simply done using a Nikon microscope.

This procedure allowed the verification of the electrode position in the hippocampus, as well as the kainate-induced hippocampal histopathology and finally the effect of the stimulation currents on hippocampal tissue.

3 QUANTIFYING STIMULATION EFFECTS

In order to assess the epileptic degree of the injected hippocampus at different instants, the same lumped features assessed computationally were measured in the real LFP signals in the absence of stimulation and at the end of stimulation. These features included the total duration, the intensity, and the number of discharges, as well as the number of detected peaks in a pre-defined time interval. To proceed, the iEEG recordings of each animal passed the following steps:

- a. Pre-selection

- b. Tagging
- c. Processing
- d. Statistical Analysis

Pre-selection. During the first step, the iEEG recordings of the considered animal were checked for the presence of episodes of restless activity (notably during the active exploration of the cage). These episodes were excluded due to the existence of iEEG movement artifacts, and consequently amplifier saturation episodes. Not to mention, during active episodes, epileptic events are rarely observed in the iEEG recordings. Consequently, only iEEG signals recorded during the restfulness of the animal were included in the study. Only the signals recorded from the injected hippocampus were studied.

Tagging. The selected iEEG recordings were then tagged for stimulation trials. After each stimulation pulse, the instant at which the stimulation artifact ends was manually tagged with stimulation pulse duration and polarity (S_1/S_2). Then, peaks were detected using the Page-Hinkley test. As aforementioned, peak detection is verified manually to avoid detecting stimulation artifacts.

Processing. The preselected signals, along with their corresponding stimulation and peak tag tables were then preprocessed as follows:

- i. A processing window length t_{win} was defined ($t_{win} = 2$ minutes).
- ii. For no stimulation iEEG recordings, the epileptic measurements were calculated over a sliding window of 2 minutes duration (0% overlap – see Figure 70-A).
- iii. As for stimulation responses, the epileptic measurements were calculated over a 2-minutes fixed interval starting at the stimulation end tag (see Figure 70-B). In other words, the response of each stimulation pulse was calculated over a single 2-minutes interval.

The pseudo code used for the tagging ongoing epileptic events over a fixed-interval window is the same as the one given in Table 5. An algorithm similar to that presented in Table 5, but with a fixed window, was used for detecting discharge time slots after stimulation pulses (Figure 70-B). Once detected, measuring the epileptic features of the iEEG signals in each time window consisted of evaluating the occurrence of epileptic dynamics, their intensity, and duration using the same algorithm used for simulated signals Table 6. However, for every t_{win} interval, the moving average of the recorded LFP signal is estimated using a window of 1 second. It is then filtered from the signal before extracting the aforementioned features. This was uniquely done on real signals in order to filter stimulation artifacts.

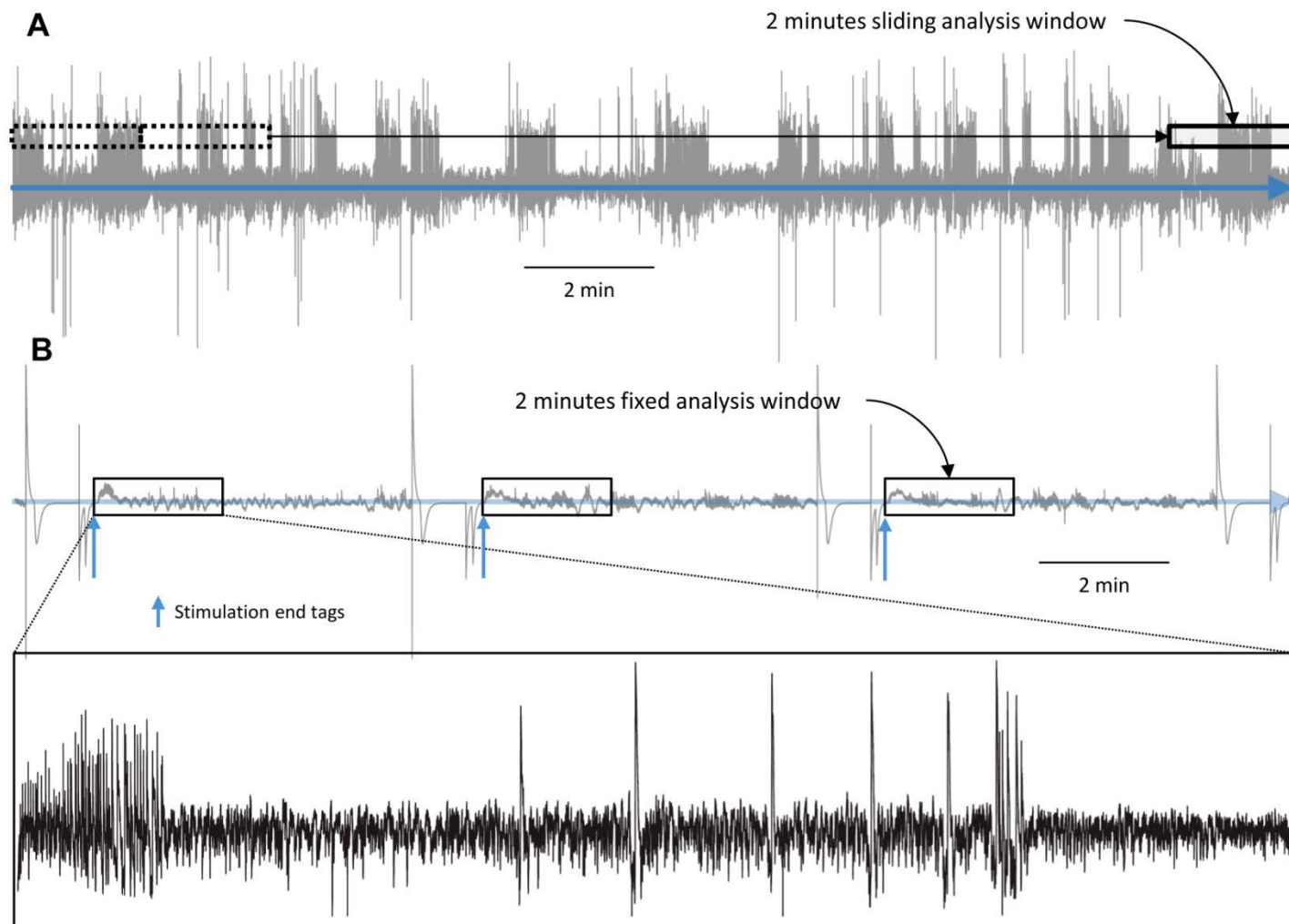


Figure 70. The processing of iEEG signals over fixed-window intervals. **(A)** Case of no stimulation, the iEEG signal is processed over a sliding fixed length 2-minute intervals (0% overlap). **(B)** Case of stimulation, fixed 2-min intervals are defined starting at the stimulation end tag of every stimulation pulse. The considered 2-min signal is then pre-processed to filter the stimulation artifact (B lower panel), before any further quantification. The same preprocessing step is applied on no stimulation intervals in to avoid preprocessing bias.

4 STATISTICAL Analysis.

For all stimulated animals, a control features dataset has been calculated, per animal, in the absence of stimulation over about 2 hours of iEEG recordings considered at different days of the protocol. These iEEG recordings generally correspond to the pre-stimulation baseline recordings. Each t_{win} minutes interval corresponding to a supposedly independent trial of the same random variable.

Then, for every animal, each stimulation response (calculated after each stimulation trial) was attributed to a stimulation group according to its polarity (S_1/S_2), and its duration (case of protocol P_3). These stimulation responses corresponded to the sum of stimulation trials done during the n stimulation sessions for a given animal. Below is a table of the number of repetitions per group per animal (Table 8).

Mouse ID	#NS	#S1	#S2	
K155	119	12	10	
K168	120	19	20	
K171	144	18	20	
K148	40 s	110	4	3
	50 s	110	2	1
K143	100 s	100	8	6

Table 8. Number of 2-min processing intervals for every animal. Only one processing window is attributed to each stimulation trial (pulse). Abbreviations, NS: No stimulation; S1: stimulation polarity S_1 ; S2: stimulation polarity S_2 .

Given the little number of stimulation repetitions, the choice of the statistical test was then limited to a non-parametric test: the Mann Whitney Wilcoxon test. Statistical testing was directly performed in Matlab® using the *ranksum* function of the statistical toolbox. Consequently, a p -value could have been calculated for each stimulation polarity and for each animal.

5 THE EXPERIMENTAL OBSERVATIONS

In view of the small number of stimulated animals versus the variants of the stimulation protocol, the results presented in this chapter can be interpreted in a preliminary perspective. In the following pages, the experimental results are presented and discussed.

5.1 IN VIVO EFFECTS

The visual inspection of the recorded iEEG signals in the absence of and directly after the end of stimulation was not sufficient to confirm an eventual effect of stimulation polarity. As for stimulation duration, one conclusion can be made: when stimulation duration is as long as 100 s, the recorded iEEG signals after stimulation seem to be less epileptic for both stimulation polarities. Figure 71 to Figure 73, illustrate sample signals recorded in the absence of stimulation (Figure 71), and others recorded after distinct stimulation trials of duration 100 s, and of polarity S_1 (Figure 72) and S_2 (Figure 73) respectively. Given that the scale is approximately doubled for Figure 72 and 9, the intensity of the present discharges of all types (isolated or continuous) is highly dampened. No further results could be concluded from the visual inspection of the signals. Sample iEEG signals for other stimulated animals are presented in Appendix B.

5.2 THE EFFECTS OF STIMULATION POLARITY

LFP signals were analyzed using the methods defined in chapter 7 over an analysis window of 120 s. Then, the computed features over the different stimulation conditions (No Stimulation (NS), S_1 stimulation and S_2 stimulation) were represented in boxplots. The boxplots (Figure 74 and Figure 75) show that an S_1 stimulation polarity tends to diminish HPD occurrence and duration when applied for 40s in mouse K148, and for 50s in mice K155 and K168. Conversely, the S_2 stimulation polarity does not seem to have an effect. As for mouse K171, the boxplots show that the S_2 stimulation polarity may provoke an antiepileptic effect when applied for 50 s. For this mouse, the S_1 stimulation duration does not seem to have an effect. As for mouse K143 (Figure 76), both stimulation polarities seem to provoke a more or less an antiepileptic effect when applied for 100 s. A hyperpolarization antiepileptic effect was assumed when a stimulation polarity diminishes the occurrence, duration, as well as the intensity of epileptic events.

Further statistical investigation using the Mann-Whitney non-parametric test (5% significance level) showed that the antiepileptic effects revealed in the boxplots of the stimulated animals are significant for mice K148, K155, and K171. For details, the statistical test was operated per animal on the total duration of HPDs feature. The results are detailed in Table 9.

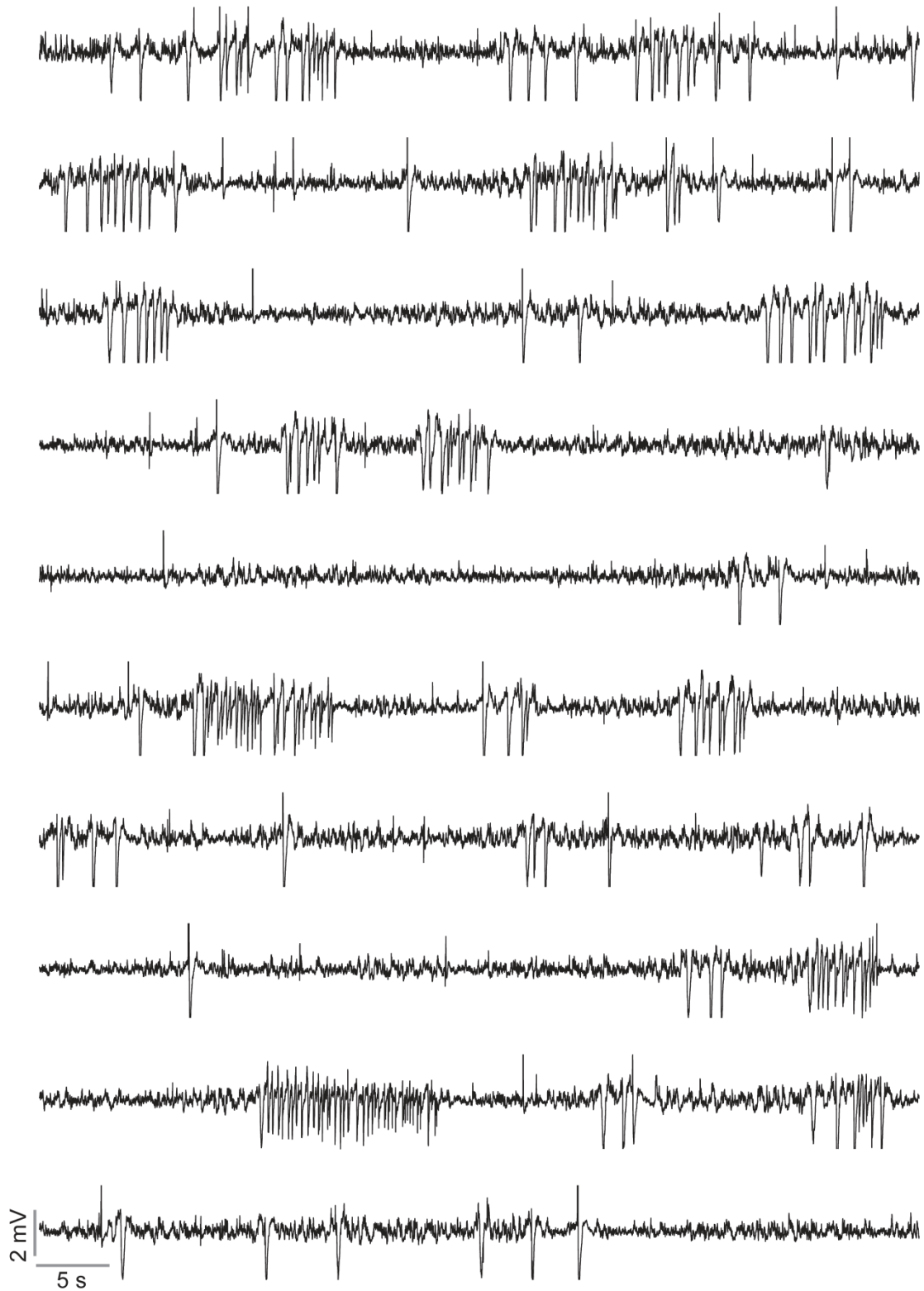


Figure 71. Example signal segments (**mouse K143**) in the absence of stimulation. Note the recurrence of HPDs and isolated sharp waves and spikes.

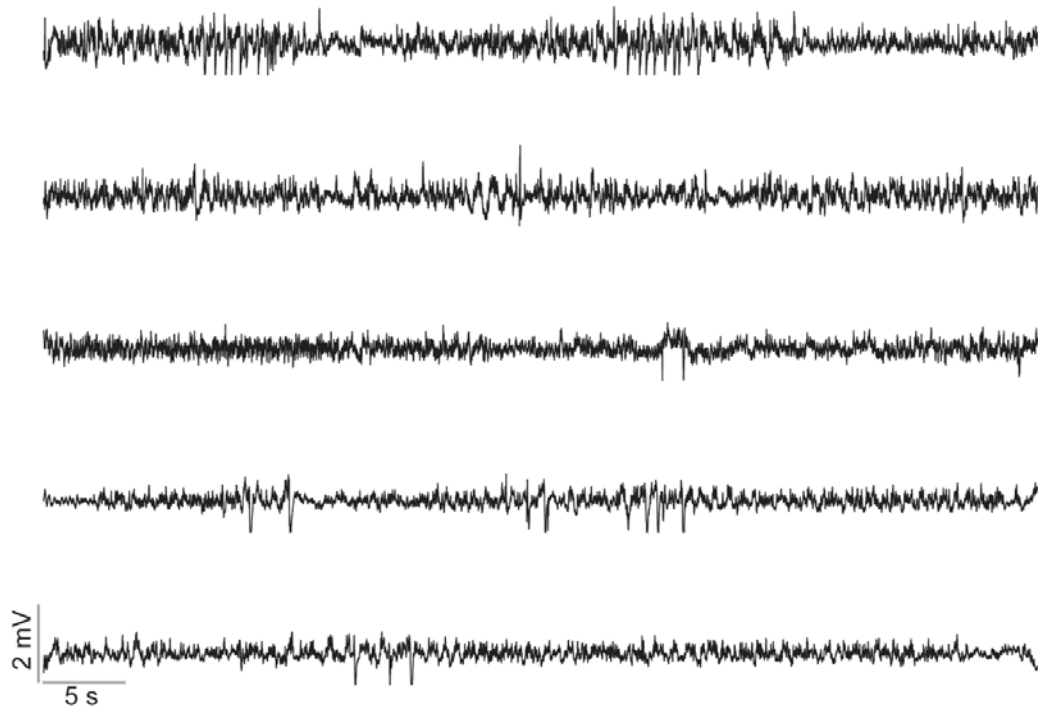


Figure 72 Signals recorded just after the end of 100 s S_1 stimulation (**mouse K143**) during different sessions. Note the reduction in number and intensity of HPDs in the recorded signals. This was observed for both polarities.

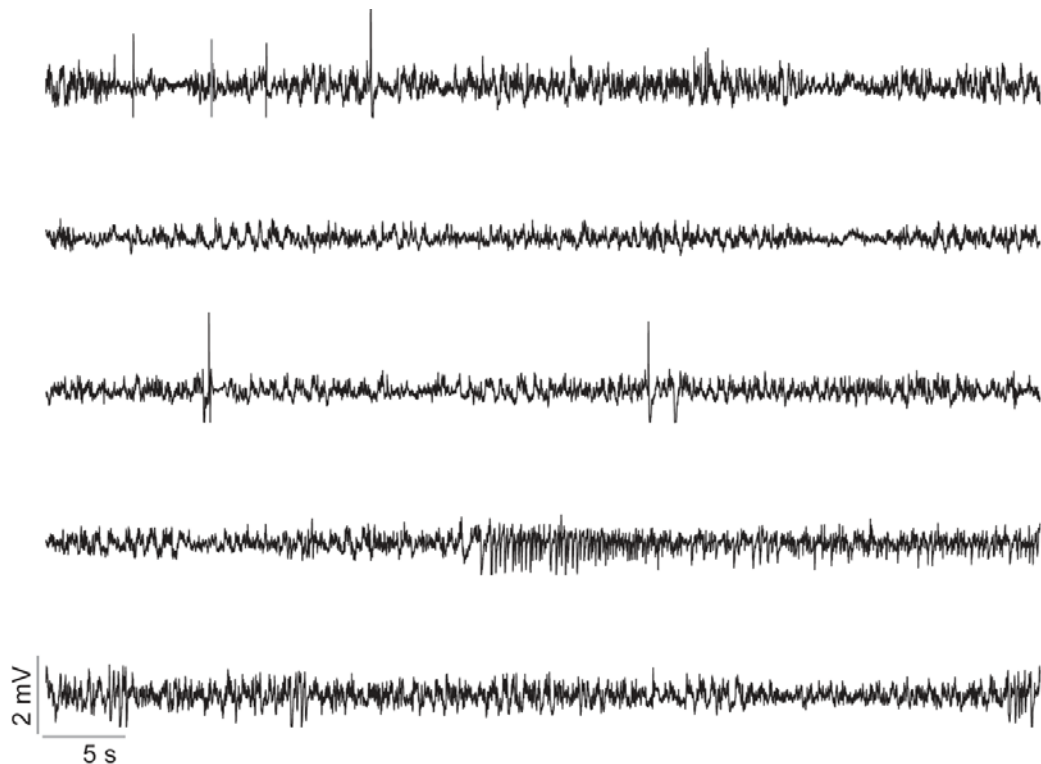


Figure 73. Signals recorded just after the end of 100 s S_2 stimulation (**mouse K143**) during different sessions. Note the reduction in number and the intensity of HPDs in the recorded signals. This was observed for both polarities.

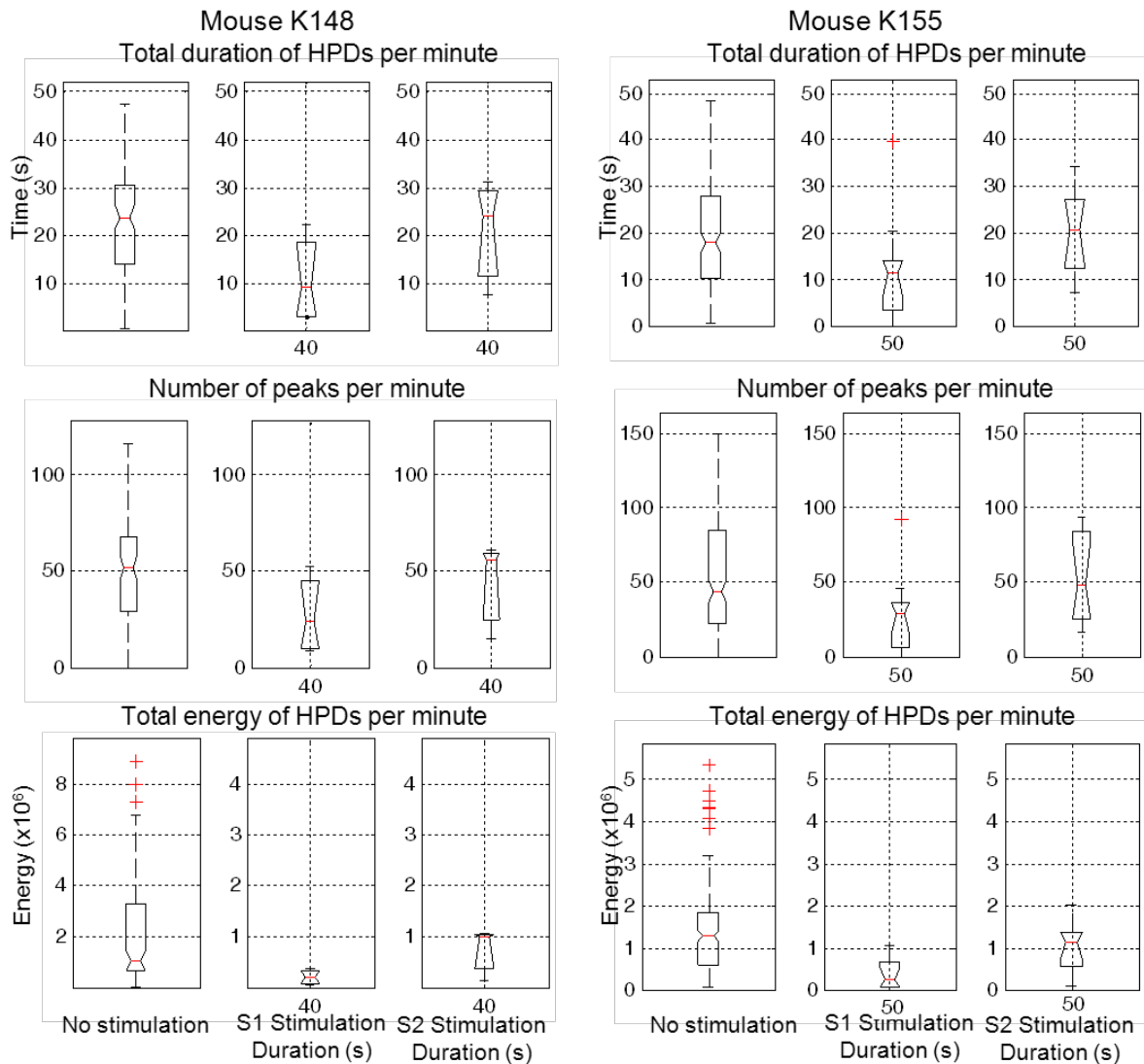


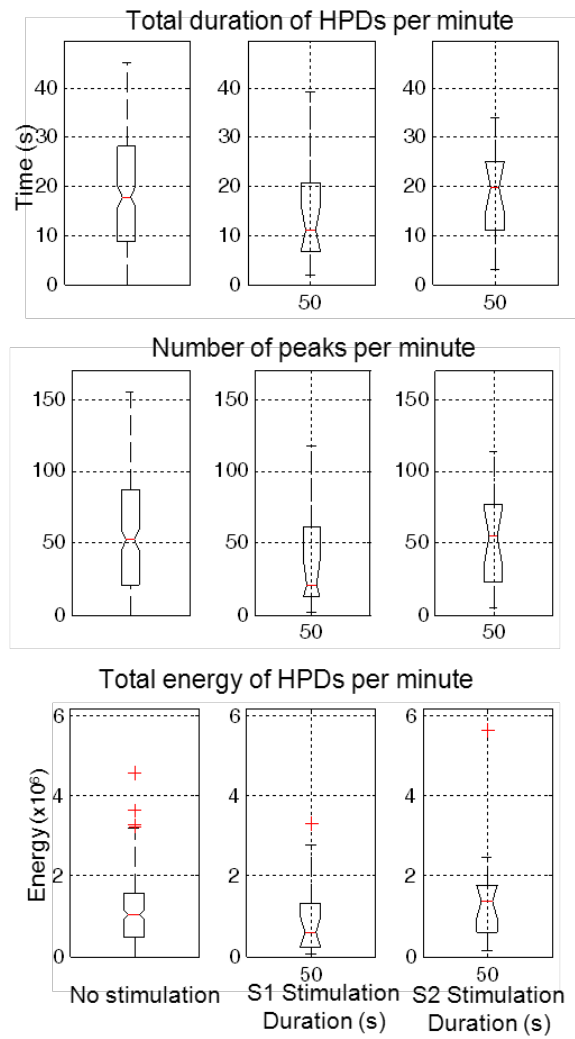
Figure 74. Boxplots of the signal features of mice K148 (number of trials: NS = 220, S1 = 4, S2 = 3) and K155 (number of trials NS = 238, S1 = 12, S2 = 10) in the absence and just after the end of a stimulation pulse of polarity S_1/S_2 . Features computed over 120 s windows. Note the visible decrease in epileptic features (HPD duration, number of peaks and total energy of HPD/minute) for an S_1 stimulation polarity in both mice. An S_2 stimulation polarity does not present a significant effect.

5.3 THE EFFECTS OF STIMULATION DURATION

Given the visual damping effect of iEEG signals after a stimulation of 100 s duration (mouse K143), a further analysis of the evolution of the discharge intensity longtime after the end of the stimulation session was performed. The results revealed an irreversible damping of the intensity of discharge/minute when the stimulation duration is of the order of 100 s. A slight recovery in the discharge intensity (1/3 of the initial value) was observed 4 days after the last stimulation session (see Figure 77). However, this recovery was annihilated by a subsequent stimulation session at Day 57. No further recovery was observed in the following month. This is probably due to the KA-provoked cell dispersion in CA1, more than 90 days after the injection. Consequently, stimulation

sessions were limited to 45 days after KA-injection. Moreover, in order to assess the contribution of the stimulation duration to stimulation effects, the protocol variant P₃ was designed and tested on mouse K148. Eventually, a more robust experimental validation should be performed in the future to verify the results illustrated in Figure 78.

Mouse K168



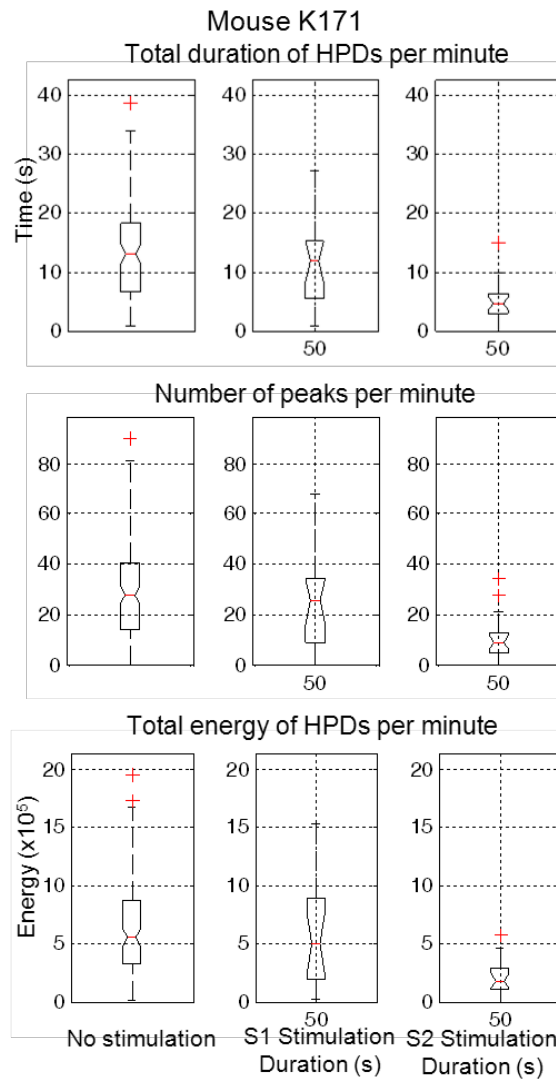


Figure 75. Boxplots of the signal features of mice K168 (number of trials: NS = 240, S1 = 19, S2 = 20) and K171 (number of trials NS = 288, S1 = 18, S2 = 20) in the absence and just after the end of a stimulation pulse of polarity S_1/S_2 . Note that the a hyperpolarizing effect of S_1 for mouse K168 is not evident. Features computed over 120 s windows. Note the visible decrease in epileptic features (HPD duration, number of peaks and total energy of HPD/minute) for an S_2 stimulation polarity in mouse 171. An S_1 stimulation polarity does not present a significant effect. On the other hand mouse K168 does not seem to respond to DC stimulation. Note that later histological verification showed the presence of the stimulation electrodes in the CA3 hippocampal region for this mouse.

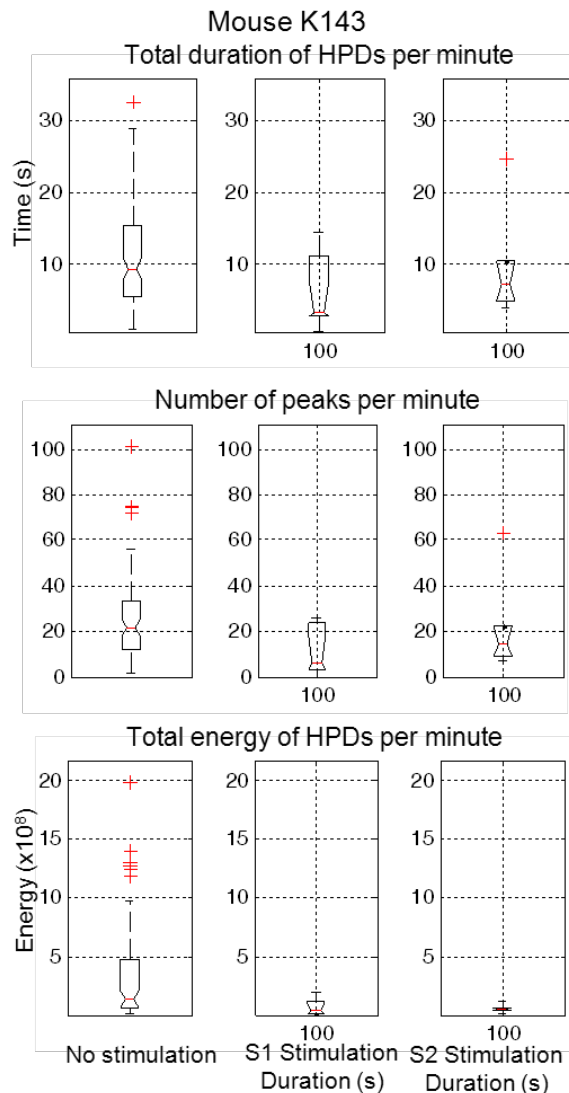


Figure 76. Boxplots of the signal features of mouse K143 (number of trials: NS = 200, S₁ = 8, S₂ = 6) in the absence and just after the end of a stimulation pulse of polarity S₁/S₂. Features computed over 120 s windows. Note the visible decrease in epileptic features (HPD duration, number of peaks and total energy of HPD/minute) for both stimulation polarities in this mouse.

Figure 78 represents the boxplots of stimulation effects in three groups, the NS group, the S₁ and the S₂ stimulation polarity group. The two latter groups represent the iEEG signal features in function of the stimulation duration [5, 10, 20, 30, 40, 50 s]. Apparently, stimulation durations as short as 5 – 20 s do not have an effect. However, a stimulation duration around 30 – 40 s seems to diminish epileptic features for an S₁ polarity, and to slightly reinforce HPD generation for an S₂ polarity. However, stimulation durations of 50 s seem to be the limit of stimulation polarity effect. Both polarities relatively diminish the epileptic features in the recorded signals. This is particularly obvious for the total duration of discharge and the number of peaks feature. As for the intensity of discharge feature, it seems that the energy of total discharge starts falling when the stimulation duration is as short as 20 s.

Souris	#NS	#S1	#S2	Ranksum_S1			Ranksum_S2			
				h	p	sum	h	P	sum	
K155	119	12	10	1	0.0161	490	0	0.9333	660	
K168	120	19	20	0	0.7475	1277	0	0.6065	1497	
K171	144	18	20	0	0.9299	1450	1	0.0221	1194	
K148	40s	110	4	3	1	0.0429	98	0	0.7546	153
	50s	110	2	1	1	0.0230	9	0	0.2958	22
K143	100s	100	8	6	1	0.0218	240	0	0.5071	272

Table 9. The results of the Mann-Whitney test per animal. Illustrated: the number of trials in the absence of stimulation (#NS), after a stimulation polarity S_1/S_2 (#S1, #S2 respect.), the p -value, the sum (Mann-Whitney test), and the null hypothesis ([0, 1] = [not rejected, rejected]). Note that the decrease in the epileptic features of the recorded LFP is significant in mice K148, K143, K155 and K171. This result seemed to be independent of the used stimulation protocol.

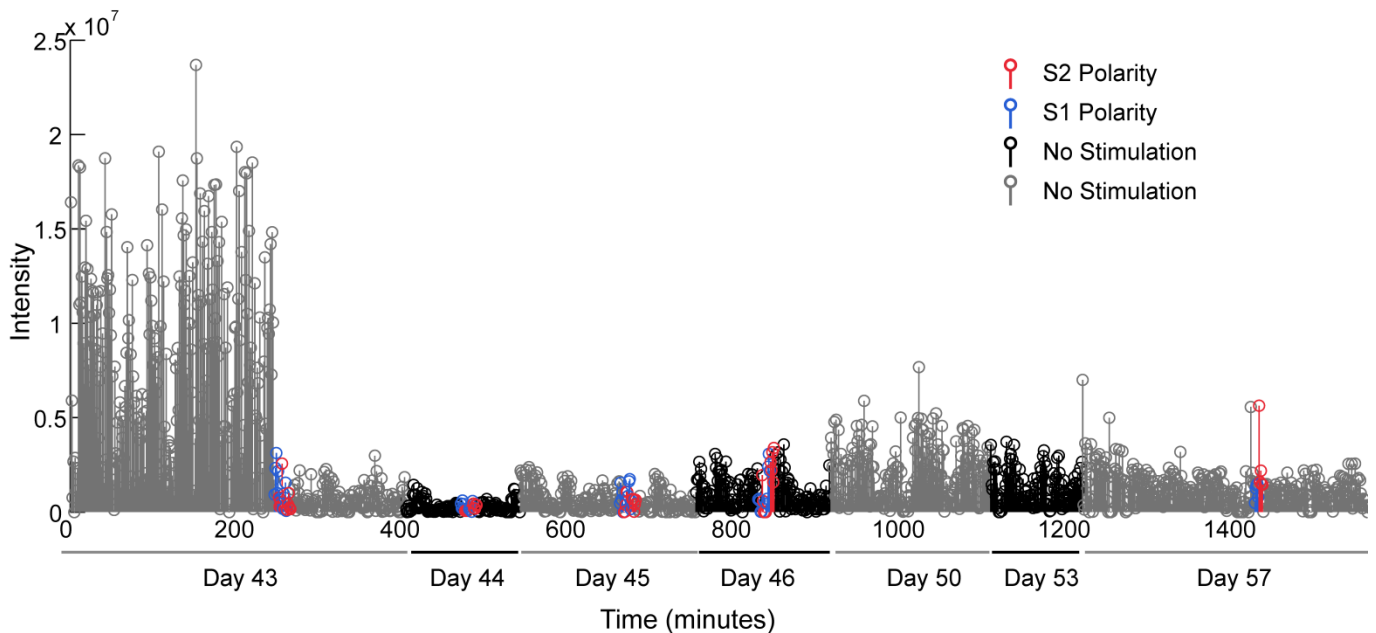


Figure 77. A unique observation of the evolution of the intensity of discharge through stimulation and baseline sessions when excessive stimulation duration is used (100 s). Each point represents the intensity of the discharge in the considered minute (sliding window 0% overlap). The blue/red points correspond to the S_1/S_2 stimulation polarities respectively. Note the brutal fall of discharge intensity following the first S_1 stimulation at Day 43 (after KA injection). The discharge intensity is never recovered due to the daily stimulation sessions between Day 43 and Day 46. However, after a 4-days stimulation pause (Day 50), the discharge intensity slightly recovers to 1/3 of its initial value. A stimulation session at Day 57 re-diminishes the discharge intensity. For this reason, stimulation duration was set to values inferior or equal to 50 s.

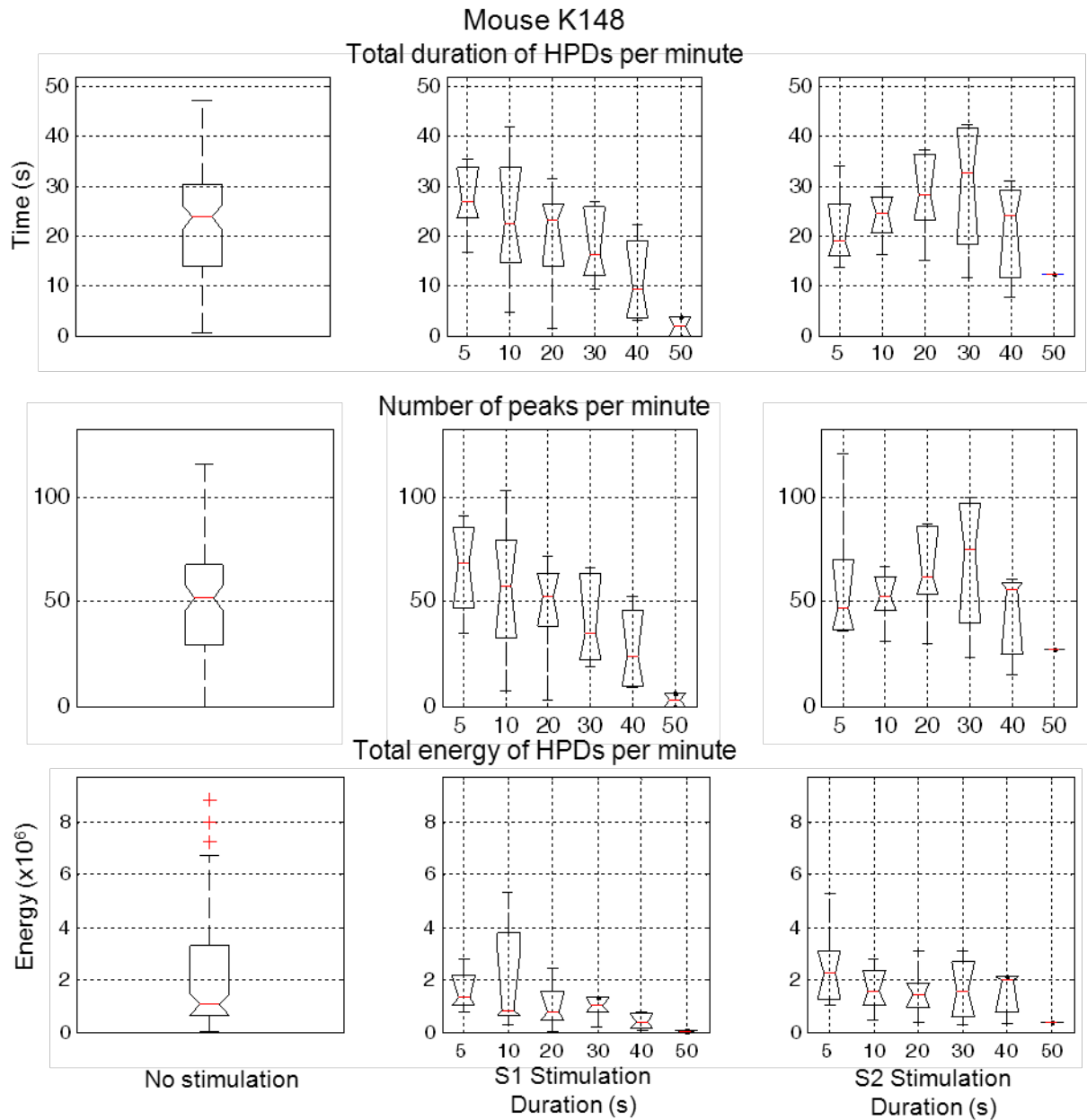


Figure 78. The effects of stimulation duration and polarity on the iEEG signal features. Results observed in mouse K148 (NS = 100; S₁: N_{5s} = 5, N_{10s} = 5, N_{20s} = 5, N_{30s} = 5, N_{40s} = 4, N_{50s} = 2; S₂: N_{5s} = 5, N_{10s} = 5, N_{20s} = 5, N_{30s} = 4, N_{40s} = 3, N_{50s} = 1). Features computed over 60 s windows.

Noteworthy, mouse K148 underwent spontaneous convulsive seizures during the 300 s inter-stimulation intervals after a stimulation pulse of polarity S₂ and of duration 5, 20, and 30 s. This was observed during one stimulation session and was not reproduced when the particular stimulation pulse was repeated later in the stimulation session. Since the 50 s stimulation repetitions are limited in number (Table 9) for mouse K148, stimulation repetitions of duration 40 s were represented in Figure 74.

5.4 ELECTRODE POSITION AND STIMULATION EFFECTS ON HIPPOCAMPAL TISSUE

The histological verification of the electrode position and the stimulation effects was not possible for 3 out of 5 mice due to unexpected problems with the cresyl violet coloration. The irreversible aspect of the Nissl staining method did not permit the re-coloration of the mal-colored sections. Figure 79 shows the only visible structure on a mal-colored coronal section of mouse K155. It probably represents the electrode trace in the stimulated lesioned hippocampus. A radial brownish neural proliferation of dimensions (300 μm x 200 μm) can be seen in this section.

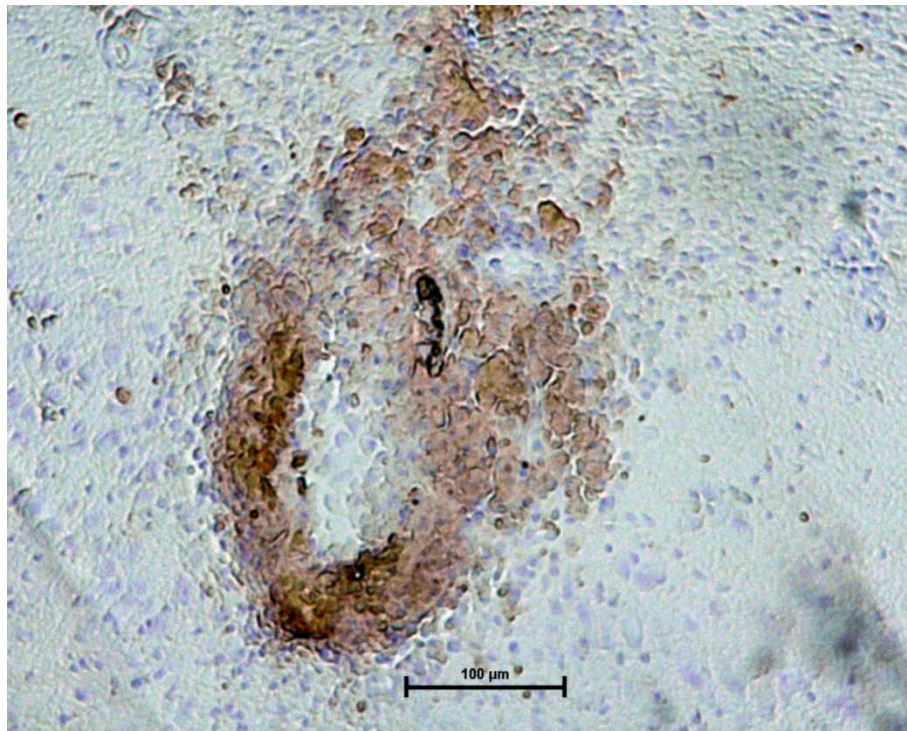


Figure 79. The electrode trace in the injected hippocampus in a mal-colored section of mouse K155. A radial gliosis can be observed around in the tissue.

Fortunately, the histological sections of mice K168 and K171 were successfully performed and stained (Figure 81 and Figure 80 respectively). Figure 80 shows selected coronal sections of mouse K171. On the first section, the two hippocampi can be seen with an arrow indicating the position of the recording electrode in the non-injected hippocampus. Note the slight cellular disorganization around this electrode (Figure 80-A). The second section shows the position of the recording/stimulation electrode in the lesioned hippocampus (right side). Visibly the purple stain (Figure 80-B) showing the trace of this electrode is much more prominent than that of the contralateral hippocampus.

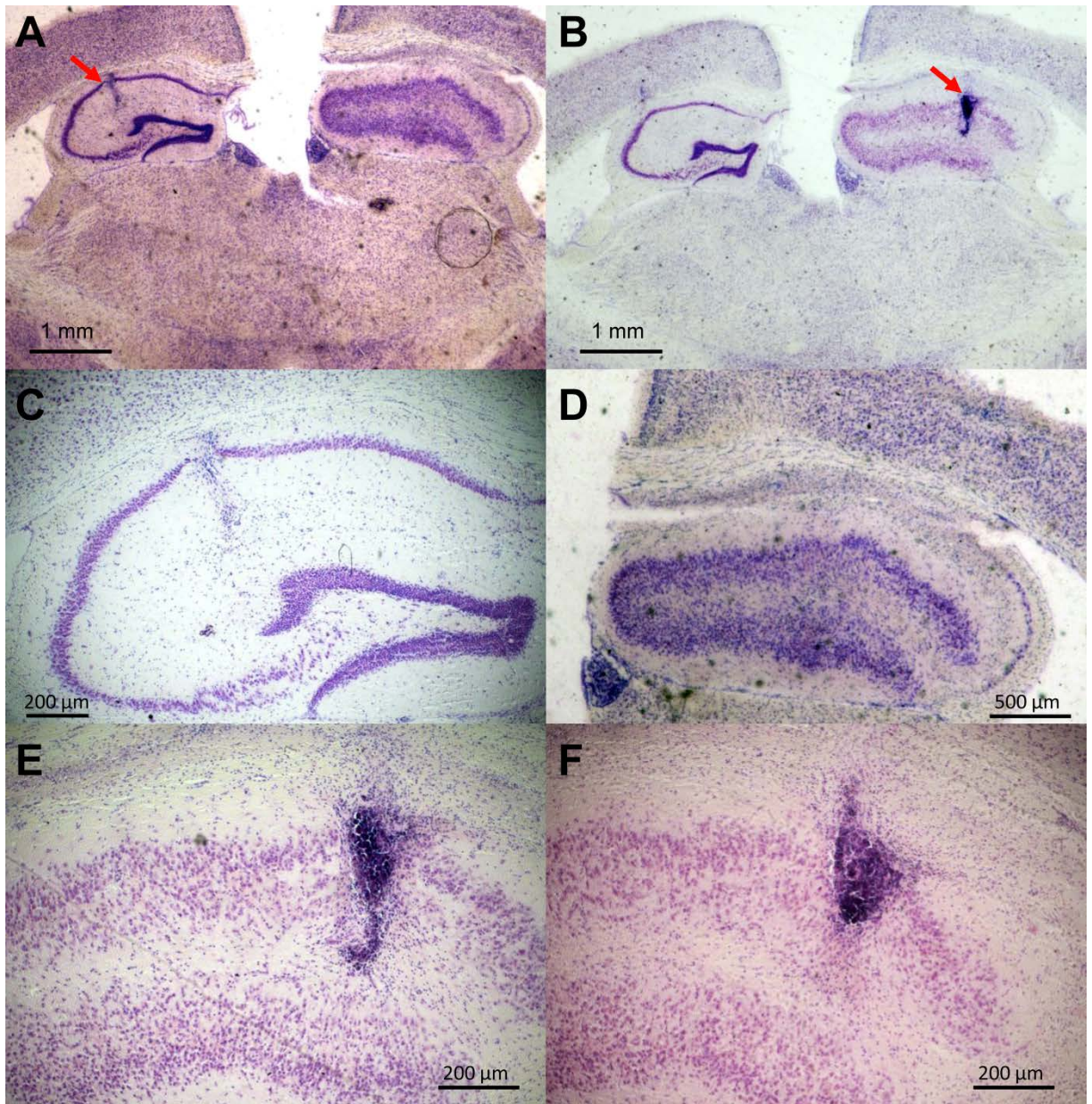


Figure 80. Histological coronal sections of mouse K171. **(A)** A coronal section showing the trace of the recording electrode of the contralateral (not injected) hippocampus (see red arrow) and **(B)** an equivalent section showing the emplacement of the stimulation electrode in the injected (right) hippocampus (see red arrow). **(C)** Zoom on the electrode trace in the contralateral hippocampus. Note the slight neural proliferation around the electrode trace. **(D)** Zoom on the injected hippocampus. Note the cell dispersion in the dentate gyrus, and the extensive cell loss in the CA1 and CA3 layers. **(E, F)** Two examples of two coronal sections showing the electrode trace in the CA1 region. This trace is consistent with the one observed in the CA3 region of mouse K168.

These sections show equally the cellular dispersion in the dentate gyrus, the CA1 and the CA3 layers of the injected hippocampus (Figure 80-D) as compared to the contralateral non-injected hippocampus (Figure 80-C). The radial violet stain at the level of the stimulation electrodes is mostly prominent with a cellular proliferation, a gliosis, between the two tips of the electrode (Figure 80-D and E).

In mouse K168, the cell dispersion in the injected hippocampus could be verified. As for the electrode position, it happened to be in the CA3 region rather than in the CA1 region (Figure 81-A). This may explain the less significant stimulation results obtained for this mouse. Around the electrode position, a spherical cellular proliferation of radius 250 μm can also be reported (Figure 81-B).

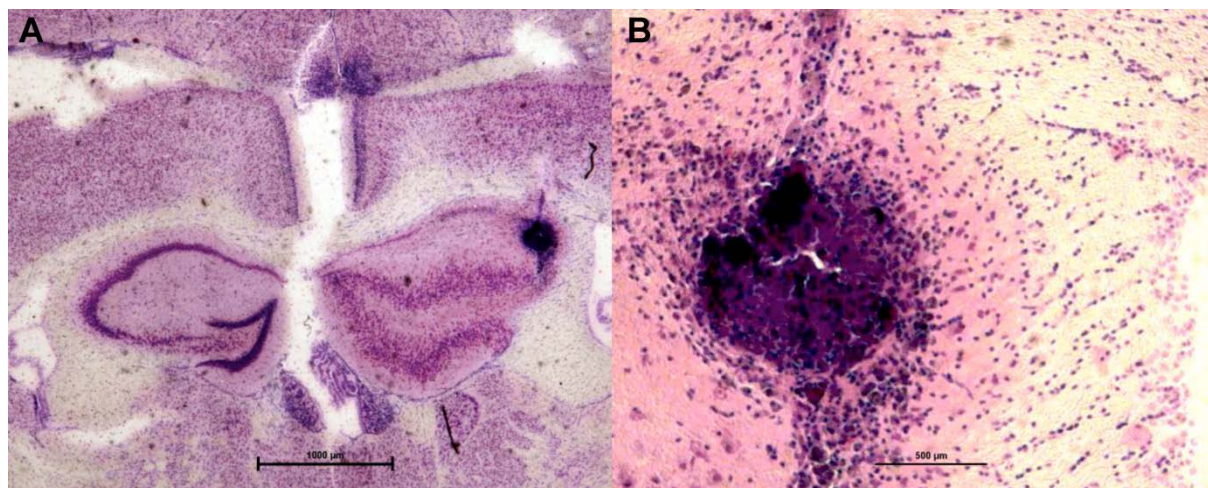


Figure 81. Histological coronal sections of mouse K168. **(A)** Electrode position in the CA3 region of the injected hippocampus. Note the cell dispersion in the right hippocampus (KA-injected). **(B)** Electrode trace in the CA3 region. Note the radial pattern of cell proliferation probably induced between the two tips of the stimulation electrode.

5.5 IN VITRO VERIFICATION

Extracellular recordings provide a lumped measurement of the underlying neuronal activity. Therefore, only based on LFP recordings, it is difficult to guarantee that the observed changes in HPDs are only caused by membrane polarization effects. The absence of some other mechanisms also participating into these HPD changes cannot be completely ruled out. Thus, *in vivo* recordings were complemented by *in vitro* experiments in order to better assess cell- and network-related mechanisms occurring under low-intensity DC stimulation.

Moreover, to our knowledge, the effects of radial long-duration (> 1 s) electric fields, induced by microwires, on the membrane potential of stimulated neurons have never been studied. For these two reasons, the following *in vitro* verification of the intracellular effects underlying the measured *in vivo* stimulation effects was undertaken. Rat organotypic hippocampal slices were then used in order to verify the existence of DC stimulation polarizing effects in the context of radial currents. Patch clamp recordings in whole cell configuration were done. The cells were patched in the pyramidal layer. A bipolar stimulation electrode was placed on either side of the CA1 layer (e.g. one electrode tip in the stratum oriens and the other in the Stratum radiatum layer).

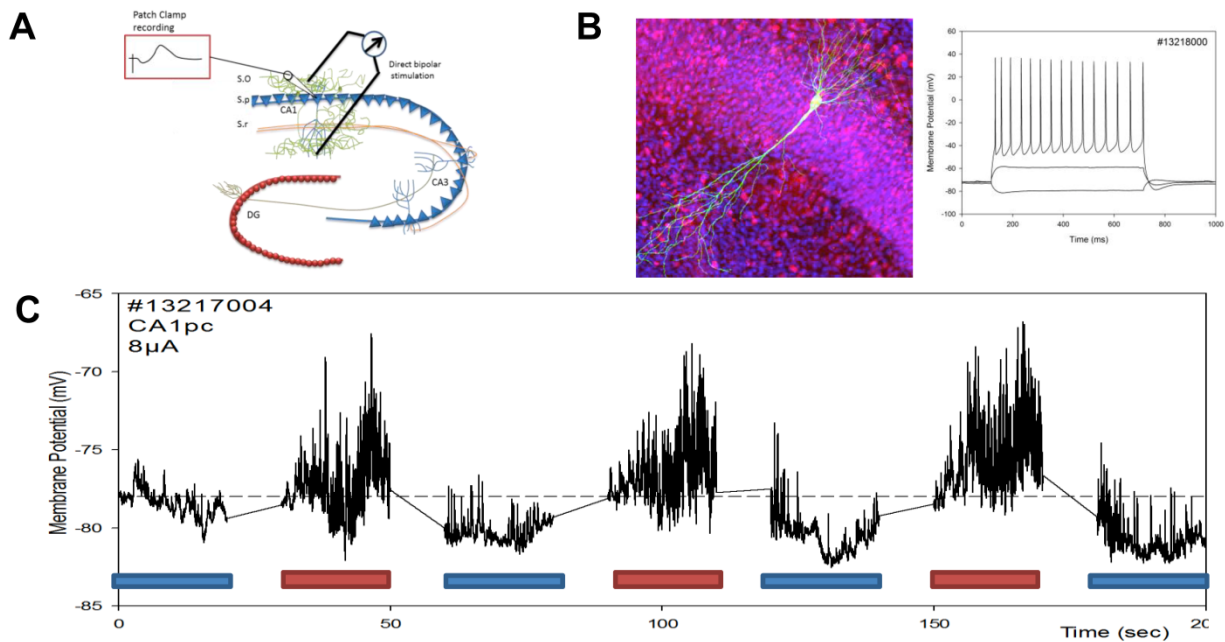


Figure 82. Patch Clamp recordings in whole cell configuration of organotypic rat hippocampal slices from pyramidal CA1 neurons. **(A)** The experimental setup. Cells were patched in the pyramidal layer. A bipolar stimulation electrode was placed on either side of the pyramidal cell layer. **(B)** Pyramidal neurons were injected with Biocytin and were recorded in current clamp mode. The resting membrane potential, the cellular morphology and the presence of dendritic spine were the identifying characteristics of a pyramidal cell. **(C)** In normal excitability condition (ACSF), the value of the resting membrane potential of a CA1 pyramidal cell is increased or decreased depending of stimulation polarity.

Intracellular cell recordings were performed using a glass pipette containing a microelectrode. In normal excitability conditions (ACSF), a DC stimulation current of $8\mu\text{A}$ was delivered by pulses of alternating phases of 30 s each. The recorded membrane potential of a pyramidal CA1 cell was then modulated by the current polarity, increasing during negative polarity and slightly decreasing during the positive one (Figure 82-C). Otherwise, in high excitability conditions (decrease in extracellular Mg^{2+} concentrations with $10\mu\text{M}$ of Bicuculine), the effects were slightly altered. A positive polarity 100 s stimulation pulse at $15\mu\text{A}$ did not change the resting membrane potential whereas a negative polarity 100 s stimulation pulse elicited enormous spike-like events (Figure 83-A). Similarly, the intracellular recordings from a basket cell (interneuron) revealed equivalent stimulation results. While a positive polarity 100 s stimulation pulse at $15\mu\text{A}$ did not change the resting membrane potential, a negative 100 s stimulation pulse at the same intensity induced an enormous long-lasting depolarization of the resting membrane potential (see Figure 83-B).

Then, in order to verify whether the observed effects are dependent on network dynamics rather than membrane polarization, similar experiments were repeated in the presence of the voltage-gated sodium channel blocker TTX ($1\mu\text{M}$). Consequently, depolarization effects were reproduced but at significantly higher current intensities ($> 50\mu\text{A}$). When tested in basket cells, a linear relation between the current intensity and

the membrane potential deviation could be observed. Depending on the polarity, the resting membrane potential of basket cells could be either hyperpolarized or depolarized.

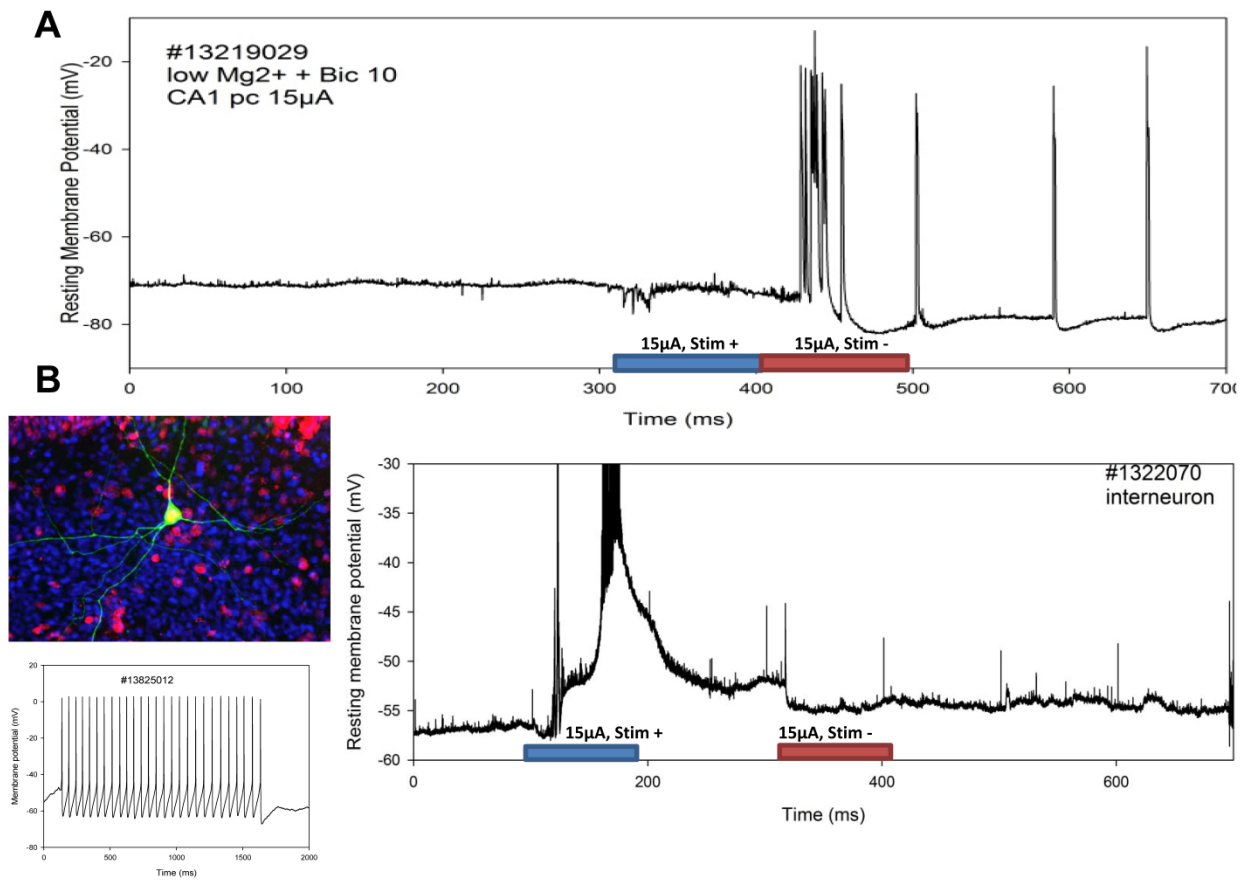


Figure 83. Patch Clamp recordings in whole cell configuration of organotypic rat hippocampal slices. **(A)** In high excitability conditions (low extracellular Mg^{2+} and $10\mu M$ Bicuculline), one stimulation polarity induced spike-like activity while the opposite polarity had no effect. **(B)** The effect of DC stimulation on a basket cell (interneuron). Basket cells were labeled with biocytin, they were characterized by the absence of dendritic spines, a more depolarized resting potential and a typical firing pattern. One polarity induced a prominent depolarization of basket cells while the other barely had an effect.

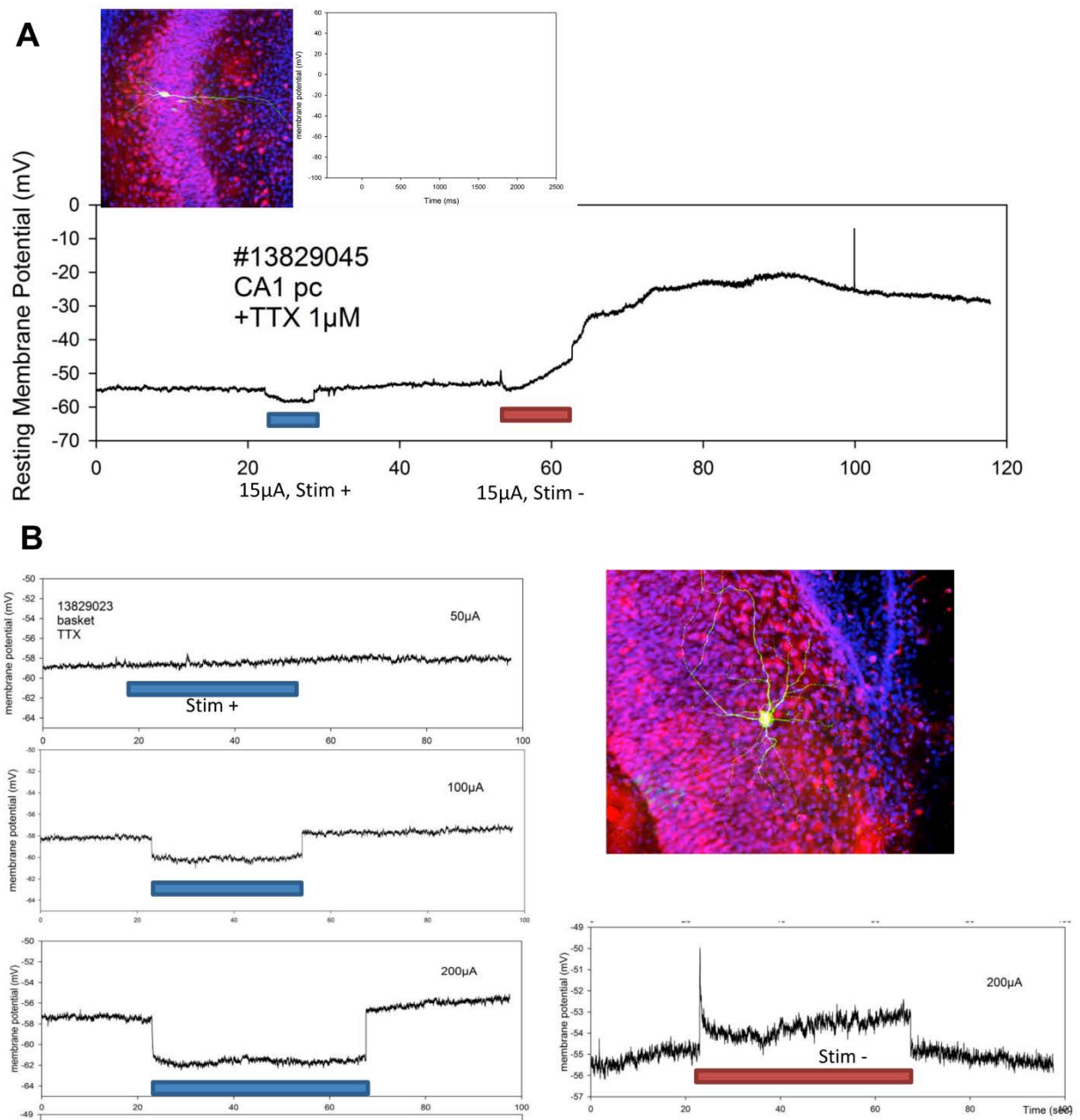


Figure 84. Patch Clamp recordings in the presence of the voltage-gated sodium channel blocker TTX (1 μ M). **(A)** Higher stimulation current intensities were necessary for inducing a direct polarization in the absence of synaptic transmission suggesting that the effects stimulation are independent of the neuronal network activity. **(B)** Hyperpolarizing basket cells was only possible for extremely high current intensities. The effect seems to increase linearly with the stimulation intensity. Inverting stimulation polarity reverses hyperpolarization to a depolarization.

Finally, this in vitro part can be resumed by the following three conclusions:

- (1) Direct bipolar DC stimulation currents can depolarize/hyperpolarize pyramidal CA1 cells.
- (2) These currents equally polarize interneurons.

(3) The major effect at low current intensities can be attributed to more complex network effects rather than the simple polarization of individual somatic transmembrane potentials. Actually, the observed effects depend on synaptic transmission. Nevertheless, a dominant effect exists leading either to an increase or a decrease of the stimulated neuronal system excitability.

Conclusion and Discussion on Part 2

1 POSITION WITH RESPECT TO EARLIER STUDIES

Except the “quenching” effects of low-intensity intracerebral DC stimulation (10 μ A – 15 minutes/day) accidentally observed in adult rats during the kindling protocol due to the stimulator leakage [242], no *in vivo* experiments of low-intensity DC stimulation has ever been reported. Conversely, a number of *in vitro* studies addressed the polarizing effects of DC stimulation [34-36, 237, 238] on CA1 neural dynamics. In the following paragraphs, our results are confronted with the state of the art of polarizing stimulation.

1.1 *IN VIVO* OBSERVATIONS

In this part, our results show that a certain polarity of long-duration (> 30 s and \leq 50s) DC current applied on the epileptogenic zone can be identified in the perspective of diminishing epileptiform discharges *in vivo*. In a similar perspective, the modulation of epileptiform activity with intra-cerebrally applied electric fields in chronically implanted animals seems to be possible according to two recent studies [266, 267]. In both studies, low frequency (\approx 9 Hz [266], 0.25 Hz [267]) applied electric fields modulated the seizure dynamics of the stimulated animals. Nevertheless, the duration of the DC stimulation pulse was inferior to 10 s in all the tested protocols [267], otherwise a sinusoidal waveform was used [266]. No histological damage was reported in the three aforementioned studies.

In fact, Richardson and his colleagues [267] showed that a cylindrical electrode placed axially in the hippocampus, induces a polarizing radial electric field that is aligned with the CA3 pyramidal cells, and can then modulate their activity. In this work, the experiments were done in freshly KA-injected rats under anesthesia. The authors report an induced excitation of the field activity of CA3 pyramidal cells exclusively for the negative phase of stimulation when a phasic stimulation of frequency 0.025 Hz, pulse width 10 s, and amplitude 1.2 mA is used. Similar results were obtained when the stimulation signal was replaced by a sinusoidal signal of frequency 0.2 Hz and amplitude 1.25 mA was used. Conversely, the authors reported the suppression of the field activity only for a phasic stimulation of 0.25 Hz, of pulse duration 1 s and of intensity 0.01 mA. The inverse phase elicited excitation.

Similarly, Sunderam and his colleagues tested the effects of low frequency induced electric fields on seizure modulation in chronically implanted rats [266]. In this study,

the authors used a low-frequency (9, 11 or 15 Hz) sinusoidal stimulation signal of amplitude 110 μA to entertain chemically induced seizures (tetanus toxin). The authors prove that the chemically-induced seizures are phase-locked to the stimulation signal. In conclusion, seizure dynamics were modulated by the stimulation signal.

Moreover, none of the preceding studies reported histological damage related to stimulation. Conversely, the histological verification presented in the previous chapter (section 5.4) showed a radial cellular proliferation around the stimulation electrodes. No further verification has been performed to study the nature of this proliferation at the moment. Yet future protocols can be designed to clarify this point.

1.2 *IN VITRO* OBSERVATIONS

Extracellular recordings of CA1 activity showed that subthreshold anodal currents, with an average amplitude of 3.9 μA (minimum 1 μA), were sufficient to suppress spontaneous epileptiform field activity [35]. Conversely, cathodal currents prolonged the duration of ictal events. Similarly, anodal electric fields exerted a similar effect on the activity of CA1 pyramidal cells in hippocampal slices [36, 238]. Field recordings showed an increase in the AP threshold of CA1 pyramidal cells placed in hyperpolarizing fields vice versa [36].

On the intracellular recordings of CA1 pyramidal cells [34] revealed a direct hyperpolarizing effect on neuronal membrane when electric currents are applied for short durations (10 ms). The suppressive effects lasted 1 s after the end of stimulation, and proved independent of field polarity and network signaling (synaptic transmission and Ca^{2+} current influx). This effect was dependent on the orientation of the induced electric field with respect to the somato-dendritic axis; the most significant effects obtained when these two are aligned. These results suggested that the prolonged suppression of epileptiform activity may be related to stimulation-induced changes in the membrane properties including the attenuation of Na^+ current dependent signals. Nevertheless, long-duration (> 20s) DC stimulation intracellular recordings were never reported in the literature. Consequently, the intracellular recordings presented in the previous chapter during 100 s stimulation episodes add up a new element to the understanding of the polarizing effects of stimulation.

Eventually, the *in vitro* results reported in this study are probably the unique reported results concerning the effect of radial long-duration electric fields on pyramidal CA1 neurons as well as interneurons measured by intracellular electrodes. These results suggest a possible polarization of neural membranes by radial stimulation currents. This polarization may affect both principal cells and interneurons. Yet, the privileged explanation of the observed effects highlights a more complex network mechanism rather than simple polarization.

2 POLARIZATION OR A NETWORK EFFECT

Actually, when analyzing jointly the *in vivo*, the *in vitro*, and the computational results presented in the previous chapter, we directly get the conclusion that the mechanisms of the diminution of the field epileptic activity may be more complicated than a simple polarity-dependent polarization of the transmembrane potential of the stimulated neurons. Hereby, the different results are confronted and analyzed.

Concerning the computational results, the model output is dependent on the polarity of the stimulation signal. This is particularly true when the inversion of the current polarity is modeled as the inversion of the sign of the impact factors on the pyramidal cell subpopulation as well as the two interneuron subpopulations. Hereby, the effect of a depolarizing 1 μA current was reflected in the increase (almost doubling) of discharge occurrence, duration and consequently intensity. Conversely, a hyperpolarizing current of the same intensity only divided by two the discharge occurrence, duration and intensity. In conclusion, depolarization effects were more marked in the model than the hyperpolarization effects.

On the experimental aspect, the *in vivo* experimental results presented earlier indicate that stimulation polarity has a preferential suppressive effect of epileptiform activity. While a certain current polarity diminishes epileptiform discharges in LFP signals, the opposite polarity does not seem to have a significant effect on discharge patterns. This is particularly true when stimulation duration is sufficiently long but inferior to 50 s. If this duration constraint is not respected, stimulation results in a suppressive effect for both stimulation current polarities.

Finally, as hinted by the preliminary *in vitro* results presented in the preceding chapter, polarizing effects are not outstanding in the normal excitability condition. They can be seen as mere positive/negative fluctuations of the transmembrane potential depending on current polarity. However, in excitable tissue, a preferential depolarization effect has been observed in both pyramidal and basket cells (a type of interneurons) for a specific polarity, the opposite polarity having barely any effect. Besides, these results demonstrate that polarization effects are more marked in the absence of synaptic transmission in the patched hippocampal slices. However, enormous current intensities ($> 50 \mu\text{A}$) had to be used in order to observe an effect.

On first sight, the reconciliation of the aforementioned results (computational and experimental: *in vivo* and *in vitro*) might seem tricky. However, if we suppose that the intensity of the electric current used *in vivo* is sufficient to provoke a local polarization (depolarization/hyperpolarization) of the pyramidal cells/interneurons theoretically lying between the two tips of the stimulation electrode, we can assume that the results obtained computationally should be theoretically observed *in vivo*. However, since this

is not the case, we can imagine that other mechanisms may be responsible. It has been reported that the LM interneurons (the interneurons of stratum lacunosum-moleculare) of the hippocampus are easily depolarized under the effect of external electric fields independently from the field polarity [36]. In which case, a class of interneurons is expected to be depolarized by the stimulation current independently from the current polarity. Therefore, the depolarization of these interneurons can be expected to compensate the depolarization of pyramidal cells during cathodal stimulation, and to reinforce the hyperpolarization effect during anodal stimulation. In the model, under this hypothesis, the depolarizing effect of cathodal stimulation can be avoided.

In conclusion, the polarization effects of low-intensity DC stimulation can be interpreted in a network perspective that necessitates the presence of the polarizing current effect alongside with the intrinsic network components in order to suppress epileptiform activity.

3 FUTURE IMPLICATIONS OF THE RESULTS

During the stimulation protocol, it was observed that 4 pulses of hyperpolarizing stimulation of duration 50 s and intensity 1 μ A distributed over an interval of 20 min allowed the attenuation of the occurrence of epileptic paroxysmal discharges in the following 30 – 45 minutes. This implies a reversible relatively long-lasting suppressive effect of stimulation. Consequently, three aspects need to be better-defined and verified before this protocol can be used in clinics. The first one concerns the precision in the stimulation electrode implantation site. The second consists of the validation of the polarity-effect relationship. The third consists of a further verification of safety issues. That is, once the hyperpolarizing stimulation polarity is well-defined and validated experimentally, the adapted monophasic stimulation bipolar electrode characteristics should be chosen to minimize any possible faradaic electrode polarization on the long-term. Only then, chronic closed-loop low-intensity DC stimulation protocols can be tested for efficacy and long-term safety issues.

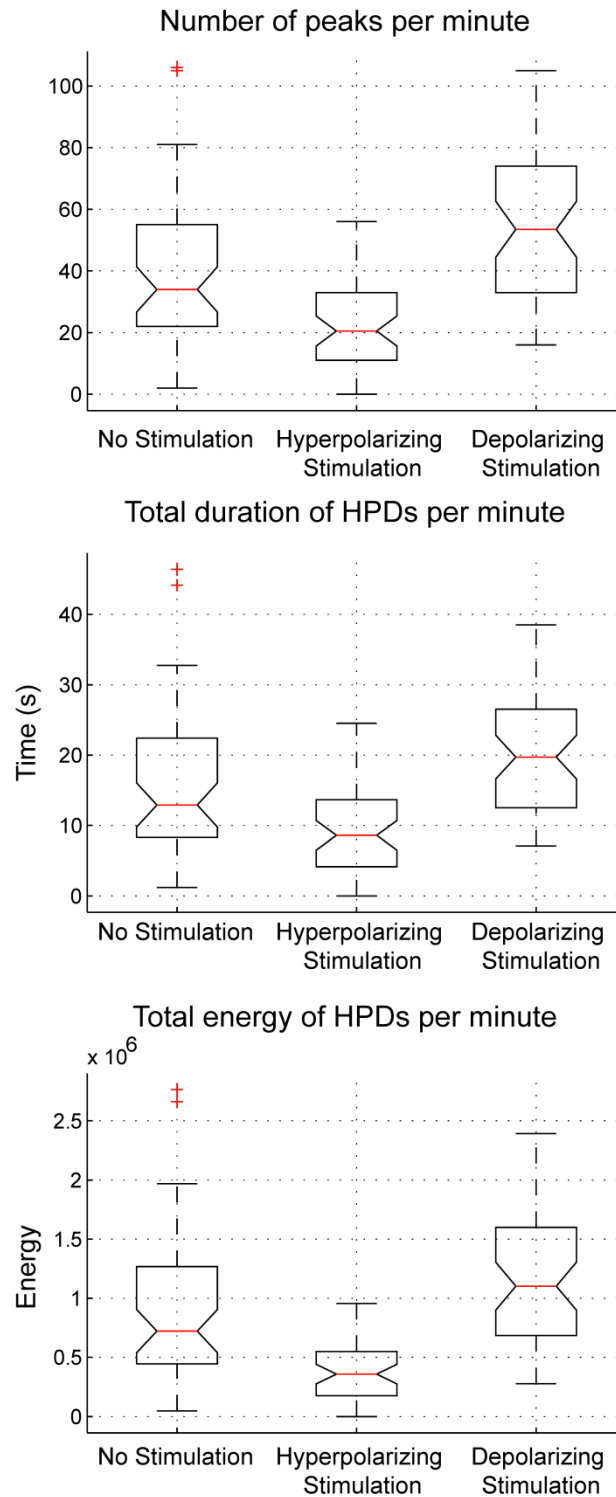


Figure 85. Simulated Boxplots of HPD occurrence during polarizing stimulation under the hypothesis that FSI are always depolarized by stimulation. It can be deduced that the effect of the depolarizing stimulation is less marked than the one shown in the previous simulated boxplot (Figure 63). This is a potential element to take into consideration in a future study.

Another less invasive clinical implication of the presented results can be imagined. It concerns the application of transcranial polarizing long-duration DC stimulation (tDCS)

on focal epileptogenic lesions such as focal cortical dysplasias (such as the clinical case presented in Chapter 4).

4 LIMITATIONS AND PERSPECTIVES

Eventually, this study has some limitations that can be outcome in the future. First, the manual electrode implantation procedure and kainate injection result in an imprecision in the electrode emplacement with respect to the CA1 level. As demonstrated earlier in Chapter 6, if the two tips of the stimulating electrode are placed both above or below the CA1 layer, polarizing field directions will be most likely inverted. Consequently, the definition of a hyperpolarizing, respectively depolarizing, polarity depends on the exact electrode position. If ever this technical difficulty is impossible to overcome, different pre-stimulation test protocols should be defined in order to define these polarities.

Whenever this first issue is resolved, an elaborated experimental protocol can be defined to overcome the present variability in the protocol variants. The simplest protocol would be to define two groups of animals each of $n = 10$. Each group receives a unique polarity, duration and intensity stimulation pulses. After a defined number of stimulation sessions, LFP signals will be quantified in order to verify the exactitude of the polarity-antiepileptic effect relationship. It is expected that one group experiences a global diminution in discharge occurrence in response to stimulation whereas the other experiences no significant change at best. Histological verifications should be meticulously performed over all stimulated animals in order to verify the safety of the chosen stimulation parameters.

Even when the efficacy and the histological safety of the protocol are verified, one more elaborated test should be performed before a potential clinical translational path is possible; behavioral tests. This would be the only way to verify that this type of stimulation does not have adverse side effects on memory, learning or even motor functions.

General Conclusion and Perspectives

In this thesis, the effects of stimulation on neuronal epileptic activity were addressed from a well-balanced computational-experimental/clinical coupled approach. This approach allied computational modeling, signal processing, nonlinear dynamical systems analysis and experimental data analysis/acquisition. This permitted the further exploration of the effects and mechanisms of stimulation currents as a function of their consequent parameters. Two parts describe this investigation in two distinct stimulation configurations: indirect AC stimulation and direct DC stimulation.

The first part of the manuscript investigated the frequency-dependent effects of thalamic deep brain stimulation (DBS) on cortical dynamics. This is probably one of the most used indirect stimulation settings in the clinical context of focal epilepsy. An adequate model of the involved cerebral network, thalamocortical loop, has been developed (Chapter 3). Two major mechanisms of neural adaptation in the thalamocortical network, feedforward inhibition and short term depression, were equally implemented. The development of a matching pursuit based algorithm permitted the quantification of the frequency content of a rare dataset of thalamic DBS in a patient with drug-resistant epilepsy (Chapter 4). Consequently, the quantified data was used to optimize the model's parameters in the absence as well as during stimulation. This algorithm proved more precise than classical FFT-based characterization.

The results (Chapter 5) of this first study quantitatively proved the frequency-dependent effects of AC indirect stimulation in the thalamocortical network as observed in the clinical dataset. Computationally, the proposed model successfully reproduced the observed epileptic dynamics as well as stimulation effects. Then, the study of the dynamical system's behavior in the phase plane of two major model variables, thalamic firing and cortical LFP, showed that the stimulation input induces in the model the same bifurcations observed due to stimulation in the actual dataset. Furthermore, the quantification of the intermittency of the same two variables on an extended stimulation frequency range (0.5 – 150 Hz), given by the high-to-low firing ratio (*HtoLR*), showed that stimulation frequency can abruptly change the model's behavior. A critical frequency range (20 – 60 Hz) was identified to reinforce undesired pathological epileptic oscillations in the thalamocortical system. Moreover, frequency-dependent stimulation mechanisms were identified in the model.

The rare clinical context of thalamic DBS did not allow the recruitment of other patients with drug-resistant focal epilepsy. However, despite the insufficient availability of

clinical data, it can be assumed that this model can be used patient-wise conjointly with a clinical exploratory thalamic stimulation session for establishing comparable simulated epileptic dynamics, and a consequent frequency-*HtoLR* pattern starting from three different actual stimulation frequencies. This would allow a conjoint clinical-computational approach for optimizing stimulation frequency. Nevertheless, the applicability of such proposition remains bound to a solid experimental validation that should be performed in advance.

The second part of this dissertation provides a more complete study of the polarity-dependent effects of direct DC hippocampal stimulation in the context of MTLE. This investigation starts with a computational study of these effects in a well-established model of hippocampal dynamics already developed in our team (Chapter 6). Two innovative amendments are added to this model. Firstly, a new implementation of HPD occurrence depending on the statistical identification of HPD onset and duration probability from experimental data was proposed. And secondly, a more plausible electrochemical representation of stimulation inputs inspired from previous descriptions of the electrode-electrolyte interface was implemented. Furthermore, to accomplish this computational study, a spike-detection and quantification algorithm based in the Page-Hinkley algorithm was adopted.

The computational results (Chapter 7) suggest a clear polarity-dependence of stimulation effects in the model. The depolarization of principal cells by cathodal stimulation with the slight concurrent hyperpolarization of the interneuron subpopulations during a 50 s DC pulse resulted in an increase of epileptic features (HPD duration and intensity as well as peak occurrence) in the simulated LFP. Conversely, the opposite stimulation polarity induced a decrease in these three quantitative features.

Two preliminary experimental protocols were then proposed in order to verify the exactitude of polarity-dependent effects *in vivo* and to further validate the underlying membrane polarization mechanisms *in vitro* using intracellular recordings (Chapter 8). The *in vivo* results showed the existence of a privileged polarity for significantly diminishing the occurrence of electrophysiological epileptic biomarkers in the recorded LFP signals. Nevertheless, the opposite polarity did not induce a significant effect in these signals. The histological verification of the electrode position indicated an induced cellular proliferation at the stimulation site that was proved to be not of thermal origin. The consequent cellular recordings of transmembrane potential under the effect of radial stimulation currents showed that somatic membrane polarization is only possible for high stimulation currents. Furthermore, they indicated the possible existence of a more complex complimentary network mechanism inducing the *in vivo* observed effects.

In the perspectives of this study, a more detailed study of DC stimulation effects in a microscopic model of the hippocampus is probably worth considering. A more physiological modeling of membrane polarization as a function of the position from the stimulation

electrode can be performed. Besides, a more extended experimental study is also planned on a larger number of animals and with less variant protocol definitions. This new study should take into consideration the electrode position a priori. Moreover, each group of animals will receive only one stimulation polarity in order to discard the hypothesis of effect overlapping and accumulation among consecutive stimulation pulses of varying polarities. In the same perspective, a more elaborated *in vitro* study on a higher number of neurons can be also planned.

References

- [1] J. A. De Carlos and J. Borrell, "A historical reflection of the contributions of Cajal and Golgi to the foundations of neuroscience," *Brain Research Reviews*, vol. 55, pp. 8-16, 2007.
- [2] L. Lapique, "Recherches quantitatives sur l'excitation électrique des nerfs traitée comme une polarisation," *J Physiol Pathol Gen*, vol. 9, pp. 620-635, 1907.
- [3] A. L. Hodgkin and A. F. Huxley, "A quantitative description of membrane current and its application to conduction and excitation in nerve," *The Journal of Physiology*, vol. 117, pp. 500-544, August 28 1952.
- [4] A. L. Hodgkin, A. F. Huxley, and B. Katz, "Measurement of current-voltage relations in the membrane of the giant axon of Loligo," *J Physiol*, vol. 116, pp. 424-448, April 28, 1952 1952.
- [5] K. S. Cole, "Dynamic electrical characteristics of the squid axon membrane.," *Arch. Sci. Physiol.*, vol. 3, pp. 253-25, 1949.
- [6] D. Golomb, C. Yue, and Y. Yaari, "Contribution of persistent Na⁺ current and M-type K⁺ current to somatic bursting in CA1 pyramidal cells: combined experimental and modeling study," *J Neurophysiol*, vol. 96, pp. 1912-26, Oct 2006.
- [7] M. Migliore, M. Ferrante, and G. A. Ascoli, "Signal propagation in oblique dendrites of CA1 pyramidal cells," *J Neurophysiol*, vol. 94, pp. 4145-55, Dec 2005.
- [8] R. Traub and R. Wong, "Cellular mechanism of neuronal synchronization in epilepsy," *Science*, vol. 216, pp. 745-747, May 14, 1982 1982.
- [9] V. B. Mountcastle, "Modality and topographic properties of single neurons of cat's somatic sensory cortex," *J Neurophysiol*, vol. 20, pp. 408-34, Jul 1957.
- [10] D. H. Hubel and T. N. Wiesel, "Shape and arrangement of columns in cat's striate cortex," *J Physiol*, vol. 165, pp. 559-68, Mar 1963.
- [11] H. R. Wilson and J. D. Cowan, "Excitatory and inhibitory interactions in localized populations of model neurons," *Biophys J*, vol. 12, pp. 1-24, Jan 1972.
- [12] W. J. Freeman, "Tutorial on neurobiology: From single neurons to brain chaos," *International Journal of Bifurcation and Chaos*, vol. 02, pp. 451-482, 1992.
- [13] H. R. Wilson and J. D. Cowan, "Excitatory and Inhibitory Interactions in Localized Populations of Model Neurons," *Biophysical Journal*, vol. 12, pp. 1-24, 1972.
- [14] W. J. Freeman, "A model of the olfactory system. In M. A. B. Brazier, D. O. Walter, & D. Schneider (Eds.), *Neural modeling*, pp. 41-62. Los Angeles: Univ. of California.," 1973.
- [15] W. J. Freeman, "Measurement of oscillatory responses to electrical stimulation in olfactory bulb of cat," *J Neurophysiol*, vol. 35, pp. 762-79, Nov 1972.
- [16] W. J. Freeman, "Depth recording of averaged evoked potential of olfactory bulb," *J Neurophysiol*, vol. 35, pp. 780-96, Nov 1972.
- [17] W. J. Freeman, "Simulation of chaotic EEG patterns with a dynamic model of the olfactory system," *Biol Cybern*, vol. 56, pp. 139-50, 1987.
- [18] F. H. Lopes da Silva, A. Hoeks, H. Smits, and L. H. Zetterberg, "Model of brain rhythmic activity. The alpha-rhythm of the thalamus," *Kybernetik*, vol. 15, pp. 27-37, May 31 1974.
- [19] P. L. Nunez, "The brain wave equation: a model for the EEG," *Mathematical biosciences*, vol. 21, pp. 279-297, 1974.
- [20] J. J. Wright, R. R. Kydd, and G. J. Lees, "State-changes in the brain viewed as linear steady-states and non-linear transitions between steady-states," *Biol Cybern*, vol. 53, pp. 11-7, 1985.

- [21] B. H. Jansen, G. Zouridakis, and M. E. Brandt, "A neurophysiologically-based mathematical model of flash visual evoked potentials," *Biol Cybern*, vol. 68, pp. 275-83, 1993.
- [22] C. J. Stam, J. P. Pijn, P. Suffczynski, and F. H. Lopes da Silva, "Dynamics of the human alpha rhythm: evidence for non-linearity?," *Clin Neurophysiol*, vol. 110, pp. 1801-13, Oct 1999.
- [23] I. Bojak and D. T. Liley, "Modeling the effects of anesthesia on the electroencephalogram," *Phys Rev E Stat Nonlin Soft Matter Phys*, vol. 71, p. 041902, Apr 2005.
- [24] F. Wendling, F. Bartolomei, J. J. Bellanger, and P. Chauvel, "Epileptic fast activity can be explained by a model of impaired GABAergic dendritic inhibition," *Eur J Neurosci*, vol. 15, pp. 1499-508, May 2002.
- [25] F. Wendling, J. J. Bellanger, F. Bartolomei, and P. Chauvel, "Relevance of nonlinear lumped-parameter models in the analysis of depth-EEG epileptic signals," *Biol Cybern*, vol. 83, pp. 367-78, Oct 2000.
- [26] P. A. Robinson, C. J. Rennie, and D. L. Rowe, "Dynamics of large-scale brain activity in normal arousal states and epileptic seizures," *Phys Rev E Stat Nonlin Soft Matter Phys*, vol. 65, p. 041924, Apr 2002.
- [27] P. Suffczynski, S. Kalitzin, and F. H. Lopes Da Silva, "Dynamics of non-convulsive epileptic phenomena modeled by a bistable neuronal network," *Neuroscience*, vol. 126, pp. 467-84, 2004.
- [28] D. T. Liley and I. Bojak, "Understanding the transition to seizure by modeling the epileptiform activity of general anesthetic agents," *J Clin Neurophysiol*, vol. 22, pp. 300-13, Oct 2005.
- [29] L. Wang, P. Y. Kim, D. E. McCarty, C. Frilot li, A. L. Chesson Jr, S. Carrubba, and A. A. Marino, "EEG recurrence markers and sleep quality," *Journal of the Neurological Sciences*, vol. 331, pp. 26-30, 2013.
- [30] C. Huneau, P. Benquet, G. Dieuset, A. Biraben, B. Martin, and F. Wendling, "Shape features of epileptic spikes are a marker of epileptogenesis," *Epilepsia*, (in press) 2013.
- [31] J. Engel, A. Pitkänen, J. A. Loeb, F. Edward Dudek, E. H. Bertram, A. J. Cole, S. L. Moshé, S. Wiebe, F. E. Jensen, I. Mody, A. Nehlig, and A. Vezzani, "Epilepsy biomarkers," *Epilepsia*, vol. 54, pp. 61-69, 2013.
- [32] T. Wyckhuys, P. J. Geerts, R. Raedt, K. Vonck, W. Wadman, and P. Boon, "Deep brain stimulation for epilepsy: knowledge gained from experimental animal models," *Acta neurologica Belgica*, vol. 109, pp. 63-80, 2009.
- [33] M. Avoli, J. Louvel, D. Mattia, A. Olivier, V. Esposito, R. Pumain, and M. D'Antuono, "Epileptiform synchronization in the human dysplastic cortex," *Epileptic Disord*, vol. 5 Suppl 2, pp. S45-50, Sep 2003.
- [34] R. Mikkelsen, M. Andreasen, and S. Nedergaard, "Suppression of epileptiform activity by a single short-duration electric field in rat hippocampus in vitro," *J Neurophysiol*, vol. 109, pp. 2720-31, Jun 2013.
- [35] R. J. Warren and D. M. Durand, "Effects of applied currents on spontaneous epileptiform activity induced by low calcium in the rat hippocampus," *Brain Res*, vol. 806, pp. 186-95, Sep 28 1998.
- [36] M. Bikson, M. Inoue, H. Akiyama, J. K. Deans, J. E. Fox, H. Miyakawa, and J. G. Jefferys, "Effects of uniform extracellular DC electric fields on excitability in rat hippocampal slices in vitro," *J Physiol*, vol. 557, pp. 175-90, May 15 2004.
- [37] G. Buzsaki, "Large-scale recording of neuronal ensembles," *Nat Neurosci*, vol. 7, pp. 446-51, May 2004.
- [38] S. Murakami and Y. Okada, "Contributions of principal neocortical neurons to magnetoencephalography and electroencephalography signals," *J Physiol*, vol. 575, pp. 925-36, Sep 15 2006.
- [39] C. Bedard, H. Kroger, and A. Destexhe, "Model of low-pass filtering of local field potentials in brain tissue," *Phys Rev E Stat Nonlin Soft Matter Phys*, vol. 73, p. 051911, May 2006.

- [40] K. E. Andreas, F. Pascal, and S. Wolf, "Dynamic predictions: Oscillations and synchrony in top-down processing," *Nature Reviews Neuroscience*, vol. 2, pp. 704-716, 2001.
- [41] A. Schnitzler and J. Gross, "Normal and pathological oscillatory communication in the brain," *Nat Rev Neurosci*, vol. 6, pp. 285-96, Apr 2005.
- [42] A. Raz, E. Vaadia, and H. Bergman, "Firing patterns and correlations of spontaneous discharge of pallidal neurons in the normal and the tremulous 1-methyl-4-phenyl-1,2,3,6-tetrahydropyridine vervet model of parkinsonism," *J Neurosci*, vol. 20, pp. 8559-8571, 2000.
- [43] R. Levy, W. D. Hutchison, A. M. Lozano, and J. O. Dostrovsky, "High-frequency Synchronization of Neuronal Activity in the Subthalamic Nucleus of Parkinsonian Patients with Limb Tremor," *The Journal of Neuroscience*, vol. 20, pp. 7766-7775, October 15, 2000 2000.
- [44] P. Dietmar and T. K. Stephen, "A basal ganglia pacemaker formed by the subthalamic nucleus and external globus pallidus," *Nature*, vol. 400, pp. 677-682, 1999.
- [45] C. J. Stam, A. M. van Cappellen van Walsum, Y. A. Pijnenburg, H. W. Berendse, J. C. de Munck, P. Scheltens, and B. W. van Dijk, "Generalized synchronization of MEG recordings in Alzheimer's Disease: evidence for involvement of the gamma band," *Journal of clinical neurophysiology : official publication of the American Electroencephalographic Society*, vol. 19, pp. 562-574, 2002.
- [46] T. Koenig, L. Prichep, T. Dierks, D. Hubl, L. O. Wahlund, E. R. John, and V. Jelic, "Decreased EEG synchronization in Alzheimer's disease and mild cognitive impairment," *Neurobiology of Aging*, vol. 26, pp. 165-171, 2005.
- [47] C. J. Stam, Y. Van Der Made, Y. A. L. Pijnenburg, and P. Scheltens, "EEG synchronization in mild cognitive impairment and Alzheimer's disease," *Acta Neurologica Scandinavica*, vol. 108, pp. 90-96, 2003.
- [48] A. Crespel, P. Gélisse, M. Bureau, and P. Genton, "Atlas de l'électroencéphalographie." vol. II: Les épilepsies de l'EEG aux syndromes, J. L. Eurotext, Ed., ed Paris, 2006.
- [49] M.-F. Kuo and M. A. Nitsche, "Effects of Transcranial Electrical Stimulation on Cognition," *Clinical EEG and Neuroscience*, vol. 43, pp. 192-199, July 1, 2012 2012.
- [50] B. Krause, J. Marquez-Ruiz, and R. C. Kadosh, "The effect of transcranial direct current stimulation: a role for cortical excitation/inhibition balance?," *Front Hum Neurosci*, vol. 7, p. 602, 2013.
- [51] C. S. Herrmann, S. Rach, T. Neuling, and D. Struber, "Transcranial alternating current stimulation: a review of the underlying mechanisms and modulation of cognitive processes," *Front Hum Neurosci*, vol. 7, p. 279, 2013.
- [52] B. Krause and R. Cohen Kadosh, "Can transcranial electrical stimulation improve learning difficulties in atypical brain development? A future possibility for cognitive training," *Developmental Cognitive Neuroscience*.
- [53] M. A. Nitsche and W. Paulus, "Sustained excitability elevations induced by transcranial DC motor cortex stimulation in humans," *Neurology*, vol. 57, pp. 1899-901, Nov 27 2001.
- [54] M. A. Nitsche, M. S. Nitsche, C. C. Klein, F. Tergau, J. C. Rothwell, and W. Paulus, "Level of action of cathodal DC polarisation induced inhibition of the human motor cortex," *Clin Neurophysiol*, vol. 114, pp. 600-4, Apr 2003.
- [55] D. R. McNeal, "Analysis of a Model for Excitation of Myelinated Nerve," *Biomedical Engineering, IEEE Transactions on*, vol. BME-23, pp. 329-337, 1976.
- [56] S. Joucla and B. Yvert, "Modeling extracellular electrical neural stimulation: from basic understanding to MEA-based applications," *J Physiol Paris*, vol. 106, pp. 146-58, May-Aug 2012.
- [57] C. C. McIntyre and W. M. Grill, "Finite element analysis of the current-density and electric field generated by metal microelectrodes," *Ann Biomed Eng*, vol. 29, pp. 227-35, Mar 2001.

- [58] C. C. McIntyre and W. M. Grill, "Extracellular stimulation of central neurons: influence of stimulus waveform and frequency on neuronal output," *J Neurophysiol*, vol. 88, pp. 1592-604, Oct 2002.
- [59] S. Joucla and B. Yvert, "Improved focalization of electrical microstimulation using microelectrode arrays: a modeling study," *PLoS One*, vol. 4, p. e4828, 2009.
- [60] D. M. Durand and M. Bikson, "Suppression and control of epileptiform activity by electrical stimulation: a review," *Proceedings of the IEEE*, vol. 89, pp. 1065-1082, 2001.
- [61] D. Tranchina and C. Nicholson, "A model for the polarization of neurons by extrinsically applied electric fields," *Biophys J*, vol. 50, pp. 1139-56, Dec 1986.
- [62] F. Rattay, "Analysis of models for external stimulation of axons," *IEEE Trans Biomed Eng*, vol. 33, pp. 974-7, Oct 1986.
- [63] A. Datta, M. Elwassif, F. Battaglia, and M. Bikson, "Transcranial current stimulation focality using disc and ring electrode configurations: FEM analysis," *J Neural Eng*, vol. 5, pp. 163-74, Jun 2008.
- [64] N. Yousif and X. Liu, "Investigating the depth electrode–brain interface in deep brain stimulation using finite element models with graded complexity in structure and solution," *Journal of Neuroscience Methods*, vol. 184, pp. 142-151, 2009.
- [65] G. Pizzolato and T. Mandat, "Deep brain stimulation for movement disorders," *Front Integr Neurosci*, vol. 6, p. 2, 2012.
- [66] F. Fröhlich and D. A. McCormick, "Endogenous Electric Fields May Guide Neocortical Network Activity," *Neuron*, vol. 67, pp. 129-143, 2010.
- [67] M. H. Adhikari, J. H. Heeroma, M. di Bernardo, B. Krauskopf, M. P. Richardson, M. C. Walker, and J. R. Terry, "Characterisation of cortical activity in response to deep brain stimulation of ventral-lateral nucleus: modelling and experiment," *Journal of neuroscience methods*, vol. 183, pp. 77-85, Sep 30 2009.
- [68] C. Beurrier, B. Bioulac, J. Audin, and C. Hammond, "High-frequency stimulation produces a transient blockade of voltage-gated currents in subthalamic neurons," *J Neurophysiol*, vol. 85, pp. 1351-6, Apr 2001.
- [69] J. O. Dostrovsky, R. Levy, J. P. Wu, W. D. Hutchison, R. R. Tasker, and A. M. Lozano, "Microstimulation-induced inhibition of neuronal firing in human globus pallidus," *J Neurophysiol*, vol. 84, pp. 570-4, Jul 2000.
- [70] M. Filali, W. D. Hutchison, V. N. Palter, A. M. Lozano, and J. O. Dostrovsky, "Stimulation-induced inhibition of neuronal firing in human subthalamic nucleus," *Exp Brain Res*, vol. 156, pp. 274-81, Jun 2004.
- [71] L. D. Liu, I. A. Prescott, J. O. Dostrovsky, M. Hodaie, A. M. Lozano, and W. D. Hutchison, "Frequency-dependent effects of electrical stimulation in the globus pallidus of dystonia patients," *J Neurophysiol*, vol. 108, pp. 5-17, Jul 2012.
- [72] L. Garcia, J. Audin, G. D'Alessandro, B. Bioulac, and C. Hammond, "Dual effect of high-frequency stimulation on subthalamic neuron activity," *J Neurosci*, vol. 23, pp. 8743-51, Sep 24 2003.
- [73] C. C. McIntyre, W. M. Grill, D. L. Sherman, and N. V. Thakor, "Cellular effects of deep brain stimulation: model-based analysis of activation and inhibition," *J Neurophysiol*, vol. 91, pp. 1457-69, Apr 2004.
- [74] H. L. Kendall, L. H. Frederick, C. Su-Youne, C. L. Dongchul, W. R. David, C. M. Cameron, and C. L. James, "High frequency stimulation abolishes thalamic network oscillations: an electrophysiological and computational analysis," *Journal of Neural Engineering*, vol. 8, p. 046001, 2011.
- [75] D. Ukueberuwa and E. M. Wassermann, "Direct Current Brain Polarization: A Simple, Noninvasive Technique for Human Neuromodulation," *Neuromodulation: Technology at the Neural Interface*, vol. 13, pp. 168-173, 2010.

- [76] A. L. Benabid and N. Torres, "New targets for DBS," *Parkinsonism & Related Disorders*, vol. 18, Supplement 1, pp. S21-S23, 2012.
- [77] M. D. Johnson, S. Miocinovic, C. C. McIntyre, and J. L. Vitek, "Mechanisms and targets of deep brain stimulation in movement disorders," *Neurotherapeutics*, vol. 5, pp. 294-308, Apr 2008.
- [78] P. Brown and D. Williams, "Basal ganglia local field potential activity: character and functional significance in the human," *Clin Neurophysiol*, vol. 116, pp. 2510-9, Nov 2005.
- [79] R. Levy, W. D. Hutchison, A. M. Lozano, and J. O. Dostrovsky, "Synchronized neuronal discharge in the basal ganglia of parkinsonian patients is limited to oscillatory activity," *J Neurosci*, vol. 22, pp. 2855-61, Apr 1 2002.
- [80] R. Levy, W. D. Hutchison, A. M. Lozano, and J. O. Dostrovsky, "High-frequency synchronization of neuronal activity in the subthalamic nucleus of parkinsonian patients with limb tremor," *J Neurosci*, vol. 20, pp. 7766-75, Oct 15 2000.
- [81] C. Hammond, H. Bergman, and P. Brown, "Pathological synchronization in Parkinson's disease: networks, models and treatments," *Trends in neurosciences*, vol. 30, pp. 357-364, 2007.
- [82] M. Magnin, A. Morel, and D. Jeanmonod, "Single-unit analysis of the pallidum, thalamus and subthalamic nucleus in parkinsonian patients," *Neuroscience*, vol. 96, pp. 549-64, 2000.
- [83] P. A. Pahapill and A. M. Lozano, "The pedunculopontine nucleus and Parkinson's disease," *Brain*, vol. 123, pp. 1767-1783, September 1, 2000 2000.
- [84] R. Hassler, T. Riechert, F. Mundinger, W. Umbach, and J. A. Ganglberger, "Physiological observations in stereotaxic operations in extrapyramidal motor disturbances," *Brain*, vol. 83, pp. 337-50, 1960.
- [85] A. L. Benabid, S. Chabardes, J. Mitrofanis, and P. Pollak, "Deep brain stimulation of the subthalamic nucleus for the treatment of Parkinson's disease," *The Lancet Neurology*, vol. 8, pp. 67-81, 2009.
- [86] A. L. Benabid, P. Pollak, E. Seigneuret, D. Hoffmann, E. Gay, and J. Perret, "Chronic VIM thalamic stimulation in Parkinson's disease, essential tremor and extra-pyramidal dyskinesias," *Acta Neurochir Suppl (Wien)*, vol. 58, pp. 39-44, 1993.
- [87] J. P. Hubble, K. L. Busenbark, S. Wilkinson, R. Pahwa, G. W. Paulson, K. Lyons, and W. C. Koller, "Effects of thalamic deep brain stimulation based on tremor type and diagnosis," *Movement Disorders*, vol. 12, pp. 337-341, 1997.
- [88] P. Limousin, P. Krack, P. Pollak, A. Benazzouz, C. Ardouin, D. Hoffmann, and A.-L. Benabid, "Electrical Stimulation of the Subthalamic Nucleus in Advanced Parkinson's Disease," *New England Journal of Medicine*, vol. 339, pp. 1105-1111, 1998.
- [89] J. Vesper, F. Klostermann, F. Stockhammer, T. Funk, and M. Brock, "Results of chronic subthalamic nucleus stimulation for Parkinson's disease: a 1-year follow-up study," *Surgical Neurology*, vol. 57, pp. 306-311, 2002.
- [90] A.-L. Benabid, A. Koudsié, A. Benazzouz, V. Fraix, A. Ashraf, J. F. Le Bas, S. Chabardes, and P. Pollak, "Subthalamic Stimulation for Parkinson's Disease," *Archives of Medical Research*, vol. 31, pp. 282-289, 2000.
- [91] C. Hamani, E. Richter, J. M. Schwalb, and A. M. Lozano, "Bilateral subthalamic nucleus stimulation for Parkinson's disease: a systematic review of the clinical literature," *Neurosurgery*, vol. 56, pp. 1313-21; discussion 1321-4, Jun 2005.
- [92] K. Østergaard, N. Sunde, and E. Dupont, "Effects of bilateral stimulation of the subthalamic nucleus in patients with severe Parkinson's disease and motor fluctuations," *Movement Disorders*, vol. 17, pp. 693-700, 2002.
- [93] P. Brown, "Abnormal oscillatory synchronisation in the motor system leads to impaired movement," *Curr Opin Neurobiol*, vol. 17, pp. 656-664, 2007.

- [94] S. Little and P. Brown, "What brain signals are suitable for feedback control of deep brain stimulation in Parkinson's disease?," *Ann N Y Acad Sci*, vol. 1265, pp. 9-24, 2012.
- [95] P. Afshar, A. Khambhati, S. Stanslaski, D. Carlson, R. Jensen, S. Dani, M. Lazarewicz, J. Giftakis, P. Stypulkowski, and T. Denison, "A translational platform for prototyping closed-loop neuromodulation systems," *Frontiers in Neural Circuits*, vol. 6, 2013-January-22 2013.
- [96] A. L. Benabid, L. Minotti, A. Koudsie, A. de Saint Martin, and E. Hirsch, "Antiepileptic effect of high-frequency stimulation of the subthalamic nucleus (corpus luyisi) in a case of medically intractable epilepsy caused by focal dysplasia: a 30-month follow-up: technical case report," *Neurosurgery*, vol. 50, pp. 1385-91; discussion 1391-2, Jun 2002.
- [97] R. S. Fisher, S. Uematsu, G. L. Krauss, B. J. Cysyk, R. McPherson, R. P. Lesser, B. Gordon, P. Schwerdt, and M. Rise, "Placebo-controlled pilot study of centromedian thalamic stimulation in treatment of intractable seizures," *Epilepsia*, vol. 33, pp. 841-51, Sep-Oct 1992.
- [98] G. D. Wright, D. L. McLellan, and J. G. Brice, "A double-blind trial of chronic cerebellar stimulation in twelve patients with severe epilepsy," *J Neurol Neurosurg Psychiatry*, vol. 47, pp. 769-74, Aug 1984.
- [99] I. S. Cooper, I. Amin, and S. Gilman, "The effect of chronic cerebellar stimulation upon epilepsy in man," *Trans Am Neurol Assoc*, vol. 98, pp. 192-6, 1973.
- [100] S. Saittel, M. Langlois, B. Feddersen, L. Minotti, L. Vercueil, S. Chabardes, O. David, A. Depaulis, C. Deransart, and P. Kahane, "Manipulating the epileptic brain using stimulation: a review of experimental and clinical studies," *Epileptic Disord*, vol. 11, pp. 100-12, Jun 2009.
- [101] J. D. Putzke, R. E. Wharen, Jr., Z. K. Wszolek, M. F. Turk, A. J. Strongosky, and R. J. Uitti, "Thalamic deep brain stimulation for tremor-predominant Parkinson's disease," *Parkinsonism Relat Disord*, vol. 10, pp. 81-8, Dec 2003.
- [102] J. L. Vitek, T. Hashimoto, J. Peoples, M. R. DeLong, and R. A. E. Bakay, "Acute stimulation in the external segment of the globus pallidus improves parkinsonian motor signs," *Movement Disorders*, vol. 19, pp. 907-915, 2004.
- [103] I. S. Cooper, "Effect of chronic stimulation of anterior cerebellum on neurological disease," *Lancet*, vol. 1, p. 206, Jan 27 1973.
- [104] C. Boëx, S. Vulliëmoz, L. Spinelli, C. Pollo, and M. Seeck, "High and low frequency electrical stimulation in non-lesional temporal lobe epilepsy," *Seizure*, vol. 16, pp. 664-669, 2007.
- [105] A. Pasnicu, Y. Denoyer, C. Haegelen, E. Pasqualini, and A. Biraben, "Modulation of paroxysmal activity in focal cortical dysplasia by centromedian thalamic nucleus stimulation," *Epilepsy Research*, p. in press, 2013.
- [106] R. Fisher, V. Salanova, T. Witt, R. Worth, T. Henry, R. Gross, K. Oommen, I. Osorio, J. Nazzaro, D. Labar, M. Kaplitt, M. Sperling, E. Sandok, J. Neal, A. Handforth, J. Stern, A. DeSalles, S. Chung, A. Shetter, D. Bergen, R. Bakay, J. Henderson, J. French, G. Baltuch, W. Rosenfeld, A. Youkilis, W. Marks, P. Garcia, N. Barbaro, N. Fountain, C. Bazil, R. Goodman, G. McKhann, K. Babu Krishnamurthy, S. Papavassiliou, C. Epstein, J. Pollard, L. Tonder, J. Grebin, R. Coffey, N. Graves, and S. S. G. the, "Electrical stimulation of the anterior nucleus of thalamus for treatment of refractory epilepsy," *Epilepsia*, vol. 51, pp. 899-908, 2010.
- [107] P. Boon, K. Vonck, V. De Herdt, A. Van Dycke, M. Goethals, L. Goossens, M. Van Zandijcke, T. De Smedt, I. Dewaele, R. Achten, W. Wadman, F. Dewaele, J. Caemaert, and D. Van Roost, "Deep brain stimulation in patients with refractory temporal lobe epilepsy," *Epilepsia*, vol. 48, pp. 1551-60, Aug 2007.
- [108] F. Velasco, M. Velasco, C. Ogarrio, and G. Fanghanel, "Electrical stimulation of the centromedian thalamic nucleus in the treatment of convulsive seizures: a preliminary report," *Epilepsia*, vol. 28, pp. 421-30, Jul-Aug 1987.
- [109] A. L. Velasco, F. Velasco, M. Velasco, D. Trejo, G. Castro, and J. D. Carrillo-Ruiz, "Electrical Stimulation of the Hippocampal Epileptic Foci for Seizure Control: A Double-Blind, Long-Term Follow-Up Study," *Epilepsia*, vol. 48, pp. 1895-1903, 2007.

- [110] M. Miatton, D. Van Roost, E. Thiery, E. Carrette, A. Van Dycke, K. Vonck, A. Meurs, G. Vingerhoets, and P. Boon, "The cognitive effects of amygdalohippocampal deep brain stimulation in patients with temporal lobe epilepsy," *Epilepsy Behav*, vol. 22, pp. 759-64, Dec 2011.
- [111] A. Valentin, E. Garcia Navarrete, R. Chelvarajah, C. Torres, M. Navas, L. Vico, N. Torres, J. Pastor, R. Selway, R. G. Sola, and G. Alarcon, "Deep brain stimulation of the centromedian thalamic nucleus for the treatment of generalized and frontal epilepsies," *Epilepsia*, Sep 13 2013.
- [112] A. Palmi, A. Gambardella, F. Andermann, F. Dubeau, J. C. da Costa, A. Olivier, D. Tampieri, P. Gloor, F. Quesney, E. Andermann, and et al., "Intrinsic epileptogenicity of human dysplastic cortex as suggested by corticography and surgical results," *Ann Neurol*, vol. 37, pp. 476-87, Apr 1995.
- [113] Y. Bozzi, S. Casarosa, and M. Caleo, "Epilepsy as a neurodevelopmental disorder," *Frontiers in Psychiatry*, vol. 3, 2012-March-19 2012.
- [114] A. Palmi, "Electrophysiology of the focal cortical dysplasias," *Epilepsia*, vol. 51 Suppl 1, pp. 23-6, Feb 2010.
- [115] S. M. Sisodiya, S. Fauser, J. H. Cross, and M. Thom, "Focal cortical dysplasia type II: biological features and clinical perspectives," *Lancet Neurol*, vol. 8, pp. 830-43, Sep 2009.
- [116] A. Gambardella, A. Palmi, F. Andermann, F. Dubeau, J. C. Da Costa, L. F. Quesney, E. Andermann, and A. Olivier, "Usefulness of focal rhythmic discharges on scalp EEG of patients with focal cortical dysplasia and intractable epilepsy," *Electroencephalogr Clin Neurophysiol*, vol. 98, pp. 243-9, Apr 1996.
- [117] S. Noachtar, O. Bilgin, J. Remi, N. Chang, I. Midi, C. Vollmar, and B. Feddersen, "Interictal regional polyspikes in noninvasive EEG suggest cortical dysplasia as etiology of focal epilepsies," *Epilepsia*, vol. 49, pp. 1011-7, Jun 2008.
- [118] W. O. t. Tatum, "Mesial temporal lobe epilepsy," *J Clin Neurophysiol*, vol. 29, pp. 356-65, Oct 2012.
- [119] J. Engel, Jr., "Introduction to temporal lobe epilepsy," *Epilepsy Res*, vol. 26, pp. 141-50, Dec 1996.
- [120] N. C. de Lanerolle, J. H. Kim, A. Williamson, S. S. Spencer, H. P. Zaveri, T. Eid, and D. D. Spencer, "A retrospective analysis of hippocampal pathology in human temporal lobe epilepsy: evidence for distinctive patient subcategories," *Epilepsia*, vol. 44, pp. 677-87, May 2003.
- [121] A. Bragin, C. L. Wilson, R. J. Staba, M. Reddick, I. Fried, and J. Engel, Jr., "Interictal high-frequency oscillations (80-500 Hz) in the human epileptic brain: entorhinal cortex," *Ann Neurol*, vol. 52, pp. 407-15, Oct 2002.
- [122] J. Jacobs, P. LeVan, C.-É. Châtillon, A. Olivier, F. Dubeau, and J. Gotman, "High frequency oscillations in intracranial EEGs mark epileptogenicity rather than lesion type," *Brain*, vol. 132, pp. 1022-1037, April 1, 2009 2009.
- [123] J. F. Tellez-Zenteno and S. Wiebe, "Hippocampal Stimulation in the Treatment of Epilepsy," *Neurosurgery clinics of North America*, vol. 22, pp. 465-475, 2011.
- [124] T. Wyckhuys, P. J. Geerts, R. Raedt, K. Vonck, W. Wadman, and P. Boon, "Deep brain stimulation for epilepsy: knowledge gained from experimental animal models," *Acta Neurol Belg*, vol. 109, pp. 63-80, Jun 2009.
- [125] X.-L. Zhong, J.-T. Yu, Q. Zhang, N.-D. Wang, and L. Tan, "Deep brain stimulation for epilepsy in clinical practice and in animal models," *Brain Research Bulletin*, vol. 85, pp. 81-88, 2011.
- [126] K. Vonck, P. Boon, E. Achten, J. De Reuck, and J. Caemaert, "Long-term amygdalohippocampal stimulation for refractory temporal lobe epilepsy," *Ann Neurol*, vol. 52, pp. 556-565, 2002.

- [127] R. Fisher, V. Salanova, T. Witt, R. Worth, T. Henry, R. Gross, K. Oommen, I. Osorio, J. Nazzaro, D. Labar, M. Kaplitt, M. Sperling, E. Sandok, J. Neal, A. Handforth, J. Stern, A. DeSalles, S. Chung, A. Shetter, D. Bergen, R. Bakay, J. Henderson, J. French, G. Baltuch, W. Rosenfeld, A. Youkilis, W. Marks, P. Garcia, N. Barbaro, N. Fountain, C. Bazil, R. Goodman, G. McKhann, K. Babu Krishnamurthy, S. Papavassiliou, C. Epstein, J. Pollard, L. Tonder, J. Grebin, R. Coffey, N. Graves, and S. S. Group, "Electrical stimulation of the anterior nucleus of thalamus for treatment of refractory epilepsy," *Epilepsia*, vol. 51, pp. 899-908, May 2010.
- [128] R. S. McLachlan, S. Pigott, J. F. Tellez-Zenteno, S. Wiebe, and A. Parrent, "Bilateral hippocampal stimulation for intractable temporal lobe epilepsy: Impact on seizures and memory," *Epilepsia*, vol. 51, pp. 304-307, 2010.
- [129] C. Boex, M. Seeck, S. Vulliemoz, A. O. Rossetti, C. Staedler, L. Spinelli, A. J. Pegna, E. Pralong, J. G. Villemure, G. Foletti, and C. Pollo, "Chronic deep brain stimulation in mesial temporal lobe epilepsy," *Seizure*, vol. 20, pp. 485-90, Jul 2011.
- [130] P. Bondallaz, C. Boëx, A. O. Rossetti, G. Foletti, L. Spinelli, S. Vulliemoz, M. Seeck, and C. Pollo, "Electrode location and clinical outcome in hippocampal electrical stimulation for mesial temporal lobe epilepsy," *Seizure*, vol. 22, pp. 390-395, 2013.
- [131] M. Z. Koubeissi, E. Kahriman, T. U. Syed, J. Miller, and D. M. Durand, "Low-frequency electrical stimulation of a fiber tract in temporal lobe epilepsy," *Ann Neurol*, pp. n/a-n/a, 2013.
- [132] A. Cukiert, C. M. Cukiert, J. A. Burattini, and A. M. Lima, "Seizure outcome after hippocampal deep brain stimulation in a prospective cohort of patients with refractory temporal lobe epilepsy," *Seizure*.
- [133] R. S. Fisher, G. L. Krauss, E. Ramsay, K. Laxer, and J. Gates, "Assessment of vagus nerve stimulation for epilepsy: report of the Therapeutics and Technology Assessment Subcommittee of the American Academy of Neurology," *Neurology*, vol. 49, pp. 293-7, Jul 1997.
- [134] M. J. Morrell and R. N. S. S. i. E. S. Group, "Responsive cortical stimulation for the treatment of medically intractable partial epilepsy," *Neurology*, vol. 77, pp. 1295-304, Sep 27 2011.
- [135] S. Sunderam, B. Gluckman, D. Reato, and M. Bikson, "Toward rational design of electrical stimulation strategies for epilepsy control," *Epilepsy Behav*, vol. 17, pp. 6-22, Jan 2010.
- [136] K. H. Lee, F. L. Hitti, S. Y. Chang, D. C. Lee, D. W. Roberts, C. C. McIntyre, and J. C. Leiter, "High frequency stimulation abolishes thalamic network oscillations: an electrophysiological and computational analysis," *J Neural Eng*, vol. 8, p. 046001, Aug 2011.
- [137] E. Kim, B. Owen, W. R. Holmes, and L. M. Grover, "Decreased afferent excitability contributes to synaptic depression during high-frequency stimulation in hippocampal area CA1," *J Neurophysiol*, vol. 108, pp. 1965-76, Oct 2012.
- [138] C. C. McIntyre, M. Savasta, L. Kerkerian-Le Goff, and J. L. Vitek, "Uncovering the mechanism(s) of action of deep brain stimulation: activation, inhibition, or both," *Clin Neurophysiol*, vol. 115, pp. 1239-48, Jun 2004.
- [139] A. R. Rezai, A. M. Lozano, A. P. Crawley, M. L. Joy, K. D. Davis, C. L. Kwan, J. O. Dostrovsky, R. R. Tasker, and D. J. Mikulis, "Thalamic stimulation and functional magnetic resonance imaging: localization of cortical and subcortical activation with implanted electrodes. Technical note," *J Neurosurg*, vol. 90, pp. 583-90, Mar 1999.
- [140] A. O. Ceballos-Baumann, "Functional imaging in Parkinson's disease: activation studies with PET, fMRI and SPECT," *J Neurol*, vol. 250 Suppl 1, pp. I15-23, Feb 2003.
- [141] J. S. Perlmutter, J. W. Mink, A. J. Bastian, K. Zackowski, T. Hershey, E. Miyawaki, W. Koller, and T. O. Videen, "Blood flow responses to deep brain stimulation of thalamus," *Neurology*, vol. 58, pp. 1388-94, May 14 2002.
- [142] A. Benazzouz, D. M. Gao, Z. G. Ni, B. Piallat, R. Bouali-Benazzouz, and A. L. Benabid, "Effect of high-frequency stimulation of the subthalamic nucleus on the neuronal activities of the

- substantia nigra pars reticulata and ventrolateral nucleus of the thalamus in the rat," *Neuroscience*, vol. 99, pp. 289-95, 2000.
- [143] C. H. Tai, T. Boraud, E. Bezard, B. Bioulac, C. Gross, and A. Benazzouz, "Electrophysiological and metabolic evidence that high-frequency stimulation of the subthalamic nucleus bridges neuronal activity in the subthalamic nucleus and the substantia nigra reticulata," *FASEB J*, vol. 17, pp. 1820-30, Oct 2003.
- [144] M. E. Anderson, N. Postupna, and M. Ruffo, "Effects of high-frequency stimulation in the internal globus pallidus on the activity of thalamic neurons in the awake monkey," *J Neurophysiol*, vol. 89, pp. 1150-60, Feb 2003.
- [145] T. Hashimoto, C. M. Elder, M. S. Okun, S. K. Patrick, and J. L. Vitek, "Stimulation of the subthalamic nucleus changes the firing pattern of pallidal neurons," *J Neurosci*, vol. 23, pp. 1916-23, Mar 1 2003.
- [146] K. Z. Shen, Z. T. Zhu, A. Munhall, and S. W. Johnson, "Synaptic plasticity in rat subthalamic nucleus induced by high-frequency stimulation," *Synapse*, vol. 50, pp. 314-9, Dec 15 2003.
- [147] E. Kim, B. Owen, W. R. Holmes, and L. M. Grover, "Decreased afferent excitability contributes to synaptic depression during high frequency stimulation in hippocampal area CA1," *J Neurophysiol*, Jul 5 2012.
- [148] B. Jiang, Y. Akaneya, Y. Hata, and T. Tsumoto, "Long-term depression is not induced by low-frequency stimulation in rat visual cortex in vivo: a possible preventing role of endogenous brain-derived neurotrophic factor," *J Neurosci*, vol. 23, pp. 3761-70, May 1 2003.
- [149] W. J. Speechley, J. L. Hogsden, and H. C. Dringenberg, "Continuous white noise exposure during and after auditory critical period differentially alters bidirectional thalamocortical plasticity in rat auditory cortex in vivo," *Eur J Neurosci*, vol. 26, pp. 2576-84, Nov 2007.
- [150] S. Chung, X. Li, and S. B. Nelson, "Short-term depression at thalamocortical synapses contributes to rapid adaptation of cortical sensory responses in vivo," *Neuron*, vol. 34, pp. 437-46, Apr 25 2002.
- [151] G. V. Goddard, "Development of epileptic seizures through brain stimulation at low intensity," *Nature*, vol. 214, pp. 1020-1, Jun 3 1967.
- [152] H.-Y. Lai, J. R. Younce, D. L. Albaugh, Y.-C. J. Kao, and Y.-Y. I. Shih, "Functional MRI reveals frequency-dependent responses during deep brain stimulation at the subthalamic nucleus or internal globus pallidus," *NeuroImage*, vol. 84, pp. 11-18, 2014.
- [153] D. R. Merrill, M. Bikson, and J. G. R. Jefferys, "Electrical stimulation of excitable tissue: design of efficacious and safe protocols," *Journal of Neuroscience Methods*, vol. 141, pp. 171-198, 2005.
- [154] B. Piallat, S. Chabardès, A. Devergnas, N. Torres, M. Allain, E. Barrat, and A. L. Benabid, "Monophasic But Not Biphasic Pulses Induce Brain Tissue Damage During Monopolar High-Frequency Deep Brain Stimulation," *Neurosurgery*, vol. 64, pp. 156-163 10.1227/01.NEU.0000336331.88559.CF, 2009.
- [155] F. Wendling, F. Bartolomei, F. Mina, C. Huneau, and P. Benquet, "Interictal spikes, fast ripples and seizures in partial epilepsies – combining multi-level computational models with experimental data," *European Journal of Neuroscience*, vol. 36, pp. 2164-2177, 2012.
- [156] W. W. Lytton, "Computer modelling of epilepsy," *Nat Rev Neurosci*, vol. 9, pp. 626-37, Aug 2008.
- [157] C. C. McIntyre, S. Miocinovic, and C. R. Butson, "Computational analysis of deep brain stimulation," *Expert Rev Med Devices*, vol. 4, pp. 615-22, Sep 2007.
- [158] F. Wendling, F. Bartolomei, F. Mina, C. Huneau, and P. Benquet, "Interictal spikes, fast ripples and seizures in partial epilepsies - combining multi-level computational models with experimental data," *Eur J Neurosci*, vol. 36, pp. 2164-77, Jul 2012.

- [159] A. L. Taylor, J.-M. Goaillard, and E. Marder, "How Multiple Conductances Determine Electrophysiological Properties in a Multicompartment Model," *The Journal of Neuroscience*, vol. 29, pp. 5573-5586, April 29, 2009.
- [160] S. Krstulovic and R. Gribonval, "Mptk: Matching Pursuit Made Tractable," in *IEEE International Conference on Acoustics, Speech and Signal Processing*, Toulouse, 2006, pp. 496 - 499.
- [161] F. Wendling, F. Bartolomei, J. J. Bellanger, and P. Chauvel, "Epileptic fast activity can be explained by a model of impaired GABAergic dendritic inhibition," *European Journal of Neuroscience*, vol. 15, pp. 1499-1508, 2002.
- [162] R. S. Fisher, W. van Emde Boas, W. Blume, C. Elger, P. Genton, P. Lee, and J. Engel, Jr., "Epileptic seizures and epilepsy: definitions proposed by the International League Against Epilepsy (ILAE) and the International Bureau for Epilepsy (IBE)," *Epilepsia*, vol. 46, pp. 470-2, Apr 2005.
- [163] J. R. Huguenard and D. A. McCormick, "Thalamic synchrony and dynamic regulation of global forebrain oscillations," *Trends Neurosci*, vol. 30, pp. 350-6, Jul 2007.
- [164] B. Greenstein and A. Greenstein, *Color Atlas of Neuroscience*. Stuttgart . New York, 2000.
- [165] N. D. Woodward, H. Karbasforoushan, and S. Heckers, "Thalamocortical dysconnectivity in schizophrenia," *Am J Psychiatry*, vol. 169, pp. 1092-9, Oct 2012.
- [166] S. G. Ewing and A. A. Grace, "Deep brain stimulation of the ventral hippocampus restores deficits in processing of auditory evoked potentials in a rodent developmental disruption model of schizophrenia," *Schizophrenia Research*, vol. 143, pp. 377-383, 2013.
- [167] M. Breakspear, J. A. Roberts, J. R. Terry, S. Rodrigues, N. Mahant, and P. A. Robinson, "A unifying explanation of primary generalized seizures through nonlinear brain modeling and bifurcation analysis," *Cereb Cortex*, vol. 16, pp. 1296-313, Sep 2006.
- [168] J. A. Roberts and P. A. Robinson, "Modeling absence seizure dynamics: Implications for basic mechanisms and measurement of thalamocortical and corticothalamic latencies," *J Theor Biol*, vol. 253, pp. 189-201, 2008.
- [169] V. Crunelli, D. W. Cope, and J. R. Terry, "Transition to absence seizures and the role of GABA(A) receptors," *Epilepsy Res*, vol. 97, pp. 283-9, Dec 2011.
- [170] P. A. Robinson, C. J. Rennie, and J. J. Wright, "Propagation and stability of waves of electrical activity in the cerebral cortex," *Physical Review E*, vol. 56, pp. 826-840, 1997.
- [171] J. J. Wright, P. A. Robinson, C. J. Rennie, E. Gordon, P. D. Bourke, C. L. Chapman, N. Hawthorn, G. J. Lees, and D. Alexander, "Toward an integrated continuum model of cerebral dynamics: the cerebral rhythms, synchronous oscillation and cortical stability," *Biosystems*, vol. 63, pp. 71-88, 2001.
- [172] P. Suffczynski, S. Kalitzin, G. Pfurtscheller, and F. H. Lopes da Silva, "Computational model of thalamo-cortical networks: dynamical control of alpha rhythms in relation to focal attention," *Int J Psychophysiol*, vol. 43, pp. 25-40, Dec 2001.
- [173] F. H. Lopes da Silva, "Event-related neural activities: what about phase?," in *Prog Brain Res* vol. Volume 159, N. Christa and K. Wolfgang, Eds., ed: Elsevier, 2006, pp. 3-17.
- [174] F. H. Lopes da Silva, "Event-related neural activities: what about phase?," in *Progress in brain research*. vol. Volume 159, N. Christa and K. Wolfgang, Eds., ed: Elsevier, 2006, pp. 3-17.
- [175] J. A. Roberts and P. A. Robinson, "Modeling absence seizure dynamics: Implications for basic mechanisms and measurement of thalamocortical and corticothalamic latencies," *Journal of theoretical biology*, vol. 253, pp. 189-201, 2008.
- [176] V. Crunelli, D. W. Cope, and J. R. Terry, "Transition to absence seizures and the role of GABA(A) receptors," *Epilepsy Research*, vol. 97, pp. 283-9, Dec 2011.
- [177] M. E. Calcagnotto, M. F. Paredes, T. Tihan, N. M. Barbaro, and S. C. Baraban, "Dysfunction of Synaptic Inhibition in Epilepsy Associated with Focal Cortical Dysplasia," *The Journal of Neuroscience*, vol. 25, pp. 9649-9657, October 19, 2005.

- [178] J. S. Nettleton and W. J. Spain, "Linear to Supralinear Summation of AMPA-Mediated EPSPs in Neocortical Pyramidal Neurons," *J Neurophysiol*, vol. 83, pp. 3310-3322, June 1, 2000 2000.
- [179] B. Molaee-Ardekani, J. Marquez-Ruiz, I. Merlet, R. Leal-Campanario, A. Gruart, R. Sanchez-Campusano, G. Birot, G. Ruffini, J. M. Delgado-Garcia, and F. Wendling, "Effects of transcranial Direct Current Stimulation (tDCS) on cortical activity: A computational modeling study," *Brain Stimul*, Feb 28 2012.
- [180] B. Molaee-Ardekani, P. Benquet, F. Bartolomei, and F. Wendling, "Computational modeling of high-frequency oscillations at the onset of neocortical partial seizures: from 'altered structure' to 'dysfunction'," *Neuroimage*, vol. 52, pp. 1109-22, Sep 2010.
- [181] F. Marten, S. Rodrigues, O. Benjamin, M. P. Richardson, and J. R. Terry, "Onset of polyspike complexes in a mean-field model of human electroencephalography and its application to absence epilepsy," *Philos Transact A Math Phys Eng Sci*, vol. 367, pp. 1145-61, Mar 28 2009.
- [182] D. Pinault, "The thalamic reticular nucleus: structure, function and concept," *Brain research reviews*, vol. 46, pp. 1-31, 2004.
- [183] D. L. Meinecke and A. Peters, "GABA immunoreactive neurons in rat visual cortex," *J Comp Neurol*, vol. 261, pp. 388-404, Jul 15 1987.
- [184] J. S. Isaacson and M. Scanziani, "How inhibition shapes cortical activity," *Neuron*, vol. 72, pp. 231-43, Oct 20 2011.
- [185] L. L. Glickfeld and M. Scanziani, "Distinct timing in the activity of cannabinoid-sensitive and cannabinoid-insensitive basket cells," *Nat Neurosci*, vol. 9, pp. 807-15, Jun 2006.
- [186] C. C. Stokes and J. S. Isaacson, "From dendrite to soma: dynamic routing of inhibition by complementary interneuron microcircuits in olfactory cortex," *Neuron*, vol. 67, pp. 452-65, Aug 12 2010.
- [187] D. P. Lloyd, "Facilitation and inhibition of spinal motoneurons," *J Neurophysiol*, vol. 9, pp. 421-38, Nov 1946.
- [188] H. A. Swadlow, "Fast-spike Interneurons and Feedforward Inhibition in Awake Sensory Neocortex," *Cerebral Cortex*, vol. 13, pp. 25-32, January 1, 2003 2003.
- [189] H. A. Swadlow, T. Bezdudnaya, and A. G. Gusev, "Spike timing and synaptic dynamics at the awake thalamocortical synapse," *Prog Brain Res*, vol. 149, pp. 91-105, 2005.
- [190] F. Pouille and M. Scanziani, "Enforcement of temporal fidelity in pyramidal cells by somatic feed-forward inhibition," *Science*, vol. 293, pp. 1159-63, Aug 10 2001.
- [191] B. V. Atallah and M. Scanziani, "Instantaneous modulation of gamma oscillation frequency by balancing excitation with inhibition," *Neuron*, vol. 62, pp. 566-77, May 28 2009.
- [192] M. H. Hennig, "Theoretical models of synaptic short term plasticity," *Front Comput Neurosci*, vol. 7, p. 45, 2013.
- [193] J. Xu and L.-G. Wu, "The Decrease in the Presynaptic Calcium Current Is a Major Cause of Short-Term Depression at a Calyx-Type Synapse," *Neuron*, vol. 46, pp. 633-645, 2005.
- [194] D. L. Brody and D. T. Yue, "Release-independent short-term synaptic depression in cultured hippocampal neurons," *J Neurosci*, vol. 20, pp. 2480-94, Apr 1 2000.
- [195] L. J. Bindman, O. C. Lippold, and J. W. Redfearn, "The Action of Brief Polarizing Currents on the Cerebral Cortex of the Rat (1) during Current Flow and (2) in the Production of Long-Lasting after-Effects," *J Physiol*, vol. 172, pp. 369-82, Aug 1964.
- [196] P. C. Miranda, L. Correia, R. Salvador, and P. J. Basser, "Tissue heterogeneity as a mechanism for localized neural stimulation by applied electric fields," *Phys Med Biol*, vol. 52, pp. 5603-17, Sep 21 2007.
- [197] A. Pasnicu, Y. Denoyer, C. Haegelen, E. Pasqualini, and A. Biraben, "Modulation of paroxysmal activity in focal cortical dysplasia by centromedian thalamic nucleus stimulation," *Epilepsy Research*, vol. 104, pp. 264-268, 2013.
- [198] A. L. Velasco, F. Velasco, F. Jiménez, M. Velasco, G. Castro, J. D. Carrillo-Ruiz, G. Fanghänel, and B. Boleaga, "Neuromodulation of the Centromedian Thalamic Nuclei in the Treatment of

- Generalized Seizures and the Improvement of the Quality of Life in Patients with Lennox–Gastaut Syndrome," *Epilepsia*, vol. 47, pp. 1203-1212, 2006.
- [199] F. Velasco, A. L. Velasco, M. Velasco, F. Jimenez, J. D. Carrillo-Ruiz, and G. Castro, "Deep brain stimulation for treatment of the epilepsies: the centromedian thalamic target," *Acta Neurochir Suppl*, vol. 97, pp. 337-42, 2007.
- [200] F. Velasco, M. Velasco, A. L. Velasco, F. Jimenez, I. Marquez, and M. Rise, "Electrical stimulation of the centromedian thalamic nucleus in control of seizures: long-term studies," *Epilepsia*, vol. 36, pp. 63-71, Jan 1995.
- [201] M. Velasco, F. Velasco, and A. L. Velasco, "Centromedian-thalamic and hippocampal electrical stimulation for the control of intractable epileptic seizures," *J Clin Neurophysiol*, vol. 18, pp. 495-513, Nov 2001.
- [202] M. Velasco, F. Velasco, A. L. Velasco, F. Brito, F. Jimenez, I. Marquez, and B. Rojas, "Electrocortical and behavioral responses produced by acute electrical stimulation of the human centromedian thalamic nucleus," *Electroencephalogr Clin Neurophysiol*, vol. 102, pp. 461-71, Jun 1997.
- [203] M. Velasco, F. Velasco, A. L. Velasco, F. Jimenez, F. Brito, and I. Marquez, "Acute and chronic electrical stimulation of the centromedian thalamic nucleus: modulation of reticulo-cortical systems and predictor factors for generalized seizure control," *Arch Med Res*, vol. 31, pp. 304-15, May-Jun 2000.
- [204] S. G. Mallat and Z. Zhifeng, "Matching pursuits with time-frequency dictionaries," *Signal Processing, IEEE Transactions on*, vol. 41, pp. 3397-3415, 1993.
- [205] P. J. Franaszczuk, G. K. Bergey, P. J. Durka, and H. M. Eisenberg, "Time–frequency analysis using the matching pursuit algorithm applied to seizures originating from the mesial temporal lobe," *Electroencephalogr Clin Neurophysiol*, vol. 106, pp. 513-521, 1998.
- [206] P. J. Durka, D. Ircha, and K. J. Blinowska, "Stochastic time-frequency dictionaries for matching pursuit," *Signal Processing, IEEE Transactions on*, vol. 49, pp. 507-510, 2001.
- [207] F. Marten, S. Rodrigues, P. Suffczynski, M. P. Richardson, and J. R. Terry, "Derivation and analysis of an ordinary differential equation mean-field model for studying clinically recorded epilepsy dynamics," *Phys Rev E Stat Nonlin Soft Matter Phys*, vol. 79, p. 021911, Feb 2009.
- [208] B. Molaee-Ardekani, J. Márquez-Ruiz, I. Merlet, R. Leal-Campanario, A. Gruart, R. Sánchez-Campusano, G. Birot, G. Ruffini, J.-M. Delgado-García, and F. Wendling, "Effects of transcranial Direct Current Stimulation (tDCS) on cortical activity: A computational modeling study," *Brain Stimul*, vol. 6, pp. 25-39, 2013.
- [209] T. Radman, R. L. Ramos, J. C. Brumberg, and M. Bikson, "Role of cortical cell type and morphology in subthreshold and suprathreshold uniform electric field stimulation in vitro," *BRAIN STIMULATION: Basic, Translational, and Clinical Research in Neuromodulation*, vol. 2, pp. 215-228.e3, 2009.
- [210] P. Suffczynski, S. Kalitzin, F. L. da Silva, J. Parra, D. Velis, and F. Wendling, "Active paradigms of seizure anticipation: computer model evidence for necessity of stimulation," *Phys Rev E Stat Nonlin Soft Matter Phys*, vol. 78, p. 051917, Nov 2008.
- [211] M. H. Adhikari, J. H. Heeroma, M. di Bernardo, B. Krauskopf, M. P. Richardson, M. C. Walker, and J. R. Terry, "Characterisation of cortical activity in response to deep brain stimulation of ventral-lateral nucleus: modelling and experiment," *J Neurosci Methods*, vol. 183, pp. 77-85, Sep 30 2009.
- [212] G. Matteo, L. Micaela, A. Francesca, and D. I. Guglielmo, "Modeling electromagnetic fields detectability in a HH-like neuronal system: stochastic resonance and window behavior," *Biol Cybern*, 2005.
- [213] J. Modolo, A. W. Thomas, and A. Legros, "Neural mass modeling of power-line magnetic fields effects on brain activity," *Front Comput Neurosci*, vol. 7, 2013.

- [214] E. Niedermayer and F. H. Lopes da Silva, *Electroencephalography Basic Principles, Clinical Applications and Related Fields*, 1999.
- [215] D. L. Rowe, P. A. Robinson, and C. J. Rennie, "Estimation of neurophysiological parameters from the waking EEG using a biophysical model of brain dynamics," *Journal of theoretical biology*, vol. 231, pp. 413-33, Dec 7 2004.
- [216] P. J. Durka, "From wavelets to adaptive approximations: time-frequency parametrization of EEG," *Biomed Eng Online*, vol. 2, p. 1, Jan 6 2003.
- [217] C. C. McIntyre and P. J. Hahn, "Network perspectives on the mechanisms of deep brain stimulation," *Neurobiol Dis*, vol. 38, pp. 329-337, 2010.
- [218] M. E. Calcagnotto, M. F. Paredes, T. Tihan, N. M. Barbaro, and S. C. Baraban, "Dysfunction of synaptic inhibition in epilepsy associated with focal cortical dysplasia," *J Neurosci*, vol. 25, pp. 9649-57, Oct 19 2005.
- [219] L. Gabernet, S. P. Jadhav, D. E. Feldman, M. Carandini, and M. Scanziani, "Somatosensory integration controlled by dynamic thalamocortical feed-forward inhibition," *Neuron*, vol. 48, pp. 315-27, Oct 20 2005.
- [220] J. Talairach, J. Bancaud, G. Szikla, A. Bonis, S. Geier, and C. Vedrenne, "[New approach to the neurosurgery of epilepsy. Stereotaxic methodology and therapeutic results. 1. Introduction and history]," *Neurochirurgie*, vol. 20 Suppl 1, pp. 1-240, Jun 1974.
- [221] P. Jayakar, L. A. Alvarez, M. S. Duchowny, and T. J. Resnick, "A safe and effective paradigm to functionally map the cortex in childhood," *J Clin Neurophysiol*, vol. 9, pp. 288-93, Apr 1992.
- [222] R. J. Racine, "Modification of seizure activity by electrical stimulation. II. Motor seizure," *Electroencephalogr Clin Neurophysiol*, vol. 32, pp. 281-94, Mar 1972.
- [223] C. C. McIntyre, M. Savasta, L. Kerkerian-Le Goff, and J. L. Vitek, "Uncovering the mechanism(s) of action of deep brain stimulation: activation, inhibition, or both," *Clinical Neurophysiology*, vol. 115, pp. 1239-48, Jun 2004.
- [224] M. Steriade, D. A. McCormick, and T. J. Sejnowski, "Thalamocortical oscillations in the sleeping and aroused brain," *Science*, vol. 262, pp. 679-85, Oct 29 1993.
- [225] C. Hammond, H. Bergman, and P. Brown, "Pathological synchronization in Parkinson's disease: networks, models and treatments," *Trends Neurosci*, vol. 30, pp. 357-64, Jul 2007.
- [226] B. Degos, J. M. Deniau, A. M. Thierry, J. Glowinski, L. Pezard, and N. Maurice, "Neuroleptic-induced catalepsy: electrophysiological mechanisms of functional recovery induced by high-frequency stimulation of the subthalamic nucleus," *J Neurosci*, vol. 25, pp. 7687-96, Aug 17 2005.
- [227] A. D. Dorval, G. S. Russo, T. Hashimoto, W. Xu, W. M. Grill, and J. L. Vitek, "Deep brain stimulation reduces neuronal entropy in the MPTP-primate model of Parkinson's disease," *J Neurophysiol*, vol. 100, pp. 2807-18, Nov 2008.
- [228] P. A. Schwartzkroin and H. J. Wenzel, "Are developmental dysplastic lesions epileptogenic?," *Epilepsia*, vol. 53 Suppl 1, pp. 35-44, Jun 2012.
- [229] M.-C. Lee, G.-M. Kim, Y.-J. Woo, M.-K. Kim, J.-H. Kim, S.-C. Nam, J.-J. Suh, W.-K. Chung, J.-S. Lee, H.-I. Kim, H.-Y. Choi, and S. U. Kim, "Pathogenic significance of neuronal migration disorders in temporal lobe epilepsy," *Human Pathology*, vol. 32, pp. 643-648, 2001.
- [230] Commission on Neurosurgery of the International League Against Epilepsy, H. G. Wieser, W. T. Blume, D. Fish, E. Goldensohn, A. Hufnagel, D. King, M. R. Sperling, H. Lüders, and T. A. Pedley, "Proposal for a New Classification of Outcome with Respect to Epileptic Seizures Following Epilepsy Surgery," *Epilepsia*, vol. 42, pp. 282-286, 2001.
- [231] J. Maher and R. S. McLachlan, "Febrile convulsions: Is seizure duration the most important predictor of temporal lobe epilepsy?," *Brain*, vol. 118, pp. 1521-1528, December 1, 1995 1995.

- [232] G. W. Mathern, T. L. Babb, B. G. Vickrey, M. Melendez, and J. K. Pretorius, "The clinical-pathogenic mechanisms of hippocampal neuron loss and surgical outcomes in temporal lobe epilepsy," *Brain*, vol. 118 (Pt 1), pp. 105-18, Feb 1995.
- [233] F. Cendes, F. Andermann, F. Dubeau, P. Gloor, A. Evans, M. Jones-Gotman, A. Olivier, E. Andermann, Y. Robitaille, I. Lopes-Cendes, and et al., "Early childhood prolonged febrile convulsions, atrophy and sclerosis of mesial structures, and temporal lobe epilepsy: an MRI volumetric study," *Neurology*, vol. 43, pp. 1083-7, Jun 1993.
- [234] J. Engel, Jr., "Mesial temporal lobe epilepsy: what have we learned?," *Neuroscientist*, vol. 7, pp. 340-52, Aug 2001.
- [235] C. Y. Chan, J. Hounsgaard, and C. Nicholson, "Effects of electric fields on transmembrane potential and excitability of turtle cerebellar Purkinje cells in vitro," *J Physiol*, vol. 402, pp. 751-71, Aug 1988.
- [236] R. S. Ghai, M. Bikson, and D. M. Durand, "Effects of applied electric fields on low-calcium epileptiform activity in the CA1 region of rat hippocampal slices," *J Neurophysiol*, vol. 84, pp. 274-80, Jul 2000.
- [237] J. G. Jefferys, J. Deans, M. Bikson, and J. Fox, "Effects of weak electric fields on the activity of neurons and neuronal networks," *Radiat Prot Dosimetry*, vol. 106, pp. 321-3, 2003.
- [238] J. Lian, M. Bikson, C. Sciortino, W. C. Stacey, and D. M. Durand, "Local suppression of epileptiform activity by electrical stimulation in rat hippocampus in vitro," *J Physiol*, vol. 547, pp. 427-34, Mar 1 2003.
- [239] C. P. Taylor and F. E. Dudek, "Excitation of hippocampal pyramidal cells by an electrical field effect," *J Neurophysiol*, vol. 52, pp. 126-42, Jul 1984.
- [240] J. G. Jefferys, "Influence of electric fields on the excitability of granule cells in guinea-pig hippocampal slices," *J Physiol*, vol. 319, pp. 143-52, 1981.
- [241] S. R. y. Cajal, *Histologie du système nerveux de l'homme & des vertébrés*. Paris, 1911.
- [242] S. R. Weiss, A. Eidsath, X. L. Li, T. Heynen, and R. M. Post, "Quenching revisited: low level direct current inhibits amygdala-kindled seizures," *Exp Neurol*, vol. 154, pp. 185-92, Nov 1998.
- [243] R. D. Traub and R. K. Wong, "Cellular mechanism of neuronal synchronization in epilepsy," *Science*, vol. 216, pp. 745-7, May 14 1982.
- [244] P. F. Pinsky and J. Rinzel, "Intrinsic and network rhythmogenesis in a reduced Traub model for CA3 neurons," *J Comput Neurosci*, vol. 1, pp. 39-60, Jun 1994.
- [245] S. Demont-Guignard, P. Benquet, U. Gerber, and F. Wendling, "Analysis of intracerebral EEG recordings of epileptic spikes: insights from a neural network model," *IEEE Trans Biomed Eng*, vol. 56, pp. 2782-95, Dec 2009.
- [246] F. Suzuki, M. P. Junier, D. Guilhem, J. C. Sorensen, and B. Onteniente, "Morphogenetic effect of kainate on adult hippocampal neurons associated with a prolonged expression of brain-derived neurotrophic factor," *Neuroscience*, vol. 64, pp. 665-74, Feb 1995.
- [247] S. T. Murakami, Tsunematsu; Shimizu, Zensho, "The effective principle of Digenea simplex Aq. I. Separation of the effective fraction by liquid chromatography," *Yakugaku Zasshi*, vol. 73, pp. 1026-8 1956.
- [248] J. R. Simon, J. F. Contrera, and M. J. Kuhar, "Binding of [3H] kainic acid, and analogue of Lglutamate, to brain membranes," *J Neurochem*, vol. 26, pp. 141-7, Jan 1976.
- [249] V. Bouilleret, F. Loup, T. Kiener, C. Marescaux, and J. M. Fritschy, "Early loss of interneurons and delayed subunit-specific changes in GABA(A)-receptor expression in a mouse model of mesial temporal lobe epilepsy," *Hippocampus*, vol. 10, pp. 305-24, 2000.
- [250] V. Riban, V. Bouilleret, B. T. Pham-Le, J. M. Fritschy, C. Marescaux, and A. Depaulis, "Evolution of hippocampal epileptic activity during the development of hippocampal sclerosis in a mouse model of temporal lobe epilepsy," *Neuroscience*, vol. 112, pp. 101-11, 2002.

- [251] P. Vincent and C. Mulle, "Kainate receptors in epilepsy and excitotoxicity," *Neuroscience*, vol. 158, pp. 309-23, Jan 12 2009.
- [252] C. Heinrich, S. Lahtinen, F. Suzuki, L. Anne-Marie, S. Huber, U. Haussler, C. Haas, Y. Larmet, E. Castren, and A. Depaulis, "Increase in BDNF-mediated TrkB signaling promotes epileptogenesis in a mouse model of mesial temporal lobe epilepsy," *Neurobiol Dis*, vol. 42, pp. 35-47, Apr 2011.
- [253] R. Harner, "Automatic EEG spike detection," *Clin EEG Neurosci*, vol. 40, pp. 262-270, 2009.
- [254] J. Bourien, J. J. Bellanger, F. Bartolomei, P. Chauvel, and F. Wendling, "Mining reproducible activation patterns in epileptic intracerebral EEG signals: application to interictal activity," *Biomedical Engineering, IEEE Transactions on*, vol. 51, pp. 304-315, 2004.
- [255] E. S. PAGE, "CONTINUOUS INSPECTION SCHEMES," *Biometrika*, vol. 41, pp. 100-115, June 1, 1954 1954.
- [256] J. Bourien, "Analyse de distributions spatio-temporelles de transitoires dans des signaux vectoriels. Application à la détection-classification d'activités paroxystiques intercritiques dans des observations EEG," PhD, UFR Sciences et Propriétés de la matière, Université Rennes 1, Rennes, 2003.
- [257] P. Suffczynski, F. H. L. da Silva, J. Parra, D. N. Velis, B. M. Bouwman, C. M. van Rijn, P. Van Hese, P. Boon, H. Khosravani, M. Derchansky, P. Carlen, and S. Kalitzin, "Dynamics of epileptic phenomena determined from statistics of ictal transitions," *Biomedical Engineering, IEEE Transactions on*, vol. 53, pp. 524-532, 2006.
- [258] D. Johnston and T. H. Brown, "The synaptic nature of the paroxysmal depolarizing shift in hippocampal neurons," *Annals of Neurology*, vol. 16 Suppl, pp. S65-71, 1984.
- [259] G. Schmid, G. Neubauer, and P. R. Mazal, "Dielectric properties of human brain tissue measured less than 10 h postmortem at frequencies from 800 to 2450 MHz," *Bioelectromagnetics*, vol. 24, pp. 423-430, 2003.
- [260] M. M. Elwassif, A. Datta, A. Rahman, and M. Bikson, "Temperature control at DBS electrodes using a heat sink: experimentally validated FEM model of DBS lead architecture," *J Neural Eng*, vol. 9, p. 046009, Aug 2012.
- [261] V. R. Khan and I. R. Brown, "The effect of hyperthermia on the induction of cell death in brain, testis, and thymus of the adult and developing rat," *Cell stress & chaperones*, vol. 7, pp. 73-90, 2002.
- [262] H. M. Hoffmann and V. E. Dionne, "Temperature dependence of ion permeation at the endplate channel," *The Journal of General Physiology*, vol. 81, pp. 687-703, May 1, 1983 1983.
- [263] F. R. Pierau, M. R. Klee, and F. W. Klussmann, "Effect of temperature on postsynaptic potentials of cat spinal motoneurons," *Brain research*, vol. 114, pp. 21-34, 1976.
- [264] M. M. Elwassif, Q. Kong, M. Vazquez, and M. Bikson, "Bio-heat transfer model of deep brain stimulation-induced temperature changes," *J Neural Eng*, vol. 3, pp. 306-15, Dec 2006.
- [265] F. Velasco, J. D. Carrillo-Ruiz, F. Brito, M. Velasco, A. L. Velasco, I. Marquez, and R. Davis, "Double-blind, Randomized Controlled Pilot Study of Bilateral Cerebellar Stimulation for Treatment of Intractable Motor Seizures," *Epilepsia*, vol. 46, pp. 1071-1081, 2005.
- [266] S. Sunderam, N. Chernyy, J. Mason, N. Peixoto, S. L. Weinstein, S. J. Schiff, and B. J. Gluckman, "Seizure modulation with applied electric fields in chronically implanted animals," *Conf Proc IEEE Eng Med Biol Soc*, vol. 1, pp. 1612-5, 2006.
- [267] K. A. Richardson, B. J. Gluckman, S. L. Weinstein, C. E. Glosch, J. B. Moon, R. P. Gwinn, K. Gale, and S. J. Schiff, "In vivo modulation of hippocampal epileptiform activity with radial electric fields," *Epilepsia*, vol. 44, pp. 768-77, Jun 2003.

TABLE OF CONTENTS

Introduction	5
Chapter 1: Neuronal Systems – Structure, Function and Control: Background	9
1 Neuronal Dynamics: A Systems View	9
1.1 Discovering the Concept of The Neuron.....	9
1.2 The Earliest Models of Neuronal Dynamics.....	10
1.3 Populations of Single Neuron Models	12
1.4 Neural Mass Models	12
2 Assessing Neuronal Function Using Electrophysiology.....	14
2.1 Intracellular Electrophysiological Recordings.....	15
2.2 Extracellular Electrophysiological Recordings	16
2.3 Assessing Function/Dysfunction Using Extracellular Signals (EEG/iEEG).....	17
2.3.1 Electrophysiological Oscillatory Signatures of Neuronal Pathology (Movement and Neuropsychiatric disorders).....	17
2.3.2 Electrographic Signatures of Epileptic Dynamics.....	18
3 Controlling (Patho-)physiological Neuronal Dynamics by Electrical Stimulation: State of The Art	20
3.1 Stimulation-Induced Electric Field	21
3.1.1 In a Volume Conductor	21
3.1.2 In The Vicinity of Excitable Tissue	22
3.2 Electrical Stimulation Categories	23
3.2.1 Intracerebral versus Transcranial Current Stimulation.....	23
3.2.2 AC versus DC Stimulation.....	24
3.2.3 Direct versus Indirect Stimulation	25
3.3 Stimulation for Movement Disorders.....	25
3.3.1 The Network Structure of Movement disorders.....	26
3.3.2 Modulatory Effects of Electrical Stimulation	27
3.4 Stimulation for Epilepsy.....	28
Chapter 2: Problem Statement and Objectives.....	35
1 Problem Statement: Stimulation Parameters, Outcome and Mechanisms.....	35
1.1 The Variability.....	35
1.2 The Poorly-Understood Mechanisms	36
1.3 How to Optimize Stimulation	38
2 Objectives: Optimize Stimulation Outcome.....	38
2.1 Optimize Stimulation Parameters and Effects.....	39

2.1.1	Case of indirect AC intracerebral Stimulation.....	39
2.1.2	Case of direct DC intracerebral Stimulation	39
3	General Methodology.....	40
3.1	Computational Modeling.....	40
3.2	Electrophysiological Data Acquisition/Experimentation and Signal Processing.....	41
3.3	Nonlinear System Analysis.....	42
3.4	General overview of the work accomplished during this PhD thesis	42
Chapter 3: A Computational Model of the Thalamocortical Loop		47
1	Mesoscopic Models of the Thalamocortical Loop	47
1.1	The Thalamocortical Loop	47
1.2	Thalamocortical Models: State of The Art.....	49
2	Implementing a Stimulation-Driven Model of Thalamocortical Dynamics.....	50
2.1	Model Architecture	50
2.1.1	From a Global Network View.....	50
2.1.2	On The Level of a Subpopulation	50
2.1.3	The Cortical Module.....	53
2.1.4	The Thalamic Module	55
2.1.5	The Reticular Module.....	55
2.2	Implementing Physiologically-Relevant Mechanisms	55
2.2.1	Feed-forward Inhibition.....	55
2.2.2	Short Term Depression	60
2.2.3	Stimulation Inputs.....	63
Chapter 4: Electrophysiological Observations and Signal Analysis for Model Optimization.....		67
1	The Clinical Observation	67
2	Signal Processing.....	69
2.1	General Algorithm	69
2.2	Matching Pursuit	70
2.3	The Model Optimization Algorithm for Simulating Epileptic FCD Activity	72
2.4	Model Tuning for Simulating Stimulation Effects.....	73
Chapter 5: Results of Part 1.....		75
1	Quantification of Stimulation Effects in Real Signals	75
1.1	Energy Distribution.....	75
1.1.1	Spontaneous Interictal Activity (LFPs _{FCD})	75
1.1.2	Stimulation Effects.....	76
1.2	Three Stimulation Groups.....	78
1.2.1	The 3D Space	78

1.2.2	Feature Vector Classification and Stimulation Clusters	79
2	Reproduction of Real Epileptic LFPs During and in the Absence of Stimulation.....	80
2.1	Simulating Epileptic FCD Activity	80
2.2	Simulating Stimulation Effects.....	81
3	Model Analysis.....	82
3.1	Indicative Study of Parameter Sensitivity.....	82
3.2	Model Phase Portraits	85
3.3	Quantifying Model Bifurcations: The High to Low Firing Ratio (HtoLR)	86
3.4	The Necessary Elements.....	88
4	The Mechanisms: Computational Insights.....	89
4.1	The No Stimulation “Interictal” Dynamics.....	89
4.2	Low-Frequency Stimulation (LFS, $f < 20$ Hz)	90
4.3	Intermediate-Frequency Stimulation (IFS, $20 < f < 70$ Hz).....	91
4.4	High-Frequency Stimulation (HFS, $f > 70$ Hz).....	91
	Conclusion and Discussion on Part 1.....	93
1	The Model’s Architecture	93
2	Signal Processing and Representation	95
2.1	Using FFT – Comparing the Optimal Model Outputs.....	95
2.2	Classical Time Frequency Approaches – The Limitations	97
2.3	The Advantages of Matching Pursuit (MP).....	99
2.4	The 3D Space	101
3	The Frequency-Dependence of The Identified Mechanisms	102
3.1	The No Stimulation Condition	102
3.2	The Low-Frequency Stimulation Condition	102
3.3	The Intermediate-Frequency Stimulation Condition.....	103
3.4	The High-Frequency Stimulation Condition.....	104
3.5	The Stimulation Effects Curve	104
4	The Limitations.....	105
5	Conclusion.....	105
	Chapter 6: Low-Intensity DC Stimulation of the Ictal Onset Zone – Computational Tools	109
1	DC Stimulation Protocols	110
1.1	<i>In Vitro</i> Effects of DC Electric Fields: State of The Art	110
1.2	The Hypothetical Basis of Neuronal Polarization by DC Currents	112
2	A Computational Model of Temporal Lobe Epilepsy	115
2.1	Computational Model of The Hippocampus	116
2.1.1	General Architecture	117

3	An Experimental Model of Mesio-Temporal Lobe Epilepsy.....	117
3.1	Kainate Model of Mesio-Temporal Lobe Epilepsy.....	117
3.1.1	Model Description	117
3.1.2	Hippocampal Paroxysmal Discharges: Specific Biomarkers of Epileptogenicity.....	118
3.2	Experimental Kainate Protocol and Signal Acquisition.....	120
4	Methods for Epileptic Signal Analysis	121
4.1	iEEG Signal Quantification	121
4.1.1	Detection of HPDs Using The Page-Hinkley Method	121
5	Model Adaptation for the Generation of HPDs	126
5.1	Experimentally identifying the duration and frequency of occurrence of HPDs.....	126
5.2	Implementing dynamical changes of HPDs in the model.....	129
6	Implementing the Stimulation Inputs.....	130
7	Computational Analysis of Stimulation Effects.....	134
7.1	Quantifying Epileptic Features in Simulated LFP Signals	134
	Chapter 7: Computational Results of Part 2.....	137
1	Simulating HPDs.....	137
1.1	Model Activity Maps.....	137
1.2	Simulated Stimulation Effects.....	140
1.3	The Theoretical Equipotential Lines Induced By Stimulation	141
	Chapter 8: Experimental Validation	149
1	Preliminary Safety Test: Stimulation-Induced Heating.....	149
2	The Experimental Protocol	152
2.1	The Protocol Variants	152
2.2	Database.....	154
2.3	Histological Verification.....	155
3	Quantifying Stimulation Effects	155
4	Statistical Analysis.....	158
5	The Experimental Observations.....	158
5.1	In Vivo Effects	159
5.2	The Effects of Stimulation Polarity	159
5.3	The Effects of Stimulation Duration	162
5.4	Electrode Position and Stimulation Effects on Hippocampal Tissue	168
5.5	In Vitro Verification	171
	Conclusion and Discussion on Part 2.....	177
1	Position with Respect to Earlier Studies	177
1.1	<i>In Vivo</i> Observations.....	177

1.2	<i>In Vitro</i> Observations	178
2	Polarization or a Network Effect	179
3	Future Implications of the Results	180
4	Limitations and Perspectives	182
	General Conclusion and Perspectives	183
	References.....	187
	Table of Contents	203
	Table of Figures	209
	Appendix A. Thalamocortical Model Simulink Implementation	213
	Appendix B. Experimental Signals (Part 2)	219
	Appendix C. Publications.....	227

TABLE OF FIGURES

Figure 1. Golgi staining method applied on hippocampal tissue (work of Golgi: http://neurophilosophy.wordpress.com/2006/08/29/the-discovery-of-the-neuron).	10
Figure 2. Initial integrate-and-fire model. Adapted from Lapique in 1907 [2].	11
Figure 3. High-density recording of unit activity in the somatosensory cortex of the rat ([37] no requested permission).	16
Figure 4. Different Types of epileptic EEG patterns. Adapted and translated from [48]. No permission requested.	19
Figure 5. The cerebral network involved in the pathologic dynamics of movement disorders as presented in [77].	26
Figure 6. Electrophysiology of focal cortical dysplasia (FCD).	32
Figure 7. A schematic representation of the general methodology.	41
Figure 8. Major contributions and organization of the presented work.	43
Figure 9. The Thalamic Nuclei (http://en.wikipedia.org/wiki/Thalamic_reticular_nucleus).	48
Figure 10. Generic architecture of the thalamocortical model.	49
Figure 11. Modeling the thalamocortical loop.	51
Figure 12. The form of the model's functions in the cortical module.	53
Figure 13. The Simulink implementation of the cortical module.	54
Figure 14. Cortical inhibitory circuits.	56
Figure 15. The temporal considerations of feedforward inhibition.	58
Figure 16. Feedforward inhibition in the model (sample simulations).	59
Figure 17. Rapid adaptation of cortical LFP to thalamic input at whisker stimulation of 4 Hz (adapted from [150]).	61
Figure 18. Dynamical response of the $\kappa(t)$ function to one pulse of duration (0.5 ms).	62
Figure 19. Dynamical response of the $\kappa(t)$ function to a series of pulses arriving at a 1.5 Hz frequency.	63
Figure 20. Biphasic versus monophasic pulse stimulation in the model.	64
Figure 21. MRI of the Patient showing the location of the focal cortical dysplasia in the premotor cortex of the patient.	67
Figure 22. Frequency-dependent stimulation effects: real data.	68
Figure 23. Feature extraction for parameter optimization. (A) The feature extraction algorithm. (B) The parameter optimization algorithm.	71
Figure 24. Energy Distribution (%) of Pathological (LFP _{FCD}) Signal vs. Normal Signal.	75
Figure 25. Reconstructed Signal vs. Sum of Major Bands ($\delta + \theta_1$, α , and γ).	76
Figure 26. Frequency-dependent modulation of the signal's energy distribution during stimulation. Each graph represents the distribution of given stimulation condition as compared to the <i>no stimulation</i> condition. Note the absence of effect for the 50 Hz stimulation condition.	77
Figure 27. 3D Space and Clustering.	79
Figure 28. Normalized Euclidian distance between $V_{F,real}$ and $V_{F,model}$.	80
Figure 29. Real and simulated signals for the different stimulation conditions.	81
Figure 30. The feature vectors of simulated signals (triangles) projected in 3D frequency space with the feature vectors of real iEEG signals (Squares).	82
Figure 31. Indicative Study of Parameter Sensibility.	83
Figure 32. Quantitative Representation of model output when $\mu = 0.05$.	84
Figure 33. Phase portraits (FCD activity vs. CM firing) for the four stimulation conditions: NS, LFS (2 Hz), IFS (50 Hz), and HFS (100 Hz).	86
Figure 34. Model intermittency.	86
Figure 35. Conditions to reproduce frequency-dependent stimulation effects.	88

Figure 36. Frequency-dependent mechanisms underlying DBS.	90
Figure 37. Optimizing the model output: MP vs. FFT.....	96
Figure 38. The dyadic scale used for the DWT and the corresponding decomposed frequency bands	98
Figure 39. The 3D frequency space as made possible by the DWT transform.....	99
Figure 40. MP precisely detects different signal components.	100
Figure 41. PCA automatic dimension reduction from 9D to 3D feature vectors.	101
Figure 42. Schematic representation of the hippocampal organization [241].	110
Figure 43. Effects of uniform weak DC electric field on single CA1 neurons.	111
Figure 44. Computational effects of current polarity on neural excitability.....	112
Figure 45. Schematic representation of the effects of injected currents on neuronal excitability as a function of electrode types and polarity. In the case of large field electrodes:	113
Figure 46. Schematic representation of the stimulation electrodes ideally situated on the two sides of the CA1 region.	114
Figure 47. The architecture of the hippocampus model as presented by [161].	116
Figure 48. The different electrographic signatures of the different stages of epileptogenesis defined by Heinrich and his colleagues in [252].	119
Figure 49. Distinct epileptic events observed in the iEEG of the recorded animals.	124
Figure 50. The Page-Hinkley Test.	125
Figure 51. The experimental identification of the statistical laws of ΔHPD and ΔBKG	127
Figure 52. Flowchart of HPD simulation diagram.	129
Figure 53. Block diagram of the model indicating the emplacement of stimulation inputs before the sigmoidal function of each population, as well as that of the PSD (paroxysmal depolarization shift) input.	131
Figure 54. The implementation of the electrode-electrolyte interface in the model.....	132
Figure 55. Modeling the electrode-electrolyte solution.	133
Figure 56. Modeling HPDs.....	138
Figure 57. Model activity maps representing the average number of peaks (calculated over 5 simulations) in the minute following a stimulation pulse of duration 50 s and intensity 1 μA for different values of k_1, k_2 and k_3	139
Figure 58. Model activity maps representing the average duration (s) of discharge (calculated over 5 simulations) in the minute following a stimulation pulse of duration 50 s and intensity 1 μA for different values of k_1, k_2 and k_3	140
Figure 59. Model activity maps representing the average energy of discharge (calculated over 5 simulations) in the minute following a stimulation pulse of duration 50 s and intensity 1 μA for different values of k_1, k_2 and k_3	142
Figure 60. Ten examples of possible model dynamics in the absence of stimulation.	144
Figure 61. Ten examples of the model output when “depolarizing” stimulation is applied.....	145
Figure 62. Ten examples of the model output when “hyperpolarizing stimulation” is applied.	146
Figure 63. Boxplots of simulated iEEG signals in the absence and during hyperpolarizing and depolarizing stimulation.	147
Figure 64. The theoretical equipotential lines induced during the 1 μA DC stimulation, for an intra-electrode distance of 350 μm in a homogenous medium of conductance 0.35 S/m. The red and blue spheres represent the anode and the cathode emplacements respectively. The numbers on the potential lines indicate their corresponding value in mV. The maximum induced voltage gradient between the two electrode tips is of the order of 10 mV.	148
Figure 65. The electric field lines induced by stimulation superimposed over the induced potential map (V).	148
Figure 66. Verifying temperature rise during stimulation.	149
Figure 67. The thermal heating recorded for different stimulation current intensities applied for 100s.	150
Figure 68. Thermal heating produced by high current intensity DC stimulation (4 mA)	151
Figure 69. The different stimulation protocols used in this study.	154

Figure 70. The processing of iEEG signals over fixed-window intervals.....	157
Figure 71. Example signal segments (mouse K143) in the absence of stimulation.	160
Figure 72. Signals recorded just after the end of 100 s S_1 stimulation (mouse K143) during different sessions.....	161
Figure 73. Signals recorded just after the end of 100 s S_2 stimulation (mouse K143) during different sessions.....	161
Figure 74. Boxplots of the signal features of mice K148 (number of trials: NS = 220, S_1 = 4, S_2 = 3) and K155 (number of trials NS = 238, S_1 = 12, S_2 = 10) in the absence and just after the end of a stimulation pulse of polarity S_1/S_2	162
Figure 75. Boxplots of the signal features of mice K168 (number of trials: NS = 240, S_1 = 19, S_2 = 20) and K171 (number of trials NS = 288, S_1 = 18, S_2 = 20) in the absence and just after the end of a stimulation pulse of polarity S_1/S_2	165
Figure 76. Boxplots of the signal features of mouse K143 (number of trials: NS = 200, S_1 = 8, S_2 = 6) in the absence and just after the end of a stimulation pulse of polarity S_1/S_2	166
Figure 77. A unique observation of the evolution of the intensity of discharge through stimulation and baseline sessions when excessive stimulation duration is used (100 s).....	167
Figure 78. The effects of stimulation duration and polarity on the iEEG signal features. Results observed in mouse K148 (NS = 100; S_1 : N_{5s} = 5, N_{10s} = 5, N_{20s} = 5, N_{30s} = 5, N_{40s} = 4, N_{50s} = 2; S_2 : N_{5s} = 5, N_{10s} = 5, N_{20s} = 5, N_{30s} = 4, N_{40s} = 3, N_{50s} = 1).....	168
Figure 79. The electrode trace in the injected hippocampus in a mal-colored section of mouse K155.....	169
Figure 80. Histological coronal sections of mouse K171.....	170
Figure 81. Histological coronal sections of mouse K168.....	171
Figure 82. Patch Clamp recordings in whole cell configuration of organotypic rat hippocampal slices from pyramidal CA1 neurons.....	172
Figure 83. Patch Clamp recordings in whole cell configuration of organotypic rat hippocampal slices.....	173
Figure 84. Patch Clamp recordings in the presence of the voltage-gated sodium channel blocker TTX (1 μ M).....	174
Figure 85. Simulated Boxplots of HPD occurrence during polarizing stimulation under the hypothesis that FSI are always depolarized by stimulation.....	181

Appendix A. Thalamocortical Model Simulink Implementation

In this appendix the block diagrams corresponding to Simulink® implementation of the thalamocortical model are presented. The implemented version can be provided upon request. Table A1-1 shows the values of the model parameters. Figure A1-1 shows the general model architecture. Four basic blocks are illustrated in the model diagram: the three modules and the synaptic depression block.

The diagram of the cortical module is previously presented in Chapter 3, and will not be included in this appendix.

Parameter	Value	Interpretation
A_C	6 (optimized, pathological) 3 (normal) mV	Amplitude of the cortical average EPSP
A_C'	$\kappa(t).A_C$ mV	Amplitude of the cortical average EPSP in response to thalamic input (only on subpopulation P)
B_C	14 (optimized, pathological) 50 (normal) mV	Amplitude of the cortical average IPSP (GABA _{A,slow} mediated currents)
G_C	16.5 (optimized, pathological) 22 (normal) mV	Amplitude of the cortical average IPSP (GABA _{A,fast} mediated currents)
A_{Th}	3.5 mV	Amplitude of the thalamic average EPSP
B_{Th}	30 mV	Amplitude of the thalamic average IPSP (GABA _{A,slow} and GABA _B receptors)
G_{Th}	22 mV	Amplitude of the thalamic average IPSP (GABA _{A,fast} receptors)
A_{Rt}	3.5 mV	Amplitude of the reticular average EPSP
τ_{ac}	1/80 s	Time constant of cortical glutamate-mediated synaptic transmission.
τ_{bc}	1/35 s	Time constant of cortical GABA-mediated synaptic transmission (GABA _{A,slow} receptors)
τ_{gc}	1/180 s	Time constant of cortical GABA-mediated synaptic transmission (GABA _{A,fast} receptors)
τ_{aTh}	1/100 s	Time constant of thalamic glutamate-mediated synaptic transmission
τ_{bTh}	1/20 s	Time constant of thalamic GABA-mediated synaptic transmission (GABA _{A,slow} and GABA _B receptors)
τ_{gTh}	1/150 s	Time constant of thalamic GABA-mediated synaptic

τ_{aRt}	1/100 s	transmission (GABA _{A,fast} receptors) Time constant of reticular glutamate-mediated synaptic transmission
v_0, e_0, r	$v_0 = 6 \text{ mV}, e_0 = 2.5 \text{ s}^{-1},$ $r = 0.56 \text{ mV}^{-1}$	Parameters of the nonlinear sigmoid function (transforming the average membrane potential to an average density of action potentials)
C_{P-P_I}	135	Collateral excitation connectivity constant
C_{P_I-P}	108	Collateral excitation connectivity constant
$C_{P-I_2^c}$	33.75	P to I_2^c connectivity constant
$C_{I_2^c-P}$	33.75	I_2^c to P connectivity constant
$C_{P-I_1^c}$	40.5	P to I_1^c connectivity constant
$C_{I_1^c-I_2^c}$	13.5	I_1^c to I_2^c connectivity constant
$C_{I_1^c-P}$	91.125	I_1^c to P connectivity constant
C_{TC-P}	120	TC to P connectivity constant
$C_{TC-I_1^c}$	30	TC to I_1^c connectivity constant
$C_{TC-I_2^c}$	45	TC to I_2^c connectivity constant
$C_{TC-I_1^{Rt}}$	20	TC to I_1^{Rt} connectivity constant
$C_{TC-I_2^{Rt}}$	20	TC to I_2^{Rt} connectivity constant
$C_{P-I_1^{Rt}}$	30	P to I_1^{Rt} connectivity constant
$C_{P-I_2^{Rt}}$	30	P to I_2^{Rt} connectivity constant
C_{P-TC}	20	P to TC connectivity constant
$C_{I_1^{Rt}-TC}$	35	I_1^{Rt} to TC connectivity constant
$C_{I_2^{Rt}-TC}$	5	I_2^{Rt} to TC connectivity constant
μ_{P1}	0	Mean of nonspecific cortical input
μ_{P2}	70	Mean of nonspecific subcortical input
σ_{P1}	20.√6	Standard deviation of nonspecific cortical input
σ_{P2}	35.√6	Standard deviation of nonspecific subcortical input
S_{TC}	5	Stimulation impact on subpopulation TC
S_{Rt1}	4	Stimulation impact on subpopulation I_{Rt}^1
S_{Rt2}	4	Stimulation impact on subpopulation I_{Rt}^2
f_s	1Hz – 150Hz	Frequency of the stimulation signal (pulse train)
A_{fs}	1	Stimulation signal amplitude

Table A1. Model Parameters

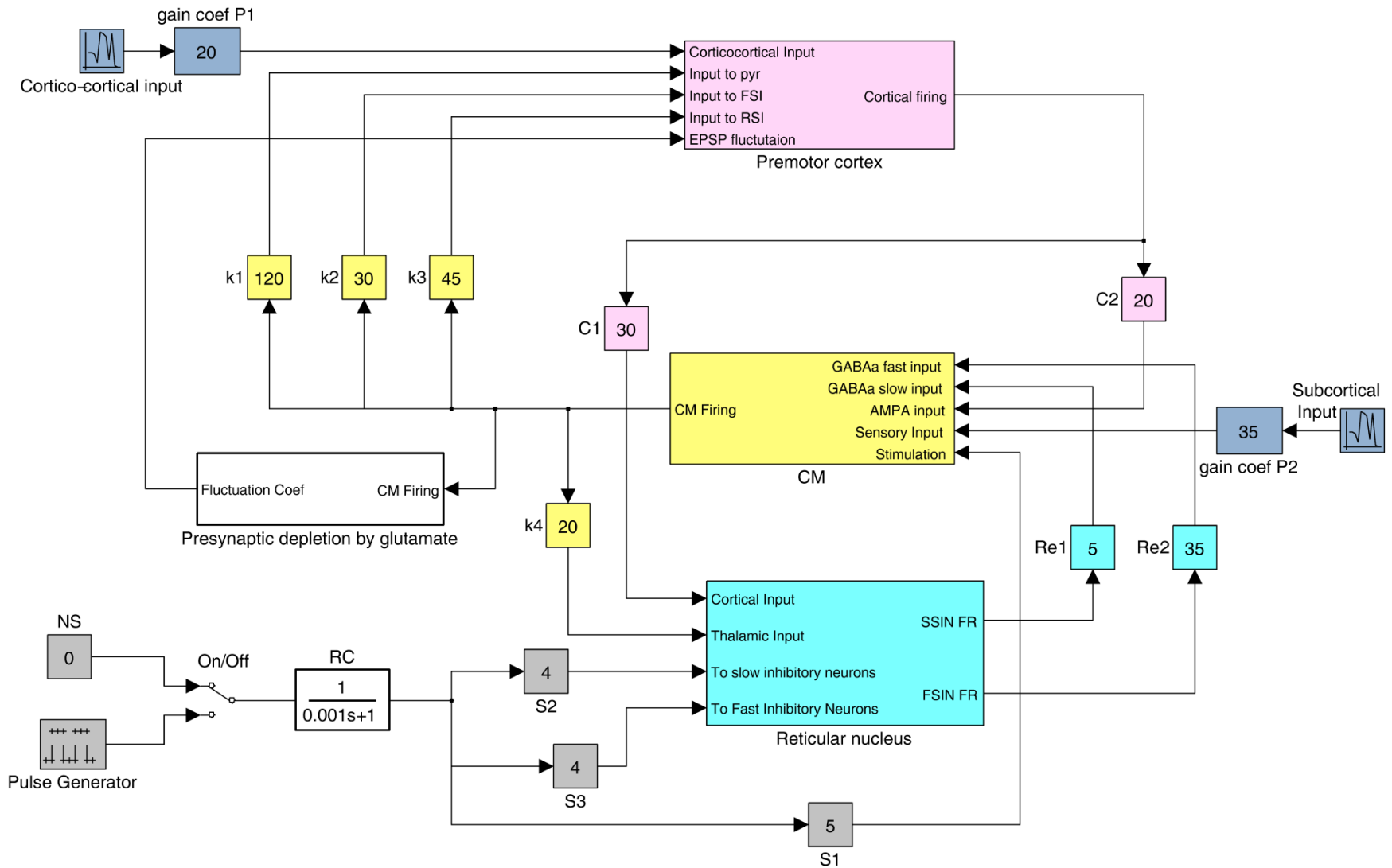


Figure A2. The model's block diagram in Simulink®. It is composed of four basic blocks: the three modules and the synaptic depletion block.

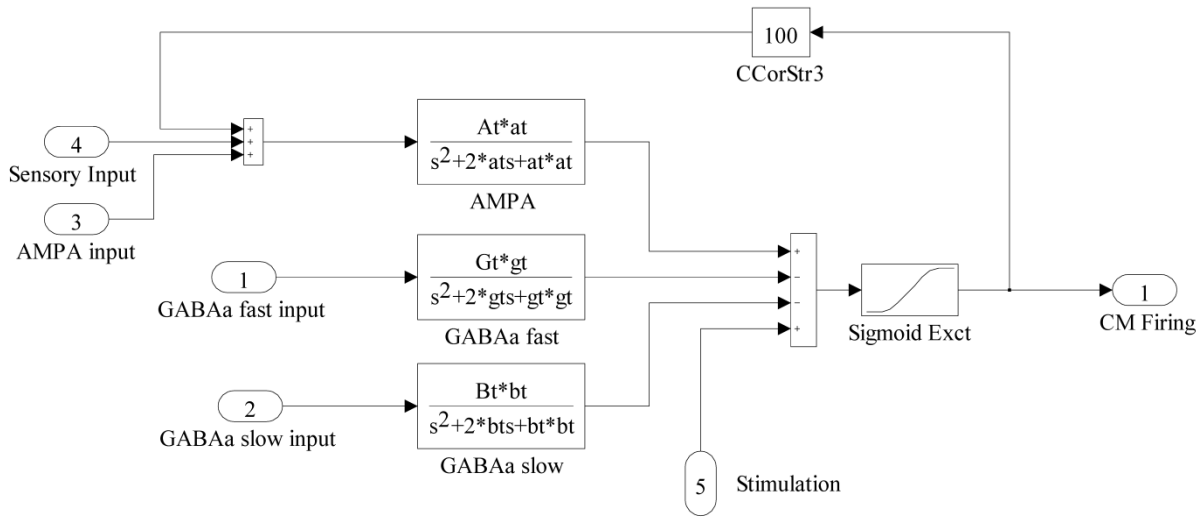


Figure A3. The implementation details of the CM block (thalamic module in the model's formal description).

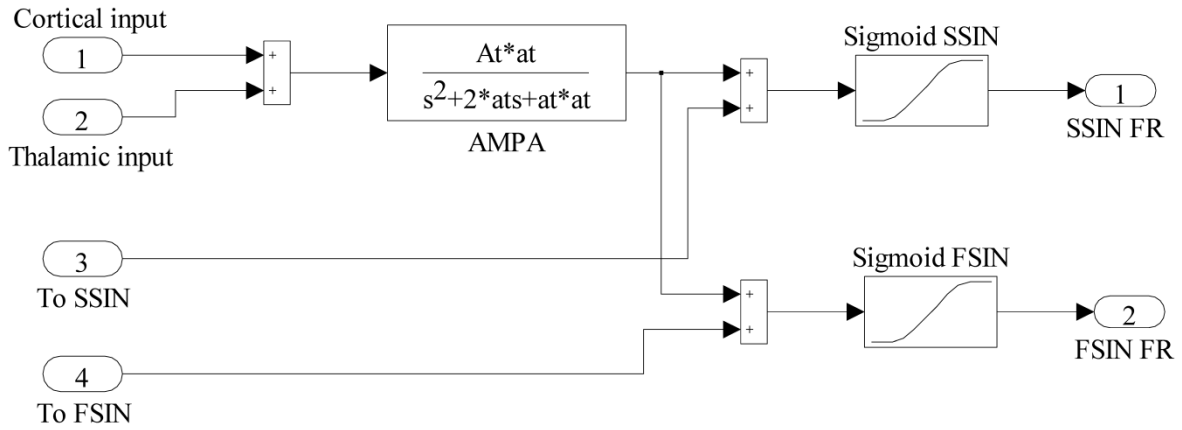


Figure A4. The implementation details of the reticular nucleus block (reticular module in the model's formal description).

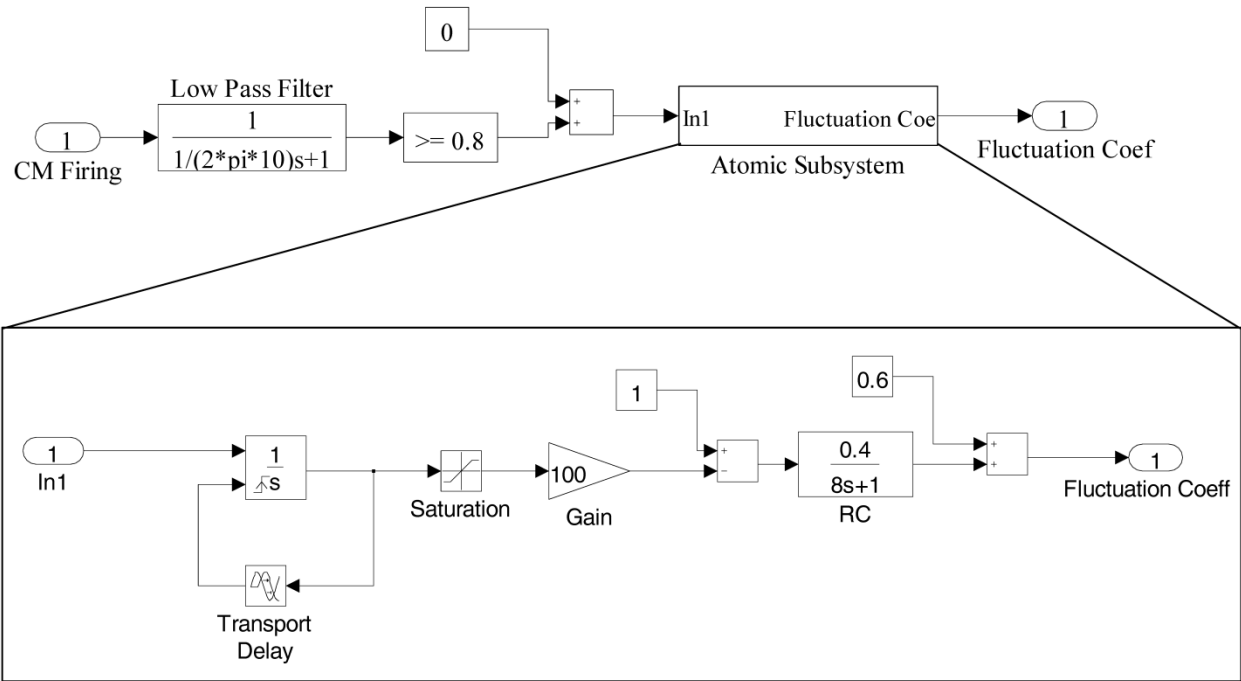


Figure A5. The implementation details of the short term depression (by synaptic depletion) block. Upper panel, the thalamic firing is low-pass filtered (10 Hz). Then it is compared to a certain threshold (0.8 in this figure), representing the upper limit of permissible firing with no STD effects. This parameter has been tuned manually. The subsequent subsystem calculates the fluctuation coefficient. Lower panel, whenever the filtered thalamic firing overpasses the threshold a step response of duration transport delay (0.45 s) is input to an RC circuit. This calculates an exponentially decreasing function varying between 1 and 0.6 in order to represent the decrease in synaptic efficacy. This function denoted “fluctuation coeff” in the block’s diagram is dynamically multiplied with the thalamocortical EPSPs arriving at the principal cell population of the cortical module. It represents function $\kappa(t)$ analytically detailed in chapter 3 section 2.2.2, and given in Table A1 in this appendix.

Appendix B. Experimental Signals (Part 2)

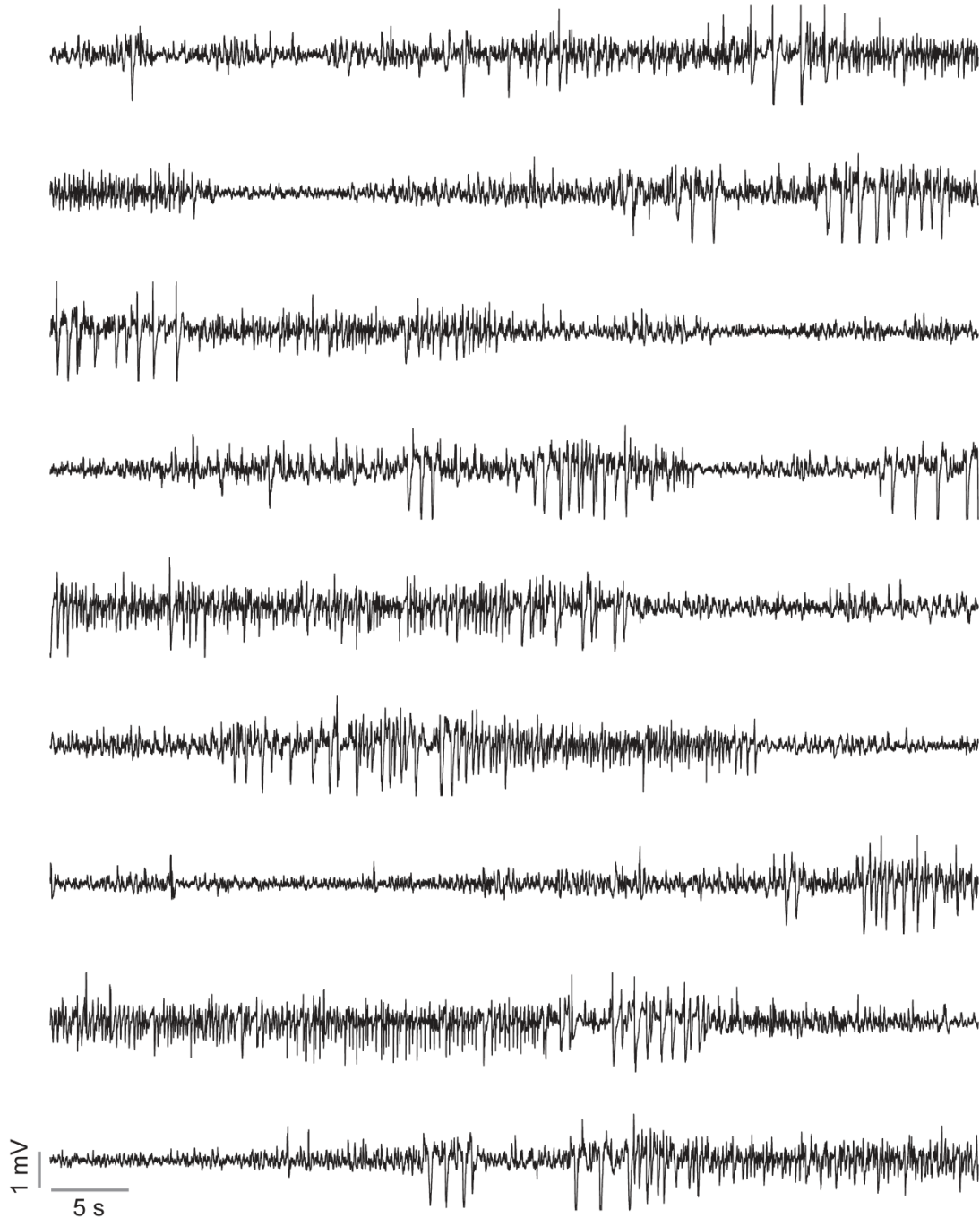


Figure B1. Spontaneous epileptiform discharges in K148

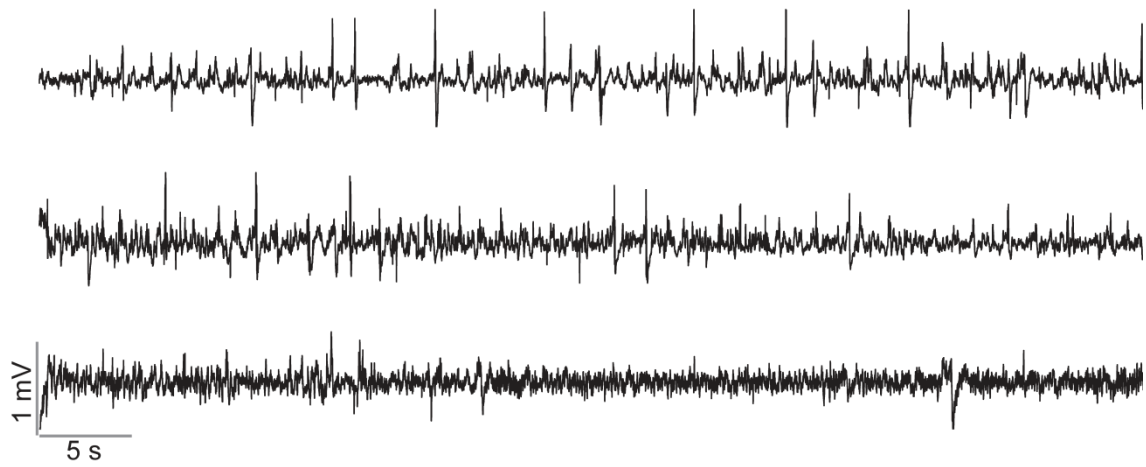


Figure B2. Recorded LFP in K148 after 40s S_1 stimulation pulses. Note the visual change in discharge patterns after a stimulation pulse of polarity S_1 .

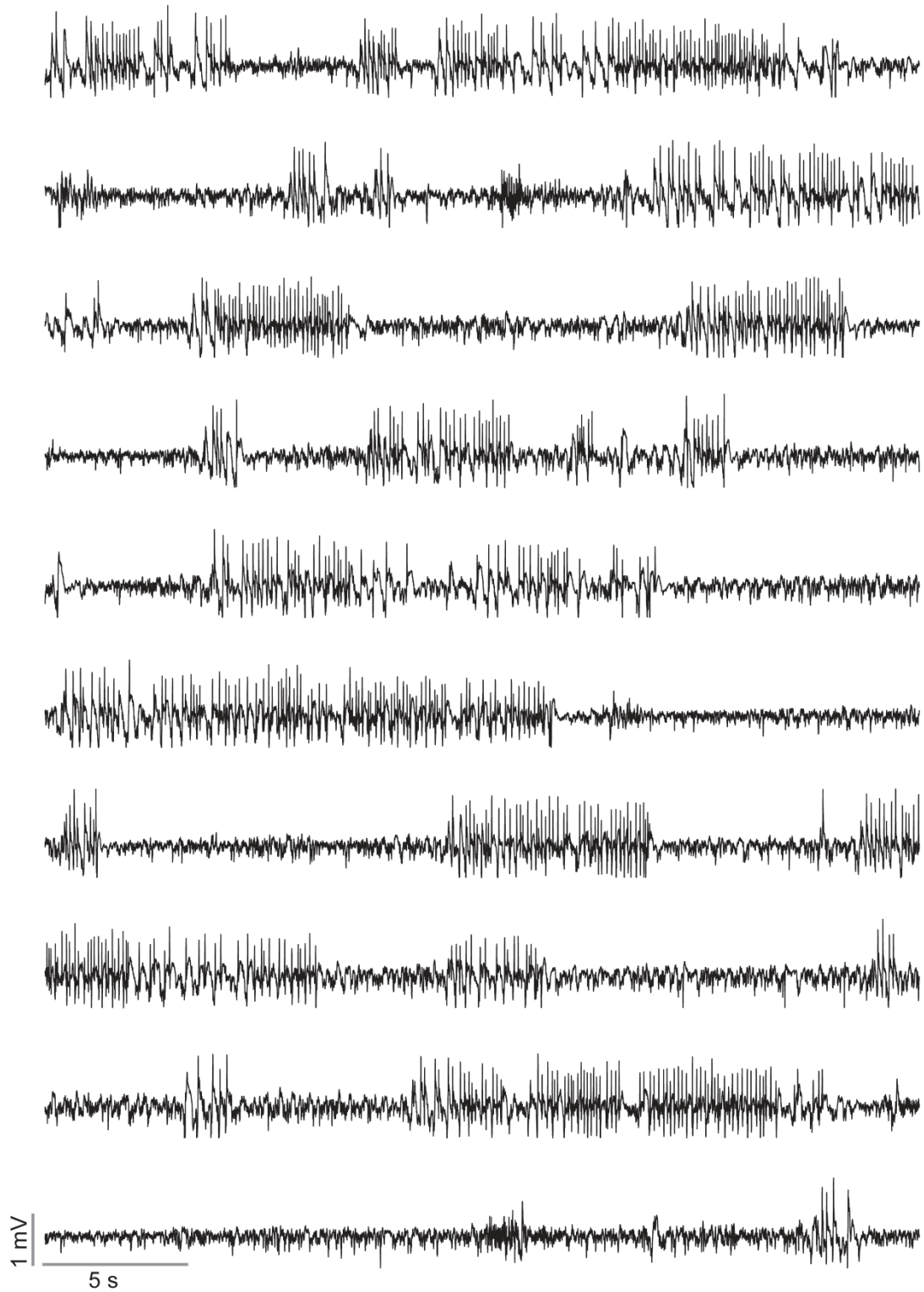


Figure B4. Spontaneous epileptiform discharges in K155

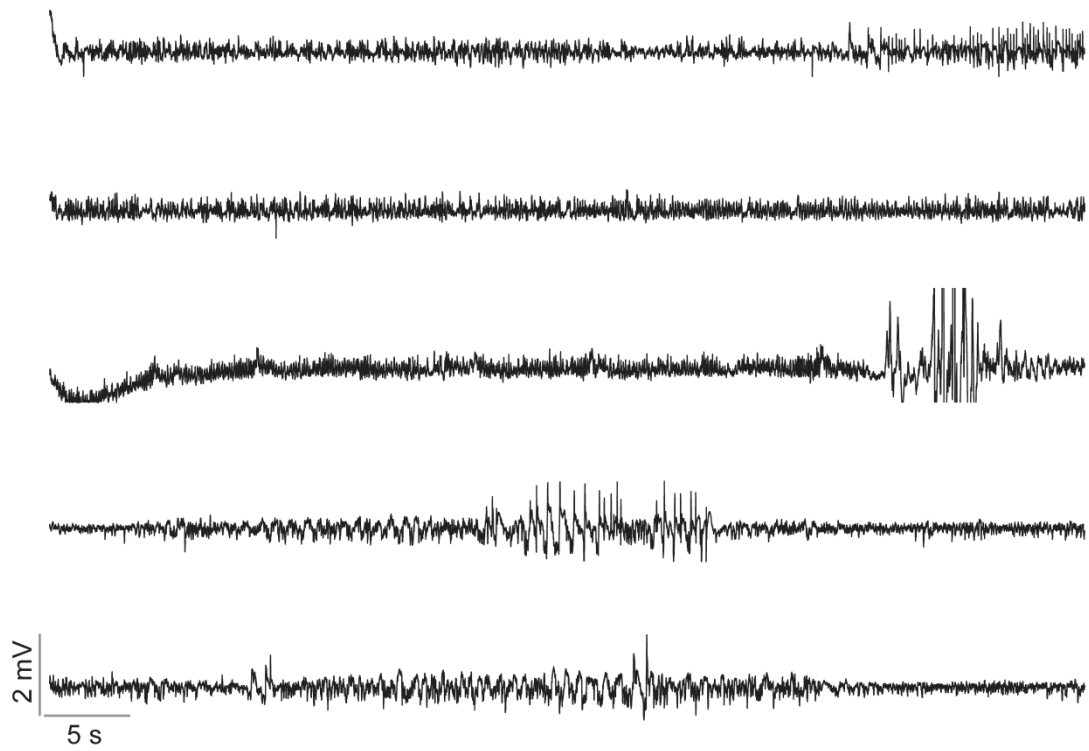


Figure B5. Recorded LFP in K155 after 50s S1 stimulation pulses. Note the damping of HPDs

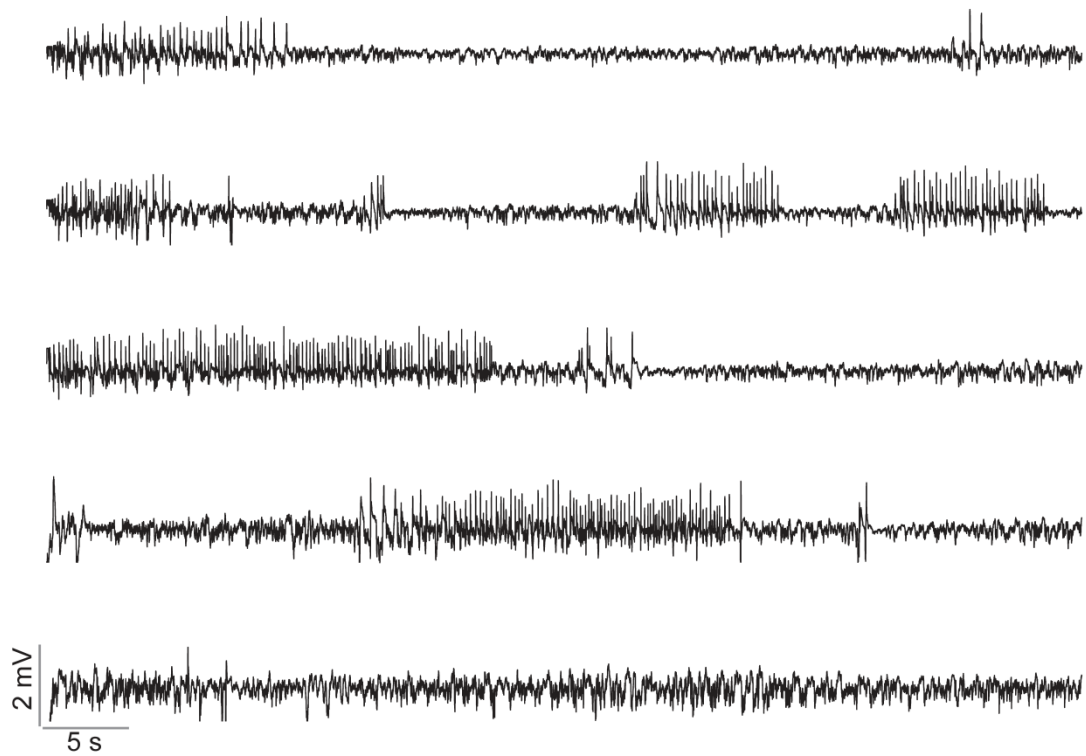


Figure B6. Recorded LFP in K155 after 50s S2 stimulation pulses. Note the recurrence of HPDs

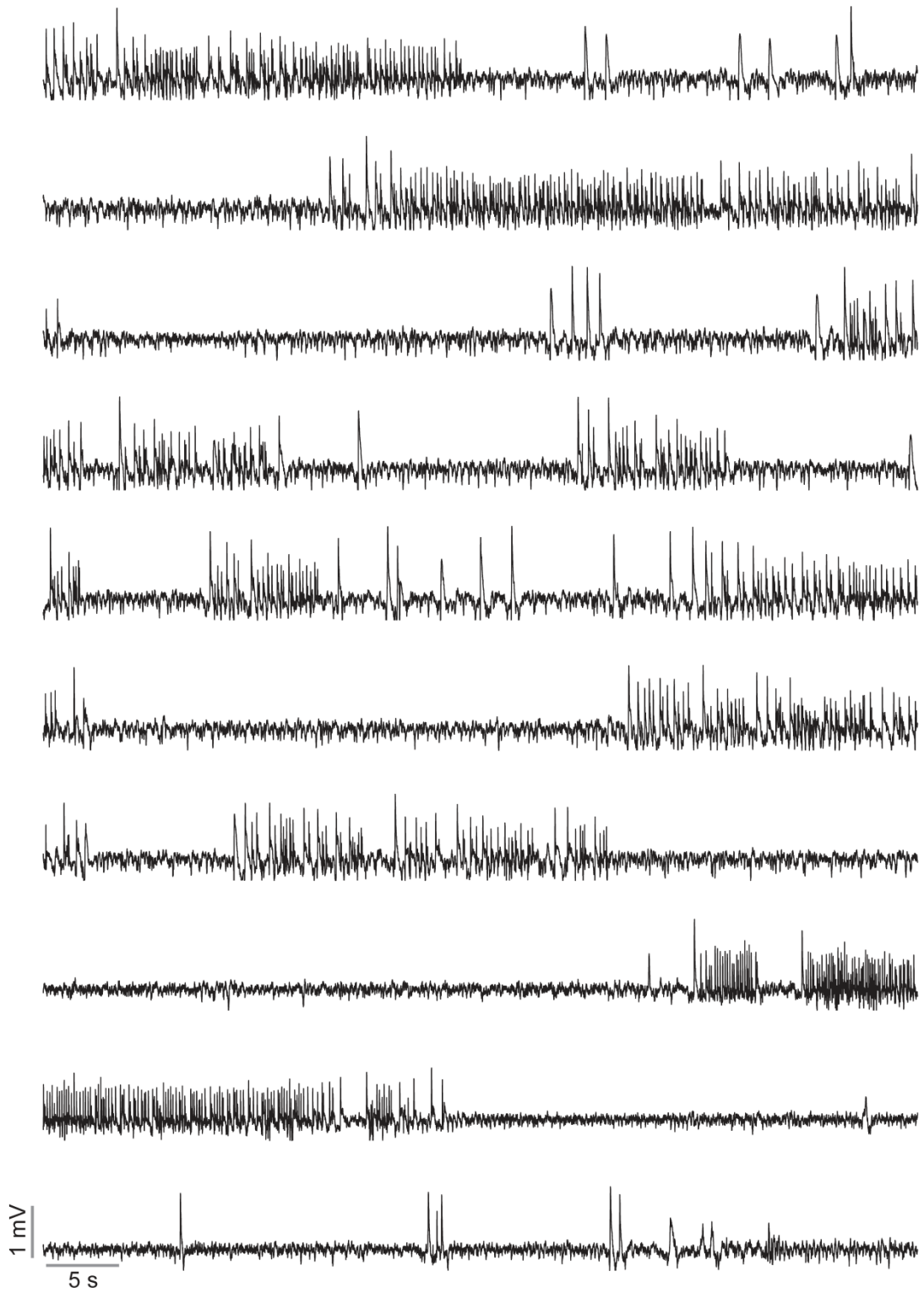


Figure B7. Spontaneous epileptiform discharges in K168

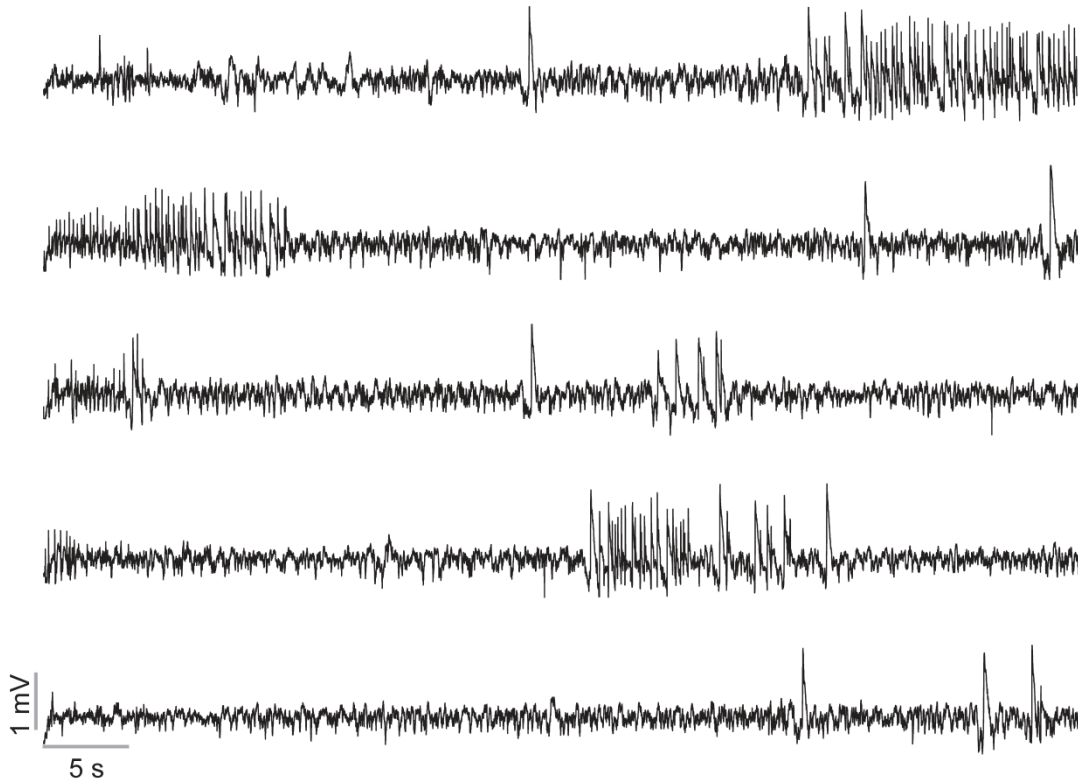


Figure B8. Recorded LFP in K168 after 50s S1 stimulation pulses. No significantly visible effect.

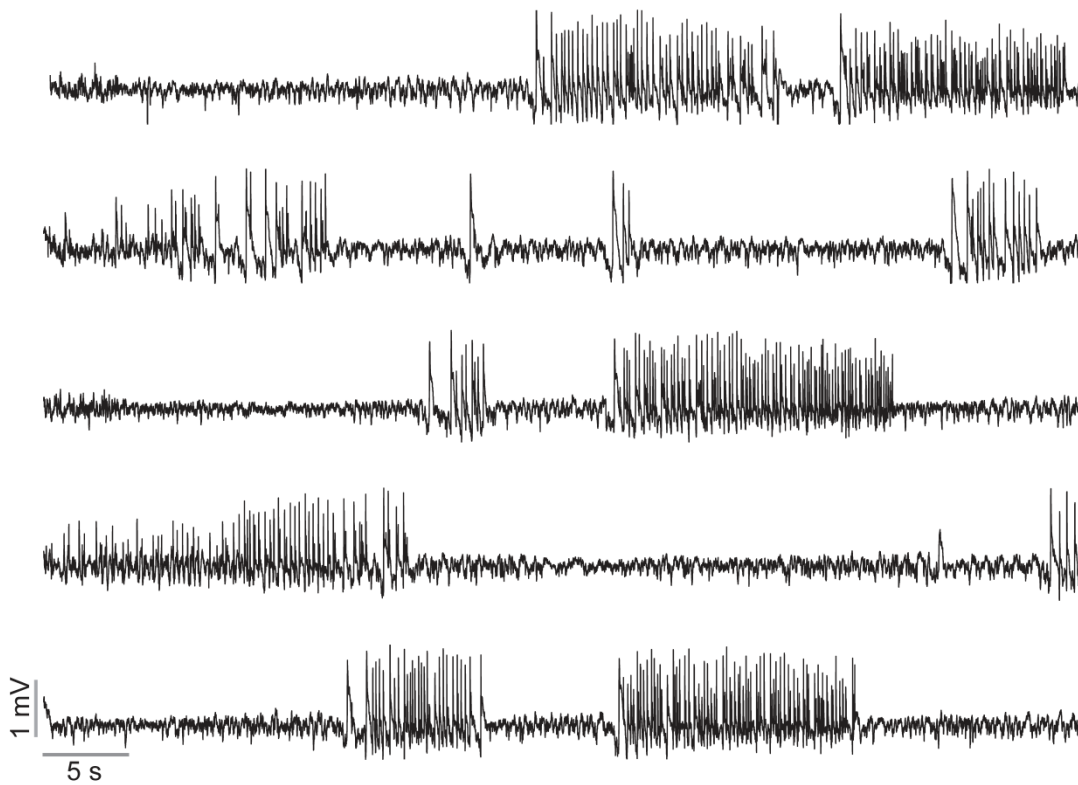


Figure B9. Recorded LFP in K168 after 50s S2 stimulation pulses. No significantly visible effect

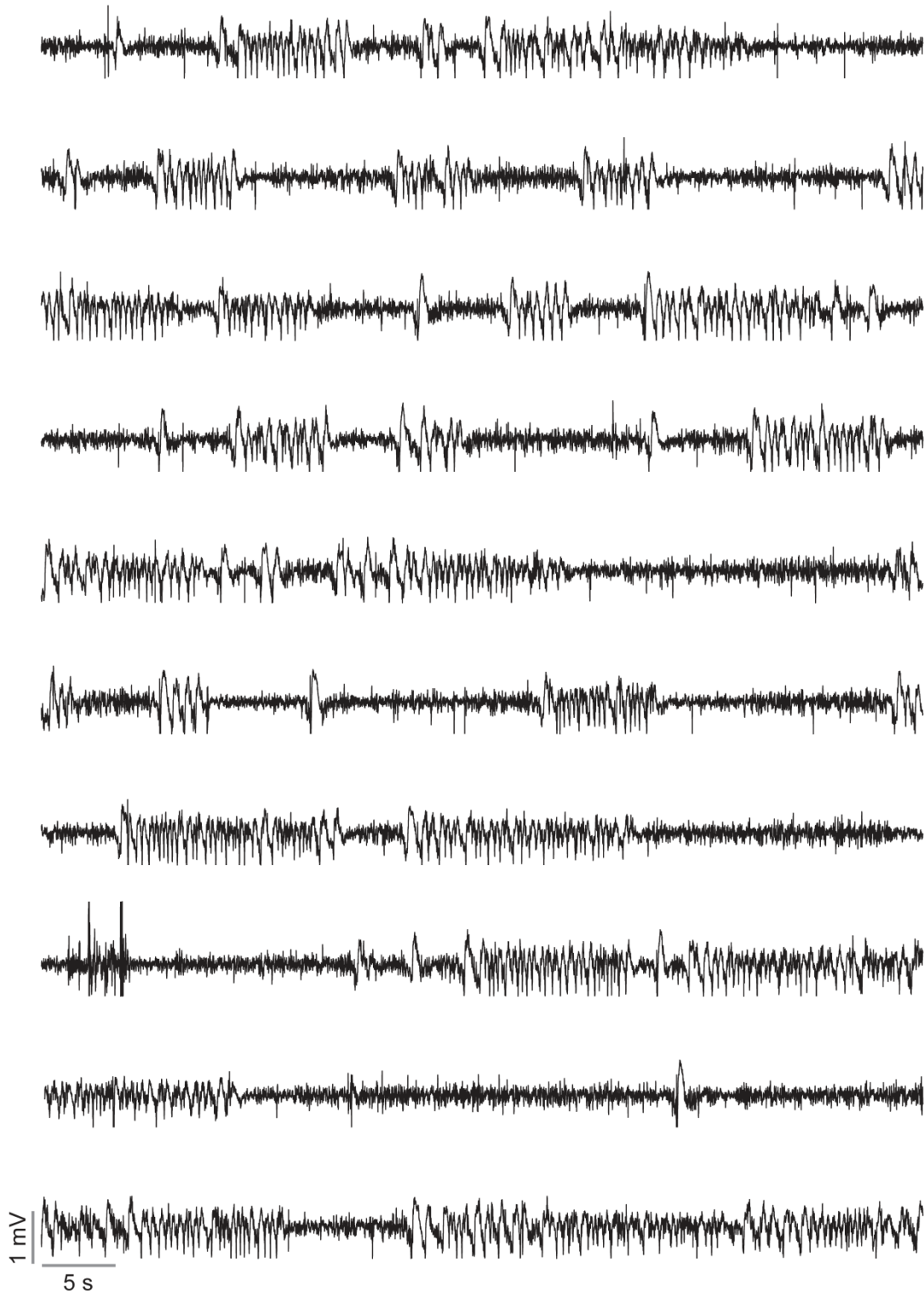


Figure B10. Spontaneous epileptiform discharges in K171

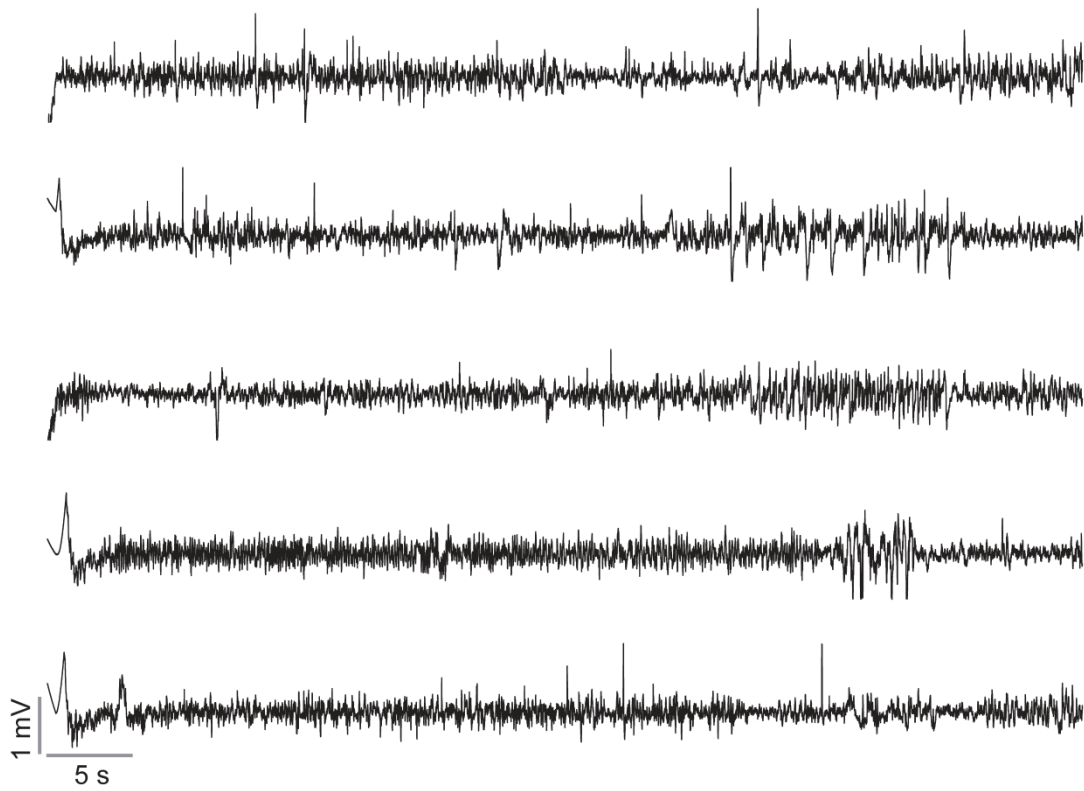


Figure B11. Recorded LFP in K171 after 50s S1 stimulation pulses.

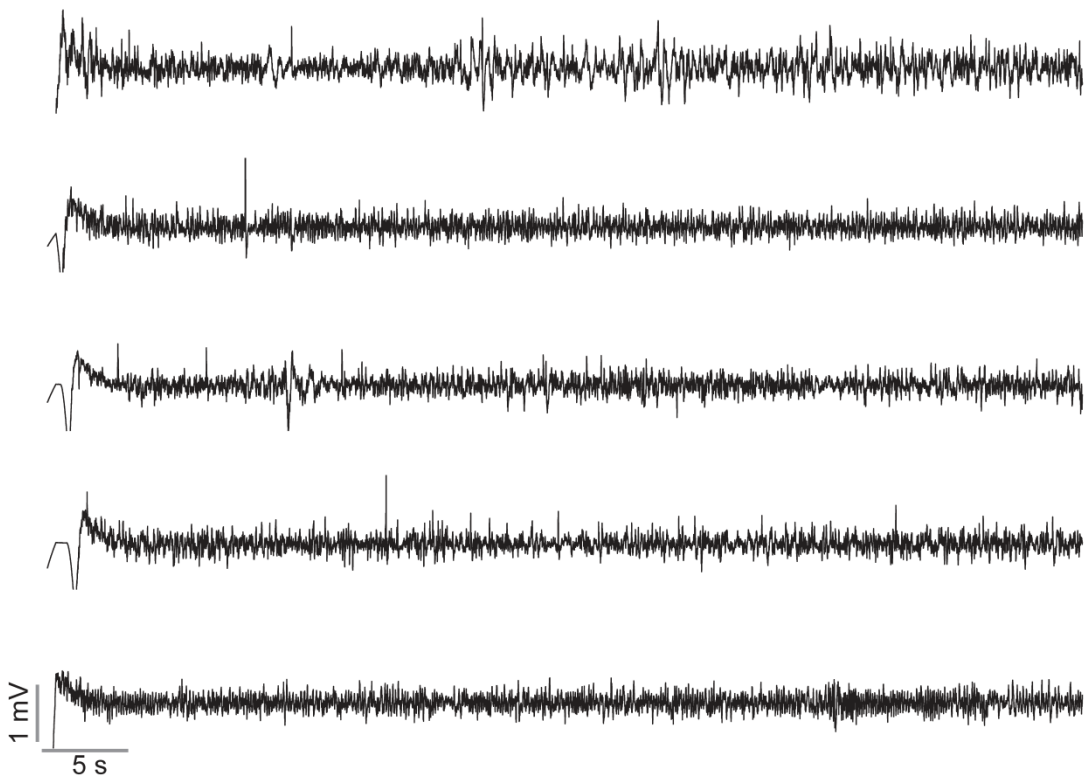


Figure B12. Recorded LFP in K171 after 50s S2 stimulation pulses. Note the decrease in HPD generation.

Appendix C. Publications



Modulation of epileptic activity by deep brain stimulation: a model-based study of frequency-dependent effects

Faten Mina^{1,2}, Pascal Benquet^{1,2}, Anca Pasnicu³, Arnaud Biraben^{1,2,3} and Fabrice Wendling^{1,2*}

¹ INSERM, U1099, Université de Rennes 1, Rennes, France

² Laboratoire Traitement du Signal et de L'Image, Université de Rennes 1, Rennes, France

³ Unité d'Épileptologie, Service de Neurologie, CHU, Rennes, France

Edited by:

Peter Robinson, University of Sydney, Australia

Reviewed by:

Peter Robinson, University of Sydney, Australia

Anthony Burkitt, University of Melbourne, Australia

*Correspondence:

Fabrice Wendling, Laboratoire Traitement du Signal et de L'Image, INSERM, Université de Rennes 1, Campus de Beaulieu, Bat. 22 - 35042 Rennes Cedex, France
e-mail: fabrice.wendling@univ-rennes1.fr

A number of studies showed that deep brain stimulation (DBS) can modulate the activity in the epileptic brain and that a decrease of seizures can be achieved in “responding” patients. In most of these studies, the choice of stimulation parameters is critical to obtain desired clinical effects. In particular, the stimulation frequency is a key parameter that is difficult to tune. A reason is that our knowledge about the frequency-dependant mechanisms according to which DBS indirectly impacts the dynamics of pathological neuronal systems located in the neocortex is still limited. We address this issue using both computational modeling and intracerebral EEG (iEEG) data. We developed a macroscopic (neural mass) model of the thalamocortical network. In line with already-existing models, it includes interconnected neocortical pyramidal cells and interneurons, thalamocortical cells and reticular neurons. The novelty was to introduce, in the thalamic compartment, the biophysical effects of direct stimulation. Regarding clinical data, we used a quite unique data set recorded in a patient (drug-resistant epilepsy) with a focal cortical dysplasia (FCD). In this patient, DBS strongly reduced the sustained epileptic activity of the FCD for low-frequency (LFS, < 2 Hz) and high-frequency stimulation (HFS, > 70 Hz) while intermediate-frequency stimulation (IFS, around 50 Hz) had no effect. Signal processing, clustering, and optimization techniques allowed us to identify the necessary conditions for reproducing, in the model, the observed frequency-dependent stimulation effects. Key elements which explain the suppression of epileptic activity in the FCD include: (a) feed-forward inhibition and synaptic short-term depression of thalamocortical connections at LFS, and (b) inhibition of the thalamic output at HFS. Conversely, modeling results indicate that IFS favors thalamic oscillations and entrains epileptic dynamics.

Keywords: DBS, thalamocortical model, computational, centromedian nucleus, FCD, premotor cortex, epilepsy

INTRODUCTION

Deep brain stimulation (DBS) for Parkinson's disease (PD) and other movement and psychiatric disorders—including dystonia, tremor, and depression—is clinically used today as a conventional therapeutic procedure for the alleviation of symptoms (Sillay and Starr, 2009). Since the early 90s, neurologists also attempted to apply DBS to other neurological disorders, typically to intractable epilepsies in order to suppress—or at least dramatically reduce—the occurrence of seizures [see recent review in Boon et al. (2009)]. These studies followed early scientific evidence showing potentially beneficial effects of DBS on epileptic neural dynamics in animal models (Reimer et al., 1967; Hablitz, 1976) as well as in patients (Cooper et al., 1973; Davis et al., 1982; Wright and

Weller, 1983). However, contrary to PD, the optimal “antiepileptic parameters” of DBS for reducing the frequency of seizures are much more variable among patients and the number of non-responders to stimulation still perplexes scientists. Moreover, in responding patients, the fine tuning of stimulation parameters in a patient-specific manner remains indispensable for maximizing antiepileptic effects. On that account, many fundamental questions are frequently raised: where and when to stimulate, at which frequency, at which current intensity, and with which current waveform?

The answers to these questions remain bound to our current, and still limited, understanding of the mechanisms by which DBS modulates neuronal dynamics, whether normal or pathological. Today, the precise mechanisms of neuronal modulation by DBS remain elusive. In addition, these mechanisms are controversial as observed effects are sometimes opposite (McIntyre et al., 2004b). Among the many studies reported over the last decade, identified mechanisms regarding HFS include: local depolarization blockade by HFS (Beurrier et al., 2001), synaptic depression due to neurotransmitter depletion (Shen et al., 2003; Kim et al., 2012), synaptic inhibition (Filali et al., 2004), disruption of

Abbreviations: CMN, Centromedian Nucleus; DBS, Deep Brain Stimulation; EPSP, Excitatory Postsynaptic Potentials; FCD, Focal Cortical Dysplasia; FFI, Feed-Forward Inhibition; GPi, Globus Pallidus; HFS, High Frequency Stimulation; iEEG, Intracerebral EEG (depth electrodes); IFS, Intermediate Frequency Stimulation; IPSP, Inhibitory Postsynaptic Potentials; LFP, Local Field Potential; LFPs_{FCD}, Local Field Potentials recorded in the FCD; LFS, Low Frequency Stimulation; NS, No Stimulation; PMC, Premotor cortex; RtN, Reticular thalamic Nucleus, STD, Short-Term Depression; STN, Subthalamic Nucleus.

the thalamocortical network's dysrhythmia (McIntyre and Hahn, 2010; Kendall et al., 2011). As far as LFS is concerned, some studies described a transient synaptic depression that alters synaptic transmission (Jiang et al., 2003; Speechley et al., 2007). Finally, IFS is routinely used in the context of presurgical evaluation of patients with drug resistant epilepsy to map epileptogenic and functional brain areas. It has long been observed that this type of stimulation is prone to trigger epileptic afterdischarges (Goddard, 1967). This brief overview shows that the spectrum of involved mechanisms is very large and that distinct stimulation frequencies trigger distinct cellular/network processes. More precise insights into these processes will come with increased knowledge about both biophysical and neurophysiological effects of stimulation currents on underlying neuronal systems.

However, the access to cellular and network mechanisms induced by DBS is rather difficult in animal models of epilepsy and (almost) impossible in patients especially in large-scale systems like the thalamocortical loop. An alternative approach is the use of computational models based on physiological data to first reproduce and then explain changes in cerebral activity as a function of stimulation conditions (stimulation site, intensity, and frequency). This is precisely the objective of this study, with a special focus on the distinct effects of DBS frequency on cortical epileptic dynamics.

Our investigation combines computational modeling and clinical data. We explored stimulation effects in a lumped-parameter mesoscopic neural mass model of the thalamocortical loop, inspired from previously published models (Suffczynski et al., 2004; Lopes Da Silva, 2006; Roberts and Robinson, 2008; Crunelli et al., 2011).

Although these models are lumped representations of underlying neuronal systems, they offer a number of advantages in the context of this study. First, neural mass models include subpopulations of principal excitatory cells and inhibitory interneurons. Second, these models were shown to produce realistic activity as observed in LFPs or EEG under normal (Freeman, 1973; Lopes Da Silva et al., 1974) or epileptic conditions [review in Lytton (2008); Wendling (2008)]. Third, main parameters (mean membrane potential and firing rate) provide access to the investigation of several stimulation-induced (patho)physiological mechanisms. For instance, a neural mass model was successfully used in the context of direct low-intensity pulse stimulation in the hippocampus to explain the behavior of evoked responses during the transition to seizures (Suffczynski et al., 2008).

In particular, using this model, we analyzed the neurophysiological effects induced by direct thalamic stimulation on epileptic cortical dynamics at low frequency (LF, < 20 Hz), intermediate frequency (IF, 20–70 Hz) and high frequency (HF, 70–130 Hz). Model parameters were tuned to reproduce a typical pathological oscillatory activity observed in a neocortical lesion (focal cortical dysplasia, or FCD) in a patient with drug-resistant epilepsy. Intracerebral EEG (iEEG) signals observed during thalamic stimulation (centromedian nucleus) of this patient revealed particularly pronounced frequency-dependent modulation of the FCD pathological activity. Therefore, this data set offered the unique opportunity to identify key model parameters for which such a frequency-dependent modulation could be reproduced and,

subsequently to get insights regarding the mechanisms underlying the modulatory effects, in the FCD, of thalamic stimulation. Results revealed that LFS favors feed-forward inhibition and short-term depression at the cortical level and that HFS inhibits the thalamic activity, while IFS reinforces reticulothalamic oscillations thus entraining cortical pathological epileptic dynamics.

MATERIALS AND METHODS

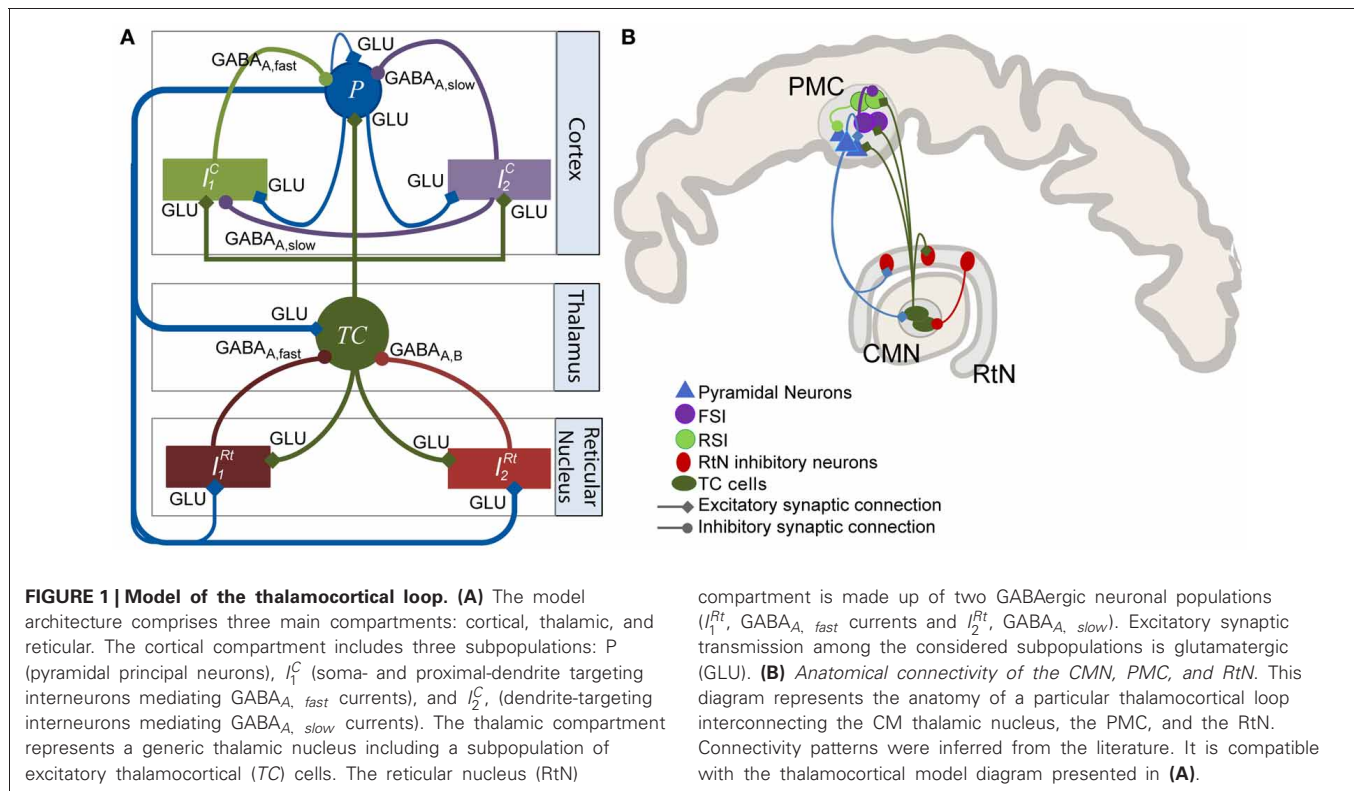
In this section, we present (1) the neurophysiologically-relevant computational model that we developed to study thalamic DBS, (2) the real depth-EEG dataset used for model tuning and, (3) the signal processing methods used for characterizing real and simulated EEG signals.

MODEL OF THE THALAMOCORTICAL LOOP

In order to study the effects of thalamic DBS on cortical dynamics, we implemented a physiologically-plausible mesoscopic model of the thalamocortical loop. This model accounts for the average activity of both cortical and thalamic compartments which include various types of neuronal populations interacting via synaptic transmission. This modeling approach was first proposed in the early 70s (Wilson and Cowan, 1972) and further enriched in order to interpret electrophysiological recordings and study brain dynamics, in the olfactory (Freeman, 1973) and the thalamocortical (Lopes Da Silva et al., 1974) system, for instance, as well as the dynamics of cortical oscillations (Nunez, 1974). This approach was then developed by other research groups in the context of state changes in brain dynamics (Wright et al., 1985), visual evoked potentials (Jansen et al., 1993), dynamics of the human alpha rhythm (Stam et al., 1999) or pathophysiological mechanisms of ictal transitions in epilepsy (Wendling et al., 2000, 2002; Suffczynski et al., 2001; Robinson et al., 2002; Liley and Bojak, 2005; Breakspear et al., 2006). Later, neural mass models were also used in studies dealing with the connectivity among cortical regions and the impact of model parameters on the power spectrum of EEG or MEG signals (Robinson et al., 1997; David and Friston, 2003; Zavaglia et al., 2006).

Model architecture

The model architecture was inspired from previously published models of the thalamocortical loop (Suffczynski et al., 2004; Lopes Da Silva, 2006; Roberts and Robinson, 2008; Crunelli et al., 2011). In a global view, the model was built of three interconnected compartments: a cortical compartment, a thalamic compartment, and a reticular compartment, in accordance with previously published models (Figure 1A) and with anatomical data (Figure 1B). Each compartment includes one or several subpopulation(s) of neurons, either excitatory or inhibitory. Generally speaking, the input/output functions of a considered subpopulation are represented by two mathematical equations that were respectively named “pulse-to-wave” (input) and “wave-to-pulse” (output) by Walter Freeman (Freeman, 1992). The former is a linear transfer function that converts the presynaptic average density of afferent action potentials into an average postsynaptic membrane potential (PSP), either excitatory (EPSP) or inhibitory (IPSP). The output function is a static nonlinear function (sigmoid) that



provides the average pulse density of action potentials fired by neurons depending on the sum of EPSPs and IPSPs at the input. This non-linear function accounts for threshold and saturation effects that take place at the somas and initial axonal segments of considered cells.

Formally, the input function is represented by a second order low-pass filter $H(s) = W/(s+1/\tau_w)^2$ (where s is the Laplace variable). The impulse response of this filter is given by

$$h(t) = \frac{W}{\tau_w} \cdot t \cdot e^{-t/\tau_w} \quad (1)$$

Parameters W and τ_w are tuned such that $h(t)$ approximates the shape of real excitatory (glutamatergic) or inhibitory (GABAergic) postsynaptic potentials (Lopes Da Silva et al., 1976). The quantity $W \cdot \tau_w^2$ is the static gain of filter h . Lumped parameter τ_w (expressed in s) is linked to the kinetics of synaptic currents. It determines both the rise time ($t_{rise} = \tau_w$) and the decay time ($t_{decay} = 3.146\tau_w$) of the second order filter impulse response h and it is usually adjusted with respect to the physiological rise and decay times of actual PSPs (Molae-Ardekani et al., 2010). Given the time constant τ_w , parameter W can be used to adjust the sensitivity of synapses (the maximal PSP amplitude is $W \cdot e^{-1}$). An alternative implementation of the h function was introduced in Bojak and Liley (2005) and is described in detail in Molae-Ardekani et al. (2013). It is based on a bi-exponential pulse-to-wave function with two time constant parameters. This implementation allows for the separate adjustment of the rise and decay times of PSPs, and therefore a better approximation of actual PSPs in some circumstances. Besides, the output function

is represented by $S(v) = \frac{2e_0}{1+e^{r(v_0-v)}}$, where $2e_0$ is the maximum firing rate, v_0 is the postsynaptic potential corresponding to a firing rate of e_0 and r is the steepness of the sigmoid.

The cortical compartment

The cortical compartment was inspired from an existing model of the neocortex which proved its capability of generating both normal and epileptiform activity. Readers may refer to Molae-Ardekani et al. (2010) for details. In brief, the cortical compartment integrates a subpopulation of pyramidal cells (P , $W = A_C$, $\tau_w = \tau_{ac}$ in Equation 1) and two inhibitory neuronal populations (I_1^C and I_2^C , **Figure 1A**) representing soma- and proximal-dendrite targeting interneurons ($GABA_{A, fast}$ currents, $W = G_C$, $\tau_w = \tau_{gc}$ in Equation 1) and dendrite-targeting interneurons ($GABA_{A, slow}$ currents, $W = B_C$, $\tau_w = \tau_{bc}$ in Equation 1), respectively. Pyramidal collateral excitation was implemented as in Jansen et al. (1993).

In addition, these three cortical subpopulations receive excitatory input from the thalamic compartment. Therefore, feed-forward inhibition (FFI) is represented in the model as the two subpopulations of interneurons project to the pyramidal subpopulation (see *The Thalamic and Reticular Compartments* paragraph below).

Short-term synaptic depression (STD)

STD is present in the neocortex (Boudreau and Ferster, 2005). It can be potentially involved in the context of direct stimulation of the thalamus as TC cells directly project to cortical pyramidal cells. Consequently, this mechanism was implemented at the interface of thalamic/cortical compartments. To our knowledge,

an implementation of STD in neural mass models has not been proposed before.

In our model, we represented a modulatory effect of the amplitude of the average EPSP (parameter A_C') at the level of subpopulation P depending on the density of action potentials [$d_{AP}(t)$] coming from the thalamic compartment. This modulatory effect was obtained by multiplying A_C' by a time-varying coefficient $\kappa(t) \in [0.6, 1]$ where the function describing the evolution of $\kappa(t)$ was derived from Chung et al. (2002). This study shows that: (i) cortical EPSPs drop by 40% under periodic low-frequency intense thalamocortical (TC) cell firing and, (ii) this drop in cortical EPSP is directly linked to transient depression of thalamocortical monosynaptic projections to pyramidal neurons.

In line with these observations, STD was implemented as follows. First, signal $d_{AP}^f(t)$ is low-pass filtered (cutoff frequency = 10 Hz) to restrict the STD effect to LFS. Then, from each time t_η at which the filtered signal $d_{AP}^f(t)$ exceeds a firing rate equal to η , the $\kappa(t)$ coefficient undertakes an exponential decay given by $\kappa(t) = \kappa_\eta \cdot e^{-t/\tau}$ where $\kappa_\eta = \kappa(t_\eta^-)$ and where t_η^- is the time instant that just precedes t_η . The decrease of $\kappa(t)$ is limited to the time interval [$t_\eta + 0.45$ s] and cannot exceed 40%, total. Parameters η and τ were set to 0.8 and 8 s, respectively.

The thalamic and reticular compartments

The thalamic compartment was limited to one population of excitatory neurons (known as glutamatergic thalamocortical - TC - cells) receiving glutamatergic EPSPs ($W = A_{Th}$, $\tau_w = \tau_{aTh}$ in Equation 1) from cortical pyramidal cells (P) and GABAergic IPSPs with slow ($W = B_{Th}$, $\tau_w = \tau_{bTh}$ in Equation 1) and fast ($W = G_{Th}$, $\tau_w = \tau_{gTh}$ in Equation 1) kinetics from the reticular compartment (RtN). Here, we increased the time constant (τ_{bTh}) with respect to τ_{bc} to account for both GABA_A, slow- and GABA_B-receptor mediated currents in a single variable. TC cells directly target both cortical pyramidal cells and interneurons. The activation of these GABAergic interneurons subsequently promotes inhibition of pyramidal cells after a di-synaptic delay. Therefore, TC cells activation induces first an EPSP followed later on by an IPSP on cortical pyramidal cells, resulting in feed-forward inhibition (FFI). The RtN compartment comprised two inhibitory subpopulations, namely I_1^{RT} and I_2^{RT} which both receive excitatory input from the cortical ($W = A_{Rt}$, $\tau_w = \tau_{aRt}$ in Equation 1) and the thalamic ($W = A_{Rt}$, $\tau_w = \tau_{aRt}$ in Equation 1) compartments.

Simulation of stimulation effects

Stimulation currents induce a perturbation of the membrane potential of neurons. At cellular level, this effect can be accounted for by the “ λE model”, which is well grounded in the biophysics of compartment models (Rattay, 1998; McIntyre et al., 2004a; Manola et al., 2005, 2007) (see Miranda et al., 2009 for a review) and supported by *in vitro* experiments (Bikson et al., 2004; Frohlich and McCormick, 2010). This model $\Delta V \approx \tilde{\lambda} \cdot \vec{E}$ approximates the membrane potential variation ΔV as a linear function of the electrical field \vec{E} induced by stimulation ($\tilde{\lambda}$ representing the membrane space constant). In our neural mass model, the situation is less straightforward as space is not explicitly represented, conversely to detailed or mean-field models. However, within a certain range of intensity values, it has been shown that

the membrane potential variation ΔV is modified in a linear way with respect to the electrical field which is itself proportional to the stimulation intensity (Bikson et al., 2004). These considerations led us to also assume a linear variation for the mean membrane potential as a function of stimulation intensity, in stimulated sub-populations of neurons. In addition, stimulation was represented by a train of periodic monophasic depolarizing pulses. The pulse width was fixed to 1 ms (as in clinics). Pulses were low-pass filtered to account for the average time of repolarization (set to 4.8 ms) in stimulated sub-populations of cells. The resulting stimulation signal was added to the mean membrane potential of neuronal sub-populations included in the thalamic (TC) and reticular (I_1^{RT} and I_2^{RT}) compartments of the proposed model. The depolarizing effect was weighted by three coefficients S_{TC} , S_{Rt1} and S_{Rt2} (Table 1) accounting for the possibly different stimulation impact at the thalamic and reticular level.

Model parameters, outputs, and implementation

Parameter values as well as physiological interpretation are provided in Table 1. Note that each synaptic connection in the model is weighted by a connectivity constant denoted by $C_{SP1-SP2}$ where $SP1$ and $SP2$, respectively, denote the source and target subpopulations. In addition, two Gaussian noise inputs $p_P(t) \sim N(\mu_P, \sigma_P)$ and $p_{TC}(t) \sim N(\mu_{TC}, \sigma_{TC})$ were used to represent nonspecific inputs on pyramidal and thalamocortical cell subpopulations. Finally, signals simulated at the level of pyramidal cells in the cortical compartment and at the level of TC cells in the thalamic compartment were chosen as model outputs. They correspond to the sum of PSPs at each compartment respectively. The temporal dynamics of these signals provide a good approximation of actual LFPs. The model was implemented in Simulink®, and all other complementary scripts were implemented in MATLAB®.

REAL DATA FOR MODEL TUNING

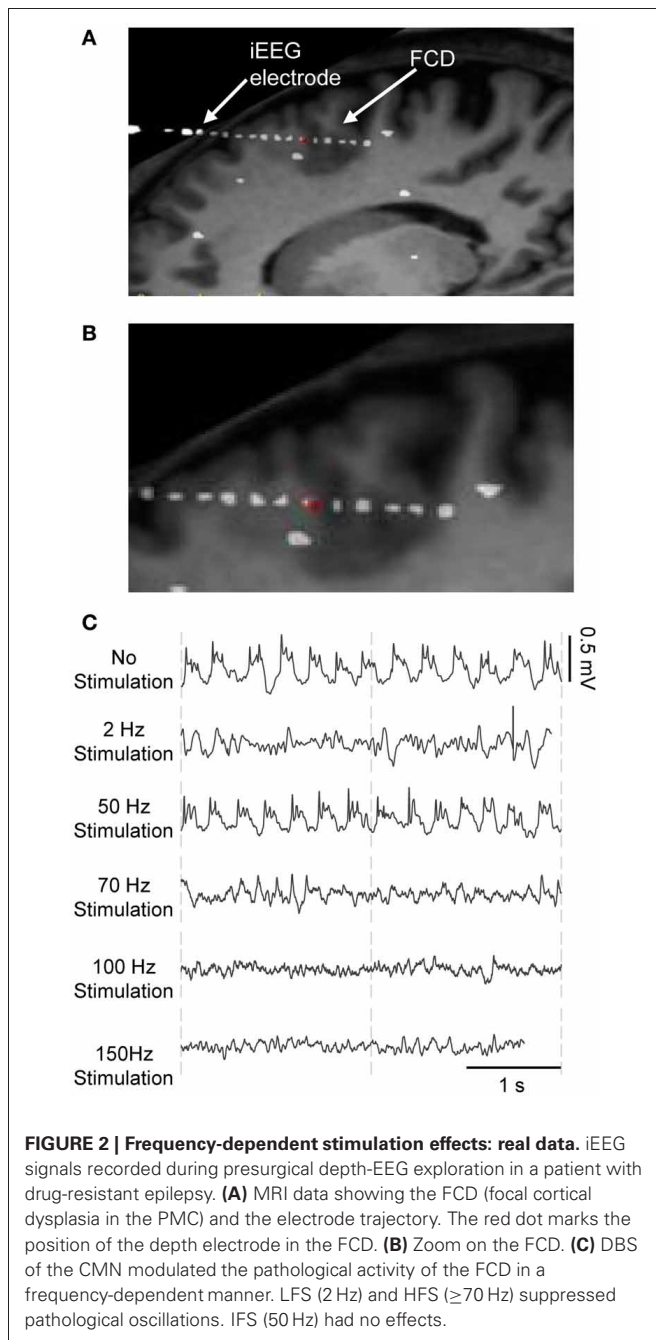
We used real clinical data to tune the model into a functioning mode which simulates pathological activity. The clinical data set was limited to a unique patient who underwent thalamic DBS during the presurgical intracerebral EEG exploration (iEEG performed with depth electrodes implanted under stereotaxic conditions) at the Epilepsy Surgery Unit, Rennes University Hospital. This particular patient was chosen for two main reasons: (1) the pronounced frequency-dependent stimulation effects observed during his preoperative diagnostic iEEG exploration at LF, IF and HF in addition to (2) the existence of an epileptogenic zone in a limited area of the premotor cortex (PMC).

In brief, this patient suffered from partial drug-resistant epilepsy since the age of two. MRI scans and EEG recordings pointed out the existence of a neuronal malformation known as FCD in the PMC at the origin of seizures. This type of cortical malformation is known for its epileptogenic features like neuronal hyperexcitability and hypersynchronization and its characteristic epileptiform discharges (continuous, rhythmic or semirhythmic spikes, and polyspikes) (Avoli et al., 2003; Palmini, 2010) as shown in Figure 2C. Based on various clinical studies reporting the modulation of epileptic cortical activity by the

Table 1 | Model parameters, values and interpretation.

Parameter	Value	Interpretation
A_C	6 (optimized, pathological) 3 (normal) mV	Amplitude of the cortical average EPSP
A_C'	$\kappa(t).A_C$ mV	Amplitude of the cortical average EPSP in response to thalamic input (only on subpopulation P)
B_C	14 (optimized, pathological) 50 (normal) mV	Amplitude of the cortical average IPSP (GABA _{A,slow} mediated currents)
G_C	16.5 (optimized, pathological) 22 (normal) mV	Amplitude of the cortical average IPSP (GABA _{A,fast} mediated currents)
A_{Th}	3.5 mV	Amplitude of the thalamic average EPSP
B_{Th}	30 mV	Amplitude of the thalamic average IPSP (GABA _{A,slow} and GABA _B receptors)
G_{Th}	22 mV	Amplitude of the thalamic average IPSP (GABA _{A,fast} receptors)
A_{Rt}	3.5 mV	Amplitude of the reticular average EPSP
τ_{ac}	1/80 s	Time constant of cortical glutamate-mediated synaptic transmission.
τ_{bc}	1/35 s	Time constant of cortical GABA-mediated synaptic transmission (GABA _{A,slow} receptors)
τ_{gc}	1/180 s	Time constant of cortical GABA-mediated synaptic transmission (GABA _{A,fast} receptors)
τ_{aTh}	1/100 s	Time constant of thalamic glutamate-mediated synaptic transmission
τ_{bTh}	1/20 s	Time constant of thalamic GABA-mediated synaptic transmission (GABA _{A,slow} and GABA _B receptors)
τ_{gTh}	1/150 s	Time constant of thalamic GABA-mediated synaptic transmission (GABA _{A,fast} receptors)
τ_{aRt}	1/100 s	Time constant of reticular glutamate-mediated synaptic transmission
v_0, e_0, r	$v_0 = 6\text{mV}, e_0 = 2.5\text{ s}^{-1}$ $r = 0.56\text{mV}^{-1}$	Parameters of the nonlinear sigmoid function (transforming the average membrane potential to an average density of action potentials)
$C_{P-P'}$	135	Collateral excitation connectivity constant
$C_{P'-P}$	108	Collateral excitation connectivity constant
$C_{P-I_2^C}$	33.75	P to I_2^C connectivity constant
$C_{I_2^C-P}$	33.75	I_2^C to P connectivity constant
$C_{P-I_1^C}$	40.5	P to I_1^C connectivity constant
$C_{I_1^C-P}$	13.5	I_1^C to P connectivity constant
$C_{I_1^C-I_2^C}$	91.125	I_1^C to I_2^C connectivity constant
C_{TC-P}	120	TC to P connectivity constant
$C_{TC-I_1^C}$	30	TC to I_1^C connectivity constant
$C_{TC-I_2^C}$	45	TC to I_2^C connectivity constant
$C_{TC-I_1^{Rt}}$	20	TC to I_1^{Rt} connectivity constant
$C_{TC-I_2^{Rt}}$	20	TC to I_2^{Rt} connectivity constant
$C_{P-I_1^{Rt}}$	30	P to I_1^{Rt} connectivity constant
$C_{P-I_2^{Rt}}$	30	P to I_2^{Rt} connectivity constant
C_{P-TC}	20	P to TC connectivity constant
$C_{I_1^{Rt}-TC}$	35	I_1^{Rt} to TC connectivity constant
$C_{I_2^{Rt}-TC}$	5	I_2^{Rt} to TC connectivity constant
μ_{P1}	0	Mean of nonspecific cortical input
μ_{P2}	70	Mean of nonspecific subcortical input
σ_{P1}	20. $\sqrt{6}$	Standard deviation of nonspecific cortical input
σ_{P2}	35. $\sqrt{6}$	Standard deviation of nonspecific subcortical input
S_{TC}	5	Stimulation impact on subpopulation TC
S_{Rt1}	4	Stimulation impact on subpopulation I_1^{Rt}
S_{Rt2}	4	Stimulation impact on subpopulation I_2^{Rt}
f_s	1Hz – 150Hz	Frequency of the stimulation signal (pulse train)
A_{fs}	1	Stimulation signal amplitude

Model parameters used to reproduce LFPs_{FCD}. Stimulation impact parameters S_{TC} , S_{Rt1} and S_{Rt2} are set to zero during the simulation of the NS scenario. These parameters are held constant for all other stimulation scenarios.



stimulation of the CM nucleus (Velasco et al., 1995, 1997, 2000, 2001, 2007), it was decided by neurologists and neurosurgeons to implant a depth electrode in this nucleus, as potentially beneficial for the patient who gave his informed consent.

During the presurgical exploration, the stimulation of the thalamic CM nucleus (CMN) induced frequency-dependent modulation of the pathologic activity of the FCD (Figure 2). Readers may refer to (Pasnicu et al., 2013) for detailed information. Interestingly, LFS (2 Hz, 4 mA) and HFS (70, 100, and 150 Hz, 0.8 mA) desynchronized the pathological activity of the FCD, while IFS (50 Hz, 0.8 mA) barely affected it. These segments of

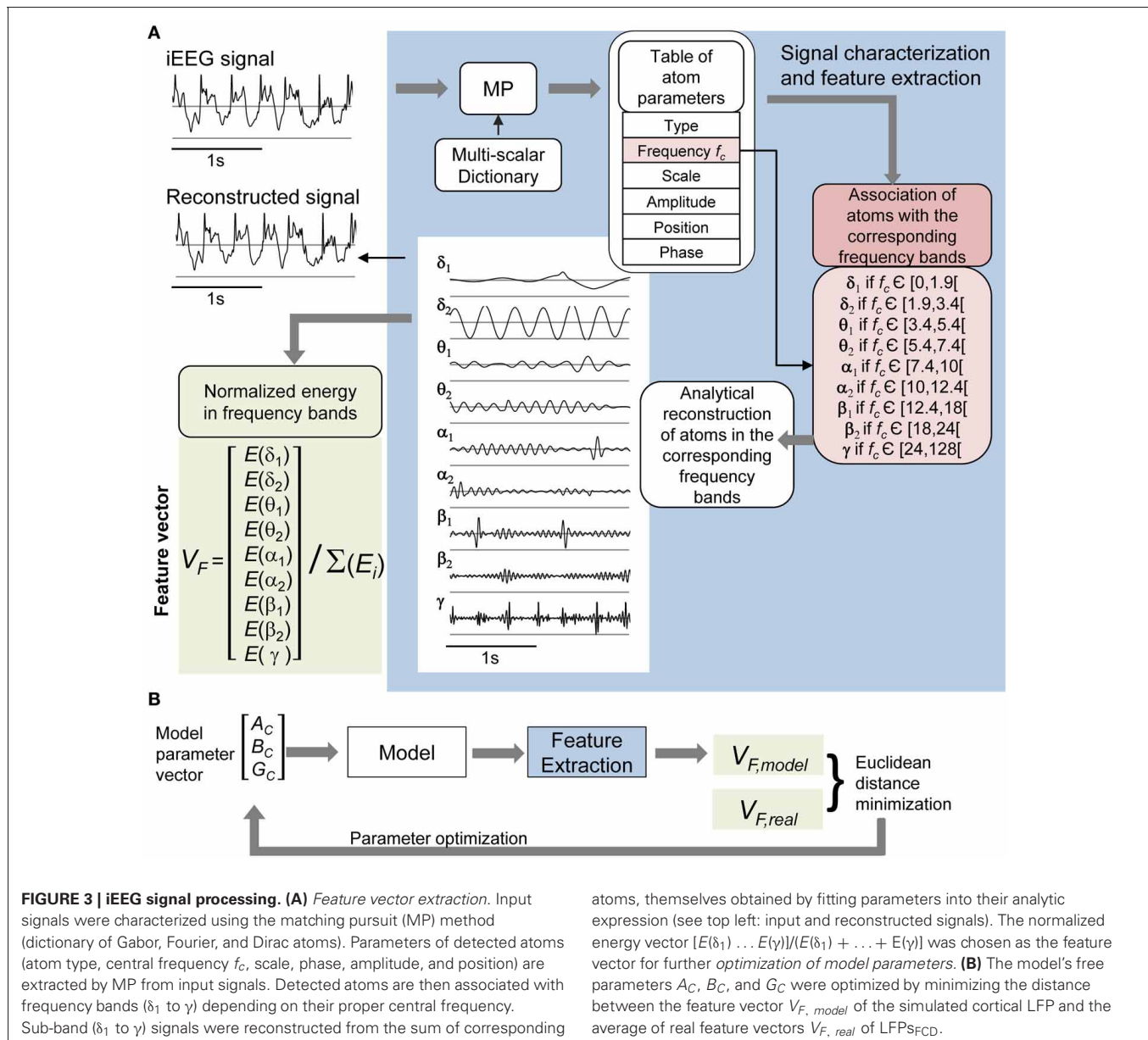
signals corresponding to either typical pathological activity or modulated activity (depending on stimulation conditions) were used to optimize the model parameters.

PROCESSING OF REAL AND SIMULATED SIGNALS

The use of signal processing techniques was necessary (i) to quantify the above-described effects of stimulation in real iEEG signals, and (ii) to define a feature-vector-based cost function for model parameter optimization. Figure 3A illustrates the feature extraction methodology. iEEG signals recorded in the FCD in absence of stimulation (LFP_{FCD}) and under different stimulation conditions were decomposed using an orthogonal matching pursuit algorithm [matching pursuit toolkit—MPTK—(Krstulovic and Gribonval, 2006)]. First introduced in 1993 (Mallat and Zhifeng, 1993), matching pursuit is signal processing algorithm used to decompose any time series into a linear sum of waveforms selected from a predefined dictionary based on a mother wavelet. To proceed, a proper multi-scalar dictionary of Gabor, Fourier, and Dirac atoms was first defined to account for real iEEG signal components (time-frequency atoms are waveforms well localized in both the time and the frequency domains). In line with (Krstulovic and Gribonval, 2006), the multi-scalar dictionary was formed by translation in time and amplitude/frequency modulation of atoms (defined as Gabor and Fourier functions in our case), over ten different user-defined time scales (i.e. the atom durations, ranging from 0.125 to 5 s). Then, the algorithm provided a table of time-frequency parameters associated to the detected atoms (atom type, central frequency, phase, scale, amplitude, position). Identified atoms were reconstructed using the extracted parameter table and their analytical expression. They were then associated to a given frequency band depending on their central frequency. These frequency bands corresponded to the classical EEG bands as defined in normal adults (δ_1 [0 – 1.9 Hz], δ_2 [1.9 – 3.4 Hz], θ_1 [3.4 – 5.4 Hz], θ_2 [5.4 – 7.4 Hz], α_1 [7.4 – 10 Hz], α_2 [10 – 12 Hz], β_1 [12 – 18 Hz], β_2 [18 – 24 Hz], γ [24 – 128 Hz]) (Figure 3A, blue). Finally, a 9D feature vector V_F was defined from the normalized energy distribution in these frequency bands, itself computed as the sum of averaged (over time) atom energies relative to the total signal energy (Figure 3A, green).

MODEL OPTIMIZATION UNDER THE “NO STIMULATION” CONDITION

In order to simulate LFP_{FCD} , we optimized the excitation/inhibition ratio of the cortical compartment. Thus, the average EPSP/IPSP amplitude parameters of the cortical compartment $\{A_C, B_C, G_C\}$ were considered as free parameters while all other model parameters were set to fixed values (Table 1). The optimization method is illustrated in Figure 3B. For each triplet $\{A_C, B_C, G_C\}$, the feature vector $V_{F, model}$ of the model's output signal (cortical compartment's LFP) was calculated and compared to $V_{F, real}$, i.e., the feature vector computed from the average of the 20 feature vectors, each computed on a 5 s signal segment of real LFP_{FCD} . Feature vectors $V_{F, model}$ and $V_{F, real}$ were computed as described in section Processing of Real and Simulated Signals. The optimization procedure aimed at finding the triplet $\{\widehat{A}_C, \widehat{B}_C, \widehat{G}_C\}$ that minimizes a cost function simply corresponding to the Euclidean



distance $d(V_{F,real}, V_{F,model})$ when parameters A_C , B_C , and G_C span pre-defined ranges of values according to a Brute-Force procedure.

RESULTS

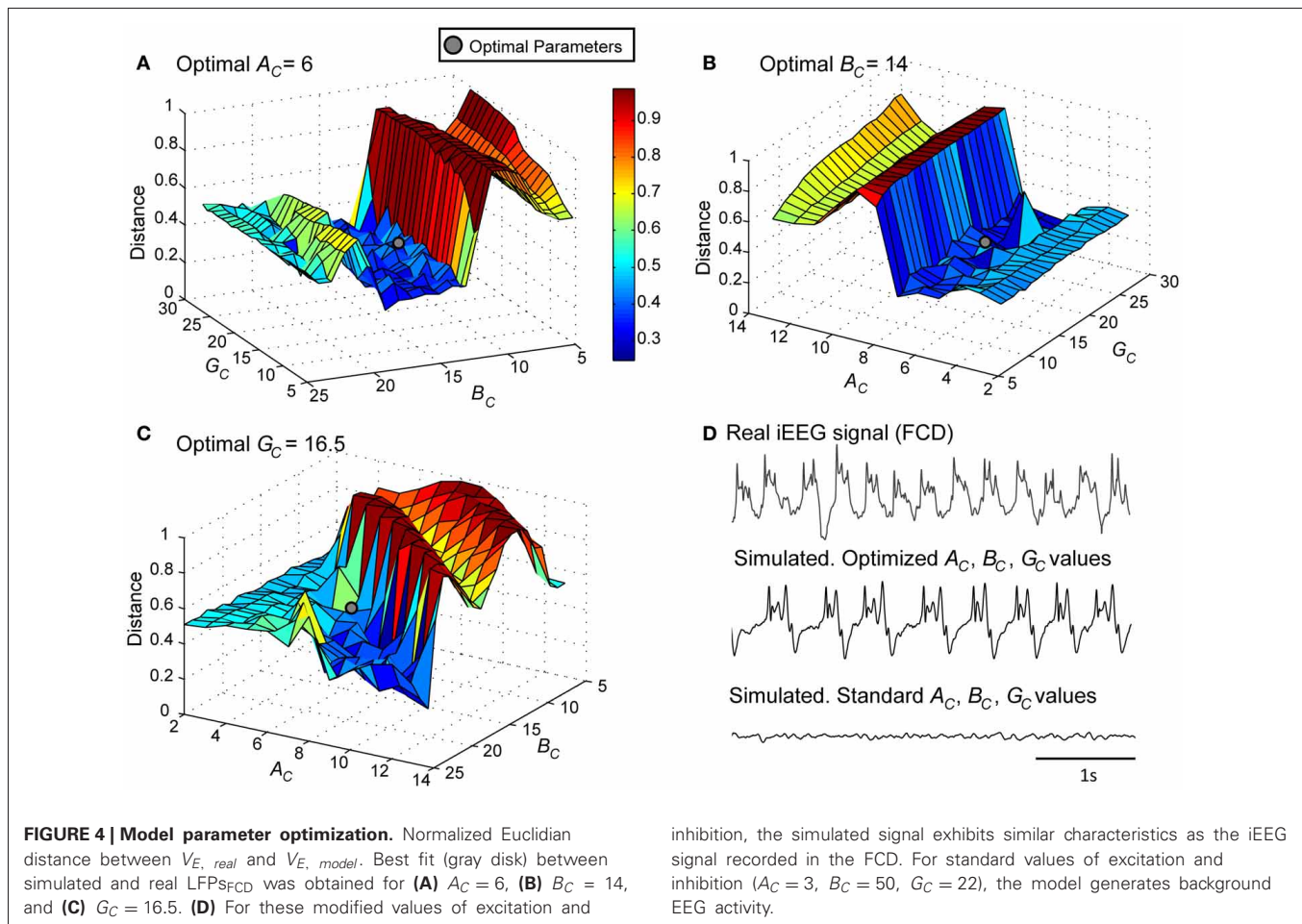
In this section, results regarding the identification of cellular mechanisms underlying the modulation of cortical activity by thalamic DBS are reported. First, the model capability to reproduce signals similar to those recorded from the FCD in the patient was assessed, under two conditions (no stimulation and during stimulation). Three mechanisms contributing to frequency-dependant stimulation effects could be identified. Then, simulations were performed to analyze the marginal or joint contribution of these mechanisms at low, intermediate or high frequency stimulation.

SIMULATION OF LFPs_{FCD} UNDER NO STIMULATION CONDITION

As a first step, we verified the ability of the model to generate signals that resemble those recorded from the FCD in the considered patient (LFPs_{FCD}). This procedure, described in sections Processing of Real and Simulated Signals and Model Optimization Under the “No Stimulation” Condition, led us to identify a minimal distance (**Figures 4A–C**) and thus an optimal parameter vector $\{\widehat{A}_C, \widehat{B}_C, \widehat{G}_C\} = \{6, 14, 16.5\}$ for which simulated signals under the no stimulation condition have similar features as compared with those of real signals (**Figure 4D**).

SIMULATION OF LFPs_{FCD} UNDER STIMULATION CONDITIONS

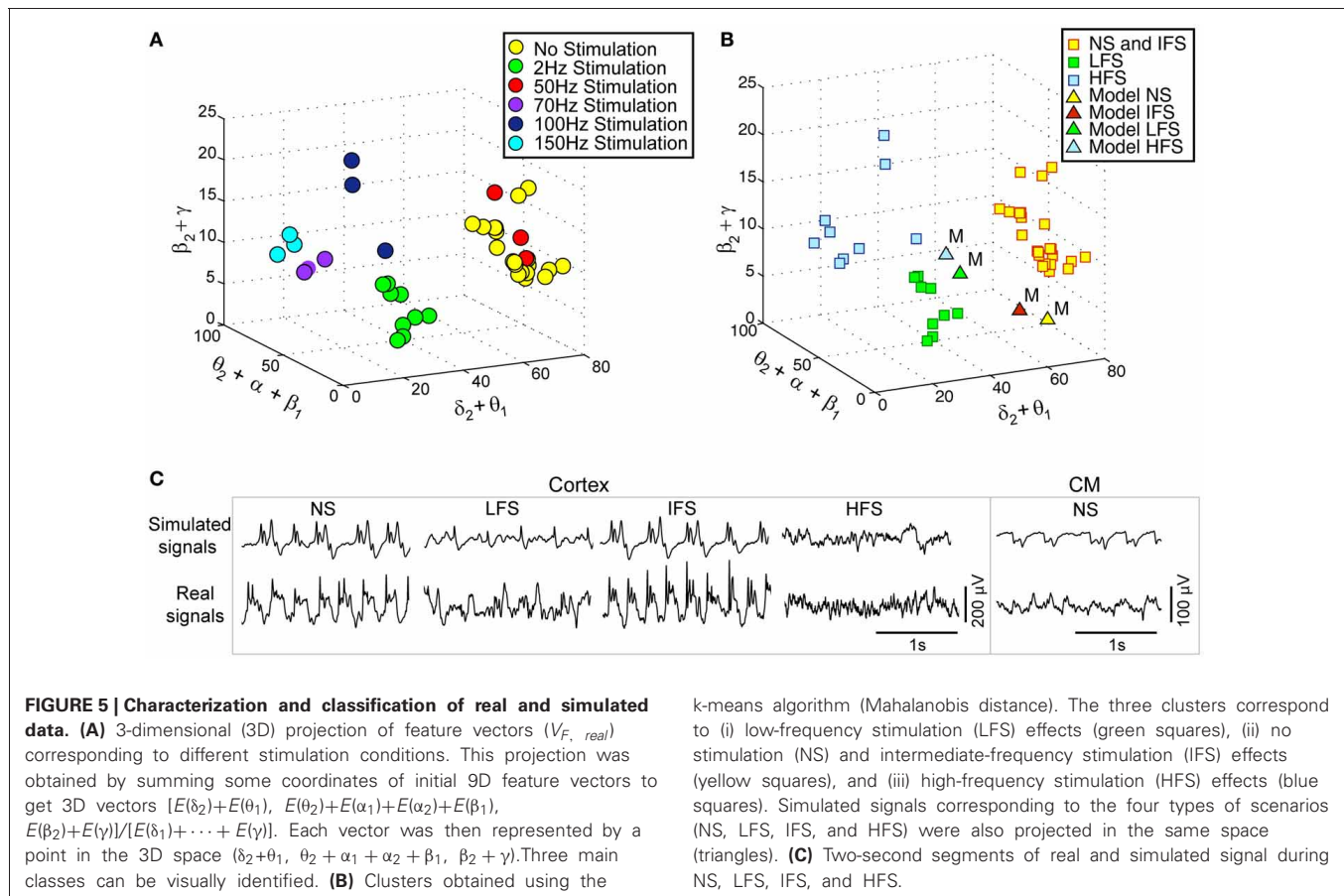
Actual LFPs_{FCD} recorded at various stimulation frequencies (2, 50, 70, 100, and 150 Hz) were first characterized using the matching pursuit method described in section Processing of



Real and Simulated Signals (Figure 3A). Results are shown in Figure 5A where feature vectors of segments of LFPs_{FCD} are represented in a 3D space where axes correspond to merged typical EEG frequency bands (δ_2 to θ_1 , θ_2 to β_1 , β_2 to γ). Results show that the distribution of points in the 3D frequency space is not random but clustered, indicating that the frequency content of LFPs_{FCD} segments depends on the stimulation frequency. In addition, some clusters are very close. This is typically the case for i) the no stimulation (yellow) and the 50 Hz stimulation conditions (red) on the one hand, and ii) the 70 Hz (violet) and 150 Hz (cyan) stimulation conditions on the other hand. To go beyond the qualitative clustering performed by visual inspection of 3D plots, a K-means clustering algorithm implemented in MATLAB and using a Mahalanobis distance was used to automatically detect the three types of stimulation effects. Initial centroids were randomly chosen. The optimal clustering that globally minimizes intra-cluster inertia is presented in Figure 5B. LFPs_{FCD} segments were automatically classified into three subgroups. The first subgroup contains LFPs_{FCD} segments obtained for low-frequency stimulation (LFS). The second subgroup gathers all segments recorded for high frequency stimulations (HFS, > 70 Hz). And finally, in the third subgroup, segments obtained under the no stimulation and the intermediate stimulation frequency (IFS, 50 Hz) conditions are merged

together, suggesting that this stimulation frequency does not reduce the “epileptiform aspect” of the activity reflected in the LFP.

Based on this characterization of local field potentials recorded in the FCD (LFPs_{FCD}), parameters S_{TC} , S_{R1} and S_{R2} were manually tuned to lead the model to generate simulated signals which have spectral characteristics similar to those of actual LFPs_{FCD}. Such a manual procedure was sufficient to reproduce stimulation effects observed in one patient. However, extending the study to a larger group of patients would have made imperative an automated parameter fitting procedure based on the spectral characteristics of real EEG signals as in Rowe et al. (2004). Figure 5B shows the projection of representative simulated LFPs_{FCD} in the 3D frequency space (“M” triangles). As depicted, simulated signals obtained for LFS, IFS and HFS were close to corresponding clusters obtained from real signals for the exact same computation of feature vectors. Shown in Figure 5C, these representatives simulated LFPs_{FCD} do not perfectly match actual signals. However, qualitatively similar bifurcations were observed in the model when the stimulation conditions are changed. Indeed, under the no stimulation (NS) and the IFS condition the model generates rhythmic slow oscillations (δ) with superimposed faster activity (β , γ), as observed in real data. For LFS and HFS conditions, strong modulation of this activity was also obtained in the model.



At LFS, in the model, the slow wave activity was strongly reduced but spike events occurred in the signals at the instant times of stimulation, mimicking, to some extent, comparable events also present in actual LFPs_{FCD}. Finally, at HFS, slow oscillations (δ) were abolished in the model which generates quasi-normal background activity. This simulated activity was also comparable to real activity observed for HFS stimulation but disclosed less γ activity. Note that these are the effects which were quantified in **Figure 5B**. The qualitative optimization procedure of parameters S_{TC} , S_{Rt1} , and S_{Rt2} was then complemented by an evaluation of parameter sensitivity aimed at studying the impact of random changes affecting the parameter vector $\Theta = \{A_C, B_C, G_C, A_{Th}, B_{Th}, G_{Th}, A_{Rt}\}$ on simulated signals. Parameter vector Θ determines the excitability properties in the three model compartments. As shown in **Figure 6**, results show that the simulated signals obtained under the four stimulation conditions (NS, LFS, IFS, HFS) stay “quite robust” (in the sense that waveforms are conserved) when parameters stay in the range $[\hat{\Theta} \pm \zeta, \hat{\Theta}]$ with $0 \leq \zeta \leq 0.2$.

MECHANISMS UNDERLYING FREQUENCY-DEPENDANT STIMULATION EFFECTS

Three main mechanisms implemented in the model are required to mimic actually observed effects of the CM nucleus stimulation. These mechanisms are the following: (i) the presence of feed-forward inhibition (FFI) at the level of thalamic projections

to the FCD, (ii) the presence of short-term depression (STD) at the level of the thalamocortical glutamatergic synapses and, (iii) the depolarization of RtN inhibitory interneurons targeting TC cells.

This result raises an additional question: to what extent the joint effect of these mechanisms is necessary to reproduce frequency-dependant stimulation effects (LFS, IFS, and HFS). In order to assess their individual contribution, we performed simulations where each mechanism was either present in—or removed from—the model (the model parameters remaining unchanged). Results are displayed in **Figure 7**. First, they confirmed that both FFI and STD mechanisms are jointly necessary in the model to suppress the epileptic activity in the FCD when LFS is being used since the withdrawal of either STD or FFI leads the model to generate epileptic activity at LFS. Second, results indicated that the RtN inhibitory interneurons targeting TC cells (both I_1^{RT} and I_2^{RT} subpopulations) must be affected (i.e., depolarized) by the stimulation to obtain a suppression of epileptic activity when HFS is being used, as observed in the patient. Third, and interestingly, an unexpected effect was observed at IFS when the depolarization of I_2^{RT} interneurons was removed from the model. Indeed, epileptic activity was abolished in this case, which is really unlikely to occur during actual stimulation as both subtypes of neurons are expected to be affected by the direct stimulation of the CM nucleus.

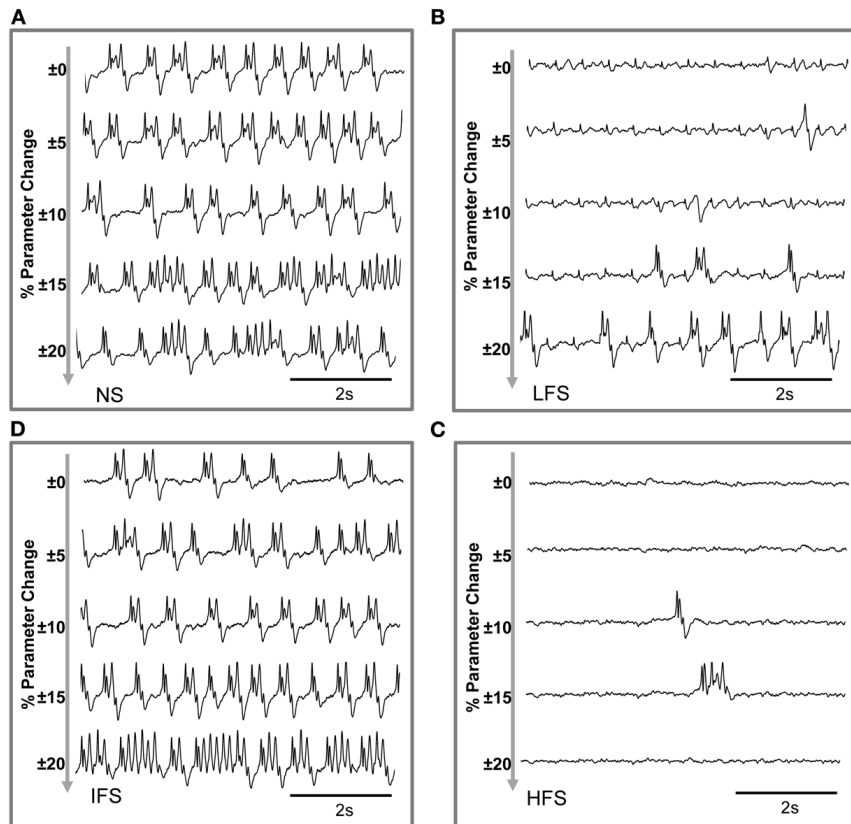


FIGURE 6 | Evaluation of parameter sensitivity. Model output sensitivity to variations of excitatory and inhibitory key parameters. Realizations of parameter vector $\Theta = \{A_C, B_C, G_C, A_{Th}, B_{Th}, G_{Th}, A_{Rt}\}$ were randomly (uniform law) generated around the optimal parameter vector Θ_0 over a

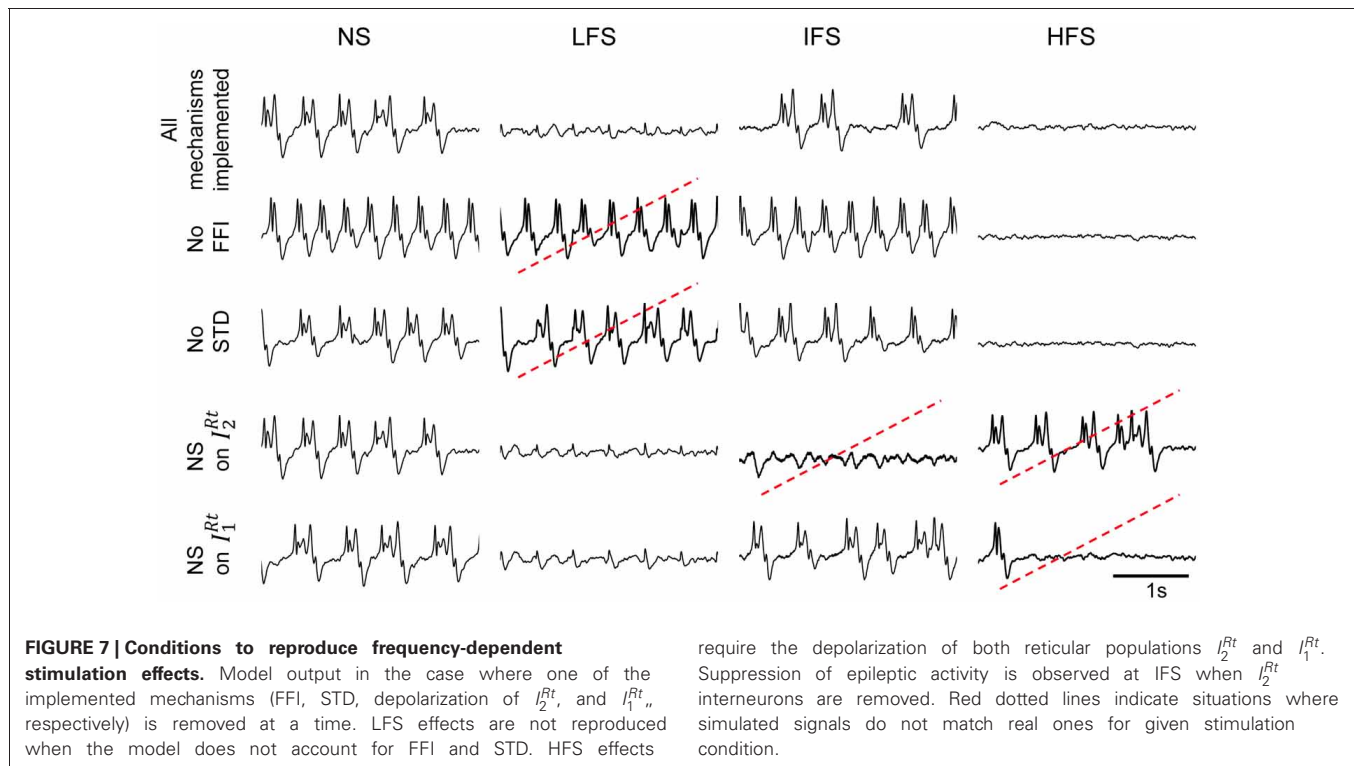
variation domain defined by $(1 \pm \zeta) \cdot \Theta_0$. For $\zeta \leq 0.2$ ($\pm 20\%$ variation), stimulation effects are preserved in the model for **(A)** no stimulation, **(B)** low-frequency stimulation, **(C)** intermediate-frequency stimulation, and **(D)** high-frequency stimulation.

These results were complemented by a deeper analysis of the thalamic output (i.e., the firing rate of *TC* cells) in response to stimulation at low, intermediate and high frequency. Results are provided in **Figure 8**. First, they showed that the thalamic output dramatically differs depending on the stimulation frequency (**Figure 8A**). Under the no stimulation condition, the firing rate continuously oscillates around a certain value (referred to as Λ , **Figure 8A**). At LFS, the firing rate was found to be lower, except at the stimulation times where it abruptly and transiently increased. At IFS, a balance was observed between time intervals for which the *TC* firing is above and below Λ . Finally, at HFS, the output of *TC* cells was found to be very low, i.e., systematically under the threshold Λ . From these observations, we could define (i) two time intervals, $\Delta 1$ and $\Delta 2$, for which the *TC* cells firing rate is either below Λ ($\Delta 1$) or above Λ ($\Delta 2$) and (ii) a “high to low firing” ratio (*HtoLR*) which provides an indication on the amount of time the *TC* cells spend firing (up state) relatively to the amount of time they do not fire (down state). **Figure 8B** provides the evolution of the *HtoLR* when the stimulation frequency is progressively changing from 0 to 150 Hz in the model. As depicted, these simulations indicated that three stimulation frequency ranges have dramatic effects on the firing of *TC* cells. First, from 0 to 20 Hz, the down state

is predominant. Then, an abrupt jump was observed around 22 Hz indicating that beyond this value, the firing rate dramatically increased. Interestingly, from 55 to 65 Hz, a progressive decrease of the *HtoLR* was observed. Then, after 70 Hz, the ratio is equal to zero indicating that *TC* cells did not fire anymore. Finally, in order to relate the thalamic activity with the cortical activity, we plotted the phase portraits (*TC* cell firing vs. cortical LFP) as illustrated in **Figure 8C**. Results confirmed the visual inspection of signals simulated at the two sites. For the no stimulation (NS) and for the intermediate frequency stimulation (IFS) conditions, phase portraits were found to be quite similar. They indicated the presence of mixed slow/fast oscillations in both signals. For the low frequency stimulation (LFS) condition, oscillations in the simulated LFP in the FCD were reduced. They came along with short-duration, abrupt and rhythmic augmentations of the *TC* firing corresponding to stimulation pulses. Finally, for the high frequency stimulation (HFS) condition, oscillations in both types of activity stayed confined to small amplitude values.

DISCUSSION

We modeled the thalamocortical loop in order to investigate frequency-dependent effects of electrical stimulation performed



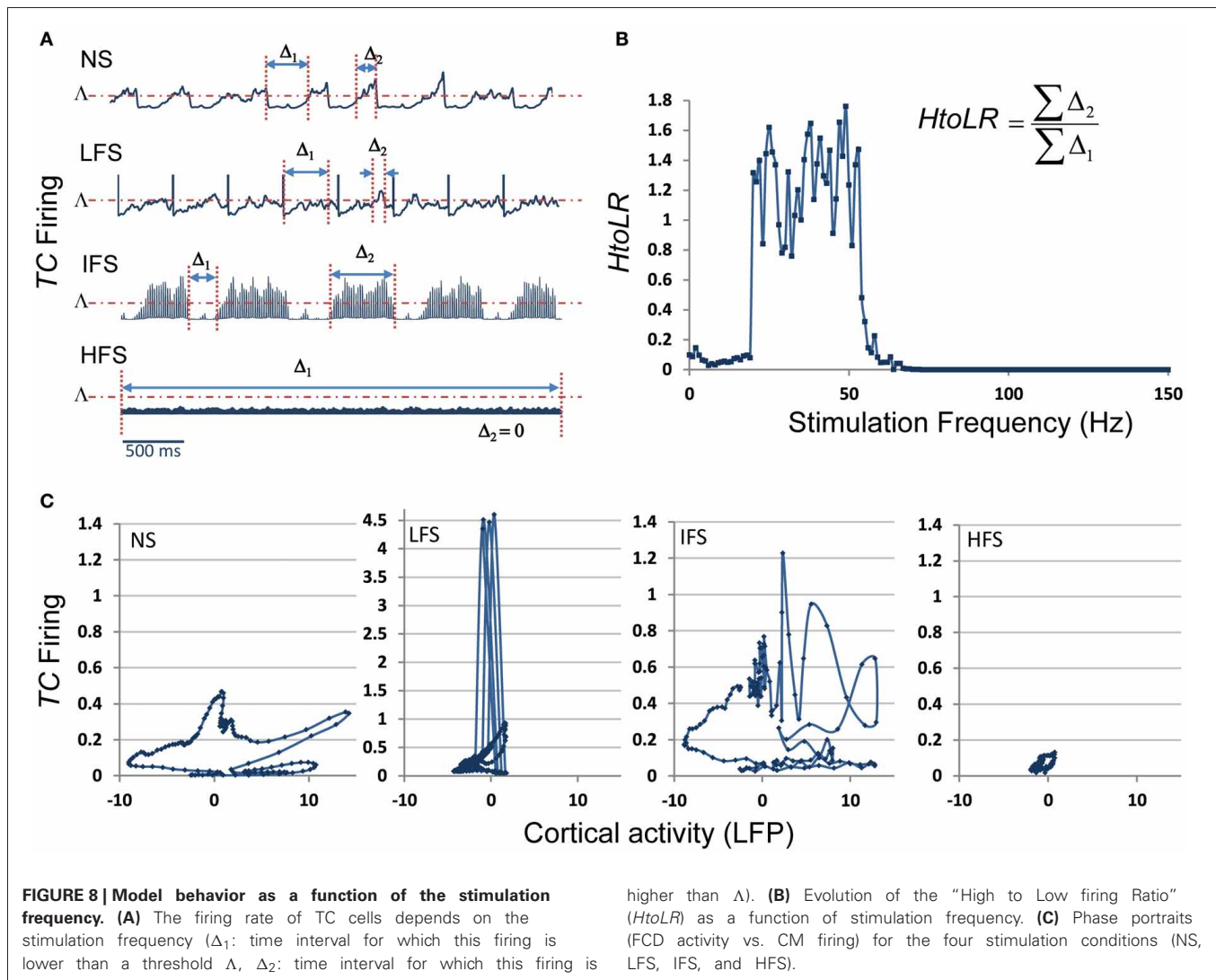
in the thalamus and aimed at modulating the neocortical activity. We chose to elaborate our model at a mesoscopic level, i.e., intermediate between microscopic and macroscopic.

Regarding the model architecture, we followed a similar approach to that used in previously proposed models of the thalamocortical loop (Robinson et al., 2002; Suffczynski et al., 2004; Breakspear et al., 2006; Roberts and Robinson, 2008; Marten et al., 2009; Crunelli et al., 2011). Our model includes three main compartments: cerebral cortex, reticular nucleus and thalamic relay. Subpopulations of neurons and interneurons located in these three structures interact via excitatory and/or inhibitory synaptic connections. The novelty with respect to aforementioned studies is threefold. First, we modified the cortical compartment in order to better approximate the temporal dynamics of epileptic signals recorded in the FCD. This modification consisted in the use of two types of interneurons (mediating GABAergic IPSPs with slow and fast kinetics on cortical principal cells), as reported in a previous study (Molae-Ardekani et al., 2010). Second, our model accounts for the direct effects of electrical stimulation. At this stage, we used the $\Delta V \approx \lambda \cdot \vec{E}$ assumption according to which the perturbation of the mean membrane potential of neurons is a linear function of the electrical field magnitude induced by bipolar stimulation. This “ λE ” assumption was already used in neural mass models in the context of low-intensity direct hippocampal stimulation to anticipate seizures (Suffczynski et al., 2008) as well as in the analysis of the stimulus-response relationship of DBS in healthy animals (Adhikari et al., 2009). However, it is worth mentioning that in our model, the three subtypes of neurons (TC cells and both subpopulations of inhibitory neurons in the RtN) are depolarized by the stimulation, as suggested in

(Molae-Ardekani et al., 2013) and conversely to (Adhikari et al., 2009) where only principal cells are impacted. And third, our model includes two well-known mechanisms at the cortical level: feed-forward inhibition (FFI) and short-term depression (STD).

As in any modeling approach, our approach has some limitations. First, the chosen modeling level does not allow for analyzing sub-cellular mechanisms involved in stimulation-evoked changes. Similarly, it does not account for direct activation of axons by stimulation versus somatic inhibition (McIntyre et al., 2004b), nor for the mechanisms of orthodromic/antidromic propagation of action potentials due to stimulation (Degos et al., 2005; Hammond et al., 2007; Dorval et al., 2008). Second, a strong assumption in the type of model we used (neural mass) is related to the intrinsic synchronization among neurons included in a given sub-population. This assumption does not allow for representing either de- or weakly-synchronized firing patterns that may be observed during epileptic activity, in particular during high frequency oscillations that can be encountered in FCDs (Brázdil et al., 2010). Nevertheless, we could accurately reproduce the abnormal rhythms generated in the FCD suggesting that main pyramidal cells have a relatively synchronized activity in this epileptogenic tissue. Third, regarding plasticity-related mechanisms, we only implemented short-term effects (i.e., STD) and neglected long-term plastic changes that may be induced by DBS (Shukla et al., 2013).

Despite these limitations, we could identify a number of mesoscopic factors which could explain the frequency-dependent mechanisms of thalamic stimulation. The model was tuned using electrophysiological data recorded in a patient in whom the centromedian nucleus (CMN) stimulation was particularly efficient



to reduce the epileptic activity of a FCD located in the premotor cortex, in a frequency-specific manner. The main findings are summarized in **Figure 9**.

“NO STIMULATION” (NS) CONDITION

In the model, under the NS condition, excitation among pyramidal cells had to be increased and inhibition had to be reduced in the cortical compartment for producing “pathological” oscillatory rhythms, as observed in the FCD. The thalamocortical loop was found to be responsible for these pathological dynamics, characteristic of FCDs. These findings are in line with histological studies showing that these typical oscillations are generated in altered brain tissue, where inhibition is partially deteriorated or dysfunctioning (Calcagnotto et al., 2005), and where excitation is heavily increased (Avoli et al., 2003). In addition to neuron alterations in the dysplastic tissue (Sisodiya et al., 2009), FCD keeps sufficient projections to—and input from—other brain structures to propagate pathological dynamics (Avoli et al., 2003). As mentioned, the presence of connections with subcortical structures was a necessary condition in the model for producing

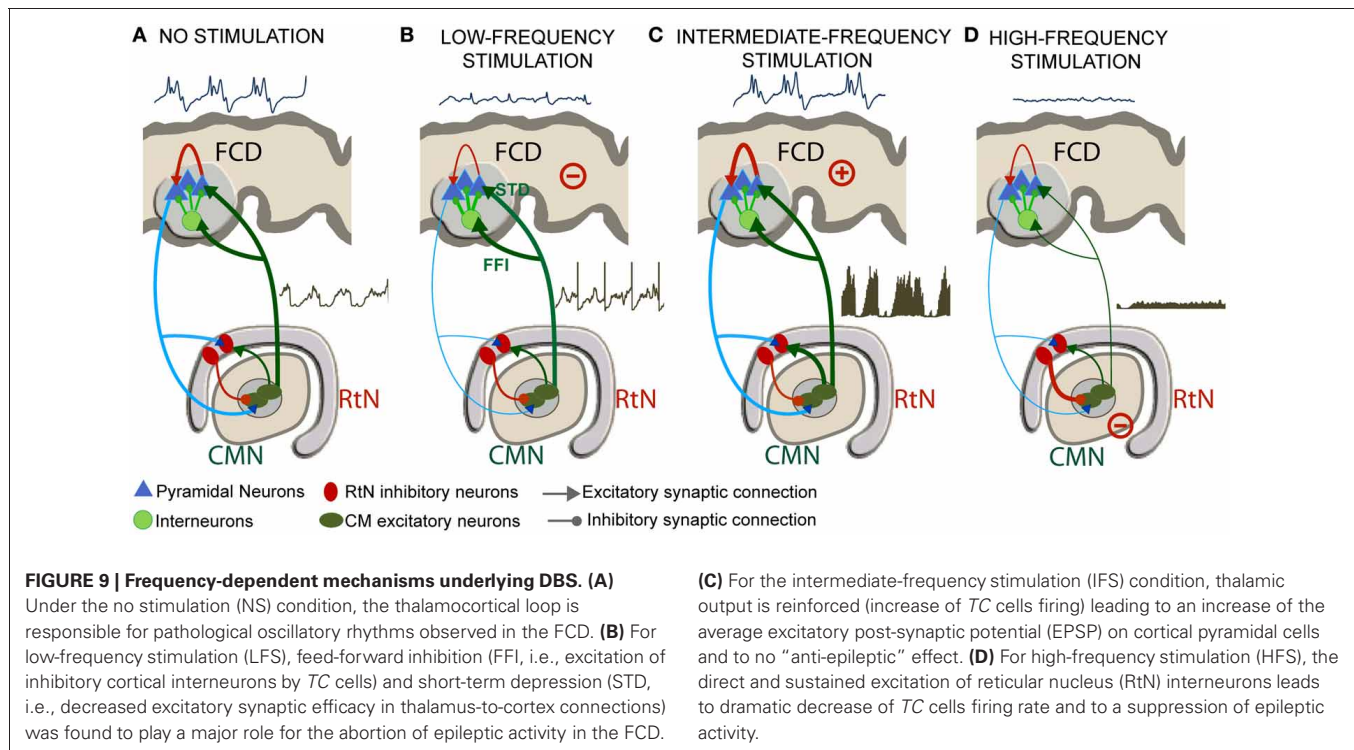
pathological oscillations resembling those actually recorded in the FCD (**Figure 9A**).

LOW-FREQUENCY STIMULATION (LFS) CONDITION

For the low-frequency stimulation (LFS, $f < 20$ Hz) condition, two mechanisms were found to play a major role for the abolition of epileptic activity in the FCD: short-term depression (STD, i.e., decreased excitatory synaptic efficacy in thalamus-to-cortex connections) and feed-forward inhibition (FFI, i.e., excitation of inhibitory cortical interneurons by TC cells) (**Figure 9B**).

STD was reported in previous studies concerning cortical adaptation to thalamic stimulation, and suggesting that electrical LFS of TC cell axons *in vivo* resulted in a 40% reduction in cortical EPSPs (Chung et al., 2002). In the same context, LFS trains in adult anaesthetized rats provoked transient long-term depression of thalamocortical synapses; this was measured by up to 40% drop in cortical EPSPs after LFS trains and under the effect of GABA antagonist (Speechley et al., 2007).

As mentioned above, the LFS effects could not be reproduced by the model without incorporating also FFI. Actually,



thalamocortical ascending fibers directly target pyramidal neurons as well as cortical GABAergic interneurons inducing EPSPs in both cell types (Pouille and Scanziani, 2001). In the model, while less efficient (STD) thalamic EPSPs arrive directly onto pyramidal neurons, IPSPs induced by thalamic stimulation also arrive on pyramidal neurons (FFI) lagging by 1–2 ms. This short latency between the onset of thalamocortical excitation and the onset of feed-forward inhibition presents a temporal “window of opportunity” for pyramidal cells to integrate excitatory and inhibitory inputs, thus keeping the transmembrane potential below firing threshold. In the literature, neuroanatomical and neurophysiological studies (Isaacson and Scanziani, 2011) showed the functional importance of FFI in regulating cortical dynamics by controlling cortical excitability (Gabernet et al., 2005). Our study suggests that LFS regulates cortical excitability by a dual mechanism of FFI and STD (Figure 9B).

INTERMEDIATE-FREQUENCY STIMULATION (IFS) CONDITION

For the intermediate-frequency stimulation (IFS, $20 < f < 70$ Hz) condition, results indicated that the thalamic output is reinforced (increase of TC cells firing) and leads to an increase of the average excitatory post-synaptic potential (EPSP) on cortical pyramidal cells (Figure 9C). This effect corresponds to an increase of the spatiotemporal summation of unitary EPSPs. In this case, both the cortical excitability and the gain in the excitatory thalamocortical loop is increased, leading to “no anti-epileptic” effect. We did not find much studies using DBS stimulation in the intermediate frequency range of (20–60 Hz) in the context of epilepsy. Nevertheless, it is noteworthy that 50 Hz stimulation frequency is classically used during the presurgical evaluation of patient with intractable partial epilepsy in order to

trigger seizures and delineate the epileptogenic zone (Talairach et al., 1974; Jayakar et al., 1992). The same frequency range is also known to provoke afterdischarges and was actually used in the kindling model of epilepsy (Goddard, 1967; Racine, 1972).

HIGH-FREQUENCY STIMULATION (HFS) CONDITION

Finally, for the high-frequency stimulation (HFS, $f > 70$ Hz) condition, the direct and sustained excitation of reticular nucleus (RtN) interneurons leads to strong inhibition of TC cells and thus to dramatic decrease of their firing rate. Despite the fact that TC neurons are also affected by stimulation, the response of reticular GABAergic neurons to stimulation and the higher efficiency of GABA-mediated currents ensure that IPSPs override EPSPs on TC cells. In this case, the reduced excitatory input to cortical pyramidal cells also leads to a suppression of epileptic activity (Figure 9D). This result corroborates reported stimulation studies where HFS (>100 Hz) was associated with significant decrease in epileptiform discharges *in vitro*, and reduction in seizure frequency in responding patients (Velasco et al., 2006; Fisher et al., 2010). This hypothesis is in line with recent findings suggesting that HFS of the globus pallidus (GPi) in dystonia patients decreased its firing by stimulation-evoked GABA release from afferent fibers and thereby the enhancement of inhibitory synaptic transmission by HFS (Liu et al., 2012). Similarly, HFS (100 Hz–130 Hz) of the STN neurons *in vitro* showed a suppression of the activity of the majority of neurons by the reinforcement of inhibitory responses (Filali et al., 2004). Other HFS studies also provided evidence on the inhibition of GPi output during HFS in human patients (Dostrovsky et al., 2000) as well as the disruption thalamocortical network’s dysrhythmia (McIntyre and Hahn, 2010; Kendall et al., 2011).

CONCLUSION

In epilepsy research, it is well-admitted that there is, unfortunately, a lack of tangible results regarding the effects of electrical stimulation in the brain. Therefore, the very crucial issue of choosing the “optimal” stimulation parameters remains unsolved, whatever the stimulation procedure. Although computational models are always based on a number of simplifying assumptions, we think that they provide an efficient framework to (i) account for the many and essential factors that may intervene during stimulation procedures and (ii) analyze the links between these factors in a formal manner. This approach is particularly fruitful when models are well grounded in experimental/clinical data (Wendling et al., 2012). This is somehow a weak point of this study since we could make use of data sets recorded in one patient only. However, it should be mentioned that these very informative data sets stay relatively rare since many conditions have to be met (patient candidate to surgery, FCD, electrodes positioned in appropriate structures).

At this stage, the face value of the model is satisfactory. The next step is obviously to test the model predictions using animal

models. Experiments can be undertaken in rodents with electrodes implanted in the cerebral cortex and in the thalamus. First, we could start with control animals to assess the modulation of cortical rhythms during/after direct thalamic stimulation at various frequencies and for controlled vigilance states (sleep, awake, resting, exploratory). In these controls, some drugs can be used to alter some parameters related to synaptic transmission (in a more or less specific manner) which have a correspondence in the model, on the other hand. Then, refined experimental models could be introduced to get closer to the epilepsy context including models of developmental dysplastic lesions [see review in Schwartzkroin and Wenzel (2012)]. Hopefully, this combined computational/experimental approach will help us to disclose some of the highly intricate effects of DBS either at local or at network level.

ACKNOWLEDGMENTS

This study was supported by Region Bretagne, France. The first author benefits from a research allocation (ARED) in the context of the project entitled “STIMULE.”

REFERENCES

- Adhikari, M. H., Heeroma, J. H., Di Bernardo, M., Krauskopf, B., Richardson, M. P., Walker, M. C., et al. (2009). Characterisation of cortical activity in response to deep brain stimulation of ventral-lateral nucleus: modelling and experiment. *J. Neurosci. Methods* 183, 77–85. doi: 10.1016/j.jneumeth.2009.06.044
- Avoli, M., Louvel, J., Mattia, D., Olivier, A., Esposito, V., Pumain, R., et al. (2003). Epileptiform synchronization in the human dysplastic cortex. *Epileptic Disord.* 5(Suppl. 2), S45–S50.
- Beurrier, C., Bioulac, B., Audin, J., and Hammond, C. (2001). High-frequency stimulation produces a transient blockade of voltage-gated currents in subthalamic neurons. *J. Neurophysiol.* 85, 1351–1356.
- Bikson, M., Inoue, M., Akiyama, H., Deans, J. K., Fox, J. E., Miyakawa, H., et al. (2004). Effects of uniform extracellular DC electric fields on excitability in rat hippocampal slices *in vitro*. *J. Physiol.* 557, 175–190. doi: 10.1113/jphysiol.2003.055772
- Bojak, I., and Liley, D. T. (2005). Modeling the effects of anesthesia on the electroencephalogram. *Phys. Rev. E Stat. Nonlin. Soft Matter Phys.* 71:041902. doi: 10.1103/PhysRevE.71.041902
- Boon, P., Raedt, R., De Herdt, V., Wyckhuys, T., and Vonck, K. (2009). Electrical stimulation for the treatment of epilepsy. *Neurotherapeutics* 6, 218–227. doi: 10.1016/j.nurt.2008.12.003
- Boudreau, C. E., and Ferster, D. (2005). Short-term depression in thalamocortical synapses of cat primary visual cortex. *J. Neurosci.* 25, 7179–7190. doi: 10.1523/JNEUROSCI.1445-05.2005
- Brázdil, M., Halánek, J., Jurák, P., Daniel, P., Kuba, R., Chrástina, J., et al. (2010). Interictal high-frequency oscillations indicate seizure onset zone in patients with focal cortical dysplasia. *Epilepsy Res.* 90, 28–32. doi: 10.1016/j.eplepsyres.2010.03.003
- Breakspear, M., Roberts, J. A., Terry, J. R., Rodrigues, S., Mahant, N., and Robinson, P. A. (2006). A unifying explanation of primary generalized seizures through nonlinear brain modeling and bifurcation analysis. *Cereb. Cortex* 16, 1296–1313. doi: 10.1093/cercor/bhj072
- Calcagnotto, M. E., Paredes, M. F., Tihan, T., Barbaro, N. M., and Baraban, S. C. (2005). Dysfunction of synaptic inhibition in epilepsy associated with focal cortical dysplasia. *J. Neurosci.* 25, 9649–9657. doi: 10.1523/JNEUROSCI.2687-05.2005
- Chung, S., Li, X., and Nelson, S. B. (2002). Short-term depression at thalamocortical synapses contributes to rapid adaptation of cortical sensory responses *in vivo*. *Neuron* 34, 437–446. doi: 10.1016/S0896-6273(02)00659-1
- Cooper, I. S., Amin, I., and Gilman, S. (1973). The effect of chronic cerebellar stimulation upon epilepsy in man. *Trans. Am. Neurol. Assoc.* 98, 192–196.
- Crunelli, V., Cope, D. W., and Terry, J. R. (2011). Transition to absence seizures and the role of GABA(A) receptors. *Epilepsy Res.* 97, 283–289.
- David, O., and Friston, K. J. (2003). A neural mass model for MEG/EEG: coupling and neuronal dynamics. *Neuroimage* 20, 1743–1755. doi: 10.1016/j.neuroimage.2003.07.015
- Davis, R., Engle, H., Kudzma, J., Gray, E., Ryan, T., and Dushnak, A. (1982). Update of chronic cerebellar stimulation for spasticity and epilepsy. *Appl. Neurophysiol.* 45, 44–50.
- Degos, B., Deniau, J. M., Thierry, A. M., Glowinski, J., Pezard, L., and Maurice, N. (2005). Neuroleptic-induced catalepsy: electrophysiological mechanisms of functional recovery induced by high-frequency stimulation of the subthalamic nucleus. *J. Neurosci.* 25, 7687–7696. doi: 10.1523/JNEUROSCI.1056-05.2005
- Dorval, A. D., Russo, G. S., Hashimoto, T., Xu, W., Grill, W. M., and Vitek, J. L. (2008). Deep brain stimulation reduces neuronal entropy in the MPTP-primate model of Parkinson’s disease. *J. Neurophysiol.* 100, 2807–2818. doi: 10.1152/jn.90763.2008
- Dostrovsky, J. O., Levy, R., Wu, J. P., Hutchison, W. D., Tasker, R. R., and Lozano, A. M. (2000). Microstimulation-induced inhibition of neuronal firing in human globus pallidus. *J. Neurophysiol.* 84, 570–574.
- Filali, M., Hutchison, W. D., Palter, V. N., Lozano, A. M., and Dostrovsky, J. O. (2004). Stimulation-induced inhibition of neuronal firing in human subthalamic nucleus. *Exp. Brain Res.* 156, 274–281. doi: 10.1007/s00221-003-1784-y
- Fisher, R., Salanova, V., Witt, T., Worth, R., Henry, T., Gross, R., et al. (2010). Electrical stimulation of the anterior nucleus of thalamus for treatment of refractory epilepsy. *Epilepsia* 51, 899–908. doi: 10.1111/j.1528-1167.2010.02536.x
- Freeman, W. J. (1973). “A model of the olfactory system,” in *Neural Modeling*, eds M. A. B. Brazier, D. O. Walter, and D. Schneider (Los Angeles, CA: University of California), 41–62.
- Freeman, W. J. (1992). Tutorial on neurobiology: from single neurons to brain chaos. *Int. J. Bifurcat. Chaos* 2, 451–482. doi: 10.1142/S0218127492000653
- Frohlich, E., and McCormick, D. A. (2010). Endogenous electric fields may guide neocortical network activity. *Neuron* 67, 129–143. doi: 10.1016/j.neuron.2010.06.005
- Gabernet, L., Jadhav, S. P., Feldman, D. E., Carandini, M., and Scanziani, M. (2005). Somatosensory integration controlled by dynamic thalamocortical feed-forward inhibition. *Neuron* 48, 315–327. doi: 10.1016/j.neuron.2005.09.022
- Goddard, G. V. (1967). Development of epileptic seizures through brain stimulation at low intensity. *Nature* 214, 1020–1021. doi: 10.1038/2141020a0
- Hablitz, J. J. (1976). Intramuscular penicillin epilepsy in the cat: effects of chronic cerebellar stimulation. *Exp. Neurol.* 50, 505–514. doi: 10.1016/0014-4886(76)90022-4
- Hammond, C., Bergman, H., and Brown, P. (2007). Pathological synchronization in Parkinson’s disease:

- networks, models and treatments. *Trends Neurosci.* 30, 357–364. doi: 10.1016/j.tins.2007.05.004
- Isaacson, J. S., and Scanziani, M. (2011). How inhibition shapes cortical activity. *Neuron* 72, 231–243. doi: 10.1016/j.neuron.2011.09.027
- Jansen, B. H., Zouridakis, G., and Brandt, M. E. (1993). A neurophysiologically-based mathematical model of flash visual evoked potentials. *Biol. Cybern.* 68, 275–283. doi: 10.1007/BF00224863
- Jayakar, P., Alvarez, L. A., Duchowny, M. S., and Resnick, T. J. (1992). A safe and effective paradigm to functionally map the cortex in childhood. *J. Clin. Neurophysiol.* 9, 288–293. doi: 10.1097/00004691-199204010-00009
- Jiang, B., Akaneya, Y., Hata, Y., and Tsumoto, T. (2003). Long-term depression is not induced by low-frequency stimulation in rat visual cortex *in vivo*: a possible preventing role of endogenous brain-derived neurotrophic factor. *J. Neurosci.* 23, 3761–3770.
- Kendall, H. L., Frederick, L. H., Su-Youne, C., Dongchul, C. L., David, W. R., Cameron, C. M., et al. (2011). High frequency stimulation abolishes thalamic network oscillations: an electrophysiological and computational analysis. *J. Neural Eng.* 8:046001. doi: 10.1088/1741-2560/8/4/046001
- Kim, E., Owen, B., Holmes, W. R., and Grover, L. M. (2012). Decreased afferent excitability contributes to synaptic depression during high frequency stimulation in hippocampal area CA1. *J. Neurophysiol.* 108, 1965–1976. doi: 10.1152/jn.00276.2011
- Krstulovic, S., and Gribonval, R. (2006). “Mptk: Matching Pursuit Made Tractable,” in: *IEEE International Conference on Acoustics, Speech and Signal Processing*, (Toulouse), 496–499.
- Liley, D. T., and Bojak, I. (2005). Understanding the transition to seizure by modeling the epileptiform activity of general anesthetic agents. *J. Clin. Neurophysiol.* 22, 300–313.
- Liu, L. D., Prescott, I. A., Dostrovsky, J. O., Hodaie, M., Lozano, A. M., and Hutchison, W. D. (2012). Frequency-dependent effects of electrical stimulation in the globus pallidus of dystonia patients. *J. Neurophysiol.* 108, 5–17. doi: 10.1152/jn.00527.2011
- Lopes Da Silva, F. H. (2006). Event-related neural activities: what about phase? *Prog. Brain Res.* 159, 3–17. doi: 10.1016/S0079-6123(06)59001-6
- Lopes Da Silva, F. H., Hoeks, A., Smits, H., and Zetterberg, L. H. (1974). Model of brain rhythmic activity. The alpha-rhythm of the thalamus. *Kybernetik* 15, 27–37. doi: 10.1007/BF00270757
- Lopes Da Silva, F. H., van Rotterdam, A., Barts, P., van Heusden, E., and Burr, W. (1976). Models of neuronal populations: the basic mechanisms of rhythmicity. *Prog. Brain Res.* 45, 281–308. doi: 10.1016/S0079-6123(08)60995-4
- Lytton, W. W. (2008). Computer modelling of epilepsy. *Nat. Rev. Neurosci.* 9, 626–637. doi: 10.1038/nrn2416
- Mallat, S. G., and Zhifeng, Z. (1993). Matching pursuits with time-frequency dictionaries. *Signal Processing, IEEE Transactions* 41, 3397–3415. doi: 10.1109/78.258082
- Manola, L., Holsheimer, J., Veltink, P., and Buiteweg, J. R. (2007). Anodal vs cathodal stimulation of motor cortex: a modeling study. *Clin. Neurophysiol.* 118, 464–474. doi: 10.1016/j.clinph.2006.09.012
- Manola, L., Roelofsen, B. H., Holsheimer, J., Marani, E., and Geelen, J. (2005). Modelling motor cortex stimulation for chronic pain control: electrical potential field, activating functions and responses of simple nerve fibre models. *Med. Biol. Eng. Comput.* 43, 335–343. doi: 10.1007/BF02345810
- Marten, F., Rodrigues, S., Benjamin, O., Richardson, M. P., and Terry, J. R. (2009). Onset of polyspike complexes in a mean-field model of human electroencephalography and its application to absence epilepsy. *Philos. Trans. A Math. Phys. Eng. Sci.* 367, 1145–1161. doi: 10.1098/rsta.2008.0255
- McIntyre, C. C., Grill, W. M., Sherman, D. L., and Thakor, N. V. (2004a). Cellular effects of deep brain stimulation: model-based analysis of activation and inhibition. *J. Neurophysiol.* 91, 1457–1469.
- McIntyre, C. C., and Hahn, P. J. (2010). Network perspectives on the mechanisms of deep brain stimulation. *Neurobiol. Dis.* 38, 329–337. doi: 10.1016/j.nbd.2009.09.022
- McIntyre, C. C., Savasta, M., Kerkerian-Le Goff, L., and Vitek, J. L. (2004b). Uncovering the mechanism(s) of action of deep brain stimulation: activation, inhibition, or both. *J. Clin. Neurophysiol.* 115, 1239–1248.
- Miranda, P. C., Wendling, F., Ruffini, G., Merlet, I., Molaee-Ardekani, B., Dunne, S., et al. (2009). *Brain Stimulation: Models, Experiments and Open Questions, Deliverable D1.1: Review of the State of the Art in Currents Distribution and Effects HIVE* (FET Open FP7 EU project), Available online at: <http://hive-eu.org>
- Molaee-Ardekani, B., Benquet, P., Bartolomei, F., and Wendling, F. (2010). Computational modeling of high-frequency oscillations at the onset of neocortical partial seizures: from ‘altered structure’ to ‘dysfunction’. *Neuroimage* 52, 1109–1122. doi: 10.1016/j.neuroimage.2009.12.049
- Molaee-Ardekani, B., Marquez-Ruiz, J., Merlet, I., Leal-Campanario, R., Gruart, A., Sanchez-Campusano, R., et al. (2013). Effects of transcranial Direct Current Stimulation (tDCS) on cortical activity: a computational modeling study. *Brain Stimul.* 6, 25–39. doi: 10.1016/j.brs.2011.12.006
- Nunez, P. L. (1974). The brain wave equation: a model for the EEG. *Math. Biosci.* 21, 279–297. doi: 10.1016/0025-5564(74)90020-0
- Palmini, A. (2010). Electrophysiology of the focal cortical dysplasias. *Epilepsia* 51(Suppl. 1), 23–26. doi: 10.1111/j.1528-1167.2009.02437.x
- Pasnicu, A., Denoyer, Y., Haegelen, C., Pasqualini, E., and Biraben, A. (2013). Modulation of paroxysmal activity in focal cortical dysplasia by centromedian thalamic nucleus stimulation. *Epilepsy Res.* 104, 264–268. doi: 10.1016/j.eplepsyres.2012.10.012
- Pouille, F., and Scanziani, M. (2001). Enforcement of temporal fidelity in pyramidal cells by somatic feed-forward inhibition. *Science* 293, 1159–1163. doi: 10.1126/science.1060342
- Racine, R. J. (1972). Modification of seizure activity by electrical stimulation. II. Motor seizure. *Electroencephalogr. Clin. Neurophysiol.* 32, 281–294. doi: 10.1016/0013-4694(72)90177-0
- Rattay, F. (1998). Analysis of the electrical excitation of CNS neurons. *IEEE Trans. Biomed. Eng.* 45, 766–772. doi: 10.1109/10.678611
- Reimer, G. R., Grimm, R. J., and Dow, R. S. (1967). Effects of cerebellar stimulation on cobalt-induced epilepsy in the cat. *Electroencephalogr. Clin. Neurophysiol.* 23, 456–462. doi: 10.1016/0013-4694(67)90188-5
- Roberts, J. A., and Robinson, P. A. (2008). Modeling absence seizure dynamics: implications for basic mechanisms and measurement of thalamocortical and corticothalamic latencies. *J. Theor. Biol.* 253, 189–201. doi: 10.1016/j.jtbi.2008.03.005
- Robinson, P. A., Rennie, C. J., and Rowe, D. L. (2002). Dynamics of large-scale brain activity in normal arousal states and epileptic seizures. *Phys. Rev. E Stat. Nonlin. Soft Matter Phys.* 65:041924. doi: 10.1103/PhysRevE.65.041924
- Robinson, P. A., Rennie, C. J., and Wright, J. J. (1997). Propagation and stability of waves of electrical activity in the cerebral cortex. *Phys. Rev. E Stat. Nonlin. Soft Matter Phys.* 56, 826–840. doi: 10.1103/PhysRevE.56.826
- Rowe, D. L., Robinson, P. A., and Rennie, C. J. (2004). Estimation of neurophysiological parameters from the waking EEG using a biophysical model of brain dynamics. *J. Theor. Biol.* 231, 413–433. doi: 10.1016/j.jtbi.2004.07.004
- Schwartzkroin, P. A., and Wenzel, H. J. (2012). Are developmental dysplastic lesions epileptogenic? *Epilepsia* 53(Suppl. 1), 35–44. doi: 10.1111/j.1528-1167.2012.03473.x
- Shen, K. Z., Zhu, Z. T., Munhall, A., and Johnson, S. W. (2003). Synaptic plasticity in rat subthalamic nucleus induced by high-frequency stimulation. *Synapse* 50, 314–319. doi: 10.1002/syn.10274
- Shukla, A. W., Moro, E., Gunraj, C., Lozano, A., Hodaie, M., Lang, A., et al. (2013). Long-term subthalamic nucleus stimulation improves sensorimotor integration and proprioception. *J. Neurol. Neurosurg. Psychiatry*. doi:10.1136/jnnp-2012-304102. [Epub ahead of print].
- Sillay, K., and Starr, P. (2009). “Chapter 42 - deep brain stimulation in Parkinson’s Disease,” in *Neuromodulation*, eds E. S. Krames, P. H. Peckham, and A. R. Rezai (San Diego, CA: Academic Press), 539–548.
- Sisodiya, S. M., Fauser, S., Cross, J. H., and Thom, M. (2009). Focal cortical dysplasia type II: biological features and clinical perspectives. *Lancet Neurol.* 8, 830–843. doi: 10.1016/S1474-4422(09)70201-7
- Speckley, W. J., Hogsdon, J. L., and Dringenberg, H. C. (2007). Continuous white noise exposure during and after auditory critical period differentially alters bidirectional thalamocortical plasticity in rat auditory cortex *in vivo*. *Eur. J. Neurosci.* 26, 2576–2584. doi: 10.1111/j.1460-9568.2007.05857.x
- Stam, C. J., Pijn, J. P., Suffczynski, P., and Lopes Da Silva, F. H. (1999). Dynamics of the human alpha rhythm: evidence for non-linearity? *Clin. Neurophysiol.* 110, 1801–1813.

- Suffczynski, P., Kalitzin, S., Da Silva, F. L., Parra, J., Velis, D., and Wendling, F. (2008). Active paradigms of seizure anticipation: computer model evidence for necessity of stimulation. *Phys. Rev. E Stat. Nonlin. Soft Matter Phys.* 78:051917. doi: 10.1103/PhysRevE.78.051917
- Suffczynski, P., Kalitzin, S., and Lopes Da Silva, F. H. (2004). Dynamics of non-convulsive epileptic phenomena modeled by a bistable neuronal network. *Neuroscience* 126, 467–484. doi: 10.1016/j.neuroscience.2004.03.014
- Suffczynski, P., Kalitzin, S., Pfurtscheller, G., and Lopes Da Silva, F. H. (2001). Computational model of thalamo-cortical networks: dynamical control of alpha rhythms in relation to focal attention. *Int. J. Psychophysiol.* 43, 25–40. doi: 10.1016/S0167-8760(01)00177-5
- Talairach, J., Bancaud, J., Szikla, G., Bonis, A., Geier, S., and Vedrenne, C. (1974). [New approach to the neurosurgery of epilepsy. Stereotaxic methodology and therapeutic results. 1. Introduction and history]. *Neurochirurgie* 20(Suppl. 1), 1–240.
- Velasco, A. L., Velasco, F., Jiménez, F., Velasco, M., Castro, G., Carrillo-Ruiz, J. D., et al. (2006). Neuromodulation of the centromedian thalamic nuclei in the treatment of generalized seizures and the improvement of the quality of life in patients with Lennox–Gastaut syndrome. *Epilepsia* 47, 1203–1212. doi: 10.1111/j.1528-1167.2006.00593.x
- Velasco, F., Velasco, A. L., Velasco, M., Jimenez, F., Carrillo-Ruiz, J. D., and Castro, G. (2007). Deep brain stimulation for treatment of the epilepsies: the centromedian thalamic target. *Acta Neurochir. Suppl.* 97, 337–342. doi: 10.1007/978-3-211-33081-4_38
- Velasco, F., Velasco, M., Velasco, A. L., Jimenez, F., Marquez, I., and Rise, M. (1995). Electrical stimulation of the centromedian thalamic nucleus in control of seizures: long-term studies. *Epilepsia* 36, 63–71. doi: 10.1111/j.1528-1157.1995.tb01667.x
- Velasco, M., Velasco, F., and Velasco, A. L. (2001). Centromedian-thalamic and hippocampal electrical stimulation for the control of intractable epileptic seizures. *J. Clin. Neurophysiol.* 18, 495–513. doi: 10.1097/00004691-200111000-00001
- Velasco, M., Velasco, F., Velasco, A. L., Brito, F., Jimenez, F., Marquez, I., et al. (1997). Electroconvulsive and behavioral responses produced by acute electrical stimulation of the human centromedian thalamic nucleus. *Electroencephalogr. Clin. Neurophysiol.* 102, 461–471. doi: 10.1016/S0013-4694(96)95203-0
- Velasco, M., Velasco, F., Velasco, A. L., Jimenez, F., Brito, F., and Marquez, I. (2000). Acute and chronic electrical stimulation of the centromedian thalamic nucleus: modulation of reticulo-cortical systems and predictor factors for generalized seizure control. *Arch. Med. Res.* 31, 304–315. doi: 10.1016/S0188-4409(00)00085-0
- Wendling, F. (2008). Computational models of epileptic activity: a bridge between observation and pathophysiological interpretation. *Expert Rev. Neurother.* 8, 889–896. doi: 10.1586/14737175.8.6.889
- Wendling, F., Bartolomei, F., Bellanger, J. J., and Chauvel, P. (2002). Epileptic fast activity can be explained by a model of impaired GABAergic dendritic inhibition. *Eur. J. Neurosci.* 15, 1499–1508. doi: 10.1046/j.1460-9568.2002.01985.x
- Wendling, F., Bartolomei, F., Mina, F., Huneau, C., and Benquet, P. (2012). Interictal spikes, fast ripples and seizures in partial epilepsies - combining multi-level computational models with experimental data. *Eur. J. Neurosci.* 36, 2164–2177. doi: 10.1111/j.1460-9568.2012.08039.x
- Wendling, F., Bellanger, J. J., Bartolomei, F., and Chauvel, P. (2000). Relevance of nonlinear lumped-parameter models in the analysis of depth-EEG epileptic signals. *Biol. Cybern.* 83, 367–378. doi: 10.1007/s004220000160
- Wilson, H. R., and Cowan, J. D. (1972). Excitatory and inhibitory interactions in localized populations of model neurons. *Biophys. J.* 12, 1–24. doi: 10.1016/S0006-3495(72)86068-5
- Wright, G. D., and Weller, R. O. (1983). Biopsy and post-mortem findings in a patient receiving cerebellar stimulation for epilepsy. *J. Neurol. Neurosurg. Psychiatr.* 46, 266–273. doi: 10.1136/jnnp.46.3.266
- Wright, J. J., Kydd, R. R., and Lees, G. J. (1985). State-changes in the brain viewed as linear steady-states and non-linear transitions between steady-states. *Biol. Cybern.* 53, 11–17. doi: 10.1007/BF00355686
- Zavaglia, M., Astolfi, L., Babiloni, F., and Ursino, M. (2006). A neural mass model for the simulation of cortical activity estimated from high resolution EEG during cognitive or motor tasks. *J. Neurosci. Methods* 157, 317–329. doi: 10.1016/j.jneumeth.2006.04.022

Conflict of Interest Statement: The authors declare that the research was conducted in the absence of any commercial or financial relationships that could be construed as a potential conflict of interest.

Received: 07 December 2012; paper pending published: 23 March 2013; accepted: 23 June 2013; published online: 16 July 2013.

Citation: Mina F, Benquet P, Pasicu A, Biraben A and Wendling F (2013) Modulation of epileptic activity by deep brain stimulation: a model-based study of frequency-dependent effects. *Front. Comput. Neurosci.* 7:94. doi: 10.3389/fncom.2013.00094

Copyright © 2013 Mina, Benquet, Pasicu, Biraben and Wendling. This is an open-access article distributed under the terms of the Creative Commons Attribution License, which permits use, distribution and reproduction in other forums, provided the original authors and source are credited and subject to any copyright notices concerning any third-party graphics etc.

Interictal spikes, fast ripples and seizures in partial epilepsies – combining multi-level computational models with experimental data

Fabrice Wendling,^{1,2} Fabrice Bartolomei,^{3,4} Faten Mina,^{1,2} Clément Huneau^{1,2} and Pascal Benquet^{1,2}

¹INSERM, U642, Rennes F-35000, France

²Université de Rennes 1, LTSI, Rennes F-35000, France

³INSERM, U751, Marseille, France

⁴AP-HM, Hôpital de la Timone, Service de Neurophysiologie Clinique, Marseille, France

Keywords: computational, epilepsy, fast ripples, interictal spikes, models, seizures

Abstract

Epileptic seizures, epileptic spikes and high-frequency oscillations (HFOs) are recognized as three electrophysiological markers of epileptogenic neuronal systems. It can be reasonably hypothesized that distinct (hyper)excitability mechanisms underlie these electrophysiological signatures. The question is ‘What are these mechanisms?’. Solving this difficult question would considerably help our understanding of epileptogenic processes and would also advance our interpretation of electrophysiological signals. In this paper, we show how computational models of brain epileptic activity can be used to address this issue. With a special emphasis on the hippocampal activity recorded in various experimental models (*in vivo* and *in vitro*) as well as in epileptic patients, we confront results and insights we can get from computational models lying at two different levels of description, namely macroscopic (neural mass) and microscopic (detailed network of neurons). At each level, we show how spikes, seizures and HFOs can (or cannot) be generated depending on the model features. The replication of observed signals, the prediction of possible mechanisms as well as their experimental validation are described and discussed; as are the advantages and limitations of the two modelling approaches.

Introduction

Drug-resistant partial epilepsies refer to a group of chronic neurological disorders that cannot be treated pharmacologically. By definition, partial epilepsies are characterized by recurrent seizures generated in a focal or multi-focal zone relatively well circumscribed in the brain and often referred to as the epileptogenic zone (EZ). From the clinical point of view, the accurate delineation of the EZ is the essential diagnostic step in prospect of surgery, which is, to date, the only therapeutic option that can lead to a total suppression of seizures.

In some specialized Epilepsy Surgery Units, a direct exploration of brain regions is performed using intracerebral (i.e. depth) electrodes [stereo-electroencephalogram (EEG) or depth-EEG recordings; Bancaud & Talairach, 1973]. This method has long been considered as the ‘gold standard’ for EZ identification. It provides data about both interictal and ictal brain activity with an excellent temporal resolution in the form of time series signals corresponding to local field potentials (LFPs) generated by explored regions.

Although the direct recording of LFPs from brain regions has dramatically advanced the assessment of the EZ, the demand is still high for diagnostic methods allowing for better interpretation of these signals, in terms of underlying pathophysiological mechanisms (Stefan *et al.*, 2006).

Generally speaking, three main types of electrophysiological events are observed in depth-EEG signals recorded from the epileptic brain,

namely seizures, spikes and high-frequency oscillations (HFOs). In partial epilepsies, seizures involving temporo-mesial and/or neocortical structures are most often characterized by a tonic onset phase (so-called rapid discharges) followed by a clonic phase marked by a highly rhythmic activity synchronized across vast and distant regions. Rapid discharges (classically in the upper beta and gamma bands of the EEG, i.e. 25–100 Hz) have long been considered as the hallmark of the EZ (Talairach & Bancaud, 1966; Fisher *et al.*, 1992; Wendling *et al.*, 2003; Bartolomei *et al.*, 2008). Epileptic spikes have also been recognized as potentially useful markers of epileptogenic areas as these transient paroxysmal events are being generated in very early stages in experimental models of epileptogenesis (White *et al.*, 2010) and are very often (if not always) observed during interictal periods in patients (review in Rodin *et al.*, 2009). However, the diagnostic value of epileptic spikes remains controversial as their relation to seizures is not elucidated yet (Hufnagel *et al.*, 2000; Asano *et al.*, 2003; Avoli *et al.*, 2006; Marsh *et al.*, 2010; Staley *et al.*, 2011). Finally, over the past decade, the significance of HFOs in epilepsy, especially fast ripples (FRs), has been a topic of increasing interest (recent review in Zijlmans *et al.*, 2011). FRs are transient low-amplitude fast oscillations (250–600 Hz) observed in signals recorded with intracerebral electrodes. Seminal studies reported the presence of FRs in experimental models of epilepsy (Bragin *et al.*, 1999b), as well as in the human epileptic brain (Bragin *et al.*, 1999a). FRs were also hypothesized as unique to brain areas capable of generating spontaneous seizures (Jacobs *et al.*, 2009), and their clinical value has been confirmed in recent papers (Jacobs *et al.*, 2010; Worrell & Gotman, 2011).

Correspondence: Dr F. Wendling, ¹INSERM, U642, as above.
E-mail: fabrice.wendling@univ-rennes1.fr

Received 5 December 2011, revised 9 January 2012, accepted 17 January 2012

In the light of results reported in aforementioned studies, one can reasonably assume that seizures, epileptic spikes and HFOs correspond to distinct mechanisms of (hyper)excitability within underlying neuronal networks that generate observed electrophysiological signals. The question is 'Which ones?'. Solving this difficult question would considerably help our understanding of epileptogenic processes and would also advance our interpretation of the above-mentioned electrophysiological signatures of these processes.

In this paper, we address this issue through the use of computational models of brain epileptic activity developed in our team. But our intent is to go beyond the simple review of models we introduced over the past 10 years. For the first time, we confront results and insights we got from such models lying at different levels of description, namely macro- and microscopic. At each level, we show how spikes, seizures and HFOs can (or cannot) be generated depending on the model features. With a special emphasis on the hippocampal activity, the replication of observed signals, the prediction of possible mechanisms and their experimental validation are described and discussed; as are the advantages and limitations of the two modelling approaches.

Materials and methods

Experimental data recorded from hippocampus

The objective of this section is to present the electrophysiological features of epileptic events under study (epileptic spikes, FRs and seizures). The events shown in this study were extracted from electrophysiological data collected in animal models (*in vivo*, *in vitro*) and in a patient with temporal lobe epilepsy (TLE), as described below.

In vivo data

Experiments were conducted on 80 ± 5 -day-old C57BL/6J (B6) male mice. All animal procedures were conducted in accordance with the European Communities Council Directive of 24 November 1986 (86/609/EEC). Mice were stereotaxically injected under general anaesthesia (chloral hydrate 400 mL/kg i.p.) with low dose of kainic acid (KA; 50 nL of a 20 mM solution in 0.9% NaCl) into the right dorsal hippocampus (anteroposterior = -2; mediolateral = -1.5; dorsoventral = -2 mm), with bregma as reference according to the Franklin & Paxinos atlas (Paxinos & Franklin, 2001). Control mice were injected with saline solution under the same protocol. After intrahippocampal injection, all mice were implanted with a bipolar electrode inserted into the injected hippocampus (anteroposterior = -2; mediolateral = -1.5; dorsoventral = -1.9 mm), and two monopolar surface electrodes were placed over the right frontoparietal cortex and over the cerebellum (reference electrode). LFPs were recorded on a video-EEG monitoring system (Deltamed™). Signals were sampled at 2048 Hz (16 bits). Upon completion of the experiments, histological analyses were performed to verify the location of the KA injection, the location of the hippocampal electrode and the pattern of neuronal loss/dispersion of dentate gyrus granule cells. This mouse model of TLE was previously described (Suzuki *et al.*, 1995) to reproduce histological characteristics similar to those found in hippocampal sclerosis described in human mesial TLE, such as cell loss, granule cell dispersion, astrogliosis and mossy fibre sprouting (Bouilleret *et al.*, 1999). Moreover, studies of epileptogenesis in this model revealed that sporadic epileptic spikes change as a function of time as the brain evolves towards the chronic epileptic state characterized by the repetition of spontaneous seizures (Huneau *et al.*, 2010).

Hippocampal organotypic slices

Hippocampal slice cultures were prepared from 6-day-old Wistar rats as described previously (Gahwiler *et al.*, 1997), following a protocol approved by the Veterinary Department of the Canton of Zurich. Briefly, hippocampi were dissected and transverse slices (375 μ m thick) were maintained on a glass coverslip in individual tubes filled with culture medium. Each tube was then placed in a roller drum in an incubator at 36 °C for 2 weeks. After 2–3 weeks *in vitro* slices were transferred to a recording chamber on an upright microscope (Axioscope FS, Zeiss, Oberkochen, Germany). Hippocampal slice cultures are a particularly valuable *in vitro* model to study some cellular mechanisms of epilepsy. Because of the inevitable damaging of axons during the preparation of acute brain slices (*ex vivo*), many projection pathways are kept more intact in cultured slices as compared with *ex vivo* slices. Indeed, during the preparation of brain slice culture, the density of synapses first decreases just after the brain cut, but then synaptic structures gradually redevelop (*in situ* synaptogenesis). Therefore, the degree of connectivity between neurons in culture increases with time. It is more prominent than that of acute brain slices and it was shown to be closer to the *in vivo* situation (Gahwiler *et al.*, 1997). The hippocampal circuitry within these cultures is well preserved and is able to support synchronized network activity. The cellular network develops in such a way that synaptic inhibition and excitation are balanced appropriately (Thompson *et al.*, 2005). Thus, the high degree of interneuronal and pyramidal connectivity in organotypic slice cultures, and the spontaneous synaptic activity, facilitate the induction of epileptic activity. Indeed, applications of convulsivants, including bicuculline, picrotoxin, tetraethylammonium, or low Mg^{2+} - or high K^{+} -containing saline, can trigger both interictal and ictal-like burst discharges that are synchronized throughout large cell populations (Scanziani *et al.*, 1994). These bursts appear essentially identical to those evoked *in vivo* or in acutely prepared hippocampal slices (Thompson *et al.*, 2005).

Both intracellular and extracellular recordings were performed to measure interictal- and ictal-like activity in organotypic slices. Intracellular activity of CA1 pyramidal neurons was recorded in the whole cell configuration of the patch-clamp technique. Recording pipettes (3–6 M Ω) were filled with an intracellular solution containing the following (in mM): K-gluconate, 135; KCl, 4; HEPES, 10; Na₂-phosphocreatine, 10; Mg-ATP, 4; Na-GTP, 0.3; pH 7.2, 291–293 mOsm. Simultaneous field recordings were obtained with an extracellular electrode [glass pipette filled with normal artificial cerebrospinal fluid (ACSF), 1 M Ω] positioned in CA1 stratum radiatum. The field recording pipette was placed into the same area as the patch-clamp pipette (4–6 M Ω). Current-clamp mode was used and signals were amplified with an Axopatch 200B amplifier (Axon Instruments, Foster City, CA, USA), filtered at 2 kHz, stored and visualized with pClamp9 software (Axon Instruments). Signals were analogue-filtered at 10 kHz and sampled at 100–300 kHz. Stimulation (100 μ s, 10–40 μ A, every 10 s) was applied with a glass pipette filled with ACSF placed in CA3 pyramidal layer. When requested, recordings were performed continuously in gap-free mode in order to obtain an entire period of spontaneous ictal- and interictal-like activity. Slices were superfused continuously at a rate of 1–2 mL/min with normal ACSF equilibrated with 95% O₂/5% CO₂ containing (in mM): NaCl, 124; KCl, 2.5; NaHCO₃, 26; NaH₂PO₄, 1.25; glucose, 10; CaCl₂, 3; MgCl₂, 2; pH 7.4, at a bath temperature of 34 °C.

Guinea-pig-isolated brain preparation

For the purpose of this study, we used data recorded from an isolated brain preparation that is an acute model of temporal lobe ictogenesis

(courtesy of Dr M. de Curtis, Istituto Neurologico Carlo Besta, Milan, Italy). Brains of Hartley guinea-pigs (150–200 g; Charles River, Calco, Italy) were isolated and maintained *in vitro* according to the standard procedure described elsewhere (Muhlethaler *et al.*, 1993; Avoli *et al.*, 2006). In brief, animals were anaesthetized with sodium tiopental (125 mg/kg *i.p.*, Farmotal; Pharmacia) and transcardially perfused with a cold (4–10 °C) oxygenated (95% O₂, 5% CO₂) complex saline solution composed of (in mM): NaCl, 126; KCl, 3; KH₂PO₄, 1.2; MgSO₄, 1.3; CaCl₂, 2.4; NaHCO₃, 26; glucose, 15; HEPES, 2.1; 3% dextran M.W. 70 000 (pH 7.1). Brains were rapidly dissected out and transferred in the recording chamber where they were perfused through the basilar artery with the same solution (5.5 mL/min, pH 7.3, 15 °C). The experiments were performed at 32 °C after gradually raising the temperature by steps of 0.2 °C/min. Extracellular recordings were performed in the hippocampus (CA1 region) with 16-channels silicon probes (100 µm contact separation; CNCT, University of Michigan, Ann Arbor, MI, USA). Probes were inserted in the tissue as perpendicular as possible to the lamination of the structure according to a guinea-pig stereotaxic atlas. At the end of the electrophysiological experiments, electrolytic lesions were made by passing a 30 µA current for 30 s between the two deepest contacts of the silicon probes. Brains were then fixed and cut with a vibratome in 75–100-µm-thick coronal sections to verify the position of the electrodes. The experimental protocol was reviewed and approved by the Committee on Animal Care and Use, and by Ethics Committee of the Istituto Nazionale Neurologico.

Clinical data

The intracerebral stereo-EEG recording used in this study was performed in a patient with mesial TLE. For simplicity, only signals recorded from contacts located in the hippocampus (Amon's horn) are shown and analysed in the present study. It is worth mentioning that these signals are very representative of those recorded from the hippocampus in mesial TLE. Signals were recorded on a 128-channel Deltamed™ system and were sampled at 1024 Hz. The positioning of electrodes was determined from available non-invasive information and hypotheses about the localization of the patient's EZ. Implantation accuracy was per-operatively controlled by telemetric X-ray imaging. A post-operative computer tomography (CT) scan without contrast product was used to verify both the absence of bleeding and the precise 3D location of electrode contacts. After stereo-EEG exploration, intracerebral electrodes were removed, and magnetic resonance imaging (MRI) was performed on which the trajectory of each electrode remained visible. Finally, a CT-scan/MRI data fusion was performed to anatomically locate each contact along each electrode trajectory. The stereo-EEG exploration was carried out as part of normal clinical care of the patient who gave informed consent about the use of data for research purposes.

Electrophysiological features of epileptic spikes, FRs and seizures

Sporadic epileptic spikes could be observed in the above-described experimental models (*in vivo* and *in vitro*), as well as in depth-EEG signals recorded from a patient with mesial TLE. Typical examples are shown in Fig. 1A. As depicted (first three boxes), these spikes recorded from the hippocampus have common morphological features. Their onset is characterized by an initial fast component (the spike) followed by a slow negative (w.r.t. baseline) wave. The duration (from onset to baseline return) is of the same order of

magnitude (about one or two hundreds of ms) in the three considered situations (mouse *in vivo*, rat *in vitro* and human). As described in the Results, we could reproduce the spike shape, both in the lumped-parameter and in the detailed model of the hippocampus (Fig. 1A, fourth and fifth box), which are both presented in the next section.

FRs were also observed in real data (experimental and clinical), as shown in Fig. 1B. As revealed by time–frequency representations (spectrograms in Fig. 1B), FRs are transient events characterized by low-amplitude HFOs occurring in a frequency sub-band ranging from 250 to 600 Hz (approximately). Some similarities could also be found across experimentally or clinically recorded FRs, but to a lesser extent than epileptic spikes, which really have a stereotyped shape. In particular, their duration is about a few tens of ms. As also described in the Results, we recently managed to simulate FRs in a detailed model of hippocampal activity (presented in the next section). Interestingly, such a simulation could not be obtained when the lumped-parameter modelling approach was followed.

Finally, electrophysiological signals recorded during the transition from interictal to ictal activity in experimental models of epilepsy and in the considered patient are displayed in Fig. 2. As depicted, the general time-course of electrophysiological signals recorded in human (Fig. 2A), in the epileptic freely-moving mouse (Fig. 2B) and in the isolated guinea-pig brain (Fig. 2C) is quite reproducible. Indeed, these signals are very typical of those recorded in mesial TLE, particularly from the hippocampus. Usually, interictal and preictal spikes are observed before the onset of the seizure marked by the appearance of higher frequency oscillations (20–30 Hz), which persist for a few seconds (typically 5–10 s). This early tonic phase of the seizure is then followed by a clonic phase characterized by the appearance of a slower and very rhythmic activity (5–10 Hz) of larger amplitude. So far, as illustrated in Fig. 2D, we could reproduce the above-described features in the lumped-parameter model (described in the next section). Finally, Fig. 2E provides time–frequency representations focused on the onset of seizures for clinical, experimental and simulated data. As observed, the fast-onset activity is always present (white arrows in spectrograms), its duration is reduced in the mouse (about 1 s).

Computational models

Computational neuroscience is an interdisciplinary field of research at the interface of neurophysiology, neurobiology, mathematics and physics. In the field of epilepsy, computational modelling approaches are considerably developed, and models are more and more accepted by clinicians and research scientists as they provide an efficient way to gather information into manageable representations of neuronal systems, to articulate knowledge and to bridge between disciplines (Lytton, 2008; Soltesz & Staley, 2008; Wendling, 2008). Models are also recognized as efficient tools for tackling the complexity of epileptic phenomena as they can account for the many non-linear mechanisms taking place at multiple levels in neuronal systems, from sub-cellular to organ levels. Over the past three decades, two computational modelling approaches have been developing, either at the lumped (neural mass) or detailed (network of neurons) level. Readers may refer to Suffczynski *et al.* (2006), Deco *et al.* (2008), Ullah & Schiff (2009) and Coombes (2010) for background and details about the concepts that led to both modelling approaches. In brief, the central issue is the scale at which the neuronal population is considered. According to the lumped-parameter approach (macroscopic level), which stems from the pioneering work of Wilson & Cowan (1972), Freeman (1973) and Lopes da Silva *et al.* (1974), the

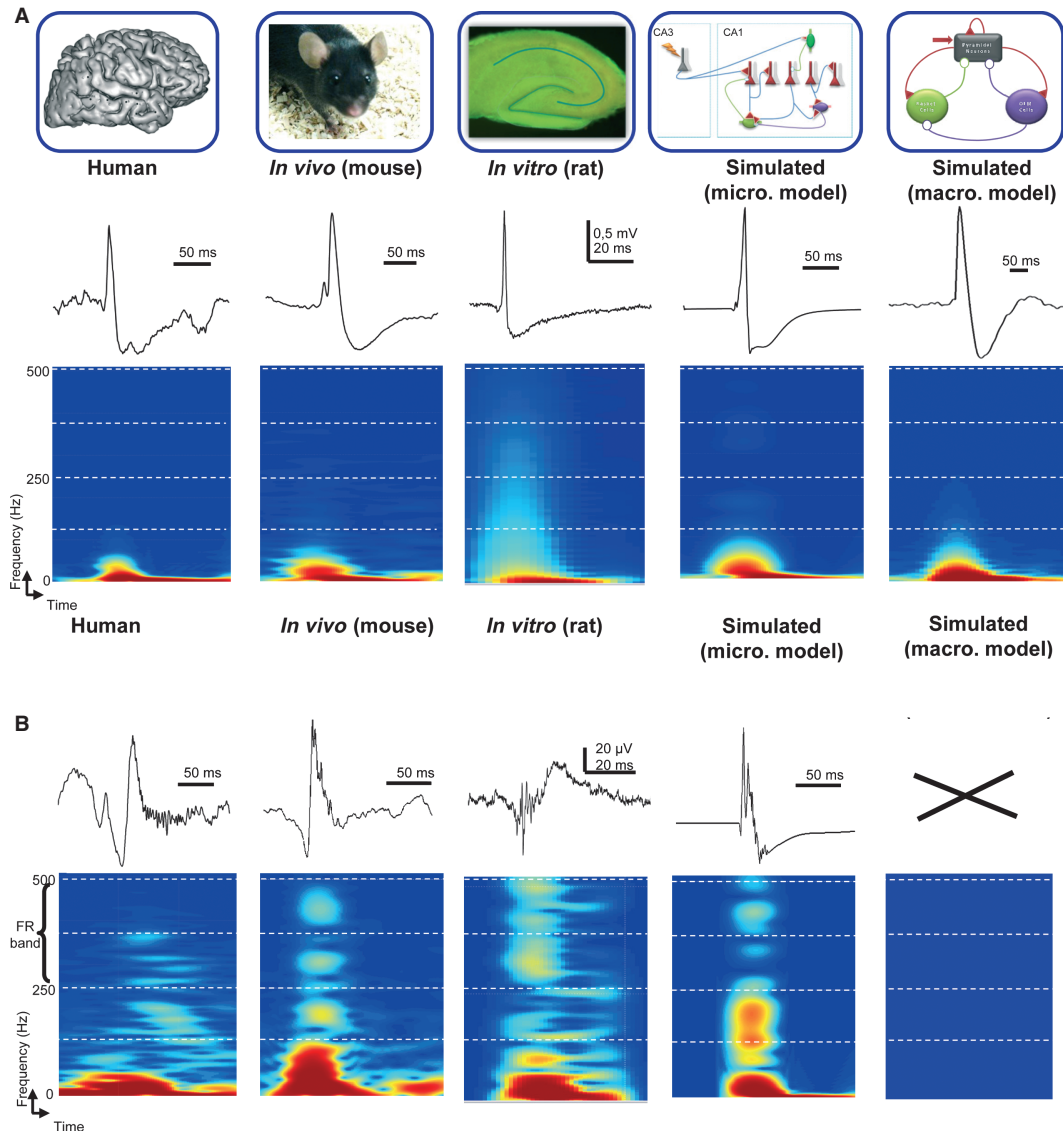


FIG. 1. Epileptic spikes and fast ripples (FRs). (A) Human (hippocampus), *in vivo* (mouse, hippocampus) and *in vitro* (rat organotypic hippocampal slice) interictal spikes recorded with extracellular electrodes. Simulated LFPs generated from microscopic (cellular level) and macroscopic (neuronal population level) computational models of the hippocampal CA1 subfield. (B) Human (hippocampus), *in vivo* (mouse, hippocampus) and *in vitro* (rat organotypic hippocampal slice) FRs recorded with extracellular electrodes. Simulated LFPs generated by the macroscopic model. Colour-coded maps are time–frequency representations (spectrograms) of corresponding signals. Hot (respectively, cold) colours correspond to the presence (respectively, absence) of signal energy at a given time (X -axis) and frequency (Y -axis) point in the time–frequency plane.

neuronal population is assumed to be composed of sub-populations of cells (typically main cells and interneurons) interacting through synaptic transmission. This approach aims at describing the ‘average activity’ of the population without explicit representation of signals generated at the cellular level [typically action potentials (APs) and single postsynaptic potentials (PSPs)]. This is why the two relevant variables in lumped-parameter models are: (i) the average density of APs (i.e. firing rate); and (ii) the average PSPs (either excitatory or inhibitory) generated at the level of each sub-population included in the whole population. Conversely, the detailed approach starts from a finer description of neurons that are then interconnected via synapses or gap junctions to form networks. This description accounts for the active and passive properties of the excitable membrane of neurons. It can be either simple (one compartment) or more sophisticated (i.e. multi-compartmental) if dendrites, soma and axons are to be accurately represented, for instance. Most of the detailed models are

still based on Hodgkin & Huxley, (1952) mathematical equations governing transmembrane currents via voltage-dependent ion channels (Hodgkin *et al.*, 1952). In the field of epilepsy, the detailed approach started with Traub’s work (Traub, 1979) and progressively developed, partly helped by the tremendous increase in computer performance (computing time and memory) since the 1980s.

A lumped-parameter model of the hippocampal CA1 circuit

Following the lumped-parameter approach, we developed a model for the hippocampal CA1 subfield. Readers may refer to Wendling *et al.* (2002, 2005) for details. Briefly, the neuronal population of CA1 is assumed to consist of three sub-populations of neurons corresponding to main (pyramidal) cells and to two types of local inhibitory interneurons [oriens-lacunosum moleculare (OLM) and basket cells] projecting to either the peri-dendritic or the peri-somatic region of

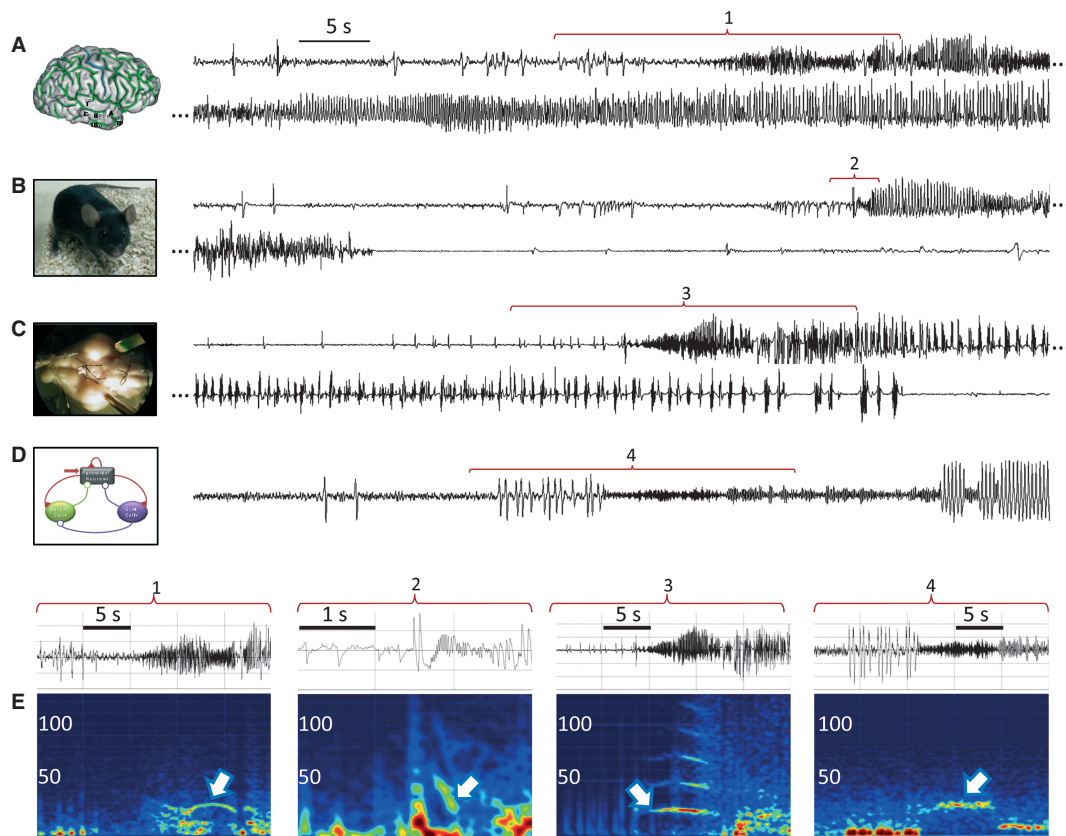


FIG. 2. Electrophysiological signals recorded during the interictal to ictal transition. (A) Depth-EEG signal recorded from the hippocampus in a patient with TLE. (B) LFP recorded in a freely-moving chronic epileptic mouse with micro-electrodes implanted in the hippocampus, 4 weeks after the KA injection. (C) LFP recorded with intra-hippocampal electrode in an isolated brain preparation (guinea-pig) after transient arterial perfusion of bicuculline. (D) LFP simulated with the macroscopic model when inhibition-related parameter is gradually decreased as a function of time. Total durations of signals shown in (A), (B) and (C) is 120 s. Duration of signal (D) is 60 s. (E) Time–frequency diagrams focusing on the fast-onset activity (tonic phase of the seizure) for upper signals.

pyramidal cells, as described in White *et al.* (2000) and Cossart *et al.* (2001). An inhibitory connection from OLM to basket cells is also represented in the model (White *et al.*, 2000), as depicted in the schematic diagram provided in Fig. 3A. Input to interneurons is excitatory (glutamate receptor mediated). Feedback to pyramidal cells is either excitatory (glutamate receptor mediated) or inhibitory [γ -aminobutyric acid (GABA) receptor mediated]. Slow ($\text{GABA}_{A,\text{slow}}$) and fast ($\text{GABA}_{A,\text{fast}}$) kinetics are associated to inhibitory PSPs depending on the location of GABA receptors, either in the peridendritic or peri-somatic region of pyramidal cells (Banks *et al.*, 2000; Klausberger & Somogyi, 2008). In each sub-population, the mean membrane potential is converted into an average pulse density of potentials fired by the neurons using a static non-linear function (asymmetric sigmoid curve), referred to as the ‘wave-to-pulse’ function. Conversely, the average pulse density of afferent APs is changed into an average inhibitory or excitatory postsynaptic membrane potential using a linear dynamic transfer function. The impulse response of this ‘pulse-to-wave’ function was shown to approximate that of actual PSPs (van Rotterdam *et al.*, 1982). In the model, these ‘pulse-to-wave’ functions introduce the three main parameters that, respectively, correspond to the amplitude of average (i) excitatory PSPs (EXC); (ii) slow dendritic inhibitory PSPs (SDI); and (iii) fast somatic inhibitory PSPs (FSI). Besides, the model also accounts for the average number of synaptic connections among the three sub-populations. Finally, the model output corresponds to the summation of these average PSPs on pyramidal cells, which is assumed to be the principal contribution to LFPs. A block diagram of the model as well

as the value and the meaning of each model parameter are provided in (Wendling & Chauvel, 2008; see fig. 23.12 and table 23.3).

A detailed model of the hippocampal CA1 network

More recently and following the detailed approach, we developed a neuronal network model for the hippocampal CA1 subfield (Demont-Guignard *et al.*, 2009). We started by developing a two-compartment ‘reduced’ model of the CA1 pyramidal cell in line with Pinsky & Rinzel, (1994) work on CA3 cells. This single neuron model is minimal but still biologically inspired. The objective was to find a good compromise between physiological relevance and computing time. Based on the Hodgkin & Huxley, (1952) formalism (Hodgkin *et al.*, 1952), the model entails distinct somatic and dendritic membrane properties. Transmembrane currents were selected based on a review of the literature. A validation was performed using intracellular data recorded in an experimental model (organotypic rat hippocampal slices). A schematic diagram of the neuron model is shown in Fig. 3B. In brief, the shape of the AP is mainly controlled by voltage-dependent sodium, potassium and calcium currents (I_{Na} , I_{KDR} , I_{Ca} , low and high threshold). In addition, to replicate physiological firing rates potassium channels activated by intracellular calcium ions were added (after-hyperpolarization current I_{AHP}). Similarly, we also included a rapidly inactivated potassium current (I_{KA} , dendritic compartment; Hoffman *et al.*, 1997; to reproduce the change of density of ion channels along the membrane) in consideration of its potential role in epileptiform activity, as well as a hyperpolarization-

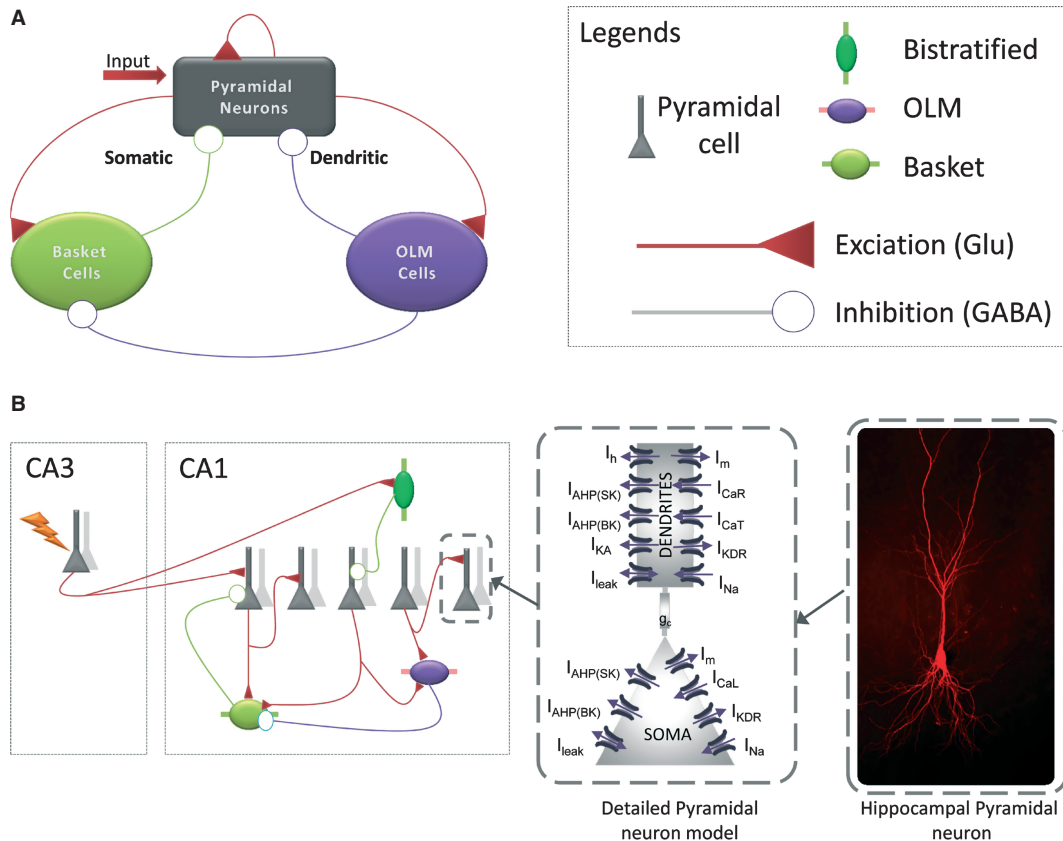


FIG. 3. Computational models intended to reproduce the hippocampal activity (CA1 subfield). (A) Lumped-parameter model of CA1. The neuronal population was assumed to consist of three sub-populations of neurons corresponding to main (pyramidal) cells and to two types of local inhibitory interneurons [oriens-lacunosum moleculare (OLM) and basket cells] projecting to either the peri-dendritic or the peri-somatic region of pyramidal cells. Input to interneurons is excitatory (Glutamatergic). Feedback to pyramidal cells is either excitatory (Glutamatergic) or inhibitory (GABAergic). Slow ($GABA_{A,slow}$) and fast ($GABA_{A,fast}$) kinetics are associated to IPSPs depending on the location of GABA receptors, either in the peri-dendritic or peri-somatic region of pyramidal cells. (B) Detailed model in which each cell is explicitly represented (CA1 pyramidal cell – two-compartment model; OLM, bistratified basket cells – one-compartment model). The CA1 pyramidal cell was created based on a precise selection of distinct types of dendritic and somatic ionic channels, according to the literature. Physiological properties of ionic channels such as kinetic of activation and inactivation, voltage dependence and reversal potential were respected. Single neuron models are synaptically (AMPA-, NMDA- and GABA-ergic synapses) interconnected into network (about 800 neurons and 200 interneurons). To mimic the excitatory input from CA3 to CA1, the network model was stimulated with an afferent volley of APs coming from an ‘external array of cells’. GABA, γ -aminobutyric acid; Glu, Glutamatergic.

activated cationic current (I_h , dendrite compartment; Mayer & Westbrook, 1983) and a muscarinic potassium current (I_m ; Lancaster & Adams, 1986; Lancaster & Nicoll, 1987). Regarding basket and OLM interneurons, we implemented single-compartment models published in the literature (Hajos *et al.*, 2004). Single neuron and interneuron models were interconnected via glutamatergic [α -amino-3-hydroxy-5-methyl-4-isoxazolepropionic acid (AMPA) and *N*-methyl-D-aspartate (NMDA)] and GABAergic synapses in accordance with commonly accepted assumptions about location of synapses and receptors (somatic vs. dendritic) and connectivity patterns in CA1 (Andersen *et al.*, 2007). Finally, the network model is stimulated with an afferent volley of APs coming from an ‘external array of cells’ (Fig. 3B). The objective was to mimic the excitatory input from CA3 to CA1. In practice, this stimulation of the CA1 network depends on two parameters: (i) the number of cells, randomly and uniformly selected in CA1, that are contacted by axons firing APs; and (ii) the value of the delay between these APs that follows a Gaussian distribution with mean and standard deviation allowing for adjusting the synchronicity of APs.

Regarding the model output, we used the dipole theory for computing the LFP generated by the network. According to this theory, field signals due to individual neurons and recorded at a distance from the electrode are proportional to the magnitude of the

net intracellular current dipole in each contributing cell (Geselowitz, 1967; Murakami & Okada, 2006). To proceed, we made three assumptions. First, the main contribution to the LFP comes from pyramidal cells due to their spatial arrangement ‘in palisades’. Second, each pyramidal cell is considered as a point source (current dipole formed by a sink and a source) positioned within a volume conductor characterized by a homogeneous conductivity. Third, according to the superposition theorem, the contributions of all pyramidal cells sum up instantaneously at the level of the extracellular recording electrode, placed at the centre of the modelled network. For each cell, this contribution depends on the cell–electrode distance as well as the associated dipole moment and orientation.

Lumped-parameter and the detailed model of the hippocampal CA1 network – implementation details

For the macroscopic model, equations are provided in previously published papers (Wendling *et al.*, 2002, 2005). A didactic presentation of this class of models can also be found in a book chapter (Wendling & Chauvel, 2008). In addition, the source code can be downloaded from the Yale Model Database (<http://senselab.med.yale.edu/modeldb/showmodel.asp?model=97983>). For the micro-

scopic model, equations are fully described in the 2-pp. appendix published in Demont-Guignard *et al.* (2009).

Results

A first requirement in the development of models is to reproduce the observed phenomena, typically an extracellular activity that closely resembles that actually recorded. In the case of epileptic spikes, the 'close resemblance' means that the simulated events should have the same morphological features (sharpness and the spike, duration of the negative wave, in particular) as real spikes. For FRs, simulated signals should contain oscillations occurring in the 'correct' (i.e. actually observed) frequency band (250–600 Hz). For seizures, models should reproduce the fast-onset activity observed during the initial tonic phase as well as the slower activity recorded during the clonic phase. A second requirement is that model parameters for which a more or less accurate replication of actual signals is obtained should stay in 'physiological' ranges of values. But, this capability to replicate observations is not sufficient to guarantee that the mechanisms embedded in the model are those actually occurring in real neuronal systems. In Marder's group (Taylor *et al.*, 2009), it has been recently shown that about 1300 different configurations of a four-compartment computational model (out of ~600 000) were able to well approximate the electrophysiological properties of a biological neuron, as simple as the lateral pyloric (LP) neuron of the stomatogastric ganglion of decapod crustaceans. Thus, mimicking and replicating the interictal or ictal-like activity of an epileptic neuronal network by computational modelling is not sufficient. In all cases, further model validation is also required. This validation can be obtained by translating model predictions into experimentally testable hypotheses and, of course, by performing the tests. At least some of the predictions of the computational model have to be experimentally tested and validated.

In the following sections, we report the results we could get from the above-described models in terms of generating spikes, FRs or seizures. Then, we show examples for which some experimental validation of model-based assumptions on underlying mechanisms could be obtained.

Model predictions

Lumped-parameter approach

As mentioned in the Materials and methods, the macroscopic model is characterized by three main parameters related to synaptic transmission: (i) average EXC; (ii) average SDI; and (iii) average FSI. We conducted a parameter sensitivity analysis in the 3D-space defined by (EXC, SDI, FSI), as reported in Wendling *et al.* (2002). The basic procedure is: (i) to perform exhaustive simulations when the three parameters vary over physiological ranges of values step-by-step; and (ii) to classify segments of simulated activity obtained for each triplet based on spectral features. Six different classes were found: background activity; sporadic spikes; rhythmic spikes; fast-onset activity; ictal-like activity (alpha range); and ictal-like activity (theta range). This procedure allowed us to map the activity generated by the model into the 3D-space corresponding to excitation- and inhibition-related parameters.

Results showed that the model (Fig. 3A) was able to generate transient events that closely resemble those recorded either in the human hippocampus or in animal models (*in vivo* and *in vitro*), as shown in fifth column of Figs 1A and 4B. The simulated epileptic spike is composed of a first and relatively sharp peak of positive

polarity (w.r.t. baseline) followed by a slower wave of negative polarity. It was obtained under two conditions – parameter EXC must be increased and parameter SDI must be decreased, indicating that epileptic spikes occur in the model for: (i) increased collateral excitation among pyramidal neurons and increased excitatory drive onto interneurons; and (ii) decreased inhibitory drive onto pyramidal neurons from dendritic-projecting interneurons [slow GABA_A receptor-mediated inhibitory postsynaptic potentials (IPSPs)]. The model was also found to generate a fast activity (about 25 Hz; Fig. 4C), mimicking that observed at the onset of seizure in the hippocampus, either in patients or in animal models of TLE (Fig. 2). This fast-onset activity could be obtained when parameter SDI was decreased again, to a large extent. As illustrated in Fig. 4C, this important drop of parameter SDI led to a situation where: (i) somatic-projecting projecting interneurons (producing fast GABA_A receptor-mediated IPSPs) were not inhibited anymore; and (ii) they still received excitatory drive from pyramidal cells. Finally, a clonic ictal-like activity could also be reproduced when a slight re-increase of parameter SDI occurred in the model whilst parameter FSI decreased. Two types of ictal-like activity could be simulated with a dominant frequency either about 10 Hz or about 5 Hz (Fig. 4D). A strong resemblance with the actual clonic activity recorded in the hippocampus was noticed (see Fig. 4D vs. Fig. 2). Interestingly, we were not able to produce very HFOs in this lumped-parameter model, typically beyond the gamma frequency (> 80 Hz). Some fast oscillations could be produced by modifying the rise and decay times of average PSPs but to unrealistic values, i.e. much lower than those characterizing actual glutamatergic or GABAergic PSPs. This result suggests that the simulation of FRs is impossible to achieve in our model under the constraint that physiological values for time-related parameters (rise and decay time values of PSPs) are respected.

Detailed approach

As mentioned in the Materials and methods, we built our own CA1 pyramidal cell model, after an accurate selection of dendritic and somatic ionic currents (and associated conductances) from the literature. This single pyramidal neuron model was evaluated by comparing the simulated intracellular activity with real intracellular activity recorded from pyramidal cells in the *in vitro* model. Taking advantage of the abundant literature about the neurophysiological properties of CA1 pyramidal cells, we tried to respect as much as possible some of the physiological properties of ionic channels, such as the kinetics of activation and inactivation, the voltage dependence and the reversal potentials. This single cell model, although reduced to two compartments, and extremely simplified compared with a real neuron, was found to generate fairly realistic signals, as reported in Demont-Guignard *et al.* (2009). Qualitatively, our CA1 pyramidal cell model is able to reproduce basic electrophysiological properties of real CA1 pyramidal cells, such as AP shape and threshold, spike rate adaptation upon depolarizing current, sag plus rebound upon hyperpolarization, an increase in spiking rate upon I_{KA} inhibition (Demont-Guignard *et al.*, 2009). The CA1 network was built by connecting these CA1 pyramidal cells in accordance with commonly accepted assumptions about connectivity patterns (location of synapses and receptors, synaptic strength, inter-cell distances). The percentage of pyramidal cells was set at 80%, that of interneurons at 20%, as *in vivo* (Andersen *et al.*, 2007). Two main differences between detailed and lumped models have to be pointed out: (i) the detailed model allows for topological repartition of individual pyramidal cells and for possible asynchrony in the activity of simulated neurons; (ii) the detailed model can simultaneously simulate both the extracellular LFP

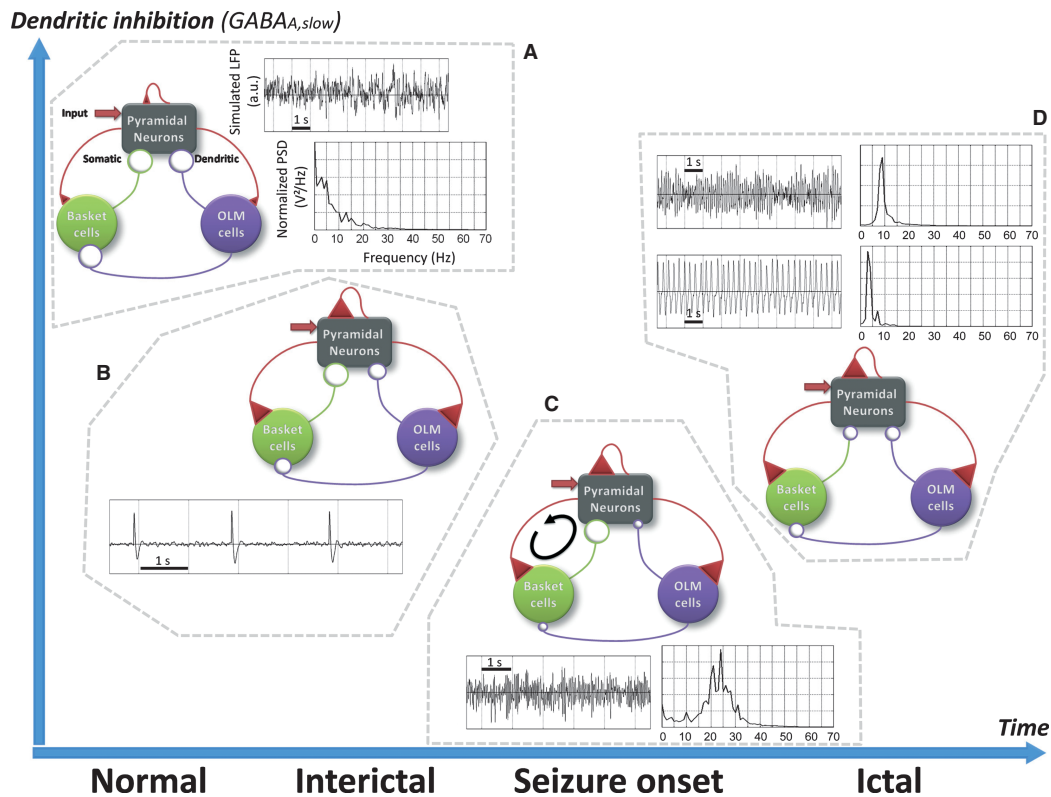


FIG. 4. Macropscopic (lumped-parameter) model. Simulation of the transition from interictal to ictal activity. For increased excitation (amplitude of average EPSPs) and gradual decrease of inhibition (amplitude of average IPSPs), dramatic changes are observed in simulated local field potentials (LFPs). (A) Background activity. (B) Sporadic spikes. (C) Fast-onset activity. (D) Rhythmic ictal activity. GABA, γ -aminobutyric acid; OLM, oriens-lacunosum moleculare; PSD, power spectral density.

and the intracellular activity of virtually thousands of individual cells. Thanks to these two properties, we have found that FRs are generated by small clusters of hyperexcitable and slightly asynchronous bursting pyramidal cells surrounded by hyperpolarized neurons, as shown in Fig. 5B. The origin of the hyperexcitability was due to a moderate increase of glutamatergic conductances (AMPA and NMDA), to a slight decrease of conductances associated with GABAergic currents, and to a shift of the GABA reversal potential toward more depolarized values (Demont-Guignard *et al.*, 2011). The low number of hyperexcitable neurons, the degree of synchronicity and the network topology (clustered) was found to be critical to produce FRs about 250 Hz and up to 500 Hz. The model was also able to reproduce epileptic spikes relatively similar to human or animal epileptic spikes (Fig. 1), again not spontaneously but for a physiologically relevant stimulation mimicking the input from CA3 to CA1, reminding the 'CA3-driven interictal activity' (Avoli *et al.*, 2002). The model could generate epileptic spikes for a sufficiently large subset (i.e. > 30% of the total number of cells) of quasi-synchronously firing CA1 pyramidal cells. To produce realistic epileptic spikes the reversal potential for GABA_A receptor has also been modified to more depolarized values in some pyramidal cells (Demont-Guignard *et al.*, 2011).

Overall, the number and spatial distribution of involved pyramidal cells, their degree of excitability and level of synchronization are critical factors that strongly modify the morphology of the induced epileptic event that reflects in the LFP (Fig. 5). Interestingly, as previously reported (Demont-Guignard *et al.*, 2011), a continuum between 'normal' population spike, FR and epileptic spike could be found depending on synaptic transmission parameters. For increase of the AMPA and NMDA conductances and decrease of the GABA conductance, simulated events progressively shifted from normal

population spikes to FRs, from FRs to interictal epileptic spikes (IESs), and then from IESs to ictal-like activity (not shown). As presented in the next section, this model prediction could be verified experimentally.

Model validation

Lumped-parameter approach

An interesting prediction of the lumped-parameter model is related to the generation of a fast activity that satisfactorily approximates that observed at the onset of seizures in TLE (human data), in an experimental model of TLE and in an experimental model of temporal lobe ictogenesis (guinea-pig), as illustrated in Fig. 2. In the computational model, this fast activity is obtained when: (i) dendritic-projecting interneurons do not generate slow IPSPs (GABA_A receptor-mediated) anymore; and (ii) somatic-projecting interneurons still receive some excitatory drive from pyramidal cells and, in turn, generate fast IPSPs (GABA_A receptor-mediated) onto pyramidal cells. In other words, and as already reported in Wendling *et al.* (2002), the model predicts: (i) a crucial role of inhibitory networks during the transition to seizures in the hippocampus; and (ii) a prominent contribution of the fast inhibitory feedback loop in the generation of high-beta, low-gamma (20–30 Hz) activity, as quantified in the simulated LFP. To some extent, an experimental validation of these modelling results was recently brought by M. de Curtis and colleagues (Gnatkovsky *et al.*, 2008), although these authors focused on the entorhinal cortex (EC), which is also a limbic structure frequently involved in human TLE (Molae-Ardekani *et al.*, 2010a). The objective of these authors was to analyse the cellular and network mechanisms underlying the gener-

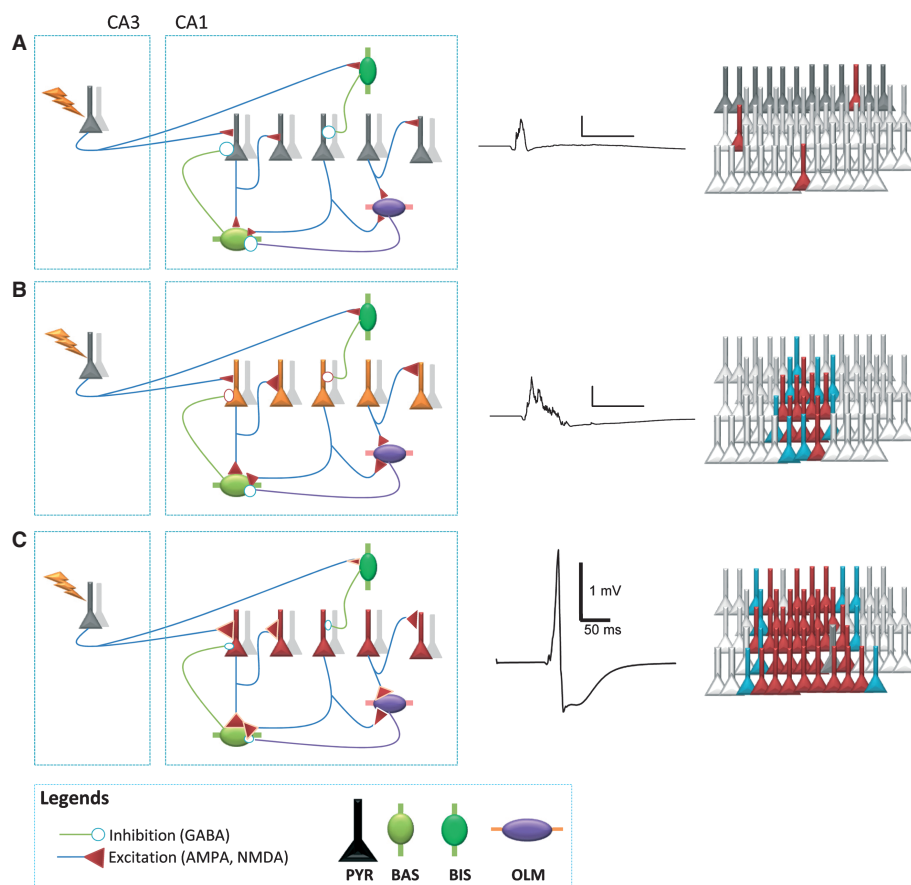


FIG. 5. Microscopic (detailed) model. The number and spatial distribution of involved pyramidal cells, their degree of excitability and the network synchronization are critical factors that strongly modify the morphology of epileptic events induced in the LFP. (A) Field EPSP simulated for 'normal' conditions. (B) FR simulated for altered excitability conditions (small cluster of hyperexcitable pyramidal cells, slightly increased excitation and slightly decreased inhibition). (C) Epileptic spike simulated for another alteration of excitability conditions (large cluster of hyperexcitable pyramidal cells, markedly increased excitation and decreased inhibition). AMPA, α -amino-3-hydroxy-5-methyl-4-isoxazolepropionic acid; BAS, basket cell; BIS, bistratified cell; GABA, γ -aminobutyric acid; NMDA, *N*-methyl-D-aspartate; OLM, oriens-lacunosum moleculare; PYR, pyramidal cell.

ation of 20–30 Hz oscillations recorded at the onset of TLE seizures. First, the *in vitro* isolated guinea-pig brain, they could reproduce such a pattern in the EC that is quite similar to that observed in the hippocampus (see example in Fig. 2C and E), i.e. a narrow band activity characterized by a dominant frequency at about 25 Hz. During the transition to seizure induced by a transient arterial perfusion of bicuculline, they performed simultaneous intracellular and extracellular electrophysiological recordings in the EC (deep and superficial layers). As a major result, they observed that principal neurons did not generate APs during the fast-onset activity observed in the LFP, whilst a sustained firing could be revealed in non-principal neurons that were likely to be interneurons (so-called 'putative' interneurons). In addition, during the fast activity, they could detect some rhythmic oscillations in the membrane potential of principal neurons. Results strongly suggested that these oscillations were due to rhythmic IPSPs that progressively decreased in amplitude as the fast-onset activity progressively changed into the slower clonic activity. Coming back to the lumped-parameter model, we analysed the firing rates of the sub-populations of neurons during the simulated transition from interictal to ictal activity obtained for gradual variation of the SDI parameter, as described in the Results. Very interestingly, the model showed that the average firing rate at the pyramidal cell sub-population increased during preictal spikes, dramatically decreased during the fast activity before increasing again as the ictal clonic activity started. It is also

worth mention that a strong increase of the average firing rate of the sub-population of interneurons (producing fast IPSPs onto pyramidal cells) was generated by the model (Fig. 6), corroborating the above-described experimental observations.

Detailed approach

As mentioned in the Materials and methods, we used rat organotypic hippocampal slices to perform experimental validation because they offer a number of advantages, among which the preserved connectivity of both excitatory and inhibitory neurons. In these slices, depending on experimental procedure, we could produce normal field potentials, epileptic spikes, FRs or ictal-like activity. For example, application of 4-AP (100 μ M) produced both interictal and ictal-like activity in 98% of the slices ($n = 34$, data not shown), as already observed in Albus *et al.* (2008). Simultaneous intracellular (patch-clamp whole-cell recordings) and extracellular (field recordings) were performed in the CA1 region (Fig. 7A). To reproduce the conditions used in the detailed computational model, we stimulated the CA3 area and recorded responses intracellularly from the CA1 pyramidal layer and extracellularly from CA1 stratum radiatum. When superfused with control ACSF, stimulation of CA3 axons induced a field PSP (Fig. 7B), through release of glutamatergic neurotransmitters (AMPA/NMDA). To follow the prediction of the detailed computational

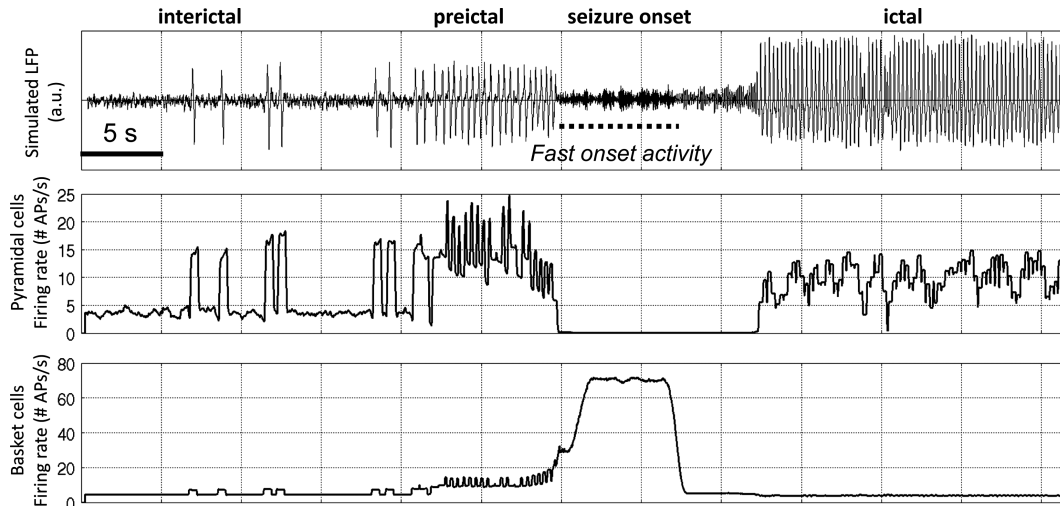


FIG. 6. Macroscopic model of hippocampal activity. The fast-onset activity observed at the onset of seizures is explained by the sustained firing of somatic-projecting projecting interneurons (fast GABA_A receptor-mediated IPSPs). During this fast-onset activity, the average firing rate in the pyramidal cell sub-population is dramatically reduced. Experimental validation of these findings were reported in Gnatkovsky *et al.* (2008), although authors focused on the EC. APs, action potentials; LFPs, local field potentials.

model, we complemented the above-described stimulation (activation of AMPA receptors and NMDA receptors): (i) by a reduction GABA-current by using low concentration of GABA receptor antagonist bicuculline; and (ii) by an indirect increase of NMDA current (by lowering the extracellular magnesium concentration from 1.2 to 0.3 mM). These procedures led to a fairly reproducible induction of FRs in LFP recordings (Fig. 7C, top trace), associated with a strong slow depolarization (on top of which APs were produced) in simultaneous intracellular recordings (Fig. 7C, bottom trace). During this stimulation protocol, the further increase of the slice excitability through the activation of AMPA receptors (supplementary bath application of a low dose of AMPA) led to the generation of epileptic spikes as predicted by the computational model (Fig. 7D). Finally, we could also observe that the additional increase of the excitability of the slice (bath application of 4-AP, 50–100 μ M) or high concentration of the GABA_A receptors antagonist (bicuculline, 50 μ M) led to the generation of ictal-like activity (Fig. 7E).

Discussion and perspectives

The imbalance between excitation and inhibition has long been a leading concept in epilepsy research (Bernard *et al.*, 1998). According to this concept, the epileptic tissue is characterized by either an increase of excitation or a decrease of inhibition at the level of principal cells, or both. This characteristic property of the epileptic tissue is probably true. However, we think that the excitation/inhibition concept is somehow too simplistic, as a plethora of mechanisms most often non-linear and highly interlinked can lead to hyperexcitability in neuronal systems. We also think that this is precisely on this issue that computational models can help epilepsy research. Indeed, biologically inspired models provide a very efficient framework to integrate many of these mechanisms into a system of constraints based on neurophysiological knowledge. In addition, when these computational models are intimately linked with experimental models, not only those mechanisms potentially leading to epileptic activity can be more easily identified but also a finer interpretation of observations can be derived. This model-based interpretation could progressively lead to a new era where our way of looking at electrophysiological signals

(LFPs, EEG) would change and would get closer to underlying mechanisms. More particularly, in the context of typical epilepsy-related signatures (interictal spikes and FRs, seizures) analysed in this paper, we could get a number of insights regarding hyperexcitability from both macro- and microscopic computational models. These insights are discussed below, from a comparative perspective. Then, the limitations of the present study are addressed and some perspectives to this work are presented.

Hyperexcitability mechanisms in spikes, FRs and seizures – what do we learn from models?

In the macroscopic (lumped) model, excitatory processes must definitely be increased and inhibitory processes must be decreased in order to produce interictal spikes and ictal activity. Increased excitation was achieved by increasing the amplitude of average excitatory postsynaptic potentials (EPSPs) at each glutamatergic synaptic transmission site in the model (pyramidal to pyramidal cells, pyramidal cells to interneurons). Regarding inhibition, the situation is not as simple. The model predicted that GABA_A receptor-mediated inhibition is a crucial factor (as reviewed in Avoli & de Curtis, 2011), but also that two types (slow and fast) of inhibition (possibly corresponding to dendritic and somatic inhibition) were necessary to reproduce the typical phases and the corresponding signal dynamics observed during the interictal to ictal transition. Inhibition had to be indeed gradually lowered in the model to get to seizure activity, but this disinhibition (achieved via the amplitude of slow GABA_A IPSPs) was, in the model, dendritic. The faster peri-somatic inhibition (fast GABA_A IPSPs) had to be maintained at seizure onset in order to produce fast oscillations in the simulated LFP. It is worth mentioning that some recent experimental findings support the hypothesis according to which the fast-onset activity is closely related to the generation of fast IPSPs onto pyramidal cells (Gnatkovsky *et al.*, 2008). An interesting finding in the macroscopic model is the impossibility to generate FRs under the constraint that rise and decay times of PSPs stay in appropriate physiological ranges. This model ‘incompleteness’ can be explained by several properties of macroscopic models, among which the fact that individual cells (and thus

Decrease of GABAergic inhibition

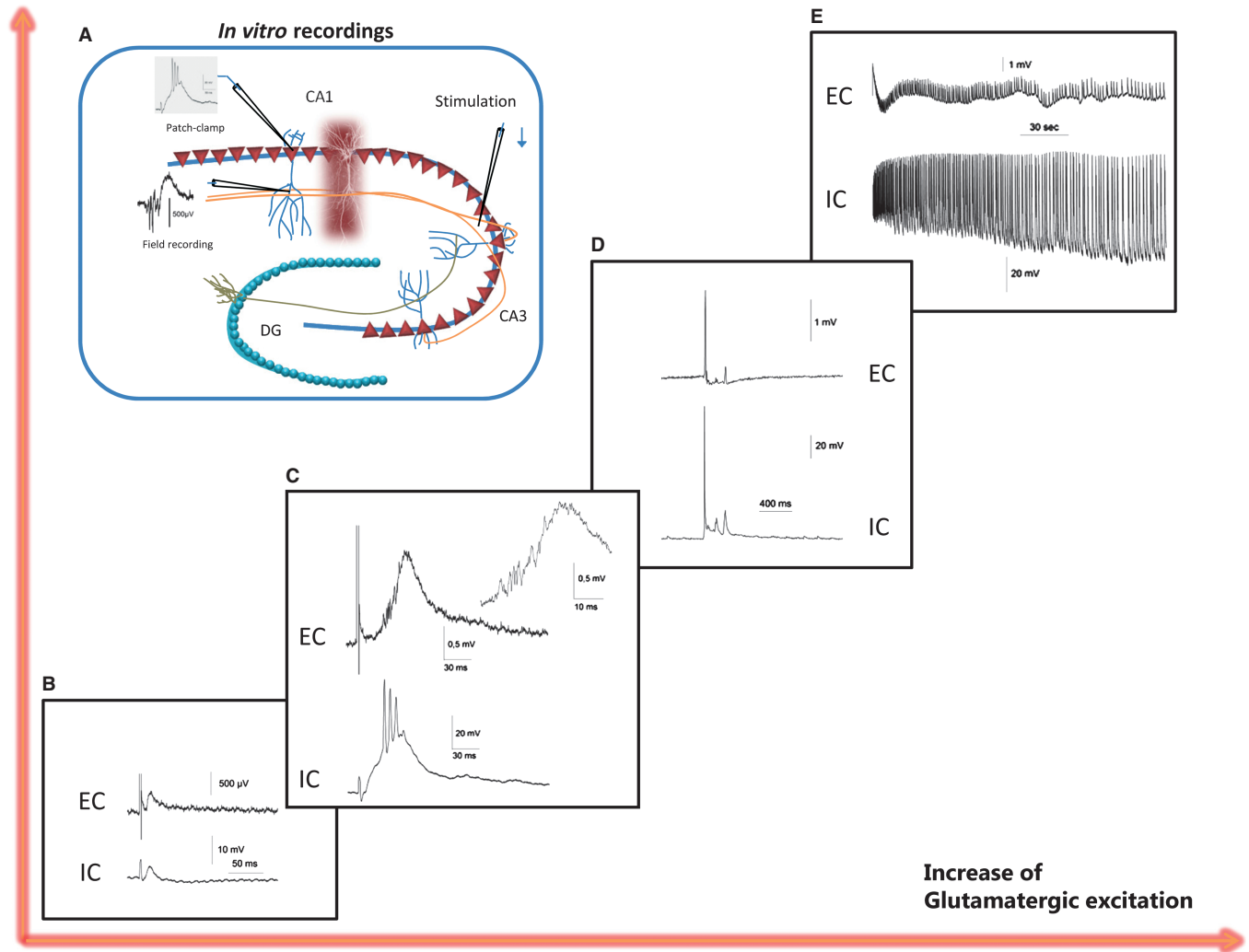


FIG. 7. Experimental validation of the detailed model predictions. (A) *In vitro* recordings were performed to test the model prediction about the effect of network excitability (respective role of glutamatergic and GABAergic neurotransmission) on the generation of distinct interictal (spikes or FRs) and ictal-like activity. (B) Under control condition (normal excitability), no FRs or epileptic spikes could be generated. (C) As predicted by the model, evoked FRs could be generated with a moderate increase of excitability, while (D) epileptic spikes could be obtained when excitability was significantly increased. (E) Further increase of excitability induced seizure-like activity. CA1 responses were induced by electrical stimulation of the CA3–CA1 pathway. Increase of excitability was obtained by the lowering magnesium level (unblocked NMDA receptors) and adding low concentration of GABA_A receptor antagonist (2–4 μM bicuculline). Evoked epileptic spikes could be generated by adding AMPA (4–6 μM) to the previous condition. Transient seizure-like activity followed by spontaneous epileptic spikes could be obtained by using either 4-AP (100 μM) or high concentration of bicuculline (40 μM). DG, dentate gyrus; EC, extracellular; GABA, γ -aminobutyric acid; IC, intracellular.

firing patterns) are not explicitly represented. Indeed, this type of model assumes a hypersynchronization of the activity of cells ‘merged’ together into a given sub-population. This result indicates that this hypersynchronization assumption is probably correct for the spiking, the fast-onset (20–30 Hz) and the rhythmic ictal activity, and that it may not hold when HFOs like FRs (250–500 Hz) are to be generated. Recently, we studied ‘chirp-like’ rapid discharges (70–100 Hz) observed in neocortical seizures using a macroscopic model similar to that presented here but adapted to the cerebral cortex (Molae-Ardekani *et al.*, 2010a). We noticed that it was somehow difficult to go beyond 110–120 Hz while respecting physiological values for the kinetics of EPSPs and IPSPs.

In the microscopic (detailed) model, we do not have, at this stage, many results regarding the simulation of the interictal to ictal transition (see limitations below). This work-in-progress issue will be addressed

in future studies. Regarding the generation of interictal spikes and FRs, we learnt that the excitation/inhibition ratio should also be increased to produce electrophysiological events resembling those actually observed. But here again, our results show that there are multiple manners to alter this ratio, and that subtle changes in the hyperexcitability of simulated neuronal networks can lead to either spikes or FRs. In particular, the number of hyperexcitable cells (small vs. large clusters) is a first determinant factor. In our model, the fact that GABAergic currents may become depolarizing is also an important factor in the generation of FRs and, to some extent, in the generation of spikes. This result corroborates those reported in Cohen *et al.* (2002) and shows that depolarizing GABAergic events in subicular pyramidal cells contribute to interictal-like activity in an *in vitro* human subiculum preparation. The weak synchronization of firing patterns of pyramidal cells in the generation of FRs is also an

interesting prediction of the model that corroborates recently published findings (Ibarz *et al.*, 2010). Finally, our conductance-related parameter sensitivity analysis revealed that subtle changes in the synaptic transmission (increase of g_{AMPA} and g_{NMDA} , decrease of g_{GABA}) could lead to different electrophysiological events (population spikes, interictal-like spikes, FRs or sustained seizure-like activity) in the LFP. This prediction, which was experimentally verified, is interesting as the increase of g_{AMPA} can be interpreted in different ways. At a postsynaptic level, it can correspond to changes in the properties of AMPA receptors (subunit alteration, phosphorylation, etc.) or to an increased number of channels (insertion of new channels, synaptic plasticity, long-term potentiation). At a presynaptic level, it can describe an increased neurotransmitter release. All these mechanisms are encountered in the epileptic brain.

Macroscopic or microscopic?

Although epilepsy is a complex dynamical disease, it is generally admitted that epileptic activity corresponds to caricatured quasi-deterministic mechanisms. For this reason, we think that computational modelling is particularly adapted to epileptic processes because these processes are much less subtle than those involved in normal brain activity. To model epilepsy-related mechanisms, both macro- and microscopic approaches have their own advantages and limitations. The structure of macroscopic models as well as their parameters can be relatively easily adapted to the specific cyto-architecture of brain structures (for instance, the EC; Labyt *et al.*, 2007). They make it possible to simulate quite extended neuronal systems like the olfactory system (Freeman, 1978) or the thalamo-cortical loop (Suffczynski *et al.*, 2001), among others. The recent past years have witnessed a considerable increase of interest for such approaches. This is probably because epilepsy is a disease that often involves relatively extended areas or systems that can hardly be represented at a cellular level, given the still limited power of computers for simulating large-scale neuronal networks with explicit representation of all neurons. However, parameters governing these models are themselves macroscopic and are not directly related to cellular or sub-cellular levels, by definition. In addition, they assume a synchronous activity of cells in the sub-populations interconnected to model the considered neuronal population. Our results show that this assumption may not always hold for all epileptic events. Therefore, we also need more detailed approaches that provide access to cellular parameters among which some are hardly accessible experimentally (like the properties of voltage-dependent or leak channels, ionotropic channels, etc.). A nice feature of detailed models is also to simultaneously generate intracellular and extracellular activity, for all cell types represented in the network. However, difficulties in parameter identification increase with the level of detail, in particular regarding the network topology (Dyhrfeld-Johnsen *et al.*, 2007). In addition, there is an inherent compromise between building more and more detailed models vs. being able to compute them in short time and using them in practical situations. To give an idea, in the detailed hippocampus model, each pyramidal cell is represented by a two-compartment model accounting for 16 different ionic currents (each based on Hodgkin–Huxley formalism). We simulated networks including up to 3000 cells and also accounting for three types of synapses (AMPA, NMDA and GABA). In such networks, the time required to generate 1 s of activity on a quad-core PC is about half an hour. In addition, the number of parameters is quite high and appropriate strategies must be defined to ‘globally’ (i.e. at the level of all cells and synaptic interactions in the network) change the parameters values.

Limitations of this study and future work

In this study, we did not explicitly address the important issue of interrelating the two described models, as this issue would deserve a specific study itself. In particular, it may be interesting to investigate whether mathematical approaches (equation-free, statistical neurodynamics, aggregation of variables) can help us: (i) to reduce the detailed model into an aggregated model; (ii) to identify the macrodynamic variables and equations; and (iii) to determine to what extent these variables and equations correspond to those governing the lumped-parameter model.

This work is still to be done. What we can do, at this stage, is to establish some qualitative relations between both models. First, because the two models are intended to reproduce the same neuronal system (the hippocampal CA1 subfield), they share a number of features. Both models include main pyramidal cells and different types of interneurons, although the detailed model adds a subset of bistratified cells that is not presented in the lumped model. The connectivity patterns (pyr-pyr, pyr-in, in-pyr, in-in) are comparable. Regarding the synaptic transmission, both models include glutamatergic and GABAergic synapses. However, a distinction between AMPA and NMDA receptors is accounted for in the detailed model, conversely to the lumped model in which the average EPSP is characterized by a single kinetics. Second, both models have some limitations. At this stage, none of them implements plasticity-related effects, although these could be obtained by making some relevant parameters time-dependent (for instance, the amplitude of PSPs at macro-level or the conductance values at micro-level). Interneurons are simplified and limited to two or three types. The input to CA1 is restricted to CA3. Finally, models do not account for metabolic variables or for interactions with glial cells that may also be important in epilepsy.

Nevertheless and, despite these limitations, we could find some similarities in the LFPs generated by both models. In the microscopic model, we noticed that some model parameter configurations could lead to sustained rhythmic activity that could correspond to ictal-like activity. So far, we have not analysed this model bifurcation in detail. Therefore, at this stage, any comparison with the ictal-like activity generated by the macroscopic model would be pure speculation. Conversely, for epileptic spikes, we could simulate quite similar ‘LFP events’ from both models. Therefore, we are in a situation where the same system (the hippocampus CA1 subfield), modelled at two different scales (cellular and population), can produce similar spikes. In this context, the identification of some relationships between parameter sets at considered levels of description (cellular and population) seems achievable. These relationships would help us to better understand the meaning of aggregated parameters in macroscopic models as a function of microscopic ones. We think that this simulation framework is a first step toward the development of across-scale approaches and further toward multi-level models.

Acknowledgements

This work was supported by ‘Region Bretagne’ (CREATE 2009, ‘EPIGONE’ project). The authors are grateful to Dr Marco de Curtis for providing the data recorded from the guinea-pig isolated brain preparation.

Abbreviations

ACSF, artificial cerebrospinal fluid; AMPA, α -amino-3-hydroxy-5-methyl-4-isoxazolepropionic acid; AP, action potential; CT, computer tomography; EC, entorhinal cortex; EEG, electroencephalogram; EPSP, excitatory postsynaptic potential; EXC, excitatory; EZ, epileptogenic zone; FR, fast ripple; FSI, fast somatic inhibitory; GABA, γ -aminobutyric acid; HFOs, high-frequency oscillations; IES, interictal epileptic spike; IPSP, inhibitory postsynaptic potential; KA, kainic acid; LFP, local field potential; MRI, magnetic resonance imaging; NMDA, *N*-methyl-D-aspartate; OLM, oriens-lacunosum moleculare; PSP, postsynaptic potential; SDI, slow dendritic inhibitory; TLE, temporal lobe epilepsy.

References

- Albus, K., Wahab, A. & Heinemann, U. (2008) Standard antiepileptic drugs fail to block epileptiform activity in rat organotypic hippocampal slice cultures. *Br. J. Pharmacol.*, **154**, 709–724.
- Andersen, P., Morris, R., Amaral, D., Bliss, T. & O'Keefe, J. (2007) *The Hippocampus Book*. Oxford University Press, New York.
- Asano, E., Muzik, O., Shah, A., Juhasz, C., Chugani, D.C., Sood, S., Janisse, J., Ergun, E.L., Ahn-Ewing, J., Shen, C., Gotman, J. & Chugani, H.T. (2003) Quantitative interictal subdural EEG analyses in children with neocortical epilepsy. *Epilepsia*, **44**, 425–434.
- Avoli, M. & de Curtis, M. (2011) GABAergic synchronization in the limbic system and its role in the generation of epileptiform activity. *Prog. Neurobiol.*, **95**, 104–132.
- Avoli, M., Biagini, G. & de Curtis, M. (2006) Do interictal spikes sustain seizures and epileptogenesis? *Epilepsy Curr.*, **6**, 203–207.
- Avoli, M., D'Antuono, M., Louvel, J., Kohling, R., Biagini, G., Pumain, R., D'Arcangelo, G. & Tancredi, V. (2002) Network and pharmacological mechanisms leading to epileptiform synchronization in the limbic system in vitro. *Prog. Neurobiol.*, **68**, 167–207.
- Bancaud, J. & Talairach, J. (1973) [Methodology of stereo EEG exploration and surgical intervention in epilepsy]. *Rev. Otoneuroophthalmol.*, **45**, 315–328.
- Banks, M.I., White, J.A. & Pearce, R.A. (2000) Interactions between distinct GABA(A) circuits in hippocampus. *Neuron*, **25**, 449–457.
- Bartolomei, F., Chauvel, P. & Wendling, F. (2008) Epileptogenicity of brain structures in human temporal lobe epilepsy: a quantified study from intracerebral EEG. *Brain*, **131**, 1818–1830.
- Bernard, C., Esclapez, M., Hirsch, J.C. & Ben-Ari, Y. (1998) Interneurons are not so dormant in temporal lobe epilepsy: a critical reappraisal of the dormant basket cell hypothesis. *Epilepsy Res.*, **32**, 93–103.
- Bouillere, V., Ridoux, V., Depaulis, A., Marescaux, C., Nehlig, A. & Le Gal La Salle, G. (1999) Recurrent seizures and hippocampal sclerosis following intrahippocampal kainate injection in adult mice: electroencephalography, histopathology and synaptic reorganization similar to mesial temporal lobe epilepsy. *Neuroscience*, **89**, 717–729.
- Bragin, A., Engel, J. Jr, Wilson, C.L., Fried, I. & Buzsaki, G. (1999a) High-frequency oscillations in human brain. *Hippocampus*, **9**, 137–142.
- Bragin, A., Engel, J. Jr, Wilson, C.L., Fried, I. & Mathern, G.W. (1999b) Hippocampal and entorhinal cortex high-frequency oscillations (100–500 Hz) in human epileptic brain and in kainic acid – treated rats with chronic seizures. *Epilepsia*, **40**, 127–137.
- Cohen, I., Navarro, V., Clemenceau, S., Baulac, M. & Miles, R. (2002) On the origin of interictal activity in human temporal lobe epilepsy in vitro. *Science*, **298**, 1418–1421.
- Coombes, S. (2010) Large-scale neural dynamics: simple and complex. *Neuroimage*, **52**, 731–739.
- Cossart, R., Dinocourt, C., Hirsch, J.C., Merchán-Pérez, A., De Felipe, J., Ben-Ari, Y., Esclapez, M. & Bernard, C. (2001) Dendritic but not somatic GABAergic inhibition is decreased in experimental epilepsy. *Nat. Neurosci.*, **4**, 52–62.
- Deco, G., Jirsa, V.K., Robinson, P.A., Breakspear, M. & Friston, K. (2008) The dynamic brain: from spiking neurons to neural masses and cortical fields. *PLoS Comput. Biol.*, **4**, e1000092.
- Demont-Guignard, S., Benquet, P., Gerber, U. & Wendling, F. (2009) Analysis of intracerebral EEG recordings of epileptic spikes: insights from a neural network model. *IEEE Trans. Biomed. Eng.*, **56**, 2782–2795.
- Demont-Guignard, S., Benquet, P., Gerber, U., Biraben, A., Martin, B. & Wendling, F. (2011) Distinct hyperexcitability mechanisms underlie fast ripples and epileptic spikes. *Ann. Neurol.*, in press, <http://onlinelibrary.wiley.com/doi/10.1002/ana.22610/abstract>.
- Dyhrfeld-Johnsen, J., Santhakumar, V., Morgan, R.J., Huerta, R., Tsimring, L. & Soltesz, I. (2007) Topological determinants of epileptogenesis in large-scale structural and functional models of the dentate gyrus derived from experimental data. *J. Neurophysiol.*, **97**, 1566–1587.
- Fisher, R.S., Webber, W.R., Lesser, R.P., Arroyo, S. & Uematsu, S. (1992) High-frequency EEG activity at the start of seizures. *J. Clin. Neurophysiol.*, **9**, 441–448.
- Freeman, W.J. (1973) A model of the olfactory system. In Brazier, M.A.B., Walter, D.O. & Schneider, D. (Eds), *Neural Modeling*. University of California, Los Angeles, CA, pp. 41–62.
- Freeman, W.J. (1978) Models of the dynamics of neural populations. *Electroencephalogr. Clin. Neurophysiol. Suppl.*, **34**, 9–18.
- Gahwiler, B.H., Capogna, M., Debanne, D., McKinney, R.A. & Thompson, S.M. (1997) Organotypic slice cultures: a technique has come of age. *Trends Neurosci.*, **20**, 471–477.
- Geselowitz, D.B. (1967) On bioelectric potentials in an inhomogeneous volume conductor. *Biophys. J.*, **7**, 1–11.
- Gnatkovsky, V., Librizzi, L., Trombin, F. & de Curtis, M. (2008) Fast activity at seizure onset is mediated by inhibitory circuits in the entorhinal cortex in vitro. *Ann. Neurol.*, **64**, 674–686.
- Hajos, M., Hoffmann, W.E., Orban, G., Kiss, T. & Erdi, P. (2004) Modulation of septo-hippocampal Theta activity by GABAA receptors: an experimental and computational approach. *Neuroscience*, **126**, 599–610.
- Hodgkin, A.L. & Huxley, A.F. (1952) The components of membrane conductance in the giant axon of *Loligo*. *J. Physiol.*, **116**, 473–496.
- Hodgkin, A.L., Huxley, A.F. & Katz, B. (1952) Measurement of current-voltage relations in the membrane of the giant axon of *Loligo*. *J. Physiol.*, **116**, 424–448.
- Hoffman, D.A., Magee, J.C., Colbert, C.M. & Johnston, D. (1997) K⁺ channel regulation of signal propagation in dendrites of hippocampal pyramidal neurons. *Nature*, **387**, 869–875.
- Hufnagel, A., Dumpelmann, M., Zentner, J., Schijns, O. & Elger, C.E. (2000) Clinical relevance of quantified intracranial interictal spike activity in presurgical evaluation of epilepsy. *Epilepsia*, **41**, 467–478.
- Huneau, C., Demont-Guignard, S., Benquet, P., Martin, B. & Wendling, F. (2010) Time-domain features of epileptic spikes as potential bio-markers of the epileptogenesis process. *Conf. Proc. IEEE Eng. Med. Biol. Soc.*, **2010**, 6007–6010.
- Ibarz, J.M., Foffani, G., Cid, E., Inostroza, M. & Menendez de la Prida, L. (2010) Emergent dynamics of fast ripples in the epileptic hippocampus. *J. Neurosci.*, **30**, 16249–16261.
- Jacobs, J., Levan, P., Chatillon, C.E., Olivier, A., Dubeau, F. & Gotman, J. (2009) High frequency oscillations in intracranial EEGs mark epileptogenicity rather than lesion type. *Brain*, **132**, 1022–1037.
- Jacobs, J., Zijlmans, M., Zemann, R., Chatillon, C.E., Hall, J., Olivier, A., Dubeau, F. & Gotman, J. (2010) High-frequency electroencephalographic oscillations correlate with outcome of epilepsy surgery. *Ann. Neurol.*, **67**, 209–220.
- Klausberger, T. & Somogyi, P. (2008) Neuronal diversity and temporal dynamics: the unity of hippocampal circuit operations. *Science*, **321**, 53–57.
- Labyt, E., Frogerais, P., Uva, L., Bellanger, J.J. & Wendling, F. (2007) Modeling of entorhinal cortex and simulation of epileptic activity: insights into the role of inhibition-related parameters. *IEEE Trans. Inf. Technol. Biomed.*, **11**, 450–461.
- Lancaster, B. & Adams, P.R. (1986) Calcium-dependent current generating the afterhyperpolarization of hippocampal neurons. *J. Neurophysiol.*, **55**, 1268–1282.
- Lancaster, B. & Nicoll, R.A. (1987) Properties of two calcium-activated hyperpolarizations in rat hippocampal neurons. *J. Physiol.*, **389**, 187–203.
- Lopes da Silva, F.H., Hoeks, A., Smits, H. & Zetterberg, L.H. (1974) Model of brain rhythmic activity. The alpha-rhythm of the thalamus. *Kybernetik*, **15**, 27–37.
- Lytton, W.W. (2008) Computer modelling of epilepsy. *Nat. Rev. Neurosci.*, **9**, 626–637.
- Marsh, E.D., Peltzer, B., Brown, M.W. 3rd, Wusthoff, C., Storm, P.B. Jr, Litt, B. & Porter, B.E. (2010) Interictal EEG spikes identify the region of electrographic seizure onset in some, but not all, pediatric epilepsy patients. *Epilepsia*, **51**, 592–601.
- Mayer, M.L. & Westbrook, G.L. (1983) A voltage-clamp analysis of inward (anomalous) rectification in mouse spinal sensory ganglion neurones. *J. Physiol.*, **340**, 19–45.
- Molae-Ardekani, B., Benquet, P., Bartolomei, F. & Wendling, F. (2010a) Computational modeling of high-frequency oscillations at the onset of neocortical partial seizures: from 'altered structure' to 'dysfunction'. *Neuroimage*, **52**, 1109–1122.
- Muhlethaler, M., de Curtis, M., Walton, K. & Llinas, R. (1993) The isolated and perfused brain of the guinea-pig in vitro. *Eur. J. Neurosci.*, **5**, 915–926.
- Murakami, S. & Okada, Y. (2006) Contributions of principal neocortical neurons to magnetoencephalography and electroencephalography signals. *J. Physiol.*, **575**, 925–936.
- Paxinos, G. & Franklin, K.B.J. 2001. *The Mouse Brain in Stereotaxic Coordinates*, 2nd Edn. Academic Press, San Diego, CA.
- Pinsky, P.F. & Rinzel, J. (1994) Intrinsic and network rhythmogenesis in a reduced Traub model for CA3 neurons. *J. Comput. Neurosci.*, **1**, 39–60.
- Rodin, E., Constantino, T., Rampp, S. & Wong, P.K. (2009) Spikes and epilepsy. *Clin. EEG Neurosci.*, **40**, 288–299.
- van Rotterdam, A., Lopes da Silva, F.H., van den Ende, J., Viergever, M.A. & Hermans, A.J. (1982) A model of the spatial-temporal characteristics of the alpha rhythm. *Bull. Math. Biol.*, **44**, 283–305.

- Scanziani, M., Debanne, D., Müller, M., Gähwiler, B.H. & Thompson, S.M. (1994) Role of excitatory amino acid and GABAB receptors in the generation of epileptiform activity in disinhibited hippocampal slice cultures. *Neuroscience*, **61**, 823–832.
- Soltesz, I. & Staley, K.J. (2008) *Computational Neuroscience in Epilepsy*. Elsevier Academic Press, London.
- Staley, K.J., White, A. & Dudek, F.E. (2011) Interictal spikes: harbingers or causes of epilepsy? *Neurosci. Lett.*, **497**, 247–250.
- Stefan, H., Lopes da Silva, F.H., Loscher, W., Schmidt, D., Perucca, E., Brodie, M.J., Boon, P.A., Theodore, W.H. & Moshe, S.L. (2006) Epileptogenesis and rational therapeutic strategies. *Acta Neurol. Scand.*, **113**, 139–155.
- Suffczynski, P., Kalitzin, S., Pfurtscheller, G. & Lopes da Silva, F.H. (2001) Computational model of thalamo-cortical networks: dynamical control of alpha rhythms in relation to focal attention. *Int. J. Psychophysiol.*, **43**, 25–40.
- Suffczynski, P., Wendling, F., Bellanger, J.-J. & Da Silva, F.H.L. (2006) Some insights into computational models of (Patho)physiological brain activity. *Proc. IEEE*, **94**, 784–804.
- Suzuki, F., Junier, M.P., Guilhem, D., Sorensen, J.C. & Onteniente, B. (1995) Morphogenetic effect of kainate on adult hippocampal neurons associated with a prolonged expression of brain-derived neurotrophic factor. *Neuroscience*, **64**, 665–674.
- Talairach, J. & Bancaud, J. (1966) Lesion, “irritative” zone and epileptogenic focus. *Confin. Neurol.*, **27**, 91–94.
- Taylor, A.L., Goaillard, J.M. & Marder, E. (2009) How multiple conductances determine electrophysiological properties in a multicompartiment model. *J. Neurosci.*, **29**, 5573–5586.
- Thompson, S., Cai, X., Dinocourt, C. & Nestor, M. (2005) The use of brain slice cultures for the study of epilepsy. In Pitkänen, A., Schwartzkroin, P.A. & Moshé, S.L. (Eds), *Models of Seizures and Epilepsy*. Elsevier Academic Press, Burlington, San Diego, London, pp. 45–58.
- Traub, R.D. (1979) Neocortical pyramidal cells: a model with dendritic calcium conductance reproduces repetitive firing and epileptic behavior. *Brain Res.*, **173**, 243–257.
- Ullah, G. & Schiff, S. (2009) Models of epilepsy. *Scholarpedia*, (http://www.scholarpedia.org/article/Models_of_epilepsy), **4**, 1409.
- Wendling, F. (2008) Computational models of epileptic activity: a bridge between observation and pathophysiological interpretation. *Expert Rev. Neurother.*, **8**, 889–896.
- Wendling, F. & Chauvel, P. (2008) Transition to ictal activity in temporal lobe epilepsy: insights from macroscopic models. In Soltesz, I. & Staley, K. (Eds), *Computational Neuroscience in Epilepsy*. Elsevier Academic Press, London, pp. 356–386.
- Wendling, F., Bartolomei, F., Bellanger, J.J. & Chauvel, P. (2002) Epileptic fast activity can be explained by a model of impaired GABAergic dendritic inhibition. *Eur. J. Neurosci.*, **15**, 1499–1508.
- Wendling, F., Bartolomei, F., Bellanger, J.J., Bourien, J. & Chauvel, P. (2003) Epileptic fast intracerebral EEG activity: evidence for spatial decorrelation at seizure onset. *Brain*, **126**, 1449–1459.
- Wendling, F., Hernandez, A., Bellanger, J.J., Chauvel, P. & Bartolomei, F. (2005) Interictal to ictal transition in human temporal lobe epilepsy: insights from a computational model of intracerebral EEG. *J. Clin. Neurophysiol.*, **22**, 343–356.
- White, J.A., Banks, M.I., Pearce, R.A. & Kopell, N.J. (2000) Networks of interneurons with fast and slow gamma-aminobutyric acid type A (GABAA) kinetics provide substrate for mixed gamma-theta rhythm. *Proc. Natl. Acad. Sci. USA*, **97**, 8128–8133.
- White, A., Williams, P.A., Hellier, J.L., Clark, S., Edward Dudek, F. & Staley, K.J. (2010) EEG spike activity precedes epilepsy after kainate-induced status epilepticus. *Epilepsia*, **51**, 371–383.
- Wilson, H.R. & Cowan, J.D. (1972) Excitatory and inhibitory interactions in localized populations of model neurons. *Biophys. J.*, **12**, 1–24.
- Worrell, G. & Gotman, J. (2011) High-frequency oscillations and other electrophysiological biomarkers of epilepsy: clinical studies. *Biomark. Med.*, **5**, 557–566.
- Zijlmans, M., Jiruska, P., Zelmann, R., Leijten, F., Jefferys, J. & Gotman, J. (2011) High frequency oscillations as a new biomarker in epilepsy. *Ann. Neurol.*, in press, <http://onlinelibrary.wiley.com/doi/10.1002/ana.22548/abstract>.

How Deep Brain Stimulation Modulates Cortical Epileptic Dynamics – Insights from Computational Modeling*

F. Mina, P. Benquet, A. Pasnicu, A. Biraben, F. Wendling

Abstract— Despite the growing scientific evidence that supports the efficacy of deep brain stimulation (DBS) for controlling epileptic seizure dynamics, further research remains mandatory to optimize DBS parameters for an efficient clinical use. In particular, progress can be expected from detailed study of the still poorly understood mechanisms that are responsible for the modulation of neural activity by DBS. In this work, a computational model of the thalamocortical loop was developed to explore the mechanisms of thalamic DBS and its effects on cortical dynamics. The model was tuned using real intracerebral EEG (iEEG) signals recorded in an epileptic patient. Results confirmed the dependence of DBS activated mechanisms on the choice of stimulation frequency. They revealed that short-term depression, feed-forward inhibition, and stimulation-induced depolarization of inhibitory reticular neurons seem to be key factors of frequency-dependent effects.

I. INTRODUCTION

The last decade has witnessed a remarkable advance in deep brain stimulation (DBS) technologies for movement and neurological disorders. Particularly in epilepsy, clinical trials showed that DBS effects remain largely variable from a patient to another ([1] for review). These effects depend on the choice of stimulation parameters which are patient-specifically tuned. Indeed, four fundamental issues should be resolved to optimize stimulation outcome: the choice of 1) the brain structure to be stimulated, 2) the stimulation current waveform 3) its frequency and finally 4) its intensity. As the choice of current waveform (usually biphasic pulse train) and intensity is often restrained for safety considerations, this study addresses the frequency-dependence of DBS effects and mechanisms in the thalamocortical loop – a brain system often targeted by clinical DBS protocols. On that account, a coupled clinical/computational approach was adopted in this work. First, a computational mesoscopic model of the thalamocortical loop was developed based on the literature [2, 3]. Intracerebral EEG (iEEG) signals recorded in an epileptic patient were used to tune the model parameters in order to assess the model face value, and to generate mechanistic insights about the impact of DBS on epileptic activity.

*The first author is supported by regional research allocations (AREC) from the region of Brittany France.

F. Mina, P. Benquet, A. Biraben and F. Wendling are with the LTSI (Laboratoire Traitement du Signal et de l'Image), Inserm, U1099, Beaulieu campus, University of Rennes 1, Rennes, France (faten.mina@univ-rennes1.fr, fabrice.wendling@univ-rennes1.fr; +33223235605).

A. Pasnicu and A. Biraben are with the epilepsy unit of the university hospital of Rennes, France. Rue Henri Le Guilloux, 35033, Rennes, France.

II. METHODS

A. Neural Mass Model of the Thalamocortical Loop

We implemented a mesoscopic neural mass model of the thalamocortical loop to study the mechanisms underlying the modulation of cortical epileptic dynamics by thalamic stimulation. This model was inspired from existing models [2, 3] and thus followed the general three-module architecture; a thalamic, a reticular and a cortical module, each composed of one or several neural subpopulations (Figure 1). Moreover, three new features were explicitly integrated into the model: 1) the implementation of an extended cortical module as in [4] including two types of GABAergic interneurons, 2) the incorporation of stimulation inputs following the “ λE ” model at the thalamic and reticular level [5], thus assuming that stimulation current linearly affects the transmembrane potential of the impacted subpopulations due to the current-induced electric field, and 3) the implementation of two mechanisms potentially activated by stimulation: thalamocortical feed-forward inhibition (FFI) and synaptic short-term depression (STD).

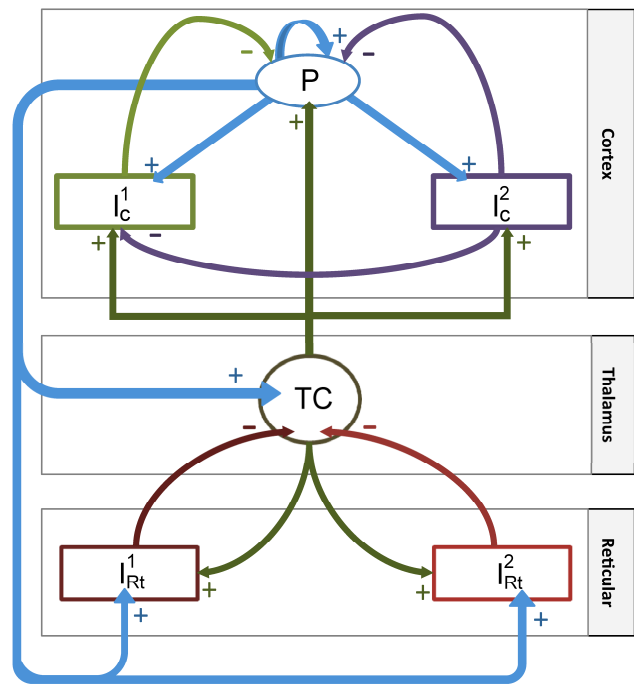


Figure 1. Model architecture.

Feed-forward inhibition. FFI implied that the TC cells of the thalamic module extend excitatory projections not only to

the pyramidal neurons (P) of the cortical module but also to the two inhibitory populations I_c^1 and I_c^2 . Thereby, the three cortical populations receive glutamatergic input from the same presynaptic source, i.e. TC cells. In response to their activation by thalamocortical firing, I_c^1 and I_c^2 produce inhibitory postsynaptic potentials (IPSP) onto the P subpopulation. Thus, the latter receives two types of input due to thalamic firing, an excitatory input followed by an inhibitory input lagging by a synaptic delay. The inhibitory input designates FFI. Nowadays, FFI is a well-admitted mechanism in thalamocortical circuitry probably responsible for input normalization and sensory integration [6], yet little is known about its role in antiepileptic thalamic DBS.

Short-term depression. Short-term plasticity is a mechanism of transient activity-dependent modulation of synaptic efficacy. It is often related to cellular interactions lying at the presynaptic terminal. As for short-term depression, experimental evidence as well as previous implementations in microscopic neural models suggest that it is particularly related to vesicle depletion after episodes of intense/repetitive firing (see [7] for review). To our knowledge, such a short-term cellular mechanism has never been implemented at the mesoscopic or macroscopic levels.

Our model accounts for STD at thalamocortical synapses ($TC \rightarrow P$) following evidence [8] that low-frequency stimulation (LFS) trains can provoke up to 40% depression in cortical EPSPs recorded in the absence of GABAergic inhibition. We consequently implemented a vesicle depletion-based STD mechanism at the level of glutamatergic cortical synapses formed between subpopulations TC and P . This implementation suggested that intense low-frequency thalamic firing provokes a transient short-term depression in the efficacy of these synapses. Formally, STD was modeled as a time varying-function $\kappa(t)$, that varies between 0.6 and 1 following the intensity/frequency of the mean density of thalamic action potentials $d_{AP}(t)$. $\kappa(t)$ is multiplied by the amplitude (A_c) of thalamocortical EPSPs at $TC \rightarrow P$ synapses and thus dynamically modulates their efficacy.

Technically, the implemented mechanism of STD involves two steps. First $d_{AP}(t)$ is filtered by a low-pass filter (cutoff frequency $f_c = 10$ Hz) to limit the effects to low-frequency stimulation. Then, the filtered signal $d_{AP}^f(t)$ is compared to a mean firing threshold λ in order to assure that STD is produced following a high release of cortical glutamate. Every supra-threshold firing of TC cells at instant t_0 ($d_{AP}^f(t_0) > \lambda$), entrains an exponential decrease ($\tau = 8$ s) of $\kappa(t)$ from $\kappa(t_0)$ to 0.6. The duration of this decrease was extended to 0.5s after each thalamic supra-threshold firing. $\kappa(t)$ is formally described by the following dynamics:

$$\kappa(t) = \begin{cases} 0.4(d_{AP}^f(t) > \lambda) \cdot \frac{(u(t) - u(t - 0.5))}{2} e^{-t/\tau} + 0.6 \\ 0.4(d_{AP}^f(t) < \lambda) \cdot (1 - e^{-t/\tau}) + 0.6 \end{cases}$$

where $u(t)$ is the Heaviside function.

B. Clinical Data to Tune Model Parameters

To assure a realistic epileptic model output, model parameters were optimized using real iEEG signals recorded during the pre-surgical evaluation of a patient with drug-resistant epilepsy at the epilepsy surgery unit of the

university hospital of Rennes, France [9]. This particular dataset was used for two reasons. Firstly, the patient had recording electrodes implanted in a cortical malformation (focal cortical dysplasia; FCD) particularly known for characteristic epileptic discharges [10], and in a thalamic nucleus reported as a potentially antiepileptic target for DBS [11] (centromedian thalamic nucleus; CMN). Secondly, the stimulation of this nucleus during the pre-surgical iEEG evaluation modulated the epileptic activity of the FCD in a frequency-dependent manner. Briefly, low-frequency (LFS, < 2 Hz) as well as high-frequency (HFS, > 70 Hz) stimulation suppressed the almost continuous epileptic activity observed in the FCD, while intermediate-frequency stimulation (IFS, 50Hz) showed no effect.

C. Signal Processing and Parameter Optimization

The matching pursuit algorithm (Matching Pursuit Toolkit - MPTK [12] available online at <http://mptk.irisa.fr/>) was used to decompose real and simulated iEEG activity into time-frequency components using a multi-scalar dictionary of Gabor, Fourier, and Dirac atoms (10 different scales ranging from 0.125 to 5s). The atom parameters (type, scale ζ , frequency f , amplitude C , phase ϕ , position p) extracted by MPTK were used to analytically reconstruct the corresponding atoms in predefined frequency bands depending on their characteristic frequency. The general analytic expression used for the Gabor atom reconstruction is of the form

$$C \cdot e^{-\pi((t-p)/\zeta)^2} \cdot \cos(2\pi ft + \phi)$$

A Dirac is reconstructed if the scale ζ is null at position p and of amplitude C . The decomposition algorithm follows exactly the one summarized in [12]. As for the frequency bands, they represent the classic EEG bands defined as follows: δ_1 [0 – 1.9Hz], δ_2 [1.9 – 3.4 Hz], θ_1 [3.4 – 5.4 Hz], θ_2 [5.4 – 7.4 Hz], α_1 [7.4 – 10 Hz], α_2 [10 – 12 Hz], β_1 [12 – 18 Hz], β_2 [18 – 24 Hz] and γ [24 – 128 Hz].

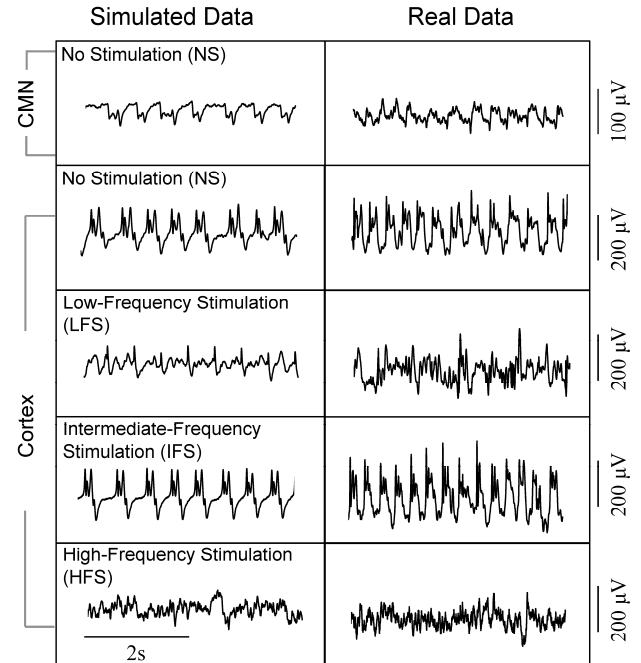


Figure 2. Simulated and real iEEG signals.

Finally, 9D feature vectors \vec{V}_c representing the normalized energy distribution in these frequency bands were used to characterize real and simulated signals. They were extracted as follows:

$$\vec{V}_c(i) = \frac{1}{N} \sum_{j=1}^N s_i(j)^2 \bigg/ \sum_{i=1}^9 \vec{V}_c(i)$$

where s_i is the reconstructed signal in the i^{th} frequency band and N is the number of samples in the initial signal.

Free model parameters were limited to cortical excitability and inhibition coefficients [A_c, B_c, G_c], while all other parameters were fixed. Brute-Force optimization (over pre-defined physiological ranges) was used to adjust the model parameters during the no stimulation (NS) condition. The cost function was defined as the distance between the aforementioned feature vectors \vec{V}_c as computed on simulated and real iEEG signals in the absence of stimulation.

III. RESULTS

A. Simulating Epileptic Dynamics and Stimulation Effects

Model parameter optimization allowed the definition of a triplet $\theta_0 = [A_c, B_c, G_c]$ necessary for generating qualitatively similar epileptic dynamics as those observed in real iEEG recordings (Figure 2). Actually, the output of both cortical and thalamic modules exhibited features comparable to those observed in real iEEG signals.

The different stimulation-induced effects observed in actual iEEG signals were reproduced in the model by simulating the thalamic stimulation input. The manual tuning of the parameters [$S_{TC}, S_{Irl}, S_{Irl2}$] – representing the multiplicative impact coefficients of stimulation on the neural populations of both subcortical modules (TC, I_{Rt}^1 and I_{Rt}^2) – allowed the qualitative reproduction of the real cortical activity observed during the different stimulation conditions (Figure 2). Interestingly, comparable stimulation effects could not be reproduced if stimulation effects were limited to the thalamic module (S_{Irl} and S_{Irl2} set to zero).

B. Stable Model Output

In order to assess the resemblance of simulated and real iEEG signals, and to check the stability of the model output, five random simulations (uniform distribution $U(\theta_0 - 0.05 \cdot \theta_0, \theta_0 + 0.05 \cdot \theta_0)$) of each of the different stimulation conditions were generated using a 5% interval around the optimal parameters θ_0 . The 9D feature vector \vec{V}_c of each signal, real and simulated, was then reduced into a 3D feature vector \vec{V}_{c3D} accounting for the energy in the lower ($\delta_2 + \theta_1$), medium ($\theta_2 + \alpha + \beta_1$), and higher iEEG bands ($\beta_2 + \gamma$). The resulting feature vectors of real signals were then classified into 3 groups using k-means and projected in the same 3D space with the feature vectors of simulated signals. Results are depicted in Figure 3. Each point represents the 3D feature vector of real (circles) and simulated (asterisks) iEEG. The simulated signals are visibly close to the corresponding k-means clusters of real signals. A net decrease in the low-frequency signal component can be affirmed for LFS and HFS in real and simulated signals, whereas the real and simulated signals corresponding to IFS

closely resemble those of the NS (no stimulation) condition and were thus classified in the same group.

C. Model Phase Portraits

Figures 2 and 3 show that, in the model, stimulation induced qualitatively comparable effects as those observed in the patient's iEEG signals. To highlight this fact, the phase portraits of two key variables in the model, thalamic firing and cortical activity (designating the sum of input EPSPs/ IPSP arriving to the population P), were plotted in the four different conditions NS, LFS, IFS and HFS (Figure 4). Similar frequency ranges as those used in the clinical context were used for illustration. As depicted, in the absence of stimulation (NS condition), the thalamocortical system oscillates on a limit cycle. During the LFS (4 Hz) condition, cortical oscillations are largely diminished while the thalamic firing was transiently increased following stimulation pulses and diminished afterwards. On the other hand, the IFS (40 Hz) stimulation condition seems to be the least efficient for model bifurcation. It actually increased thalamic firing while the system continued to oscillate on a limit cycle. Finally, HFS (130 Hz) completely changed the system's behavior from limit cycle to fixed point. The consequent simulated cortical LFP resembles actual normal iEEG activity.

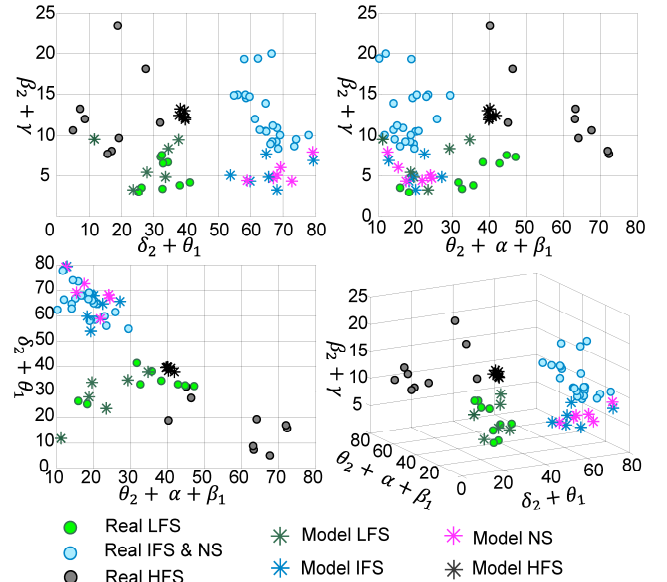


Figure 3. Real signal k-means classification of reduced 3D feature vectors \vec{V}_{c3D} under NS (no stimulation), low-frequency (LFS), intermediate-frequency (IFS), and high-frequency (HFS) stimulation conditions. Simulated signal feature vectors are projected in the same space.

D. Mechanisms of Action

Supplementary simulations were run in order to evaluate the necessity of the implemented mechanisms for the reproduction of the observed stimulation effects. For this, the implemented mechanisms were deactivated one at a time. Effectively, the implementation of FFI and STD proved necessary to simulate LFS effects. Only coupled, these two mechanisms diminish thalamocortical oscillations. Unexpectedly, the absence of effects of IFS necessitates the depolarization of slow reticular inhibitory neurons I_{Rt}^2 by stimulation.

Actually, when simulated, if stimulation impacts only the TC and/or I_{Rt}^1 neural populations, the model bifurcates to a normal functioning mode during IFS. Finally, the depolarization of both fast and slow reticular inhibitory populations I_{Rt}^1 and I_{Rt}^2 was necessary to reproduce HFS effects. Otherwise, HFS cannot modulate epileptic dynamics.

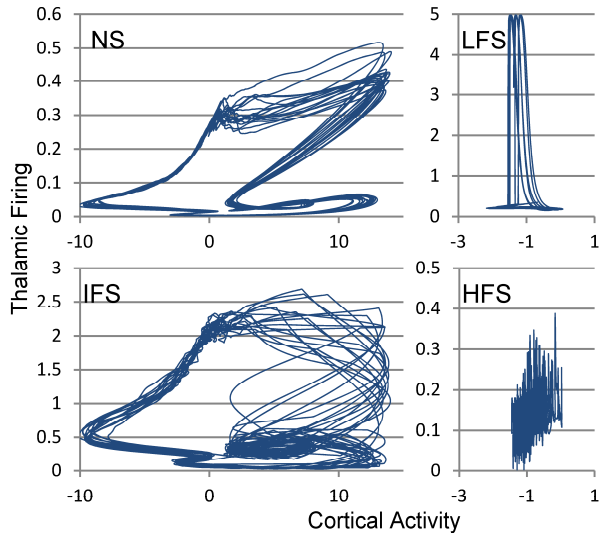


Figure 4. Phase portraits of cortical activity vs. thalamic firing. During the no stimulation (NS) condition, the system oscillates on a limit cycle. Cortical activity is diminished during low-frequency stimulation (LFS; 4 Hz), whereas thalamic firing increases transiently following stimulation pulses. Cortical activity barely changes during intermediate-frequency stimulation (IFS; 40 Hz) whereas thalamic firing increases. High-frequency stimulation (HFS; 130 Hz) switches the model from a limit cycle functioning mode to a more normal fixed point functioning mode.

IV. DISCUSSION AND CONCLUSION

The originality of this study resides in the fact that it explores the effects of thalamic DBS on epileptic cortical dynamics over a wide range of stimulation frequencies (LFS, IFS, and HFS), thus evoking the frequency-dependence of stimulation effects.

As for LFS, its effects engage two capital mechanisms, STD and FFI. In the presence of GABA antagonist, repetitive trains of thalamic LFS provoked a 40% decrease in cortical EPSPs *in vivo* [8]. Actually, LFS effects could not be reproduced by the model in the absence of STD implementation. The use of IFS (50 Hz) is well-reputed for its epileptic potential in the kindling model [13]. The model-revealed paradox resides in the fact that slow inhibitory reticular neurons should be depolarized by stimulation in order to maintain the epileptic character of this stimulation. On the other hand, HFS condition requires the depolarization of both inhibitory reticular populations to suppress epileptic activity. The depolarization of these neurons actually participates to the diminution of TC firing and thus the diminution of cortical epileptic discharges. The suppression of the output of the stimulated target during HFS has been reported in several previous studies as in [14]. Moreover, the use of real iEEG signals to tune the model allowed the identification of capital parameters responsible of the epileptogenicity of the focal cortical dysplasia (FCD; cortical malformation). Actually, cortical excitation parameter A_c had

to be doubled whereas the inhibition parameters B_c and G_c had to be diminished by 72% and 25% respectively in order to generate epileptic discharges rather than normal iEEG signals. The deterioration or dysfunction of inhibition has already been reported in dysplastic tissue [10].

Indeed, while the effects of IFS and HFS seem to be less controversial, LFS antiepileptic effects remain more investigational. More complex stimulation protocols might be needed to provoke therapeutic effects using LFS [15]. Experimental validation of the proposed mechanisms would be helpful to verify the model's predictions. Such experiments can be performed in rodents. Electrodes can be implanted in the thalamus and in the cortex to 1) verify the reproducibility of these effects in control/epileptic animals and 2) therefore, experimentally investigate and validate the proposed mechanisms.

REFERENCES

- [1] P. Boon, R. Raedt, V. de Herdt, *et al.*, "Electrical stimulation for the treatment of epilepsy," *Neurotherapeutics*, vol. 6, pp. 218-27, Apr 2009.
- [2] P. Suffczynski, S. Kalitzin, G. Pfurtscheller, *et al.*, "Computational model of thalamo-cortical networks: dynamical control of alpha rhythms in relation to focal attention," *Int J Psychophysiol*, vol. 43, pp. 25-40, Dec 2001.
- [3] P. A. Robinson, C. J. Rennie, and D. L. Rowe, "Dynamics of large-scale brain activity in normal arousal states and epileptic seizures," *Phys Rev E Stat Nonlin Soft Matter Phys*, vol. 65, p. 041924, Apr 2002.
- [4] B. Molaee-Ardekani, P. Benquet, F. Bartolomei, *et al.*, "Computational modeling of high-frequency oscillations at the onset of neocortical partial seizures: from 'altered structure' to 'dysfunction'," *Neuroimage*, vol. 52, pp. 1109-22, Sep 2010.
- [5] P. C. Miranda, F. Wendling, G. Ruffini, *et al.*, *Brain stimulation: models, experiments and open questions, Deliverable D1.1: review of the state of the art in currents distribution and effects* HIVE (FET Open FP7 EU project), Available at <http://hive-eu.org>, 2009.
- [6] L. Gabernet, S. P. Jadhav, D. E. Feldman, *et al.*, "Somatosensory integration controlled by dynamic thalamocortical feed-forward inhibition," *Neuron*, vol. 48, pp. 315-27, Oct 20 2005.
- [7] M. H. Hennig, "Theoretical models of synaptic short term plasticity," *Front Comput Neurosci*, vol. 7, p. 45, 2013.
- [8] W. J. Speechley, J. L. Hogsden, and H. C. Dringenberg, "Continuous white noise exposure during and after auditory critical period differentially alters bidirectional thalamocortical plasticity in rat auditory cortex *in vivo*," *Eur J Neurosci*, vol. 26, pp. 2576-84, Nov 2007.
- [9] A. Pasnicu, Y. Denoyer, C. Haegelen, *et al.*, "Modulation of paroxysmal activity in focal cortical dysplasia by centromedian thalamic nucleus stimulation," *Epilepsy Research*, p. in press, 2013.
- [10] M. Avoli, J. Louvel, D. Mattia, *et al.*, "Epileptiform synchronization in the human dysplastic cortex," *Epileptic Disord*, vol. 5 Suppl 2, pp. S45-50, Sep 2003.
- [11] F. Velasco, A. L. Velasco, M. Velasco, *et al.*, "Deep brain stimulation for treatment of the epilepsies: the centromedian thalamic target," *Acta Neurochir Suppl*, vol. 97, pp. 337-42, 2007.
- [12] S. Krstulovic and R. Gribonval, "Mptk: Matching Pursuit Made Tractable," in *IEEE International Conference on Acoustics, Speech and Signal Processing*, 2006, pp. 496 - 499.
- [13] G. V. Goddard, "Development of epileptic seizures through brain stimulation at low intensity," *Nature*, vol. 214, pp. 1020-1, Jun 3 1967.
- [14] L. D. Liu, I. A. Prescott, J. O. Dostrovsky, *et al.*, "Frequency-dependent effects of electrical stimulation in the globus pallidus of dystonia patients," *J Neurophysiol*, vol. 108, pp. 5-17, Jul 2012.
- [15] P. A. Tass, L. Qin, C. Hauptmann, *et al.*, "Coordinated reset has sustained aftereffects in Parkinsonian monkeys," *Annals of neurology*, vol. 72, pp. 816-820, 2012.

Effets de la stimulation électrique intracérébrale sur l'activité corticale : apport de la modélisation biomathématique

FATEN MINA^{1,2}, PASCAL BENQUET^{1,2}, ANCA PASNICU³, ARNAUD BIRABEN^{1,2,3}, FABRICE WENDLING^{1,2}

¹ INSERM, U1099, Rennes, F-35000, France

² Université de Rennes 1, LTSI, F-35000, France

³ Unité d'Épileptologie, Service de Neurologie, CHU, Rennes, F-35000, France

faten.mina@univ-rennes1.fr, pascal.benquet@univ-rennes1.fr,

fabrice.wendling@univ-rennes1.fr

Résumé – Plusieurs études récentes mettent en évidence le potentiel antiépileptique de la stimulation électrique intracérébrale. Cependant, pour la plupart de ces études, le choix des paramètres de stimulation reste souvent déterminant pour empêcher l'activité épileptique. La mise au point des paramètres est déterminée de manière empirique, non optimisée, s'explique par une connaissance incomplète des mécanismes d'action de la stimulation électrique profonde. Cette étude adresse cette problématique en couplant la modélisation biomathématique aux données cliniques. Elle concerne plus particulièrement les effets de la stimulation thalamique sur l'activité corticale épileptique. Les résultats montrent que l'activité épileptique corticale est fortement modulée en fonction de la fréquence de stimulation thalamique. Les différents mécanismes cellulaires responsables de cette modulation sont ensuite identifiés et étudiés.

Abstract – Recent clinical trials and animal studies highlight the antiepileptic potential of Deep Brain Stimulation (DBS) on epileptic neural dynamics. However, for the majority of these studies, the choice of stimulation parameters remains critical for obtaining antiepileptic effects. This suboptimal empirical approach is due to our limited knowledge about the mechanisms by which DBS modulates neuronal dynamics. This study addresses this issue with a coupled computational/clinical approach. In particular, we study the effects of thalamic stimulation on epileptic cortical activity. The results show that epileptic cortical activity is modulated by thalamic stimulation in a frequency-dependent manner. The different cellular mechanisms responsible for this modulation are then identified and studied.

1 Introduction

Depuis deux décennies, plusieurs études (voir [1] pour une revue) se sont intéressées aux effets antiépileptiques de la stimulation intracérébrale, notamment pour diminuer la survenue des crises. Ceci est particulièrement utile dans le cas des épilepsies partielles pharmaco-résistantes. Pourtant, les approches empiriques employées dans ces études n'ont pas répondu aux questions les plus fondamentales concernant l'optimisation des paramètres de stimulation : à quel endroit faut-il stimuler, à quelle fréquence, à quelle intensité du courant ? Cet empirisme est en partie dû à une compréhension très incomplète des mécanismes cellulaires qui sous-tendent la stimulation électrique [2], et particulièrement dans le contexte des activités épileptiques humaines.

Dans cette étude, un modèle biomathématique basé sur les connaissances neurophysiologiques actuelles est proposé pour étudier les effets de la stimulation électrique sur les dynamiques neuronales épileptiques. Le couplage de ce modèle avec des données cliniques a permis l'identification de certains facteurs clés responsables de la modulation – observée en clinique – de l'activité corticale épileptique par stimulation thalamique. Nos résultats montrent qu'en fonction de la fréquence de stimulation choisie, des mécanismes cellulaires distincts sont déclenchés suite à la stimulation thalamique.

2 Méthodes et Matériaux

2.1 Modélisation biomathématique

Dans ce travail, les effets de la stimulation électrique intracérébrale sur la dynamique neuronale de la boucle thalamocorticale (particulièrement visée en clinique) sont étudiés. Pour se faire, un modèle méso-scopique de cette structure cérébrale a été implémenté. L'architecture du modèle proposé (Fig. 1) est inspirée des modèles précédemment publiés de la boucle thalamocorticale [3, 4]. Il se compose de 3 modules principaux, cortical, thalamique et réticulaire, chacun comportant des sous-populations de neurones. Cependant, les aspects nouveaux de ce modèle se situent dans : 1) l'intégration des entrées de stimulation au niveau des modules thalamique et réticulaire, 2) l'implémentation d'un module cortical [5] plus complet par rapport aux modèles précédents de la boucle thalamocorticale afin de mieux reproduire les dynamiques épileptiques observées dans les signaux de stéréo-électro-encéphalographiques (SEEG) réels, et enfin 3) l'implémentation de deux mécanismes potentiellement impliqués pendant la stimulation à l'interface des modules thalamique et cortex cérébral, à savoir l'inhibition antérograde ($TC \rightarrow I_c^1$ et $TC \rightarrow I_c^2$) et la dépression synaptique à court terme ($TC \rightarrow P$).

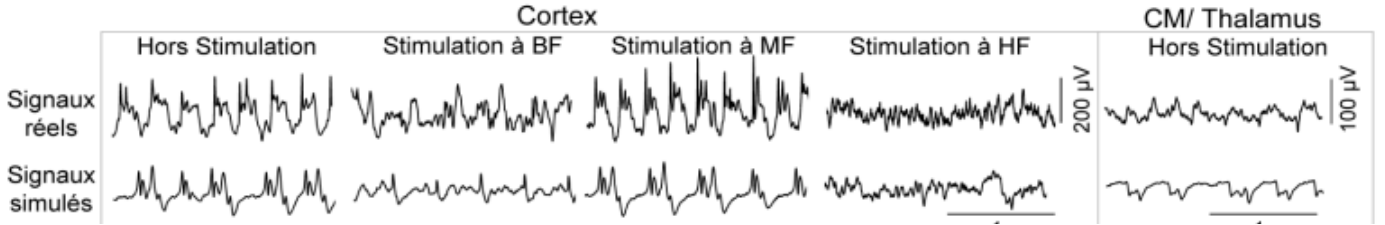


Figure 2 : Signaux réels et simulés sous les différentes conditions de stimulation

étape. Ensuite, un vecteur 9D de caractéristiques (\vec{V}_c) a été défini, correspondant à la distribution normalisée de l'énergie du signal (s_i ; $i = \{1, 2, \dots, 9\}$) dans les neuf sous-bandes fréquentielles $\{\delta_1, \delta_2, \dots, \gamma\}$.

$$\vec{V}_c(i) = \frac{\frac{1}{N} \sum_{j=1}^N s_i(j)^2}{\sum_{i=1}^9 \vec{V}_c(i)}$$

N est le nombre d'échantillons dans le signal s_i , i définit l'indice de \vec{V}_c et désigne une sous-bande fréquentielle. La sortie du modèle a été optimisée par une recherche exhaustive menée sur trois paramètres clés du modèle : l'excitation (A_c) et l'inhibition corticale (B_c, G_c). La distance euclidienne entre la moyenne des vecteurs de caractéristiques des signaux réels hors stimulation $\vec{V}_{c,réel}$ et le vecteur de caractéristiques du signal ainsi simulé $\vec{V}_{c,simulé}$ pour un triplet donné [A_c, B_c, G_c] représente ainsi la fonction du coût choisie pour optimiser la sortie du modèle hors stimulation. Par conséquent, le triplet [A_c, B_c, G_c] = argmin ($d(\vec{V}_{c,réel}, \vec{V}_{c,simulé})$) qui a permis de minimiser cette fonction de coût a été retenu comme le triplet optimal et nécessaire pour simuler une activité épileptique semblable à celle enregistrée chez le patient.

3 Résultats

3.1 Simulation de l'activité corticale hors et pendant la stimulation

L'optimisation des 3 paramètres corticaux a permis la reproduction d'une activité simulée « réaliste », c'est à dire comparable à celle observée dans la dysplasie hors stimulation (Fig. 2). Le triplet [A_c, B_c, G_c] optimal présente une augmentation de l'excitation corticale (100% de la valeur de A_c) et une diminution de

l'inhibition (72% et 25% de la valeur de B_c et de G_c respectivement) par rapport à un triplet attribué à une dynamique normale.

Pour simuler les signaux observés sous différentes conditions de stimulation, trois paramètres désignant l'impact de la stimulation sur les sous-populations thalamique et réticulaire S_{TC} , S_{R11} et S_{R12} ont été manuellement réglés. Ces trois paramètres étaient considérés constants pendant toutes les simulations. Le signal de stimulation utilisé pour les simulations était un train de pulses de durée constante et de fréquence réglable selon la condition de stimulation. La sortie du modèle montre trois zones de fonctionnement qui coïncident avec la stimulation à basse fréquence (BF, < 20 Hz), la stimulation à moyenne fréquence (MF, $20 - 70$ Hz) et la stimulation à haute fréquence (HF, ≥ 70 Hz).

3.2 Bifurcations du modèle et mécanismes impliqués

La Figure 3 montre les portraits de phase du modèle : taux de décharge de la sous-population thalamique TC en fonction de l'amplitude de l'activité corticale (à la sortie de sous-population P) dans les différentes conditions étudiées. La stimulation induit, dans le modèle, le même type de bifurcations que celles observées lors de la stimulation chez le patient. A basse fréquence (Fig. 3B), le taux de décharge de la sous-population TC augmente considérablement alors que l'amplitude de l'activité corticale diminue. A moyenne fréquence (Fig. 3C), le portrait de phase est similaire à celui obtenu hors stimulation (Fig. 3A), indiquant que cette gamme de fréquence a peu d'effets. Enfin, à haute fréquence (Fig. 3D), on observe une réduction importante des deux quantités représentées avec une

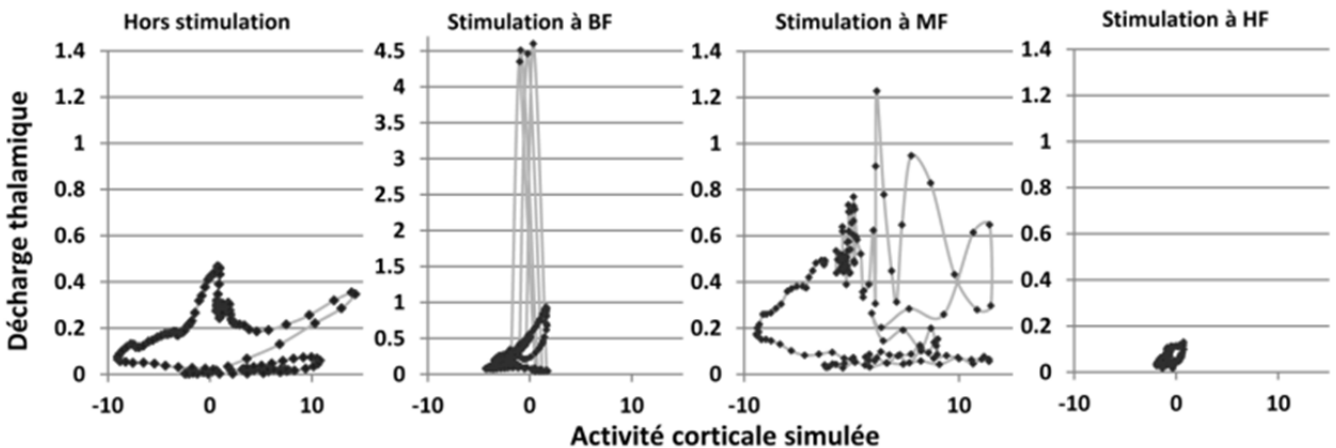


Figure 3 : Portrait de phase. Taux de décharge de la sous-population thalamique (TC) en fonction de l'amplitude de l'activité corticale (somme des potentiels post-synaptiques au niveau de la sous-population P)

suppression quasi-complète des oscillations. Une analyse détaillée des mécanismes impliqués dans ces trois configurations a conduit aux résultats suivants. Pendant la stimulation à basse fréquence, la diminution de l'amplitude de l'activité corticale est causée une dépression synaptique à court terme ($TC \rightarrow P$) qui s'ajoute à une inhibition antérograde ($TC \rightarrow IC$) renforcée. A haute fréquence, la stimulation induit une inhibition locale qui supprime la sortie thalamique conduisant ainsi à une baisse de l'excitabilité corticale. Enfin, à moyenne fréquence, la dépolarisation des neurones thalamiques (TC) renforce les oscillations pathologiques observées au niveau du cortex.

4 Discussion et conclusion

Les résultats présentés dans ce travail sont en conformité avec des études précédentes concernant les effets de la stimulation à basse [9], moyenne [12], et haute fréquence [13]. L'intérêt de cette étude concerne l'utilisation d'une approche computationnelle-clinique basé sur des hypothèses neurobiologiques récentes pour expliquer les effets sur les dynamiques épileptiques, de la stimulation électrique de la boucle thalamocorticale sur une plage étendue de fréquences de stimulation. Cette étude révèle des hypothèses originales quant aux mécanismes cellulaires impliqués dans les effets fréquence-dépendants de la stimulation électrique intracérébrale.

5 Références

[1] P. Boon, et al., Electrical stimulation for the treatment of epilepsy, *Neurotherapeutics*, Vol. 6, pp. 218-27, 2009.
 [2] C. C. McIntyre, et al., Uncovering the mechanism(s) of action of deep brain stimulation: activation, inhibition, or both, *Clinical Neurophysiology*, Vol. 115, pp. 1239-48, 2004.
 [3] J. A. Roberts and P. A. Robinson, Modeling absence seizure dynamics: Implications for basic mechanisms and measurement of thalamocortical and corticothalamic

latencies, *Journal of theoretical biology*, Vol. 253, pp. 189-201, 2008.

[4] P. Suffczynski, et al., Dynamics of non-convulsive epileptic phenomena modeled by a bistable neuronal network, *Neuroscience*, Vol. 126, pp. 467-84, 2004.

[5] B. Molaee-Ardekani, et al., Computational modeling of high-frequency oscillations at the onset of neocortical partial seizures: from 'altered structure' to 'dysfunction', *Neuroimage*, Vol. 52, pp. 1109-22, 2010.

[6] M. Bikson, et al., Effects of uniform extracellular DC electric fields on excitability in rat hippocampal slices in vitro, *J Physiol*, Vol. 557, pp. 175-90, 2004.

[7] P. C. Miranda, et al., Brain stimulation: models, experiments and open questions, Deliverable D1.1: review of the state of the art in currents distribution and effects HIVE (FET Open FP7 EU project), Available at <http://hive-eu.org>, 2009.

[8] F. Pouille and M. Scanziani, Enforcement of temporal fidelity in pyramidal cells by somatic feed-forward inhibition, *Science*, Vol. 293, pp. 1159-63, 2001.

[9] S. Chung, et al., Short-term depression at thalamocortical synapses contributes to rapid adaptation of cortical sensory responses in vivo, *Neuron*, Vol. 34, pp. 437-46, 2002.

[10] A. Pasnicu, et al., Modulation of paroxysmal activity in focal cortical dysplasia by centromedian thalamic nucleus stimulation, *Epilepsy research*, 2012.

[11] S. Krstulovic and R. Gribonval, Mptk: Matching Pursuit Made Tractable, *IEEE International Conference on Acoustics, Speech and Signal Processing* vol. 3, pp. 496 - 499, 2006.

[12] G. V. Goddard, Development of epileptic seizures through brain stimulation at low intensity, *Nature*, Vol. 214, pp. 1020-1, 1967.

[13] H. L. Kendall, et al., High frequency stimulation abolishes thalamic network oscillations: an electrophysiological and computational analysis, *Journal of Neural Engineering*, Vol. 8, p. 046001, 2011.



Modulation of intracerebral EEG signals from premotor cortical focal dysplasia by thalamic deep brain stimulation: Quantified analysis and mechanisms insights from computational modeling

F. Mina^{1,2}, P. Benquet^{1,2}, A. Pasnicu³, E Pasqualini³, A. Biraben^{1,2,3}, F. Wendling^{1,2}

1 INSERM, U642, Rennes, F-35000, France – Equipe SESAME « Systèmes Epileptogènes : Signaux et Modèles »
2 – University of Rennes 1, LTSI, F-35000, France
3 - Epileptology Unit, Neurological department, CHU Rennes; Rennes, F-35000, France

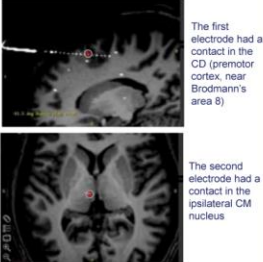
www.ltsi.univ-rennes1.fr





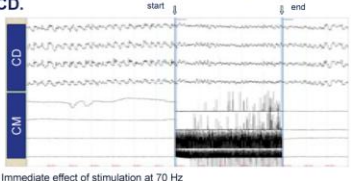

Context

- Numerous studies claim that deep brain stimulation (DBS) can be a potential therapy for medically refractory focal epilepsy.
- Yet, the mechanisms underlying its effects remain unclear.
- Our study concerns a pre-surgical depth-EEG exploration of a patient suffering partial refractory epilepsy related to a focal cortical dysplasia (FCD).
- The activity recorded in FCD
 1. Is very different from normal background neocortical activity
 2. Is highly rhythmic
 3. Presents nested δ and α rhythms with spikes and sharp waves
- DBS of the Centromedian (CM) nucleus showed strong modulatory effects of the abnormal electrophysiological activity recorded in the FCD.



The first electrode had a contact in the CD (premotor cortex, near Brodmann's area 8)

The second electrode had a contact in the ipsilateral CM nucleus.



Immediate effect of stimulation at 70 Hz



Modulation of intracerebral EEG signals in a focal dysplasia by thalamic deep brain stimulation

F. Mina^{1,2}, P. Benquet^{1,2}, A. Pasnicu³, E Pasqualini³, A. Biraben^{1,3}, F. Wendling^{1,2}

1 – INSERM, U642, Rennes, F-35000, France
2 – University of Rennes 1, LTSI, F-35000, France
3 - Epileptology Unit; Neurological department; CHU Rennes; Rennes, F-35000, France

www.ltsi.univ-rennes1.fr

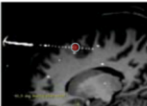




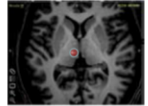

Context

□ Despite the numerous studies that claim deep brain stimulation (DBS) can be a potential therapy for medically refractory focal epilepsy, the underlying mechanisms of action remain unclear.

□ Our study concerns a pre-surgical depth-EEG exploration of a patient suffering partial refractory epilepsy related to focal cortical dysplasia (FCD).

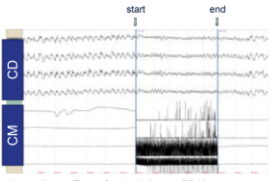


The first electrode had a contact the CD (premotor cortex, near Brodmann's area 8)

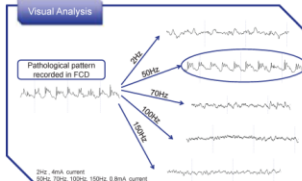


The second electrode had a contact in the ipsilateral CM nucleus

□ DBS of the Centromedian (CM) nucleus provoked modulator effects of the pathologic patterns recorded in FCD.



Immediate effect of stimulation at 70 Hz



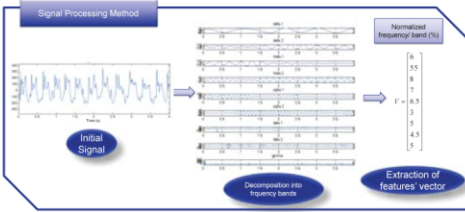
Objectives

□ Uncover the time-frequency content of the stimulation induced signals in the FCD in function of stimulation parameters.

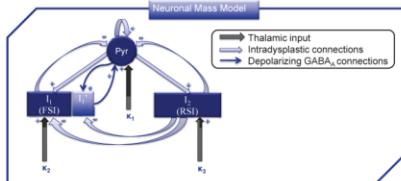
□ Explain, from a neurophysiologic point of view, the observed effects and their dependence on stimulation parameters.

Methods

□ We used time-frequency signal processing techniques to quantify signal content.

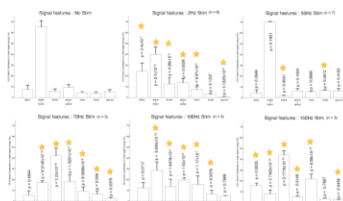


□ We introduced a physiologically relevant computational model of the cortex in order to identify the key parameters engendering the observed effects.



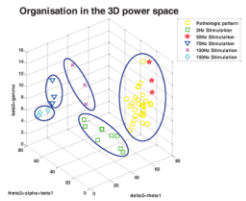
Results

□ Signal Processing confirmed pathological pattern modulation as measured by the variations of the energy contribution of frequency bands to signals' total energy in function of stimulation parameters.

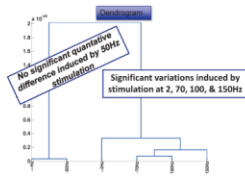


Significant changes include :

1. An increase in the band β_1 (12-18Hz) proportional to the increase of stimulation frequency.
2. A decrease in the band $\delta_2 + \theta_1$ (1.9 - 5.4Hz).

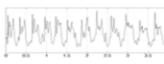


Organisation in the 3D power space



□ Preliminary model results show that dysplastic activity could be a result of an excitation/inhibition imbalance in FCD that might be caused by several hypotheses that we are currently checking.

□ The pathologic pattern has been simulated by the model by incorporating a depolarizing GABA_A sub population.

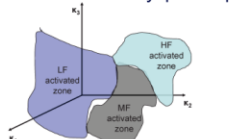



Conclusion and Perspective

□ Cortical dysplastic patterns can be modulated by thalamic stimulation as verified by signal processing results.

□ Model preliminary results evoked several hypotheses to be scrutinized:

1. Stimulation frequency determines the type of neuronal cells (pyramidal, fast spiking interneurons, regular spiking interneurons).
2. Low frequency stimulation favors feed forward inhibition by activating excitatory thalamocortical projection neurons that excite FSI.
3. Depolarizing interneurons may play a key role in the generation of the dysplastic pattern.



Some References

- McIntyre C. et al. Uncovering the mechanisms of deep brain stimulation: activation, inhibition, or both? *Clinical Neurophysiology*, 2004, 115: 1238-1248
- Pasnicu A. et al. Modulating the cortico-thalamo-cortical stimulation: a review of experimental and clinical studies. *Epileptic Disorders* 2009, 11 (2) : 102-112
- Pasnicu A. et al. Time-frequency analysis of cortical activity: a neurophysiological model from experimental animal models. *Acta Neurologica Belgica* 2009, 109: 63-80
- Pasnicu A. et al. Modulation of the epileptic activity in a premotor dysplasia by stimulation of the ipsilateral centromedian thalamic nucleus during a pre-surgical stereo-EEG exploration for partial drug-resistant epilepsy. *Epilepsia* 2010 Review
- Wendling F. et al. Neurostimulation of the centromedian thalamic nucleus in the treatment of generalized tonic-clonic and partial seizures: the improvement of the quality of life in patients with Lennox-Gastaut syndrome. *Epilepsia* 2006, 47: 1703-1712
- Poiré J., Courvaux A. et al. Stochastic Time-Frequency Clustering for Mapping Functional EEG Networks on Signal Processing, Vol. 49, No. 1, pp. 167-170, March 2011

Frequency-Dependent Modulation of Epileptic Cortical Dynamics by Thalamic Deep Brain Stimulation: A Computational Study

Faten MINA^{1,2}, Pascal Benquet^{1,2}, Anca Pasnicu³, Arnaud Biraben^{1,2,3}, Fabrice Wendling^{1,2}



¹Inserm, U1099, Rennes, F-35000, France
²Université de Rennes 1, LTSI, F-35000, France
³Unité d'Epileptologie, Service de Neurologie, CHU, Rennes, F-35000, France



Context and Objectives

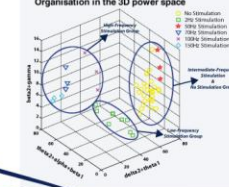
Clinical and experimental studies showed that **thalamic deep brain stimulation** is efficient in modulating pathological brain dynamics in a number of neurological disorders including refractory epilepsies.

The choice of stimulation frequency remains essential in determining stimulation effects. Antiepileptic effects are sometimes attributed to **high-frequency (>70Hz) stimulation** [1, 2]. Similar effects were reported for **low-frequency (<10Hz) stimulation** [3, 4]. Nevertheless, **intermediate-frequency (50Hz to 60Hz) stimulation** was often correlated with epileptic discharges and seizure initiation [5, 6].

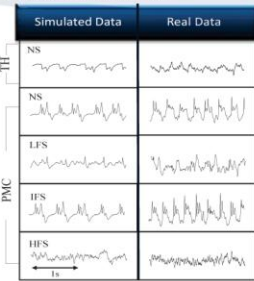
Our study aims at studying the **frequency-dependent mechanisms of thalamic deep brain stimulation** on epileptic cortical dynamics. Our approach couples **computational modeling & clinical data**.

Results

Three classes of stimulation effects were automatically detected in the clinically observed data.



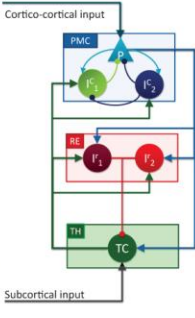
Model simulations of the observed cortical activity in the FCD of the patient in absence of stimulation as well as during low-frequency, intermediate-frequency, and high-frequency stimulation of the thalamic centromedian nucleus.



Our computational study allowed us to deduce capital insights on the frequency-dependent cellular mechanisms of thalamic deep brain stimulation.

Materials & Methods

Implementation of a mesoscopic model of the **thalamocortical loop** including a premotor cortical module (PMC), a reticular module (RE), and a thalamic module (TH).



Model parameters were optimized to reproduce clinically-observed data by decreasing the distance between the feature vectors of the simulated signals & the recorded in-depth EEG signals.



Conclusion

Further computational results provided us with more insights concerning the frequency-dependent modulation of cortical activity by deep brain stimulation, in particular:

1. LFS modulates pathological cortical activity by a dual mechanism of feed-forward inhibition coupled to short-term depression of glutamatergic cortical synapses formed on cortical principal cells.
2. IFS favors pathological cortical oscillations by provoking reticulo-thalamic oscillations.
3. HFS incites faster GABAergic responses in the reticular neurons, enough to override the stimulation-provoked EPSPs in the thalamic module (CM in the figure above).

References:

- [1] Velasco, A.L. et al. (2006). Neurostimulation of the Centromedian Thalamic Nuclei in the Treatment of Generalized Seizures and the Improvement of the Quality of Life in Patients with Lennox-Gastaut Syndrome. *Epilepsia* 47, 1203-1212.
- [2] Fisher, K. et al. (2010). Electrical stimulation of the anterior nucleus of thalamus for treatment of refractory epilepsy. *Epilepsia* 51, 899-908.
- [3] Jerger, K. and Schiff, S.J. (1995). Periodic pacing in an in vitro epileptic focus. *J Neurophysiol* 73, 876-879.
- [4] D'Arcangelo, G., Panuccio, G., Tancredi, V., and Avoli, M. (2005). Repetitive low-frequency stimulation reduces epileptiform synchronization in limbic neuronal networks. *Neurobiology of Disease* 19, 119-128.
- [5] Goddard, G.V. (1967). Development of epileptic seizures through brain stimulation at low intensity. *Nature* 214, 1020-1021.
- [6] Talbot, J. et al. (1974). New approach to the neurosurgery of epilepsy. Stereotaxic methodology and therapeutic results. 1. (Introduction and history). *Neurochirurgie* 20 Suppl 1, 1-240.
- [7] Kristulovic, S., and Grbavac, R. (2006). "Mpsk: Matching Pursuit Made Tractable", in: *IEEE International Conference on Acoustics, Speech and Signal Processing* 3, 496 - 499.



How Deep Brain Stimulation Modulates Cortical Epileptic Dynamics

- Insights from Computational Modeling

Faten MINA^{1,2}, Pascal Benquet^{1,2}, Anca Pasnicu³, Arnaud Biraben^{1,2,3}, Fabrice Wendling^{1,2}

¹Inserm, U1099, Rennes, F-35000, France
²Université de Rennes 1, LTSI, F-35000, France
³Unité d'Epileptologie, Service de Neurologie, CHU, Rennes, F-35000, France






Context and Objectives

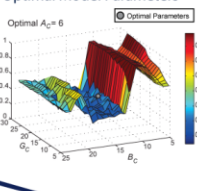
Clinical and experimental studies showed that **thalamic deep brain stimulation** is efficient in modulating pathological brain dynamics in a number of neurological disorders including refractory epilepsies.

The choice of stimulation frequency remains essential in determining stimulation effects. Antiepileptic effects are sometimes attributed to **high-frequency (>70Hz) stimulation** [1, 2]. Similar effects were reported for **low-frequency (<10Hz) stimulation** [3, 4]. Nevertheless, **intermediate-frequency (50Hz to 60Hz) stimulation** was often correlated with epileptic discharges and seizure initiation [5, 6].

Our study aims at studying the **frequency-dependent mechanisms of thalamic deep brain stimulation** on epileptic cortical dynamics. Our approach couples **computational modeling & clinical data**.

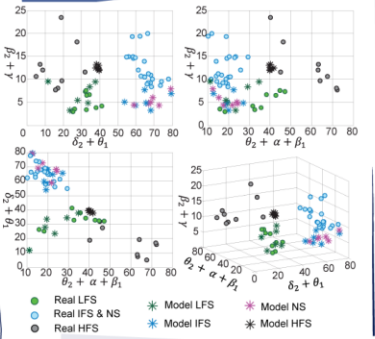
Results

Identification of Optimal Model Parameters

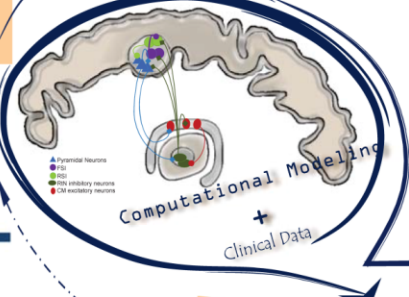


Optimal $A_1 = 6$

Three classes of stimulation effects were automatically detected in the clinically observed data.



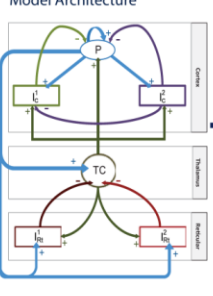
● Real LFS ● Model LFS
 ● Real IFS & NS ● Model IFS
 ● Real HFS ● Model HFS



Materials & Methods

Implementation of a mesoscopic model of the **thalamocortical loop** including a cortical, a reticular and a thalamic module.

Model Architecture



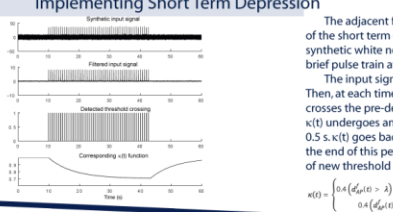
Optimization of model output
 "to reproduce pathological dynamics of a focal cortical dysplasia (FCD) observed in a patient's PM".

Model parameters were optimized to reproduce clinically-observed data by decreasing the distance between the feature vectors of the simulated signals & the recorded in-depth EEG signals.

Our computational study allowed us to deduce capital insights on the frequency-dependent cellular mechanisms of thalamic deep brain stimulation.

The stimulation frequencies used in this illustration below are in the same range as those used in the clinical context. For LFS, we used a frequency of 4 Hz, as for IFS, we used 40 Hz, and for HFS, 130 Hz.

Implementing Short Term Depression



The adjacent figure shows the response of the short term depression block to a synthetic white noise signal including a brief pulse train at 1.5 Hz. The input signal d_{in} is low-pass filtered. Then, at each time the filtered signal d_{in} crosses the pre-defined threshold, function $\kappa(t)$ undergoes an exponential decrease of 0.5 s. $\kappa(t)$ goes back exponentially to 1 at the end of this period and in the absence of new threshold crossings.

$$\kappa(t) = \begin{cases} 0.5 & \text{if } (d_{in}(t) > \lambda) \\ 0.4(d_{in}(t) < \lambda) \cdot (1 - e^{-t/\tau}) + 0.6 & \text{else} \end{cases}$$

	Simulated Data	Real Data
CM	NS	
	IFS	
	HFS	
Cortex	NS	
	LFS	
	HFS	

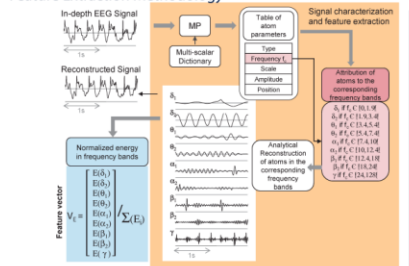
Stimulation induces in the model the same type of bifurcations observed in the real signals. The phase portraits of cortical LFP and thalamic firing show that the model oscillates on a cycle during the NS condition. Moreover, LFS reduces this cycle. IFS aggravates the spontaneous oscillations and HFS suppresses them.

Conclusion

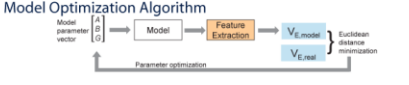
Further computational results provided us with more insights concerning the frequency-dependent modulation of cortical activity by deep brain stimulation, in particular :

- LFS modulates pathological cortical activity by a dual mechanism of feed-forward inhibition coupled to short-term depression of glutamatergic cortical synapses formed on cortical principal cells.
- IFS favors pathological cortical oscillations by provoking reticulo-thalamic oscillations.
- HFS incites faster GABAergic responses in the reticular neurons, enough to override the stimulation-provoked EPSPs in the thalamic module (CM in the figure above). Thalamic activity is inhibited by HFS, and so are cortical oscillations.

Feature Extraction Methodology



Model Optimization Algorithm



References

[1] Velasco, A.L. et al. (2006). Neurostimulation of the Centromedian Thalamic Nuclei in the Treatment of Generalized Seizures and the Improvement of the Quality of Life in Patients with Lennox-Gastaut Syndrome. *Epilepsia* 47, 1203-1212.

[2] Fisher, R. et al. (2010). Electrical stimulation of the anterior nucleus of thalamus for treatment of refractory epilepsy. *Epilepsia* 51, 899-908.

[3] Jørgen, K. and Schiff, S.J. (1995). Periodic pacing in an in vitro epileptic focus. *J. Neurophysiol* 73, 876-879.

[4] D'Arcangelo, G., Pasnicu, A., Tancède, V., and Avoni, M. (2005). Repetitive low frequency stimulation reduces epileptiform synchronization in limbic neuronal networks. *Neurobiology of Disease* 19, 119-128.

[5] Goddard, G.V. (1967). Development of epileptic seizures through brain stimulation at low intensity. *Nature* 214, 1020-1021.

[6] Talbot, L. et al. (1974). New approach to the neurosurgery of epilepsy. Stimulatory methodology and therapeutic results. 1. Introduction and history. *Neurosurgery* 20 Suppl 1, 1-240.

[7] Kristulovic, S. and Grubisic, R. (2006). "Mipic: Matching Pursuit Made Tractable", in: *IEEE International Conference on Acoustics, Speech and Signal Processing* 4, 496-499.

